A Database of Damaging Earthquakes of Moment Magnitude from 4.0 to 5.5

Cecilia Inés Nievas, Helen Crowley, Michail Ntinalexis & Julian J Bommer

General Introduction

Earthquakes are complex phenomena which can have large impact on the people living in the vicinity of the epicenter. This can include damage to buildings ranging from cracks to collapse, damage to infra-structure and psychological effects on the community. Case studies of historical earthquakes can therefore contribute to the understanding of the diversity of the effects earthquakes can have on the built environment, the natural environment, the local economy, the community and individual people.

Many case histories of earthquakes are available, but these focus primarily on larger earthquakes, like the 1906 earthquake in San Francisco and the 1960 earthquake in Chile. These tectonic earthquakes are considerably larger than the earthquakes expected to contribute to the hazard of induced earthquakes in Groningen.

Detailed case histories for earthquakes in the magnitude range relevant for Groningen are more difficult to find and often concentrate on the deep sub-surface seismological description and offer less insight into the effects of these earthquakes. NAM has therefore asked at team of academics to compile and thesaurus of earthquake case studies. This report contains the first 6 case studies of earthquakes with magnitude in the range from 4 to 5.5.

No single earthquake case will be in all respects similar to the induced earthquakes in this study, but the collection of case studies of earthquakes is thought to provide additional insights.

Together with the report; "Human Induced Earthquakes" by Gillian R. Foulger, Miles Wilson, Jon Gluyas & Richard Davies., this documents the activity to acquire an overview of earthquakes relevant for Groningen and learn from these. Both reports can be downloaded from:

www.namplatform.nl/feiten-en-cijfers/onderzoeksrapporten

NAM

Title	A Database of Damaging Earthquakes of Moment Magnitude from 4.0 to 5.5		Date	June 2016
			Initiator	NAM
Author(s)	Cecilia Inés Nievas, Helen Crowley, Michail Ntinalexis & Julian J Bommer	**Editors**	Jan van Elk Dirk Doornhof	
Organisation	Team of Academic Experts	**Organisation**	NAM	
Place in the Study and Data Acquisition Plan	Study Theme: Hazard and Risk Assessment Comment: Case studies of historical earthquakes can contribute to the understanding of the diversity of the effects earthquakes can have on the built environment, the natural environment, the local economy and people. Many case histories of earthquakes are available, for tectonic earthquakes which are considerably larger than the earthquakes expected to contribute to the hazard of induced earthquakes in Groningen. NAM has therefore asked at team of academics to compile and thesaurus of earthquake case studies. This report contains the first 6 case studies of earthquakes with magnitude in the range from 4 to 5.5. No single earthquake case will be in all respects similar to the induced earthquakes in this study, but the collection of case studies of earthquakes is thought to provide additional insights.			
Directly linked research	(1) Report "Human Induced Earthquakes, Gillian R. Foulger, Miles Wilson, Jon Gluyas & Richard Davies, Department of Earth Sciences, Durham University, Durham, U.K., Executive Office, Newcastle University, Newcastle upon Tyne, U.K.			
Used data	Open Literature.			
Associated organisation	Team of Academic Experts			
Assurance	Report is based on compilation of academic papers and open literature.			

A Database of Damaging Earthquakes of Moment Magnitude from 4.0 to 5.5

A report to NAM

Cecilia Inés Nievas, Helen Crowley, Michail Ntinalexis & Julian J Bommer

Version 1

22 June 2016

Table of Contents

1. INTRODUCTION

Gas production in the Groningen field in the northern Netherlands is leading the occurrence of earthquakes in a region for which there is no evidence for any perceptible levels of natural seismicity. The largest induced event to date occurred on 16th August 2012 near the village of Huizinge and was reported by KNMI to have a magnitude of 3.6.

In response to these induced earthquakes, NAM is conducting probabilistic assessments of the seismic hazard and risk, building on the preliminary assessments presented as part of the Winningsplan submitted in late 2013. The current hazard and risk studies are focused on the next Winningsplan that is due in mid-2016. These studies will also inform the programme for structural upgrading of vulnerable buildings in and around the gas field.
.
In probabilistic seismic hazard analyses (PSHA) conducted to define seismic design loads for new structures, the integrations are truncated at a lower magnitude limit, M_{min}, which is selected on the basis of smaller earthquakes producing insufficiently energetic motions to pose a threat to engineered structures. The rationale for M_{min} (sometimes referred to as m_0) was stated in the landmark paper by Cornell (1968) that set out the basic formulation for PSHA:

> "….and m_o *is some magnitude small enough, say 4, that events of lesser magnitude may be ignored by engineers.*"

Numerous statements conveying the same rationale can be found in basic texts on engineering seismology and earthquake engineering, such as Reiter (1990):

> "*The lower bound, or minimum, magnitude represents that level of earthquake size below which there is no engineering interest.*"

The textbook on *Geotechnical Earthquake Engineering* by Kramer (1996) makes the following statements:

> "*For engineering purposes, the effects of very small earthquakes are of little interest and it is common to disregard those that are not capable of causing significant damage.*"

The imposition of an abrupt truncation of the magnitude distribution does not mean that all earthquakes of M_{min} or greater are potentially damaging to engineered structures, but rather that no earthquake smaller than this level could be considered capable of causing distress to the structures being designed. In essence, therefore, it is about the nature of the motions generated rather than the absolute size of the earthquakes. Reiter (1990) stated the following in his discussion of minimum magnitude:

> "*If, for example, probabilistic seismic hazard analysis were sufficiently sophisticated to allow separation between non-damaging peak accelerations from small*

earthquakes and more damaging peak accelerations from large earthquakes, lower bound magnitudes could be extended as low as the data allowed."

Such an approach, based on a ground-motion filter rather than a magnitude cut-off, is precisely what is involved with the use of CAV (cumulative absolute velocity) filters as an alternative to M_{min}. Based on values of CAV predicted as conditional on PGA (peak ground acceleration), all M-R-ε (magnitude-distance-epsilon, where the latter refers to the number of standard deviations above the median prediction from a ground-motion prediction equation, or GMPE) contributions leading to motions that fall below a specified level of CAV, are excluded from the calculation of annual exceedance frequency of PGA and spectral accelerations (EPRI, 2005).

Values of M_{min} used in practice are generally in the range from 4 to 5, with the upper limit being common to PSHA studies for nuclear sites. The value of 5 for M_{min} was recommended in EPRI (1989), a 360-page document arising from a 3-day workshop conducted by the Electric Power Research Institute specifically "*to establish a lower-bound earthquake magnitude, below which the potential for damage to nuclear plants is negligible.*" The approach that EPRI adopted to address this goal was summarised as follows:

> "*The objective of the workshop was to consider a broad range of issues that could provide insight to the engineering significance of ground motion generated by small-magnitude earthquakes. Based on the presentations at the meeting it was intended to develop a strategy to select a lower-bound magnitude for use in seismic hazard assessments. An Advisory Committee reviewed the information presented at the workshop and provided recommendations concerning the level of earthquake magnitude that may be damaging to nuclear power plant structures and equipment and a strategy to establish a sound basis to determine the lower bound magnitude.*"

The use of 5 as the lower bound of magnitude 5.0 is not, however, limited to nuclear applications: this same value of M_{min} is used, for example, in the hazard mapping that forms the basis of seismic design codes in the USA (Petersen *et al.*, 2008). The European hazard map produced in the SHARE project (www.share-eu.org) was generated with a lower magnitude limit of 4.5.

The rationale for not inflating high-frequency design accelerations with contributions from frequent small-magnitude earthquakes—producing motions of very short duration and low energy content—is perfectly defensible when considering new engineered structures. For the assessment of risk to existing buildings, however—and in particular buildings whose design did not include any consideration of earthquake loading, as is the case for dwellings in the Groningen region—it would not be justifiable to exclude earthquakes in the range from magnitude 4-5 from consideration. Consequently, in the hazard and risk calculations for the Groningen field, the range of magnitudes considered is currently from **M**3.5 to **M**6.5. The upper limit is inferred from the highly improbably scenario of the maximum field compaction (at the end of production, which is currently at about the ¾ mark) being

expressed as co-seismic slip in a single event. The lower limit is based on the fact that the threshold for catalogue completeness is **M**1.5, but sensitivity analyses have shown that contributions to both hazard and risk from the first unit of magnitude are practically negligible. Given that a Monte Carlo approach is being used to perform the calculations, the computational burden of considering these very small earthquakes is worth avoiding if possible.

Disaggregations of the hazard (at the 475-year return period) and risk (in terms of 'inside local personal risk') estimates at the centre of the compaction bowl indicate dominant contributions from earthquakes in the range from **M**4 to **M**5 and a little higher. This is not a surprising result given that the contrary trends of earthquake recurrence rates decreasing with increasing magnitude (and doing so very sharply as M_{max} is approached) and accelerations increasing with increasing magnitude (at a diminishing rate due to non-linearity in the scaling) generally lead to dominant contributions from earthquakes somewhere in the middle of the considered range, depending on the annual exceedance frequency being considered.

The primary focus of both the risk modelling and the structural upgrading programmes, at least at this stage, is life safety. In other words, the main focus of the risk model is to estimate the numbers of people who could be injured or killed by structural damage caused by ground shaking. The motivation for compiling this database of damaging earthquakes with magnitudes in the same range as those dominating the hazard and risk estimates is to provide a basis for comparing and evaluating the estimated losses, or in other words, to provide a 'sanity check'. The database should provide insight to the precedents for loss of life and damage due to earthquakes of moderate magnitude, which will be helpful in assessing the reliability of the risk calculations. This is not to say that if greater losses are estimated than have been observed in other earthquakes of comparable magnitude it would automatically invalidate the risk model, but rather it would require explanation of the specific features of the Groningen field—whether related to the seismicity rates, the ground motions, or the fragility of the exposed building stock—leading to exceptionally high estimates of expected losses. Similarly, for those cases where small-to-moderate earthquakes elsewhere in the world have resulted in unexpectedly high impact in terms of damage and casualties, the study will attempt to identify the specific features that led to this outcome; the team responsible for developing the Groningen hazard and risk model would then need to address the question of whether any of these same features could be expected to be present in the Groningen case. While this purpose of providing a basis for assessing the estimated seismic risk in terms of precedents is the primary objective of this database, the information gathered will also be of benefit in informing the development of various elements of the hazard and risk models.

The core of this study is the database of earthquakes with magnitudes in the range from 4 to 5.5 that are reported to have caused appreciable damage or casualties. The listing of these earthquakes is presented in Appendix I. The information is retrieved from a wide variety of sources, of varying degrees of reliability, but all earthquakes for which a report of damage is encountered are included in the listing, providing the magnitude falls within the

specified range. A key question in this regard is the magnitude scale to be used. Ultimately, the intention would be include earthquakes with a moment magnitude, **M**, in the range from 4 to 5.5, since both the seismological model and the GMPEs for Groningen will be expressed in terms of this magnitude scale. However, seismic moments are not routinely calculated for smaller earthquakes, so in the first instance damaging earthquakes are included if they are reported to have a magnitude on any scale that falls within the specified range, unless there is an estimate of moment magnitude that falls above the limit of **M**5.5. For example, the earthquake that struck San Salvador, capital city of the Central American republic of El Salvador, on 10th October 1986 caused the collapse of hundreds of dwellings as well as several large engineered structures, leaving 1,500 dead and resulting in economic losses on the order of one-third of the GDP (Bommer *et al.*, 2001). On the basis of the body-wave magnitude, m_b, of 5.0 and the surface-wave magnitude, M_S, of 5.4, this event would have been included in this database, but it is excluded on the basis of its moment magnitude of **M**5.7. Events originally included on the basis of a magnitude on a scale other than moment magnitude may subsequently be removed if a larger moment magnitude is calculated or estimated.

For those earthquakes about which some degree of detailed information is available, case histories are presented summarising the nature of the event, the characteristics of the affected region, and the nature of the damage and other consequences. These case histories are presented in Appendix II for induced earthquakes and in Appendix III for tectonic earthquakes. The distinction is made since it may be expected that induced earthquakes provide a better analogy for the Groningen field for two main reasons: firstly, induced earthquakes are generally of shallower focal depth than most tectonic events, which places the source of energy release closer to exposed buildings, on the one hand, but may also mean that the earthquakes have lower stress drops (*e.g.*, Hough, 2014); secondly, induced earthquakes often occur in regions of relatively low natural seismicity and hence impact on built environments of low earthquake resistance. The case histories share a common format, which is explained in Chapter 2 of this report. Chapter 3 presents an overview of the case histories in Appendices II and III respectively. The report closes with a summary of the findings in Chapter 4.

2. STRUCTURE of CASE HISTORIES

In the Appendices of this report, numerous case histories of damaging earthquakes are described in some detail. In this Chapter, the information presented for each earthquake case history is briefly described together with an explanation of why the information is relevant to the objectives of this study.

2.1. Tectonic and seismic setting

This Section introduces the geographical setting of the earthquake in terms of the tectonics of the region and the characteristics of the natural seismicity, if any, of the area affected by the earthquake.

2.1.1. Tectonic setting

The tectonic setting of the earthquake will be noted in very simple terms such as whether the event occurred in an active or stable region. The location and characteristics of any well-known faults in the area of the earthquake are noted. The local stress field, if known at all from focal mechanisms or other sources, will be reported; this will be of particular relevance for those cases reported as being induced or triggered by anthropogenic activities.

2.1.2. Regional and local seismicity

The previous seismicity in the immediate vicinity of the earthquake, as well as in the broader region, is summarised. Here again the information is to provide context for the reported event, since in an active of elevated seismicity it is less likely that a moderate magnitude earthquake would attract much attention or be reported. Moreover, in a seismically active area, building practices are likely to take some account of seismic loading thus reducing the likelihood of damage from smaller earthquakes. On the contrary, events—particularly induced earthquakes—that occur in seismically quiet areas are more likely to affect vulnerable building stock and to be considered worthy of reporting.

2.1.3. Seismic hazard

A summary of existing seismic hazard assessments for the area, region or country where the earthquake occurred fulfils a similar role of providing context. Seismic hazard studies and seismic zonation maps are published for most parts of the world now, and wherever such information can be retrieved it should be reported. For ease of comparison, however, it will always be valuable to also include the hazard estimates provided in regional maps such as that produced for Europe in the SHARE project (www.share-eu.org), and global studies such as GSHAP (Giardini *et al.,* 1999). The digital data for the GSHAP global map, giving PGA values with a 475-year return period, can be accessed from the following site:

http://www.seismo.ethz.ch/static/gshap/

While this provides global coverage, some caution should be applied since the map was compiled from various national and regional studies of varying quality. Moreover, some areas were not covered by these studies, such as the United Arab Emirates, and in order to fill these gaps some interpolations and extrapolations were made that may have resulted in very unreliable hazard estimates (*e.g.*, Aldama-Bustos et al., 2009).

In addition to stand-alone seismic hazard maps, another source of relevant information will be national building codes where these include specifications for seismic design loads. Estimates of the short- and long-period spectral ordinates used to define seismic loading in the US International Building Code can be obtained for any location from the following web site, as another source of global information:

http://geohazards.usgs.gov/designmaps/ww/

2.2. Earthquake source characteristics

This section presents the basic features that characterise the earthquake and which are essential for its interpretation.

2.2.1. Location, depth and time

The location of the earthquake is defined by the geographical coordinates of the epicentre and the focal depth reported in kilometres below the Earth's surface. Estimates of these parameters will generally be available from multiple sources, including national, regional and global seismological agencies. The latter category includes the USGS and the ISC, the latter providing source characteristics about two years after the occurrence of each event but using more data and generally providing more reliable estimates. Additionally, there may be estimates provided in special studies of the individual earthquake. All of the estimates should be reported, together with their source, most conveniently in the form of a table. It is also very informative to plot the various epicentral locations on a map together with the affected locations. Where location parameters are reported together with uncertainty estimates, these should also be included in table.

The parameter that is generally most difficult to constrain is the focal depth, for which it is necessary to have recordings from nearby seismographs. For this reason, a local network may often provide the most reliable estimate of the focal depth even if the other source parameters are more reliably determined by regional or global agencies. It is common to find focal depths reported as 5, 10 or 33 km—without associated errors—which reflects the practice of constraining the depth to one of these values in order to obtain convergence in the location calculations. These values are not reliable indicators of the depth at which the earthquake occurred. For larger earthquakes in which the fault ruptures through the full depth of the seismogenic crust, the significance of the focal depth is relatively minor, but for small-magnitude earthquakes where the rupture dimensions are small in comparison to the

seismogenic thickness, the depth can be a controlling factor in the nature of the surface motions.

The origin time of the earthquake will be presented in both UTC and local time, the former (which is equivalent to GMT) being the global standard for reporting earthquakes. Local time is also important, however, for interpreting the impact of the event, especially since the number of casualties will be related to where the population is located, and may be more numerous at night for example, particularly in those cases where damage was experienced mainly by dwellings. This is discussed further in Section 2.6.3.

2.2.2. Magnitude

The basic measure of the strength of an earthquake, in terms of the total seismic energy radiated from the source, is the magnitude or the seismic moment. Magnitudes may be reported by several agencies and also on multiple scales, including local (or Richter) magnitude, M_L, and its variants based on the length of the signals, coda magnitude, MC, and duration magnitude, M_D. These measures are commonly available for small earthquakes that are only recorded by local or regional seismograph networks. In some cases, regional and global agencies will also report magnitudes on teleseismic scales such as body-wave magnitude, m_b, and surface-wave magnitude, M_S. The best indication of earthquake size is generally considered to be seismic moment, M_0, which may be converted to moment magnitude, which is represented by the symbol **M** or M_w (the former being strictly more correct for smaller earthquakes). All of the magnitude values reported for the earthquake, both by different agencies and on different scales, will be reported, again in tabular form. Subsequently, an attempt will be made to homogenise the magnitudes in the database and to assign a single representative value to each earthquake, but this will need to take account of the uncertainties in empirical correlations between magnitude scales and the need for these final magnitudes to be consistent with those being used to characterise seismicity in the Groningen field.

2.2.3. Style-of-faulting

Should centroid moment tensor (CMT) of fault plane solutions be available for the earthquake, these will be clearly reported. Although it is now common practice to include style-of-faulting in predictive equations for tectonic earthquakes (*e.g.*, Bommer *et al.*, 2003), the significance of style-of-faulting on the resulting motions from small-magnitude earthquakes has not been clearly established. However, knowledge of the style-of-faulting—and if known, the strike, dip and rake of the fault rupture—is useful for placing the earthquake in the context of the tectonic environment and the inferred causes of the event.

2.2.4. Stress drop

Inversions of the Fourier amplitude spectra of earthquake recordings can be used to estimate the source, path and site parameters that characterise the attenuation source spectrum defined according to a model such as that of Brune (1970). These parameters

include the stress parameter, Δσ, often—and not entirely correctly (Atkinson & Beresnev, 1997)—referred to as the stress drop. The value of the stress parameter is an indicator of the strength of the high-frequency radiation from the source (Figure 2.1). Since the parameters estimated from such inversions are invariably subjected to various trade-offs (*e.g.*, Edwards *et al.*, 2008), the extraction—and even more so, comparison between one inversion study and another—of individual parameter values requires some caution. However, whenever the stress drop has been estimated, it should be reported given its implications for the strength of the resulting ground motions. This is particularly relevant for induced seismicity, since a number of studies have suggested that shallow earthquakes—both induced and tectonic—tend to be associated with lower than average stress drops (*e.g.*, Allen, 2012; Hough, 2014).
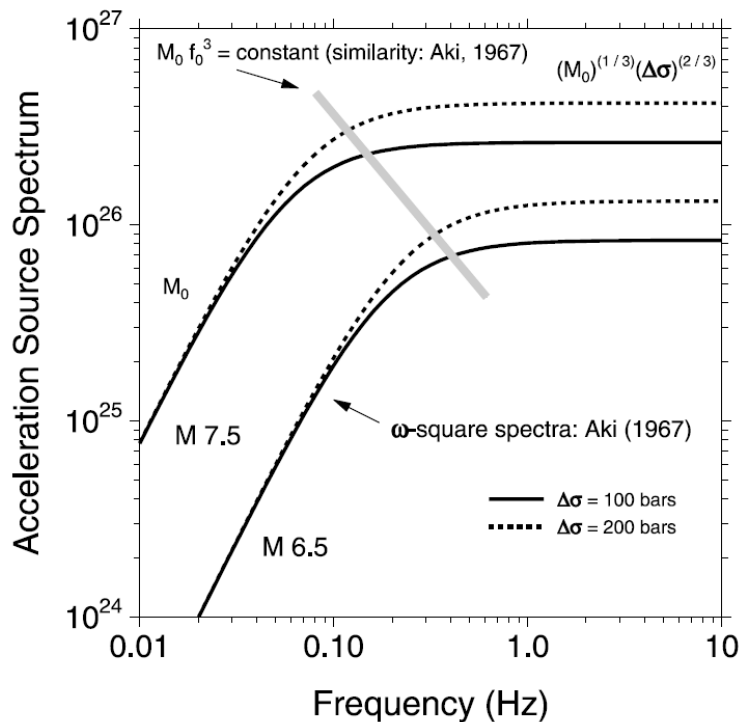
Figure 2.1. Fourier amplitude spectra of acceleration for earthquakes of **M** 6.5 and 7.5 and two values of stress drop (Boore, 2003)

2.2.5. Foreshocks and aftershocks

The document will note any felt foreshocks and aftershocks. The locations may also be shown on the same map as the epicentral locations discussed in Section 2.2.1 since they may help to constrain the source location. The primary reason for identifying felt foreshocks is that such events can prompt evacuation of buildings that results in fewer casualties when the main event strikes. The interest in aftershocks stems from both the possibility that these may compound any damage from the main shock and the fact that any prolongation of the disturbance is more likely to make it worthy of attention and reporting.

2.2.6. Nature of earthquake

In this section, we simply note whether the event was natural (*i.e.*, of tectonic, or possibly volcanic, origin) or whether it was reported to have been induced or triggered. The report will not attempt to make the discrimination between events of natural and anthropogenic origin—following published guidelines such as those proposed by Dahm *et al.* (2013)—but rather accept on face value the conclusions made in the available reports. However, in those cases where the classification has been controversial, this will be noted.

2.3. Geology and ground conditions in the affected area

The geological context of the earthquake will be very briefly summarised, the focus being primarily on how this will influence the effects of the earthquake rather than its bearing on the origin of the earthquake; the latter is already addressed in Section 2.1.1.

2.3.1. Regional geology and topography

The general geological setting of the earthquake location and the affected areas is briefly described. If there are well-known faults mapped in the area, these will be noted—and shown in map form where possible—with a note as to whether any role of these structures in the event has been inferred. The key features of interest, however, are the general age and nature of the local geology and the setting of the affected areas (*e.g.*, valleys, mountainside, plains, *etc.*). These factors are significant since they can influence both the nature and intensity of the ground shaking (Section 2.4) and also can lead to collateral hazards triggered by the ground shaking (Section 2.5).

2.3.2. Site conditions in the affected area

In addition to noting the general geological and topographical setting of the earthquake, this section will specifically focus on the nature of the surface materials in the affected areas. This is important because of the influence of the site conditions—whether hard rock or deep layers of soft soils—can have on the nature of the ground motions. The subsequent interpretation of the earthquake effects will be greatly enhanced when the recorded motions and/or the structural damage can be related to the near-surface geo-materials.

If the descriptions of the near-surface deposits in the vicinity of the epicentre and/or the affected areas indicates the presence of sand deposits, whether at the surface or at some depth, this should be noted, together with any available information regarding the depth to the phreatic level (water table). The key interest here is related to liquefaction, since it has been raised as a potential hazard in the Groningen field. Reporting of liquefaction from small-to-moderate magnitude earthquakes is rather rare (*e.g.*, Holzer *et al.*, 2010) hence a very useful by-product of this database may be 'negative evidence' regarding liquefaction triggered by such earthquakes. If in this section the presence of potentially liquefiable deposits is recorded but no liquefaction is reported (Section 2.5.3), then this may be

interpreted to indicate that either liquefaction did not occur or else that the impact of any liquefaction was sufficiently small to pass unnoticed.

2.4. Ground motions

Damage due to earthquake shaking reflects that the seismic demand (*i.e.*, strength of the shaking) exceeded the seismic capacity (or resistance) of the exposed buildings. Damage may therefore occur under low levels of shaking if the affected buildings are exceptionally susceptible, just as damage to buildings of high seismic resistance would be indicative of very intense shaking. Therefore, meaningful interpretation of damage reports is greatly enhanced by information regarding the strength and nature of the induced shaking.

2.4.1. Intensity observations

Reported intensities will be reported, whether these are just mentions of values at specific locations, mapped intensity data points (IDP) or isoseismal maps The origin of such macroseismic data will be clearly identified since practices related to the assigning of intensities varies greatly from country to country and from agency to agency, and these procedures often diverge appreciably from what might be considered good practice as defined, for example, by Musson & Cecić (2002). There have even been cases of authors of reports on a single earthquake documenting their divergent views on the assessment of intensity (*e.g.*, Sargeant *et al.*, 2008).

The scale on which the intensities have been defined must also be recorded since there are subtle differences among the various scales in use globally. Even if most of the 12-point scales are broadly comparable in their definitions, it has been found that some tend to yield different results in their application, particularly the MCS scale widely used in Italy (Musson *et al.*, 2010). In view of such differences, no attempt will be made to convert intensity observations to a common scale in the database; each data set will be reported in the scale in which the original assessment was made.

2.4.2. Ground motion recordings

Clearly, the best possible insights that can be obtained regarding the nature of the ground shaking are obtained from accelerograph recordings. If such instruments were installed and operational in the affected areas, the characteristics of the recorded motions should be reported together with as much information as possible regarding the locations of the recording instruments and the site conditions at those locations. The proximity of the recordings to both the earthquake epicentre and to the areas where damage is reported to have occurred is a key piece of information in this regard. Showing the location of the recording stations on a map with the epicentral locations and damaged areas can be an effective way of summarising this information.

If the accelerograms can be accessed, this clearly would allow a great deal of derived information to be represented, but failing this any published plots of acceleration and velocity time-series and response spectra should be reproduced in the report.

2.4.3. Inferred shaking levels

In the absence of any recordings of ground shaking in the epicentral region, there will be a temptation to infer levels of ground shaking. One option is to use empirical correlations between macroseismic intensity and instrumental ground-motion parameters to infer values of PGA, PGV and even spectral accelerations from the intensities (Dangkua & Cramer, 2011; Worden *et al.*, 2012); however, the uncertainties associated with such correlations is such as to render the results of limited value and very possibly to make them misleading. This is particularly the case when the correlations of intensity and ground-motion parameters have been derived using recordings of larger magnitude earthquakes.

Other options for inferring ground-motion levels include ShakeMap approaches and the application of GMPEs judged to be applicable to the region and magnitude range of the earthquakes. All such practices are subject to great uncertainty and with the possible exception of a well-established (and hence well calibrated) local ShakeMap facility, are likely to yield results of limited value.

Therefore, this section should be reserved only for recording any inferences on ground shaking made by others, including a brief explanation of how these inferences were made and offering an assessment of how uncertain the estimated shaking levels may be.

2.4.4. Duration of ground shaking

For both the assessment of damage to structures that experience degradation of strength and stiffness under cycling loading (*e.g.*, Bommer *et al.,* 2004) and the assessment of liquefaction hazard, the duration of the ground shaking is an important parameter. Therefore, reports of the duration of shaking can be a useful addition to the case history, but only if these have been calculated from recordings rather than based on subjective experiences of the shaking; the latter tend to exaggerate the length of the shaking episode. Given how many definitions of duration have been proposed and how different are the results that these can yield even from a single accelerogram (Bommer & Martinez-Pereira, 1999), the definition of duration should be clearly stated.

2.5. Collateral earthquake hazards

While the primary focus in this study is damage due to ground shaking—since this is generally the main cause of building damage (Bird & Bommer, 2004) and is also expected to be the primary hazard in Groningen—it is worthwhile giving brief consideration to other earthquake hazards (Figure 2.2). Some of these—in particular liquefaction in the case of Groningen—could pose a threat to infrastructure and lifelines (Bird & Bommer, 2004).

Amplified ground shaking is already covered by Sections 2.3.2 and 2.4. Clearly the possibility of tsunami hazard in the Groningen field can be safely dismissed and it is well established that the magnitude threshold for tsunamigenic earthquakes is larger than the upper limit of 5.5 considered in this review. However, the other collateral hazard are worthy of consideration and these are briefly discussed in the following three sub-sections.
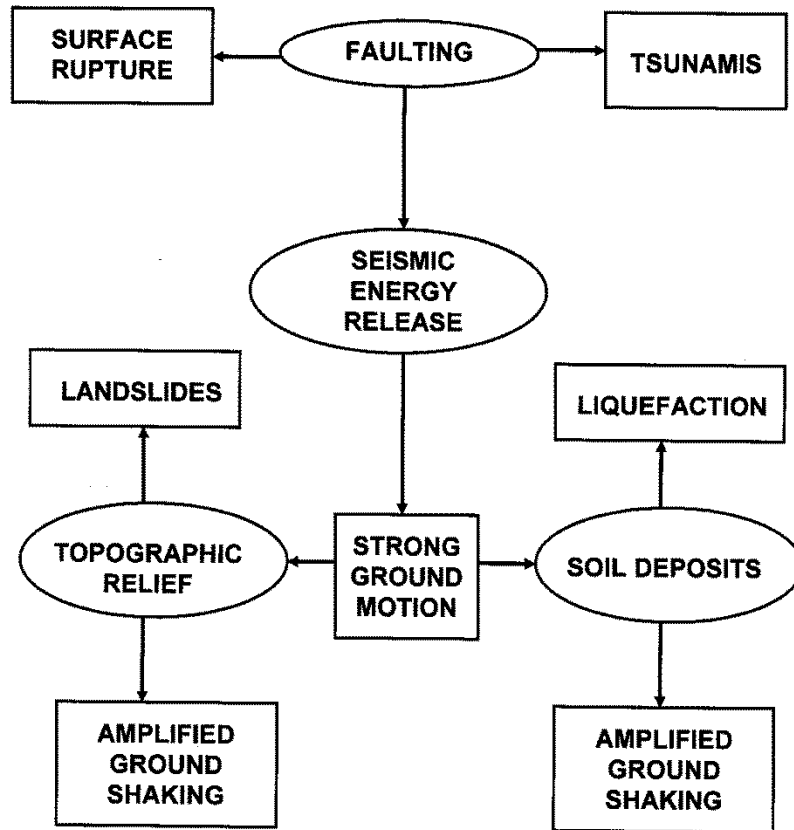
Figure 2.2. Potentially damaging earthquake effects (rectangles) associated with earthquake processes (ellipses) (Bommer & Boore, 2004)

2.5.1. Surface rupture

If the fault rupture associated with an earthquake reaches the Earth's surface, the resulting offsets can pose a very serious threat to any structures straddling the fault trace, particularly if the offset is vertical. However, the probability of surface rupture associated with earthquakes in the magnitude range covered by this study is rather low (Figure 2.3) hence it would not be expected that this hazard will be reported very often. Even in those rare cases where such surface expression of the faulting was noted, it is possible that the actual displacements may be sufficiently small to not necessarily pose a particular onerous threat. Nonetheless, for each earthquake in the database it will be noted whether or not any surface rupture was reported and, in any cases where this phenomenon was observed, if it contributed to the reported damage.
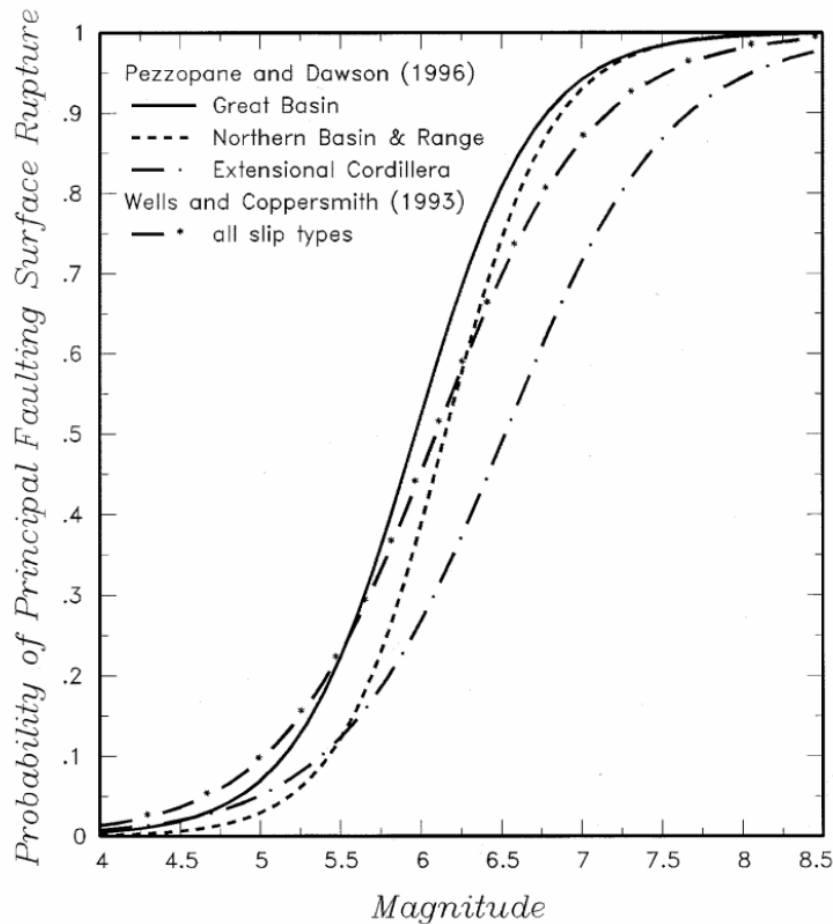
Figure 2.3. Probabilities of surface rupture as a function of earthquake magnitude
(Youngs *et al.*, 2003)

2.5.2. Landslides

Earthquake-triggered landslides can lead to additional damage if they affect the foundations of any structures located on the slope that becomes unstable or if they impact on or bury structures located downslope from the instability. Given the very flat landscape in the Groningen region—and indeed in the whole of the Netherlands—landslides are not expected to be a relevant hazard. Therefore, any damage or casualties that were associated with landsliding can be noted as examples of events that would not be expected to manifest in Groningen.

Overall relatively few landslides would be expected from earthquakes in the magnitude range of interest to this study (Figure 2.4) but this does not mean that they are impossible. Indeed, given that landslides can and do occur under static conditions, the lower bound magnitude of earthquakes that could trigger slope instability is likely to be rather small, provided that the geotechnical and hydrological conditions in the slope were sufficiently unfavourable. In summary, any landslides associated with the earthquake will be reported, with as much information as possible regarding their location, size, run out or volume, and the material in the slide as well. Any damage directly associated with landslides will be clearly documented. Otherwise, this section simply records the absence of such reports.
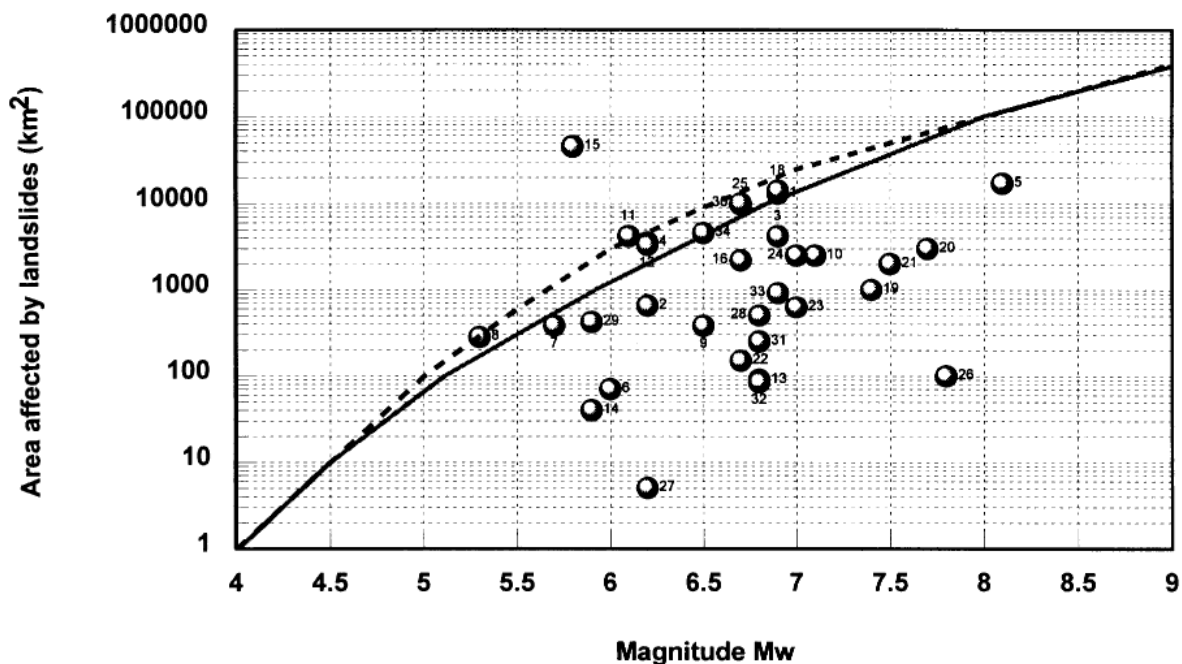
Figure 2.4. Areas affected by landsliding as a function of earthquake magnitude from the study of Rodriguez *et al.* (1999)

2.5.3. Liquefaction

This section records any observations of liquefaction and, should such cases be encountered, the nature of any damage attributable to liquefaction. For those earthquakes where the presence of potentially liquefiable soils was noted (Section 2.3.2), the absence of liquefaction reports may also be noted since this contributes useful data for the characterisation of liquefaction hazard in the Groningen field.

2.6. Exposed population

This section presents the main characteristics of the population that was exposed to the seismic event under consideration.

2.6.1. Socio-economic setting

The socio-economic conditions of the population of a certain region can exert a significant influence on the quality of construction of buildings and infrastructure. In prosperous regions and countries, people and authorities tend to carry out appropriate maintenance work, which is sometimes poor or even non-existent in under-developed areas. Further, other needs such as water, employment or security generally take precedent over seismic safety in poor regions. The socio-economic setting can thus end up controlling the vulnerability of the building stock and, by extension, whether it represents or not a threat to life. Nevertheless, the relationship between prosperity and maintenance can be far more complex than this. It is not uncommon to find less well-maintained buildings in prosperous regions with low seismicity, simply because of the lack of awareness that not being

15

exposed to high levels of hazard can entail. This latter factor can be of particular relevance for putting the influence of socio-economic settings in context when studying regions of low natural seismicity like the Netherlands.

Defining the socio-economic setting is not a trivial task. For the sake of simplicity, the Human Development Index (HDI) and the Inequality-adjusted Human Development Index (IHDI) will be the two main indices used as main indicators. The HDI is a composite statistic that combines indicators of life expectancy, education and per capita income. Its inequality-adjusted version takes into consideration inequality in these three indicators among the population. In addition to these, a brief description regarding the economic development of the region will be provided, including data such as gross domestic product (GDP) per capita and unemployment rates.

2.6.2. Population density and distribution

Interpretation of the impact of an earthquake obviously depends on the number of people and buildings exposed to the strong ground shaking. The distribution of the population and population density need not only be described in broad regional and epicentral terms but also, and more importantly, in terms of occupancy of the different building typologies within the affected areas. If the majority of the population lives and works in modern buildings constructed using a modern seismic design code, it is possible that the number of casualties observed would be less than if the population was concentrated within old pre-seismic-code constructions.

The main source of data for this section will come from specific journal publications or technical reports that describe the characteristics of the exposed population of each seismic event in the database, as well as from national and regional censuses and GEM's Global Exposure Database (Gamba, 2014), if no specific sources are available. Global data sets of population distribution such as Gridded Population of the World (GPW) and the Global Rural-Urban Mapping Project (GRUMP) will also constitute a significant source of information for events that occurred after 1990.

Where enough data are available, information regarding population density and distribution will be presented on a map.

2.6.3. Time of day of earthquake

The time of the day at which an earthquake occurs has a large influence on the number of people exposed within building typologies of varying vulnerability. For example, it is broadly recognized that the 2011 Christchurch earthquake could have caused many more casualties had it occurred during the daytime, as most of the buildings that collapsed were located in the business district of the city (*e.g.,* Galloway *et al.*, 2014). By contrast, the opposite was true in the case of the 2003 Bam earthquake, which also occurred during night time but during which residential buildings were heavily damaged and thus a high number of casualties was observed. (Ibrion *et al.*, 2015). Further, climate and seasons can

have an analogous effect, with warm pleasant weather encouraging more people to be outside and, therefore, less exposed to structural failure. This information is relevant for understanding whether a large/small number of dead or injured people is due to the characteristics of the seismic event and the exposed building stock, or to the daily and seasonal variation of occupancy of the different structures.

2.7. Characteristics of exposed building stock

A description of the buildings exposed to the seismic events under study will be provided herein.

2.7.1. Seismic design codes

Whether the building stock has been designed to some seismic code or not has a significant influence on the level of damage to be expected during a seismic event. Structural engineering practice evolved during centuries from not explicitly considering any kind of seismic load, to prescribing that buildings should be able to resist a lateral load equivalent to a pre-established percentage of its own weight, to developing proper seismic design codes based on more advanced knowledge of hazard and structural dynamics. The latter only became common practice in the second half of the twentieth century. This means that a very large proportion of the building stock worldwide has not been designed following a seismic code and, therefore, can be found to be relatively vulnerable to seismic actions. Relevant exceptions to this conclusion are those regions for which strong winds have always represented a significant hazard: buildings in these areas can be found to be able to withstand low-to-moderate levels of ground shaking due to their lateral load resistance coming from wind design considerations. All this is particularly relevant for the case of the Groningen field, a region with a low level of natural seismic hazard but constant relatively strong winds.

However, having seismic design codes in force does not necessarily translate into safe buildings, for lack of official governmental control of code-compliance can be a fundamental failure in the seismic design process and contribute significantly to the vulnerability of the building stock, as pointed out by Gülkan (2000).

Determining whether the status of the building stock of the seismic events under study is comparable to that of the Netherlands, with regards to the implementation of seismic design codes and exposure to other kinds of hazard, is relevant to understanding to what extent the consequences observed for these events could be expected in the Groningen field.

2.7.2. Building typologies

Not all buildings are expected to behave in the same way during a seismic event. Combinations of different factors such as types of materials, geometry and construction

quality, will lead to buildings with different degrees of vulnerability and different replacement/repair costs. This sub-section will contain detailed descriptions of the building typologies present at the time of the seismic events under study, at the site of interest. This information will be used to understand if the building stock of the Netherlands is comparable to that of the events in the database, both in terms of vulnerability, which will dictate the level of damage to be expected, and replacement costs. The latter will be fundamental for those cases in which only a reduced amount of information is available and values of overall unclassified economic loss need to be interpreted.

Numerous building taxonomies (*i.e.*, building classification schemes) have been proposed and used to describe building stocks in different countries and at different points in time. HAZUS (FEMA, 2003), EMS-98 (Grunthal, 1998), the World Housing Encyclopedia (EERI, 2000), and the GEM Building Taxonomy (Brzev *et al.*, 2013) are only some of the many examples. Damage statistics are directly related to the taxonomy used, as the percentages of buildings in each damage state will normally be sub-classified according to each building type, and damage scales may be specific to the typology. Given the difficulties entailed in trying to re-classify buildings starting from a certain taxonomy, with the original data being usually inaccessible, the exposed building stock will be characterised as found in the literature and relevant references of each seismic event under study.

2.7.3. Prior damage and retrofit

When describing the characteristics of the exposed building stock, it is not only relevant to include information on the buildings as they were designed, but also to understand if that original design has been strengthened by some degree of retrofit or weakened by un-repaired prior damage. It is noted that this may actually be very difficult to assess, for information of this kind will most probably not be available. Inferences will be made based on knowledge regarding previous earthquakes and the influence of other factors, such as settlement.

2.8. Damage observations

This section, together with the upcoming one, will be the core of the present study. All the information gathered in previous sections will acquire a more significant meaning in light of the consequences of the events being described. Damage to the exposed building stock will be extensively described herein, with the aim of achieving a comprehensive understanding of the impact of these small-to-moderate earthquakes and the factors contributing to their negative consequences.

2.8.1. Damage states

In order to describe the damage state of buildings affected by seismic events, there are many structural damage scales available, such as the European Macroseismic Scale (EMS-98; Grunthal, 1998), FEMA 356 (FEMA, 2000) and HAZUS (FEMA, 2003), just to

name some. It is not unusual to find publications from older events that do not report damage levels directly but describe the severity of the shaking by means of macroseismic intensity scales such as the Medvedev-Karnik-Sponheuer (MSK; Musson & Cecić, 2012) scale, the Mercalli-Cancani-Sieberg scale (MCS-1930; Sieberg, 1930) and the Modified Mercalli scale (MMI; Musson & Cecić, 2012). If no detailed information is available, macroseismic intensity can be used to infer the level of damage.

Depending on the location and date of the events under study, information will be available in terms of one scale or another. In view of the potential drawbacks of converting reported damage from one scale to a different one, no attempt will be made to carry out such conversion. As in the case of Section 2.4.1, damage state data will be reported in the scale in which the original assignment of damage states was made. Sufficient description of the scale used will be provided, so that the meaning of each damage state can be fully understood from the contrast against the whole range of damage states covered by the scale.Details on the damage scales used along the study cases are provided below.

Immediately after a damaging earthquake has occurred, it is common practice that trained engineers carry out a visual inspection of the building stock in order to determine the degree of habitability of each structure. This is indicated by means of a colour tag, which can be green, yellow or red, each symbolizing unrestricted, restricted and no access, respectively. A green tag is assigned to a structure that has either not suffered any damage or has suffered only from minor superficial damage. A yellow tag indicates that significant actions need to be put in place for the building to be fully inhabitable again but that, until that occurs, occupants can access it briefly to gather essential belongings, and technicians and engineers can access it to carry out the reparations. Finally, a red (or sometimes black) tag is assigned to those structures which have suffered extensive damage and are at risk of imminent collapse.

The European Macroseismic Scale (EMS-98; Grünthal, 1998) classifies damage into five grades, defined separately for masonry and reinforced concrete buildings. The following tables (in Figures 2.5-2.7), extracted from Grünthal (1998), define said damage grades, and the intended definitions of the qualitative expressions "few", "many" and "most".
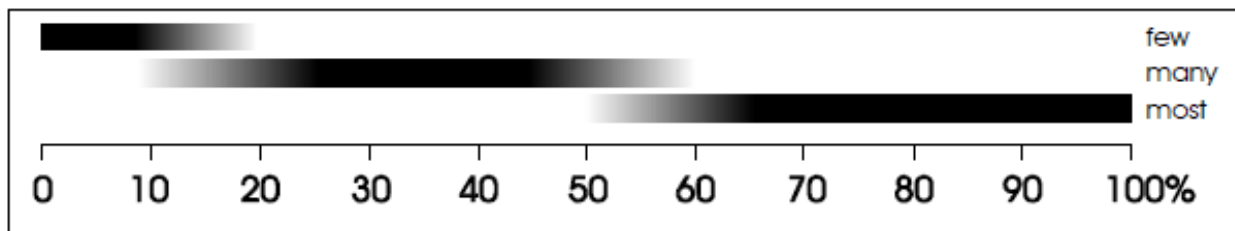
Figure 2.5. Definition of "few", "many" and "most" in EMS-98, from Grünthal (1998).

Classification of damage to masonry buildings	

	Grade 1: Negligible to slight damage
	    (no structural damage,
	    slight non-structural damage)
	Hair-line cracks in very few walls.
	Fall of small pieces of plaster only.
	Fall of loose stones from upper parts of
	buildings in very few cases.

	Grade 2: Moderate damage
	    (slight structural damage, moderate
	    non-structural damage)
	Cracks in many walls.
	Fall of fairly large pieces of plaster.
	Partial collapse of chimneys.

	Grade 3: Substantial to heavy damage
	    (moderate structural damage,
	    heavy non-structural damage)
	Large and extensive cracks in most walls.
	Roof tiles detach. Chimneys fracture at the
	roof line; failure of individual non-struc-
	tural elements (partitions, gable walls).

	Grade 4: Very heavy damage
	    (heavy structural damage,
	    very heavy non-structural damage)
	Serious failure of walls; partial structural
	failure of roofs and floors.

	Grade 5: Destruction **(very heavy structural damage)** Total or near total collapse.

Figure 2.6. Definition of EMS-98 damage grades for masonry buildings, from Grünthal (1998).
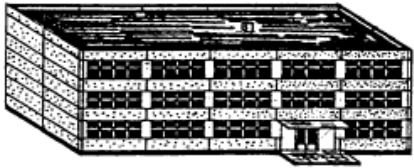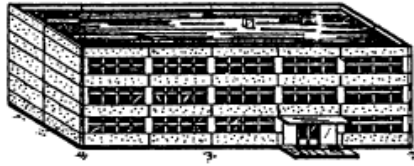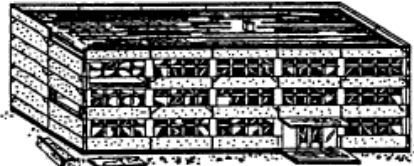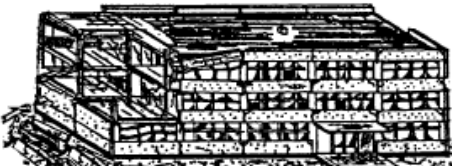
Classification of damage to buildings of reinforced concrete	
	Grade 1: Negligible to slight damage (no structural damage, slight non-structural damage) Fine cracks in plaster over frame members or in walls at the base. Fine cracks in partitions and infills.
	Grade 2: Moderate damage (slight structural damage, moderate non-structural damage) Cracks in columns and beams of frames and in structural walls. Cracks in partition and infill walls; fall of brittle cladding and plaster. Falling mortar from the joints of wall panels.
	Grade 3: Substantial to heavy damage (moderate structural damage, heavy non-structural damage) Cracks in columns and beam column joints of frames at the base and at joints of coupled walls. Spalling of conrete cover, buckling of reinforced rods. Large cracks in partition and infill walls, failure of individual infill panels.
	Grade 4: Very heavy damage (heavy structural damage, very heavy non-structural damage) Large cracks in structural elements with compression failure of concrete and fracture of rebars; bond failure of beam reinforced bars; tilting of columns. Collapse of a few columns or of a single upper floor.
	Grade 5: Destruction (very heavy structural damage) Collapse of ground floor or parts (e. g. wings) of buildings.

Figure 2.7. Definition of EMS-98 damage grades for reinforced concrete (RC) buildings, from Grünthal (1998).

2.8.2. Damage statistics

The proportion of buildings that can be assigned to each damage state will be reported here. Due note will be taken of whether the damage observed was caused directly by ground shaking or if it is a consequence of collateral earthquake hazards such those listed

21

in Section 2.5. Given that landslides are not expected to represent a significant hazard in Groningen, while liquefaction could be, and other forms of collateral hazards may be totally discarded in the Groningen field, this distinction is of great relevance for the present study.

It is noted that the proportion of the total building stock that is damaged during an earthquake is often not reported. Nevertheless, an effort will be made to describe as thoroughly as possible the damage reported as well as an estimation of the total number of buildings existing in the affected area at the moment of the event.

Apart from specific publications that can exist reporting the consequences of each seismic event in the database, relevant sources of information for this section will be the Cambridge Earthquake Impact Database, Munich Re's NatCatSERVICE and Latin American-originated Desinventar database.

2.8.3. Observed weaknesses

In those cases for which information regarding specific structural weaknesses that might have had a significant influence on the extent of damage observed is available, this information will be included herein. Structural weaknesses to be considered include, but are not limited to, soft-storeys (\, the stiffness of one storey being significantly lower than the others'), vertical and horizontal irregularities, insufficient width of seismic joints leading to pounding of neighbouring buildings, short-column effects (*i.e.*, columns with shorter effective heights than others in the structure, and consequently more prone to shear failure), lack of verticality of walls, lack of anchorage of façades, out-of-plane failure of unreinforced masonry walls, inadequate confinement of reinforced concrete members, and corrosion of reinforcement. In addition, special attention will be paid to damage of non-structural components such as chimneys and parapets, which are commonplace in ordinary buildings in the Netherlands, in view of the potential threat these elements can pose to human life. The influence of eventual systematic weaknesses on the damage observed for a specific event needs to be accounted for when interpreting the possible extrapolation of consequences from earthquakes of the database to the case of the Groningen field.

2.8.4. Damage distribution

The geographical distribution of physical damage caused by the seismic event will be reported here. This is relevant in order to form an idea of the spatial extent of those areas that could be affected by induced earthquakes of the characteristics studied herein.

Due note will be taken of cases in which a concentration of damage was observed within a certain area, identifying, where possible, the reasons for such trend. For example, if more extensive damage was observed in structures located over a hill than those of similar characteristics, located at a similar distance from the epicentre, the influence of topographic effects may be suspected. Further, even though there is still some controversy around the question of whether small-to-moderate magnitude earthquakes can be

associated to directivity effects, a number of recent publications has shown that there is evidence of high frequency directivity for moderate magnitude earthquakes (*e.g.* Chen *et al.*, 2014; Boatwright, 2007). No attempt will be made to study the potential directivity effects of the earthquakes in the present database, but note will be taken of those cases for which bibliographical sources suggest their existence.

Where enough data are available, information regarding damage distribution will be presented on a map.

2.9. Casualties and losses

As the primary focus of this study is life safety, this is one of the core sections of the present study. The number and causes of casualties, as well as estimates of the overall economic losses, will be provided.

Apart from specific journal publications or reports that may exist describing the consequences of each seismic event in the database, other relevant sources of information for this section will be the Cambridge Earthquake Impact Database, Munich Re's NatCatSERVICE, the International Disaster Database (EM-DAT), and Desinventar.

2.9.1. Numbers of dead and injured

The number of people who died or were injured by the seismic event will be reported here, ideally related to building typologies and their damage states, or to any other relevant context. These numbers will be interpreted jointly with the causes reported in the next sub-section.

2.9.2. Causes of casualties

The causes of the observed casualties will be fundamental to understanding what sort of intervention would be needed to reduce the induced seismic risk in the Netherlands, if any. As a first step, it should be established whether the casualties were a direct consequence of ground shaking or of a collateral hazard such as landslides or surface ruptures, or, even further, if they were due to subsequent physical and/or emotional trauma triggered by the stress and panic caused by the seismic event. Within those caused directly by ground shaking, it should be further determined if they had their origin in severe structural damage or collapse of specific structural typologies, or if they were the consequence of non-structural elements or equipment moving or falling. The first case would suggest the possible need for some kind of structural intervention in the building stock, while the latter would indicate that attention should be focused more on non-structural components than on structural ones.

2.9.3. Estimates of economic losses

Estimates of economic losses made by others will be reported here, and no attempt will be made to make new estimates. Where necessary, however, monetary values will be given both as originally calculated at the time of the event, and adjusted to account for the historical variation of interest and exchange rates.

Ideally, the overall economic losses should be subdivided into material losses (*i.e.*, repairing, rebuilding, etc.), downtime losses (*i.e.*, losses due to the period of time in which industries and businesses of the region affected by the seismic event could not continue normally with their economic activities) and losses due to the "value of life" (*i.e.*, the economic value assigned to fatalities).

2.10. Discussion and conclusions

In this closing section, a brief summary will be given of the impact of the particular earthquake, and an attempt will be made to explain the main factors contributing to damage, casualties and losses associated with the event. Following these brief inferences, there will be a short discussion of whether or not these same factors are expected in the case of the Groningen field.

3. OVERVIEW OF CASE HISTORIES

In this initial report, which in a sense is a pilot study for a larger endeavour to document as many of the earthquake cases listed in Appendix I as possible, only six small-magnitude damaging earthquakes have been studied in detail. This is too small a sample to allow any conclusions to be drawn that would be applicable to the potential effects of moderate-magnitude seismicity, but nonetheless several significant observations can be made regarding the nature and impact of these earthquakes.

Of the six case histories studied to date, only one is a natural earthquake whose origin was linked entirely to tectonic processes (Appendix III). This was the 1992 Roermond earthquake that occurred in the southern Netherlands, which is a region of low seismicity but this magnitude 5.4 event was not outside the range of expected earthquakes in this part of the world. The size of this earthquake places it close to the upper limit of the range considered in this study.

The Roermond earthquake caused shaking that was widely felt and did cause some damage, particularly in pre-1920 unreinforced masonry structures and old churches. This damage led to some 45 injuries; one death was reported due a heart attack, the timing of which was attributed to the earthquake. More modern code-designed buildings did not suffer distress due to the earthquake shaking. The implications for Groningen are significant although this cannot be taken as a direct analogue for the potential impact of such an event within the gas field given the differences in focal depth, upper crustal velocity structure, and near-surface geology. However, it is also important to keep in mind that the Roermond earthquake was almost two units of magnitude greater than the largest induced earthquake in Groningen to date and hence several hundred times more energetic.

One important feature of the Roermond earthquake was that the shaking caused significant liquefaction, which is another factor of relevance to Groningen (although once again the differences in magnitude need to be taken into account here). However, no building damage at all was attributed to liquefaction, which is also an important observation for the Groningen case.

Of the five cases of anthropogenically-caused earthquakes, four are triggered by high-pressure fluid injection and one by groundwater extraction. In all cases, the earthquakes occurred within a sequence of foreshocks and aftershocks, in some cases with the total number of events numbering tens or even hundreds. The two most damaging earthquakes were the 2011 magnitude 5.3 event in Trinidad, Colorado, and the 2011 magnitude 5.6 events in Prague, Oklahoma; it is noted that latter is slightly above the upper limit of the magnitude range for this study, but it was included nonetheless because of its importance as a highly-publicised case of induced seismicity. Both of these earthquakes were triggered by wastewater injection and caused shaking that was damaging to local buildings in quite sparsely-populated areas. The damage was almost exclusively to unreinforced masonry and was consistent with classical patterns of seismic response for such buildings observed in many earthquakes. Damage include the collapse of gable walls, parapets, chimneys and

brick façades. Recorded ground-motion amplitudes are not always available but records of the Trinidad earthquake show relatively low amplitudes of acceleration. However, basin amplification effects may have prolonged the duration of shaking, which could have exacerbated the damage to these weak, brittle structures.

The third earthquake associated with wastewater injection was the magnitude 4.7 Guy-Greenbrier event of 2011 in Arkansas. Interestingly, this somewhat smaller event than those in Colorado and Oklahama caused only very minor damage, which is not inconsistent with rules-of-thumb that indicate magnitude 5 to be an approximate threshold for tectonic earthquakes that can cause structural damage. However, in all of these cases, as well as taking account of the seismic vulnerability of the exposed building stock, it is also important to take cognisance of the population density and degree of urbanisation in the effected area. None of these three wastewater injection-triggered events occurred in close proximity to a large town or city.

This last observation is not true of the 2011 Lorca earthquake in southern Spain. This magnitude 5.1 earthquake occurred close to the town of Lorca, causing high levels of ground shaking that was intensified both by directivity effects and site amplification. The strong shaking affected an aged building stock as well as a few more modern buildings with significant structural deficiencies. The earthquake left 9 dead, nearly all of these the result of the collapse of non-structural elements.

The Lorca earthquake is a particularly interesting case since it has been attributed to triggering as a result of groundwater extraction. However, it occurred in a region with appreciable natural seismicity.

The final case is the 2006 Basel earthquake, which was associated with an enhanced geothermal project in this Swiss city. With a magnitude of only 3.2, this earthquake is actually below the range to be considered in this study, but it was included since it has been a high-profile and controversial case, which has raised significant concerns regarding anthropogenically-generated seismicity. The Basel earthquakes is often cited as an example of a damaging small-magnitude shallow-focus earthquake. However, the detailed study of this event has shown that at most it caused a large number of non-structural—and generally very superficial—cracking, and the large insurance claims paid out following this earthquake grossly exaggerated the actual physical impact of this earthquake on the built environment.

4. CONCLUSIONS AND FUTURE WORK

From a database of only six earthquake it would be unwisely ambitious to try to infer any general conclusions regarding the potential damage on the built environment of earthquakes in the range from magnitude 4.0 to 5.5 (especially when taking into account the fact that two of the case histories actually lie outside this range). However, from this small sample it could be inferred that magnitude 5 seems to be an approximate threshold for events that generate ground shaking that can potentially cause significant structural damage that may pose a threat to the exposed population. As the study continues, with many more case histories being examined in much greater detail, particular attention will be paid to the threshold conditions for such damage and there will be concerted efforts to obtain greater details regarding those cases where deaths and injuries have been attributed to smaller earthquakes. If such reports are confirmed, then the focus will be to establish in each case the specific causes for those casualties, with a view to determining whether such outcomes could be expected in Groningen.

Another tentative observation that can be made is that the four earthquakes among the six considered so far that did cause significant damage, which were all of magnitude greater than 5, were either natural events of tectonic origin (Roermond), were triggered by large-scale fluid injection (Prague, OK, and Trinidad, CO) or else were triggered in a region of appreciable natural seismicity where the crust may therefore be assumed to be under consdirable stress.

In terms of the question of whether much smaller earthquakes can cause significant damage, it is important to emphasise that the 2006 Basel earthquake cannot be presented as an example of such an event. There is no evidence whatsoever that any structural damage was caused by this earthquake and it is very misleading to refer to unsubstantiated insurance claims as 'damage'.

As well as attempting to identify the specific causes for each case of damage, injury or death due to a moderate-magnitude earthquake, it is also intended to undertake statistical studies to estimate the proportion of earthquakes in the 4-5.5 magnitude range that have caused such effects. This will be done by examining global seismicity data for the last few decades, using a tool such as GoogleEarth to ascertain how many of these occurred in the upper crust, on land and in close proximity to urban centres. Estimates can then be made, perhaps taking account of focal depths and bins of magnitude within the full range, of the proportion of such earthquakes that make a marked impact on the built environment (taking due account of the fact that reporting of damaging effects is, inevitably, incomplete).

In closing, it is important to emphasise that while this ongoing work is potentially of great value for providing a frame of reference for the management of induced seismic risk in the Groningen field, none of the cases can ever be considered a direct analogue. We therefore counsel against the use of such information as the basis for empirical risk assessments, supporting instead the development of analytical models for hazard and risk calibrated to data and measurements from Groningen.

5. REFERENCES

5.1. Bibliography

Aldama-Bustos, G., J.J. Bommer, C.H. Fenton & P.J. Stafford (2009). Probabilistic seismic hazard analysis for rock sites in the cities of Abu Dhabi, Dubai and Ra's Al Khaymah, United Arab Emirates. *Georisk* **3**(1), 1-29.

Allen, T.I. (2012). *Stochastic ground motion prediction equations for southeastern Australian earthquakes using updated source and attenuation parameters*. Record 2012/69, Geoscience Australia, Canberra, Australia.

Atkinson, G.M. & I. Beresnev (1997). Don't call it stress drop. *Seismological Research Letters* **68**(1), 3-4.

Bird, J.F. & J.J. Bommer (2004). Earthquake losses due to ground failure. *Engineering Geology* **75**(2), 147-179.

Boatwright, J. (2007). The persistence of directivity in small earthquakes. *Bulletin of the Seismological Society of America* **97**(6), 1850–1861.

Bommer, J.J. & D.M. Boore (2004). Engineering Seismology. *In*: Encyclopaedia of Geology, Academic Press, vol. 1, pp.499-514.

Bommer, J.J., J. Douglas & F.O. Strasser (2003). Style-of-faulting in ground motion prediction equations. *Bulletin of Earthquake Engineering* **1**(2), 171-203.

Bommer, J.J., G. Georgallides & I.J. Tromans (2001). Is there a near-field for small-to-moderate magnitude earthquakes? *Journal of Earthquake Engineering* **5**(3), 395-423.

Bommer, J.J., G. Magenes, J. Hancock & P. Penazzo (2004). The influence of strong-motion duration on the seismic response of masonry structures. *Bulletin of Earthquake Engineering* **2**(1), 1-26.

Bommer, J.J. & A. Martinez-Pereira (1999). The effective duration of earthquake strong motion. *Journal of Earthquake Engineering* **3**, 2, 127-172.

Boore, D.M. (2003). Simulation of ground motion using the stochastic method. *Pure & Applied Geophysics* **160**, 635-676.

Brzev S., C. Scawthorn, A.W. Charleson, L. Allen, M. Greene, K. Jaiswal & V. Silva (2013). *GEM building taxonomy version 2.0.* GEM Technical Report 2013-02 V1.0.0, 188 pp., GEM Foundation, Pavia, Italy, doi: 10.13117/GEM.EXP-MOD.TR2013.02.

Chen, Y., J. Letort, F. Cotton & S. Drouet (2014). High-frequency directivity effects: evidence from analysis of the Les Saintes records. *Journal of Seismology* **18**(3), 457-466.

Cornell, C.A. (1968). Engineering seismic risk analysis. *Bulletin of the Seismological Society of America* **58**(5), 1583-1606.

Dahm, T., D. Becker, M. Bschogg, S. Cesca, B. Dost, R. Fristschen, S. Hainzl, C.D. Klose, D. Kühn, S. Lasocki, Th. Meier, M. Ohrnberger, E. Rivalta, U. Wegler & S. Husen (2013). Recommendation for the discrimination of human-related and natural seismicity. *Journal of Seismology* **17**(1), 197-202.

Dangkua, D.T. & Cramer, C.H. (2011). Felt intensity versus instrumental ground motion: A difference between California and Eastern North America? *Bulletin of the Seismological Society of America* **101**(4), 1847-1858.

Edwards, B., A. Rietbrock, J.J. Bommer & B. Baptie (2008). The acquisition of source, path and site effects from micro-earthquake recordings using Q tomography: applications to the UK. *Bulletin of the Seismological Society of America* **98**(4), 1915-1935.

EPRI (1989). *Engineering characterization of small-magnitude earthquakes.* EPRI Report NP-6389, Electric Power Research Institute, Palo Alto, California,

EPRI (2005). *Use of minimum CAV in determining effects of small magnitude earthquakes on seismic hazard analyses.* EPRI Report 1012965, Electric Power Research Institute and US Department of Energy.

FEMA (2000). *Prestandard and commentary for the seismic rehabilitation of buildings.* Report No. 356. Federal Emergency Management Agency, Washington DC

FEMA (2003) *HAZUS-MH MR4 Technical Manual*, Federal Emergency Management Agency. http://www.fema.gov/media-library-data/20130726-1716-25045-6422/hazus_mr4_earthquake_tech_manual.pdf

Galloway, B., J. Hare, D. Brunsdon, P. Wood, B. Lizundia & M. Stannard (2014). Lessons from the post-earthquake evaluation of damaged buildings in Christchurch. *Earthquake Spectra* **30**(1), 451-474.

Gamba, P. (2014). Global Exposure Database: scientific features, GEM Technical Report 2014-10 V1.0.0, 46 pp., GEM Foundation, Pavia, Italy. DOI: 10.13117/GEM.EXP-MOD.TR2014.10

Giardini, D., G. Grunthal, K.M. Shedlock & P. Zhang (1999). The GSHAP global seismic hazard map. *Annali di Geofisica* **42**(6), 1225-1230.

Grunthal, G. (ed.) (1998). *European Macroseismic Scale 1998 (EMS-98).* Cahiers du Centre Europeen de Geodynamique et de Seismologie 15, Centre Europeen de Geodynamique et de Seismologie, Luxembourg.

Gülkan, P. (2000). Building code enforcement prospects: the failure of public policy. *Earthquake Spectra*: **16**(1), 351-374.

Holzer, T.L., A.S. Jayko, E. Hauksson, J.P.B. Fletcher, T.E. Noce, M.J. Bennett, C.M. Dietel, K.W. Hudnut (2010). Liquefaction caused by the 2009 Olancha, California (USA), **M**5.2 earthquake. *Engineering Geology* **116**, 184-188.

Hough, S.E. (2014). Shaking from injection-induced earthquakes in Central and Eastern United States. *Bulletin of the Seismological Society of America* **104**(5), 2619-2626.

Ibrion, M., M. Mokhtari, F. Parsizadeh & F. Nadim (2015). Timescape of the earthquake disasters in Iran: the intricacies of earthquake time and earthquake disaster risk reduction. *Geografiska Annaler: Series A, Physical Geography* **97**(1), 197-216.

Kramer, S.L. (1996). *Geotechnical Earthquake Engineering.* Prentice Hall.

Musson, R.M.W. & I. Cecić (2002). Macroseismology. *In*: International Handbook of Earthquake and Engineering Seismology, W.H.K. Lee, H. Kanamori, P.C. Jennings and C. Kisslinger (*eds.*), *International Geophysics* **81:** Part A, 49, 807-822.

Musson, R.M.W. & I. Cecić (2012). Intensity and intensity scales. In: Bormann, P. (Ed.), New Manual of Seismological Observatory Practice 2 (NMSOP-2), Potsdam : Deutsches GeoForschungsZentrum GFZ, p. 1-41.

Musson, R.M.W., G. Grünthal & M. Stucchi (2010). The comparison of macroseismic intensity scales. *Journal of Seismology* **14**, 413-428.

Petersen, M.D., A.D. Frankel, S.C. Harmsen, C.S. Mueller, K.M. Haller, R.L. Wheeler, R.L. Wesson, Y. Zeng, O.S. Boyd, D.M. Perkins, N. Luco, E.H. Field, C.J. Wills & K.S. Rukstales (2008). *Documentation for the 2008 update of the United States national seismic hazard maps*, USGS Open-File Report 2008-1128, US Geological Survey, Reston, VA. 61 pp.

Reiter, L. (1990). *Earthquake Hazard Analysis: Issues and Insights*. Columbia University Press, New York. 254 pp.

Rodríguez, C.E., J.J. Bommer & R.J. Chandler (1999). Earthquake-induced landslides 1980-1997. *Soil Dynamics & Earthquake Engineering* **18**(5), 325-346.

Sargeant, S.L., R. Lawley, P.J. Stafford, G. Weatherill, A-J.S. Weston, J.J. Bommer, P. Burton, M. Free, R.M.W. Musson & T. Rossetto (2008). The felt effects of the Folkstone, UK, earthquake of 28 April 2007. *Seismological Research Letters* **79**(5), 672-687.

Sieberg, A. (1930). Geologie der Erdbeben, *Handbuch der Geophysik* **2**(4), 552-555

Worden, C.B., Gerstenberger, M.C., Rhoades, D.A. & Wald, D.J. (2012). Probabilistic relationships between ground-motion parameters and Modified Mercalli Intensity in California. *Bulletin of the Seismological Society of America* 102(1), 204-221.

Youngs, R.R., W.J. Arabasz, R.E. Anderson, A.R. Ramelli, J.P. Ake, D.B. Slemmons, J.P. McCalpin, D.I. Doser, C.J. Fridrich, F.H. Swan, A.M. Rogers, J.C.. Yount, L.W. Anderson, K.D. Smith, R.L. Bruhn, P.L.K. Knuepfer, R.B. Smith, C.M. dePolo, D.W. O'Leary, K.J. Coppersmith, S.K. Pezzopane, D.P. Schwartz, J.W. Whitney, S.S. Olig & G.R. Toro (2003). A methodology for probabilistic fault displacement hazard analysis (PFDHA). *Earthquake Spectra* **19**(1), 191-219.

5.2. Web References

Cambridge Earthquake Impact Database: http://www.ceqid.org/CEQID/Home.aspx

Desinventar Database: http://www.desinventar.org/en/database

Global Rural-Urban Mapping Project (GRUMP): http://sedac.ciesin.columbia.edu/data/collection/grump-v1

Gridded Population of the World (GPW): http://sedac.ciesin.columbia.edu/data/collection/gpw-v3

International Disaster Database: http://www.emdat.be/

Munich Re's NatCatSERVICE: http://www.munichre.com/natcatservice

World Housing Encyclopedia. www.world-housing.net

I. APPENDIX I: Listing of damaging earthquakes of M4-5.5

Date	UTC	Location	M[1]	Depth (km)	MMI	Loss[2]	Cause	Dead	Injured	Buildings damaged[3]
10/06/2016	08:04	SW US (Borrego Springs)	5.2	12	VII					
15/02/2016	18:55	Greece (Krestena, Peloponnese)	5.1	5	V					
07/11/2015	06:58	N. South America (Langunillas/Merida, Venezuela)	5.3	15	VI			1	4	
14/03/2015	06:13	China (Henan - Anhui, Fuyang)	4.8	10					13	155
26/02/2015	21:59	Indian Subcontinent (Battagram)	5.4	29				2	5	
22/02/2015	06:42	China (Shawan, Xinjiang)	5.2	16		14,650,000				
20/02/2015	22:37	China – Yunnan	4.6	10						
12/11/2014	15:40	SE US (Kansas)	4.9	4	VII					
27/09/2014	02:35	Peru (Paccha, Peru)	4.9	43				7	8	45
20/09/2014	04:26	SE Asia (Barangay Luayon)	5.2	19					1	32
12/08/2014	19:57	N. South America (Quito)	5.1	5	VI			4	8	
05/08/2014	10:22	S. Africa (Orkney)	5.5	10	IX		Anthropogenic	1	2	1
17/05/2014	16:46	N. Europe (Darmstadt, Hesse)	4.1	10		1,360,000				70
08/05/2014	22:51	Indian Subcontinent (Nawabshah)	4.5	15				2	70	
14/04/2014	05:07	Central America (Managua, Ciudad Sandino)	5.1	10						7
04/04/2014	22:40	China - Yunnan (Xiluodu)	5.4	26					21	
28/03/2014	08:03	SW US (La Habra)	5.1	7.5	VII	10,800,000				
02/01/2014	20:13	Iran (Bastak)	5.5	10				1	30	800
22/10/2013	05:40	Indonesia (Banda Aceh)	5.3	48	V			1	2	
07/08/2013	09:06	Greece (Reggini, Phthiotis)	5.1	15						100
17/07/2013	03:00	W. Med. - NW Africa (Hammam Melouane)	4.8	10	VI				11	

Date	UTC	Location	M[1]	Depth (km)	MMI	Loss[2]	Cause	Dead	Injured	Buildings damaged[3]
22/06/2013	05:42	Indonesia (Lombok)	5.1	47					50	5400
18/06/2013	23:02	Russia (Kemerovo)	5.3	10	VII					
19/05/2013	09:07	W. Med. - NW Africa (Algiers)	4.9	7					5	
24/04/2013	09:25	Central Asia (Kama)	5.5	64				18	141	
11/03/2013	03:01	China (Xinjian)	5.1	10						
03/03/2013	05:41	China - Yunnan (Dali)	5.4	8		60,000,000			30	1400
22/02/2013	21:01	South Peru	5.3	8						
19/02/2013	02:47	China - Yunnan (Qiaojia	4.9	10					8	72
20/07/2012	12:11	China (Yangzhou, Jiangsu)	4.9	10				1	2	13
24/06/2012	07:59	China - Sichuan & Yunnan (Lijiang-Yanyuan,)	5.5	10		30,000,000		4	394	
14/06/2012	05:52	Asia Minor (Sirnak)	5.3	5	VI				23	
17/05/2012	03:12	SE US (Timpson, East Texas)	4.8	5	VII		Anthropogenic			
19/01/2012	12:35	Iran (Neishabour, Khorasan-E-Razavi)	5.1	8					238	
07/11/2011	09:43	SE Asia (Mindanao, Bukidnon)	5	46					31	
20/10/2011	07:24	SE US (Beeville)	4.8	3	VII		Anthropogenic			
20/10/2011	17:18	Indian Subcontinent (Gujarat)	5	15.5	IV				34	
23/08/2011		Trinidad, Colorado (Raton Basin Sequence)	5.3	4.3	IX	1,000,000	Anthropogenic			
29/06/2011	23:16	Japan	4.9	10				7		
20/06/2011	10:16	China - Yunnan	5.3	39				4		
08/06/2011	01:53	China	5.3	21				8		50
11/05/2011	16:47	W. Med. - SE Spain (Lorca)	5.1	1	VII	700,000,000	Anthropogenic	9	400	1500
10/03/2011	04:58	China - Yunnan (Yingilang, Pingyuan)	5.5	10					250	1039
27/02/2011	11:01	Guy-Greenbrier (2010-11 Arkansas swarm)	4.7	3.8	V		Anthropogenic			
01/02/2011	07:11	Central Asia (Myanmar - China border)	4.8	31				1		229
05/01/2011	16:32	Iran (Sepidan, Fars)	4.5	24					16	

Date	UTC	Location	M[1]	Depth (km)	MMI	Loss[2]	Cause	Dead	Injured	Buildings damaged[3]
12/11/2010	09:37	Indian Subcontinent	4.7	27					12	
06/11/2010	03:52	Iran	4.9	5					104	
03/11/2010	00:56	SE Europe (Kraljevo)	5.5	0	VI	140,000,000			100	5000
13/10/2010	14:06	SE US	4.4	13					2	
10/10/2010	21:44	Indian Subcontinent (Khanpur, Haripur)	5.2	33					15	100
29/08/2010	00:53	China - Yunnan	4.9	35					14	1000
30/07/2010	13:50	Iran (Torbet-I-Heydariyeh, Razavi Khorasan)	5.4	24					274	
14/05/2010	12:29	W. Med. - NW Africa (Beni Yellman)	5.2	2					43	
20/04/2010	00:17	Oceania (Kalgoorlie – Boulder)	5.2	0			Anthropogenic		3	
25/02/2010	04:56	China - Yunnan	5.2	10					11	
30/01/2010	21:36	China - Sichuan (Moxi, Suining)	5.1	10					15	200
17/01/2010	09:37	China (Guizhou)	4.4	26					9	
15/01/2010	18:00	N. South America	5.5	8					11	3
10/01/2010	00:25	Indonesia (Java Garout)	5.1	65	V				2	
31/12/2009	09:57	China - Yunnan	5.5	10					2	700
17/12/2009	23:45	Japan	4.9	6					7	20
03/11/2009	23:26	Iran (Bandar Abbas)	5.1	14					269	
01/11/2009	21:07	China - Yunnan	5	24					28	1000
03/10/2009	01:16	SW US (Olancha)	5.2							
13/06/2009	17:17	Central Asia	5.4	11						
02/05/2009	01:11	SW US	4.1	14					1	
16/04/2009	21:27	Central Asia (Nangarhar, Safed Koh)	5.5	5					51	
09/04/2009	01:46	Indian Subcontinent	5.1	44					6	
07/04/2009	17:47	N. Italy	5.5	15						
26/03/2009	04:44	Indian Subcontinent	4.1	10					5	
20/02/2009	03:48	Indian Subcontinent Kashmir	5.5	12					44	
04/01/2009	05:10	Greece	4.3	10					1	

33

Date	UTC	Location	M[1]	Depth (km)	MMI	Loss[2]	Cause	Dead	Injured	Buildings damaged[3]
25/12/2008	20:20	SE Asia, China - Yunnan (Ruili)	4.8	35		1,000,000			21	126
09/12/2008	18:53	China Sichuan	5.1	24					3	
07/12/2008	13:36	Iran	5.4	15		50,000			5	1
22/11/2008		N. Europe	4.1 (M_L)			50,000		2	3	
25/10/2008	20:17	Iran	5.4	28		10,000			9	1
16/09/2008	21:47	Indian Subcontinent	5	10		1,000,000			20	1
09/09/2008	03:07	Indonesia	5.2	25						
11/08/2008		N. South America	5.2	13		100,000				
29/07/2008	18:42	SW US	5.5	14		500,000		8	5	1
26/07/2008	18:51	China - Yunnan	4.8	17					25	
01/07/2008	00:17	Peru (Oxapampa)	5.5	33	VI	500,000			45	60
17/06/2008	05:51	China	4.8	10				1		
06/06/2008	20:02	W. Med. - NW Africa	5.5	4		100,000			30	1
06/06/2008		Indian Subcontinent	3.8 (mb)			50,000			2	
01/05/2008	00:15	Iran	4.5	16		20,000			100	
26/04/2008		Central Asia	5.5			100,000				12
30/03/2008		China	5			300,000				
29/03/2008	12:51	Peru	5.3	51		50,000		1	1	
23/03/2008		Iran	5(M_L			100,000				30
21/03/2008		China	5(M_L)			1,000,000				27
27/02/2008	00:56	N. Europe (Market Rasen, Lincolnshire)	4.8	18	VI	50,000,000			1	
27/02/2008		China	4.7			50,000				
18/02/2008		SE US	2.1 (mb)			500,000	Anthropogenic		5	1
15/02/2008	10:36	East Med.	5.1	10		50,000			10	
14/02/2008	02:07	C. Africa	5.3	10		100,000		3	59	
13/02/2008	20:55	Iran	4.5	14		50,000			10	
08/02/2008		Central America	5.4			200,000				
06/02/2008	06:09	Indian Subcontinent	4.3	10		50,000			50	
01/02/2008	07:33	W. Med. - NW Africa	4.6	10				3		
09/01/2008	22:24	W. Med. - NW Africa	4.6	10		10,000				
26/12/2007		Asia Minor	5.3(mb)	10		2,000,000				

Date	UTC	Location	M[1]	Depth (km)	MMI	Loss[2]	Cause	Dead	Injured	Buildings damaged[3]
26/12/2007		Asia Minor	5.2(M_L)	47		50,000				
09/12/2007	02:03	Brazil	4.9	10		250,000			6	6
20/11/2007	05:20	Iran	4.8	7		10,000			30	
07/11/2007	07:10	Indian Subcontinent	5.5	28		10,000			10	
07/11/2007	04:12	SE Asia	5.3	71						
06/11/2007	09:38	Indian Subcontinent	5.1	10		50,000			5	
29/10/2007		Asia Minor	5 (M_L)			200,000				
26/10/2007	06:50	Indian Subcontinent	5.2	10		100,000			12	110
15/09/2007		Central America	5.5			100,000				
09/09/2007	18:36	Indonesia	4.9	35		500,000			13	
06/09/2007		Indian Subcontinent	4.1 (M_L)			10,000			2	
25/08/2007	04:24	Iran	5	10		10,000			4	
06/08/2007		SW US	4.2 (mb)			50,000	Anthropogenic	3	6	
04/08/2007	22:21	Russia	4.9	9				2		
22/07/2007	23:02	Indian Subcontinent	5.1	19		50,000		3		
21/07/2007	22:44	Central Asia	5.2	10		200,000			3	174
20/07/2007		SW US	4.2			500,000				
19/07/2007		SE Asia	5.5 (M_L)		VI	100,000			3	10
08/05/2007		NW US	4.5			500,000				
28/04/2007	07:18	N. Europe (Folkestone, Kent)	4.6	6	VI	60,000,000			1	
16/04/2007		SE Europe	4 (M_L)			500,000				
15/04/2007	03:19	Japan	5.1	15					12	
10/04/2007		Greece	5.4 (M_L)			50,000				
13/03/2007		China	4.7 (M_L)			20,000,000				
13/03/2007		S. Africa	4.5			10,000	Anthropogenic		6	
06/03/2007	13:05	N. South America	5.2	43		500,000			9	9
06/03/2007	22:32	Iran	4.7	16		20,000			35	
03/03/2007		Indonesia	5.3 (M_L)			50,000				
09/02/2007		Asia Minor	5.3 (M_L)			50,000			35	
31/01/2007		Central Asia	5 (M_L)			50,000				
26/01/2007		Asia Minor	4.7 (M_L)			10,000				
21/01/2007	07:38	Asia Minor	5.2	3		500,000			2	
09/01/2007	14:49	China (Lanzhou, Baiyin)	4.7	33		5,000,000				2

Date	UTC	Location	M[1]	Depth (km)	MMI	Loss[2]	Cause	Dead	Injured	Buildings damaged[3]
08/01/2007		Central Asia	5 (M_L)			200,000				
31/12/2006		N. Europe	4.2 (M_L)			2,000,000				
17/12/2006		Central America	4.6			5,000,000		1		
13/12/2006		SE Asia	5.1 (M_L)			100,000				
08/12/2006	16:48	N. Europe (Basel, Switzerland)	3.4	5	V	9,000,000	Anthropogenic			
03/11/2006	06:21	China (Nei Mongol)	4.7	10		2,000,000				5586
09/10/2006	05:12	Indian Subcontinent	4.4	10		10,000			3	
03/10/2006		NE US	3.9			100,000				
29/09/2006	18:23	N. South America	5.5	52						
25/08/2006	05:51	China - Sichuan (Eastern Sichuan)	5	21		35,000,000		31	66	
16/08/2006		Indian Subcontinent	4.4			50,000			4	
29/07/2006		Indian Subcontinent	5.2			200,000		2	14	50
22/07/2006	01:10	China - Yunnan (Yanjin)	4.9	55		10,000,000			106	1400
20/06/2006	16:52	China	4.9	24		1,000,000			5	5
13/06/2006	14:15	SE Europe	4.5	10		20,000			1	12
03/06/2006	07:15	Iran	5.1	12				4		
24/05/2006		Indonesia	4.6 (M_L)			10,000		1		
07/05/2006	06:20	Iran	5	14		150,000			70	
04/04/2006	09:12	Indian Subcontinent	4.6	10		50,000			28	
31/03/2006		China	5 (M_L)			100,000				
20/03/2006	19:44	W. Med. - NW Africa (Laalam)	5.2	10		200,000		9	68	32
10/03/2006	07:50	Indian Subcontinent	4.9	10		50,000			22	
07/03/2006	18:20	Indian Subcontinent	5.5	10				7		
20/02/2006	17:20	SE Europe	4.6	10		200,000			2	
14/02/2006	00:55	Indian Subcontinent	5.3	30		1,000,000			2	
12/01/2006		China - Yunnan (Mijiang)	5 (M_L)			7,000,000			1	
10/01/2006		Central Asia	4			1,000,000			95	
24/12/2005	02:01	Japan	4.7	43				1		
14/12/2005	07:09	Indian Subcontinent	5.1	44		10,000			4	1
26/11/2005	00:49	China Ruichang (Jiujiang)	5.2	11	VI	50,000,000			8000	8000

Date	UTC	Location	M[1]	Depth (km)	MMI	Loss[2]	Cause	Dead	Injured	Buildings damaged[3]
12/11/2005		N. Europe	4.1 (M_L)	20		500,000				
08/11/2005	07:54	SE Asia	5.3	10						
06/11/2005	02:11	Indian Subcontinent	5.1	10		50,000			7	1
31/10/2005		Peru	5.1			50,000				
27/10/2005	11:18	China	4.2	10		20,000			1	
21/10/2005		Indian Subcontinent	5.2			100,000		8	6	
16/10/2005	07:05	Japan	5	40		10,000			2	
15/10/2005	04:24	Indian Subcontinent	5.2	10						
01/10/2005	22:19	Peru	5.3	20		1,000,000			10	
21/08/2005	02:29	Japan	4.8	13				2		
13/08/2005	04:58	China	4.8	10		100,000			26	
05/08/2005	14:14	China	5.2	42		1,000,000			9	
25/07/2005	15:43	China	5	47		50,000			12	
20/06/2005	04:03	Japan	4.9	15		500,000			1	
16/06/2005	20:53	SW US	4.9	11		50,000		3		
12/06/2005		Central America	5.1			1,000,000				
12/05/2005		Asia Minor	4.7 (M_L)			50,000				
10/05/2005		S. Africa	4.3 (mb)			50,000	Anthropogenic	5	19	
03/05/2005	07:21	Iran	4.9	11		100,000			26	
01/05/2005	16:23	Japan	4.6	10				1		
30/04/2005		Peru	4.7			50,000				
19/04/2005	21:11	Japan	5.5	18		2,000,000			60	
03/04/2005		Iran	4.1 (M_L)			10,000			24	
14/03/2005	09:43	Indian Subcontinent	4.9	10		50,000			45	
09/03/2005	10:15	S. Africa (Klerksdorp, Stilfontein)	5	5	V	70,000,000	Anthropogenic		58	
02/03/2005	11:12	Indian Subcontinent	4.9	51		20,000			1	
15/02/2005	19:46	Japan	5.5	46		200,000			30	
03/02/2005		Indonesia	5.5 (M_L)			50,000			3	
02/02/2005	05:55	Indonesia	4.8	15		50,000			4	
31/01/2005		W. Med. - SE Spain (La Paca)	4.6 (M_L)			500,000			4	
25/01/2005	16:30	China - Yunnan	4.8	12		50,000			3	

Date	UTC	Location	M[1]	Depth (km)	MMI	Loss[2]	Cause	Dead	Injured	Buildings damaged[3]
10/01/2005	23:48	Asia Minor	5.5	15		10,000		1	5	
10/01/2005	18:47	Iran	5.4	31		10,000			110	
20/12/2004	23:02	Asia Minor	5.4	5		100,000			3	
09/12/2004	08:49	Indian Subcontinent	5.4	34		50,000			3	
09/12/2004		SE Europe	3.8			50,000				
05/12/2004	08:30	W. Med. - NW Africa	4.5	10		50,000			46	
02/12/2004		N. South America	5.4			20,000			1	
01/12/2004	17:42	W. Med. - NW Africa	4.5	10					15	
24/11/2004	22:59	N. Italy (Garda Area, Salo)	5.1	17	VIII	250,000,000			9	
23/11/2004		SE Europe	4.7			50,000				
22/11/2004	04:01	Iran	5	36		50,000			3	
09/11/2004	18:43	Japan	5.1	10					1	
08/11/2004	02:15	Japan	5.5	10					8	
03/11/2004	23:57	Japan	5.3	10					1	
18/10/2004	22:11	China	4.8	30		1,000,000			12	
21/09/2004	13:32	N. Europe	4.8	10		50,000			3	
15/09/2004	08:35	Indonesia	5.4	98		10,000			2	
07/09/2004	12:15	China	5.2	10		2,000,000			19	600
10/08/2004	10:26	China – Yunnan	5.4	6		50,000,000			600	18556
04/08/2004		Asia Minor	5.5			10,000			15	
30/07/2004	07:14	Asia Minor	4.8	5		50,000			6	
18/07/2004	08:31	Indian Subcontinent	5.2	10		100,000			40	100
14/07/2004		Indian Subcontinent	4.7 (mb)			1,000,000				
12/07/2004	13:04	SE Europe (Soca valley, Slovenia)	5.2	7	VII	10,000,000		5	11	2
01/07/2004	22:30	Caucasus	5.1	5					21	
08/05/2004	20:11	Indian Subcontinent	4.5	10		50,000			30	
04/05/2004	05:04	China	5.5	13						
01/05/2004	07:56	Taiwan	5.2	44		500,000		1	2	
13/04/2004	21:47	Asia Minor	4.1	5		10,000			4	
30/03/2004		Central Asia	5.3			50,000				
28/03/2004		Asia Minor	5.4			100,000			12	

Date	UTC	Location	M[1]	Depth (km)	MMI	Loss[2]	Cause	Dead	Injured	Buildings damaged[3]
24/03/2004	01:53	China - Nei Mongol (Bayan UI Hot, Uliastai)	5.5	18		75,000,000			100	
01/03/2004		Asia Minor	3.8			20,000		6	2	1
26/02/2004		Asia Minor	4.9			50,000				
24/02/2004	02:14	C. Africa	4.7	10		100,000			8	24
16/02/2004	14:44	Indonesia	5.1	55		50,000		7	13	100
14/02/2004	14:44	Indian Subcontinent - Pakistan	5.5	11		1100000			63	1420
11/02/2004	08:15	Iran	5.3	26		50,000			4	
10/01/2004	18:38	W. Med. - NW Africa	4.5	10		20,000			300	
11/12/2003	16:28	Iran	5	33		100,000		5		2
26/11/2003	23:38	China - Yunnan (Ludian)	4.7	33	V	5,000,000			20	1449
13/11/2003	02:35	China	5.1	10		50,000			30	2
14/09/2003	21:42	N. Italy	5.3	10		20,000			2	10
21/08/2003		China	5			3,000,000			6	14
16/08/2003	06:58	China - Nei Mongol	5.4	24	VIII	165,000,000			1054	8000
13/08/2003		Indian Subcontinent	5.3 (M_L)			20,000			2	
12/08/2003		Iran	4.7			10,000				
11/08/2003		Indonesia	5.3			20,000				
27/07/2003		Indian Subcontinent	5.2 (mb)			50,000		2	50	
26/07/2003	08:36	Asia Minor	5.4	10		10,000			10	
26/07/2003	01:00	Asia Minor	4.5	10						
25/07/2003	15:13	Japan	5.5	10					569	
11/07/2003		Indonesia	4.2 (mb)			10,000				
03/07/2003		Iran	4.2 (M_L)			1,000,000			1	
24/06/2003	13:01	Iran	4.6	33		50,000				
11/05/2003	15:57	Japan	5.3	66				3		
11/04/2003	09:26	N. Italy (Alessandria)	5	4		70,000,000			2	
10/04/2003		Indian Subcontinent	4.5 (mb)			50,000			1	
22/03/2003		Indonesia	4.6 (M_L)			50,000				
11/03/2003		Indian Subcontinent	4.5 (M_L)			20,000				
25/02/2003	03:52	China	5.4	10						

Date	UTC	Location	M[1]	Depth (km)	MMI	Loss[2]	Cause	Dead	Injured	Buildings damaged[3]
23/02/2003		N. Europe	4.4			40,000				
23/01/2003	00:08	Indonesia	5.5	33		50,000		2	2	
11/01/2003	17:45	Iran	5.2	33		2,000,000			2	1350
24/12/2002	17:03	Iran (Kermanshah)	5.2	33	V	2000000			15	3000
01/11/2002	22:09	Indian Subcontinent (Kashmir)	5.4	33	V	550000			65	
29/10/2002	10:02	S. Italy (Etna eruption earthquake sequence)	4.5	10					9	
25/09/2002	18:14	Central America	5.3	5		10,000			2	
22/09/2002	23:53	N. Europe Dudley	5	9		50,000		1	2	
08/08/2002		China	5.2			50,000				
06/08/2002		W. Med. - SE Spain (Bullas - La Paca)	4.5 (M_L)			50,000			2	
26/06/2002	18:18	Iran	4.6	10		50,000		2	2	
24/06/2002	01:20	W. Med. - NW Africa	5.2	10		10,000			12	1
20/06/2002	05:40	Indian Subcontinent	4.5	39		10,000			55	
14/06/2002	02:42	Japan	4.9	51				1		
24/05/2002	20:42	SE Europe	4.7	10		100,000			5	
18/05/2002	15:15	Oceania	5.5	10		100,000				
25/04/2002	22:41	Caucasus (Tbilisi)	4.8	10	VIII	350,000,000			70	
24/04/2002	19:48	Iran (Kermanshah)	5.4	33	VII	500,000			56	1
22/04/2002	04:57	Peru	4.4	66						
20/04/2002		NE US	5		VII	100,000				
14/04/2002		Indian Subcontinent	5.3 (M_L)			10,000			5	
05/04/2002		SE Europe	4.0 (M_L			100,000				
01/04/2002	06:14	Oceania	5.3	80		50,000			11	
04/03/2002		Japan	5.5			50,000				1
03/03/2002		Central Asia	4 (M_L)			20,000				2
20/02/2002	11:27	N. Europe	5	1		100,000	Anthropogenic		3	
17/02/2002	13:03	Iran	5.4	33		100,000			30	
11/02/2002		Central Asia	5 (M_L)			10,000			50	1
30/01/2002		Central America	5.1 (M_L)			20,000				1
21/01/2002	14:34	Asia Minor	4.8	10						

Date	UTC	Location	M[1]	Depth (km)	MMI	Loss[2]	Cause	Dead	Injured	Buildings damaged[3]
17/01/2002	20:01	C. Africa	4.9	15						
14/01/2002		S. South America	5 (M_L)			10,000				2
09/01/2002	06:45	Central Asia	5.3	33					50	
19/12/2001	07:54	Indian Subcontinent	4.5	10		50,000			100	1
25/11/2001		Central Asia	4.5 (M_L)			50,000				1
31/10/2001	12:33	East Med.	5.2	10					5	
08/10/2001	01:17	Iran	4.9	33		10,000			1	1
16/09/2001		Greece	5.2			100,000				
26/08/2001	00:41	Marmara	5.4	7					2	
21/08/2001		Asia Minor	4.4			50,000				
24/07/2001	17:42	S. South America	5.4	33					7	
17/07/2001	15:06	North Italy	4.7	10		1,000,000			3	1
16/07/2001	16:12	Indian Subcontinent	5	33					1	
14/07/2001	18:36	China - Yunnan	4.7	33		100,000			2	
10/07/2001	21:42	Asia Minor	5.4	33		50,000			120	17
28/06/2001	03:46	Indonesia	5	36						
25/06/2001	13:28	Asia Minor	5.5	5		100,000			130	10
21/06/2001	19:55	N. Europe	4.2	1		200,000			6	
13/06/2001		Central America	5	20		50,000				
08/06/2001		China	5.3 (M_L)			10,000			13	
07/06/2001	18:03	China - Yunnan	4.6	33					13	
02/06/2001		Indian Subcontinent	5.2 (M_L)			50,000		4	20	60
01/06/2001	14:00	Central Asia	5	62					20	
29/05/2001	13:14	Asia Minor	4.6	33		50,000			2	3
23/05/2001	21:10	China - Sichuan	5.5	33	VII	36,000,000		5	600	
03/04/2001	14:57	Japan	5.4	33		50,000			8	
09/03/2001		Indian Subcontinent	5.4			10,000			25	
19/02/2001	03:51	SE Asia (Dien Bien Phu)	4.9		VI	14,000,000			4	130
17/02/2001	20:25	Central America	4.1	10					3	
08/02/2001	16:54	Indian Subcontinent	5.1	10					40	
07/01/2001		Indian Subcontinent	4.8 (M_L)			50,000		1	2	
15/12/2000		Asia Minor	5.1 (mb)			50,000		6	41	
12/12/2000		Indian Subcontinent	5			50,000				

Date	UTC	Location	M[1]	Depth (km)	MMI	Loss[2]	Cause	Dead	Injured	Buildings damaged[3]
31/10/2000		Central Asia	4.5	33		1500000				166
30/10/2000	16:42	Japan	5.5	34		10,000			7	
08/10/2000		N. South America	5.4			50,000		2		
04/10/2000	02:33	Asia Minor	4.7	8		10,000			31	
20/09/2000	08:37	N. South America	5.5	33		50,000				1
03/09/2000	08:36	SW US (Napa, Yountville)	5	10	VII	80,000,000			70	
23/08/2000	13:41	Marmara	5.3	15				22		
21/08/2000	13:25	China - Yunnan	5.1	5.4	VII	43,000,000		1	406	
19/08/2000	21:26	Asia Minor	4.1	33				9		
17/08/2000	08:08	SE US (Amarillo swarm)	3.9		V		Anthropogenic			
27/07/2000		Pacific	5.1			100,000		2		
14/07/2000		Iran	4			500,000				
12/07/2000	01:10	Indonesia (Java)	5.4	33		5,000,000			124	2000
07/07/2000	00:15	Marmara	4.2	8		10,000			34	
06/07/2000	19:30	Central America	5.4	33					42	
17/05/2000	03:25	Taiwan	5.4	10					13	
12/05/2000	03:01	Asia Minor	4.8	10		100,000			12	
07/05/2000	23:10	Asia Minor	4.5	5		50,000		1	1	
06/04/2000	22:30	Indian Subcontinent	4.9	10				2		
15/02/2000		Marmara	5			50,000			1	
07/02/2000	19:34	S. Africa	4.5	5			I	1		
02/02/2000	22:58	Iran	5.3	33		50,000			15	100
26/01/2000	20:55	China	4.9	33		200,000		2		
11/01/2000	23:43	China	5.1	10		10,000			4	
15/12/1999	05:12	SE Asia	4.8	33						
29/11/1999	04:10	China	5.3	10		100,000				
26/11/1999		Iran	4.6			50,000				
24/11/1999	16:40	China	5	33		10,000			5	
08/11/1999		Iran	5.5 (mb)	26		50,000				12
07/11/1999	16:54	Asia Minor	5	10		10,000			1	
01/11/1999	13:25	China (Datong, Shangxi)	5.3	10	VII	44,000,000			4	700
31/10/1999	13:27	Peru	4.4	62	VI	200,000		1	30	210
31/10/1999	15:09	Iran	5.2	33		10,000			28	

Date	UTC	Location	M[1]	Depth (km)	MMI	Loss[2]	Cause	Dead	Injured	Buildings damaged[3]
05/10/1999	00:53	Asia Minor	5.2	33		50,000			103	
29/09/1999	00:13	Marmara	5.2	10						
27/09/1999		Iran	4.1			10,000				
24/09/1999		Iran	5.1			50,000			14	
14/09/1999		Iran	4.5 (M_L)			50,000				
31/08/1999	08:10	Asia Minor	5.2 (M_L)	10		20,000			166	
13/08/1999		East Med.	4.8 (mb)	33	V	100,000				
10/08/1999	19:33	Iran	4.5	33				1		
03/08/1999		Indian Subcontinent	4			100,000				
22/07/1999	10:42	Indian Subcontinent (Uttaranchal, Bay of Bengal)	5.2	10	VI	1000000			500	
18/07/1999		N. South America	5.4			100,000				65
01/07/1999	07:40	SE Europe (Central Serbia)	5.1	10	VII	10,000,000				24
04/06/1999	09:12	Caucasus	5.4	33		5,000,000			18	50
31/05/1999		Caucasus	4			10,000			1	1
05/05/1999		Peru	5.5			10,000				
30/04/1999		Iran	4.7			50,000				
23/04/1999		S. Africa	4.2			500,000	Anthropogenic	2		
07/04/1999		Indian Subcontinent	5			50,000				
05/04/1999		Iran	5.5			50,000				
02/04/1999		Central America	3.9			50,000				1
25/03/1999	23:31	Japan	5.2	82				1		
18/03/1999		Oceania	4.7	10		50,000				
11/03/1999	13:18	China	5.1	33					3	
21/02/1999	18:14	Caucasus	5.3	65		2,000,000			20	
02/02/1999	13:45	W. Med. - SE Spain (Mula)	5.2	10	VII	44,000,000			20	1
30/01/1999	12:24	N. South America	4.2	10					5	5
02/01/1999	17:55	China - Yunnan	4.5	41					2	
14/12/1998	13:06	Asia Minor	4.5	10		100,000			2	118
12/12/1998		Indian Subcontinent	5.4			50,000		5	8	1
01/12/1998	07:37	China - Yunnan	4.5	10	V	23,000,000			84	8000
26/11/1998		SW US	5.2			100,000				
13/11/1998	13:01	Iran	5.4	33					105	

Date	UTC	Location	M[1]	Depth (km)	MMI	Loss[2]	Cause	Dead	Injured	Buildings damaged[3]
26/10/1998	20:01	China	4.7	46		1,000,000			28	
18/10/1998	14:20	Central America	4.4	10		10,000		3	1	45
11/10/1998		Indonesia	5.5			50,000				
05/10/1998		Iran	5.3			100,000				
29/09/1998	22:14	SE Europe	5.5	10		50,000			17	
15/09/1998	07:24	Japan	5.1	50				1		
28/08/1998	23:46	Japan	5.4	75				2		
15/08/1998		S. Italy	4.8		VII	500,000				
12/08/1998	14:10	SW US	5.2	8		50,000		2		
28/07/1998	04:51	China (Baicheng, Xinjiang)	5.5		VI	5,000,000			24	19
28/07/1998	04:51	China	5.2	33						
04/07/1998	02:15	East Med.	5.4	33					1000	
01/07/1998		Japan	4.5			1,000,000				
28/05/1998	18:33	Asia Minor	5.5	10				1		
20/04/1998		Oceania	5	250		100,000				
13/04/1998	15:14	Asia Minor	5.3	33		50,000			13	2
12/04/1998		SE Europe	5.5			500,000			1	
03/04/1998	07:26	North Italy (Gualdo Tadino-Nocera Umbra - Umbria Marche sequence)	5.2	10	VI	7,000,000			5	
26/03/1998	16:26	S. Italy	5.4	10		100,000				1
21/02/1998	00:55	Japan	5.1	33		10,000			1	
11/02/1998	13:14	SE Asia	5.5	56					6	11
06/02/1998		S. South America	5.4			10,000				
14/11/1997	04:29	Taiwan	5.2	33				1		
06/11/1997	02:34	Canada	5.1	22						
03/11/1997	08:07	Asia Minor	4.8	33				2		
23/10/1997		China	5.3			1,000,000				
06/10/1997	23:24	N. Italy	5.5	10					4	
03/10/1997	11:28	Iran	5.3	33		10,000			6	
03/10/1997	08:55	N. Italy	5.3	10					20	
26/09/1997	05:26	China Sanshui	4.2	1		85,000,000	Anthropogenic			650
25/09/1997	00:05	S. Africa	4.5	5			Anthropogenic	3		

Date	UTC	Location	M[1]	Depth (km)	MMI	Loss[2]	Cause	Dead	Injured	Buildings damaged[3]
25/08/1997		Asia Minor	3.9			10,000				
24/08/1997	21:11	Iran	5	33		10,000			67	
13/08/1997		China - Sichuan (Chongqing)	5.3	35	V	75,000,000	Anthropogenic			
08/08/1997	02:39	Asia Minor	4.5	10		10,000		1	1	7
31/07/1997		Indian Subcontinent	5.2			50,000			2	1
30/06/1997		Pacific	5.5	14		50,000				
16/06/1997		Iran	5.5	55		20,000				1
31/05/1997		China	5.3			85,000,000				
31/05/1997		Asia Minor	4			100,000				
21/05/1997	23:50	Atlantic	5.4	18		100,000			2	
21/05/1997	08:45	S. Africa	5	5			Anthropogenic		46	
17/05/1997	03:58	China	4.9	33				1		
13/05/1997	11:42	Iran	4.5	10						
26/04/1997		SE Europe	4.7			100,000				2
23/04/1997		Iran	4.8			200,000				
18/04/1997		S. Africa	2.8			10,000	Anthropogenic	2	2	
02/04/1997	19:33	Japan	5.5	10						5
26/03/1997		East Med.	5.5			250,000				
24/03/1997		S. South America	5.3	80		200,000				
20/03/1997		Indian Subcontinent	5.4	33		10,000			3	
19/03/1997	19:57	Indian Subcontinent	4.9	50		100,000			2	2
10/03/1997		SW US	5.4			100,000				
09/03/1997		S. South America	5.4	42	VII	500,000				
06/03/1997	15:16	W. Africa	4.4	10		10,000		7	7	
04/03/1997		Indian Subcontinent	5.5	24		10,000		1	1	
28/02/1997		Iran Ardabil	5.5	39		100 Mill.		1100	3000	8500
28/02/1997		Asia Minor	4.8	5		20,000				
12/02/1997		China	5.3			1,000,000				
25/01/1997		China	5.1	87		3,000,000				
22/01/1997		East Med.	5.5			300,000		1	5	10
12/01/1997		SE Europe	4.3		V	10,000				
21/12/1996		China	5.5			50,000				
21/12/1996	01:28	Japan	5.5	44				1		

Date	UTC	Location	M[1]	Depth (km)	MMI	Loss[2]	Cause	Dead	Injured	Buildings damaged[3]
15/10/1996		N. Italy	4.8			50,000		2	10	
17/09/1996		SE Europe	5.5			50,000				
11/09/1996		N. Europe	5			100,000			1	
25/08/1996	14:09	N. South America	5.5	50				2		
27/07/1996	18:55	Greece (Konitsa)	5.2			500,000				152
15/07/1996	00:13	N. Europe (Annecy)	4.3	5	VI	50,000,000		1		
02/07/1996		China	5.2			100,000		1	10	
24/05/1996	06:35	Iran	5.2	33		50,000			20	
21/05/1996		SW US	4.7			1,000,000				
07/05/1996		Central America	4.7			50,000		1	2	
03/05/1996	04:04	NW US	5.5	4		10,000			2	
02/05/1996	06:30	SE Asia	5.5	33		10,000			3	
27/04/1996		S. Italy	4.2			50,000				
02/04/1996		Asia Minor	4.9			250,000				
15/03/1996		Peru	4.7	60		10,000				
06/03/1996		N. South America	4.2			1,000,000				
19/12/1995	20:56	Central America	5.4	10		100,000		1	1	
05/11/1995		S. South America	5.2 (mb)	57		100,000			6	
30/09/1995		S. Italy	4.5			100,000			4	
28/09/1995		SE Europe	5.1 (mb)	7	VI	100,000				
26/09/1995		Asia Minor	4.6			100,000			6	
18/08/1995		Asia Minor	4.9			500,000			1	
17/08/1995		SW US	5.1 (mb)	5	V	100,000				
21/06/1995		Peru	4.9			10,000		1		
31/05/1995		Indian Subcontinent	5.2			10,000			5	
21/05/1995	06:13	Indonesia	5.2	28		100,000		5	5	
20/05/1995		Indonesia	5.5			500,000			38	
01/04/1995	03:49	Japan	5.4	10					39	
26/03/1995		N. South America	5.2			100,000		2	50	
04/03/1995	23:23	N. South America	4.4	5		500,000			4	8
11/02/1995		N. South America	5.3			100,000			37	
28/01/1995		N. South America	5			100,000				
24/01/1995	04:14	Iran	5	33		100,000			11	

Date	UTC	Location	M[1]	Depth (km)	MMI	Loss[2]	Cause	Dead	Injured	Buildings damaged[3]
04/01/1995		China	4.5			200,000			3	26
31/12/1994	02:57	China - Yunnan	5.3	33					360	
30/12/1994	06:56	Asia Minor	4.7	10					2	
26/12/1994	14:10	SW US	5.5	23		2,000,000			2	
14/12/1994		N. Europe	4.8	10		200,000				
01/12/1994		Greece	5.2			100,000				
06/08/1994	11:03	Oceania (Ellalong)	4.7	1	VIII	30,000,000				
28/07/1994		Indian Subcontinent	4			10,000				
17/06/1994		Peru	4.5			100,000				
19/05/1994		China (Mentougou)	4.2 (M_L)				Anthropogenic			
30/03/1994	19:55	Iran	5.4	53					30	
12/03/1994		NE US	3.6 (mb)	1		100,000				
02/03/1994	03:38	Central America	5.4	59		100,000				
12/02/1994	17:06	Japan	5.4	31				1		
01/02/1994	09:30	Indian Subcontinent	5	10		50,000				32
08/12/1993		Indian Subcontinent	5 (mb)	25		100,000			1	
04/12/1993		NW US	5.2 (mb)	8	VII	1,000,000				
12/11/1993	13:27	Indian Subcontinent	4.6	10		100,000			25	100
20/10/1993	16:15	Indian Subcontinent (Nepal)	5.1	37.4	VI	5,000,000			55	
01/08/1993	00:20	East Africa	5.5	12.5		100,000			9	
17/07/1993		China	5.3 (mb)	26		23,000,000				
26/06/1993		S. Italy	4.9	13	VII	2,000,000				
22/06/1993	16:32	Iran	5.4	33						
28/04/1993		N. South America	4			100,000				
11/04/1993		SE Asia	5			2,000,000			7	
09/04/1993	07:29	SE US (Fashing)	4.3		VI		Anthropogenic			
26/03/1993	11:58	Greece (Pyrgos)	5.4	10	VII	10,000,000		2		
13/02/1993	02:25	East Africa	5.3	12.4		100,000			1	
01/02/1993		China	4.5 (M_s)	33		1,000,000		2		
31/01/1993	19:33	China - Yunnan	4.9	33						
27/01/1993	10:27	Iran	5.1	33		500,000			3	
13/01/1993	17:11	Central America	5.5	16	VII	1,000,000				
01/01/1993		N. Europe	4	25		100,000				

Date	UTC	Location	M[1]	Depth (km)	MMI	Loss[2]	Cause	Dead	Injured	Buildings damaged[3]
18/12/1992	11:21	China	5	29.9		100,000			45	
12/12/1992		N. South America	4.3 (M_L)	33		50,000				
27/11/1992		SW US	5.1 (M_L)	3	VI	100,000				
30/10/1992		W. Med. - NW Africa	5.1 (M_L)	26		500,000			50	
23/10/1992		W. Med. - NW Africa	5.3 (M_L)	29		100,000		2	45	
22/10/1992	17:39	East Med.	4.5	10		100,000			50	
08/09/1992	00:38	Iran	5.2	17.5		100,000			11	
14/07/1992		Asia Minor	4.5 (mb)	18		100,000				15
09/07/1992	01:43	SW US (Big Bear Sequence)	5.3	0.1	VI	100,000,000[2]			20	
19/05/1992	01:26	Arabian peninsula	4.5	10						
04/05/1992		S. South America	5			50,000				1
13/04/1992	01:20	Roermond, Netherlands	5.4	21.2				1	45	
20/03/1992		Central America	4.2 (mb)	18		2,000,000				
20/03/1992		Greece	4.9 (mb)	14		100,000				
04/03/1992	11:57	Iran (Lordegan, Ardal)	5.1	17.9		60,000,000			50	
14/02/1992		S. Africa	3.4 (mb)	5		10,000	Anthropogenic		4	
04/02/1992	01:58	Indonesia	5.1	58.3		2,000,000			1	
19/01/1992		W. Med. - NW Africa	5			100,000				
02/01/1992	07:45	SE US (Rattlesnake Canyon Earthquake)	5		V		Anthropogenic			
02/12/1991	08:49	SE Europe (Romania)	5.5	9	VIII				4500	
27/11/1991		N. South America		39		100,000				
22/11/1991	00:40	Arabian peninsula	4.7	10		100,000		39	39	
20/11/1991		N. Europe	4.7 (mb)	15		100,000				
18/11/1991		Asia Minor	3.9 (M_L)	27		100,000				
10/11/1991	15:19	Iran	5	43.6		100,000			15	
04/11/1991	01:50	Iran	5.4	38.5					51	
28/10/1991		SE Europe	4.6	10		100,000				
28/10/1991	01:09	Japan	5.1	17				1		
14/08/1991		SE Europe	4.6			500,000				
09/08/1991		Central America	4.7 (M_S)	5		100,000				
24/07/1991	09:45	Middle-East	5.5	25.5						

Date	UTC	Location	M[1]	Depth (km)	MMI	Loss[2]	Cause	Dead	Injured	Buildings damaged[3]
23/07/1991	19:44	Peru	5.3	5	V	500,000		30		
07/07/1991		Indian Subcontinent	3			10,000		5		
21/06/1991		Central America	5.3 (mb)	77		100,000		1	3	
26/05/1991	12:26	S. Italy	5.1	8.1		100,000			1	
26/05/1991	10:59	Indonesia	5.1	33		100,000				
16/05/1991		N. Europe	4.5	10		1,000,000	Anthropogenic			
15/05/1991	14:28	Caucasus	4.9	14	V	500,000				
24/04/1991	10:54	Asia Minor	4.5	33		100,000		3	3	
18/04/1991	09:18	Central Asia (Badakshan/Tajikistan)	5.5	33	VII	5,000,000			200	
25/03/1991	18:02	China	5.4	10		500,000			131	
13/02/1991		N. Europe	3.8 (M_L)	5		100,000		9		
12/02/1991	09:54	Marmara	4.8	10		100,000				
07/12/1990		Japan	5.1 (M_L)	21		1,600,000				
02/12/1990		Central Asia	5 (M_L)	29	VI	1,000,000				
23/10/1990		SW US	5.2 (M_L)	9		100,000				
17/10/1990		S. Africa	4	5		100,000	Anthropogenic		6	
26/09/1990	23:08	S. Africa	5	5			Anthropogenic	5		
04/09/1990		Central America	5.1 (mb)	10		100,000				
11/08/1990	02:59	N. South America	5.3	5		500,000			10	
18/07/1990		Asia Minor	5.2 (mb)	17		1,000,000				
06/07/1990	00:16	Indonesia	5.5	13.5					103	
06/07/1990	19:34	Iran	5.3	34.6		10,000		2	2	
09/06/1990	01:14	Peru	5.5	25.6						
04/06/1990		Oceania	5.1 (mb)	27		100,000				
08/05/1990		Iran	4.8			10,000				1
05/05/1990	07:21	S. Italy	5.4	10	VIII	100,000		16	30	
28/04/1990		SW US	4.3 (mb)	6		100,000				
09/02/1990	17:57	China	5	10		100,000		1		
07/02/1990		China (Taiji)	3.6 (mb)				Anthropogenic			
27/12/1989	23:26	Oceania (Newcastle)	5.4	10	VIII	1,100,000,000			100	300
20/11/1989	03:21	China	5.2	33		250,000			161	

Date	UTC	Location	M[1]	Depth (km)	MMI	Loss[2]	Cause	Dead	Injured	Buildings damaged[3]
23/10/1989		S. Italy	3.8 (mb)		VII	100,000				
18/10/1989	14:57	China (Datong)	5.3	10	VII	1000000		150	50	
13/10/1989	21:19	Japan	5.3	25.5	VI	100,000		2	2	
01/09/1989		Greece	4.7			100,000				
08/08/1989	08:13	SW US	4.9	15	VI	100,000			1	
03/08/1989	07:42	Caucasus	5	18.2		150,000			1	
09/07/1989	02:09	Japan	5.1	5		3,000,000			22	
08/06/1989	06:24	East Africa	5	18.6		100,000			1	
20/05/1989		Asia Minor	5 (mb)	34		100,000				
03/05/1989	09:13	Iran	5.1	33		500,000			4	
03/05/1989		N. South America	5.4 (mb)	10		100,000				42
30/03/1989		Caucasus	4.6 (mb)	10	VII	100,000				1
26/03/1989		Brazil	4.3 (mb)	10	VII	100,000				
13/03/1989		N. Europe	4.7 (M_S)			3,000,000	I		7	
10/03/1989		Asia Minor	4.4 (M_S)	10		500,000				10
26/02/1989		Central America	4.8 (M_S)	22	VII	100,000				
19/02/1989	12:27	Japan	5.5	60.4				1		
13/01/1989		SW US	5.2 (mb)	3	VI	100,000			1	
22/12/1988		Greece	4.6 (mb)	38	VI	1,000,000				
03/12/1988	11:38	SW US	4.4	13	VI	10,000			17	
27/11/1988	04:17	China - Yunnan	5.1	15.7				1		
21/11/1988		Atlantic	5.3 (M_S)	11	VII	100,000				
10/11/1988	01:17	China	4.6	10		100,000			71	
20/10/1988		NE US	3.9	5	VI	10,000				
16/10/1988		Atlantic	5.1 (mb)	10	VI	100,000			2	
03/10/1988		Iran	5	33		100,000				
02/09/1988		N. Europe	3.8	10		10,000		3	4	
23/08/1988		SE Europe	4.7 (mb)	10		100,000				
23/08/1988		Iran	5 (mb)	35		100,000				
07/08/1988		Iran	4.8 (mb)	40		100,000				
03/07/1988	05:20	Taiwan	4.7	21.4		10,000			11	
09/05/1988	16:23	Central America	4.5	10				3		
30/03/1988		Iran	5.2	33		100,000			24	

Date	UTC	Location	M[1]	Depth (km)	MMI	Loss[2]	Cause	Dead	Injured	Buildings damaged[3]
30/03/1988		Asia Minor	4.4 (mb)	10		100,000				
17/03/1988	20:34	Japan	5.4	103						10	
11/02/1988	15:25	SW US	4.8	12	VI	1,000,000			25	
22/01/1988	23:02	Central Asia	5.3	33						
09/01/1988		SE Europe	5.3 (mb)	24	VII	100,000			1	
03/01/1988	21:32	China	5.5	14.3					60	
22/12/1987		Oceania	4.5 (mb)	10		100,000				
24/11/1987		Iran	5.3 (mb)	41		500,000				243
18/11/1987		Japan	5.4	10		50,000			3	
04/10/1987	10:59	SW US	5.2	8						
02/10/1987	22:27	Peru	5.4	19.8						
04/09/1987	16:42	S. Italy	5.1	18.6	VIII	1,000,000			2	
14/08/1987	06:24	SE Europe	5	13.6					2	
02/08/1987	09:07	China	4.9	29		500,000			84	
20/07/1987		N. Europe	4.9 (ML)	14		100,000		1	3	
24/06/1987		Oceania	4.4 (mb)	10	VII	500,000				
10/06/1987	23:48	NE US	4.9	9.7	VI	100,000		1		
29/05/1987	06:27	Iran	4.9	40.9		100,000			50	
23/05/1987	17:09	SE Asia	5.2	32		100,000				
02/05/1987	20:43	N. Italy	4.8	10	VII	1,000,000			12	
11/04/1987	02:26	S. Italy	4.1	17.9				1		
10/04/1987		Iran	4.9 (mb)	46		100,000				
12/03/1987		N. Europe	2.6 (ML)	10		100,000			3	
09/03/1987		Oceania	5.25	26		100,000				
25/02/1987		SE Europe	4.6 (mb)	15		1,000,000				
13/02/1987		SW US	5.3 (mb)	13		100,000				
26/01/1987	11:11	W. Med. - NW Africa	4.9	10		500,000			7	
22/01/1987	05:10	N. Italy	4.2	21.6						
15/01/1987		Central America	4	10		500,000				86
11/01/1987		Iran	4.9 (mb)	10		100,000				
07/01/1987	05:47	S. South America	5	33						16
24/12/1986		SE Europe	5 (mb)	29	VII	100,000				
19/12/1986		S. South America	2.8 (ML)	33		500,000				

Date	UTC	Location	M[1]	Depth (km)	MMI	Loss[2]	Cause	Dead	Injured	Buildings damaged[3]
18/12/1986		N. Europe	4.7 (mb)	10		10,000			5	
16/12/1986		SE Europe	5.3		VIII	1,000,000				
30/11/1986	05:19	Brazil (Joao Camara sequence)	5 (mb)	-36	VII	50,000,000		1		1500
25/11/1986	13:59	SE Europe	5.5	30.2					12	
17/10/1986		Indian Subcontinent	5.2	43		100,000				
16/10/1986		SE Europe	3.2	10	VI	100,000				
11/10/1986	09:00	Asia Minor	5.5	5		500,000		3		50
28/08/1986		N. Italy	5.2			10,000				
03/08/1986		Asia Minor	5 (mb)	12		500,000				
13/07/1986		SW US	5.3 (M_L)	10		1,000,000		1	29	
13/07/1986		SE Europe	3.1 (mb)	10		500,000				1
09/06/1986		Caucasus	4.4 (mb)	33		10,000				1
15/05/1986		Indian Subcontinent	5.2 (mb)	18		10,000				
26/04/1986	07:35	Indian Subcontinent	5.5	33				30		
11/04/1986		Caucasus	5 (M_L)	10		10,000				
05/04/1986	20:14	Peru (Cuzco)	5.3	50.9	V	22,000,000			170	
31/03/1986	11:55	SW US	5.5	8					6	
25/03/1986		Iran	4.9 (mb)	33		100,000				3
03/02/1986		Central America	4.8 (mb)	16		110,000				
31/01/1986	16:46	NE US	5	10		50,000			17	
29/01/1986	11:56	Indonesia	5	33		100,000			2	
27/01/1986		Caucasus	5.3 (M_L)	71	VII	100,000				
26/01/1986		W. Med. - NW Africa	5.1			50,000		1	7	
11/01/1986	19:42	Peru	5.3	38.9	V	100000			100	20
25/12/1985	02:38	S. Italy	4.3	10	VII	50,000			14	
21/12/1985		N. Europe	5.1	10	VII	500,000				
07/11/1985	08:26	Asia Minor	5.1	33		10,000			14	
11/10/1985	03:39	Central America	4.5	5		2,000,000			10	
10/10/1985		Iran	5 (mb)			50,000				
04/10/1985	15:17	S. Africa	5.3	10					1	
28/09/1985	14:50	SE Europe	5	7.4					16	
12/08/1985		Asia Minor	4.9 (M_L)	20		10,000				13

Date	UTC	Location	M[1]	Depth (km)	MMI	Loss[2]	Cause	Dead	Injured	Buildings damaged[3]
07/08/1985	15:43	Iran	5.5	14.9		100,000			2	
04/08/1985		SW US	5.4	11	VI	10,000			6	
03/07/1985		Caucasus	4.3	33		50,000				
10/05/1985		SE Europe	5.1 (M$_L$)	10.5	VIII	100,000				
30/04/1985		Greece	3.5 (mb)	43		50,000			2	
29/03/1985	11:15	China - Sichuan (Zigong)	4.9	33		30,000,000	Anthropogenic		120	
19/03/1985	10:28	S. South America	5.5	33		10,000				
14/03/1985	23:03	S. Italy	4.3	14.6						
02/02/1985	20:52	Iran	5.3	36.8		1,000,000			92	500
26/11/1984	16:21	SW US	5.1	10				1		
14/11/1984	11:58	Indian Subcontinent	4.6	10		50,000		2	2	
25/10/1984	01:11	S. Italy	4.4	33		50,000			12	
18/10/1984	09:46	Asia Minor	5.3	60.2		2,000,000			25	1700
09/10/1984	04:30	Greece	5	27	VII	500,000			1	
05/10/1984		W. Med. - NW Africa	4.8	10		10,000				
15/09/1984	11:41	Greece	4.9	10					37	
07/09/1984	00:44	SE Europe	5.1	12.8	VIII	500,000			2	
27/08/1984	06:41	Indonesia	5.2	32.5		1,500,000			123	
24/08/1984		East Med.	5.1 (mb)		VI	1,000,000				
11/08/1984		S. Italy	3.8 (M$_L$)			50,000				1
24/06/1984	18:18	Central America	5.1	32.3						
20/06/1984		Canada	3.4	1		10,000			4	
13/05/1984	12:45	SE Europe	5.1	29.7	VIII	100,000		1	10	
11/05/1984	10:41	S. Italy	5.2	13.9	VIII	4,000,000			80	
29/04/1984	05:03	N. Italy (Perugia)	5.3	11.9				36	7500	
22/04/1984	17:39	N. Italy	4.3	15.1						
05/03/1984		Oceania	5 (mb)	9	VII	500,000				
03/03/1984	08:32	SE Europe	4.6	10				3		
13/02/1984		Japan	5.3 (mb)	37		50,000			2	
01/02/1984		Indian Subcontinent	5.8	33		5,000,000		1	35	
18/11/1983	01:15	Asia Minor	5	27.1					5	
09/11/1983	16:29	N. Italy (Parma)	5.1	36.9					100	
08/11/1983	00:49	N. Europe (Waremme, Liege)	5	10	VIII	112,500,00			26	

53

Date	UTC	Location	M[1]	Depth (km)	MMI	Loss[2]	Cause	Dead	Injured	Buildings damaged[3]
						0[2]				
21/10/1983	20:34	Asia Minor	5.1	13.9		2,000,000			4	
07/10/1983	10:18	NE US	5.1	12.5					1	
06/08/1983		Indian Subcontinent	4.7 (mb)	10		50,000				
20/07/1983	22:03	S. Italy	4.4	33					10	
03/06/1983		East Med.	5.3 (mb)			50,000				
18/05/1983		S. Italy (Phlegraean Fields Seq.)	4.1 (mb)			25,000,000			30	
21/04/1983		Asia Minor	3.7 (mb)	36		2,000,000				
12/04/1983		Peru	5.2 (mb)			100,000			10	10
06/04/1983		Asia Minor	5 (mb)	45		2,000,000				
31/03/1983	13:12	N. South America	5.5	22.2						
25/03/1983	11:57	Iran	5.2	33		1,000,000			61	
15/03/1983	17:27	Japan	5.3	43.2					2	
14/03/1983		Central Asia	5.2 (mb)	33	VII	50,000				
28/02/1983		Greece	5.1	26	VII	50,000				
25/02/1983	18:22	SE Europe (Skopje)	5.3 (M$_L$)	24	VI	14,000,000			12	
25/02/1983	18:22	SE Europe	4.7	24.4	VI	10,000				
19/02/1983		Greece	4.3 (mb)	26	VI	50,000				1
13/02/1983	16:53	Japan	5.3	46.7				2		
29/12/1982	23:53	Arabian peninsula	5.3	5		50,000			6	
16/12/1982	20:20	Central America	4.5	33		20,000			6	
17/11/1982		SE Europe	4.9			2,000,000		1	12	1100
15/11/1982	20:07	W. Med. - NW Africa	5	10		50,000			14	
25/10/1982	16:54	Iran	5.4	33		50,000				
29/09/1982	05:50	Central America	5.5	12		600,000		2		
15/08/1982		S. Italy	4.2 (mb)		VI	100,000				
28/06/1982		N. Europe	5.2 (mb)	10		50,000				
04/06/1982	10:44	N. Europe	4.6	10		200,000			10	
19/05/1982		Asia Minor	4.7 (mb)	62		5,000,000				
27/04/1982		Central America	5 (mb)	33		100,000				
27/04/1982		S. Africa	4.3 (M$_L$)			50,000	Anthropogenic		7	
19/04/1982		Asia Minor	4.5 (M$_L$)			2,000,000				

Date	UTC	Location	M[1]	Depth (km)	MMI	Loss[2]	Cause	Dead	Injured	Buildings damaged[3]
13/04/1982		S. Africa	5(M_L)	10		50,000	Anthropogenic	4	23	
23/03/1982	05:10	Peru	5.1	57		10,000				
21/03/1982		S. Italy	4.8 (mb)		VII	500,000				
24/02/1982		Indonesia	5.5	40		3,500,000			17	
10/02/1982	16:17	Indonesia	5.5	39.8					17	
20/01/1982	15:15	N. South America	5.2	69		50,000			6	
12/12/1981	20:26	Indian Subcontinent	4.6	33		50,000			12	45
02/12/1981		Caucasus	5.2 (mb)	33		50,000				
14/11/1981		SE Europe	5.4 (M_L)			500,000				
14/11/1981		Indian Subcontinent	5.2 (M_S)	10	VIII	10,000				
18/10/1981	04:31	N. South America	5.4	53.6					15	
13/08/1981	02:58	SE Europe	5.5	9	VIII	1,000,000			60	
22/06/1981	17:53	Peru	5.2	23.7					6	
13/06/1981	07:29	Central Asia	5.5	24					2	
07/06/1981	13:00	S. Italy	4.9	18.7	VII	50,000			10	20
07/05/1981		S. Africa	3.5 (M_L)			10,000	Anthropogenic	1	6	
18/04/1981	00:32	Peru	5.3	38		100,000		15	36	
07/03/1981	11:34	Greece	5.5	33					1	
14/02/1981	17:27	S. Italy	4.6	10	VII	50,000			12	3
01/02/1981		W. Med. - NW Africa	5.4	10		50,000				1
22/12/1980	12:51	Iran	5.5	41		100,000			139	
30/11/1980	07:41	S. Italy	5.1	10					1	
26/11/1980	17:35	N. South America	5	40	VI	100,000			36	2
12/11/1980	06:58	Peru	5.2	71		50,000		7	20	
08/11/1980	07:54	W. Med. - NW Africa	5.3	10					36	
18/10/1980		Caucasus	4.3 (M_S)	35		2,000,000				
23/08/1980	21:36	Indian Subcontinent	5.2	25		100,000			40	
23/08/1980	19:10	Japan	5.4	89					5	
17/08/1980		Indonesia	4.7	25		50,000				
27/07/1980	18:52	SE US	5.1	8		50,000		2		
22/07/1980	05:17	Iran	5.4	62						
15/07/1980		N. Europe	5.5 (mb)			10,000				
12/07/1980		Central Asia	4.5 (M_S)			50,000				

Date	UTC	Location	M[1]	Depth (km)	MMI	Loss[2]	Cause	Dead	Injured	Buildings damaged[3]
26/06/1980		Central Asia	4.5 (mb)	24	V	10,000				
03/06/1980		Peru	4.9 (mb)	20	VI	50,000				
02/06/1980		Greece	4.6 (mb)	8	VI	50,000				10
29/02/1980		Pyrenees	5.1 (mb)			1,000,000				
28/02/1980		Greece	4.6 (mb)	30	VIII	100,000				1
28/02/1980		S. Italy	5.4 (M$_L$)		VII	50,000				
20/02/1980	02:34	S. Italy	4.6	12		10,000			1	
05/01/1980		N. Italy	4.3 (M$_L$)		V	50,000				
06/11/1979	05:26	Greece (Igoumenitsa)	5.4	40	VII				3	
09/10/1979	07:49	Central America (Santa Rosa, Jutiapa)	5	33	VI				40	
09/07/1979	10:57	China Liyang (Jiangsu)	5.5	11	V			41	3000	
02/07/1979	16:30	Indian Subcontinent	4.5	106						
23/04/1979	13:01	East Med.	5.1	33					1	
03/09/1978	05:08	N. Europe (Albstadt)	5.3	8	VII	150,000,000[2]				
29/07/1978	14:37	Central America (Patzun)	4.9	10	VI			17		
04/07/1978	22:23	Greece	5.1	19					16	
19/06/1978	10:31	Greece	5.3	10					10	
16/06/1978	06:46	SE US (Snyder Sequence)	4.6	3	V		Anthropogenic			
03/06/1978	20:03	Japan	5.2	4					1	
11/03/1978	19:20	S. Italy (Calabria)	5	33	VII			2		
15/02/1978	03:17	Asia Minor (Erzincan)	4.8	33	VI				20	500
10/12/1977	05:46	Iran	5.1	47					15	
09/12/1977	15:53	Asia Minor	4.6	19					35	
26/05/1977	01:35	Iran (Azarbaijan)	5.4	37	VII				9	
28/04/1977		China (Taiji)	4.3 (M$_L$)		VII		Anthropogenic		12	
25/03/1977	02:39	Asia Minor (Lice-Palu)	5.2	21	VI					
21/02/1977	13:02	Asia Minor	4.6	33					15	
08/12/1976	08:38	S. Africa (Welcom)	5.2	33	V		Anthropogenic		36	
11/09/1976	16:31	N. Italy (Friuli sequence)	5.5	16	VI					
11/09/1976	16:35	N. Italy (Frilui sequence)	5.4	20	VI					
05/09/1976	22:07	Asia Minor	5.1	22					9	

Date	UTC	Location	M[1]	Depth (km)	MMI	Loss[2]	Cause	Dead	Injured	Buildings damaged[3]
19/08/1976	01:12	Asia Minor (Denizli)	5	3	VII				50	1800
09/07/1976	09:34	Asia Minor	4.2	33					4	
02/07/1976	08:50	Asia Minor	4.3	30					11	
04/06/1976	00:43	Indian Subcontinent	5.2	33					1	
29/04/1976	22:18	Caucasus	5.5	44						
02/04/1976	16:58	Caucasus	4.6	46					2	
25/03/1976	23:05	Central America	5	33					7	
25/03/1976	11:55	Caucasus	4.8	18					6	
19/03/1976	13:03	Central Asia (Shamagan)	5.5	33					50	
13/03/1976	16:30	Central America (Guatemala)	5.4	5					50	
31/12/1975	09:45	Greece Kato (Makrynou)	5.5	19	VI				10	200
30/12/1975	14:36	Asia Minor	4.6	6					14	
29/11/1975	09:19	N. South America	5	17					15	
14/11/1975	12:32	Asia Minor	4.7	41					2	
05/11/1975	17:04	Central America	5	12					8	
01/09/1975	23:15	Iran	4.9	16					3	
19/07/1975	06:10	Indian Subcontinent	5.3	40					55	
11/07/1975	07:18	W. Med. - NW Africa (Djebel Babor)	4.3	33					18	
05/04/1975	20:38	N. South America	5.5	52					5	
14/03/1975	13:56	Japan	4.9	57					9	
10/03/1975	21:00	SE Asia	5.2	53					8	
12/01/1975	04:39	Asia Minor	5	40					2	
28/06/1974	11:09	W. Med. - NW Africa	5	33					3	
20/06/1974	17:08	SE Europe	4.5	47					2	
18/04/1974	01:19	N. South America	5	24					2	
15/02/1974	08:34	SE US (Perryton 1974)	4.5	24	V		Anthropogenic			
01/02/1974	00:01	Asia Minor (Izmir)	5.2	29	VI				20	
24/11/1973	14:05	W. Med. - NW Africa	5.1	17						
23/11/1973	13:36	Atlantic (Azores)	5.1	5					3700	
11/11/1973	07:14	Iran (Qeshlagh)	5.5	11	VI					
04/11/1973	15:52	Greece (Lefkada, Preveza)	5.5	8						
09/03/1973	19:09	Oceania (Wollongong,	5.5	13		500,000[2]				

Date	UTC	Location	M[1]	Depth (km)	MMI	Loss[2]	Cause	Dead	Injured	Buildings damaged[3]
		Sydney)								
16/09/1972	03:53	SE Europe	5.1	15					1	2
16/07/1972	02:46	Asia Minor	4.9	40					10	
21/06/1972	15:06	N. Italy (Ancona swarm)	4.4	4		300,000,000[2]				
22/03/1972	00:51	Asia Minor	4.8	34					4	
04/02/1972	02:42	N. Italy(Ancona swarm)	4.8	25					2	
15/07/1971	01:33	N. Italy (Parma)	5.2	8						
16/06/1971	14:44	Indonesia (Java)	5.2	35					6	
06/02/1971	18:09	North Italy (Tuscania)	4.6	33		41,000,000[2]		24	150	40
16/01/1971	09:00	C. Africa	5	18						
12/09/1970	14:30	SW US	5.4	11					4	
07/09/1970	20:58	SE Europe	5.5	5					8	
03/09/1970	05:32	Asia Minor	5.3	23					5	
02/07/1970	02:24	Asia Minor	4.8	27						
23/04/1970	09:01	Asia Minor	5.3	18					43	
19/04/1970	13:47	Marmara	5.5	26					2	
07/04/1970	09:16	W. Med. - NW Africa	4.9	33					1	
23/03/1970	01:52	Indian Subcontinent (Broach)	5.4	3				26	200	
14/03/1970	01:51	Caucasus	5.3	23					300	
31/12/1969	13:18	SE Europe	5.1	33					10	
12/10/1969	13:34	Greece	5.1	14					1	
02/10/1969	04:56	SW US (Santa Rosa)	5.2	2	VIII	8,350,000		1		
11/08/1969	13:55	N. Italy (Perugia)	4.6	33					4	
30/04/1969	20:20	Asia Minor	5.1	9					15	
03/04/1969	22:12	Greece	5.5	33					65	
03/03/1969	08:53	SE Asia	5.1	99					1	
03/12/1968	20:57	SE Europe	4.7	7					35	
03/11/1968	04:49	SE Europe (Montenegro)	5.3	17		38,600,000[2]				
29/09/1968	17:18	Oceania	5.2	38					1	
24/09/1968	04:19	Asia Minor	5.1	14					40	
29/04/1968	17:01	Iran (Maku)	5.3	34		1,000,000		38	100	1000
15/01/1968	09:56	S. Italy (Belice sequence)	5.5	33	X			8	55	

Date	UTC	Location	M[1]	Depth (km)	MMI	Loss[2]	Cause	Dead	Injured	Buildings damaged[3]
04/01/1968	10:03	Central America (Managua)	4.6	5		2,000,000				
13/08/1967	22:07	N. Europe (Arette)	5.3	15				10	80	
09/08/1967		C. US (Denver series)	5	3	VII	1,000,000	Anthropogenic			
13/07/1967	02:10	W. Med. - NW Africa)Sig)	5	13				10	15	
11/04/1967	05:09	Indonesia (Makassar)	5.5	33						
24/01/1967	14:45	China - Sichuan	5.5							
04/09/1966	22:14	N. South America (Bogota, Colombia)	5.2	8				6		
12/07/1966	00:04	Asia Minor (Bagici)	4.6	64				12	20	
26/04/1966		Central Asia (Tashkent)	5.3			300 Mill.[2]		200	1000	78,000-95,000
20/04/1966	14:31	China (Hebei)	5.3							22
06/03/1966	00:12	China (Hebei)	5.2							
20/11/1965		C. US (Denver series)	4.3 (M_L)		VI		Anthropogenic			
29/09/1965		C. US (Denver series)	4.6 (M_L)		VI		Anthropogenic			
16/02/1965		C. US (Denver series)	4.6 (M_L)		VI		Anthropogenic			
10/02/1965	16:09	Iran (Bostanabad-e Bala)	5.1	52						
01/01/1965	21:38	W. Med. - NW Africa (M'sila)	5.5	10		2,000,000		4	38	2800
01/09/1964	22:20	China (Shanxi)	4.7							
18/02/1964	12:19	Atlantic Azores (Portuguese Isle) swarm	4.6	33						
08/01/1964	22:30	Indonesia (Pinrang, Sulawesi)	5.2	90				8	27	
02/09/1963	01:34	Indian Subcontinent (Bagdam, Kashmir)	5.3	25				80		
29/07/1963	06:10	Iran (Gahkom)	5.2	46				5		
21/02/1963	17:14	East Med. (Barce, Al Marj)	5.4	3		5,000,000[2]		300	375	
31/01/1963	02:27	Iran (Khendodzhan)	4.5	3				4		
05/10/1962	20:02	Iran (Torbat Heydariyeh)	5	8				6		
04/09/1962	22:59	Asia Minor (Igdir)	5.5					1		
25/04/1962		N. Europe (Correncon)	5.3							
10/04/1962		C. US (Denver series)	3 (M_L)				I			
04/12/1961		C. US (Denver series)	4 (M_L)				I			
19/03/1957	16:37	SE US (Gladewater Sequence)	4.7		V		I			

Date	UTC	Location	M[1]	Depth (km)	MMI	Loss[2]	Cause	Dead	Injured	Buildings damaged[3]
01/03/1954		Oceania (Adelaide)	5.5							
09/04/1952	16:29	C. US (El Reno)	5.5		VII		Anthropogenic		2	
12/03/1952	10:30	SE US (Dalhart)	5.2		VI					
11/06/1938	10:57	N. Europe (Belgium)	5 (M_S)		VII					
20/06/1936	23:24	SE US (Panhandle)	5		VI		Anthropogenic			
09/04/1932	10:17	SE US (Wortham-Mexia)	4		VI		Anthropogenic			
12/08/1929	11:24	NE US (Attica, NY)	5.2		VIII		Anthropogenic			
30/07/1925	06:17	SE US (Panhandle)	5.4		VI		Anthropogenic			
06/03/1923	10:05	SE US (El Paso)	4.7		VI		Anthropogenic	1		
08/05/1914	18:10	S. Italy (Catania, Etna)	4.9					120	500	223

Notes:

1. Magnitudes are given in M_w unless noted otherwise

2. Loss estimates in USD of the time, unless noted, in which case it is USD at 2014.

3. This column should be read taking in mind the region the earthquake was located in. In more developed countries, what is reported as damaged buildings is more often the damage claims; in developing countries what is referred to as damaged buildings will more often be more significantly damaged than the damage reported in developed countries (*i.e.* cracks would not be referred to as damage) ; in countries with censorship (*i.e.* for example in the USSR, as with the Tashkent 1966 earthquake), these numbers will not be accurate estimates of the damaged buildings but most probably a lower bound.

APPENDIX II: Case histories of induced earthquakes

Detailed information on the selected case histories can be found herein.

A2.1 December 2006 M3.2 Basel Earthquake, Switzerland

This earthquake occurred on 8th December 2006, at 16.48 UTC (17.48 local time), right under the city of Basel, northern Switzerland, six days after the start of the injection of a large volume of water at high pressures for the creation of an enhanced geothermal system (EGS) for the Deep Heat Mining Project in said city. It was the largest of a series of events that were induced in the area, and was preceded by a M_L 2.6 event that occurred in the early morning of the same day, and which led to the premature halt of the injection, and by a M_L 2.7 event in the afternoon. The creaking of woodwork and rattling of doors and windows caused by the main shock alarmed the population, though consequent damage was limited mostly to hairline cracks. The geothermal project was finally cancelled in December 2009.

A2.1.1 Tectonic and seismic setting

A2.1.1.1 Tectonic setting

Basel is located in the triple frontier comprising Switzerland, France and Germany, in the southern end of the Upper Rhine Graben, which is part of the European Cenozoic rift system (Häring *et al.*, 2008). It is limited to the east by the tabular Jura, which is related to the extensional movements of the graben (Laubscher, 2001), and to the south by the folded Jura, associated to the Alpine compression (Ferry *et al.*, 2005). The overall seismotectonic regime of Switzerland is related to the collision of the African and the European plates (Wiemer *et al.*, 2009), whose average total convergence rate is around 0.9-0.94 cm/year (Giardini *et al.*, 2004).

The stress field in the southern end of the Upper Rhine Graben is characterised by an overall strike-slip regime (Häring *et al.*, 2008). The average direction of the regional maximum compressive horizontal stress is around N144 (Deichmann & Ernst, 2009, reporting results of Kastrup, 2004) to N162 (Plenefisch & Bonjer, 1997), *i.e.*, it corresponds to a NNW-SSE orientation.

Given that Switzerland lies in a transition zone between areas of high and low seismicity in Europe, its tectonic structure is quite complex (Wiemer *et al.*, 2009). Several authors report a predominance of strike-slip and normal mechanisms (*e.g.*, Deichmann & Ernst, 2009) within the seismic catalogues, but the faults system in the area around Basel is far more heterogeneous and involves a large variety of mechanisms and orientations, as can be observed in Figure A2.1.1 and Figure A2.1.2. The distinction between active and inactive faults and the determination of the deformation rates of the former are some of the most difficult issues associated to defining the tectonics of this area.
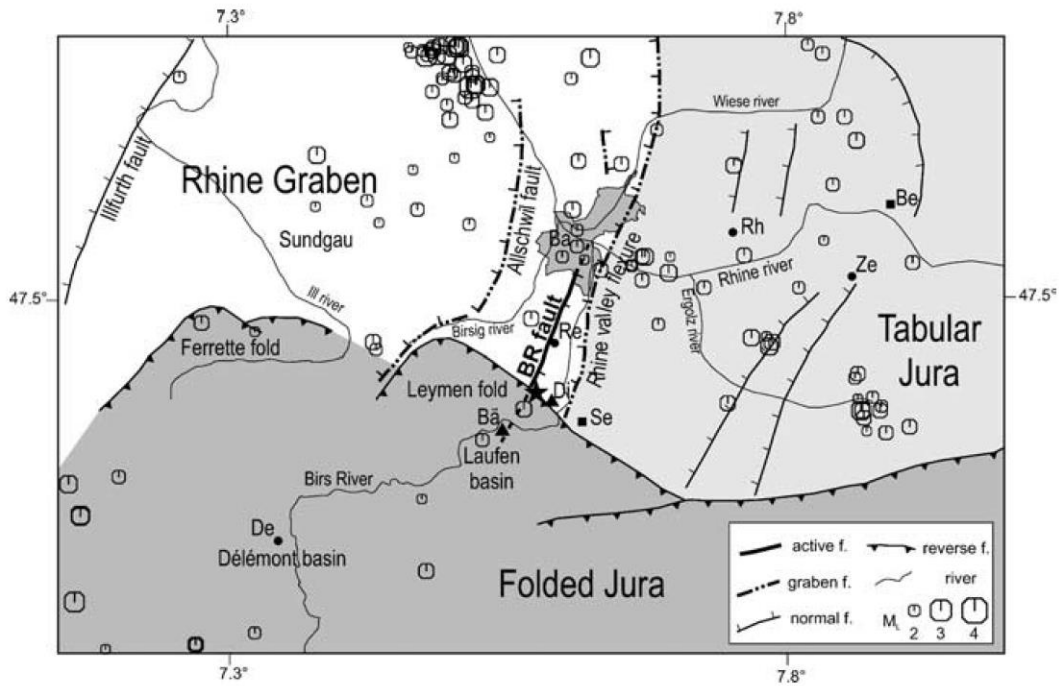
Figure A2.1.1. Seismotectonic setting of the southern end of the Upper Rhine Graben. BR: Basel-Reinach fault. Ba: Basel. Fault mechanisms shown as indicated in embedded legend. (Ferry *et al.*, 2005).
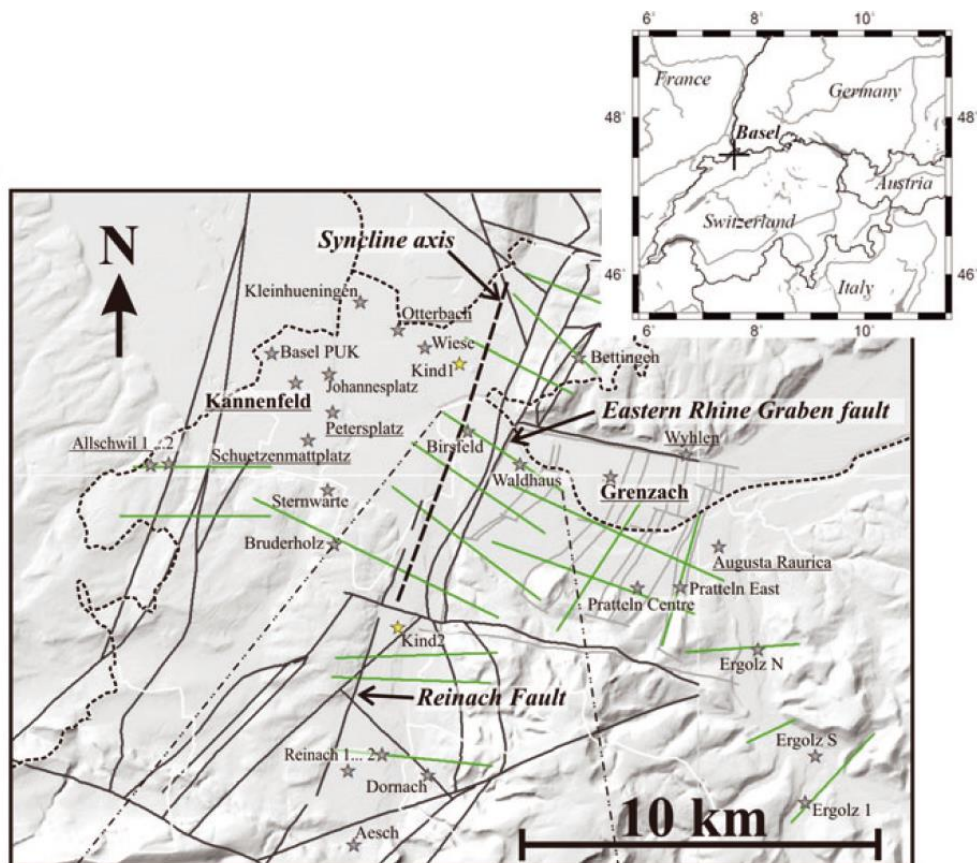
Figure A2.1.2. Seismotectonic setting of the southern Upper Rhine Graben. Dashed lines: country borders. White lines: Basel canton borders. Dark grey lines: main graben structure. Light grey lines: graben and horst structure. (Ignore green lines) (Havenith *et al.*, 2007).

A2.1.1.2 Regional and local seismicity

The area of the Upper Rhine Graben presents one of the highest seismic activity rates in Switzerland (Becker *et al.*, 2002). It sees persistent small-to-moderate seismicity and infrequent destructive events (Häring *et al.*, 2008; Wiemer *et al.*, 2009). According to the website of the Swiss Seismological Service (SED), approximately ten earthquakes with M_L between 3 and 4 occur per year in Switzerland, while an earthquake with M_L of at least 5 usually occurs every 10-20 years, and earthquakes with M_L larger than or equal to 6 occur every 100-150 years. The M_L 6.5-6.9 earthquake which severely damaged the city of Basel in 1356 is the largest known to have occurred in central-northern Europe (Häring *et al.*, 2008; Majer *et al.*, 2007). The exact return period of an event like this is not clear. Giardini *et al.* (2004) and the Swiss Seismological Service report it to be around 1,000-1,500 years, while Becker *et al.* (2002) believe it is more likely to be around 1,500-3,000 years instead.

The map in Figure A2.1.3 shows the epicentres of relevant earthquakes observed around the Basel area, while the plots in Figure A20.1.4 show the strongest earthquake magnitude and the number of earthquakes with M_L larger than 2.5 observed per year between 1975 and 2012. It is noted that the years 2006 and 2007 do not present neither the largest magnitudes nor the largest number of events with M_L larger than 2.5 of the last decades.
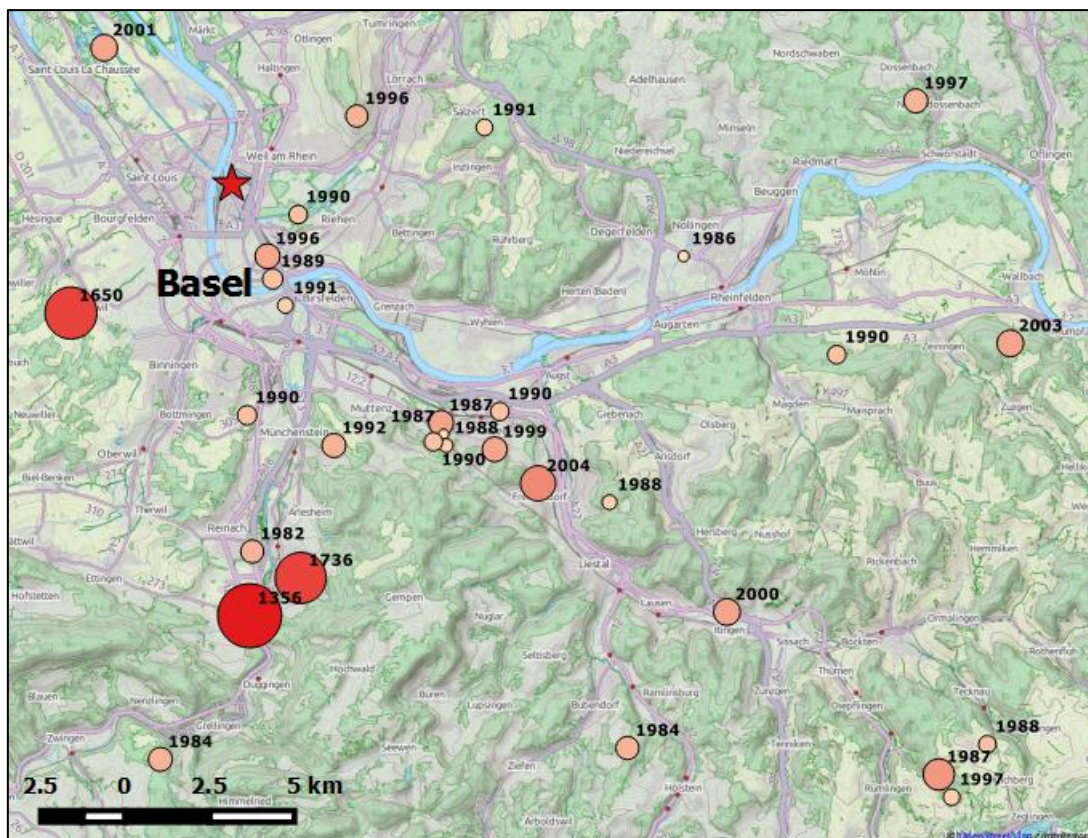
Figure A2.1.3. Epicentres of relevant earthquakes around the area of the city of Basel. The colour and diameter of the symbols is proportional to the (estimated) moment magnitude of the events. The red star corresponds to the 2006 main shock.
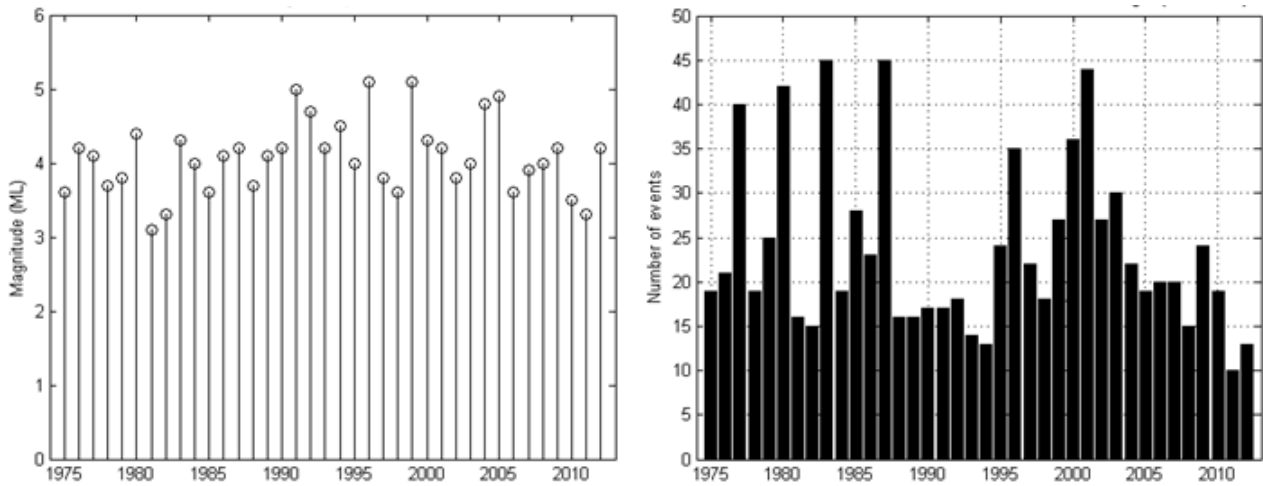
Figure A2.1.4. Magnitudes of the strongest earthquakes from 1975 to 2012 (left), and number of earthquakes with a magnitude M_L of 2.5 or greater from 1975 to 2012 (right) (Swiss Seismological Service, 2015).

A2.1.1.3 Seismic hazard

At the time of writing, Switzerland is finishing the preparation of an update to its seismic hazard maps (Wiemer *et al.*, 2014). The current hazard map was elaborated in 2004, and was the first to be the product of a fully probabilistic model to replace the previous intensity-based maps of 1978 (Wiemer *et al.*, 2009; Giardini *et al.*, 2004). The 2004 seismic hazard model provides expected pseudo-spectral accelerations for oscillator periods between 0.1 and 2.0 seconds, with a 5% damping value, for different return periods. The map in Figure A2.1.5 shows the pseudo-spectral accelerations corresponding to a 10% probability of exceedance in 50 years for an oscillator period of 0.2 seconds. As can be observed, values range between 0.05 g and 0.15 g, and, for Basel, it is around 0.12 g. Figure A2.1.6 shows the 5% damped uniform hazard spectra for Basel for different return periods.

The Eurocode-based Swiss Structural Standard SIA 261:2003 does not make direct use of the hazard maps mentioned above but, instead, divides the whole country into four seismic zones (Z1, Z2, Z3a and Z3b) and assigns a design peak ground acceleration value to each of them. For the case of Basel, this is equal to 1.3 m/s² (0.13 g, zone Z3a). This design peak ground acceleration value corresponds to a return period of 475 years, on rock, and is later used to define the design pseudo-acceleration spectrum, which also takes into consideration the soil type of the construction site.

Figure A2.1.7 shows the 5% damped uniform hazard spectrum on rock from the SHARE (Seismic Hazard Harmonization in Europe) project (Giardini *et al.*, 2013) for a point with coordinates 47.600º N and 7.582º E, which correspond approximately to the city of Basel. As can be observed, the expected pseudo-spectral acceleration for a 0.2 seconds oscillator on rock with a 10% probability of exceedance in 50 years is 0.52 g, which is significantly higher that the value provided by the Swiss seismic hazard model of 2004.
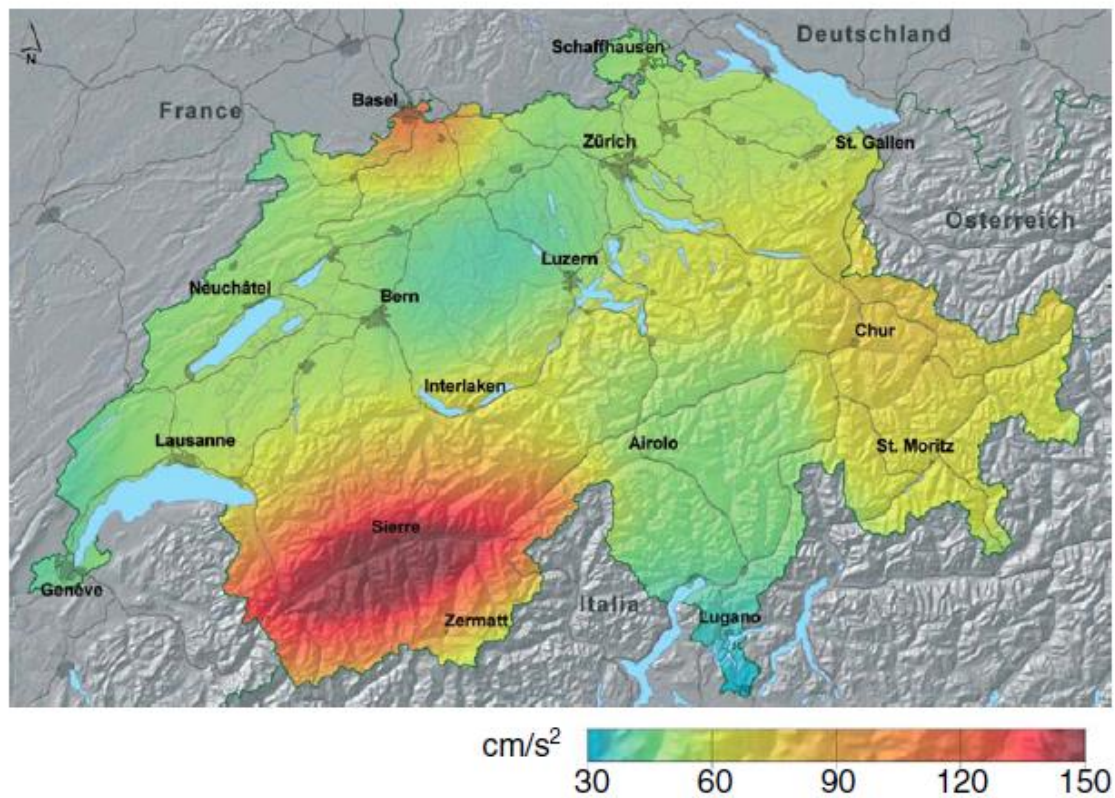
Figure A2.1.5. Seismic hazard map of Switzerland. Values correspond to 5% damped pseudo-spectral accelerations in rock for an oscillator period of 0.2 seconds with a 10% probability of exceedance in 50 years (Wiemer *et al.*, 2009).
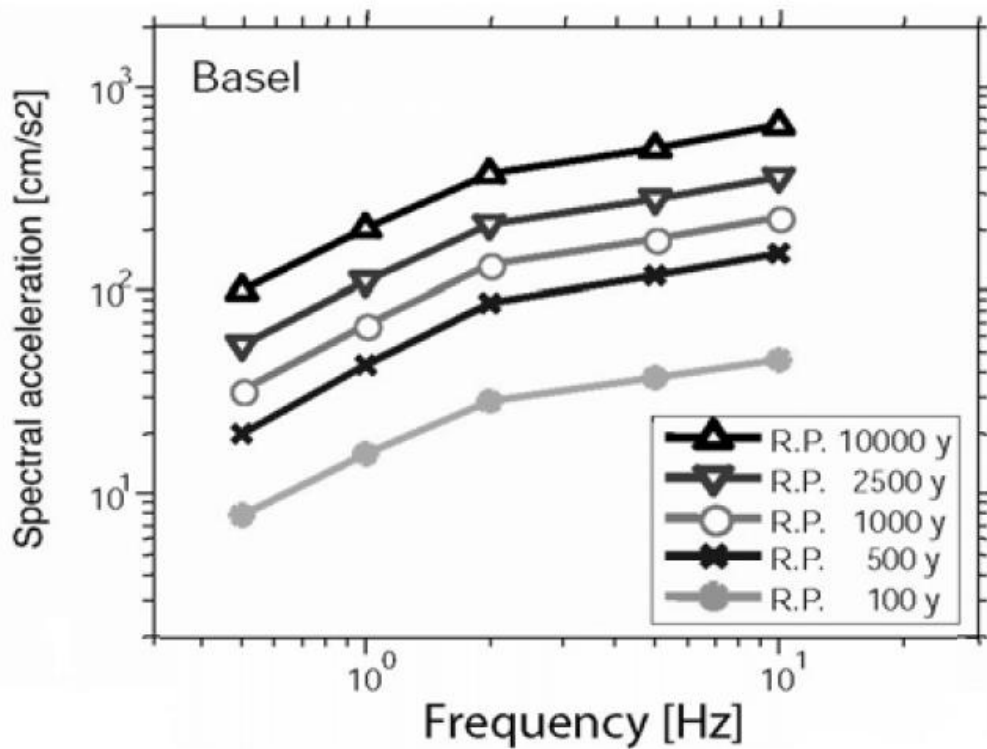
Figure A2.1.6. 5% damped uniform hazard spectra for Basel for different return periods, from Giardini *et al.* (2004).
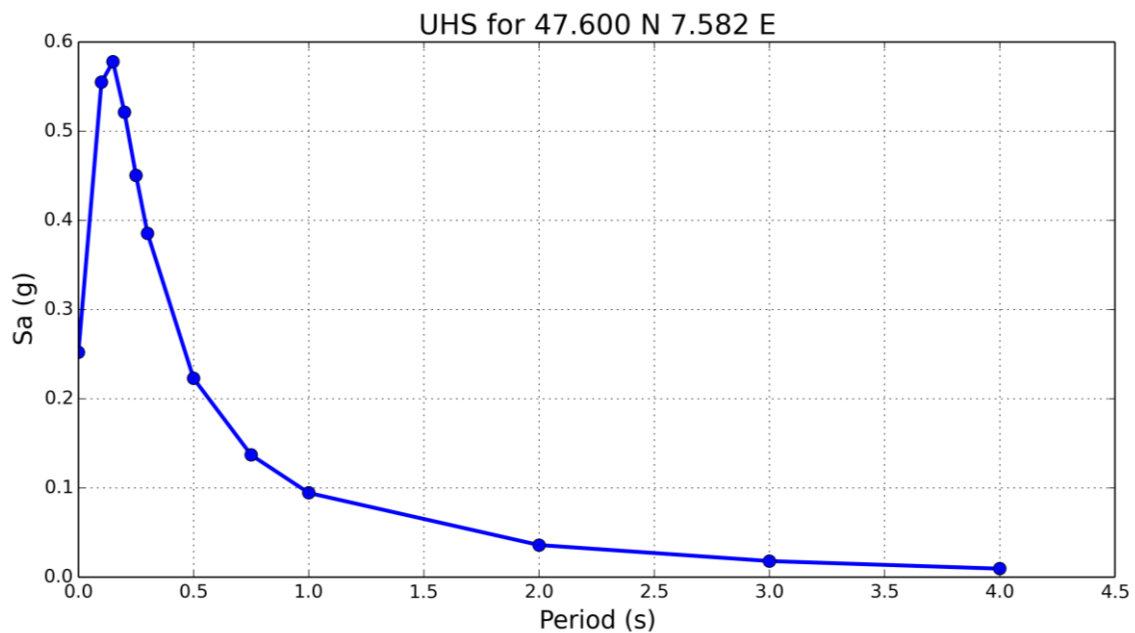
Figure A2.1.7. Uniform Hazard Spectrum for point 47.600º N 7.582º E (closest available to the city of Basel) according to SHARE. Values correspond to PGA and spectral acceleration in rock with a 10% probability of exceedance in 50 years (mean).

Results from the Global Seismic Hazard Assessment Program (GSHAP) yield an expected PGA on rock with a 10% probability of exceedance in 50 years of about 0.15 g (1.47 m/s^2) for the region around the city of Basel (Giardini *et al.*, 1999; Giardini *et al.*, 2003).

The Worldwide Seismic Design Tool of the United States Geological Survey (USGS) make use of the results from GSHAP to estimate the spectral accelerations at 0.2 and 1.0 seconds with a 2% probability of exceedance in 50 years, which, for the case of Basel, are 0.75 g and 0.30 g, respectively. It should be noted that these values result from significant approximations and are therefore classified within the lowest reliability category of the USGS database.

A2.1.2 Earthquake source characteristics

A2.1.2.1 Location, depth and time

The main shock occurred on 8th December 2006, at 16.48 UTC (17.48 local time).

Several organizations and agencies report their own estimations of the epicentral coordinates and hypocentral depth. The information reported in the websites of the Swiss Seismological Service (SED), the French Laboratoire de Détection et de Géophysique Bruyères-le-Châtel (CEA), the National Earthquake Information Center (NEIC) of the United States Geological Service (USGS), the European-Mediterranean Seismological Centre (EMSC) and the International Seismological Centre (ISC) is summarized in Table A2.1.1. Cells marked as (*f) correspond to parameters that were held fixed while inversion was carried out to retrieve those that remain. Epicentral coordinates reported by SED,

NEIC, CEA and Deichmann & Ernst (2009) are relatively consistent with each other, while those reported by the EMSC and the ISC seem to be the most inaccurate.

Table A2.1.1. Epicentral coordinates and hypocentral depths from different sources.

	Agency / Publication	Latitude	Longitude	Depth (km)
ZUR	Swiss Seismological Sevice (SED)	47.5820 ° N	7.6000 ° E	5.00
NEIC [1]	National Earthquake Information Center, USGS	47.5800 ° N	7.6000 f ° E	5.00 (*f)
EMSC	European-Mediterranean Seismological Centre	47.6100 ° N	7.6800 ° E	6.00
ISC	International Seismological Centre (inversion)	47.5821 ° N	7.5302 ° E	0.00 (*f)
DASE/CEA	Laboratoire de Détection et de Géophysique Bruyères-le-Châtel, France	47.5800 ° N	7.6000 ° E	7.00 (*f)
	Deichmann & Ernst (2009) / Deichmann & Giardini (2009)	47.5840 ° N	7.5930 ° E	4.70

(*f) fixed parameter used for inversion

(1) The USGS does not report this earthquake in its website due to its small magnitude. Values reported herein are those provided by the ISC citing the USGS as the source.

The map in Figure A2.1.8 shows the different estimations of the epicentral coordinates enumerated above, together with the epicentral locations of the 28 strongest events of the series, as reported by Deichmann & Ernst (2009) and Deichmann & Giardini (2009). According to these authors, the hypocentres of these events are located at depths between 4 and 5 km, always inside the stimulated rock volume. These depths are similar to those reported by Häring *et al.* (2008), and shown in Figure A2.1.9.
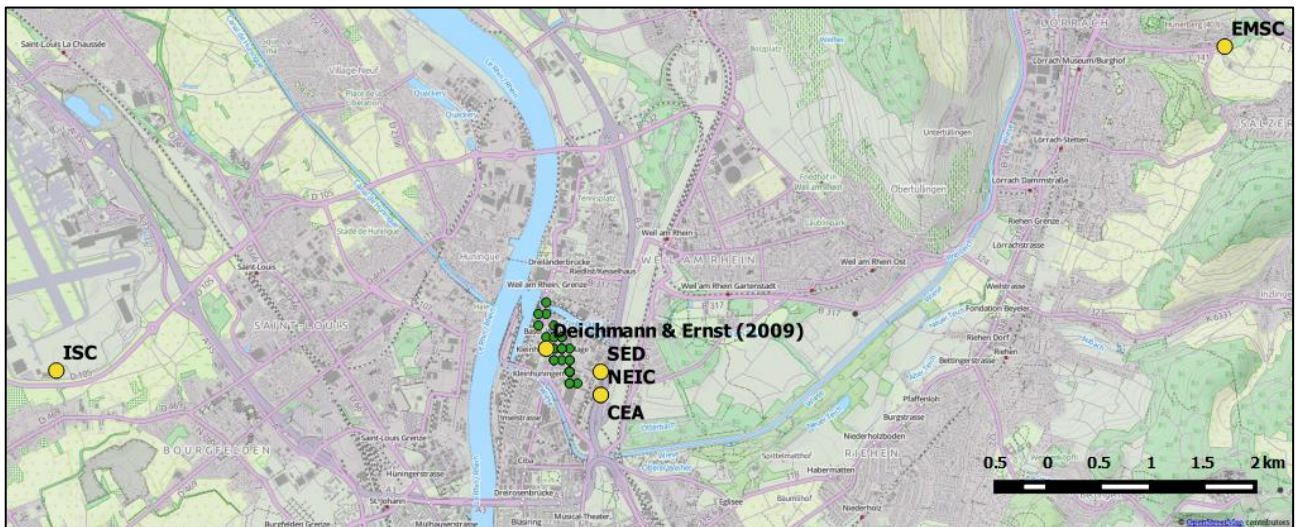
Figure A2.1.8. Estimation of epicentral coordinates (yellow circles).Green circles correspond to the epicentres of the 28 strongest events of the series, as reported by Deichmann & Ernst (2009) and Deichmann & Giardini (2009).
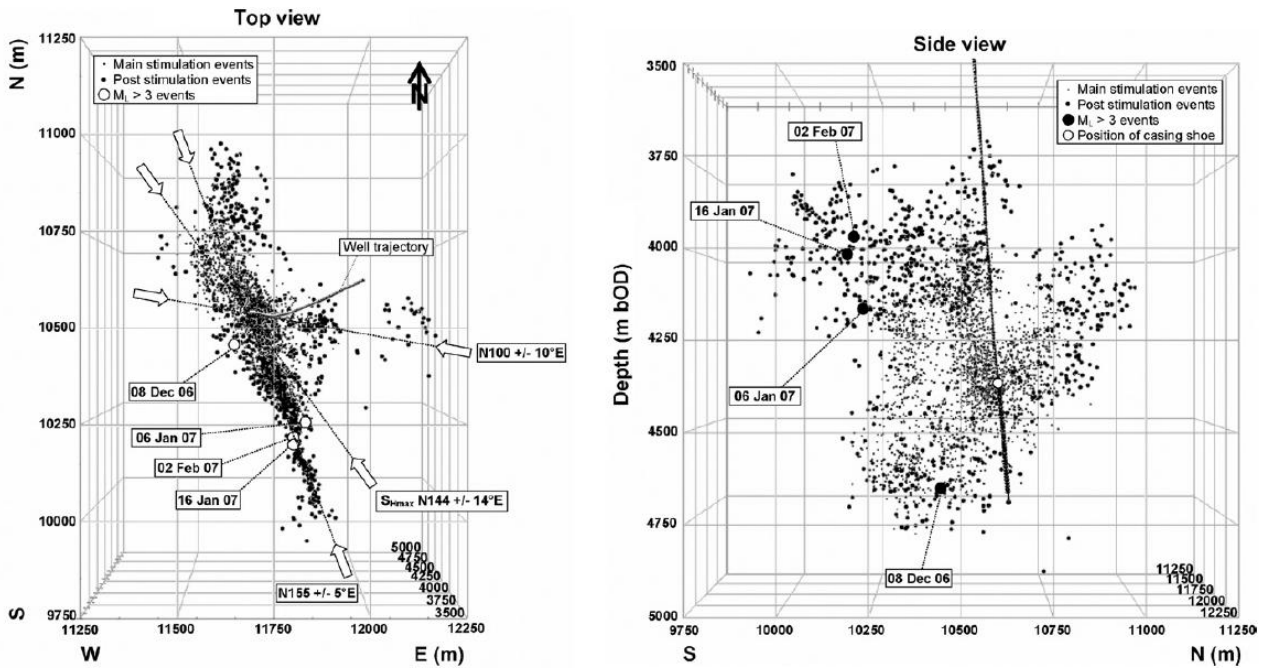
Figure A2.1.9. Locations of the seismic events that occurred between 2nd December 2006 and the end of November 2007. Depths are given in meters below Ordnance Datum (bOD), which is at 250 m depth. (Häring et al., 2008).

A2.1.2.2 Magnitude

Estimations of magnitude made by the main agencies and reported by two significant studies are reported in Table A2.1.2.

Table A2.1.2. Estimations of moment magnitude (**M**) and local magnitude (M_L).

	Agency	M	ML
ZUR	Swiss Seismological Sevice (SED)	3.17	3.4
EMSC	European-Mediterranean Seismological Centre	-	3.8
DASE/CEA	Laboratoire de Détection et de Géophysique Bruyères-le-Châtel, France	-	3.87
Deichmann & Ernst (2009) / Deichmann & Giardini (2009)		-	3.4
Bethmann et al. (2011)		2.95	-

A2.1.2.3 Style-of-faulting

Häring et al. (2008), Deichmann & Ernst (2009) and Deichmann & Giardini (2009) report the faulting mechanism of the main shock as being mostly right-lateral strike-slip, with a small normal component, as shown in Figure A2.1.10. Their fault plane solutions are summarized in Table A2.1.3. Deichmann & Giardini (2009) conclude that the main shock occurred on the WNW–ESE striking fault plane, which they say is optimally oriented with respect to the tectonic principal stress axes of the area.

68

Table A2.1.3. Fault plane solutions from different sources. Fault planes marked in gray are the preferred solution in each case.

Fault Plane 1			Fault Plane 2			Source
Strike	Dip	Rake	Strike	Dip	Rake	
12	75	-13	105	77	-165	Deichmann & Ernst (2009) / Deichmann & Giardini (2009)
12	73	-13	106	78	-163	Häring *et al*. (2008)
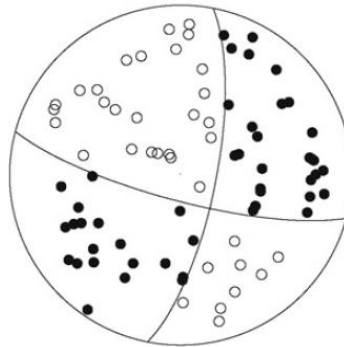
Figure A2.1.10. Fault plane solution for the main shock, from Häring *et al.* (2008).

Most of the fault mechanisms of the most significant events in the series analyzed by Häring *et al.* (2008) and Deichmann & Ernst (2009) are strike-slip, and only a few have strong normal components. According to Häring *et al.* (2008), these observations provide evidence that the place of the injection is located in a strike-slip dominated regime. It should be noted, however, that the strike of the fault plane solutions of the various events in the series reveal a complex spatial pattern that seems to be better explained by small-scale heterogeneities of the fractured rock mass and the stress field than by the activation of a single fault (Kraft & Deichmann, 2014; Deichmann *et al.*, 2014). Nevertheless, according to Deichmann & Giardini (2009), these heterogeneities would most likely correspond to pre-existing faults and not to cracking of the rock mass occurring during the water injection (hydrofracking).

A2.1.2.4 Stress drop

Goertz-Allmann *et al.* (2011) calculated the stress drop of about 1,000 earthquakes of the series. It is possible to see in Figure A2.1.11 that the estimated stress drop for the **M**2.95 (M_L 3.4) main shock is approximately 1.3 MPa, though the uncertainty is large and indicates that the true value probably lies between somewhere between 0.2 and 3.6 MPa. For the whole series, the median stress drop is 2.3 MPa. The authors note that the stress drops of individual events have been smoothed using a median filter over the closest ten events. Edwards *et al.* (2015) mention a median value closer to the upper bound of Goertz-Allmann *et al.* (2011), around 3.5 MPa, acknowledging it might vary between 0.76 and 10.4 MPa, accounting for a +/- 5% variation in the corner frequency.
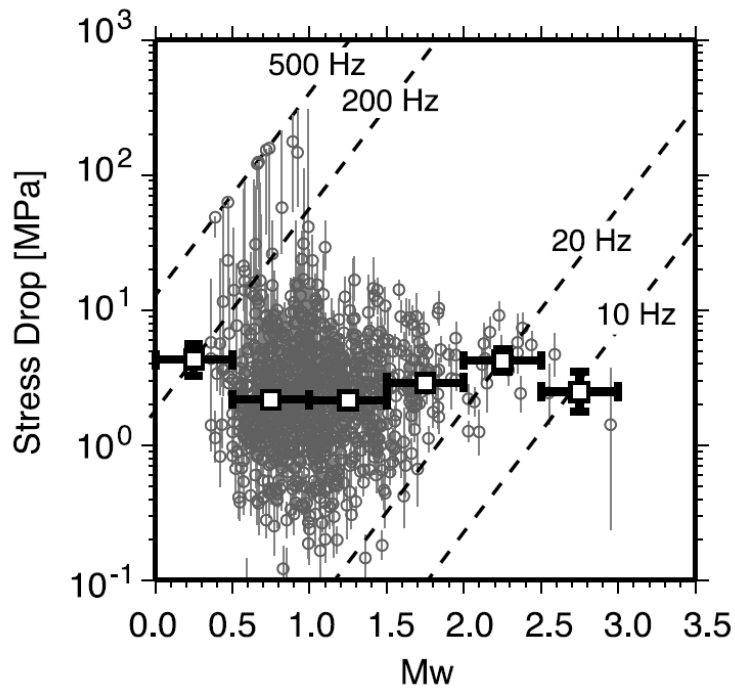
Figure A2.1.11. Stress drop versus moment magnitude for 1,000 events of the series. Thin vertical bars indicate the estimated uncertainty of the stress drop calculated for each event, due to the uncertainty in the corner frequencies. From Goertz-Allmann *et al.* (2011).

In contrast, Häring *et al.* (2008) state a stress drop of approximately 300 bar (30 MPa) for the main shock is not unlikely, given that the estimated source radius and rupture area are significantly smaller than the expected for a natural event of the same magnitude, for which typical stress drops range between 1 and 100 bar (0.1-10 MPa).

A2.1.2.5 Foreshocks and aftershocks

The **M**3.2 (M_L 3.4) event was the strongest of a large series of events directly linked to the injection of a large volume of water at high pressures for the creation of an enhanced geothermal system (EGS) in the area. According to Häring *et al.* (2008), approximately 11,200 events were detected during the phase of active stimulation, from 2nd December to 8th December 2006. In the early morning of this day, a M_L 2.6 event occurred and the injection was halted. Over 12 hours later, a M_L 2.7 event took place, and was followed one hour later by the M_L 3.4 main shock, after which the water was allowed to flow back from the well (Deichmann & Giardini, 2009). About 3,700 additional events occurred afterwards, up to the end of November 2007, three of which had magnitudes M_L larger than 3.0 (Häring *et al.*, 2008). An additional M_L 0.6 was detected in 2010, five events with M_L between 0.9 and 1.2 were detected in 2012, and two events with M_L 1.8 and 1.0 were recorded in 2013 (Deichmann *et al.*, 2014). The plot in Figure A2.1.12 shows the number of events of each magnitude recorded by the Swiss Seismological Service between 3rd December 2006 and 30th November 2007.
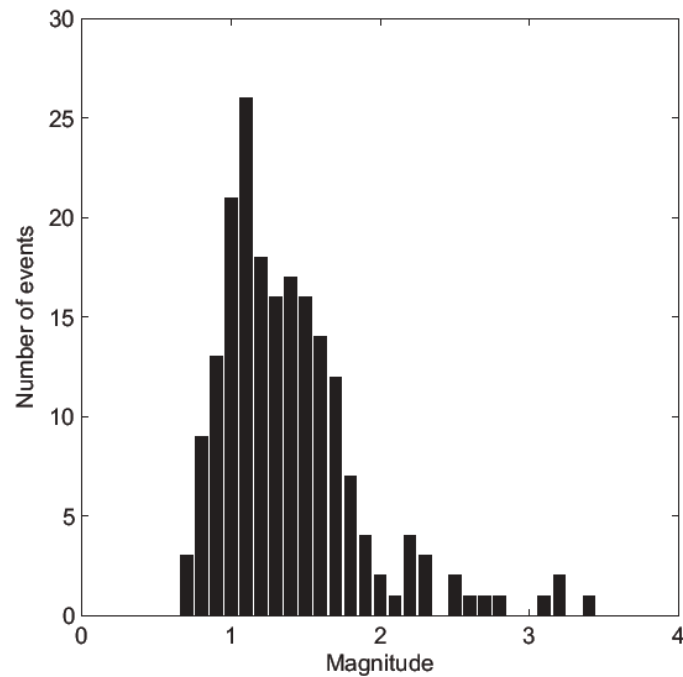
Figure A2.1.12. Number of events of each magnitude (M_L) recorded by the Swiss Seismological Service between 3rd December 2006 and 30th November 2007. From Deichmann & Giardini (2009).

A2.1.2.6 Nature of earthquake

This seismic series was induced by the injection of a large volume of water at high pressures for the creation of an enhanced geothermal system (EGS) for the Deep Heat Mining Project in Basel. An EGS consists in drilling the underground at great depths until reaching hot dry rock or magma, and injecting pressurized water into it with the aim of generating steam that can drive turbines or even be used for heating. The Basel 1 well was drilled between May and October 2006 up to a depth of 5 km, and approximately 11,500 m^3 of water were injected at high pressures between 2nd December and 8th December 2006. The injection was stopped after the occurrence of a M_L 2.6 event in the early morning of 8th December 2006, and the well was opened so as to let water flow back after a M_L 2.7 and M_L 3.4 event in the afternoon/evening, following a pre-approved seismic response plan (Häring et al., 2008). The increased seismic activity continued well after bleeding off the well, with around 15,000 events having been detected over the whole process (refer to the *Foreshocks and aftershocks* section above).

Deichmann & Giardini (2009) note, however, that these induced earthquakes do not seem to correspond to a case of hydrofracking (fracturing of the rock due to the water injection), but were caused instead by the ambient tectonic stress and shear dislocations on pre-existing faults, only triggered by the increase in pore pressure. As supporting evidence, these authors point out that, according to Häring et al. (2008), the water pressure within the rock mass did not reach the minimum stress threshold needed for hydrofracking to occur, and most of the seismic activity preceded the time at which the pressure in the well reached its maximum, and persisted for a significant duration afterwards. Nevertheless, as Catalli et al. (2013) point out, the temporary evolution of the seismic activity followed the injection rate and pressure variations in the well.

71

A2.1.3 Geology and ground conditions in the affected area

A2.1.3.1 Regional geology and topography

The city of Basel is located within a deep sedimentary basin, the Upper Rhine Graben. It is limited by the Black Forest massif to the north-east, the Vosges massif to the north-west, and the Jura mountains to the south-west (Figure A2.1.13). It is close to the Eastern Rhine Graben Fault (Figure A2.1.2), which presents a throw of about 1400 m. According to Fäh *et al.* (1997), on the (west) down-thrown side, the Mesozoic strata (Triassic to Jurassic) are covered by 500 to 1,000 m of Tertiary sediments, of which there are very few outcrops, and above which there are 5 to 50 m thick unconsolidated deposits of (Quaternary) Pleistocene and Holocene gravels. There are no Tertiary sediments to the east, where the Mesozoic sediments of the Tabular Jura (Figure A2.1.1) are covered directly by 5 to 50 m of Pleistocene and Holocene gravels and, in some parts, with an additional layer of marls. Figure A2.1.14 shows a schematic NW-SE section cutting through the Eastern Rhine Graben Fault.

Figure A2.1.13. Geographical features around the area of Basel. Image from Wikipedia
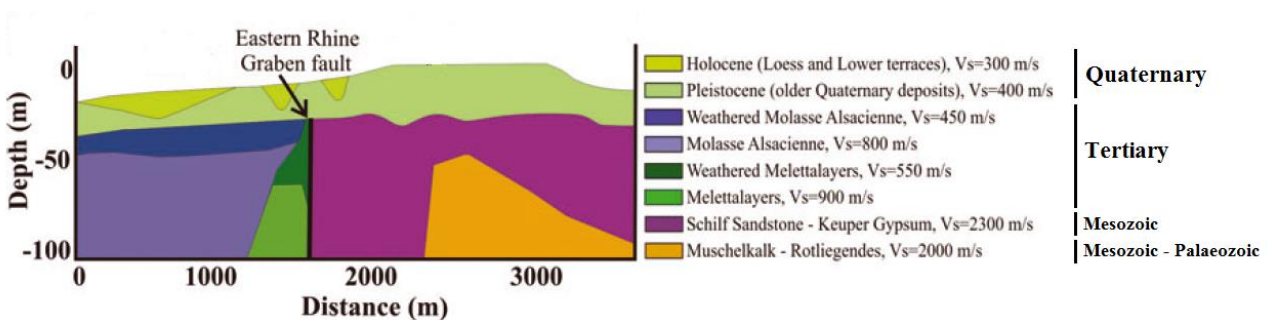
Figure A2.1.14. Geological section across the Eastern Rhine Graben Fault. (Havenith *et al.*, 2007)

The drilling of the Basel 1 well passed through over 2.4 km of Quaternary, Tertiary, Mesozoic and Permian sediments, approximately 100 m of Permian siltstone and weathered granite, and finally entered the crystalline basement at a depth of over 2.5 km (Häring *et al.*, 2008).

A2.1.3.2 Site conditions in the affected area

The map in Figure A2.1.15 shows the surficial geology of the Canton of Basel City (Basel-Stadt) and nearby areas, according to the Swiss Seismological Service. As can be observed, a large part of the city consists of gravel terraces, but there is also a significant surface covered by loess and clay.
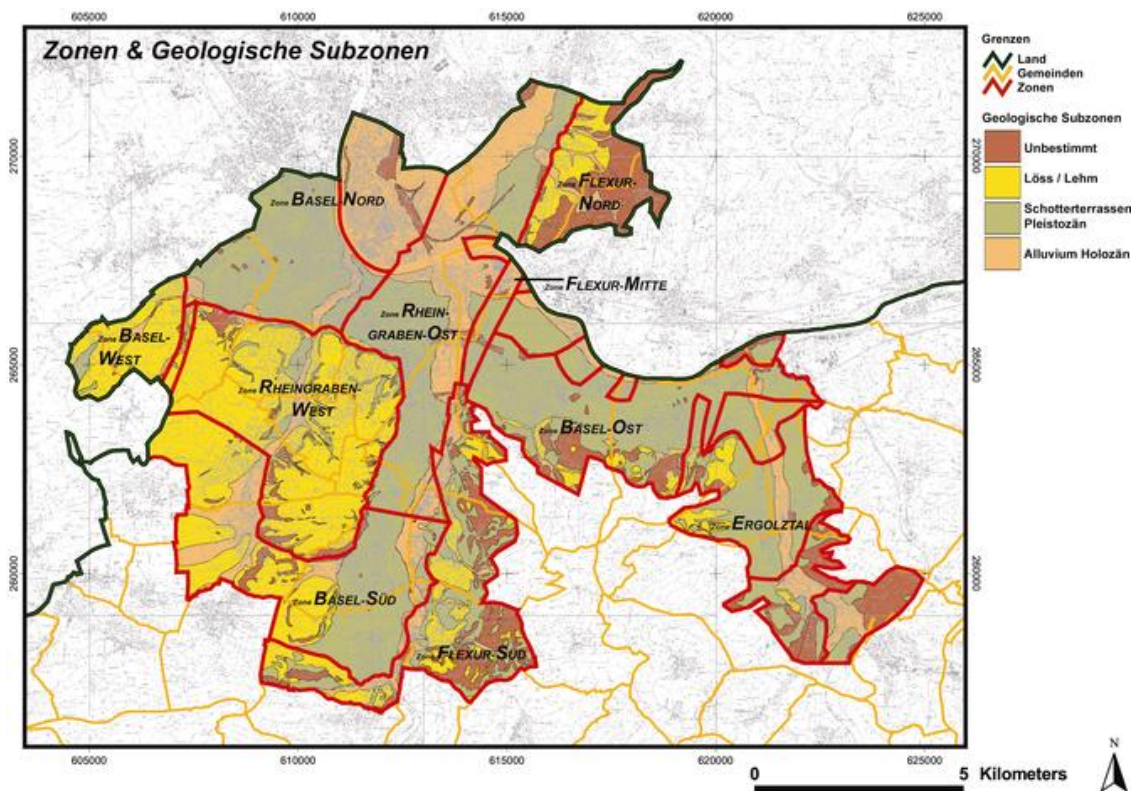
Figure A2.1.15. Surficial geology of the Canton of Basel City and nearby areas. Dark brown: rock. Yellow: loess / clay. Green: Pleistocene gravel terraces. Light brown: Holocene alluvium. Swiss Seismological Service (2015).

The online Geoportal of Basel (http://www.stadtplan.bs.ch/geoviewer/) contains an interactive version of the aforementioned map and all the associated information needed to define the design pseudo-acceleration and displacement spectra, which is summarized by Wenk & Fäh (2012). Figure A2.1.16 shows the 5%-damped design elastic pseudo-acceleration response spectra for the different microzones of the Basel area. The spectrum corresponding to the area where the Basel 1 well was located is indicated. As can be observed, the design accelerations increase significantly when taking into consideration the site conditions.

Figure A2.1.17 shows a qualitative microzonation map of the Canton of Basel City (Basel-Stadt) presented by Fäh *et al.* (2001). The colour scale represents the degree of

susceptibility of each area to site amplification effects, with red indicating an increased susceptibility and blue showing a reduced susceptibility with respect to a regional value.

According to Noack & Fäh (2015), liquefaction hazard is of minor importance for the Basel area, given that saturated sands can be found only at very few places.
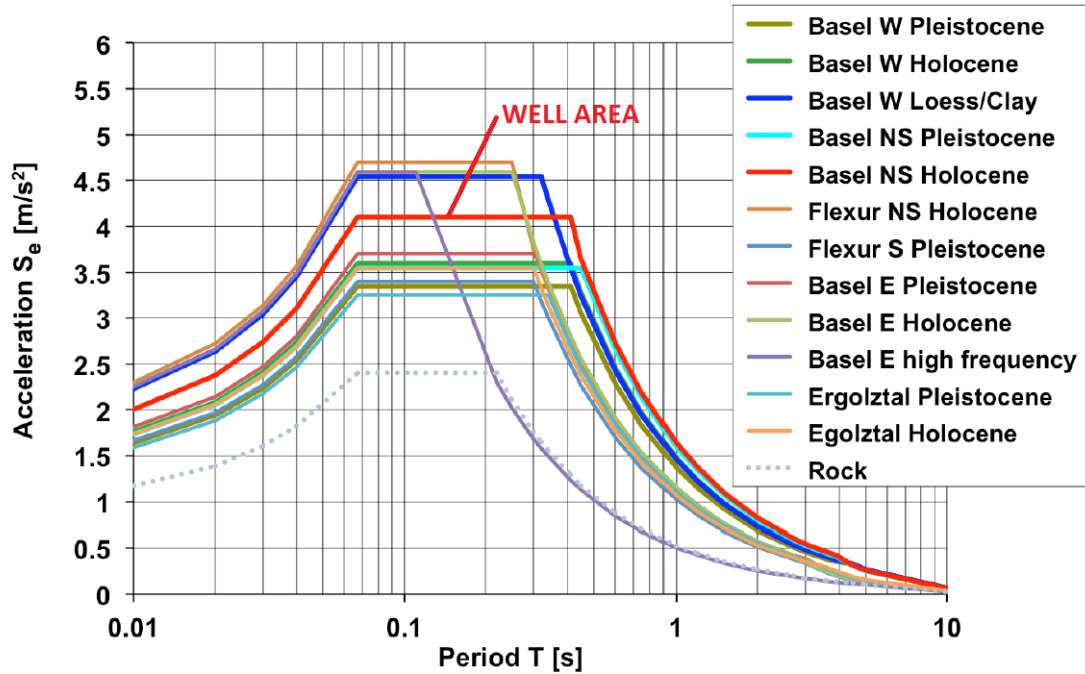
Figure A2.3.16. 5%-damped design elastic pseudo-acceleration response spectra for the microzones of the Basel area. (Wenk & Fäh, 2012).
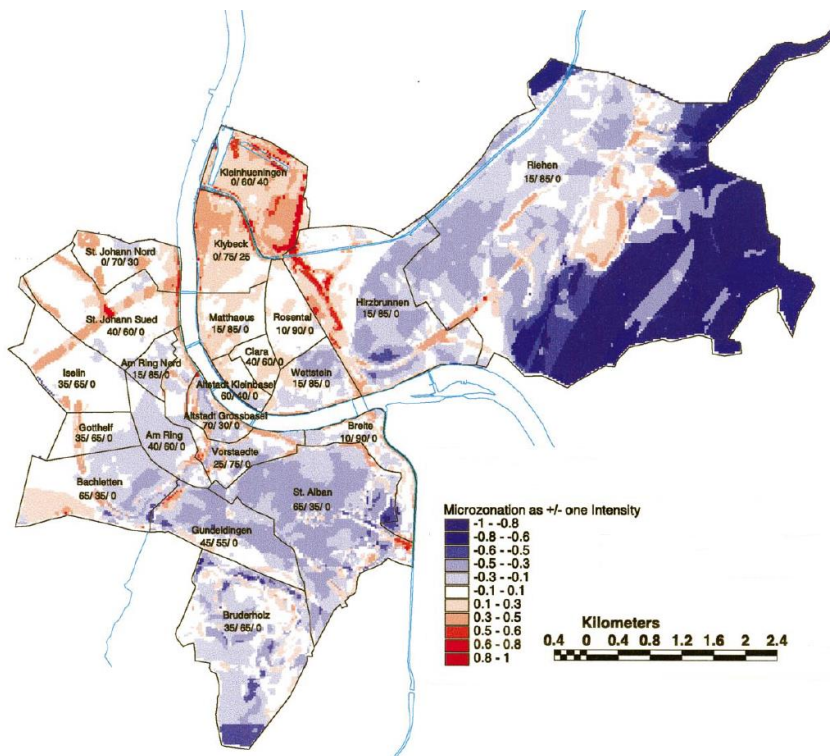
Figure A2.1.17. Qualitative microzonation map of the Canton of Basel City. Areas marked in red are more susceptible to site amplification effects (Fäh *et al.*, 2001).

74

A2.1.4 Ground motions

A2.1.4.1 Intensity observations

Baer *et al.* (2007), Deichmann & Giardini (2009) and the Swiss Seismological Service report a maximum EMS-98 (European Macroseismic Scale, Grunthal, 1998) intensity of V, which define the event as "strong", and means that it was felt indoors by most and outdoors by a few, causing some fear, and that some slight non-structural damage to the most vulnerable structures was observed. Creaking of woodwork and rattling of doors and windows were systematically reported (Deichmann & Giardini, 2009), while swinging of suspended objects and oscillations in liquid-filled containers were less frequently mentioned (Baer *et al.*, 2007). The radius of the area for which the intensity was equal to or larger than IV was 10 km, with peaks in the SSW direction and towards the east. Baer *et al.* (2007) believe the first peak is consistent with the radiation pattern expected from the focal mechanism of the event, while the second one is likely to be the consequence of site amplification due to loose alluvial terraces.

Figure A2.1.18 shows the EMS-98 macroseismic intensities determined from 865 observations of people who either filled in the online questionnaire or replied to emails directly sent to them by the Swiss Seismological Service. It should be noted that intensities assigned in French and German territories are not reliable, due to the lack of reports from these areas.
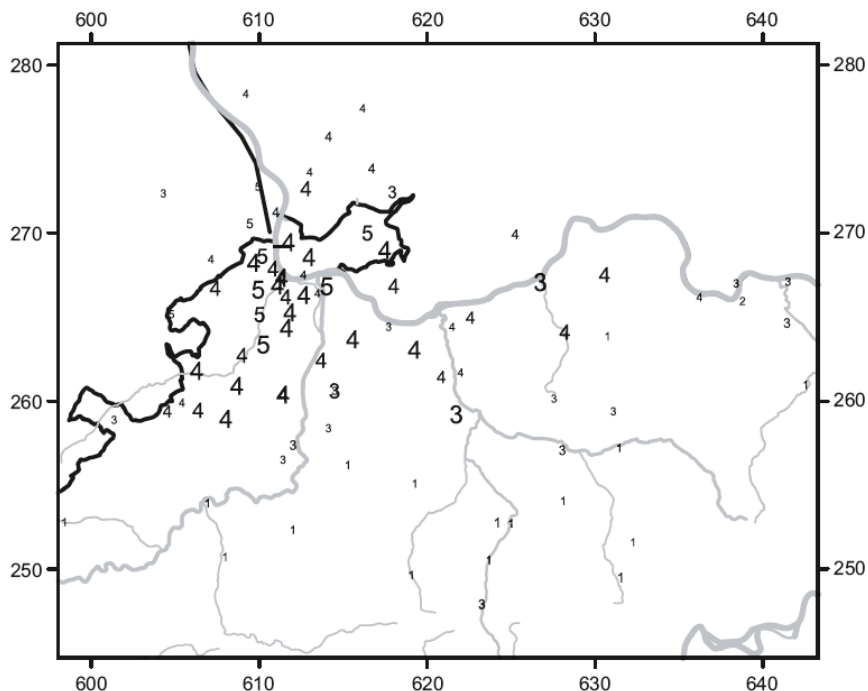
Figure A2.1.18. EMS-98 macroseismic intensities for the main shock, based on reports communicated to the Swiss Seismological Service. It is not representative of the shaking in Germany and France. The size of the number reflects the quality of the data, which can range from very poor (1-2 reports) to very good (15-60 reports). From Baer *et al.* (2007).

The observed macroseismic intensities are plotted against epicentral distance in Figure A2.1.19, and compared against median expected values from intensity prediction

equations. As can be observed, many observations are higher than the expected values, especially at short distances from the epicentre.
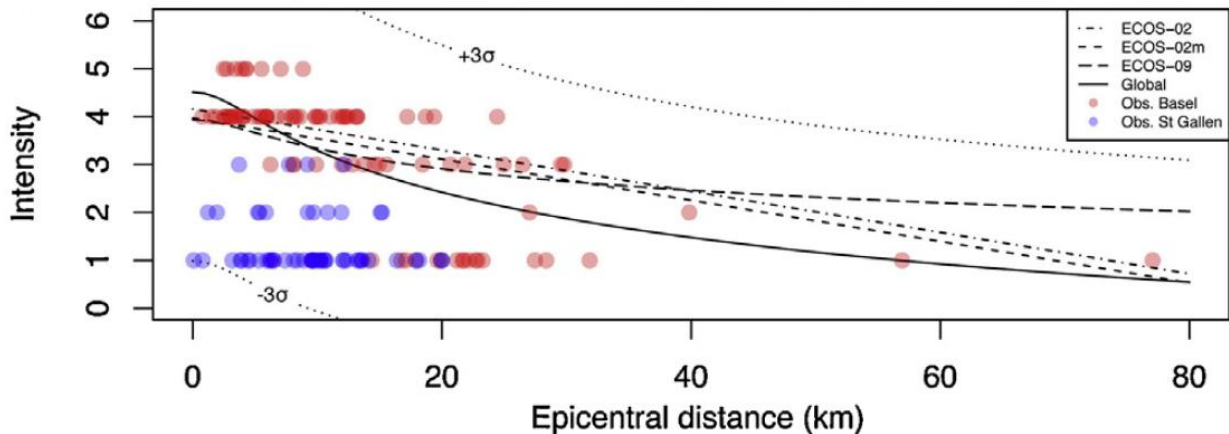
Figure A2.1.19. EMS-98 intensity versus epicentral distance: observations (red dots) and predictions from intensity prediction equations by ECOS-02 (Fäh et al., 2003), ECOS-02m (Álvarez-Rubio et al., 2012), ECOS-09 (Fäh et al., 2011) and Global (Allen et al., 2012). From Mignan *et al.* (2015).

A2.1.4.2 Ground motion recordings

The main shock of this series of events was recorded by a large number of permanent and temporary strong motion stations, even at large distances. The largest geometric mean peak ground acceleration and peak ground velocity recorded were 0.1 g and around 2 cm/s, as can be observed in Figure A2.1.20. The largest geometric mean pseudo-spectral acceleration values for oscillator periods of 0.3 and 1.0 second were 0.1 g and 0.004 g, respectively. Based on the work of Worden *et al.* (2012), Edwards *et al.* (2015) point out that these ground motions are around the onset of damage. Figure A2.1.20 also provides a comparison with respect to the median attenuation curves predicted by the Swiss stochastic model of Edwards & Fah (2013) as modified by Cauzzi *et al.* (2015) to consider an intermediate soil condition (V_{s30} of around 620 m/s), since the recorded data corresponds to several soil classes. As can be observed, the recorded data easily exceeds the median predictions, especially in the near-field. Edwards *et al.* (2015) believe that this is due to significant site amplification effects combined with the shallow depth of the hypocentre.

The largest geometric mean spectral values were observed at station SBEG (Figure A2.1.23), located in the area of Bettingen, around 5.6 km to the ESE of the epicentre, over soil with V_{s30} around 440 m/s. As can be observed in Figure A2.1.21, the geometric mean spectral acceleration and displacement demands present significant peaks in the short period range, typical of low-rise buildings. This amplification becomes more evident in Figure A2.1.22, where the geometric mean spectral acceleration is compared to the design acceleration spectra for the three types of soil that can be found in the area close to the station (10% probability of exceedance in 50 years, data obtained from the online Geoportal of Basel geoviewer and Wenk & Fäh, 2012). Other stations, such as OTTER (1.1 km from the epicentre) and CHBRI (4.8 km from the epicentre) present spectral

acceleration values of individual as-recorded components of around 0.10 and 0.06 g, respectively, at a 0.05 seconds oscillator period (Ripperger *et al.*, 2009), but do not exhibit the large amplification around 0.1 seconds as the geometric mean values of station SBEG.
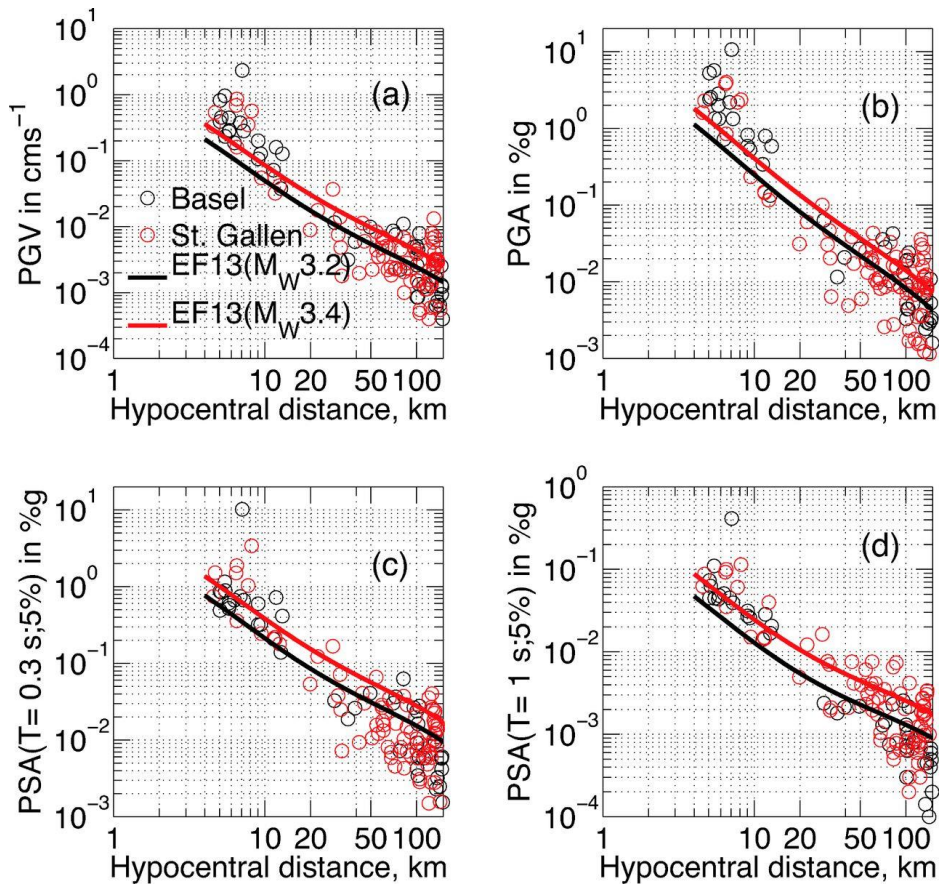
Figure A2.1.20. Attenuation of PGV (a), PGA (b) and 5%-damped pseudo-spectral acceleration at T = 0.3 s (c) and T = 1 s (d), as a function of hypocentral distance. Black circles show the geometric mean of the two horizontal components for the Basel 2006 main shock. The thick black line labeled EF13 is the median attenuation curve for events occurring in the Swiss foreland (Edwards & Fäh, 2013; Cauzzi *et al.*, 2015). Ignore red dots and red lines. (Edwards *et al.*, 2015).
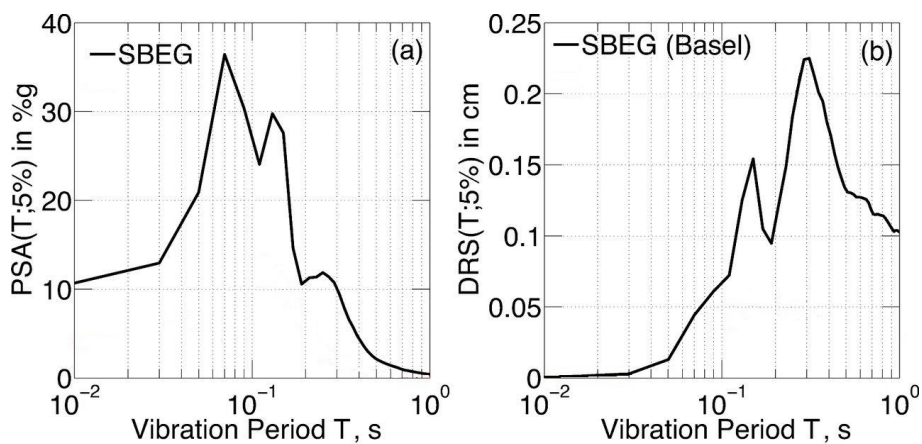
Figure A2.1.21. 5%-damped pseudo-acceleration (PSA) and displacement (DRS) spectra (geometric mean of the horizontal components) observed at station SBEG. From Edwards *et al.* (2015).
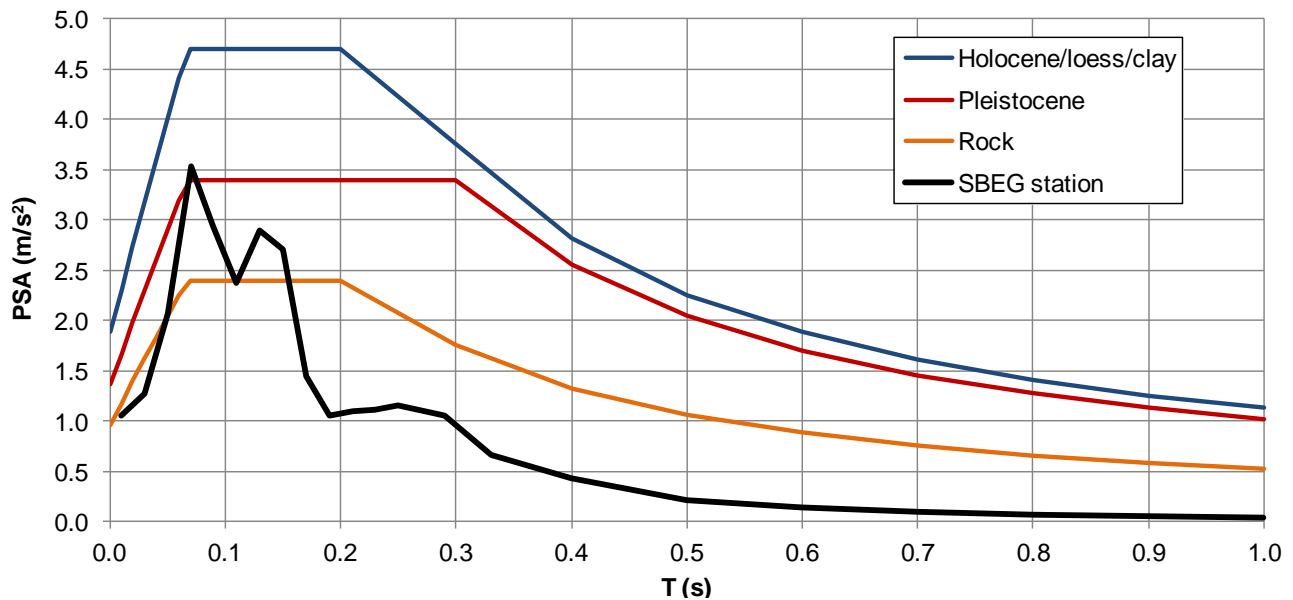
Figure A2.1.22. 5%-damped pseudo-acceleration (PSA) spectra (geometric mean of the horizontal components) observed at station SBEG compared against the design spectra for the three soil types that can be found in the area close to the station. Data for station SBEG: Edwards *et al.* (2015)

Ripperger *et al.* (2009) calculated the maximum resultant PGV from the velocity time-history of 29 stations, which range from 0.043 cm/s (CHBDO station, 12.0 km away from the epicentre) to 1.389 cm/s (SBAJ station, 2.1 km away from the epicentre). As shown in Figure A2.1.23, larger values are observed to the south and to the east of the epicentre, an observation that matches the peaks in macroseismic intensity discussed earlier (Figure A2.1.18). Figure A2.1.24 shows the velocity time histories of the four stations (out of the 29) with the largest maximum resultant PGV.

Based on the observation of some of the waveforms recorded for the largest events of the series, Häring *et al.* (2008) suggest that it is possible that these may have formed by a cascade-like rupture process either on single continuous structures or almost synchronously on several closely adjacent structures instead. Figure A2.1.25 shows how this can be observed in the waveform recorded at the OTER2 station during the main shock. A number of successive events occurring a few milliseconds apart can be distinguished after the first P-wave arrival. This staggering becomes undistinguishable at stations located farther away from the epicentre.
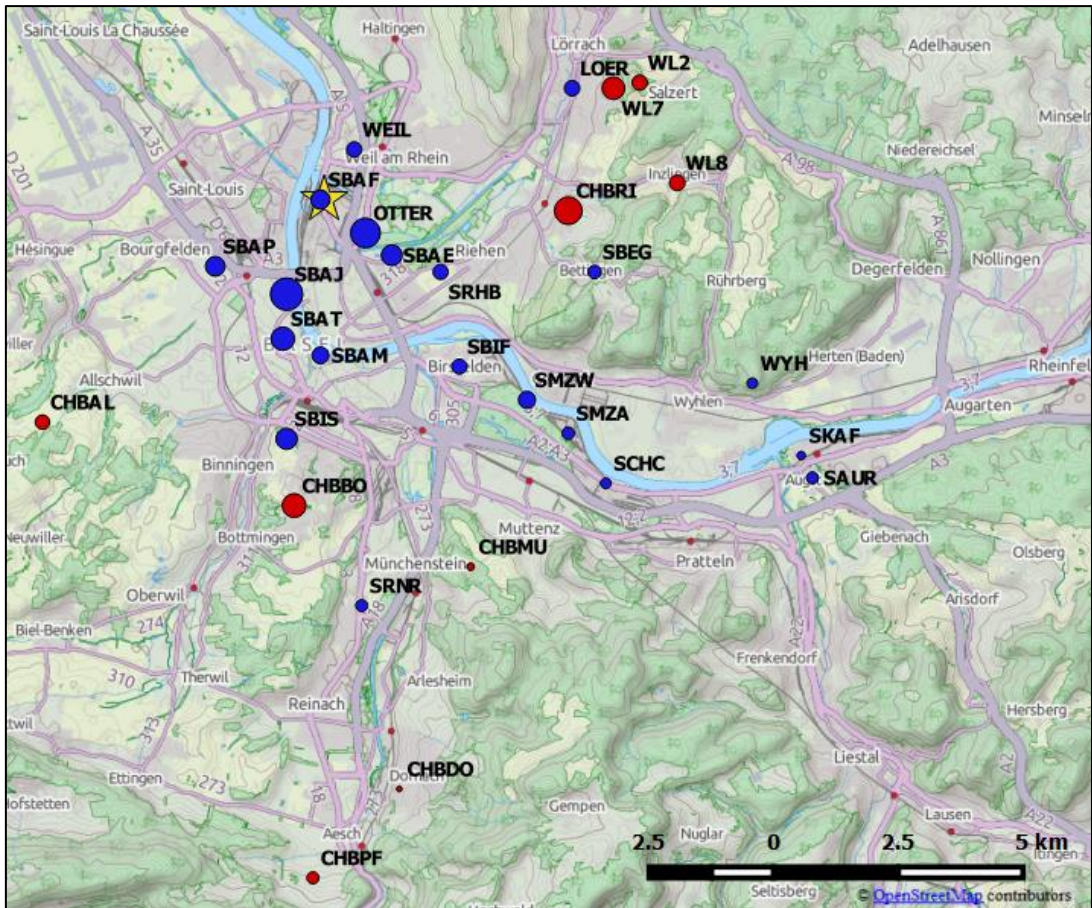
Figure A2.1.23. Maximum resultant PGV in 29 recording stations (red: temporary, blue: permanent), shown proportionally to the size of the location circles (data from Ripperger *et al.*, 2009). The yellow star shows the location of the epicentre according to Deichmann & Ernst (2009). Maximum resultant PGV: 1.389 cm/s, at SBAJ station (2.1 km from the epicentre).
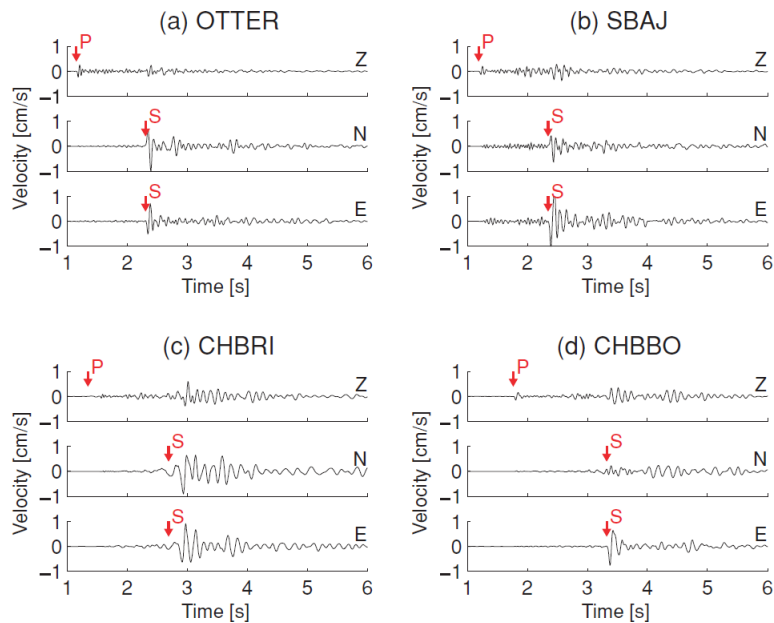
Figure A2.1.24. Velocity time histories for four stations located 1.1 km (OTTER), 2.1 km (SBAJ), 4.8 km (CHBRI) and 6.2 km (CHBBO) away from the epicentre. Stations CHBRI and CHBBO are placed over unconsolidated sediments. (Ripperger *et al.*, 2009).
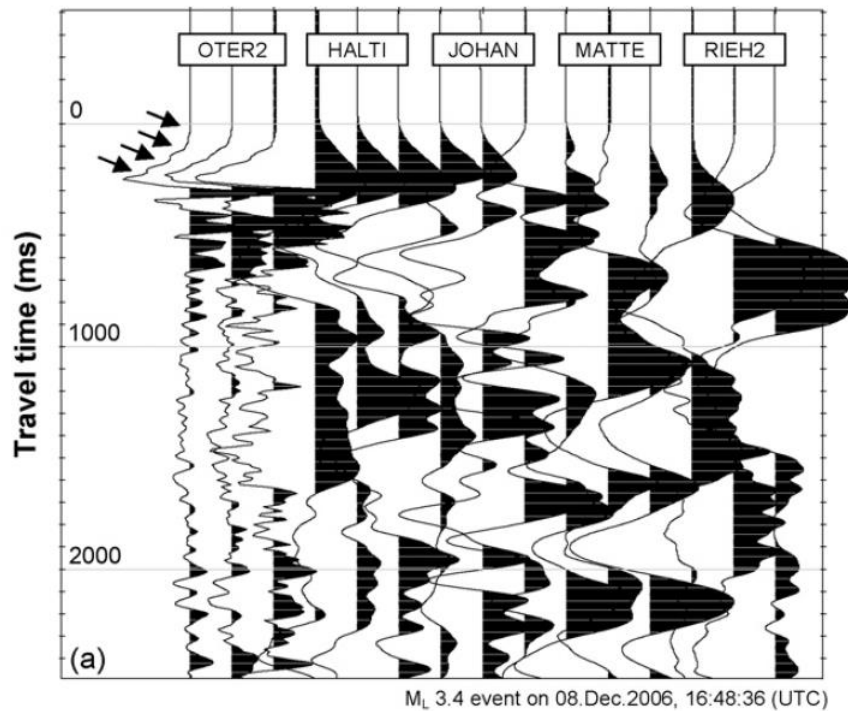
Figure A2.1.25. Raw unfiltered traces recorded during the main shock, aligned at the P-wave picks. Multiple arrivals are indicated by arrows (Häring *et al.,* 2008).

A2.1.4.3 Inferred shaking levels

As pointed out above, there is significant agreement between the maximum resultant PGV values calculated by Ripperger *et al.* (2009) and the EMS-98 intensities reported by the Swiss Seismological Service (Figure A2.1.18). Further, it is relevant to note that stations CHBRI and CHBBO, which presented two of the highest resultant PGV values, are located over unconsolidated sediments, while the other two, OTTER and SBAJ, are very close to the epicentre. Station SBEG, which experienced the largest geometric mean spectral values, is also placed over soils with a significant amplification potential.

No attempts to infer ground shaking levels within the city of Basel from macroseismic intensities have been found in the literature.

A2.1.4.4 Duration of ground shaking

According to Deichmann & Giardini (2009), people reported a short, high-frequency shaking which lasted from one to three seconds.

Estimations of earthquake significant durations can be obtained by means of prediction equations such as those of Bommer *et al.* (2009) and Kempton & Stewart (2006). Given that no details are available with respect to the locations at which the 1-3 seconds shaking was observed, a range of distances to the rupture and soil types are considered. A 0.1 km radius, as suggested by Häring *et al.* (2008), and the 4.7 km hypocentral depth of Deichmann & Ernst (2009) are assumed. Under the light of the results obtained (Figure A2.1.26), one to three seconds seems a reasonable range.
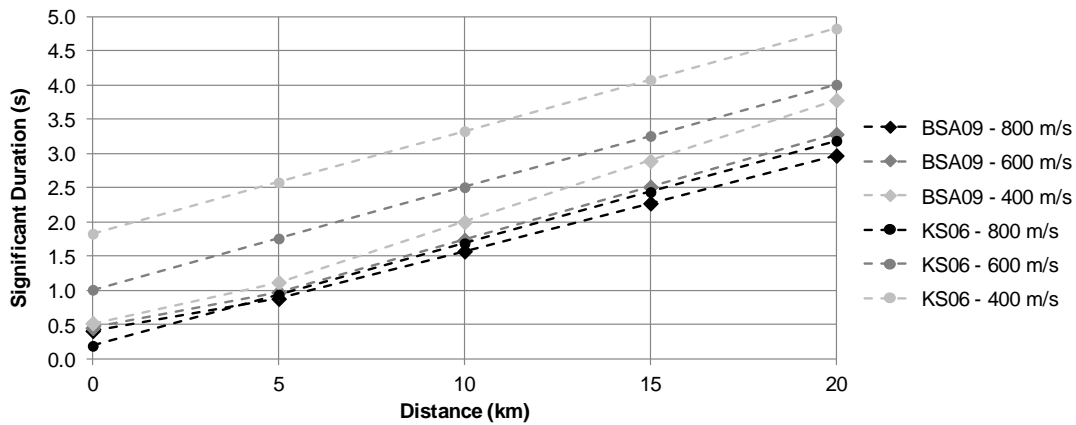
Figure A2.1.26. Estimation of the significant duration of the main shock, using prediction equations by Bommer *et al.* (2009, BSA) and Kempton & Stewart (2006, KS).

A2.1.5 Collateral earthquake hazards

A2.1.5.1 Surface rupture

No surface rupture reported.

A2.1.5.2 Landslides

No landslides reported.

A2.1.5.3 Liquefaction

No liquefaction reported.

A2.1.6 Exposed population

A2.1.6.1 Socio-economic setting

According to the 2014 Human Development Report (United Nations, 2014), the Human Development Index (HDI) for Switzerland in 2013 was 0.917, while its Inequality-adjusted HDI (IHDI) was 0.847. This located Switzerland in the 3rd place in the world's ranking, while the Netherlands ranks 4th. Table A2.1.4 compares the HDI and IHDI for both countries for a series of Human Development Reports (2006; 2008; 2009; 2014). IHDI values are not available for reports generated before 2010. The column "Adj. HDI" provides the HDI values given in the 2014 report for previous years, adjusted for data consistency in time. As can be observed, both countries present similar levels of human development.

Table A2.1.4. Human Development Index and Inequality-adjusted Human Development Index for Switzerland and the Netherlands.

Report	Data	Switzerland				Netherlands			
		HDI	IHDI	Rank	Adj. HDI	HDI	IHDI	Rank	Adj. HDI
2006	2004	0.947	-	9	-	0.947	-	10	-
2007/2008	2005	0.955	-	7	0.901	0.953	-	9	0.888
2009	2007	0.960	-	9	0.903	0.964	-	6	0.901
2014	November 2013	0.917	0.847	3	-	0.915	0.854	4	-

Switzerland has a powerful growing economy, its most important economic sectors being manufacturing and finance. Specialist chemicals, machines and electronics, and precision instruments are its main exportation products. Basel, in particular, is host to several chemical and pharmaceutical industries, and is one of the main financial centres of Switzerland (Steimen *et al.*, 2004). In 2008, the Canton of Basel City had the largest gross domestic product (GDP) per capita in Switzerland, with it being around double of the national value.

Table A2.1.5 presents a comparison between Switzerland and the Netherlands in terms of GDP, GDP per capita and unemployment rate.

Table A2.1.5. Gross domestic product (GDP), GDP per capita and unemployment rate for Switzerland and the Netherlands.

Indicator	Units	Switzerland		Netherlands	
		2006	2014	2006	2014
Gross domestic product, current prices	Billions of US dollars	377.240	712.050	663.119	866.354
Gross domestic product per capita, current prices	US dollars	51,770.607	87,475.464	40,571.399	51,372.963
Unemployment rate	% of total labor force	3.400	3.164	3.900	7.395

A2.1.6.2 Population density and distribution

The tri-national metropolitan area of Basel has a population of around 829,000 people, 65%, 8% and 27% of which live in Swiss, French and German municipalities (Figure A2.1.27). The municipality of the city of Basel itself has a population of around 170,000 inhabitants which, along with the populations of Bettingen and Riehen, make up the around 197,000 inhabitants of the Swiss Canton of Basel City (Basel-Stadt).
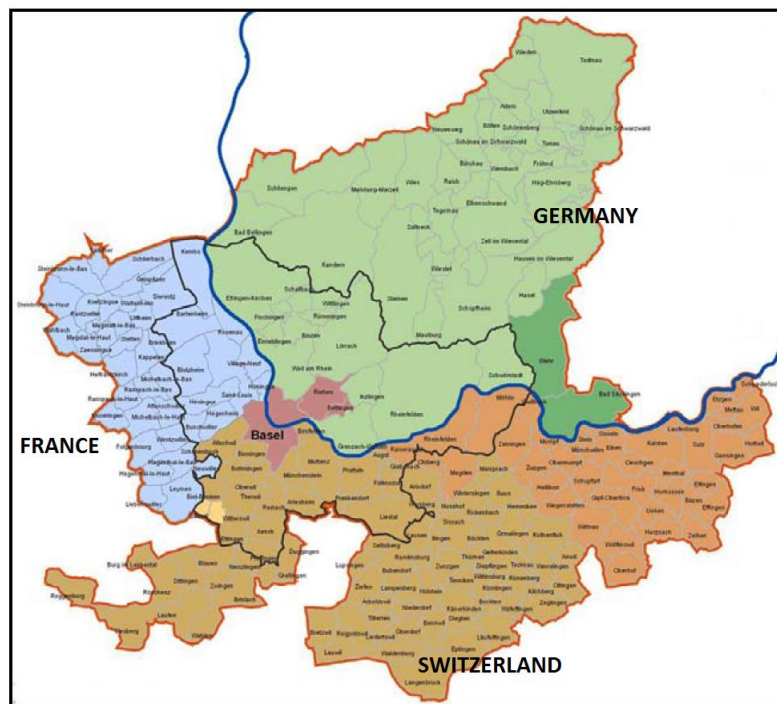
Figure A2.1.27. Basel metropolitan area: Swiss (brown), French (blue) and German (green) regions. Marked in red is the Swiss Canton of Basel City (Basel-Stadt) (Driscoll *et al.*, 2010).

A2.1.6.3 Time of day of earthquake

Given that no injuries were reported, the time at which the main shock occurred did not have any influence in its consequences for the population.

A2.1.7 Characteristics of exposed building stock

A2.1.7.1 Seismic design codes

According to Wenk & Fäh (2012), seismic requirements are generally the dominating design action for new buildings in Switzerland, though wind design codes were introduced several decades earlier than seismic ones (Badoux & Peter, 2000). As Wenk (2014) points out, the first Swiss seismic regulations were contained in the Swiss Structural Standard SIA 160:1970 introduced in 1970. They were based on allowable stress design concepts, and specified that all ordinary buildings in Switzerland be designed for a minimum horizontal load equal to 2% of their weight. They recommended that a minimum 5% be used in the regions of higher seismicity but, given that the ultimate decision was left in the hands of the local authorities, only the Canton of Basel City adopted the 5% value.

The SIA 160:1970 standards were revised in 1989, and they were modified to incorporate the first probabilistic hazard map of Switzerland, which was based on macroseismic intensity. As a result, the SIA 160:1989 standards incorporated a seismic zoning map which contained four zones, each of them finally related to a design value of horizontal ground acceleration. In this map, Basel belonged to zone 2, and was therefore associated

to a design horizontal acceleration of 0.1 g. Badoux & Peter (2000) point out that, in general, the 1989 update of the standards resulted in a significant increase in the required lateral load resistance of structures.

By 1998, the Swiss Seismological Service started the process that would lead to the 2004 non-intensity based fully-probabilistic seismic hazard assessment (PSHA) of Switzerland (Wiemer *et al.*, 2009; Giardini *et al.*, 2004). Its outcome was incorporated in the Eurocode-based new generation of Swiss Structural Standard SIA 261:2003, which replaced SIA 160:1989. Probabilistic hazard maps were generated in terms of pseudo-spectral accelerations at a number of oscillator frequencies (not peak ground accelerations), which were then combined to produce an equivalent design value of horizontal ground acceleration. The resulting seismic zoning map again divided the country into four zones, whose design acceleration values remained the same as those of SIA 160:1989, but for which the zone boundaries changed, significantly increasing the area corresponding to the higher seismicity zones. In this map, Basel belongs to zone 3a, and is thus associated to a design horizontal acceleration of 0.13 g.

According to Wenk (2014), the SIA 260:2003 - SIA 267:2003 standards were partially revised in the years 2012 to 2014, but no changes were introduced to the seismic zoning map. At the time of writing, Switzerland is finishing the preparation of an update to its seismic hazard maps (Wiemer *et al.*, 2014).

A2.1.7.2 Building typologies

According to Fäh *et al.* (2001), most of the buildings in the city of Basel were built within the last 150 years, with the exception of the old downtown area, which dates back to the Middle Ages. In general, they are mostly three to five storeys high residential buildings, with the exception of the industrial area in the north-east and two areas to the west and south in which family housing is the predominant typology (see Figure A2.1.28).

As can be observed in Figure A2.0.29, around 57% of the buildings in the metropolitan area of Basel are masonry buildings, while around 38% are made of reinforced concrete, according to the data from Mignan *et al.* (2015). Brick masonry is the most frequent type of masonry. Reinforced concrete (RC) moment-resisting frames are very infrequent, and most concrete structures consist of RC walls, either alone or combined with masonry walls too. Steel and wood structures represent a very small percentage of the overall building stock (5.6%).
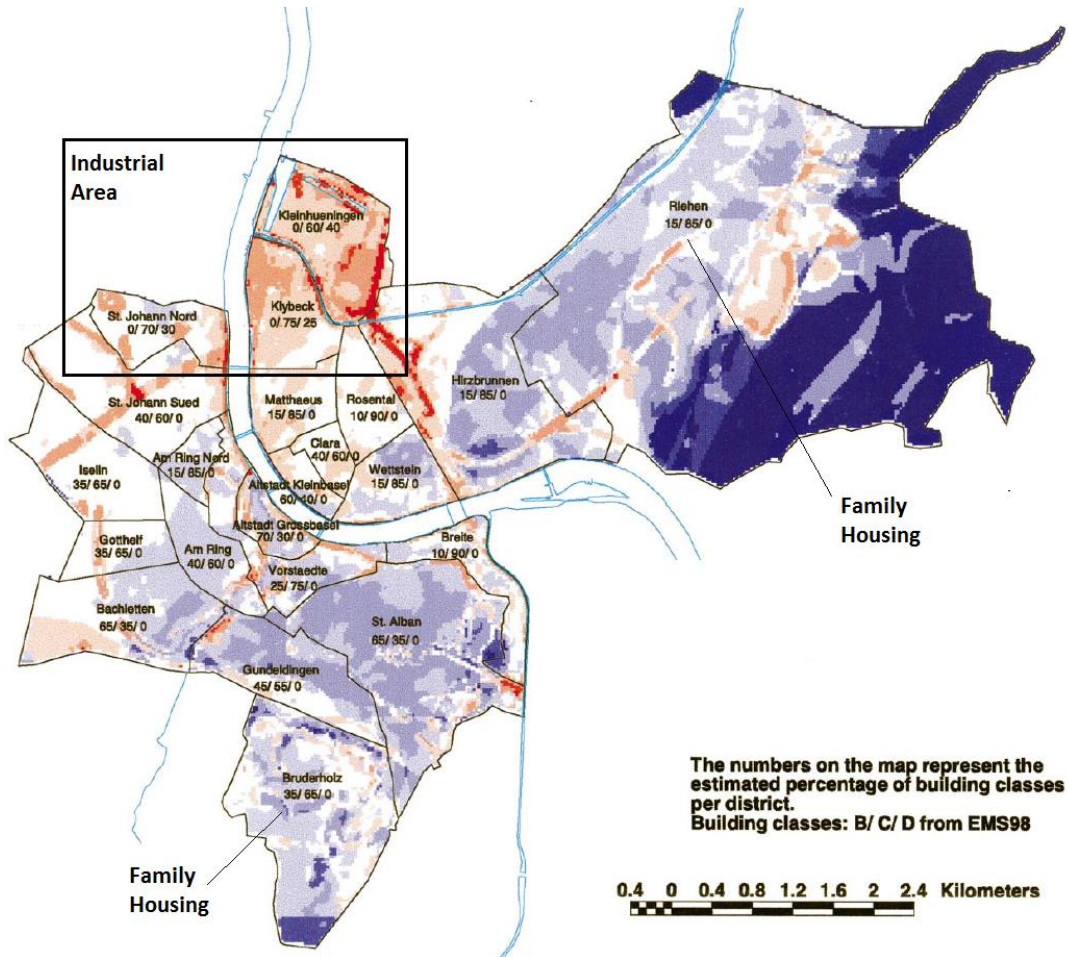
Figure A2.1.28. Distribution of EMS-98 building vulnerability classes (given in percentage with the format B/C/D). From Fäh *et al.* (2001).
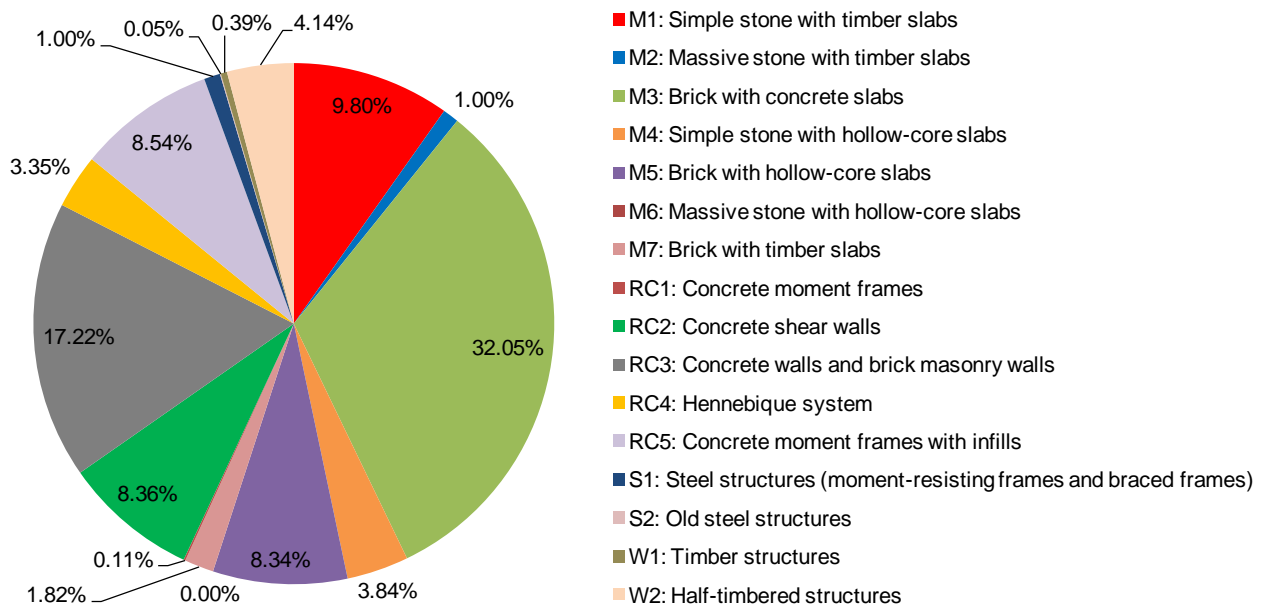
Figure A2.1.29. Percentage of buildings per building typology (data from Mignan *et al.*, 2015).

The European Macroseismic Scale (EMS-98) classifies buildings into six vulnerability classes, from A through F, with the former and the latter corresponding to the most and least vulnerable, respectively. According to Fäh *et al.* (2001) and Mignan *et al.* (2015), most of the buildings in the metropolitan area of Basel fall between classes B and D. Figure A2.1.28 shows the percentage of buildings of each district that belong to each vulnerability class (B, C or D), determined by visual inspection by Fäh *et al.* (2001). According to this map, only buildings in the industrial area are assigned to vulnerability class D. According to Mignan *et al.* (2015), typologies RC1, RC2, RC3, RC5, S2, W1 and W2 belong to this class. Masonry buildings only belong to classes B or C.

Figure A2.1.30 shows the number of buildings per administrative district of the area around the city of Basel, while Figure A2.1.31 shows the number of masonry and reinforced concrete buildings (typologies M1 to M7 and RC1 to RC5 altogether).
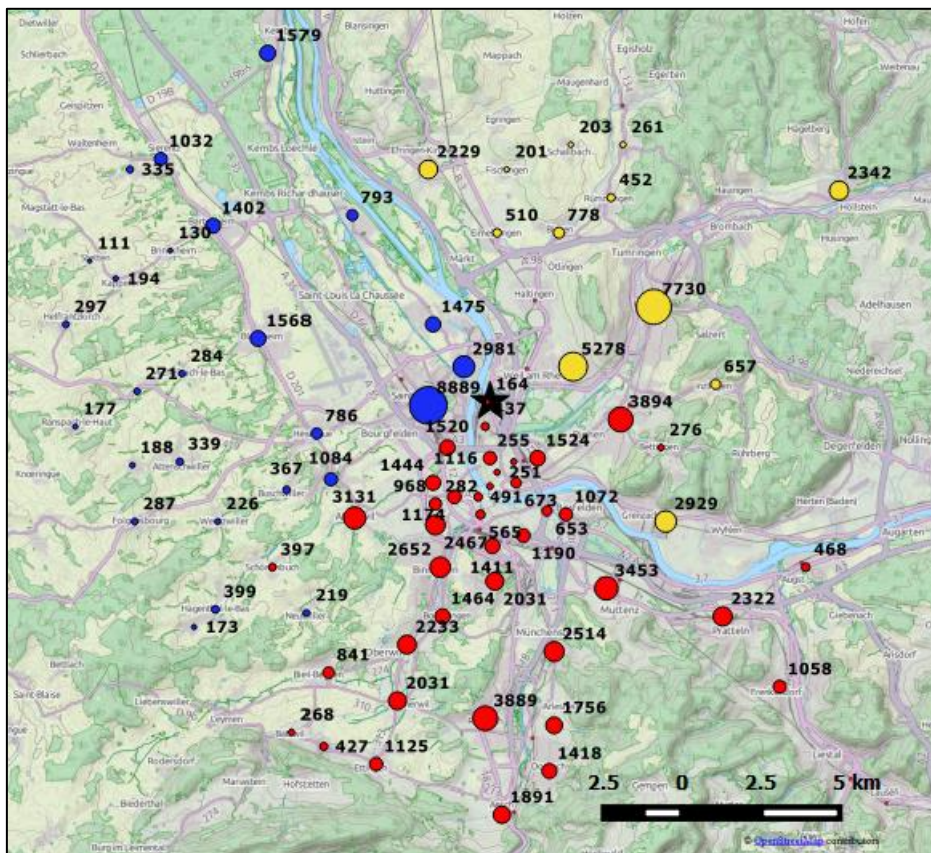
Figure A2.1.30. Total number of buildings per administrative district of Switzerland (red), France (blue) and Germany (yellow) (data from Mignan *et al.*, 2015). The black star shows the epicentre, as determined by Deichmann & Ernst (2009).

Lang & Bachmann (2004) evaluated the vulnerability of eighty-seven residential buildings of Basel using a non-linear static approach. From their results, they concluded that buildings whose structure combines reinforced concrete walls with unreinforced masonry are more vulnerable than pure unreinforced masonry buildings. They attribute this to the unfavourable layouts in plan and elevation of the former, which have very open façade planes and a very small number of lateral resisting elements, and to the practice of using unreinforced masonry in the upper storeys and reinforced concrete in the bottom ones.

Badoux & Peter (2000) studied the seismic vulnerability of Swiss RC buildings constructed between 1945 and 1989. In their assessment of a series of case studies, they observed that the thinnest RC walls found in existing buildings were 140 mm thick, slabs were 180 mm and thicker, the horizontal and vertical reinforcement ratios of RC walls was between 0.2-0.4% and 0.4-0.7%, respectively, the edges of walls were always confined with U-shaped stirrups, the overlap of the reinforcement bars was usually around 40 bar diameters, and until 1968 the anchorage of reinforcement bars was usually carried out with hooks. Based on these observations, they concluded that the basic conditions required for reinforced concrete to behave in a ductile manner appear to be met.
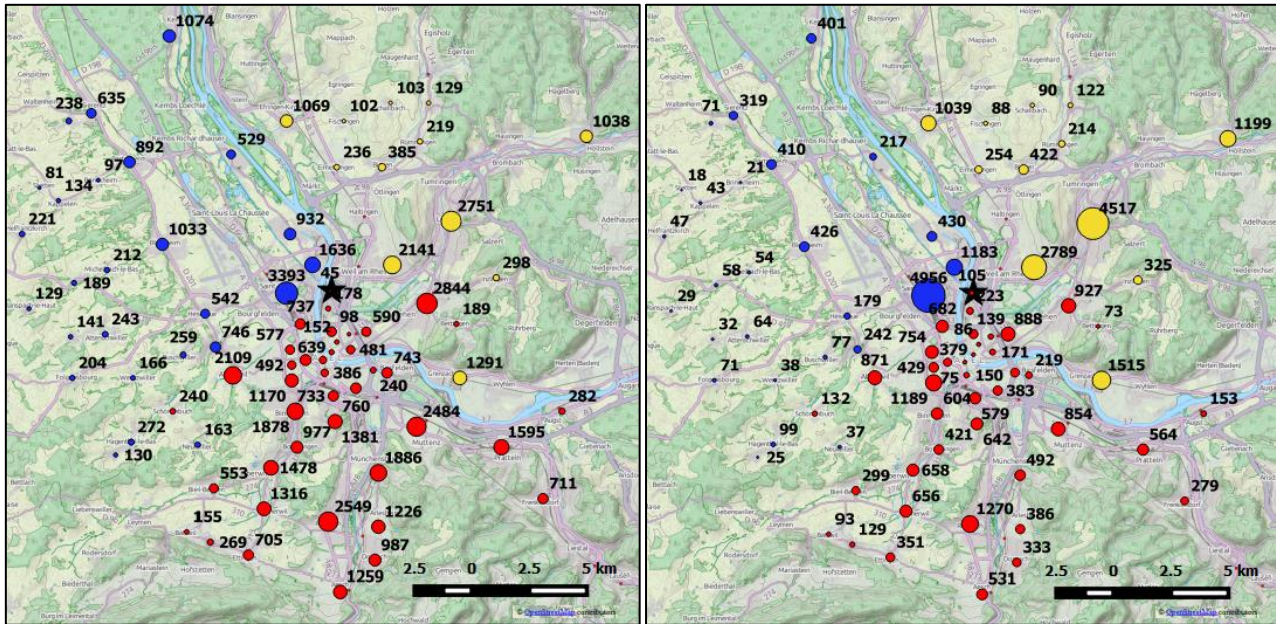
Figure A2.1.31. Number of masonry (left) and reinforced concrete (right) buildings per administrative district of Switzerland (red), France (blue) and Germany (yellow) (data from Mignan *et al*., 2015). The black star shows the epicentre, as determined by Deichmann & Ernst (2009).

A2.1.7.3 Prior damage and retrofit

No information has been found regarding prior damage and retrofit.

A2.1.8 Damage observations

A2.1.8.1 Damage states

Given the low level of damage observed, there are no reports making use of standardised damage scales for this earthquake. However, from the qualitative descriptions, it is possible to believe that all damage observed corresponded to Grade 1 in the European Macroseismic Scale (EMS-98; Grünthal, 1998). For details regarding the latter, please refer to Chapter 2.

A2.1.8.2 Damage statistics

Very slight non-structural damage, mostly fine hairline cracks to the plaster and damage to the paint at building junctions, was consistently reported for hundreds of buildings within the city of Basel and in neighbouring communities (Deichmann & Giardini, 2009).

According to Ripperger *et al.* (2009), 4.6% of the 865 observations gathered by the Swiss Seismological Service (map of macroseismic intensities, Figure A2.1.18) reported non-structural damage to buildings (3.6% hairline cracks in walls, 1% minor pieces of plaster falling down). This percentage is larger (5.7%) if only the reports coming from the area of Basel city are considered (403 reports). However, Geopower Basel, the company in charge of the geothermal project, received more than two thousand damage reports some days after the event, of which around nine hundred came from within the city of Basel. Figures A2.1.32-34 show examples of the kind of damage observed.

Figure A2.1.32. Crack in connection between wall and timber roof (left). Cracks in corner of a window (right).

Figure A2.1.33. Hairline cracks in plaster (left). Minor plaster spalling (right).

Figure A2.1.34. Crack in intersection of two perpendicular masonry elements (left). Crack parallel to the orientation of fibres in a timber element (right).

A2.1.8.3 Observed weaknesses

No particular weaknesses reported.

A2.1.8.4 Damage distribution

As pointed out earlier, the distribution of observed macroseismic intensities (Figure 0A2.1.18) presents peaks in the SSW direction and towards the east. According to Baer *et al.* (2007), the peak in the SSW direction is consistent with the radiation pattern associated with the focal mechanism of the event, while the peak generated towards the east was probably caused by site amplification due to the presence of poorly compacted alluvial terraces.

A2.1.9 Casualties and losses

A2.1.9.1 Numbers of dead and injured

No casualties were reported for this earthquake.

A2.1.9.2 Causes of casualties

No casualties were reported for this earthquake.

A2.1.9.3 Estimates of economic losses

Figures for economic losses vary between 7 million and 9 million CHF, or around 6.5 and 8.3 million USD (Baisch *et al.*, 2009; Edwards *et al.*, 2015; Giardini, 2009; Kraft *et al.*,

2009). Similar numbers are reported by newspapers such as *The New York Times* and *The Guardian*.

Giardini (2009) and Kraft *et al.* (2009) point out that these figures seem disproportionately high for a M_L 3.4 event. The two main factors contributing to a real estimation of the damage being so challenging to make are the lack of data from past small earthquakes (Giardini, 2009) and the difficulties in determining which instances of damage can be directly associated to the earthquake and which cannot, given its small magnitude. However, according to Kraft *et al.* (2009), the insurance company did not make an effort to question possibly unjustified claims.

Though the damage in each building never exceeded the usual insurance deductible value of more than 10% of the insured property, all the damage claims were paid by the liability insurance of Geopower Basel, due to the damage having been generated by a manmade event (Giardini, 2009).

A2.1.10 Discussion and conclusions

This M_L 3.4 earthquake occurred on 8th December 2006, at 16:48 UTC (17:48 local time), right under the city of Basel, northern Switzerland, six days after the start of the injection of a large volume of water at high pressures for the creation of an enhanced geothermal system (EGS) for the Deep Heat Mining Project led by Geopower Basel in said city. It was the largest of a series of little less than 15,000 events that were induced in the area, and was preceded by a M_L 2.6 event that occurred in the early morning of the same day, and which led to the premature halt of the injection, and by a M_L 2.7 event in the afternoon. The geothermal project was finally cancelled in December 2009.

The creaking of woodwork and rattling of doors and windows caused by the main shock alarmed the population, though consequent damage was limited mostly to hairline cracks in plaster and paint. Nevertheless, the company in charge of the project received more than two thousand damage reports some days after the event. Figures for economic losses vary between 7 million and 9 million CHF (6.5 to 8.3 million USD), which seem to be surprisingly high for a M_L 3.4 event. All damage claims were paid by the liability insurance of Geopower Basel.

Though the occurrence of these earthquakes was clearly related to the water injection process for the EGS, the tectonics of the area of Basel are not incapable of naturally producing seismic events of the magnitudes observed during this series and much larger. Further, they do not seem to have been the consequence of hydrofracking (fracturing of the rock due to the water injection) but of the induced activation of a complex pre-existing fault pattern.

A2.1.11 References

A2.1.11.1 Bibliography

Badoux, M. & K. Peter (2000). Seismic vulnerability of older Swiss RC buildings. In *Proceedings of the 12th World Conference on Earthquake Engineering*, Auckland, New Zealand, 30 January - 4 February.

Baer, M., N. Deichmann, J. Braunmiller, J. Clinton, S. Husen, D. Fäh, D. Giardini, P. Kästli, U. Kradolfer & S. Wiemer, S. (2007). Earthquakes in Switzerland and surrounding regions during 2006. *Swiss J. Geosci.* **100**, 517–528.

Baisch, S., D. Carbon, U. Dannwolf, B. Delacou, M. Devaux, F. Dunand, R. Jung, M. Koller, C. Martin, M. Sartori *et al.* (2009). *Deep heat mining basel: seismic risk analysis.* Ser. Group Departement Für Wirtsch. Soz. Umw. Kantons Basel-Stadt Basel.

Becker, A., C.A. Davenport & D. Giardini (2002). Palaeoseismicity studies on end-Pleistocene and Holocene lake deposits around Basle, Switzerland. *Geophys. J. Int.* **149**, 659–678.

Bommer, J.J., P.J. Stafford & J.E. Alarcón (2009). Empirical equations for the prediction of the significant, bracketed, and uniform duration of earthquake ground motion. *Bulletin of the Seismological Society of America* **99**(6), 3217-3233.

Catalli, F., M.-A. Meier & S. Wiemer (2013). The role of Coulomb stress changes for injection-induced seismicity: the Basel enhanced geothermal system. *Geophys. Res. Lett.* **40**, 72–77.

Cauzzi, C., B. Edwards, D. Fah, J. Clinton, S. Wiemer, P. Kastli, G. Cua & D. Giardini (2015). New predictive equations and site amplification estimates for the next-generation Swiss ShakeMaps. *Geophys. J. Int.* **200**, 421–438.

Deichmann, N. & J. Ernst (2009). Earthquake focal mechanisms of the induced seismicity in 2006 and 2007 below Basel (Switzerland). *Swiss J. Geosci.* **102**, 457–466.

Deichmann, N. & D. Giardini (2009). Earthquakes induced by the stimulation of an Enhanced Geothermal System below Basel (Switzerland). *Seismol. Res. Lett.* **80**, 784–798.

Deichmann, N., T. Kraft & K.F. Evans (2014). Identification of faults activated during the stimulation of the Basel geothermal project from cluster analysis and focal mechanisms of the larger magnitude events. *Geothermics* **52**, 84–97.

Driscoll, J., F. Vigier & K. Leith (2010). *The Basel Metropolitan Area: three borders - one metropolitan area.* International Centre for Local and Regional Development (ICLRD), Northern Ireland.

Edwards, B. & D. Fah (2013). A stochastic ground-motion model for Switzerland. *Bull. Seismol. Soc. Am.* **103**, 78–98.

Edwards, B., T. Kraft, C. Cauzzi, P. Kästli & S. Wiemer (2015). Seismic monitoring and analysis of deep geothermal projects in St Gallen and Basel, Switzerland. *Geophys. J. Int.* **201**, 1020–1037.

Fäh, D., E. Rüttener, T. Noack, T. & P. Kruspan (1997). Microzonation of the city of Basel. *J. Seismol.* **1**, 87–102.

Fäh, D., F. Kind, K. Lang & D. Giardini (2001). Earthquake scenarios for the city of Basel. *Soil Dyn. Earthq. Eng.* **21**, 405–413.

Ferry, M., M. Meghraoui, B. Delouis & D. Giardini (2005). Evidence for Holocene palaeoseismicity along the Basel-Reinach active normal fault (Switzerland): a seismic source for the 1356 earthquake in the Upper Rhine graben. *Geophys. J. Int.* **160**, 554–572.

Giardini, D. (2009). Geothermal quake risks must be faced. *Nature* **462**, 848–849.

Giardini, D., G. Grünthal, K.M. Shedlock & P. Zhang (1999). The GSHAP global seismic hazard map. *Annali di Geofisica* **42**(6), 1225-1228.

Giardini, D., G. Grünthal, K.M. Shedlock & P. Zhang (2003). The GSHAP global seismic hazard map. In: Lee, W., H. Kanamori, P. Jennings & C. Kisslinger (eds.): International handbook of earthquake & engineering seismology, International Geophysics Series **81**B, Academic Press, Amsterdam, 1233-1239.

Giardini, D., S. Wiemer, D. Fäh & N. Deichmann (2004). *Seismic Hazard Assessment of Switzerland, 2004*. Swiss Seismological Service, ETH Zurich.

Giardini, D., J. Woessner, L. Danciu, H. Crowley, F. Cotton, G. Gruenthal, R. Pinho, G. Valensise, S. Akkar, R. Arvidsson, R. Basili, T. Cameelbeck, A. Campos-Costa, J. Douglas, M. B. Demircioglu, M. Erdik, J. Fonseca, B. Glavatovic, C. Lindholm, K. Makropoulos, F. Meletti, R. Musson, K. Pitilakis, K. Sesetyan, D. Stromeyer, M. Stucchi & A. Rovida (2013). *Seismic Hazard Harmonization in Europe (SHARE): Online data resource*, doi:10.12686/SED-00000001-SHARE.

Goertz-Allmann, B.P., A. Goertz & S. Wiemer (2011). Stress drop variations of induced earthquakes at the Basel geothermal site. *Geophys. Res. Lett.* **38**, 5 pp.

Grünthal, G. (ed.) (1998). *European Macroseismic Scale 1998 (EMS-98)*. Cahiers du Centre Europeen de Geodynamique et de Seismologie 15, Centre Europeen de Geodynamique et de Seismologie, Luxembourg.

Häring, M.O., U. Schanz, F. Ladner & B.C. Dyer (2008). Characterisation of the Basel 1 enhanced geothermal system. *Geothermics* **37**, 469–495.

Havenith, H.-B., D. Fäh, U. Polom & A. Roullé (2007). S-wave velocity measurements applied to the seismic microzonation of Basel, Upper Rhine Graben. *Geophys. J. Int.* **170**, 346–358.

Kastrup, U. (2004). Stress field variations in the Swiss Alps and the northern Alpine foreland derived from inversion of fault plane solutions. *J. Geophys. Res.* **109**, 22 pp.

Kempton, J.J. & J.P. Stewart (2006). Prediction equations for significant duration of erthquake ground motions considering site and near-source effects. Earthquake Spectra **22**(4), 985-1013.

Kraft, T. & N. Deichmann (2014). High-precision relocation and focal mechanism of the injection-induced seismicity at the Basel EGS. *Geothermics* **52**, 59–73.

Kraft, T., P.M. Mai, S. Wiemer, N. Deichmann, J. Ripperger, P. Kästli, C. Bachmann, D. Fäh, J. Wössner & D. Giardini (2009). Enhanced geothermal systems: mitigating risk in urban areas. *Eos Trans. Am. Geophys. Union* **90**, 273–274.

Lang, K. & H. Bachmann (2004). On the seismic vulnerability of existing buildings: a case study of the city of Basel. *Earthq. Spectra* **20**, 43–66.

Laubscher, H. (2001). Plate interactions at the southern end of the Rhine graben. *Tectonophysics* **343**,1–19.

Majer, E.L., R. Baria, M. Stark, S. Oates, J. Bommer, B. Smith & H. Asanuma (2007). Induced seismicity associated with enhanced geothermal systems. *Geothermics* **36**, 185–222.

Mignan, A., D. Landtwing, P. Kästli, B. Mena & S. Wiemer (2015). Induced seismicity risk analysis of the 2006 Basel, Switzerland, Enhanced Geothermal System project: Influence of uncertainties on risk mitigation. *Geothermics* **53**, 133–146.

Noack, T. & D. Fäh (2015) *Earthquake Microzonation: site effects and local geology. A case study for the Kanton of Basel-Stadt.* Unpublished report.

Plenefisch, T. & K.-P. Bonjer (1997). The stress field in the Rhine Graben area inferred from earthquake focal mechanisms and estimation of frictional parameters. *Tectonophysics* **275**, 71–97.

Ripperger, J., P. Kästli, D. Fäh & D. Giardini (2009). Ground motion and macroseismic intensities of a seismic event related to geothermal reservoir stimulation below the city of Basel - observations and modelling. *Geophys. J. Int.* **179**, 1757–1771.

SIA 261 (2003). *Actions on Structures.* Swiss Standard SIA 261, Swiss Society of Engineers and Architects, Zurich.

Steimen, S., D. Fäh, D. Giardini, M. Bertogg & S. Tschudi (2004). Reliability of building inventories in seismic prone regions. *Bull. Earthq. Eng.* **2**, 361–388.

United Nations, ed. (2006). *Human Development Report 2006 - Beyond scarcity: power, poverty and the global water crisis.* Report of the United Nations Development Programme (UNDP). Palgrave Macmillan, New York, United States.

United Nations, ed. (2008). *Human Development Report 2007/2008 - Fighting climate change: human solidarity in a divided world.* Report of the United Nations Development Programme (UNDP). Palgrave Macmillan, New York, United States.

United Nations, ed. (2009). *Human Development Report 2009 - Overcoming barriers: human mobility and development.* Report of the United Nations Development Programme (UNDP). Palgrave Macmillan, New York, United States.

United Nations, ed. (2014). *Human Development Report 2014 - Sustaining human progress: Reducing vulnerabilities and building resilience.* Report of the United Nations Development Programme (UNDP). Palgrave Macmillan, New York, United States.

Wenk, T. (2014). *Seismic zoning map of Switzerland.* DGEB Workshop: Results of the European Project SHARE: Seismic Harmonization in Europe, pp. 43–52.

Wenk, T. & D. Fäh (2012). Seismic microzonation of the Basel area. In *Proceedings of the 15th World Conference on Earthquake Engineering,* Lisbon, Portugal, September 24-28.

Wiemer, S., D. Giardini, D. Fäh, N. Deichmann & S. Sellami (2009). Probabilistic seismic hazard assessment of Switzerland: best estimates and uncertainties. *J. Seismol.* **13**, 449–478.

Wiemer, S., S. Hiemer, J. Woessner, L. Danciu, D. Fäh, B. Edwards, C. Cauzzi, C. Michel, V. Poggi, E. Kissling, P. Kaestli & D. Giardini (2014). The 2014 update of the Swiss national seismic hazard model - Key science issues. In *Proceedings of the Second European Conference on Earthquake Engineering and Seismology,* Istanbul, Turkey, August 25-29.

Worden, C.B., M.C. Gerstenberger, D.A. Rhoades & D.J. Wald (2012). Probabilistic relationships between ground-motion parameters and Modified Mercalli Intensity in California. *Bull. seism. Soc. Am.* **102**, 204-221.

A2.1.11.2 Web references

Microzonation of Basel at the Basel Geoportal: http://www.stadtplan.bs.ch/geoviewer/

Swiss Seismological Service (SED): http://www.seismo.ethz.ch/.

World Economic Outlook Database 2015:
http://www.imf.org/external/pubs/ft/weo/2015/01/ weodata/index.aspx

A2.2 February 2011 M4.7 Guy-Greenbrier (Arkansas) Earthquake, USA

This earthquake occurred on 28th February 2011, at 05.00 UTC (27th February 2011, 23:00 local time), and is one of the largest to have been registered in Arkansas outside of the New Madrid Seismic Zone. It was part of a large earthquake swarm that started around 2009 and which is believed to have been triggered by the injection of waste water at disposal wells in the vicinity of a previously unknown fault. The main shock and other strong events in the sequence were felt across a broad area, but caused only minor damage to houses, mainly in the town of Greenbrier, and no casualties.

A2.2.1 Tectonic and seismic setting

A2.2.1.1 Tectonic setting

This earthquake occurred within the Arkoma basin, in the centre of the state of Arkansas, around 60 km to the north of Little Rock, the state capital. The Arkoma basin is located just north of the Ouachita Mountains frontal faults (Figure A2.2.1), and it is bounded to the north by the Ozark Uplift (Abd *et al.*, 2012; Horton, 2012). The whole area lies within the large stable continental region of the central and eastern United States, which is characterised by a relatively lower seismic activity and low strain rates than active continental regions (Klose & Seeber, 2007), and by the fact that earthquakes tend to be felt over much larger areas (USGS).
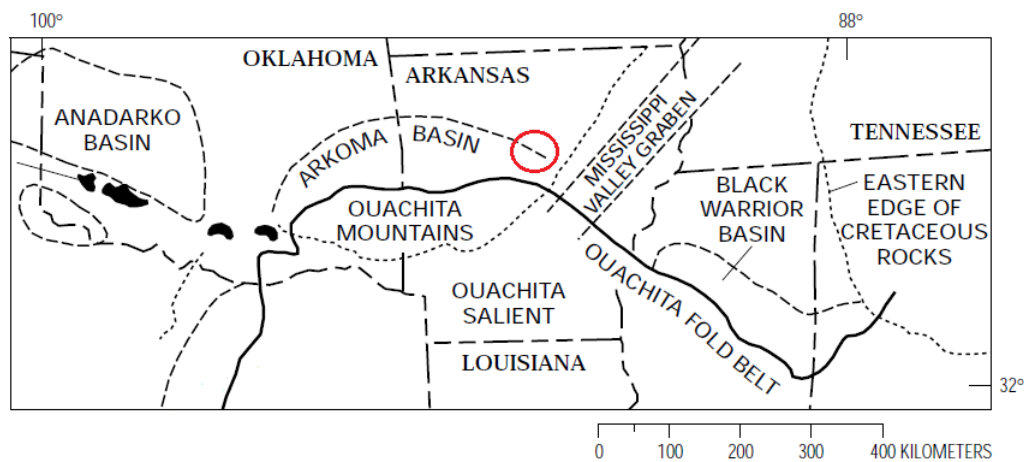
FigureA2.2.1. Tectonic map of Arkansas and surrounding areas. The red circle encloses the area around the epicentre of the 2011 Guy-Greenbrier earthquake. Modified from Perry Jr (1997).

The most relevant tectonic features of the Arkoma basin consist of normal faults, thrust faults and folds striking approximately east-west (Figure A2.2.2), originated in alternating tensional and compressional stress fields at different geological stages (Abd *et al.*, 2012). The 2011 Guy-Greenbrier earthquake sequence revealed the existence of an unknown fault striking about N30E (Figure A2.2.2) at depths between 3.0 and 7.0 km, extending from the Precambrian basement up into the Palaeozoic sedimentary rock, named "the Guy-

Greenbrier" fault by Horton (2012). This fault is suitably oriented with respect to the N60E direction of the principal compression axis of the present-day stress field in the mid-continental area for strike-slip failure (Abd *et al.*, 2012; Horton, 2012). It is noted that its orientation is similar to that of the northern segment of the New Madrid Seismic Zone, the most relevant seismic source of the state, located around 300 km to the north-east. No known seismogenic faults have surface traces within Arkansas.
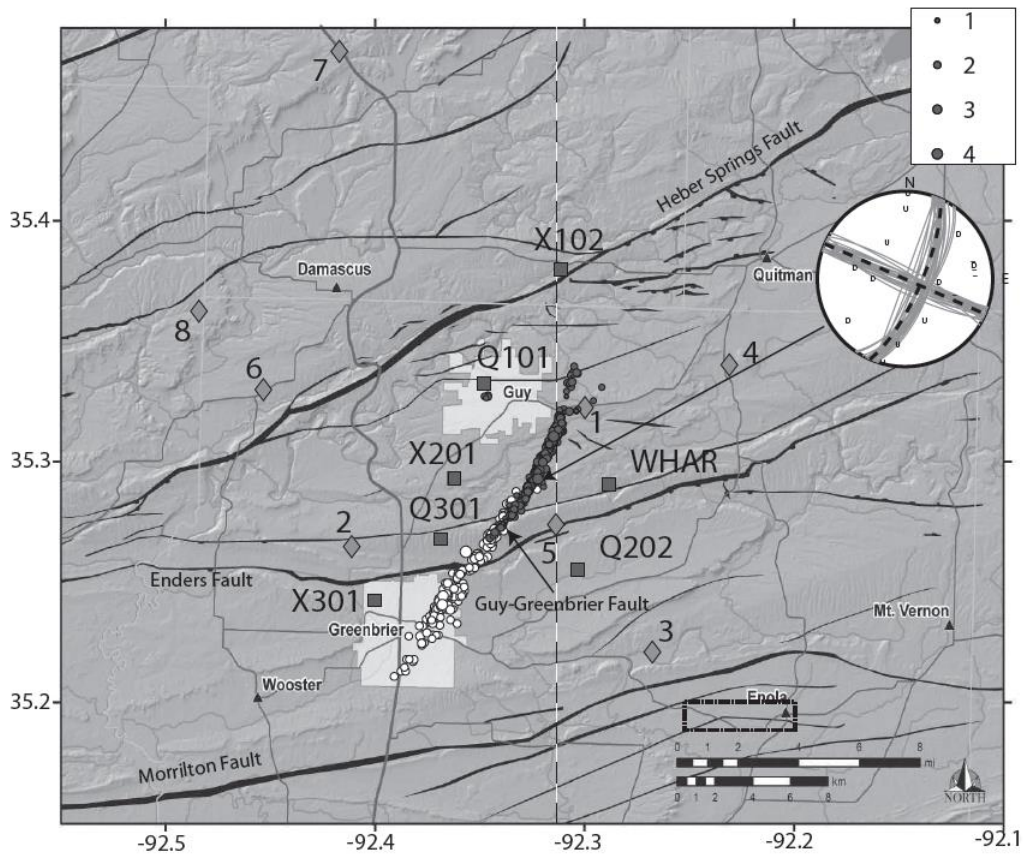
Figure A2.2.2. Known faults around the epicentral area and the newly-identified Guy-Greenbrier fault (Horton, 2012). Circles indicate the epicentres of events that occurred between 1st October 2010 and 15th February 2011 (dark gray filled) and between 16th February 2011 and 8th March 2011 (white filled). Numbered diamonds indicate waste disposal wells. First-motion focal mechanism for **M**4.0 event on 11th October 2010 shown. From Horton (2012).

A2.2.1.2 Regional and local seismicity

Seismicity rates in the area known as the central and eastern United States (CEUS) are generally low (Hough & Page, 2015). With the exception of the north-east corner of the state, which belongs to the New Madrid Seismic Zone, most of Arkansas is subject only to diffuse seismic activity consisting of scattered, isolated earthquakes, and occasional swarms (Dart & Ausbrooks, 2011; Horton, 2012). Figure A2.2.3 presents the earthquake archive catalogue of the Arkansas Geological Survey, which includes events from 1699 until 26th December 2015.

The New Madrid Seismic Zone (NMSZ) is the most hazardous fault zone to the east of the Rocky Mountains (Ausbrooks, 2010; Horton, 2012; McFarland, 2001). Four large

earthquakes with estimated magnitudes **M**7.5, **M**7.0, **M**7.3 and **M**7.5 took place in the NMSZ between 16th December 1811 and 7th February 1812, and caused extensive rise and subsidence of lands, fissures, sand blows, and large landslides, as well as damage to buildings, though limited due to the low exposure in the area. According to the United States Geological Survey (USGS), the NMSZ has produced other sequences of major earthquakes over the past 4,500 years, including several events of **M**7.0 to **M**8.0 (see Web references).
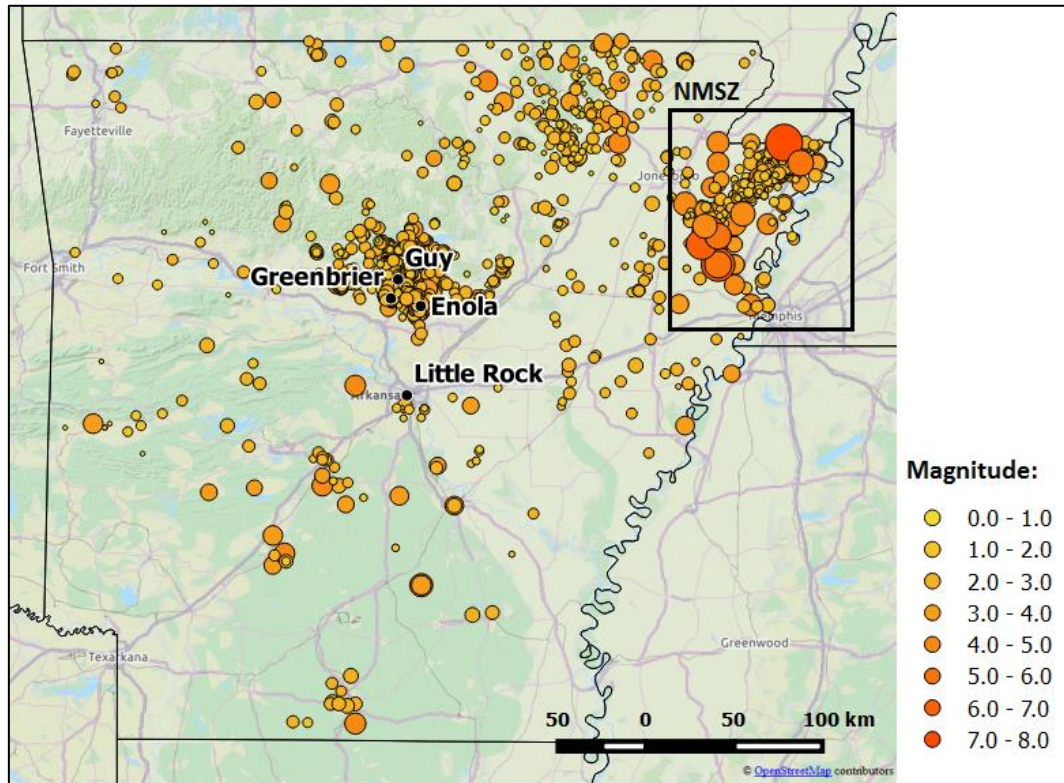
Figure A2.2.3. Earthquake catalogue (1699-2015) for Arkansas, according to the Arkansas Geological Survey. New Madrid Seismic Zone (NMSZ) marked (Arkansas Geological Survey, 2016).

Outside of the NMSZ, no earthquakes with magnitude larger than **M**4.9 have ever been recorded. Between 1699 and 2010, only twelve events with magnitudes between **M**4.0 and **M**4.9 were identified, and they actually occurred in a much narrower period of time, between 1883 and 1974. Within the Faulkner county, where Guy and Greenbrier are located, three main earthquake swarms are known to have occurred: (i) the 1982 Enola swarm, which lasted for many years and produced over 40,000 events, of which the largest was a **M**4.5, (ii) the 2001 swarm, which occurred in the same area as the 1982 one, and whose largest event was a **M**4.4, (iii) and the 2011 Guy-Greenbrier swarm itself (Abd *et al*., 2012; Ausbrooks, 2010; Horton, 2012; McFarland, 2001). The Enola swarms were located around 15.0 km to the south-east of the Guy-Greenbrier swarm. There is no report of damage from neither the 1982 nor the 2001 Enola swarms (Ausbrooks, 2010; McFarland, 2001; The Encyclopedia of Arkansas History & Culture, see Web references).

Huang & Beroza (2015) point out that even though observed seismicity along the Guy-Greenbrier fault decayed gradually after injection at the wells closer to the fault was

stopped in March 2011, it did not end abruptly but became more diffuse, and remained higher than the background seismicity rate before the 2011 sequence.

According to Horton (2012), the rupture of the entire (estimated) surface of the Guy-Greenbrier fault is capable of causing earthquakes with magnitudes up to **M**5.5-6.0, but their likelihood is unknown.

A2.2.1.3 Seismic hazard

Figure A2.2.4 shows extracts of the probabilistic seismic hazard maps for the United States of 2008 and 2014, elaborated by the United States Geological Survey (USGS). Values shown correspond to peak ground acceleration (PGA) on rock with a 10% probability of exceedance in 50 years. The area affected by the 2011 Guy-Greenbrier earthquake and the state of Arkansas are marked in red.
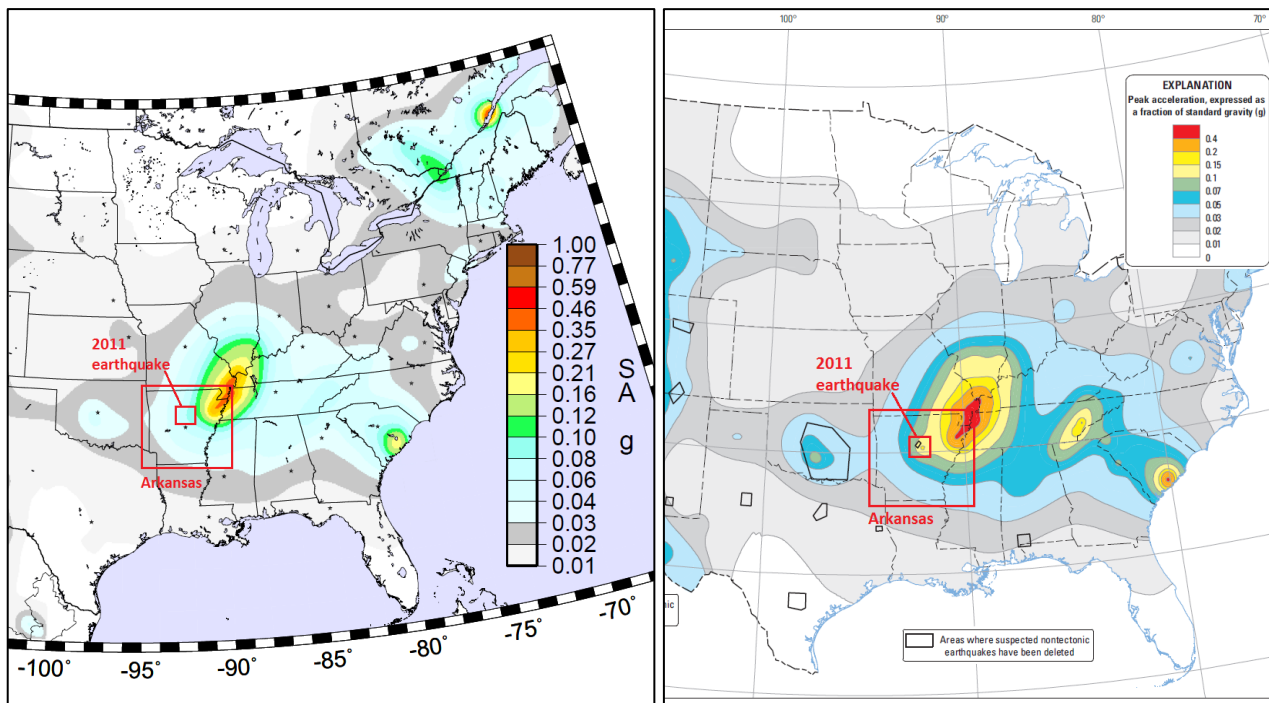
Figure A2.2.4. Extract of the 2008 (left) and 2014 (right) hazard maps for the United States, elaborated by the USGS (2016). Values correspond to peak ground acceleration (g) on rock with a 10% probability of exceedance in 50 years.

Table A2.2.1 presents a summary of the PGA values expected at Guy, Greenbrier and Little Rock. As can be observed, the expected PGA values of Guy and Greenbrier have suffered an increase of about 50% in the 2014 hazard map. The table also reports the corresponding values obtained from the Global Seismic Hazard Assessment Program (GSHAP; Giardini *et al.*, 1999; Giardini *et al.*, 2003), which are around 10% smaller than those of 2008. In spite of the discrepancies, all values support the idea that seismic hazard is moderate to low in the affected area. It should be noted that the USGS national seismic hazard maps do not take into consideration induced seismic activities.

Table A2.2.1. Peak ground acceleration (PGA, g) values on rock with a 10% probability of exceedance in 50 years according to the 2008 and 2014 USGS hazard maps, and results from the Global Seismic Hazard Assessment Program (GSHAP), at relevant locations in Arkansas.

PLACE	USA 2008	USA 2014	GSHAP
Guy	0.0750	0.1124	0.0669
Greenbrier	0.0731	0.1118	0.0641
Little Rock	0.0653	0.0802	0.0590

A2.2.2 Earthquake source characteristics

A2.2.2.1 Location, depth and time

The main shock occurred on 28th February 2011, at 05.00 UTC (27th February 2011, 23.00 local time).

Several organizations and agencies report their own estimations of the epicentral coordinates and hypocentral depth. The information reported in the websites of the National Earthquake Information Center (NEIC) of the United States Geological Service (USGS), the Global Centroid Moment Tensor Project (GCMT) and the International Seismological Centre (ISC) is summarized in Table A2.2.2. The Arkansas Geological Survey reports the same coordinates and depth as the USGS. Cells marked as (*f) correspond to parameters that were held fixed while inversion was carried out to retrieve those that remain.

Table A2.2.2. Epicentral coordinates and hypocentral depths from different sources.

	Agency / Publication	Latitude	Longitude	Depth (km)
NEIC	National Earthquake Information Center, USGS	35.2650 ° N	92.3440 °W	3.80
GCMT	Centroid Global Centroid Moment Tensor Project (**)	35.3800 ° N	92.3700 °W	12.00 (*f)
ISC	International Seismological Centre - GEM catalogue	35.3264 ° N	92.3004 °W	10.00 (*f)

(*f) fixed parameter used for inversion

(**) centroid (not-hypocentral) location

According to Horton (2012), the events recorded between late September 2010 and 4th March 2011 occurred at depths between 3.00 and 7.00 km, and the hypocentre of the main shock in particular was located at a depth of around 6.00 km. Abd *et al.* (2012) give a range of hypocentral depths between 1.00 and 7.00 km for events recorded between September 2009 and August 2011.

The map in Figure A2.2.5 shows the different estimations of the epicentral coordinates enumerated above, together with the faults identified by the USGS around the area (Stoeser *et al.*, 2007). The Guy-Greenbrier fault (shown in red) is not yet part of the USGS database because its existence was not known until after the 2011 sequence (Horton,

2012). Note that coordinates reported by the GCMT correspond to the location of the centroid, and not the hypocentre.
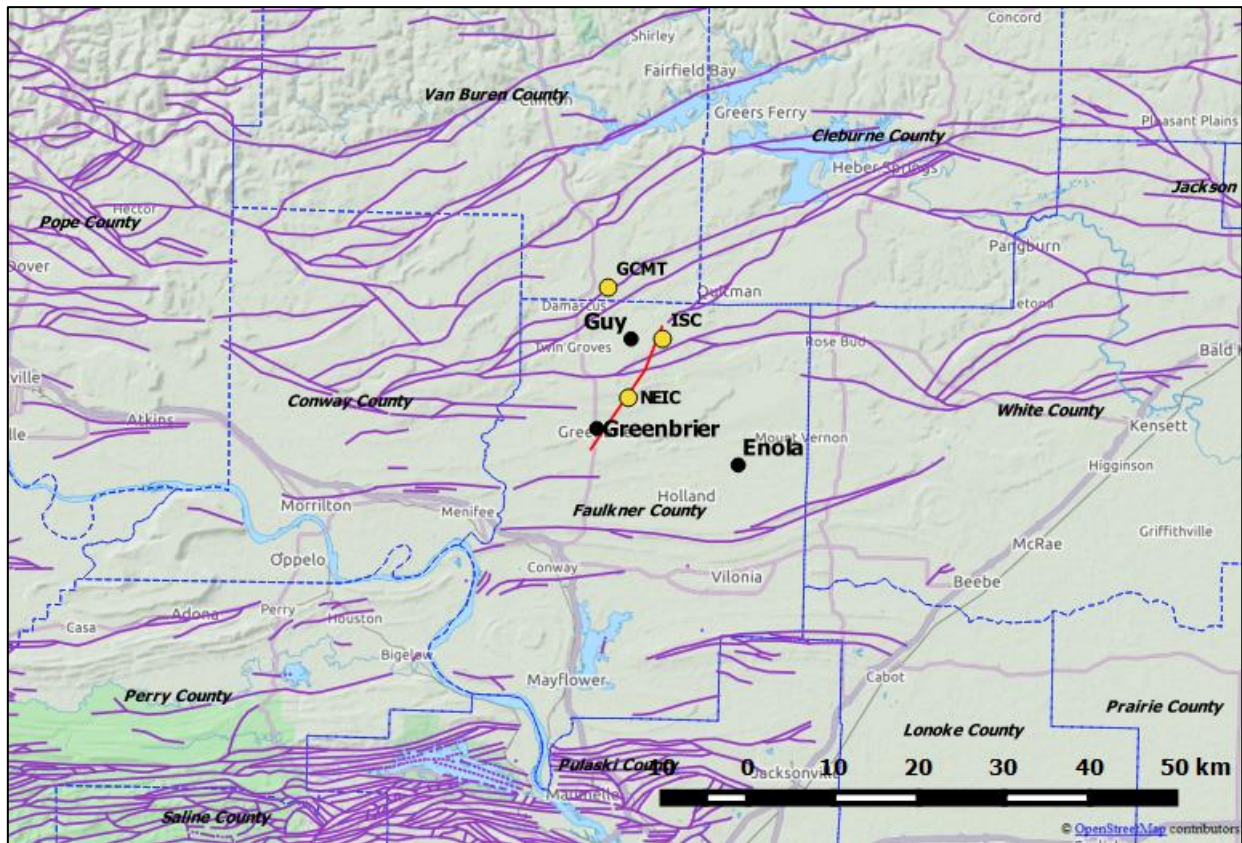
Figure A2.2.5. Estimation of epicentral coordinates (yellow circles). Faults in the area marked in violet, according to the USGS (Stoeser *et al.*, 2007; USGS, 2016). Approximate trace of the Guy-Greenbrier fault, as suggested by Horton (2012), shown in red.

A2.2.2.2 Magnitude

Estimations of magnitude made by the same agencies are reported in Table A2.2.3.

Table A2.2.3. Estimations of moment magnitude (**M**), body-wave magnitude (mb) and surface-wave magnitude (Ms).

Agency		M	mb	Ms
NEIC	National Earthquake Information Center, USGS	4.7	4.4	-
GCMT	Global Centroid Moment Tensor Project	4.8	4.4	4.8
ISC	International Seismological Service (inversion)	-	4.5	4.2

A2.2.2.3 Style-of-faulting

The fault plane solutions for the main shock indicate a right-lateral strike-slip mechanism, with a small extensional component. The Centroid Moment Tensor is significantly non-double couple, which is typical of fluid-injection triggered events, for it is an indicator of a volumetric change.

Table A2.2.4 summarizes the fault plane solutions calculated by the USGS and the GCMT, while Figure A2.2.6 shows the corresponding plot for the centroid moment tensor (GCMT) . Note that, being the dip very close to 90° in all cases, a 26° strike and a 211° strike are practically equivalent.

Table A2.2.4. Fault plane solutions and fault planes from different sources. Fault planes marked in grey are the preferred solution in each case.

Fault Plane 1			Fault Plane 2			Source
Strike	Dip	Rake	Strike	Dip	Rake	
295	80	-5	26	85	-170	Regional Moment Tensor NEIC (USGS)
301	71	1	211	89	161	GCMT
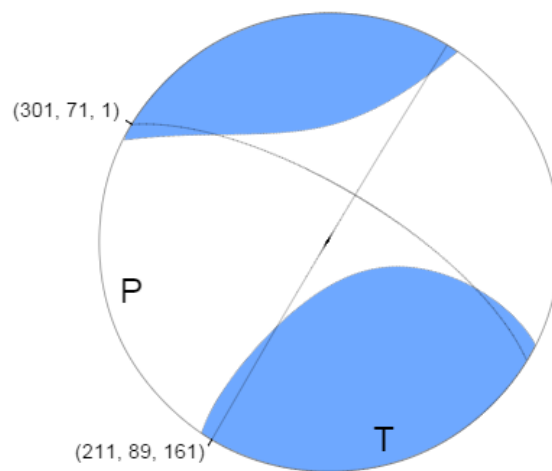
Figure A2.2.6. GCMT centroid moment tensor for the main shock. From the USGS website.

A2.2.2.4 Stress drop

No information could be found regarding the stress drop of this event. However the personal website of Dr. Yihe Huang, from Stanford University, mentions ongoing work on the subject (see Web references).

A2.2.2.5 Foreshocks and aftershocks

The exact moment at which the Guy-Greenbrier earthquake swarm started is not clear, though it is believed to be directly related to the first waste disposal well of the area becoming operational in April 2009. According to Horton (2012), there was a noticeable change in the number of earthquakes with magnitudes equal to or larger than 2.5, which increased from one in 2007 and two in 2008, to ten in 2009, 54 in 2010 and 157 in 2011. Nevertheless, Horton (2012) believes that no earthquakes occurred along the Guy-Greenbrier fault itself prior to the start of injection at well number 1 (Figure A2.2.2) on 7th July 2010. Three of the most relevant foreshocks occurred shortly after well number 5 (Figure A2.2.2) was activated in September 2010. These were a **M**4.0, a **M**3.8 and a **M**3.9,

which occurred on 11th October, 15th October and 20th November, respectively, and were widely felt across northern Arkansas and southern Missouri. After a two-month halt, seismic activity resumed by mid-February 2011. The largest foreshock of the series was a **M**4.1 event that took place on 18th February 2011.

Wells 1 and 5 were shut down on 4th March 2011, but the Guy-Greenbrier swarm did not come to a full stop immediately (Horton, 2012). The observed seismicity decayed steadily during the three months that followed but, according to Huang & Beroza (2015), it remained higher during 2012-2014 than the background seismicity rate before the 2011 sequence. Huang & Beroza (2015) detected more than 460,000 earthquakes between July 2010 and October 2011 by means of single-station template matching, a technique that allows to detect particularly small earthquakes in areas of sparse instrumentation.

A2.2.2.6. Nature of earthquake

In spite of the difficulties that exist in establishing an unequivocal link between seismic events and waste disposal wells, several authors agree that the 2011 Guy-Greenbrier earthquake sequence was a triggered swarm (Abd *et al.*, 2012; Horton, 2012; Huang & Beroza, 2015; Llenos & Michael, 2013).

Abd *et al.* (2012), found a strong correlation between fluid injection at wells 1 and 5 (Figure A2.2.2) and seismic activity. Horton (2012), Huang & Beroza (2015) and Llenos & Michael (2013) concluded that the change in seismicity rates observed in the Guy-Greenbrier area since 2009 is too significant to be due to random fluctuations in seismicity rates. In particular, Huang & Beroza (2015) observed that, during the operation of nearby injection wells, seismicity around the Guy-Greenbrier area deviated from the Gutenberg-Richter law, but returned to it after injection was halted. Apart from this temporal correlation, Horton (2012) points out that 98% of the earthquakes that occurred in the area in 2011 occurred within 6 km of one of three waste disposal wells, after the start of injection at those wells.

Within the earthquake archive catalogue of the Arkansas Geological Survey (Figure A2.2.3), the earthquakes that make up the Guy-Greenbrier earthquake sequence are tagged as "probable triggered" events.

A.2.2.3 Geology and ground conditions in the affected area

A2.2.3.1 Regional geology and topography

Guy and Greenbrier lie over the Arkansas River Valley, one of the five physiographic regions of the state (Figure A2.2.7). It is a low-lying region surrounding the Arkansas River and its major tributaries. Its Precambrian crystalline basement is overlain by thick layers of Palaeozoic sedimentary rocks (Horton, 2012). These consist of a sequence of coal-bearing sandstones and shale arranged into east-west trending open folds (anticlines and

synclines) and faults, which are a consequence of the compression stresses the area was subject to during the formation of the Ouachita orogenic system (Arkansas Geological Survey, see Web references). The Arkansas River Valley region serves as a transition zone between the Ozark plateaus, an area of fairly flat-lying rock formations, and the latter.

The sedimentary layers at the Arkansas River Valley region are part of the buried section of the Ozark aquifer, which is mainly formed by dolostone, limestone and sandstone. The Guy-Greenbrier fault partially cuts the Ozark aquifer, and penetrates 2.0-3.0 km into the Precambrian basement rock.
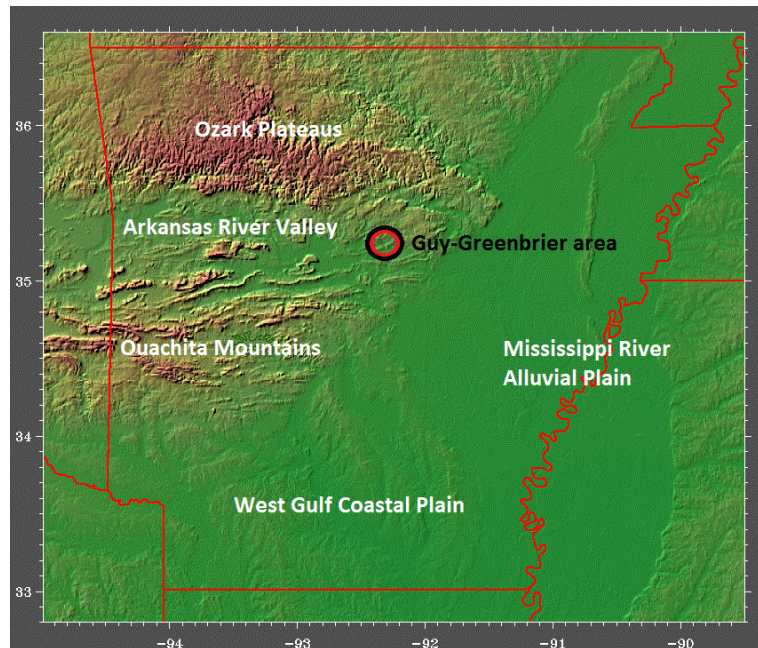
Figure A2.2.7. Topographic map and physiographic regions of the state of Arkansas. Topographic map by Ray Sterner, Applied Physics Laboratory, Johns Hopkins University (1995).

A2.2.3.2 Site conditions in the affected area

The map in Figure A2.2.8 shows the National Earthquake Hazards Reduction Program (NEHRP) soil classification map of Arkansas (Ausbrooks & Doerr, 2008a). As can be observed, the towns of Guy and Greenbrier are located over soil type B, which corresponds to rock with V_{s30} values between 760 and 1500 m/s. The map also shows that soils around the Arkansas river and in the Mississippi river alluvial plain are susceptible to liquefaction. Within the HAZUS scheme, the Guy-Greenbrier area belongs to a liquefaction susceptibility level of 1, corresponding to "very low", on a scale that goes from 0, "none", to 5, "very high" (Ausbrooks & Doerr, 2008b).
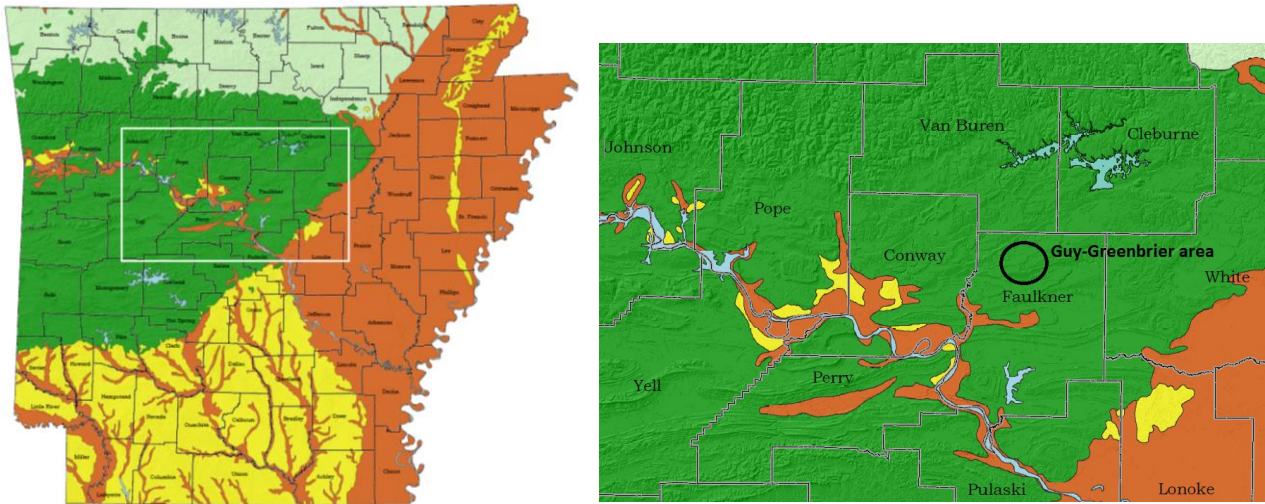
Figure A2.2.8. NEHRP soil classification map of Arkansas, by the Arkansas Geological Survey (Ausbrooks & Doerr, 2008a): rock (soil type B, dark green), regolith, weathered shales, cemented gravels, hard and/or stiff/very stiff soils (soil type C, light green), sands, silts and/or stiff/very stiff clays, loess, gravels (soil type D, yellow), and soils vulnerable to potential failure or collapse under seismic loading such as liquefiable soils, quick and highly sensitive clays, collapsible, weakly cemented soils (soil type F, brown).

A2.2.4 Ground motions

A2.2.4.1 Intensity observations

According to the written report at the USGS website, the Modified Mercalli Intensities (MMI) observed were the following: V (moderate shaking, minor damage) at Greenbrier, IV (light shaking) at Bee Branch, Clinton, Concord, Conway, Damascus, Edgemont, Enola, Glencoe, Higden, Hindsville, Judsonia, Kingston, Lepanto, Lockesburg, Oil Trough, Onia, Parthenon, Quitman, Roland, Timbo, Tuckerman, West Helena and Witts Springs, and III (weak shaking) in much of central and northern Arkansas, in parts of eastern Oklahoma and southern Missouri, and in the Memphis, Tennessee area. It was also felt in parts of Alabama, Illinois, Indiana, Kansas, Kentucky, Louisiana, Mississippi and Texas. Figure A2.2.9 shows the corresponding automatically calculated USGS ShakeMap.

A2.2.4.2 Ground motion recordings

Five three-component accelerograms are available for this event from the Center for Engineering Strong Motion Data (CESMD), with epicentral distances between 180 and 420 km. Peak ground acceleration (PGA) values for other five stations with epicentral distances between 440 and 470 km are available at the website of the USGS. The location, epicentral distance and recorded PGA values for the ten stations are summarized in Table A2.2.5. As can be observed, motion at these stations was extremely weak. As an example, the plots for the acceleration time-histories recorded at station 7404, located in Memphis, Tennesee, 211 km away from the epicentre, are shown in Figure A2.2.10. Unfortunately, no records are readily available for the near-field.
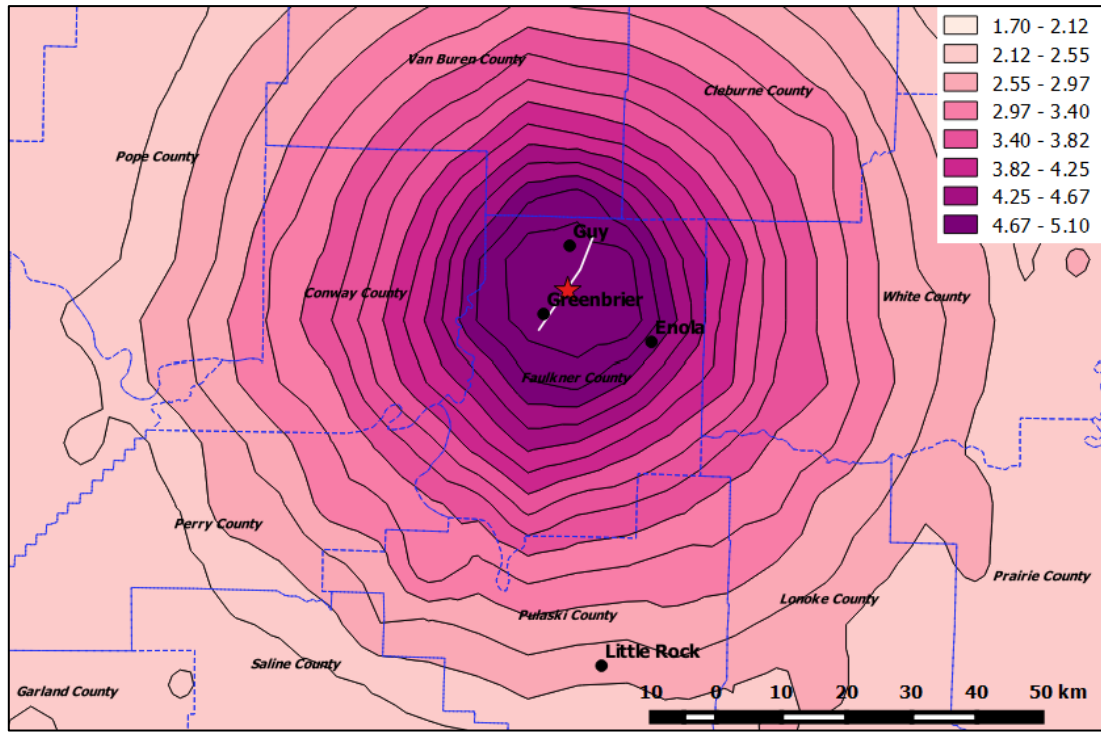
Figure A2.2.9. USGS ShakeMap in terms of Modified Mercalli Intensities (MMI), initial automatic calculation. The red star is the epicentre of the main shock, according to the USGS. Approximate trace of the Guy-Greenbrier fault shown in white.
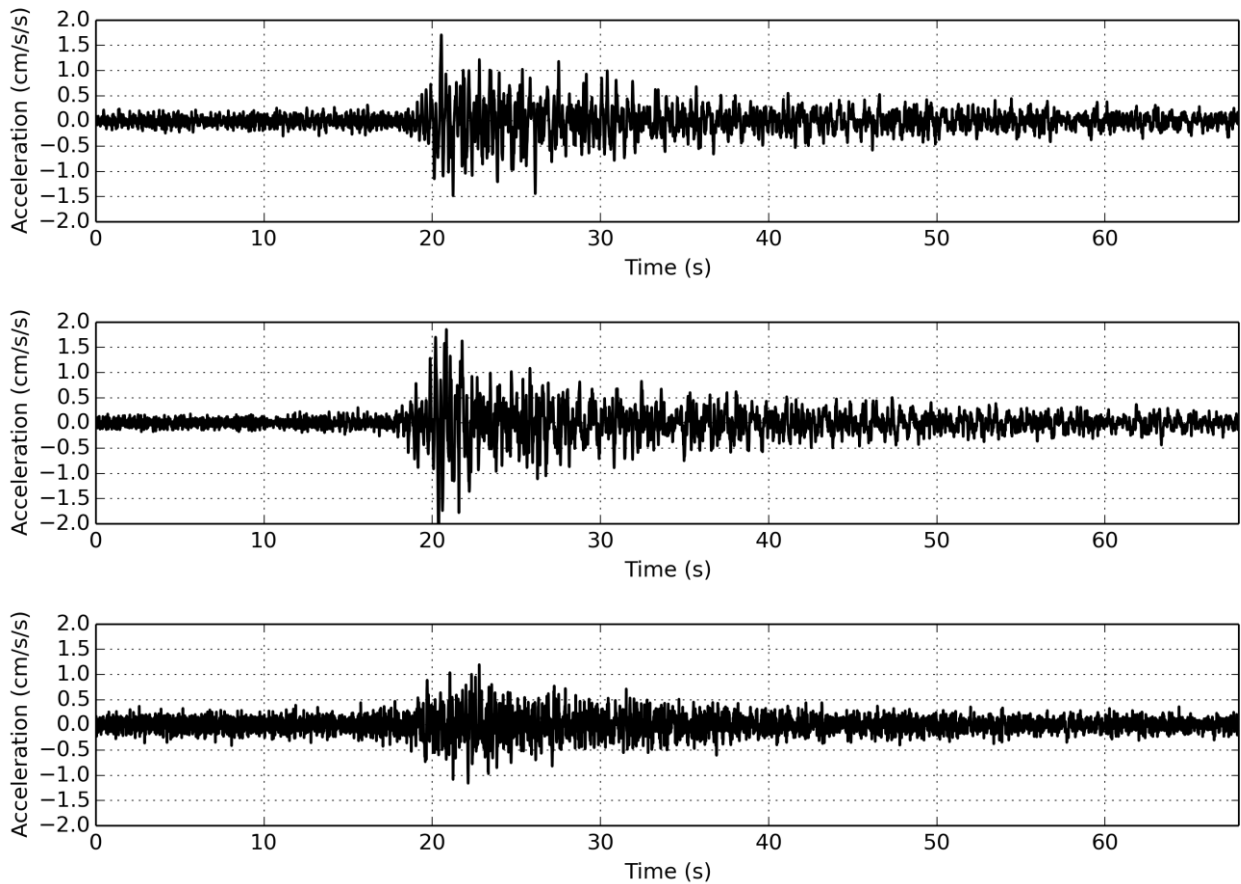
Figure A2.2.10. Horizontal (top and centre) and vertical (bottom) acceleration time-histories recorded for the main shock at station 7404, located in Memphis, Tennessee, 211 km away from the epicentre. Waveform data from the Center for Engineering Strong Motion Data (CESMD, 2016).

Figure A2.2.11 and Figure A2.2.12 show the pseudo-acceleration and displacement response spectra for the five records whose waveforms are available from the CESMD, obtained using the OpenQuake ground motion toolkit (Weatherill, 2014).

Table A2.2.5. Main characteristics of waveforms and recording stations for ten records of the main shock, available from the CESMD and the USGS. Epicentral distances as reported by the sources.

Station	Station Name	Latitude	Longitude	Epi. Dist. (km)	PGA (cm/s²)			Source
					Horiz. 1	Horiz. 2	Vertical	
2459	Paragould - Post Office	36.0570 ° N	90.4880 °W	189.3	1.546	1.945	1.089	(A)
7404	TN Memphis - VAMC, Bldg 6	35.1440 ° N	90.0260 °W	211.1	1.708	2.309	1.194	(A)
2454	Campbell - Fire Station	36.4940 ° N	90.0760 °W	245.8	1.163	1.339	0.587	(A)
2457	Dexter- Fire Station 2	36.7960 ° N	89.9660 °W	273.2	1.592	2.055	0.521	(A)
2491	St. Louis - Visitors Ctr	38.6260 ° N	90.1910 °W	419.2	1.280	1.528	0.405	(A)
OK002	Wilshire Boulevard, Harrah, OK	35.5490 ° N	97.1970 °W	442.0	0.076	0.082	0.148	(B)
OK005	Luther Middle School, Luther, OK	35.6550 ° N	97.1910 °W	442.1	0.061	0.068	0.143	(B)
OK001	Jones High School, Jones, OK	35.5610 ° N	97.2890 °W	450.4	0.061	0.071	0.103	(B)
OK009	Oakdale Elementary School, Edmond, OK	35.5810 ° N	97.4230 °W	462.6	0.418	0.282	0.560	(B)
OK004	Oklahoma Science Museum, OK	35.5230 ° N	97.4750 °W	467.1	0.055	0.076	0.097	(B)

(A) Processed records downloaded from the CESMD Strong Motion Center (http://www.strongmotioncenter.org).

(B) Data from the USGS (http://earthquake.usgs.gov/earthquakes/shakemap/global/shake/022811a/download/stationlist.txt). Waveforms not directly available.
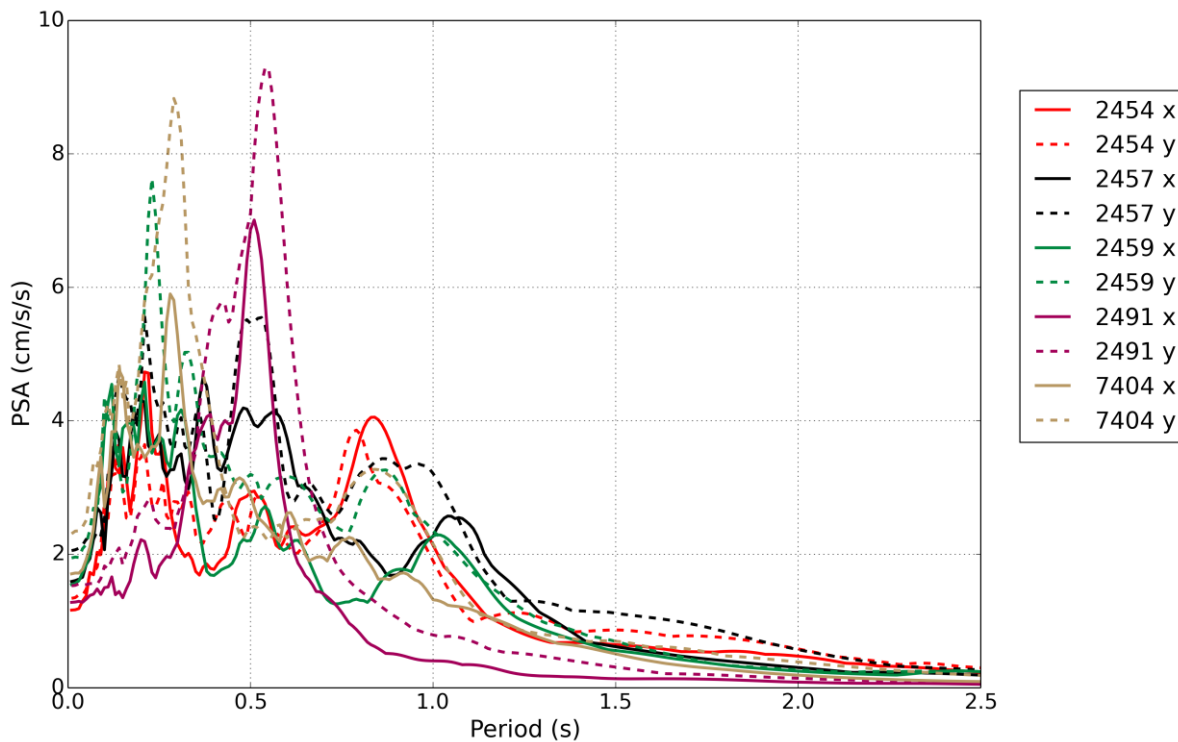
Figure A2.2.11. Pseudo-acceleration response spectra for each of the two horizontal components (x, y) of the five available accelerograms. Waveform data from the CESMD.
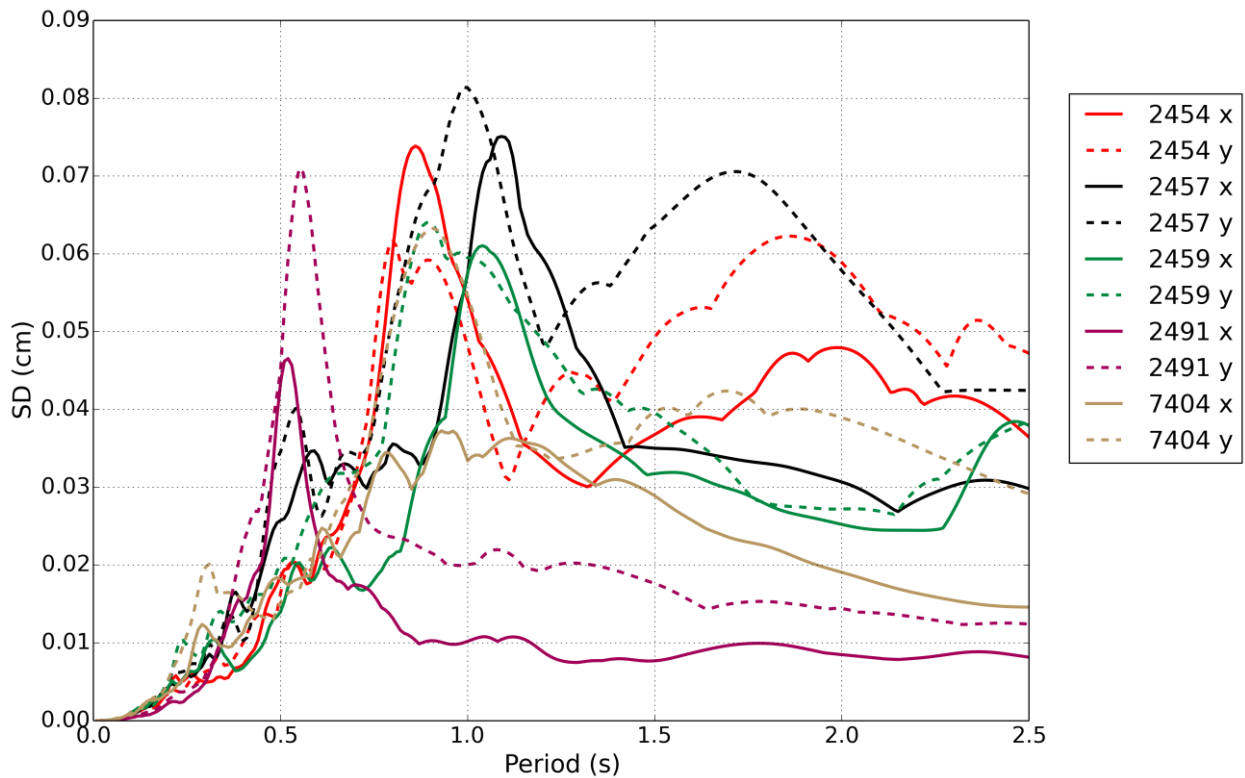
Figure A2.2.12. Pseudo-displacement response spectra for each of the two horizontal components (x, y) of the five available accelerograms. Waveform data from the CESMD.

A2.2.4.3 Inferred shaking levels

In their website, the USGS provides an estimation of the peak ground acceleration values expected to have been observed during the earthquake, based on information from reports of felt intensity and recording stations, where available. This estimation results of special interest for this event for which direct information from records is only available for epicentral distances larger than 180 km. The map on the left of Figure A2.2.13 shows the acceleration ShakeMap automatically generated by the USGS soon after the event, while the map on the right shows the acceleration contours that can be downloaded from the website. Given the difference in scale, the map on the right allows for higher values of PGA to be better appreciated. According to these maps, Guy and Greenbrier may have been subject to PGA values of around 10% g.

A2.2.4.4 Duration of ground shaking

The significant duration of a waveform is defined as the time lapse between the release of the 5% and 95% of the Arias Intensity. The significant duration of the five records from the CESMD database was calculated for each horizontal component using the OpenQuake ground motion toolkit (Weatherill, 2014). Results are shown in Table A2.2.6.
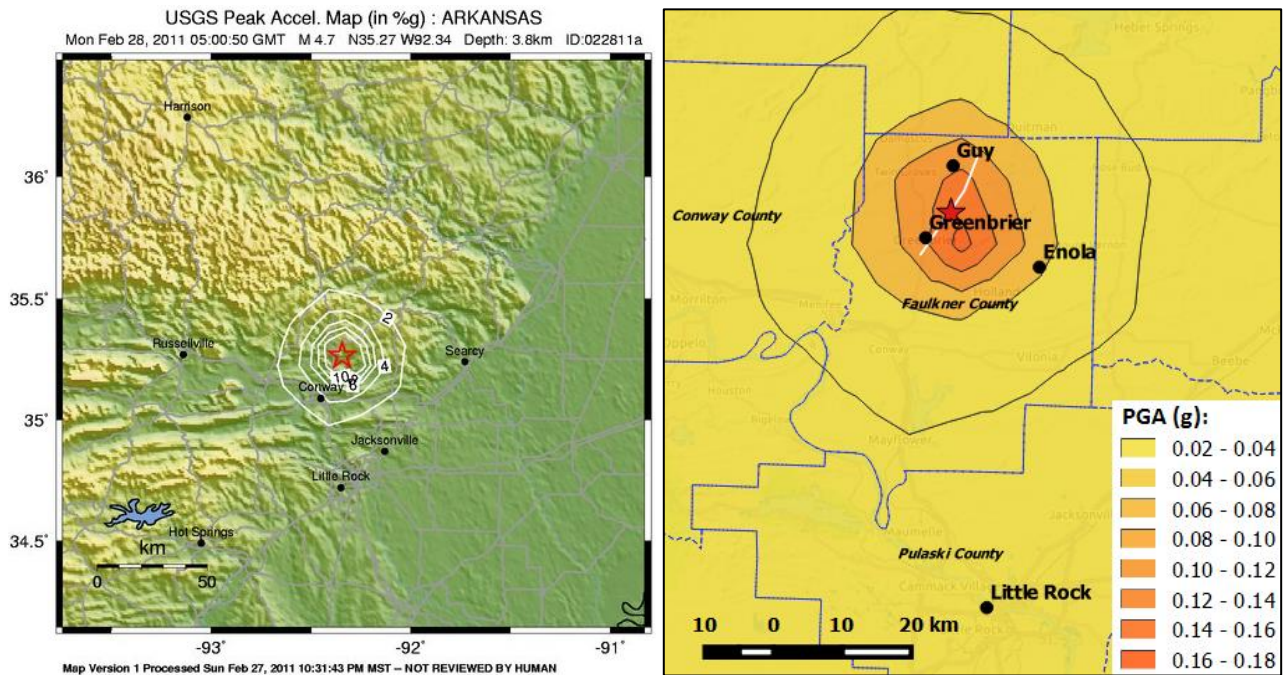
Figure A2.2.13. USGS ShakeMaps in terms of peak ground acceleration: initial automatic calculation, as reported on the USGS website (left), and contour lines shapefile downloaded from the website (right). Note the difference in scale between the two figures (USGS, 2016).

Table A2.2.6. Significant duration (in seconds) of the ground motions available from the CESMD (2016).

Station	Station Name	Latitude	Longitude	Repi (km)	X component	Y component
2459	Paragould - Post Office	36.0570 ° N	90.4880 °W	189.3	36.8	30.8
7404	TN Memphis - VAMC, Bldg 6	35.1440 ° N	90.0260 °W	211.1	35.1	32.7
2454	Campbell - Fire Station	36.4940 ° N	90.0760 °W	245.8	34.9	38.3
2457	Dexter- Fire Station 2	36.7960 ° N	89.9660 °W	273.2	38.6	33.3
2491	St. Louis - Visitors Ctr	38.6260 ° N	90.1910 °W	419.2	26.8	16.4

Estimations of earthquake significant durations can be obtained by means of prediction equations such as those of Bommer *et al.* (2009) and Kempton & Stewart (2006). Horton (2012) estimated that the area that ruptured during the main event was less than 4 km^2, which can be approximated by a square with a 2 km side, or a circle with a 2.25 km diameter. Based on these numbers, it seems reasonable to estimate the depth to the top of the rupture as the hypocentral distance minus 1 km. Two alternative values were finally considered to be used with the equation of Bommer *et al.* (2009), using the hypocentral depth reported by the USGS (3.8 - 1.0 = 2.8 km), on one hand, and that estimated by Horton (2012) (6.0 - 1.0 = 5.0 km), on the other. A series of distances were considered, including an approximation to the epicentral distances to the towns of Guy and Greenbrier (~6.00 km), and values covering the stations for which information on significant duration is available. In view of the lack of information regarding the site conditions at the recording stations, two extreme values of V_{s30} were considered: 180 m/s, the lower bound for NEHRP soil type D, which may be the soil type of station 2459, based on the NEHRP soil

classification map of Arkansas (Ausbrooks & Doerr, 2008a), and 1500 m/s, the upper bound for NEHRP soil type B, which corresponds to that of Guy and Greenbrier (see Figure A2.2.8). Results obtained are plotted in Figure A2.2.14.

As can be observed, V_{s30} has a stronger influence on the results than the depth to the top of the rupture when using the equation of Bommer *et al.* (2009). When compared to the values yielded by this equation, the significant durations of the records from stations 2459, 7404, 2454 and 2457 are closer to the curves obtained using a V_{s30} of 180 m/s. When compared to the outcome of the equation by Kempton & Stewart (2006), the durations of these stations are reasonably around the two alternative curves. It is, thus, noted that V_{s30} has a more significant influence when using the equation of Bommer *et al.* (2009) than when using that of Kempton & Stewart (2006). The significant duration of the components of station 2491 seem closer to those calculated with the equation of Bommer *et al.* (2009) using a V_{s30} value of 1500 m/s.
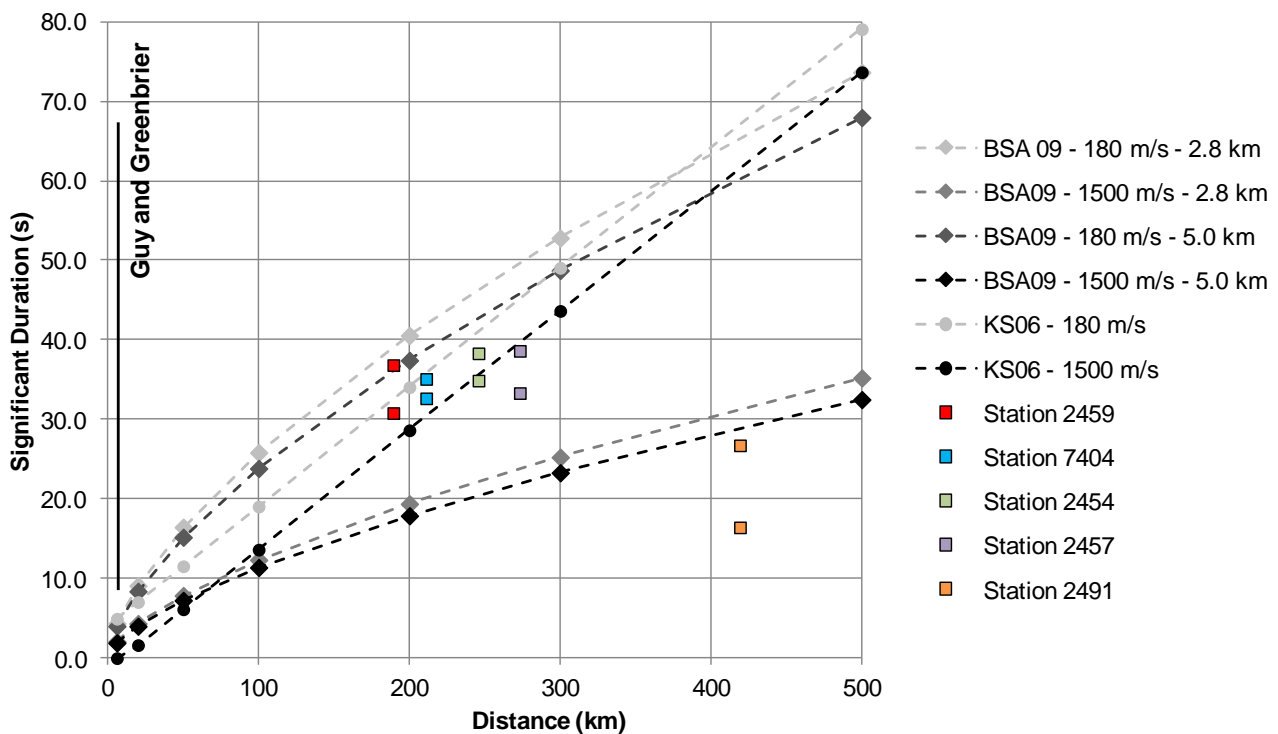
Figure A2.2.14. Estimation of the significant duration of the main shock, using prediction equations by Bommer *et al.* (2009, BSA) and Kempton & Stewart (2006, KS), and significant duration calculated for the two horizontal components of the five available accelerograms.

The Arkansas Democrat-Gazette (see Web references) reports dispatchers having said that the shaking in Greenbier lasted for about 2 seconds. The equation of Bommer *et al.* (2009) yields values of significant duration of 2.09 and 1.93 seconds, for depths to the top of the rupture of 2.8 and 5.0 km, respectively, for a closest distance to the fault rupture of 6.00 km, and V_{s30} of 1500 m/s, which is the upper bound for the type of soil conditions expected in Greenbrier (Ausbrooks & Doerr, 2008a). The equation of Kempton & Stewart (2006) cannot calculate the significant duration under these conditions, and yields negative results.

A2.2.5 Collateral earthquake hazards

A2.2.5.1 Surface rupture

According to the characterisation of the geometry of the rupture provided by Horton (2012), which can be summarized in Figure A2.2.15, this earthquake did not reach the surface. As mentioned earlier, Horton (2012) estimated that the area that ruptured during the main event was less than 4 km².
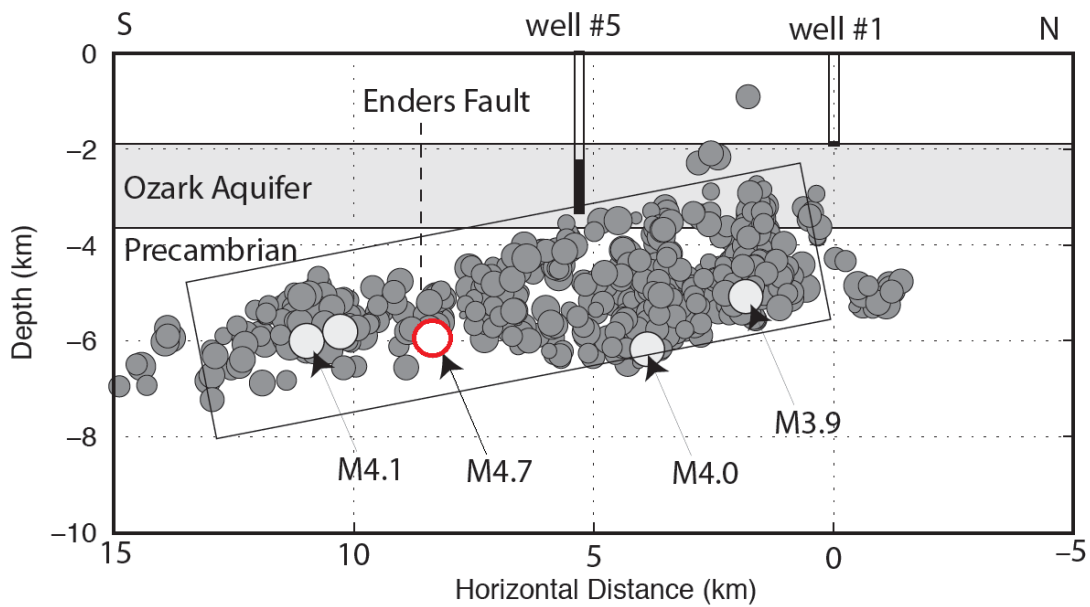
Figure A2.2.15. Cross section along the Guy-Greenbrier fault, showing the hypocentres of the **M**4.7 main shock and three foreshocks (Horton, 2012).

A2.2.5.2 Landslides

No landslides reported for this event.

A2.2.5.3 Liquefaction

No liquefaction reported for this event.

A2.2.6 exposed population

A2.2.6.1 Socio-economic setting

According to the 2014 Human Development Report (United Nations, 2014), the Human Development Index (HDI) for the United States in 2013 was 0.914, while its Inequality-adjusted HDI (IHDI) was 0.755. This located the USA in the 5th place in the world's ranking, while the Netherlands ranks 4th. The following table compares the HDI and IHDI for both countries from the last three Human Development Reports (United Nations, 2011; United Nations, 2013; United Nations, 2014). The column "Adj. HDI" provides the HDI values given in the 2014 report for previous years, adjusted for data consistency in time.

Table A2.2.7. Human Development Index and Inequality-adjusted Human Development Index for the United States and the Netherlands.

Report	Data	Unites States of America				Netherlands			
		HDI	IHDI	Rank	Adj. HDI	HDI	IHDI	Rank	Adj. HDI
2011	May 2011	0.910	0.771	4	0.911	0.910	0.846	3	0.914
2013	October 2012	0.937	0.821	3	0.914	0.921	0.857	4	0.915
2014	November 2013	0.914	0.755	5	-	0.915	0.854	4	-

Table A2.2.8 presents a comparison between the United States and the Netherlands in terms of GDP, GDP per capita and unemployment rate. During 2011, the unemployment rate in Arkansas was around 0.5% smaller than that of the US as a whole (US Bureau of Labor Statistics, see Web references).

Table A2.2.8. Gross domestic product (GDP), GDP per capita and unemployment rate for the United States and the Netherlands, according to the World Economic Outlook Database 2015.

Indicator	Units	Unites States		Netherlands	
		2011	2014	2011	2014
Gross domestic product, current prices	Billions of US dollars	15,517.925	17,418.925	894.576	866.354
Gross domestic product per capita, current prices	US dollars	49,724.999	54,596.653	53,589.909	51,372.963
Unemployment rate	% of total labor force	8.942	6.150	4.980	7.395

Though employing only 3% of its population, the agricultural sector remains fundamental to the economy of Arkansas. According to the 2012 Census of Agriculture (see Web references), 40.6% of its surface is dedicated to farming, and the state ranks 14th in the country with respect to the total value of agricultural products sold. The main industries in Arkansas include food processing, electric equipment, fabricated metal products, and paper products. According to the United States Energy Information Administration (EIA), marketed natural gas production in Arkansas has experienced a nearly six-fold increase between 2005 and 2014. The state ranked 8th in the national natural gas marketed production during 2014, accounting for 4.1% of the total marketed production of the country, and 15th in the total national energy production in 2013.

The large economic crisis that began in 2008 had a significant impact on the United States, causing high unemployment, an increasing federal debt and inflation. In 2011, the Gross Domestic Product (GDP) increased in 43 of the 50 states of the USA. The state of Arkansas was not amongst the states with the largest growth, and experienced just a 0.3% increase in its GDP, a value that positioned it within the second to lowest quintile (Bureau of Economic Analysis, U.S. Department of Commerce). During the year 2012, the state of Arkansas ranked 48th with respect to GDP per capita, with a value that was a 25% lower than that of the USA as a whole. Nevertheless, it was also the 5th cheapest state to live in and the 2nd cheapest state to do business during that same year, according to CNBC's America's Top States for Business 2012 (see Web references).

A2.2.6.2 Population density and distribution

The area around the epicentre of this event is sparsely populated. Table A2.2.9 shows the population by 1st April 2010 of some relevant towns around the epicentral area. According to the United States Census 2010 (U.S. Census Bureau, 2012), population density in the year 2010 for Faulkner County, where the epicentre was located, was 67.5 people/km^2, while the overall density for the state of Arkansas is 21.6 people/km^2. The density of housing units per area is around 29 housing units /km^2 for Faulkner County and 10 housing units /km^2 for the whole of Arkansas.

Table A2.2.9. Population of some relevant towns in the epicentral area (only urban population considered) (Quickfacts, 2016).

City	Population 1st April 2010
Guy	708
Greenbrier	4,712
Conway	58,908
Damascus	382
Enola	338
Quitman	762
Holland	557
Wooster	860
Vilonia	3,815
Menifee	302
Center Ridge	388

The USGS PAGER exposure report generated around 30 minutes after the main shock estimates that approximately thirty-five and ninety-four thousand people were exposed to shaking of intensities V and IV in the Modified Mercalli Intensity (MMI) scale, respectively, while around 1.3 million people were exposed to intensities between II and III (Figure A2.2.16). Note that these numbers are much larger than those of Table A2.2.9 because Table A2.2.9 reports strictly on the urban population of the enumerated towns, while the USGS PAGER exposure report considers all of the exposed population.
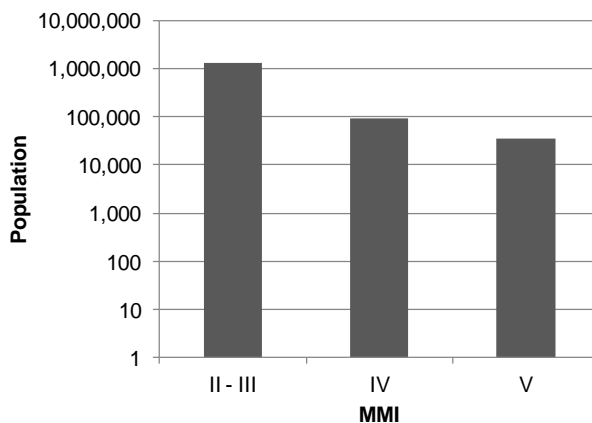
Figure A2.2.16. Estimation of total population exposed to different Modified Mercalli Intensities (MMI) 35 hours after the main shock (USGS, 2016)

A2.2.6.3 Time of day of earthquake

The main shock occurred on 28th February 2011, 23.00 local time. Given the type of damage and the absence of casualties, the time of occurrence of the event did not have a significant impact over its consequences.

A2.2.7 Characteristics of exposed building stock

A2.2.7.1 Seismic design codes

While Cutcliffe (2000) believes that it was the 1906 San Francisco earthquake which marked the start of a real interest in earthquake engineering and seismic design in the United States, Freeman (1932) stated a quarter of a century later that "the art of constructing earthquake-resisting buildings is still in the formative stage, that there are differences of opinions among experts and that there is much deficiency in important data". Further, he points at the 1925 Santa Barbara earthquake to have been more significant in raising awareness on the subject. It was this devastating event that prompted the first edition of the Uniform Building Code (UBC) in 1927, which contained the first written seismic design provisions for a regional level, but which did not become mandatory until 1961 (Beavers, 2002).

As recapitulated by Beavers (2002), the origin of seismic design codes and building codes in general in the USA started in a fragmented fashion, by regions or states. For example, the Uniform Building Code (UBC) just mentioned above was typically used west of the Mississippi river. The National Building Code of the Building Officials and Code Administrators (BOCA) (known as the BOCA Code) was, instead, used in the upper midwest and northeast. It was first published in 1950, including seismic design provisions. In the south, the Standard Building Code (SBC) of the Southern Building Code Congress International (SBCCI) was used. Seismic design provisions were included in the SBC in 1976, by referencing ANSI A58.1, but "were not mandatory unless local authorities required seismic design, which was rarely the case", until 1988. The 1987 edition of the BOCA Code also incorporated the provisions of ANSI A58.1, and made them mandatory.

The ANSI A58.1 standard of the American National Standards Institute (ANSI) was first published in 1945, and was the first standard to consider earthquake loads (Beavers, 2002). However, seismic hazard did not have a role in ANSI A58.1, which only had a map showing the locations of destructive earthquakes of the past until its 1972 edition, in which a seismic hazard description similar to the 1949 USCGS (United States Coast and Geodetic Survey) map was incorporated. The 1972 edition of ANSI A58.1 was also the first one to outline modern wind design provisions (Fratinardo & Schroeder, 2015; Ghosh, 2008), evolving from more basic guidelines developed in the 1950s (Huston, 2007).

The 1949 hazard map was the first one to encompass the whole of the contiguous USA, and it was based on "the premise that similar earthquakes will occur in the future where they have occurred in the past" (Beavers, 2002). For reasons that are not fully clear, this

map was withdrawn in 1952, and replaced with a map that only showed the location of known past significant earthquakes. In the 1970s, the responsibility of producing hazard maps passed on to the USGS (United States Geological Survey), who published the first map developed in the form of probabilistic estimates of maximum acceleration contours on rock in 1976, and which, as highlighted by Beavers (2002), represented a significant paradigm shift. It should be noted, however, that the first edition of the ATC3-06, which in 1985 evolved into the National Earthquake Hazards Reduction Program (NEHRP) Recommended Provisions for Seismic Regulations for New Buildings and Other Structures, used a truncated version of this map in 1978, not allowing for values above 0.4g to be considered. This map was used for almost 20 years, given the inability to reach consensus on a different map that took place in between 1988 and 1994. It was finally updated by the USGS in 1997, after a four-year project called Project 97, during which large efforts were invested in giving a voice to all the professionals and sectors involved. Since then, the USGS hazard map has been updated in 2002, 2008 and 2014.

The way in which seismic loads were considered evolved significantly from the simple use of a 7.5%-10.0% of the building's weight as a lateral load (1927 edition of the UBC), with the progressive incorporation of significant factors such as soil type and capacity, seismic zonation, natural period of vibration of the structure, and importance of the building.

In 1988, ANSI combined with ASCE to update and re-designate ANSI A58.1-1982 to ASCE 7, which is now the most significantly recognised standard by all earthquake regulations, codes, standards, procedures and guidelines for basic seismic design in the USA (Beavers, 2002). Furthermore, ASCE 7 is also the "de facto" national wind design standard (Fratinardo & Schroeder, 2015). The International Building Code (IBC), whose first edition in 2000 was based in the NEHRP Provisions, makes reference to ASCE 7 for the definition of seismic and wind loads. According to FEMA-543 (FEMA, 2007), the area around Guy and Greenbrier has seen around 26 tornadoes of categories F3 to F5 ("severe" to "incredible") per 10,000 km^2 between 1950 and 1998, one of the highest rates across all of the USA.

Building practise in Arkansas is regulated by the Arkansas Fire Prevention Code, which is divided into three volumes: (I) Fire, (II) Building, and (III) Residential. It is based on the International Fire Code, the International Building Code and the International Residential Code, with some adjustments carried out by local experts (Arkansas Contractors Licensing Board, Construction Market Data, see Web references; Arkansas Building Authority, 2012).

The Building Code Effectiveness Grading Schedule (BCEGS), developed by the Insurance Services Office (SO), indicates that the overall level of code enforcement across the state of Arkansas is relatively low when compared to the country as a whole and to states like California, in which awareness with respect to seismic risk is much greater. Figure A2.2.17 shows the distribution of communities by BCEGS class number for the United States as a whole and for the state of Arkansas. Within this classification schedule, classes 1-3 correspond to the maximum enforcement levels, while class 10 indicates no enforcement at all. These figures agree with statements of Beavers (2002) and Cutcliffe (2000), who

highlight that, due to their relative lack of seismic activity, the effort to incorporate good seismic design practises in building codes has been more challenging in the central and eastern USA, when compared to other areas of the country.
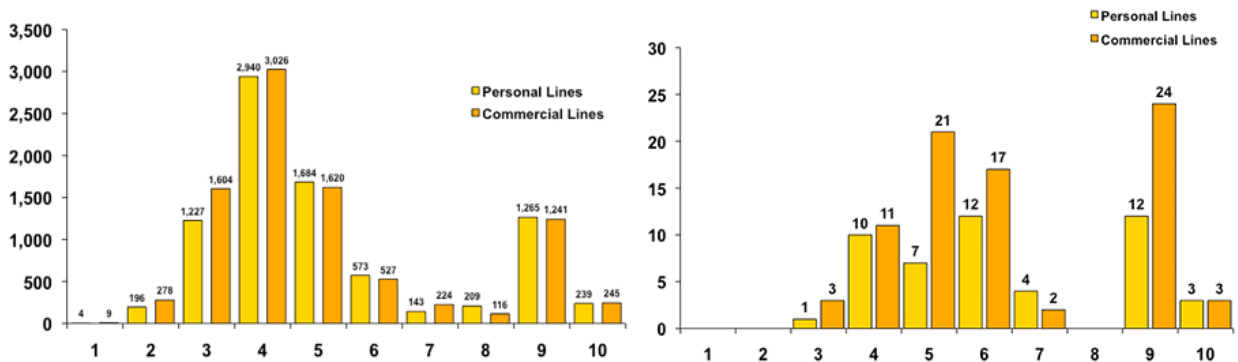
Figure A2.2.17. Distribution of communities by BCEGS class number for the whole of the United States (left) and the state of Arkansas (right). Personal lines include 1- and 2-family dwellings. Commercial lines include all other buildings. Classes 1-3: maximum enforcement. Class 10: no enforcement (ISO Mitigation, 2016).

A2.2.7.2 Building typologies

Information regarding building typologies in the state of Arkansas is scarce to null. For this reason, data regarding typologies at the country level were collected from the PAGER Inventory Database v2.0 (Jaiswal & Wald, 2008). Figure A2.2.18 shows that the structure of most of the buildings in the USA consists of light wood frames (61.2%), and unreinforced brick masonry (19.3%) in a smaller proportion. The remaining 19.4% is mostly made up of heavy wood frames and mobile homes (Figure A2.2.19). From visual inspection by means of Google Street View and from the description of damage caused by the 2011 Guy-Greenbrier earthquake that could be found, it seems possible to infer that light wood frames and unreinforced brick masonry are probably the most likely building typologies in the affected area.

- W1: Wood stud-wall frame with plywood/gypsum board sheathing.
- UFB3: Unreinforced brick masonry in lime mortar
- Other
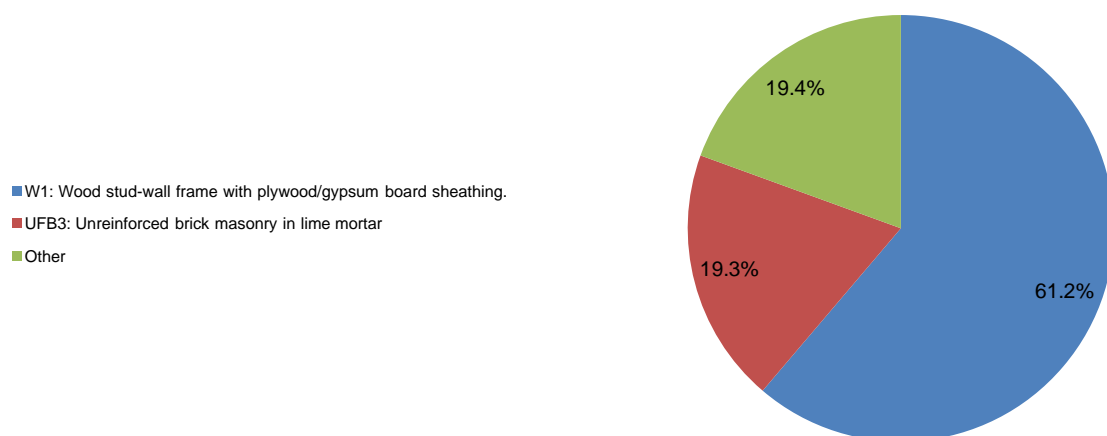
Figure A2.2.18. Proportion of buildings in the United States belonging to each typology. The subcategories within class "Other" are expanded upon in the figure below. Data from Jaiswal & Wald (2008).

115

- W2: Wood frame, heavy members (with area > 5000 sq. ft.)
- S1L: Steel moment frame low-rise
- S2L: Steel braced frame low-rise
- S3: Steel light frame
- S4L: Steel frame with cast-in-place concrete shear walls low-rise
- S5L: Steel frame with unreinforced masonry infill walls low-rise
- C1L: Ductile reinforced concrete moment frame with or without infill low-rise
- C2L: Reinforced concrete shear walls low-rise
- C3L: Nonductile reinforced concrete frame with masonry infill walls low-rise
- PC1: Precast concrete tilt-up walls
- PC2L: Precast concrete frames with concrete shear walls low-rise
- RM1L: Reinforced masonry bearing walls with wood or metal deck diaphragms low-rise
- RM2L: Reinforced masonry bearing walls with concrete diaphragms low-rise
- MH: Mobile homes

Figure A2.2.19. Breakdown of the "Other" class in the figure above. To determine the percentage that each of these sub-categories represents of the total in the USA, multiply the value in this figure by 0.194. Data from Jaiswal & Wald (2008).

A2.2.7.3 Prior damage and retrofit

No details on prior damage or retrofit available.

A2.2.8 Damage observations

A2.2.8.1 Damage states

Neither engineering reports nor relevant photographs of the damage caused by the 2011 Guy-Greenbrier earthquake seem to by publicly available. However, the qualitative descriptions found appear to correspond to Grade 2 damage in the European Macroseismic Scale (EMS-98; Grünthal, 1998). For details regarding the latter, please refer to Chapter 2.

A2.2.8.2 Damage statistics

Information regarding damage caused by the 2011 Guy-Greenbrier earthquake is scarce. The NEHRP report for the year 2011 (FEMA *et al.*, 2012) says that "the earthquake caused little damage", a statement that is supported by The New York Times' report of no "major damage" (see Web references). Nevertheless, several lawsuits were filed, mostly by residents of Greenbrier. Case number 23CV-14-84, entitled "*2010-2011 Guy-Greenbrier Earthquake Swarm Victims v. Chesapeake Operating, Inc. and BHP Billiton Petroleum (Fayetteville) LLC*", available via the archive of THV11 (see Web references) is a relevant source of information, for it gathers descriptions of damage suffered by 14 houses. Table A2.2.10 summarizes the types of damage described in the 14 cases of said lawsuit and from two additional sources, one of which mentions damage to foundations of a house located around 500 metres away from the epicentre (Reuters, see Web references), and another one that simply shows the picture of cracked bricks (Arkansas Fracking, see Web references). Fifteen of the sixteen cases considered in Table A2.2.10 correspond to

properties in Greenbrier, 6.3 km away from the epicentre, while the remaining case is from Perryville, Perry County, 61.6 km to the south-west of the epicentre. According to a litigation summary available at the website of the University of Dayton (see Web references), case number 23CV-14-84 was dismissed with prejudice, which means that the plaintiffs are barred from filing another case on the same claim.

Table A2.2.10. Type and number of cases of damage observed, from the available sources.

Type of damage	N°
Cracks in drywall	11
Cracks in exterior mortar	8
Pulling away of moulding	7
Cracks in exterior brick	7
Damage to foundations	5
Cracks in driveway	5
Cracks in walkways	5
Doorframes out of plumb	3
Damaged doors	3
Floor cracks	3
Damaged doorframes	2
Ceiling cracks	2
Front porch pulling away from the house	1
Window frames out of plumb	1
Un-levelling of front porch pillars	1
Un-levelling of interior columns	1
Waterline leaks and mold	1

A2.2.8.3 Observed weaknesses

Given the lack of information regarding damage caused by this event, no observations of systematic weaknesses can be made.

A2.2.8.4 Damage distribution

There are no details available with respect to the distribution of damage within the towns. Nevertheless, it should be noted that Greenbrier, which suffered the most damage, is a small town with a population of less than five thousand people.

A2.2.9 Casualties and losses

A2.2.9.1 Numbers of dead and injured

According to the all-hazards mitigation plan of the state of Arkansas (Arkansas Department of Emergency Management, 2013), there were no reports of casualties for this earthquake. This information matches what was reported by CNN and The Huffington Post (see Web references).

A2.2.9.2 Causes of casualties

No report of casualties found (Arkansas Department of Emergency Management, 2013).

A2.2.9.3 Estimates of economic losses

Not much information is readily available regarding the overall economic loss caused by this event.

Apart from case number 23CV-14-84 mentioned earlier, several other lawsuits were filed claiming for compensation for the damage suffered as a consequence of the 2011 Guy-Greenbrier earthquake swarm. Case 23CV-14-84 was filed in the Court of Faulkner County, Arkansas, and the amount pleaded per each of the 14 properties is 75,000 USD. According to a local newspaper, The Log Cabin Democrat (see Web references), 75,000 USD is the cut-off for Federal Court Jurisdiction. The newspaper also reports on complaints filed by about a dozen of other Greenbrier residents in Federal Court, for damages in excess of 75,000 USD each. An article by Reuters (see Web references) with date 27th August 2013, states that Emerson Poynter lawyers, who represented the plaintiffs of case 23CV-14-84, represented 35 homeowners at that point in time.

According to the estimation from USGS PAGER, the **M**4.7 main shock was most likely to cause economic losses of less than one million US dollars (65% probability), and had only a 30% chance of causing losses between one and ten million US dollars instead.

A2.2.10 Discussion and conclusions

This earthquake occurred on 28th February 2011, at 05.00 UTC (27th February 2011, 23.00 local time), and is one of the largest to have been registered in Arkansas outside of the New Madrid Seismic Zone. It was part of a large earthquake swarm that started around 2009 and which is believed to have been triggered by the injection of waste water at disposal wells in the vicinity of a previously unknown fault. Earthquakes in the area are not frequent, but three swarms have been known to occur between 1982 and 2011, including the Guy-Greenbrier sequence itself.

The main shock and other strong events in the sequence were felt across a broad area. Nevertheless, and in spite of the lack of official systematic damage and economic losses reports, it seems that the swarm caused only relatively minor damage to houses, mainly in the town of Greenbrier. The most common descriptions of damage found make reference to cracks in drywalls, masonry and moulding, and, to a lesser extent, damage to foundations, driveways and walkways. No casualties were reported.

A2.2.11 References

A2.2.11.1 Bibliography

Abd, N., H. Mahdi, H. Al-Shukri, A. Catakli, H. Chlaib & M. Su (2012). Induced Seismicity of Central Arkansas. *International Geophysical Conference and Oil & Gas Exhibition*, Istanbul, Turkey, 2012, pp. 1–4.

Arkansas Building Authority (2012). *Minimum standards & criteria*. Arkansas, USA. Available at http://aba.arkansas.gov/aboutUs/Documents/Final%202012%20Revision.pdf

Arkansas Department of Emergency Management (2013). *State of Arkansas all-hazards mitigation plan*. Arkansas, USA, 725 pp.

Ausbrooks, S.M. (2010). *The May 2001 Faulkner County earthquakes, 2nd edition*. Arkansas Geological Survey, USA.

Ausbrooks, S.M. & E. Doerr (2008a). *NEHRP Soil Classification Map of Arkansas*. Arkansas Geological Survey, USA.

Ausbrooks, S.M. & E. Doerr (2008b). *Liquefaction susceptibility map of Arkansas*. Arkansas Geological Survey, USA.

Ausbrooks, S.M. & S. Horton (2012). *Disposal of hydrofracking-waste fluid by injection into subsurface aquifers triggers earthquake swarm in central Arkansas with potential for damaging earthquakes*. Arkansas Geological Survey and the University of Memphis, USA. Presentation available online from http://www.gwpc.org/sites/default/files/event-sessions/ Ausbrooks_Scott.pdf.
Beavers, J.E. (2002). A review of seismic hazard description in US design codes and procedures. *Prog. Struct. Eng. Mater.* **4**, 46–63.

Bommer, J.J., P.J. Stafford & J.E. Alarcón (2009). Empirical equations for the prediction of the significant, bracketed, and uniform duration of earthquake ground motion. *Bulletin of the Seismological Society of America* **99**(6), 3217-3233.

Cutcliffe, S.H. (2000). Earthquake resistant building design codes and safety standards: The California experience. *GeoJournal* **51**, 259–262.

Dart, R.L. & S.M. Ausbrooks (2011). *Earthquakes in Arkansas and vicinity 1699–2010*. U.S. Geological Survey, Open-File Report 2011–1118.

FEMA (2007). *FEMA 543, Design Guide for Improving Critical Facility Safety from Flooding and High Winds: Providing Protection to People and Buildings*.

FEMA, NIST, NSF & USGS (2012). Annual report of the National Earthquake Hazards Reduction Program for fiscal year 2011. United States, 56 pp.

Fratinardo, V.F. & S.A. Schroeder (2015). Historical study of the wind design provisions of ASCE 7. *Structures Congress 2015*, 829–839.

Freeman J.R. (1932). *Earthquake Damage and Earthquake Insurance*. 1st edition. New York: McGraw-Hill.

Ghosh, S.K. (2008). Searching for simplicity: The evolution of wind provisions in standards and codes in the United States. *RCI Interface*, 13–21.

Giardini, D., G. Grünthal, K.M. Shedlock & P. Zhang (1999). The GSHAP global seismic hazard map. *Annali di Geofisica* **42**(6), 1225-1228.

Giardini, D., G. Grünthal, K.M. Shedlock & P. Zhang (2003). The GSHAP global seismic hazard map. In: Lee, W., H. Kanamori, P. Jennings & C. Kisslinger (eds.): International handbook of earthquake & engineering seismology, International Geophysics Series 81 B, Academic Press, Amsterdam, 1233-1239.

Grünthal, G. (ed.) (1998). *European Macroseismic Scale 1998 (EMS-98)*. Cahiers du Centre Europeen de Geodynamique et de Seismologie 15, Centre Europeen de Geodynamique et de Seismologie, Luxembourg.

Horton, S. (2012). Disposal of Hydrofracking Waste Fluid by Injection into Subsurface Aquifers Triggers Earthquake Swarm in Central Arkansas with Potential for Damaging Earthquake. *Seismol. Res. Lett.* **83**, 250–260.

Hough, S.E. & M. Page (2015). A Century of Induced Earthquakes in Oklahoma? *Bull. Seismol. Soc. Am.* **105**(6): 2863-2870.
Huang, Y. & G.C. Beroza (2015). Temporal variation in the magnitude-frequency distribution during the Guy-Greenbrier earthquake sequence: Variation in MFD for Induced Seismicity. *Geophys. Res. Lett.* **42**, 6639–6646.

Huston, E. (2007). SEAW's handbook of a rapid-solutions methodology for wind design. *Struct. Mag.*, 61–64.

Jaiswal, K. & D.J. Wald (2008). Creating a Global Building Inventory for Earthquake Loss Assessment and Risk Management. USGS Open File Report 2008-1160. Available electronically at http://pubs.usgs.gov/of/2008/1160/.

Kempton, J.J. & J.P. Stewart (2006). Prediction equations for significant duration of erthquake ground motions considering site and near-source effects. Earthquake Spectra **22**(4), 985-1013.

Klose, C.D. & L. Seeber (2007). Shallow seismicity in stable continental regions. *Seismol. Res. Lett.* **78**, 554–562.

Llenos, A.L. & A.J. Michael (2013). Modeling Earthquake Rate Changes in Oklahoma and Arkansas: Possible Signatures of Induced Seismicity. *Bull. Seismol. Soc. Am.* **103**, 2850–2861.

McFarland, J.D. (2001). *The May 2001 Faulkner County earthquakes, 1st edition*, Arkansas Geological Survey, USA.

Perry Jr, W.J. (1997). Structural settings of deep natural gas accumulations in the conterminous United States. Geologic Controls of Deep Natural Gas Resources in the United States, *US Geological Survey Bulletin* **2146**, 41–46.

Quickfacts: http://quickfacts.census.gov/.

Stoeser, D.B., G.N. Green, L.C. Morath, W.D. Heran, A.B. Wilson, D.W. Moore & B.S. Van Gosen (2007). *Preliminary integrated geologic map databases for the United States*. U.S. Geological Survey, Open-File Report 2005-1351. Available online at http://pubs.usgs.gov/ of/2005/1351/

Weatherill, G. A. (2014). *OpenQuake ground motion toolkit - User guide*. Global Earthquake Model (GEM). Technical Report.

A2.2.11.2 Web references

Accessed on 27 January 2016:

Arkansas Contractors Licensing Board: http://aclb.arkansas.gov/Pages/BuildingCodes .aspx

Arkansas Democrat-Gazette: http://www.arkansasonline.com/news/2011/feb/27/47-magnitude-quake-hits-central-arkansas/

Arknsas Fracking (2011): http://www.arkansasfracking.org/june24_2011_012.JPG

Arkansas Geological Survey: http://www.geology.arkansas.gov/

Arkansas Geological Survey earthquake archive: http://www.geology.arkansas.gov/xl/Earthquake_Archive.xlsx

Center for Engineering Strong Motion Data (CESMD): http://www.strongmotioncenter.org/

CNBC's America's Top States for Business 2012: http://www.cnbc.com/id/100003143.

CNN: http://edition.cnn.com/2011/US/02/28/arkansas.quake/

Construction Market Data: http://www.cmdgroup.com/building-codes/arkansas/

Dr. Yihe Huang, at Stanford: http://web.stanford.edu/~yihe/induced-eq.html

ISO Mitigation: http://www.isomitigation.com/index.php/bcegs/facts-and-figures-about-bcegs-grades-around-the-country.

Reuters: http://www.reuters.com/article/us-usa-energy-quakes-insight-idUSBRE97Q05N20130827

The Encyclopedia of Arkansas History & Culture: http://www.encyclopediaofarkansas .net/encyclopedia/entry-detail.aspx?entryID=5912

The Huffington Post: http://www.huffingtonpost.com/2011/02/28/earthquake-in-arkansas_n_829048.html

The Log Cabin Democrat: http://thecabin.net/news/local/2014-02-13#.Vqh3CjHF-Oc

The New York Times: http://www.nytimes.com/2011/03/01/us/01earthquakes.html?_r=0

THV11 archives: http://archive.thv11.com/assetpool/documents/140214060946_Earthquake%20Damage%20Lawsuit.pdf

United States Bureau of Economic Analysis: http://www.bea.gov/

United States Bureau of Labor Statistics, Economy at a Glance: http://www.bls.gov/ eag/eag.ar.htm

United States Department of Agriculture, 2012 Census of Agriculture: http://www.agcensus .usda.gov/Publications/2012/

United States Geological Survey (USGS): http://earthquake.usgs.gov/

University of Dayton, Hydraulic Fracturing Tort Litigation Summary: https://www.udayton.edu/directory/law/documents/watson/blake_watson_hydraulic_fracturing_primer.pdf

USGS, New Madrid 1811-1812 earthquakes: http://earthquake.usgs.gov/earthquakes/states/events/1811-1812.php

A2.3 May 2011 M5.1 Lorca Earthquake, Spain

This earthquake occurred on 11th May 2011, at 16.47 UTC (18.47 local time), very close to the city of Lorca, south-eastern Spain, preceded by a **M**4.5 foreshock at 15.05 UTC (17.05 local time), which caused only minor damage (Alguacil *et al.*, 2014). The main shock, on the other hand, caused significant losses to the city of Lorca, most possibly due to a combination of the proximity of the epicentre to the town, the shallowness of the hypocentre, directivity and site amplification effects, and the vulnerability of the building stock (López-Comino *et al.*, 2012; Pro *et al.*, 2014; Romão *et al.*, 2013).

A2.3.1 Tectonic and seismic setting

A2.3.1.1 Tectonic setting

The epicentre of the earthquake was located in the proximity of the city of Lorca, in the autonomous community of Murcia, south-eastern Spain, very close to the boundary between the Eurasian and the African tectonic plates, whose relative positioning is shortening in the north-northwest to south-southeast direction (Gaspar-Escribano & Benito, 2007) at an approximate rate of 4.5-5.6 mm per year (Masana *et al.*, 2004). This area constitutes the east sector of the Cordillera Bética, and it presents the highest seismic activity rate of the Iberian peninsula (Rodríguez-Escudero *et al.*, 2014). Nevertheless, this activity is quite diffuse and spread over a large number of geological structures (Masana *et al.*, 2004) with a combination of normal, strike-slip and reverse behaviour. The main southwest to northeast structures comprise over 450 km of oblique left-lateral slip faults running from Almería to Alicante, which can be subdivided into five main ones, as shown in Figure A2.3.1, which are: Carboneras fault, Palomares fault, Alhama de Murcia fault, Carrascoy fault and Bajo Segura fault. The Alhama de Murcia fault, believed by many (Alfaro *et al.*, 2012; Rodríguez-Escudero *et al.*, 2014; Rodríguez-Peces *et al.*, 2014; Cabañas Rodríguez *et al.*, 2011; Alguacil *et al.*, 2014; López-Comino *et al.*, 2012) to be responsible for the 2011 **M**5.1 Lorca earthquake, is composed, in turn, of four segments: Goñar-Lorca, Lorca-Totana, Totana- Alhama de Murcia and Alhama de Murcia-Alcantarilla (please refer to Figure A2.3.2). According to Rodríguez-Escudero *et al.* (2014), the two first segments and their inter-segment area are the ones which ruptured in May 2011.

Within the context of a seismic risk study carried out for the whole of the Murcia region, Martínez Díaz *et al.* (2005) investigated the changes in Coulomb stress induced in the area by earthquakes with **M** larger than 4.5 which occurred in between the years 1000 and 2005, and concluded that all the previous seismicity considered had increased the probability of seeing new seismic events along the westernmost segments of the Alhama de Murcia fault.
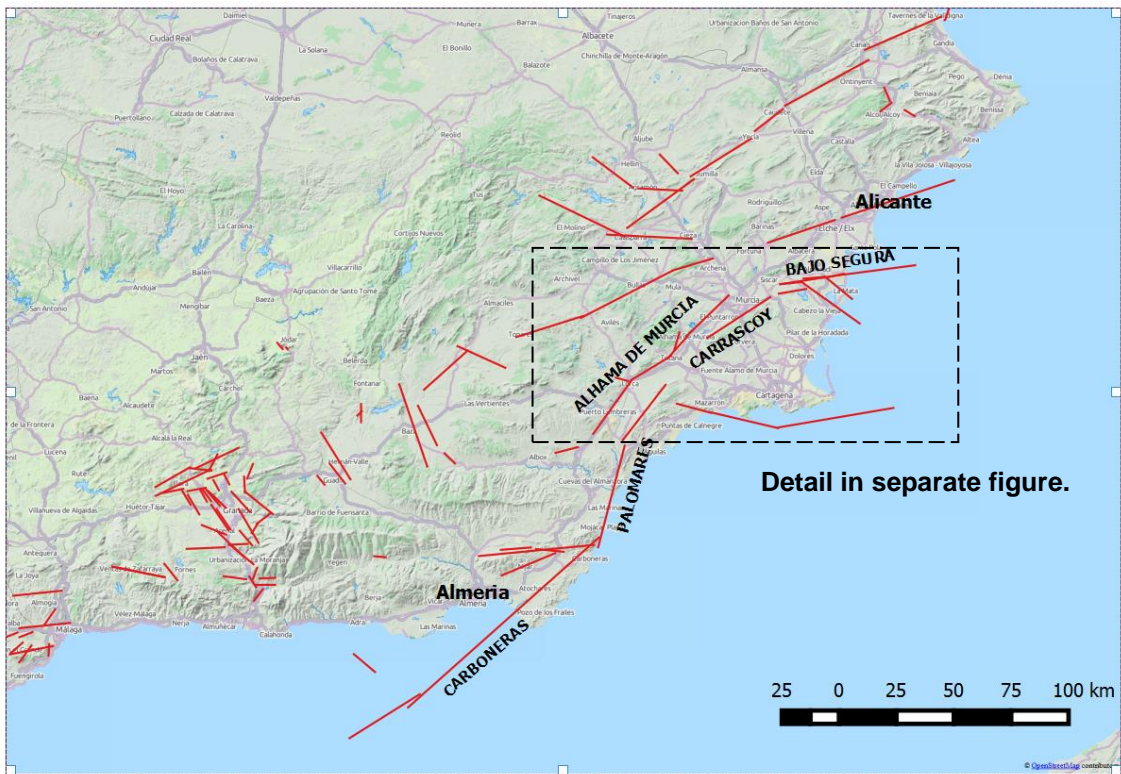
Figure A2.3.1. Main southwest to northeast structures running from Almería to Alicante. Location and dimension of faults in digital format obtained from García-Mayordomo *et al*. (2012)
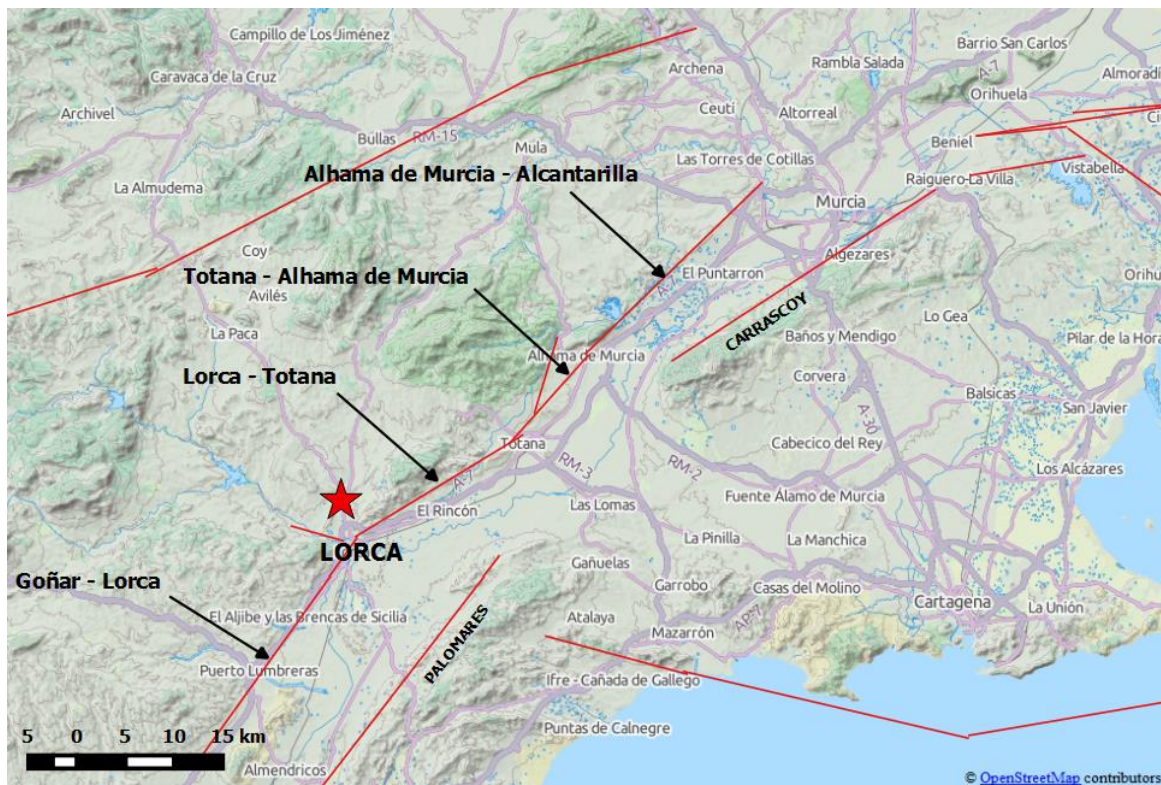
Figure A2.3.2. Segments that make up the Alhama de Murcia fault. The red star shows the location of the epicentre of the 11th May 2011 main shock, as reported by the Spanish National Geographic Institute (Instituto Geográfico Nacional, IGN). Location and dimension of faults in digital format obtained from García-Mayordomo *et al*. (2012)

It should be noted that other researchers (*e.g.*, Pro *et al.*, 2014), indicate that the 2011 Lorca earthquake was not originated within the Alhama de Murcia fault itself, but along a secondary fault parallel to the latter, located to the north of the city of Lorca, called the Cejo de los Enamorados fault. Its location is not reported in the Quaternary Active Faults Database of Iberia (QAFI, García-Mayordomo *et al.*, 2012) and it is therefore not shown in Figure A2.3.2, but it approximately coincides with the epicentre reported by the Spanish National Geographic Institute (Instituto Geográfico Nacional, IGN) shown in the figure.

A2.3.1.2 Regional and local seismicity

As mentioned above, south-eastern Spain presents the highest seismic activity rate of the Iberian peninsula. The area has experienced several seismic events that have caused a significant level of damage in the past. The city of Lorca, in particular, has experienced damage similar to that of the 2011 earthquake in 1579 and 1674 (Martínez Guevara & Fernández Navarro-Soto, 1986; Martínez Solares & Mezcua, 2002). The EMS-98 intensity of these events in the city of Lorca is estimated to have been VII ("damaging") and VIII ("heavily damaging"), respectively (Rodríguez-Escudero *et al.*, 2014). Similarly to the 2011 event, the 1674 one was preceded by a foreshock of intensity V to VI, *i.e.*, "strong" to "slightly damaging" (Cabañas Rodríguez *et al.*, 2011).

In more recent years, three significant events occurred in the vicinity of Lorca: the 1999 **M**4.7 Mula earthquake, the 2002 **M**5.0 Bullas earthquake, and the 2005 **M**4.8 La Paca sequence, which presented EMS-98 macroseismic intensities of VI ("slightly damaging"), V ("strong") and VII ("damaging"), respectively (Alfaro *et al.*, 2012; Cabañas Rodríguez *et al.*, 2011; Morales *et al.*, 2014). The epicentres of these and other relevant events can be observed in the map of Figure A2.3.3, in which the 2011 main shock is highlighted.

In spite of the moderate magnitudes of the aforementioned events, a paleoseismic study by Masana *et al.* (2004) reports the occurrence of a minimum of two but possibly three large earthquakes with moment magnitudes in between 6.1 and 7.0 along the Alhama de Murcia fault in the last 27,000 years.

A2.3.1.3 Seismic hazard

Figure A2.3.4 shows an extract of the probabilistic seismic hazard map for Spain, according to the Spanish National Geographic Institute (Instituto Geográfico Nacional, IGN). It shows the PGA values on rock with a 10% probability of exceedance in 50 years, *i.e.*, with a 475-year return period. This map was elaborated after the Lorca earthquake of 2011 and, therefore, specifies a larger design PGA than the one in force at the time of the earthquake, which was 0.12 g (NCSE-02, 2002). The current map indicates that this value should be 0.18-0.19 g instead.

Figure A2.3.5 shows the uniform hazard spectrum on rock from the SHARE (Seismic Hazard Harmonization in Europe) project (Giardini *et al.*, 2013) for a point with coordinates 37.700º N and 1.718º W, which correspond approximately to the city of Lorca. As can be

observed, the expected PGA on rock with a 10% probability of exceedance in 50 years is 0.14 g, around 17% higher than that of NCSE-02 at the time of the earthquake, but 22% smaller than that of the newest national seismic hazard map for Spain.
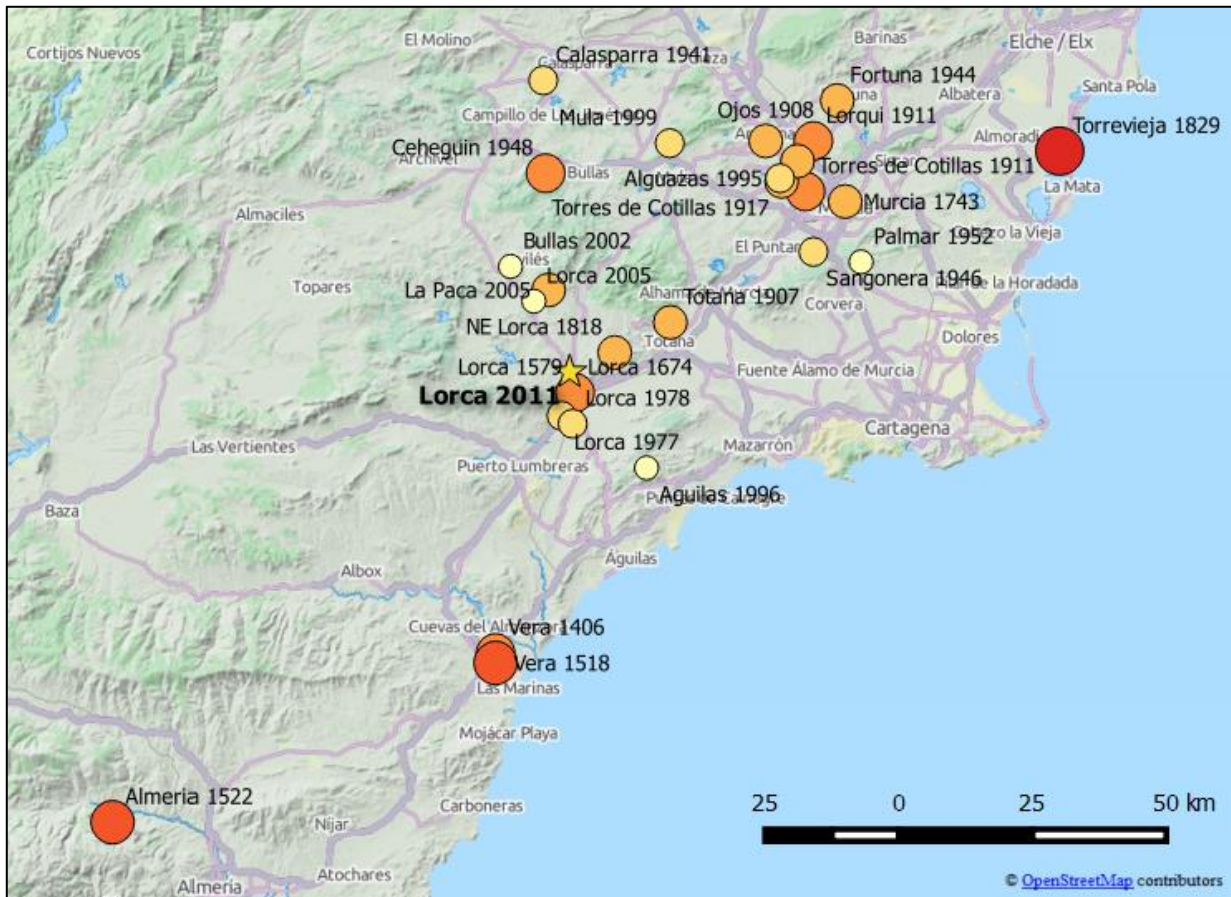
Figure A2.3.3. Epicentres of relevant earthquakes around the area of the city of Lorca. The colour and diameter of the symbols is proportional to the maximum macroseismic intensity of the event.

Results from the Global Seismic Hazard Assessment Program (GSHAP) yield an expected PGA on rock with a 10% probability of exceedance in 50 years of about 0.15 g (1.479 m/s^2) for the region around the city of Lorca (Giardini *et al.*, 1999; Giardini *et al.*, 2003). This value is around 25% higher than that of NCSE-02 at the time of the earthquake, but 17% smaller than that of the newest national seismic hazard map for Spain.

The Worldwide Seismic Design Tool of the United States Geological Survey (USGS) make use of the results from GSHAP to estimate the spectral accelerations at 0.2 and 1.0 seconds with a 2% probability of exceedance in 50 years, which, for the case of Lorca, are 0.75 g and 0.30 g, respectively. It should be noted that these values result from significant approximations and are therefore classified within the lowest reliability category of the USGS database.
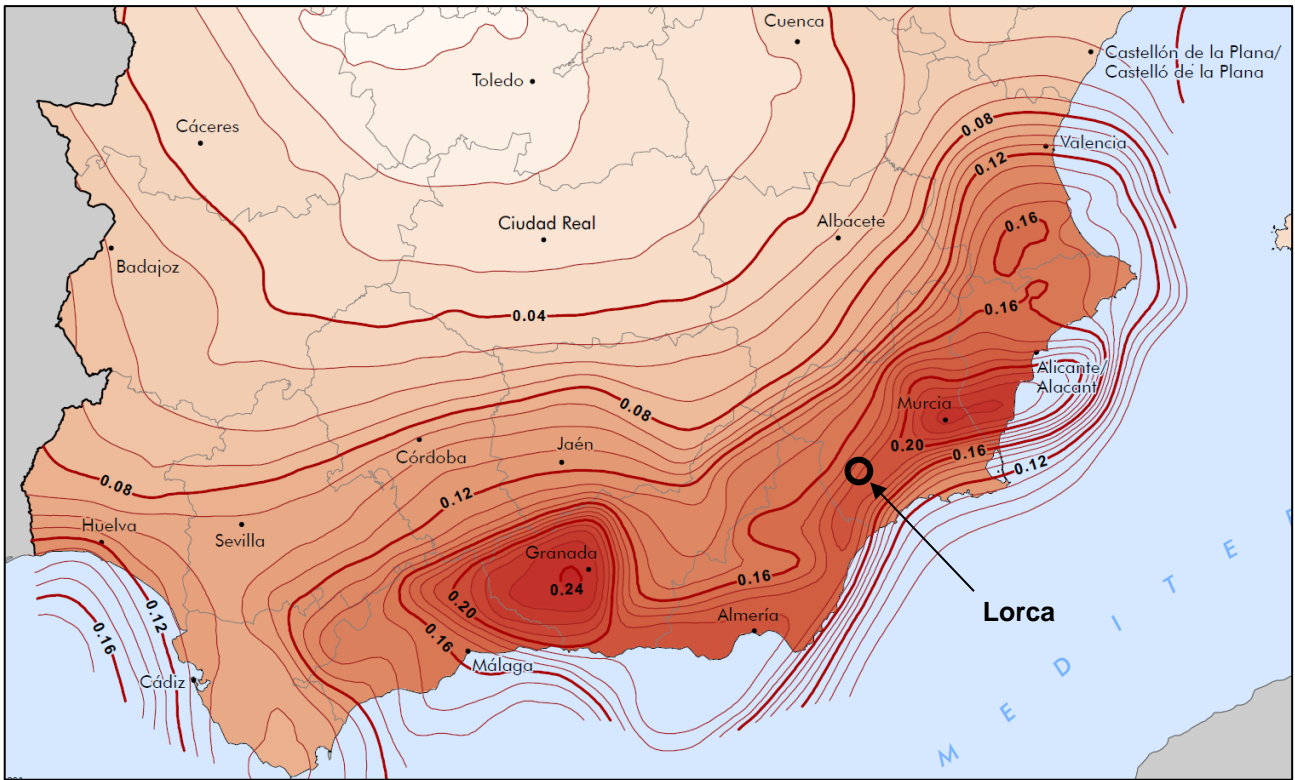
Figure A2.3.4. Extract of the seismic hazard map for Spain, according to the IGN. Values correspond to PGA on rock with a 10% probability of exceedance in 50 years (Spanish National Geographic Institute, 2016).
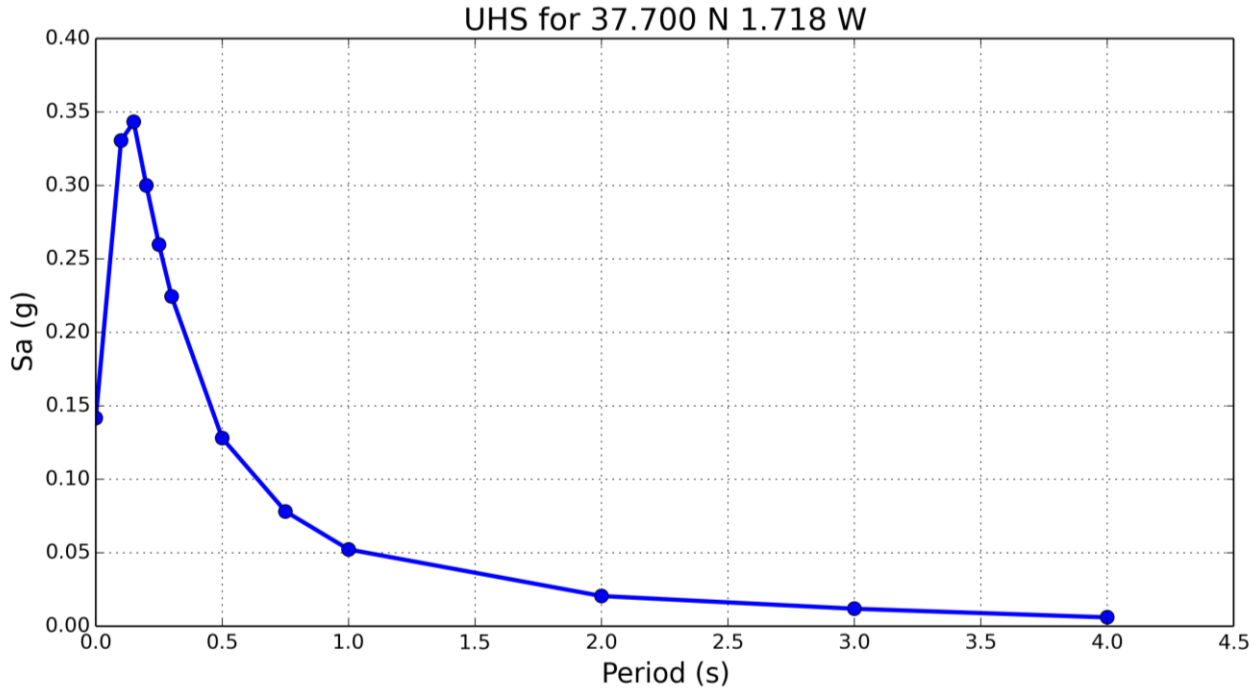
Figure A2.3.5. Uniform Hazard Spectrum for point 37.700º N 1.718º W (closest available to the city of Lorca) according to SHARE. Values correspond to PGA and spectral acceleration in rock with a 10% probability of exceedance in 50 years (mean).

A2.3.2 Earthquake source characteristics

A2.3.2.1 Location, depth and time

The main shock occurred on 11th May 2011, 16.47 UTC (18.47 local time).

Several organizations and agencies report their own estimations of the epicentral coordinates and hypocentral depth. The information reported in the websites of the Spanish National Geographic Institute (IGN), the National Earthquake Information Center (NEIC) of the United States Geological Service (USGS), the Global Centroid Moment Tensor Project (GCMT), the European-Mediterranean Seismological Centre (EMSC) and the International Seismological Centre (ISC) is summarized in Table A2.3.1. Cells marked as (*f) correspond to parameters that were held fixed while inversion was carried out to retrieve those that remain. Some discrepancy can be observed amongst the different agencies, especially regarding the hypocentral depth which is, in fact, the parameter that is most difficult to constrain. Recognizing this difficulty, Morales *et al.* (2014) and López-Comino *et al.* (2012) carried out a large effort to relocate all the events in the series, finally arriving to the values reported in Table A20.2.1.

Table A2.3.1. Epicentral coordinates and hypocentral depths from different sources.

	Agency / Publication	Latitude	Longitude	Depth (km)
IGN	Instituto Geográfico Nacional (MDD)	37.7175 ° N	1.7114 ° W	4.00 (*f)
NEIC	National Earthquake Information Center, USGS	37.6990 ° N	1.6720 ° W (*f)	1.00 (*f)
GCMT	Global Centroid Moment Tensor Project	37.7000 ° N	1.6500 ° W	12.00 (*f)
EMSC	European-Mediterranean Seismological Centre	37.6800 ° N	1.6800 ° W	2.00
ISC	International Seismological Centre (inversion)	37.6494 ° N	1.6938 ° W	6.70
Morales *et al.* (2014)		37.7300 ° N	1.6900 ° W	4.60
López-Comino *et al.* (2012)		37.7270 ° N	1.6860 ° W	4.60

(*f) fixed parameter used for inversion

Note that in some cases it is not clear whether the reported coordinates correspond to the epicentre or to the centroid of the moment tensor solution. However, given the small magnitude of the event, the difference between the two is not expected to be significant.

In spite of the large variability that can be found in the estimations regarding hypocentral depth, most journal publications regarding this earthquake make reference to a shallow event, less than 6 km below the surface (Alfaro *et al.*, 2012; Alguacil *et al.*, 2014; Basset-Salom and Guardiola-Víllora, 2014; Cabañas Rodríguez *et al.*, 2011; Feriche *et al.*, 2012; González *et al.*, 2012; López-Comino *et al.*, 2012; Morales *et al.*, 2014; Pro *et al.*, 2014; Rodríguez-Peces *et al.*, 2014; Romão *et al.*, 2013).

The map in Figure A2.3.6 shows the different estimations of the epicentral coordinates enumerated above. The Quaternary Active Faults Database of Iberia (García-Mayordomo *et al.*, 2012), indicates that the Lorca-Totana segment of the Alhama de Murcia fault is striking in the WSW direction, dipping towards the NNW. As shown in Figure A2.3.6,

hypocentral locations from the local networks (IGN) and reported in subsequent studies (López-Comino *et al.*, 2012; Morales *et al.*, 2014) are consistent with this information.
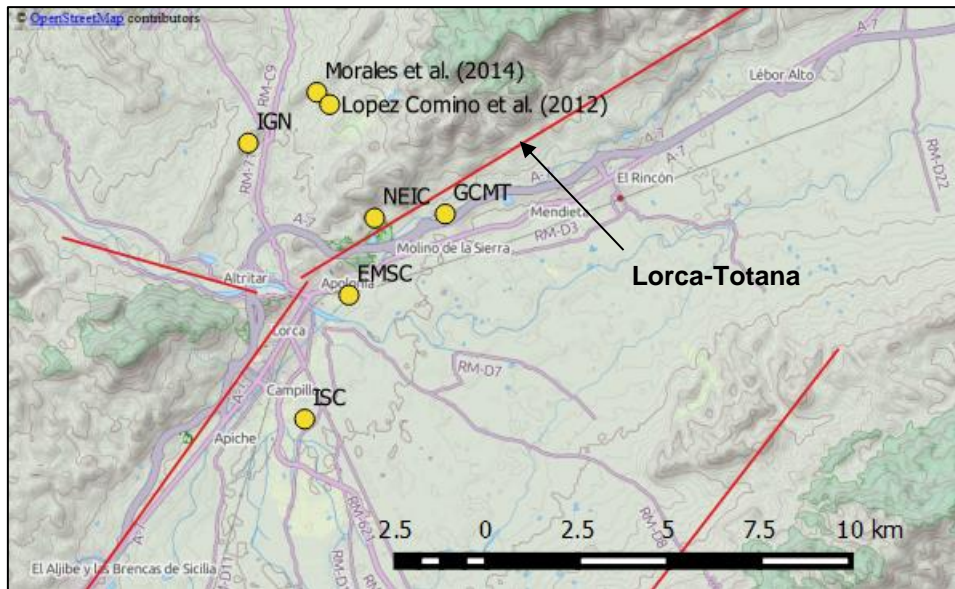
Figure A2.3.6. Estimations of the epicentral coordinates. Red lines represent the fault traces. Location and dimension of faults in digital format obtained from García-Mayordomo et al. (2012)

A2.3.1.1 Magnitude

Estimations of magnitude made by the main agencies are reported in Table A2.3.2. Most organizations agree on the moment magnitude **M** being 5.1, though several journal publications report 5.2 instead (Alguacil *et al.*, 2014; López-Comino *et al.*, 2012; Martínez-Díaz *et al.*, 2012; Rodríguez-Escudero *et al.*, 2014).

Table A2.3.2. Estimations of moment magnitude (**M**), body-wave magnitude (mb), local magnitude (M_L) and surface-wave magnitudes (Ms).

	Agency	M	mb	ML	Ms
IGN	Instituto Geográfico Nacional (MDD)	5.1	5.4 (*)	-	-
NEIC	National Earthquake Information Center, USGS	5.1	5.3	-	-
GCMT	Global Centroid Moment Tensor Project	5.1	-	-	-
EMSC	European-Mediterranean Seismological Centre	5.1	5.3	5.4	-
ISC	International Seismological Centre (inversion)	-	5.1 - 5.2	-	4.6 - 4.7

(*) mbLg

A2.3.2.3 Style-of-faulting

All the centroid moment tensor solutions from diverse sources indicate an oblique-reverse mechanism (López-Comino *et al.*, 2012; Pro *et al.*, 2014), as shown in Table A2.3.3. Based on the known tectonics and active faults in the region, nodal planes aligning to ENE-WSW would represent the likely fault plane (Martínez-Díaz *et al.*, 2012). The distribution of aftershocks supports this assertion (please refer to Foreshocks and aftershocks section).

Figure A2.3.7 plots the moment tensor solutions calculated immediately after the earthquake.

Table A2.3.3. Centroid moment tensor solutions from different sources. Fault planes marked in gray match the orientation of the Alhama de Murcia fault and parallel secondary structures in the area.

Fault Plane 1			Fault Plane 2			Source
Strike	Dip	Rake	Strike	Dip	Rake	
234	45	43	111	61	126	GCMT
245	65	58	120	40	138	GeoAzur
294	58	140	47	57	39	GFZ, reported by EMSC
230	69	33	127	59	156	IGN
220	75	50	113	42	157	NEIC (USGS)
310	76	159	45	70	15	NEIC (USGS)
238	54	59	104	46	26	Pro et al. (2014)
302	45	152	52	71	48	INGV
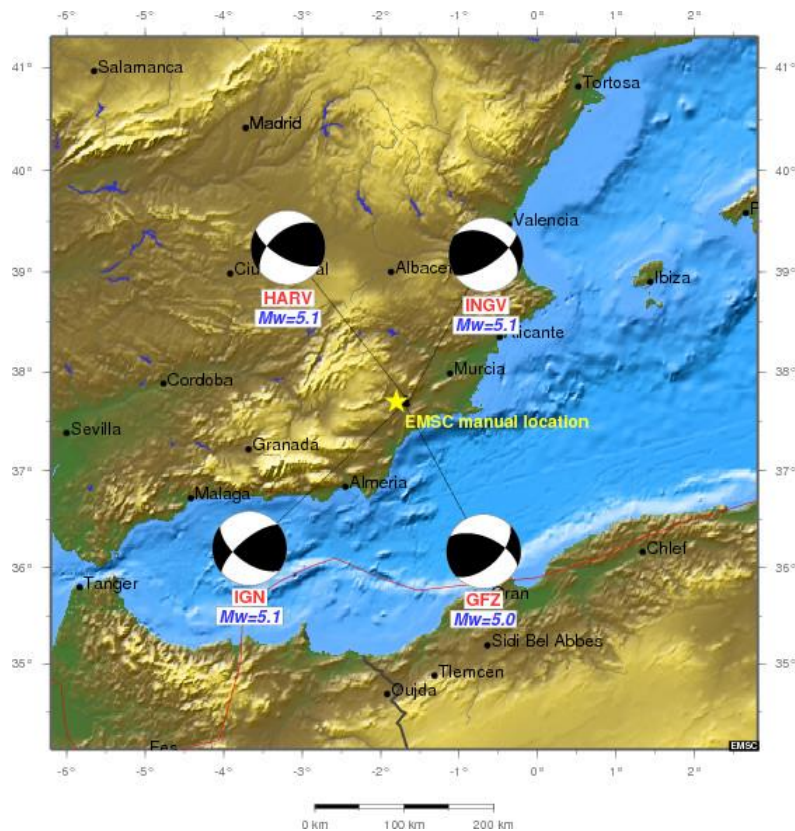
Figure A2.3.7. Moment tensor solutions calculated immediately after the earthquake, from the website of the European-Mediterranean Seismological Centre (2016).

A2.3.2.4 Stress drop

Pro *et al.* (2014) report a stress drop of 2.70 MPa, while Avouac (2012) says it has been calculated to be between 0.5 and 2.0 MPa. Morales *et al.* (2014), on the other hand, report that the dynamic stress drop was somewhere between 5.8 and 8.5 MPa.

A2.3.2.5 Foreshocks and aftershocks

The **M** 5.1 main shock was preceded by a **M** 4.5 event that occurred less than two hours earlier, on 11th May 2011, at 15.05 UTC (17.05 local time), which caused only minor damage (Alguacil *et al.*, 2014). According to Morales *et al.* (2014), the maximum EMS-98 intensity of this foreshock was VI. In between the two events, the IGN reports the occurrence of six minor events with moment magnitudes ranging from 1.3 to 2.6 (Cabañas Rodríguez *et al.*, 2011).

Several aftershocks followed the main shock. According to the IGN, around 140 earthquakes occurred in the area between 11th May and 14th July 2011, out of which sixteen were felt, one of them reaching a maximum EMS-98 intensity of IV (Cabañas Rodríguez *et al.*, 2011; Pro *et al.*, 2014). The largest aftershock was a **M**3.9 event on 11th May at 20.37 UTC (Morales *et al.*, 2014). A peak in the number of events registered per day occurred on 14th May, and a drastic decrease was observed after 16th May (Cabañas Rodríguez *et al.*, 2011; Morales *et al.*, 2014). Figure A2.3.8 shows the distribution in time of the events of the sequence, while Figure A2.3.9 shows all the events registered by the IGN between 11th May and 31st August 2011, for the region enclosed by meridians 2.0ºW and 1.2ºW and parallels 37.5ºN and 38.0ºN.
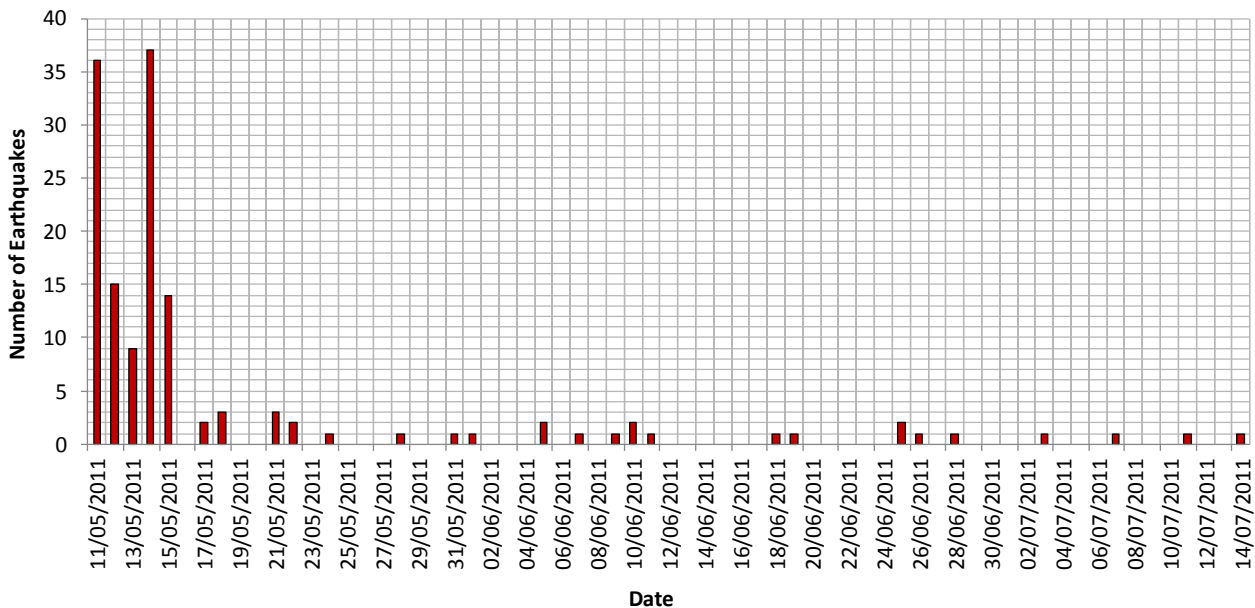
Figure A2.3.8. Distribution in time of the earthquake sequence. Data from Cabañas Rodríguez *et al.* (2011).
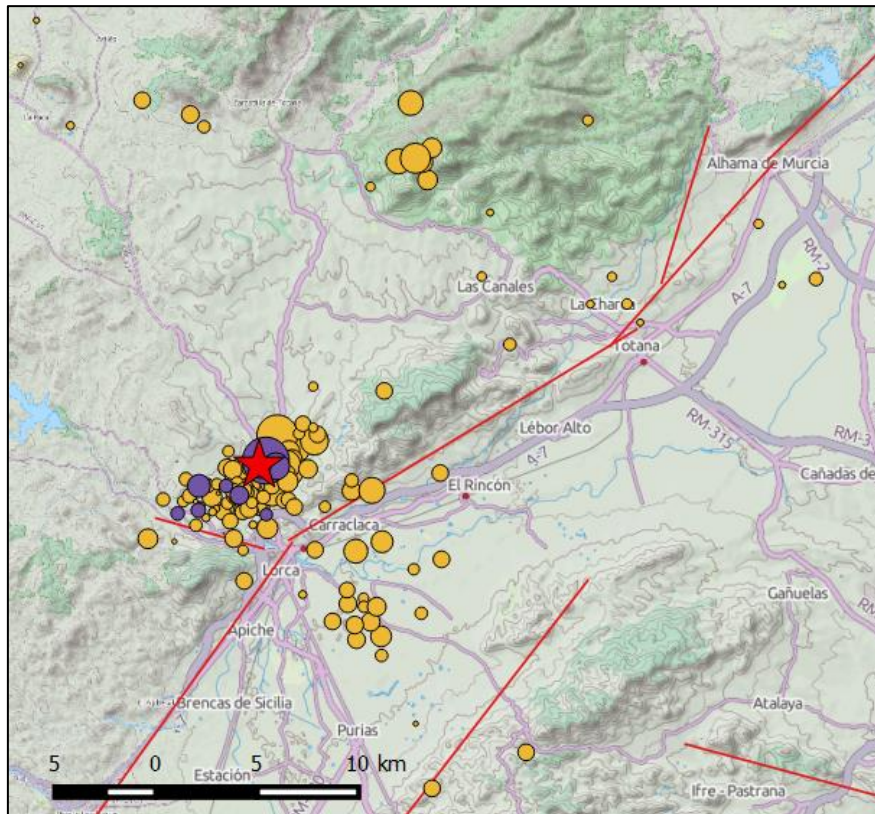
Figure A2.3.9. Epicentres of the seismic series according to the Spanish National Geographic Institute (IGN). Purple and orange circles correspond to events which occurred before and after the main shock (red star), respectively.

A2.3.2.6 Nature of earthquake

A study by González *et al*. (2012) suggests that the 2011 Lorca earthquake was triggered by the effects of groundwater extraction. These authors report a drop of around 250 metres in the phreatic level in the area of Lorca between 1960 and 2010. Furthermore, González & Fernández (2011) have determined that the Alto Guadalentín basin presents a subsidence rate of more than 10 cm per year due to long-term sustained water extraction from the underground aquifers. By means of a model of the ground deformation resulting from crustal unloading due to water extraction, González *et al*. (2012) calculated the three-dimensional Coulomb stress change and concluded that it can reasonably explain the observed fault slip pattern as well as the dynamics of the rupture.

Though agreeing with González *et al*. (2012) regarding the relevance of the influence of water extraction on the 2011 Lorca earthquake, Avouac (2012) draws attention to the fact that the stresses released during the earthquake, 0.5 to 2.0 MPa, are significantly larger than those that could have been induced by removal of underground water, and suggests that the released stresses probably built up over several centuries due to tectonic deformations, and that the role of water extraction was most likely limited to influencing the rate at which these stresses were accumulated and when and how they were released.

A2.3.3 Geology and ground conditions in the affected area

A2.3.3.1 Regional geology and topography

As described by Alfaro *et al.* (2012) and Martínez-Díaz *et al.* (2012), two mountain ranges, the Peña Rubia and Tercia ranges, are located to the northwest of the Alhama de Murcia fault, and are constituted by sedimentary and metamorphic rocks which are mainly Triassic, though some Palaeozoic and Jurassic rocks can be found as well. These two ranges are separated from each other by a pull-apart basin with sedimentary infill from the Miocene and Quaternary, known as the Lorca basin, which is where the homonymous city is located. The basin formed during an extensional phase in the Middle to Late Miocene, period in which some segments of the Alhama de Murcia fault behaved as normal faults. As described above (please refer to the Tectonic and Seismic Setting section), this sedimentary basin is subject to a NNW–SSE compressive stress field since the Upper Miocene, which causes it to be folded. The river running through the basin is called Guadalentín.

A2.3.3.2 Site conditions in the affected area

Given its location within the Lorca basin, the town of Lorca is mostly lying over sedimentary soils with a very heterogeneous structure. Navarro *et al.* (2014) carried out an extensive geological study in the area and produced a soil classification map of the city using the soil type categories of Eurocode 8 - Part 1 (CEN, 2004). As can be observed in Figure A2.3.10, a large part of the city is founded over soils type B2 and C.

Navarro *et al.* (2014) present as well two cross sections (marked as A-A' and B-B' in Figure A2.3.10, shown in Figure A2.3.11) that expose the complexity of the geology of the basin. Navarro *et al.* (2014) and Martínez-Díaz *et al.* (2011) conclude that the alluvial deposits of the basin can be responsible for amplification of ground motions.

Within the context of the RISMUR project ("Seismic Risk of the Autonomous Community of the Murcia Region", "Riesgo Sísmico de la Comunidad Autónoma de la Región de Murcia" in Spanish), Tsige Aga & García Flores (2005) produced a soil classification map for the whole of the Murcia region, according to which Lorca falls within a mid-level amplification category with respect to the whole of the autonomous community of Murcia. The authors also investigated the potential for liquefaction and concluded that though this phenomenon can take place in the region, its occurrence is expected to be isolated and non-frequent. Regarding the city of Lorca itself, the liquefaction hazard is low, especially because the phreatic level is located around 250 meters below the surface (González *et al.*, 2012). Figure A2.3.12 shows the map produced by Tsige Aga & García Flores (2005) for the whole region.
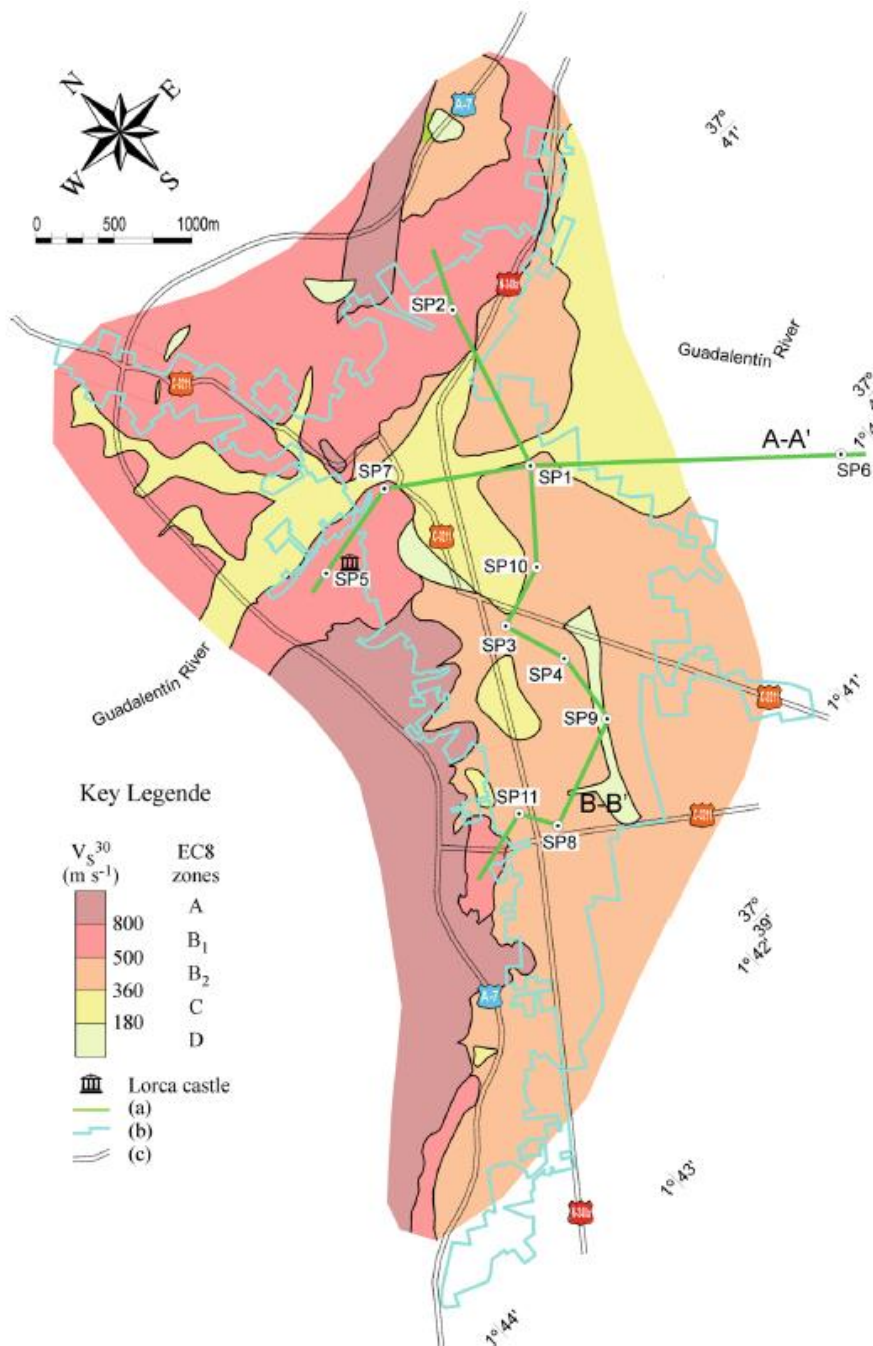
Figure A2.3.10. Soil classification map of the city of Lorca, from Navarro *et al*. (2014). The light-blue solid line shows the urban boundary. Points marked as SP(·) correspond to the location of ambient noise arrays used in the study by Navarro *et al*. (2014).
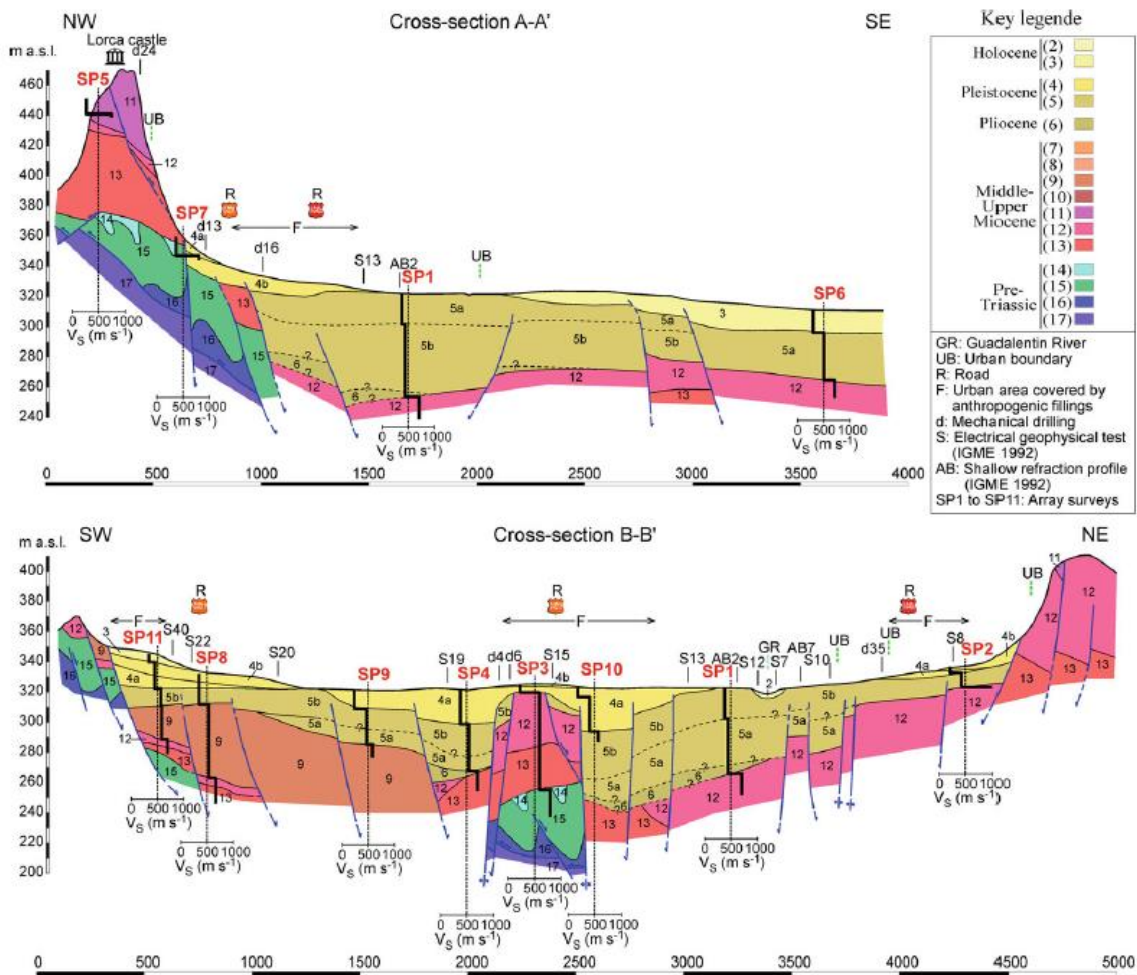
Figure A2.3.11. Geological cross sections of the city of Lorca, from Navarro *et al.* (2014).
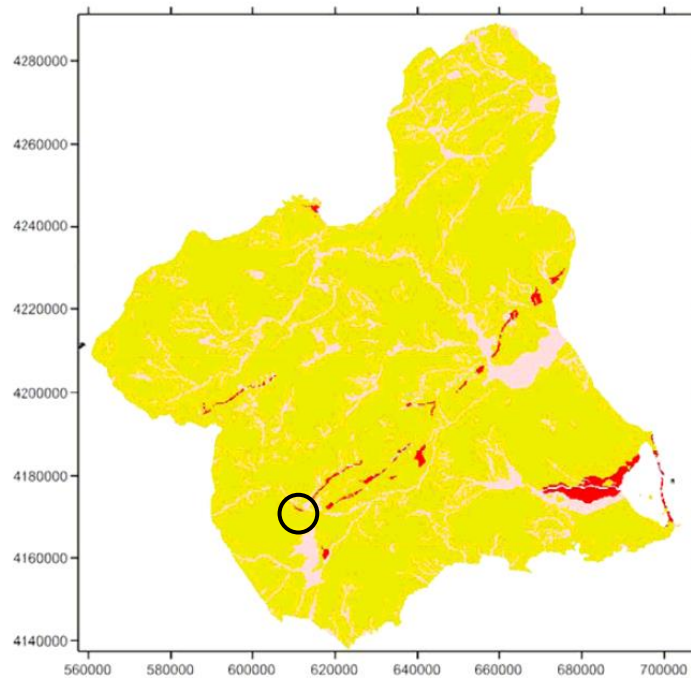
Figure A2.3.12. Liquefaction hazard map for the Murcia region, from Tsige Aga and García Flores (2005). Red: susceptible; pink: rather susceptible; yellow: not susceptible. Black circle: area around the city of Lorca.

135

A2.3.4 Ground motions

A2.3.4.1 Intensity observations

The IGN reports a maximum EMS-98 (European Macroseismic Scale, Grunthal, 1998) intensity of VII, which defines the event as "damaging". The distribution of felt intensities, as calculated from the online feedback of around six hundred users, is shown in Figure A2.3.13. The IGN provides no indication of how these intensities are calculated.
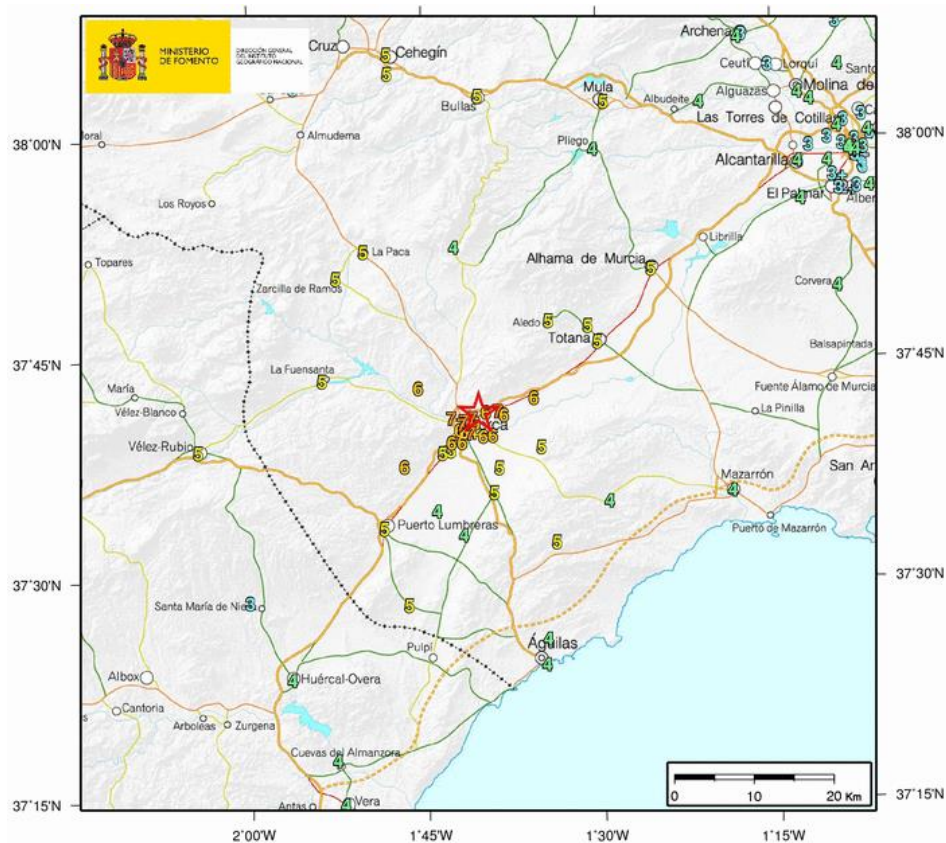
Figure A2.3.13. EMS-98 intensity levels for the 2011 Lorca main shock, from the website of the Spanish National Geographic Institute (2016), updated on 22nd March, 2012. Enlargement of the area marked in the previous figure.

In its summary of the significant earthquakes of the world which occurred during 2011, the United States Geological Service (USGS) reports a maximum MMI (Modified Mercalli Scale) intensity of VI at the city of Lorca, which corresponds to strong shaking and slight damage. Intensities assigned to other nearby locations are V ("moderate") at Alhama de Murcia and IV ("light") at Huercal-Overa, Mazarron, Murcia, Lumbreras and Totana. No details are given with respect to the computation of these values. However, within the "Did You Feel It?" report of the earthquake, an MMI of VII is assigned to the city of Lorca, as shown in Figure A2.3.14. This and the other intensity values shown on the map were calculated from the responses of around three hundred people to the corresponding online questionnaire, weighted according to the algorithm of Dengler & Dewey (1998). Figure A2.3.15 shows the MMI intensities as a function of distance, as reported by the USGS.

Note that the minimum distance considered in this plot is 10 km and, thus, information regarding the city of Lorca is not included.
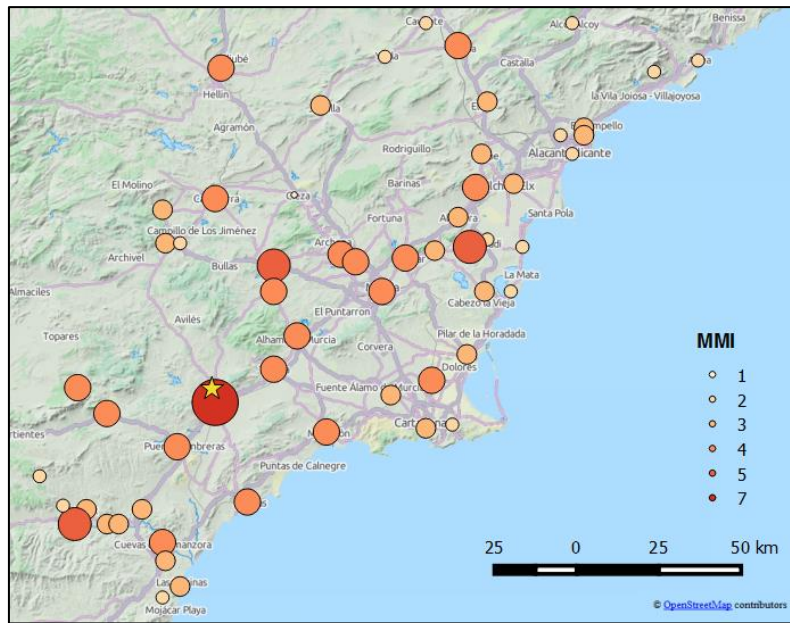
Figure A2.3.14. MMI intensity values calculated for each city from the responses to the "Did You Feel It?" questionnaire at the website of the United States Geological Service (USGS, 2016).
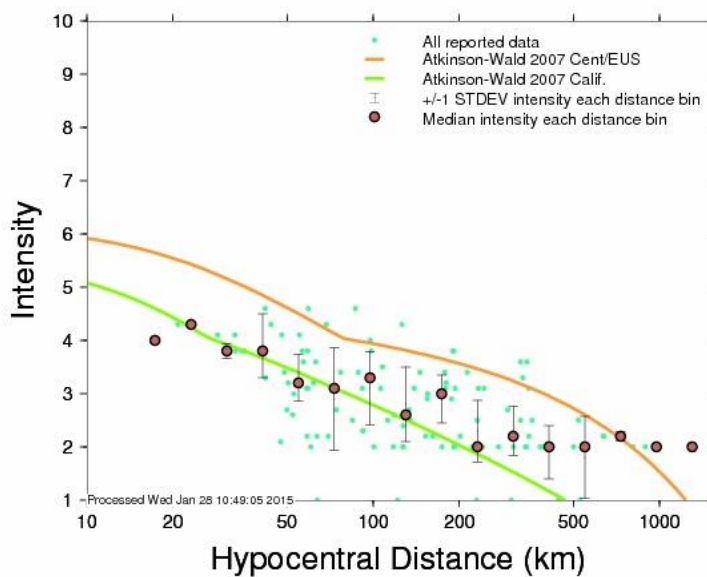
Figure A2.3.15. MMI intensity values vs. hypocentral distance, from the website of the United States Geological Service (USGS, 2016).

A2.3.4.2 Ground motion recordings

According to Cabañas Rodríguez *et al.* (2011), the foreshock was registered by five IGN stations at epicentral distances between 3 and 40 km, while the main shock was registered by seventeen IGN stations at epicentral distances between 3 and 185 km (Figure A2.3.16). The largest PGA values registered within Lorca for the foreshock and main shock were

0.275 g and 0.365 g, respectively, and they are the largest values ever recorded in the Iberian peninsula (Alfaro *et al.*, 2012). Table A2.3.4 shows the values of peak ground acceleration (PGA) and peak ground velocity (PGV) recorded at the seventeen stations for the main shock. Note that the epicentral distances provided are those reported by Cabañas Rodríguez *et al.* (2011) and they can vary depending on the estimation of the epicentral coordinates.

Table A2.3.4. Corrected PGA and PGV values recorded for the main shock, from Cabañas Rodríguez *et al.* (2011). Soil types according to classification by Mezcua *et al.* (2008): (2) firm soil, Quaternary consolidated deposits, (3) soft sedimentary deposits.

STATION	Epicentral Dist.(km)	Soil Type	E-W Component		N-S Component		Vertical Component	
			PGA(cm/s²)	PGV(cm/s)	PGA(cm/s²)	PGV(cm/s)	PGA(cm/s²)	PGV(cm/s)
LORCA	3	2	150.3	14.2	357.9	35.6	114.9	8.0
ZARCILLA DE RAMOS	24	2	31.4	2.1	25.4	2.2	25.8	1.3
ALHAMA DE MURCIA - 02	27	3	44.3	2.1	41.1	1.3	23.5	0.8
ALHAMA DE MURCIA - 01	28	N/A	7.7	0.2	9.8	0.4	9.1	0.4
VELEZ-RUBIO	36	2	9.3	0.6	10.6	0.5	5.9	0.4
MULA	42	3	41.5	1.4	35.7	1.5	20.2	0.9
VERA	53	3	7.1	0.4	5.8	0.4	4.5	0.3
LORQUÍ	57	3	7.8	0.3	7.9	0.3	3.7	0.2
MURCIA	58	3	8.4	0.4	7.0	0.4	2.6	0.1
CIEZA	64	3	2.8	0.2	2.4	0.1	1.4	0.1
OLULA DEL RÍO	67	2	4.4	0.3	2.2	0.3	1.7	0.2
FORTUNA	73	N/A	7.5	0.3	6.4	0.3	3.5	0.2
JUMILLA	92	2	5.1	0.4	3.8	0.3	3.5	0.3
GUARDAMAR DEL SEGURA	100	3	1.4	0.1	2.0	0.2	0.6	0.1
ELDA	116	2	2.7	0.2	1.7	0.2	0.9	0.1
ALBOLOTE	182	3	1.4	0.2	2.3	0.2	0.8	0.1
JAEN	186	2	2.8	0.2	2.1	0.2	1.3	0.1
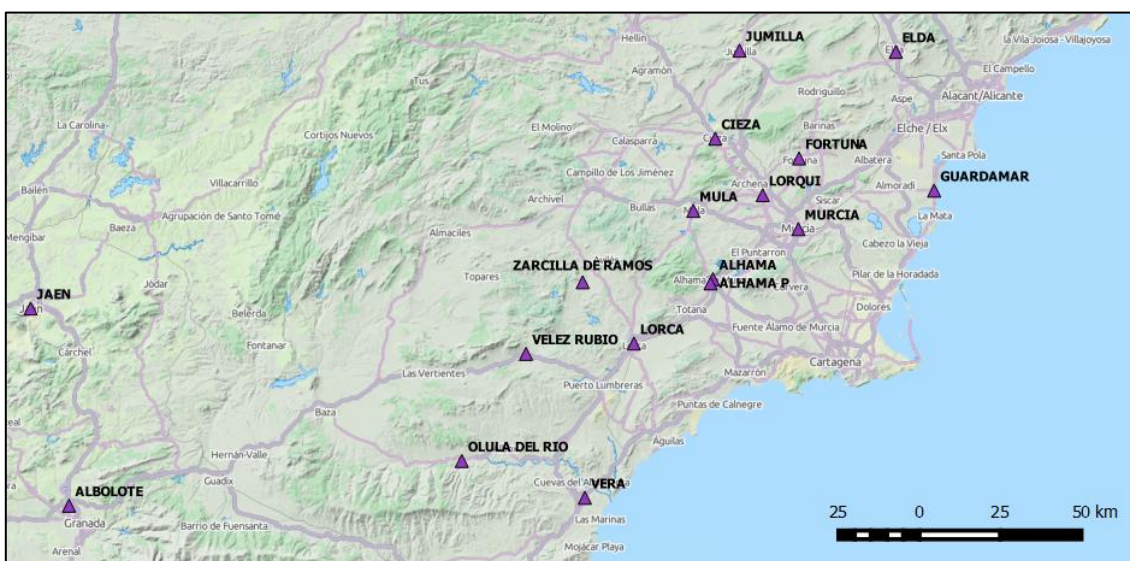
Figure A2.3.16. Location of the seventeen stations that recorded the 2011 Lorca main shock, from the website of the Spanish National Geographic Institute (2016).

According to Cabañas *et al.* (2014), most of the accelerographs deployed in South-Eastern Spain are installed in the ground floor or basement of buildings, usually no more than two or three storeys high. Detailed information regarding the type of soil in these locations is lacking, and all the available information is based on geological mapping and approximate designations. These authors assert that Lorca station can be considered to be located over soil type B (Eurocode 8), which matches what is shown in Figure A2.3.10, and that the Alhama de Murcia 02 and Mula stations are located over soil types B-C and C-D (Eurocode 8), respectively. This appears to be in reasonable agreement with the classification of Mezcua *et al.* (2008), presented in Table A2.3.4, who classified the soil types of a series of Spanish stations based on "a crude qualitative description provided for each station". However, Belvaux *et al.* (2014) state that the Lorca station is placed in the basement of a former jail in the elevated part of the ancient city, where conglomerate bedrock is seen to outcrop, and, therefore, the soil conditions might be consider to better match those of a soil type A (Eurocode 8).

The maximum recorded horizontal acceleration, 0.365 g, occurred in the N30W direction of the Lorca station (Cabañas Rodríguez *et al.*, 2011), which is almost perpendicular to the strike of the Alhama de Murcia fault (Cabañas *et al.*, 2014). This feature is interpreted as a consequence of rupture directivity in the near-field (Alguacil *et al.*, 2014). To confirm this observation, Alguacil *et al.* (2014) plot the maximum acceleration and velocity from the horizontal accelerograms recorded at the Lorca station at every possible angle, and highlight that both the maximum PGA and maximum PGV occur in the direction perpendicular to the strike of the Alhama de Murcia fault, as shown in Figure A2.3.17.

PGA max = 370 gal at 301°   PGV max = 37.5 cm/s at 111°
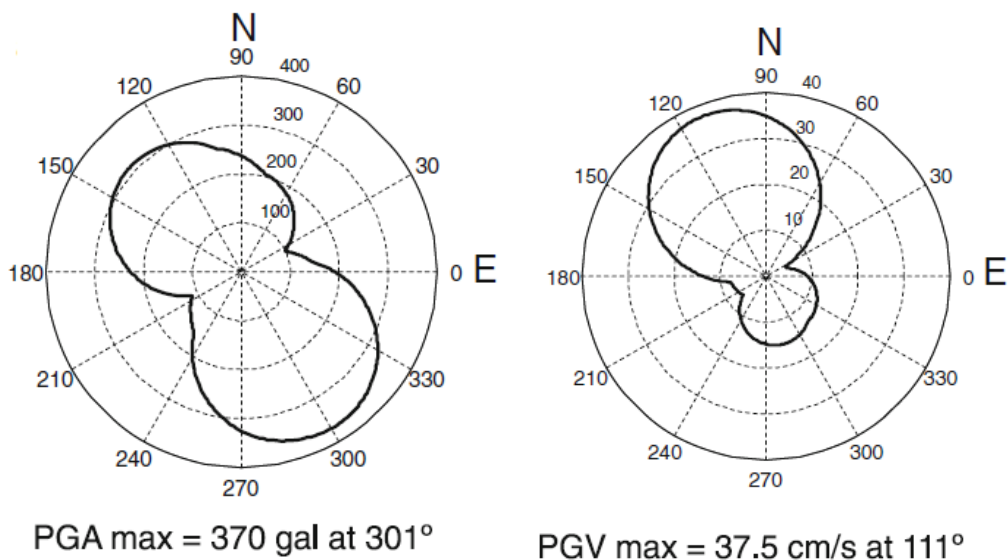
Figure A2.3.17. Polar diagrams of acceleration (left) and velocity (right) as a function of axis orientation, for the accelerograms recorded at the Lorca station, from Alguacil *et al.* (2014).

The acceleration, velocity and displacement time histories for the two components of the records with the largest PGA values are shown in the figures that follow (figures taken from Cabañas *et al.*, 2014).
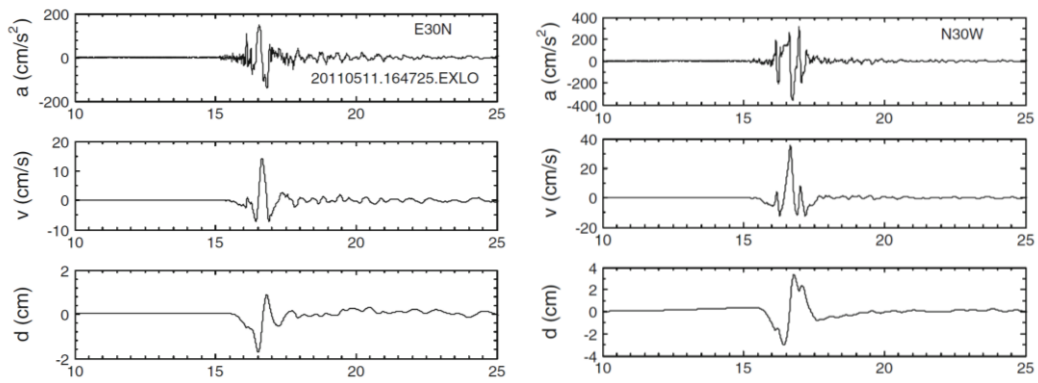
Figure A2.3.18. Horizontal corrected acceleration (top), velocity (middle) and displacement (bottom) for the two components of the Lorca station, from Cabañas *et al*. (2014).
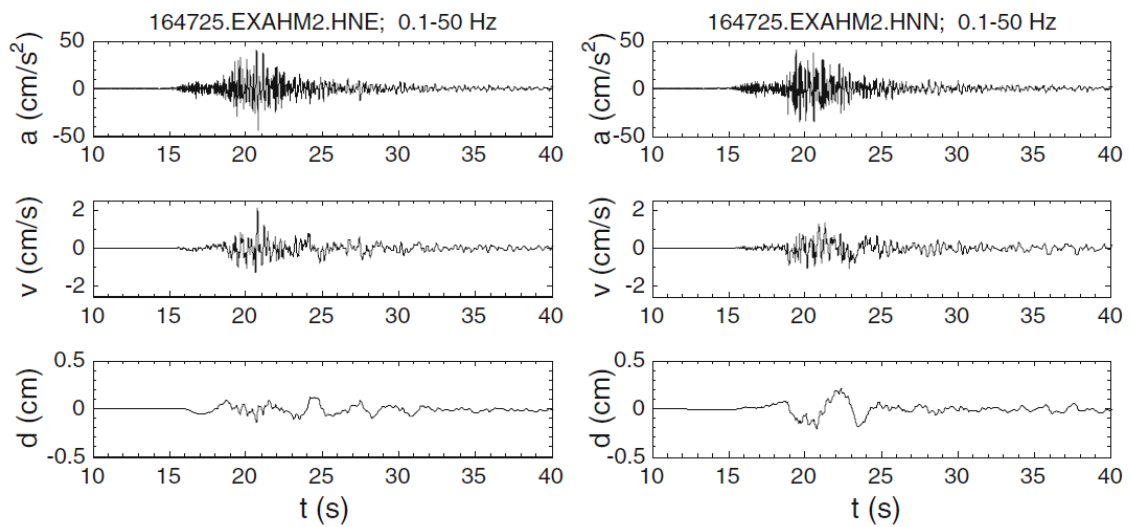
Figure A2.3.19. Horizontal corrected acceleration (top), velocity (middle) and displacement (bottom) for the two components of the Alhama de Murcia 02 station, from Cabañas *et al*. (2014).
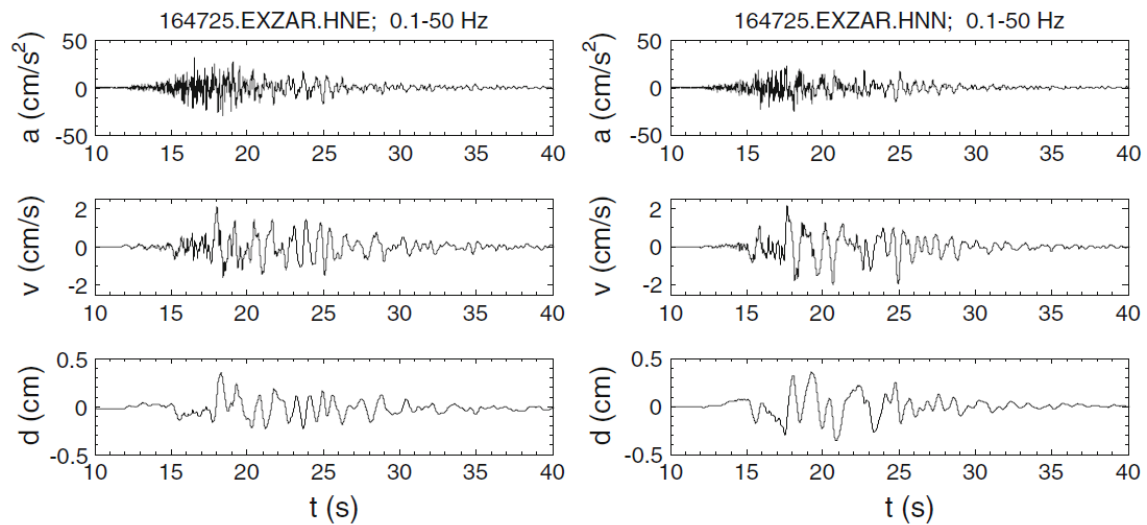
Figure A2.3.20. Horizontal corrected acceleration (top), velocity (middle) and displacement (bottom) for the two components of the Zarcilla de Ramos station, from Cabañas *et al*. (2014).
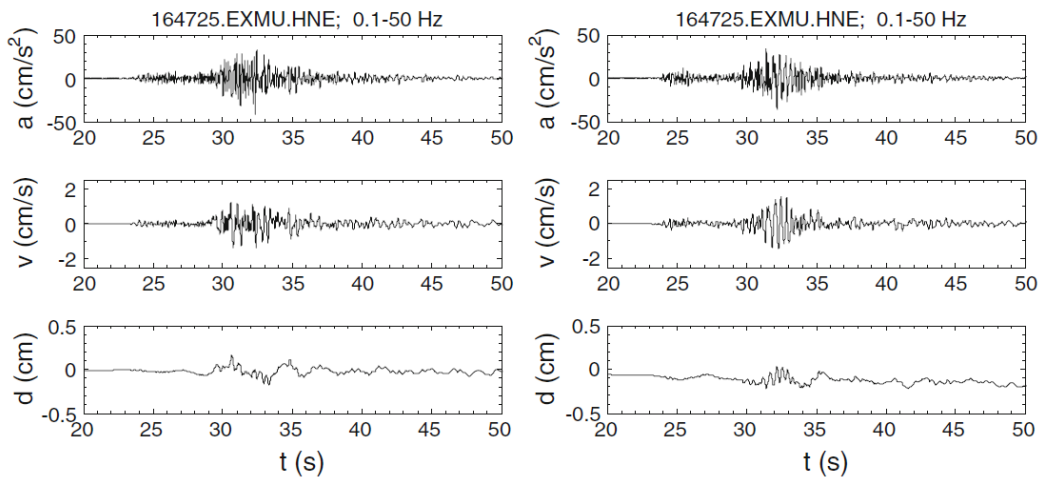
Figure A2.3.21. Horizontal corrected acceleration (top), velocity (middle) and displacement (bottom) for the two components of the Mula station, from Cabañas *et al.* (2014).

Figure A2.3.22 presents the comparisons carried out by Benito Oterino *et al.* (2012) for the PGA values recorded in the different stations with respect to those predicted by four different ground motion prediction equations (GMPEs): Abrahamson & Silva (AS08, 2008), Chiou & Youngs (CY08, 2008), Campbell & Bozorgnia (CB08, 2008) and Akkar & Bommer (AB10, 2010). All of these GMPEs consider the geometric mean of the two horizontal components: geometric mean of as-recorded components in the case of AB10, and GMRotI50 in the other three cases. In order to make the comparisons, the authors have used a V_{s30} value of 1100 m/s. In general, and with the exception of the Mula station, acceleration values recorded at distances larger than 20 km are equal to or smaller than those predicted by the GMPEs. For the case of the Lorca station, the geometric mean of the as-recorded components matches the predictions of CB08 and CY08, but each individual component is significantly different from this value.
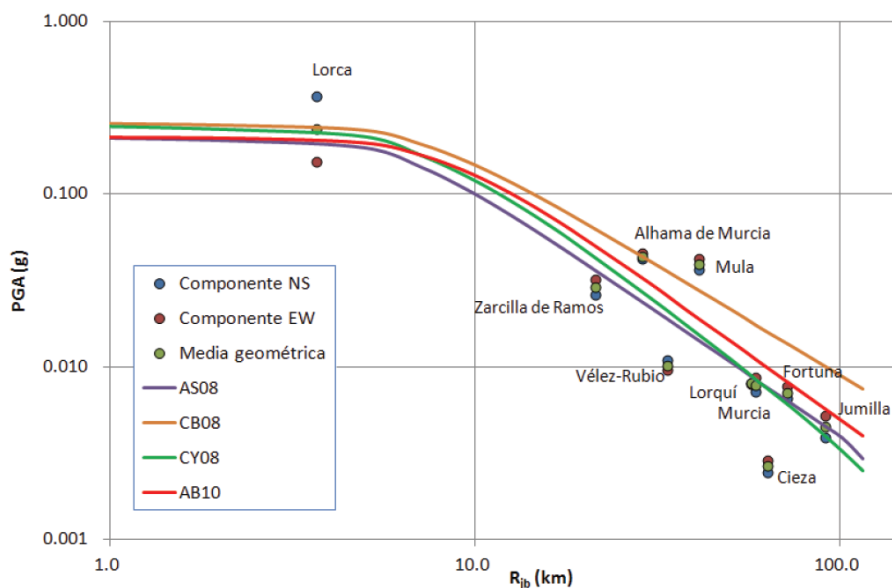
Figure A2.3.22. PGA values recorded at different stations during the main shock against estimations from ground motion prediction equations, from Benito Oterino *et al.* (2012). Blue, red and green dots correspond to north-south, east-west and geometric mean values for each record.

141

Results of the previous comparison are similar to those obtained by Belvaux *et al.* (2014) (Figure A2.3.23) using GMPEs developed for Spain: Cabañas *et al.* (1999), Tapia *et al.* (2007) and Mezcua *et al.* (2008).
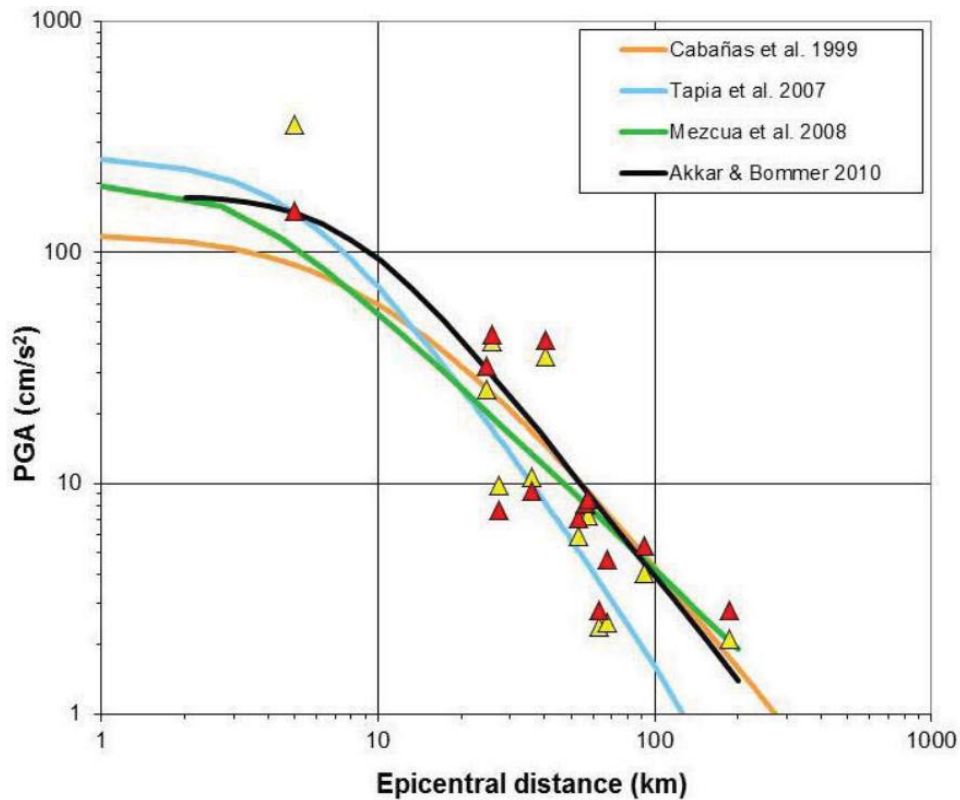
Figure A2.3.23. PGA values recorded at different stations during the main shock against estimations from ground motion prediction equations, from Belvaux *et al.* (2014).

Cabañas *et al.* (2014) have compared the pseudo-acceleration response spectra (5% critical damping) of the accelerograms recorded at the Lorca, Alhama de Murcia 02 and Mila stations with the elastic design spectra from the NCSE-02 Spanish building code for the soil types they consider representative of the site conditions at those locations. As can be observed in Figure A2.3.24, the pseudo-spectral accelerations of the N30W component of the Lorca station record largely exceed those of the design spectra in the low-period range. Some of the spectral accelerations for the E30N component exceed the design spectra as well, albeit to a lesser extent. On the other hand, both components of the Alhama de Murcia 02 and Mula stations do not exceed the spectral accelerations from the corresponding design spectra (Figure A2.3.25). It should be noted that this comparison is more appropriate for the spectral shape than for the actual values of the ordinates themselves.
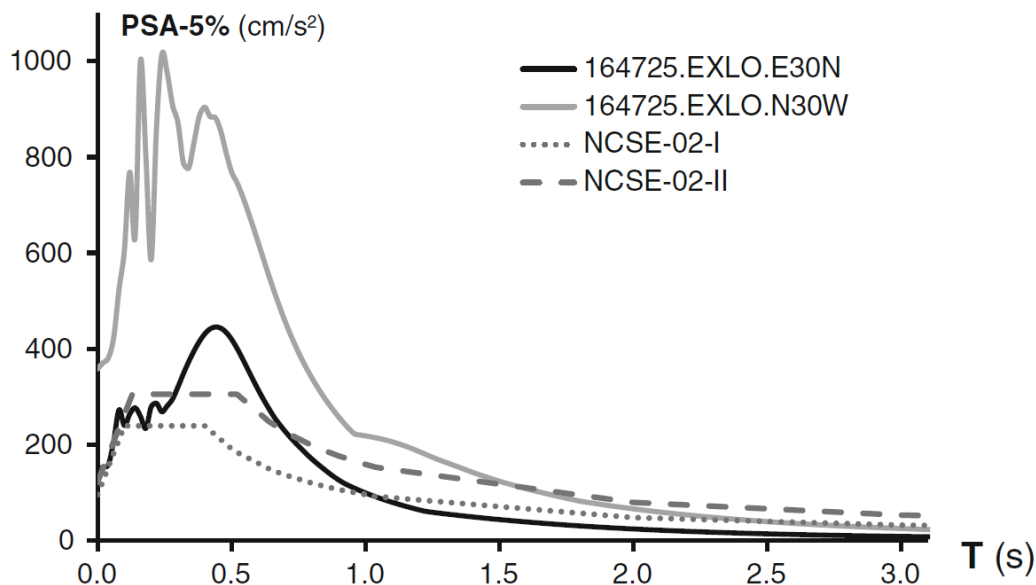
Figure A2.3.24. Pseudo-acceleration response spectra (5% critical damping) from the accelerograms recorded at the Lorca station, compared with the elastic design spectra from the NCSE-02 Spanish building code for soil types I and II (equivalent to soil classes A and B in Eurocode 8), from Cabañas *et al.* (2014).
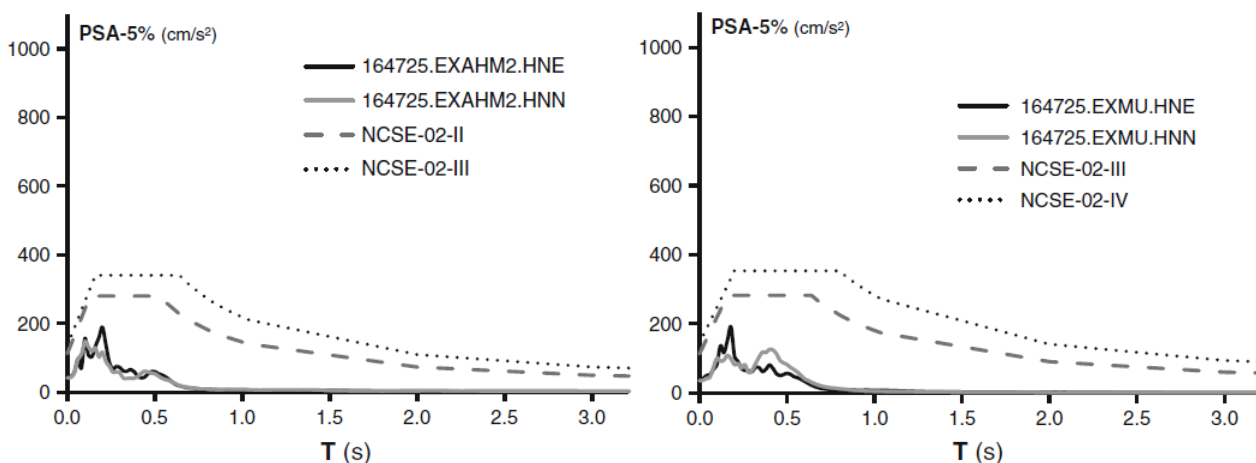
Figure A2.3.25. Pseudo-acceleration response spectra (5% critical damping) from the accelerograms recorded at the Alhama de Murcia 02 (top) and Mula (bottom) stations, compared with the elastic design spectra from the NCSE-02 Spanish building code for soil types II and III (equivalent to soil classes B and C in Eurocode 8, top) and III and IV (equivalent to soil classes C and D in Eurocode 8, bottom), from Cabañas *et al.* (2014).

Cabañas Rodríguez *et al.* (2011) have compared the pseudo-acceleration response spectrum of the N30W component of the Lorca station accelerogram with the median spectra obtained from several GMPEs for the corresponding magnitude, distance and local conditions. As can be observed in Figure A2.3.26, the spectrum of the recorded component easily exceeds all those obtained with the GMPEs.
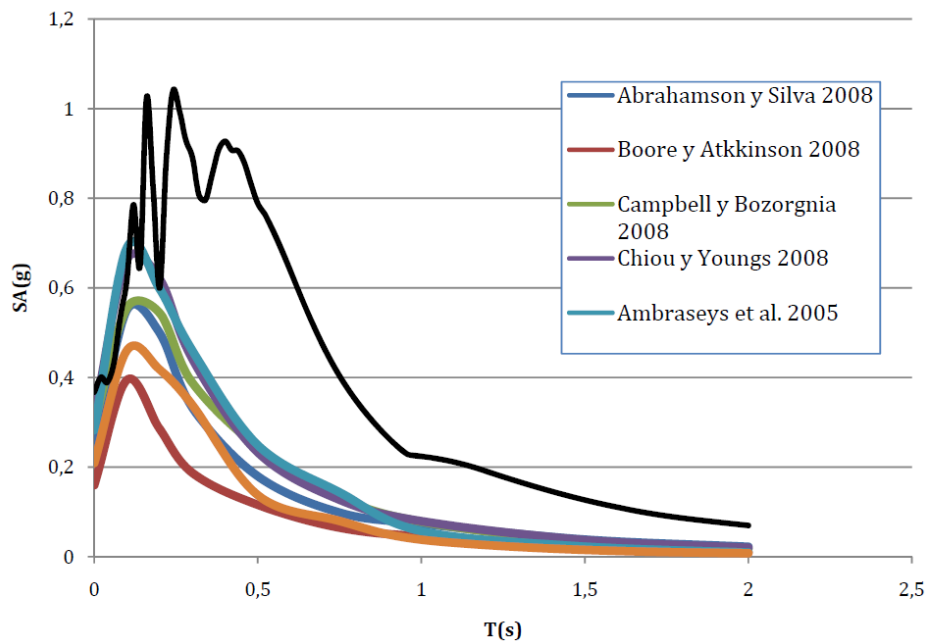
Figure A2.3.26. Pseudo-acceleration response spectra (5% critical damping) from the N30W component of the accelerogram recorded at the Lorca station, compared with mean spectra from different GMPEs, from Cabañas Rodríguez *et al.* (2011).

Cabañas Rodríguez *et al.* (2011) draw attention to the fact that the two stations located in Alhama de Murcia are located at similar distances from the epicentre of the main shock but have recorded very different PGA levels (see Table 0.2.4). The authors believe that this is probably due to one of the stations (the one with the largest recorded motion) being located over softer soils than the other one, though they acknowledge the need for a more detailed analysis.

Several authors believe that directivity effects contributed to the significant level of damage that occurred within the city of Lorca (López-Comino *et al.*, 2012; Pro *et al.*, 2014; Rueda *et al.*, 2011). Unusually well-defined pulses can be easily observed in the two components of the record from Lorca station (Figure A2.3.18). In spite of the common belief that directivity effects only take place with events larger than **M**6.5, they have been observed in other small-to-moderate magnitude events, such as the **M**5.7 1986 San Salvador earthquake (Bommer *et al.*, 2001).

Rueda *et al.* (2011) used the wavelet transform technique of Baker (2007) and identified velocity pulses due to directivity in the three components of the accelerograms recorded at the Lorca station. Figure A2.3.27 shows the pulses extracted from the recorded ground motions. A pulse period of 0.67 seconds was calculated, though this value does not match the peaks observed in both components in the response spectrum, which occur at a period of around 0.4 seconds, as shown in Figure A2.3.24 (Belvaux *et al.*, 2014).
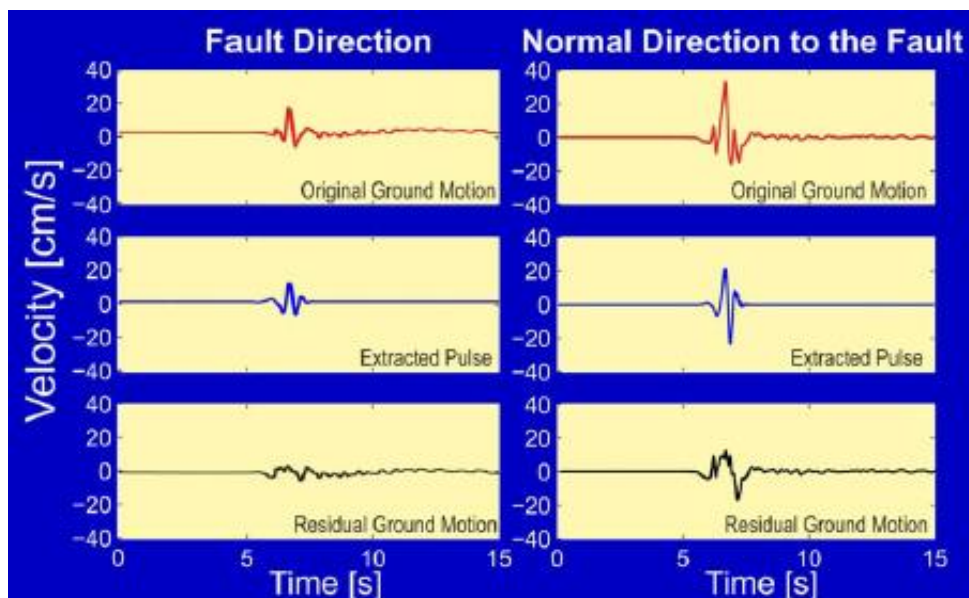
Figure A2.3.27. Original velocity time-history (top), extracted velocity pulse (middle) and residual velocity time-history (bottom) for the E30N (left) and N30W (right) components of the accelerogram recorded by the Lorca station, from Rueda *et al.* (2011).

A2.3.4.3 Inferred shaking levels

The only recording station within the city of Lorca is the Lorca station which, as mentioned earlier, is located on an elevated part of the city, over soils that could be classified as rock or very dense soil, according to different sources. As will be described later on, the most damaged areas of the city correspond to those in which softer soils are predominant, at lower altitudes. Based on the soil types and on the possible amplification due to basin effects, it is thus possible to believe that the structures might have experienced larger ground motions than those recorded at Lorca station. However, it is known that hills and ridges can cause significant amplification of ground motions as well (*e.g.* 1994 Northridge earthquake, California, Bouchon & Baker, 1996), and therefore it is also possible that the accelerations recorded at Lorca station be actually larger than those affecting the structures in the valley. No attempts to infer ground shaking levels within the city of Lorca from macroseismic intensities have been found in the literature.

A2.3.4.4 Duration of ground shaking

Benavent-Climent *et al.* (2014) and Alfaro *et al.* (2012) consistently report that the significant duration of the main shock, defined as the time lapse between the release of the 5% and 95% of the Arias Intensity, was 0.935 seconds and 1.00 second, respectively. This value is small and shows that buildings had to absorb most of the energy of the earthquake in a very short period of time, a situation which is quite common in the near-field.

Estimations of earthquake significant durations can be obtained by means of prediction equations such as those of Bommer *et al.* (2009) and Kempton & Stewart (2006). Using the rupture plane defined by Martínez-Díaz *et al.* (2012) and a range of shear wave velocities deemed appropriate for the site of the Lorca station, these equations yield values for the significant duration between 2.27 and 3.47 seconds. These are clearly larger than those

reported by Benavent-Climent *et al.* (2014) and Alfaro *et al.* (2012), though within three standard deviations, showing that the significant duration of the Lorca earthquake at Lorca station was smaller than the expected median.

A2.3.5 Collateral earthquake hazards

A2.3.5.1 Surface rupture

Martínez-Díaz *et al.* (2011) and Cabañas Rodríguez *et al.* (2011) report that a field survey carried out during three days soon after the main shock found no signs that would indicate the existence of surface rupture due to the earthquake sequence.

Detailed studies of the rupture process carried out by Pro *et al.* (2014), López-Comino *et al.* (2012) and Martínez-Díaz *et al.* (2012) support these observations and conclude that the rupture did not reach the surface, though it stopped propagating quite close to it, at a depth of around 1.5 km, an observation that can explain the strong ground motions observed. Pro *et al.* (2014) and Martínez-Díaz *et al.* (2012) report rupture planes of 12.5 km^2 and 9.0 km^2, respectively, with associated maximum slips of 27 cm and 15 cm.

A2.3.5.2 Landslides

In the 1,000 km^2 that make up their study area, Alfaro *et al.* (2012) identified 256 areas in which landslides had been induced by the earthquake sequence, with a total affected area of around 104 km^2. The authors report a prevalence of disrupted instabilities (*i.e.*, relatively highly-fragmented rocks and soil) over coherent (*i.e.*, unfragmented) ones, as defined by Keefer (1984), and highlight the fact that neither of them can be attributed to a singular event within the seismic sequence. Further, they also observed some instabilities along the Guadalentín river, which crosses the city. Those observed upstream were clearly earthquake-induced, while those downstream seemed to be the consequence of previous heavy rains, as explained by local land-owners. The maximum observed distances from the epicentre of the main shock to the landslides was 13.3 km for disrupted landslides and 4.4 km for coherent ones. Figure A2.3.28 shows the landslides they identified.

Alfaro *et al.* (2012) and Rodríguez-Peces *et al.* (2014) coincide in saying that landslides were more common in Miocene materials such as calcareous sandstones, conglomerates and marls, followed by argillites, gypsums, fine-grained soil, phyllite/slate, and coarse-grained soil.

Alfaro *et al.* (2012) do not report any damage to the building stock or casualties directly associated to the landslides, and only mention disruption in roads and communications between the city of Lorca and rural areas nearby. Rodríguez-Peces *et al.* (2014) and Martínez-Díaz *et al.* (2011) make reference to these disruptions as well and describe some damage in buildings and civil structures attributable to these instabilities. In particular, they mention that part of a wall enclosing the courtyard of a house was destroyed by a fallen

rock, at the easternmost point of the Lorca's castle cliff, and that the pavement of the road leading to the castle as well as that on the road to the Pantano de Puentes dam were seriously damaged by rock falls. Martínez-Díaz *et al.* (2011) believe that some of these areas might be related to instabilities prior to the 2011 earthquake, and highlight that both roads were open to traffic again ("with relative normality") between 24 and 48 hours after the main shock. However, Cabañas Rodríguez *et al.* (2011) indicate that circulation along the road to the Pantano de Puentes dam was still disrupted by July 2011.

Figure A2.3.28. Landslides identified by Alfaro *et al.* (2012). "LOR" makes reference to Lorca station (Alfaro *et al.*, 2012).

Martínez-Díaz *et al.* (2011) describe that some sections of the external wall of the north face of Lorca's castle collapsed due to ground instability. They also take notice that stabilization work had been carried out along the south face of the castle about three years before the earthquake, and that precautionary measures taken at that time were fundamental in avoiding further damage and losses during the 2011 events.

A2.3.5.3 Liquefaction

Liquefaction not reported for this earthquake.

A2.3.6 Exposed population

A2.3.6.1 Socio-economic setting

According to the 2014 Human Development Report (United Nations, 2014), the Human Development Index (HDI) for Spain in 2013 was 0.869, while its Inequality-adjusted HDI (IHDI) was 0.775. This located Spain in the 27th place in the world's ranking, while the

Netherlands ranks 4th. The following table compares the HDI and IHDI for both countries from the last three Human Development Reports (United Nations, 2011; United Nations, 2013; United Nations, 2014). The column "Adj. HDI" provides the HDI values given in the 2014 report for previous years, adjusted for data consistency in time.

Table A2.3.5. Human Development Index and Inequality-adjusted Human Development Index for Spain and the Netherlands.

Report	Data	Spain				Netherlands			
		HDI	IHDI	Rank	Adj. HDI	HDI	IHDI	Rank	Adj. HDI
2011	May 2011	0.878	0.799	23	0.868	0.91	0.846	3	0.914
2013	October 2012	0.885	0.796	23	0.869	0.921	0.857	4	0.915
2014	November 2013	0.869	0.775	27	-	0.915	0.854	4	-

The autonomous community of Murcia, where Lorca is located, is the region which experienced the largest economic growth between 1995 and 2008 in Spain. The mean annual growth of its gross domestic product (GDP) was 4.3% for this period, while that of Spain was 3.5% (data from the Strategic Plan of the Murcia Region 2014-2020, "Plan Estratégico de la Región de Murcia 2014-2020", 2012). This situation changed drastically in 2008, due to the significant crisis that hit Europe.

Said crisis also affected the unemployment levels significantly in the years before the 2011 Lorca earthquake. From a 7.56% unemployment rate in 2007, Murcia moved to 12.63%, 20.73% and 24.49% in 2008, 2009 and 2011, respectively. For the same years, the unemployment rates in Spain as a whole were 8.26%, 11.34%, 18.01% and 20.89%. (Sources: Wikipedia, citing the website of the Spanish National Statistics Institute (INE) website, and INE's press releases).

Figure A2.3.29 shows that, in the year 2012, the GDP per capita of Murcia was ranked 15th amongst all of the Spanish autonomous communities, and it was below the national average (data from the Spanish National Statistics Institute, Instituto Nacional de Estadística, INE).

A2.3.6.2 Population density and distribution

According to the INE, the population of the municipality of Lorca was 92,694 in 2010 and 92,869 in 2011. Around 60% and 25% of the population is located within the city of Lorca itself and its surrounding parishes (pedanías, in Spanish, Figure A2.3.30), respectively.

A2.3.6.3 Time of day of earthquake

The foreshock occurred on 11th May 2011 at 17.05 local time, while the main shock occurred on the same day at 18.47 local time. According to Goula *et al.* (2011), public offices and schools were already closed at the time of the main shock and, therefore, the number of people exposed inside these kinds of buildings was reduced. Further, said

authors highlight that the foreshock played a significant role in creating concern in the population and encouraging them to stay in open areas outside of buildings.
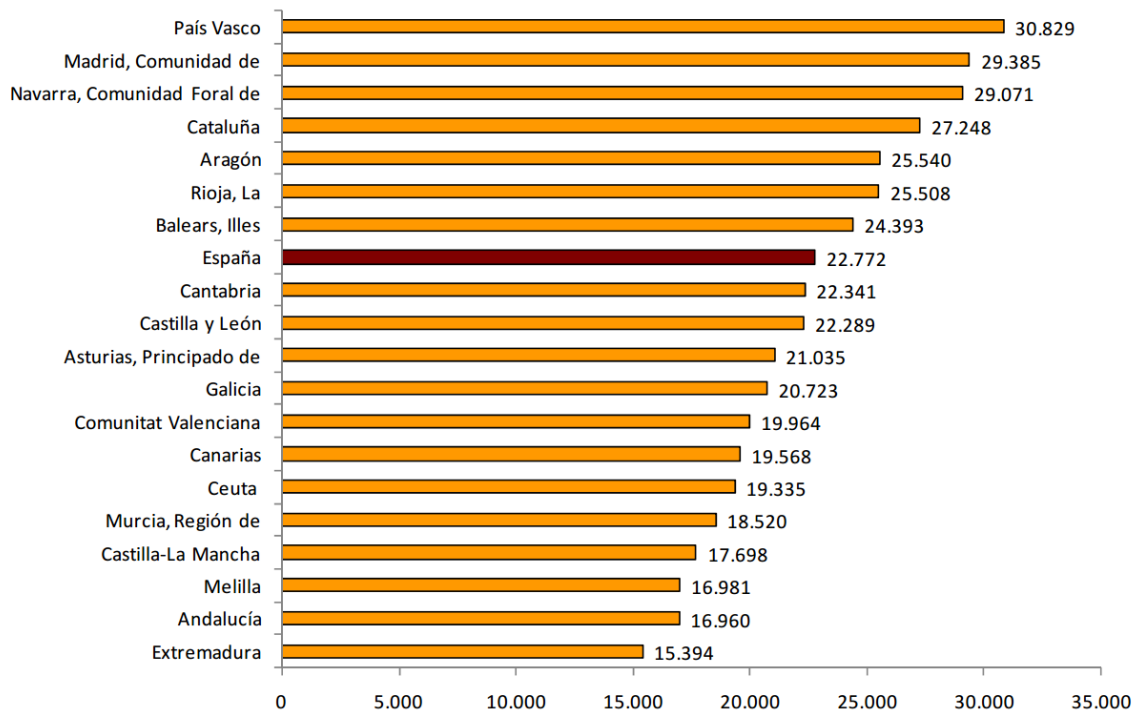
Figure A2.3.29. GDP per capita for all the autonomous communities of Spain, compared with that of the whole country (red bar), from the Spanish National Statistics Institute (2016).

Figure A2.3.30. Parishes ("pedanías") of the municipality of Lorca. The zone marked as 1 corresponds to the city of Lorca itself. Around 85% of the population of the whole municipality are located within the red circle.

A2.3.7 Characteristics of exposed building stock

Basset-Salom and Guardiola-Víllora (2014) give a brief overview of the building stock in the city of Lorca saying:

"Lorca [...] is characterized by a very rich historic heritage including not only monumental or religious buildings (towers, mansions, palaces, churches or monasteries) but also a residential stock varied in age and styles".

And:

"The city was seriously damaged by the strong 1674 earthquake which was the starting point of a long period of reconstruction: most of the building stock of the city centre, the monumental buildings and its actual urban structure belong to the following 200 years".

A2.3.7.1 Seismic design codes

The first Spanish seismic code was published in 1962, and it was updated in 1968 and 1974. In all these versions, the whole country is subdivided in seismic regions according to expected levels of macroseismic intensity. The 1962 code uses the Modified Mercalli Scale (MMS; Musson & Cecić, 2012), and assigns Lorca an intensity level of VIII. The 1968 and 1974 codes use the Medvedev-Karnik-Sponheuer scale (MSK; Musson & Cecić, 2012) instead, and the numeric value of VIII is maintained for Lorca. In all cases, the macroseismic intensity assigned to Lorca is above the threshold for which the codes needed to be applied. Seismic design was static, very basic, and carried out only for structural elements (Cabañas Rodríguez *et al.*, 2011).

The NCSE-94 code of 1994 abandoned the use of macroseismic intensities and provided, for the first time, design acceleration values calculated by means of a probabilistic seismic hazard analysis. As with modern codes, this value was used to scale a pseudo-acceleration spectrum. For the case of Lorca, the design PGA on rock with a 10% probability of exceedance in 50 years was 0.12 g. This value remained unchanged in the NCSE-02 code of 2002, the most recent seismic code of Spain, and was clearly exceeded during the 2011 Lorca earthquake. Based on a study regarding the ground motions registered during the 1999 Mula and 2005 La Paca earthquakes, Gaspar-Escribano & Benito (2007) had warned that pseudo-spectral accelerations at the intermediate-high frequencies could exceed those indicated by NCSE-02 in the Murcia region. Interestingly, a new hazard map was elaborated by the National Geographic Institute (IGN) in 2012, in which a new design PGA value in rock of around 0.18 g is specified for the city of Lorca.

After their analysis of the consequences of the 2011 Lorca earthquake, Cabañas Rodríguez *et al.* (2011) highlight as a major shortcoming of the current Spanish seismic design code (NCSE-02) the fact that it does not limit the maximum displacement of buildings in terms of absolute values.

Eurocode 8 is not yet in force for application in Spain, though it can be voluntarily applied by engineers, as long as they comply with NCSE-02 as well. According to Arnedo Pena (2010), by mid-2010 the translation of Eurocodes into Spanish had almost been finished, while the phase of elaborating the National Annex had partially started already, though 2010 was supposed to be the year for their complete implementation. The proposal for the National Annex containing the National Determined Parameters (NDPs) for the application of Euocode 8 can be downloaded from the website of the Ministerio de Fomento of Spain.

In a presentation given at the University of Costa Rica, Patrick Murphy Corella (Spanish architect, practitioner, member of the Asociación Española de Ingeniería Sísmica, AEIS) pointed out that very little seismic design concepts could be observed in the reinforced concrete (RC) buildings that suffered the most damage in Lorca. Similar comments can be found in the report by Regalado & Lloret (2011).

From personal communications with Spanish civil engineers, it appears that compliance with the NCSE-02 code is duly verified by official entities, but that this does not always translate into a well-elaborated seismic concept design of the structures.

A2.3.7.2 Building typologies

Most sources coincide in the most basic classification of the types of buildings in the city of Lorca at the time of the earthquake being a simple division between heritage (mostly churches), masonry and reinforced concrete (RC) buildings.
In their report on the 2011 Lorca earthquake, Cabañas Rodríguez *et al.* (2011) provide the most useful classification that could be found in the literature, given that they relate the six basic typologies that they describe to their equivalents in the EMS-98 (Grunthal, 1998), HAZUS (FEMA, 2003) and RISK-UE BTM (Milutinovic & Trendafiloski, 2003) classification schemes. The six typologies which, according to Cabañas Rodríguez *et al.* (2011), comprise most of the building stock of Lorca are:

- EMM: ordinary masonry walls with timber floors/roof without diaphragm effect, usually built before the 20th century
- EML: brick masonry walls with timber floors/roof without diaphragm effect, typical of the period 1921-1940
- EMH: brick masonry walls with RC floors/roof with diaphragm effect, usually built between 1941 and 1964
- EHP: RC frames constructed between 1965 and 1996
- EHP94: RC frames constructed between 1997 and 2004 (NCSE 94 building code)
- EHP02: RC frames constructed after 2004 (NCSE 02 building code)

For evident reasons, Cabañas Rodríguez *et al.* (2011) group the first and last three typologies under the names of "traditional" and "technological" constructions, respectively.

The European Macroseismic Scale (EMS-98) classifies buildings into six vulnerability classes, from A through F, with the former and the latter corresponding to the most and

least vulnerable, respectively. Cabañas Rodríguez *et al.* (2011) classify their six typologies according to the EMS-98 vulnerability scale as follows:

Table A2.3.6. EMS-98 vulnerability classes of the six building typologies identified for Lorca, according to Cabañas Rodríguez *et al.* (2011).

Typology	EMS-98
EMM	A
EML	B
EMH	C
EHP	C
EHP94	D
EHP02	D

Cabañas Rodríguez *et al.* (2011) provide as well the relationship between the typologies in Lorca and those defined by the RISK-UE Building Typology Matrix (RISK-UE BTM, Milutinovic & Trendafiloski, 2003), as well as their associated vulnerability index. Within the RISK-UE vulnerability classification scheme, each typology is assigned a basic vulnerability index between 0 and 1, which represents the vulnerability level expected for the buildings that belong to that typology. This basic vulnerability index can then be adjusted to account for the peculiarities of each building, as well as regional differences. Values close to 1 correspond to the greatest vulnerability, while values close to 0 are assigned to structures designed to high code standards. Table A2.3.7 presents the vulnerability indices and equivalence of building typologies established by Cabañas Rodríguez *et al.* (2011).

Table A2.3.7. RISK-UE typologies and vulnerability indices for the different typologies in Lorca, according to Cabañas Rodríguez *et al.* (2011).

Typology	Storeys	RISK-UE BTM and Vulnerability Index		
EMM	1-2	0.85 M11L	Rubble stone and/or fieldstone, low-rise	
	3-5	0.89 M11M	Rubble stone and/or fieldstone, mid-rise	
	+6	0.93 M11H	Rubble stone and/or fieldstone, high-rise	
EML	1-2	0.72 M31L	Wooden slabs and unreinforced masonry, low-rise	
	3-5	0.76 M31M	Wooden slabs and unreinforced masonry, mid-rise	
	+6	0.80 M31H	Wooden slabs and unreinforced masonry, high-rise	
EMH	1-2	0.59 M34L	RC slabs and unreinforced masonry, low-rise	
	3-5	0.61 M34M	RC slabs and unreinforced masonry, mid-rise	
	+6	0.67 M34H	RC slabs and unreinforced masonry, high-rise	
EHP	1-2	0.59 M34L	RC slabs and unreinforced masonry, low-rise	
	3-5	0.60 RC1M	RC moment frames, mid-rise	
	+6	0.68 RC1H	RC moment frames, high-rise	
EHP94	1-2	0.40 RC1L	RC moment frames, low-rise	
	3-5	0.44 RC1M	RC moment frames, mid-rise	
	+6	0.48 RC1H	RC moment frames, high-rise	
EHP02	1-2	0.40 RC1L	RC moment frames, low-rise	
	3-5	0.44 RC1M	RC moment frames, mid-rise	
	+6	0.48 RC1H	RC moment frames, high-rise	

Basset-Salom & Guardiola-Víllora (2014) provide a detailed description of the main characteristics of the unreinforced masonry non-heritage buildings in Lorca at the time of the earthquake, which are summarized below:

- Load bearing walls form the street façades of a corner building, or the main façade and the interior courtyard façade, and load bearing party walls.
- Façade walls are between 30 and 80 cm thick.
- Walls between adjacent buildings (party walls) are between 20 and 30 cm thick, usually shared by the two structures, with the consequence of these behaving as a whole.
- In general, interior walls are non-structural, thinner and poorly connected to exterior and party walls.
- The following fabric typologies can be found:
    - Small or medium sized rubble or poorly cut stone with lime-mortar, typical of the 18th and 19th centuries, for one or two storeys buildings.
    - Brick masonry fabric (20x10x3/4 cm bricks before 1950, 24x12x4/5 cm bricks afterwards) with lime or cement mortar, typical of the 19th and 20th centuries, for buildings of up to four storeys.
    - Isolated cases of rubble stone masonry with binding brick courses.

- Horizontal systems are usually one of the following:
    - Timber beams for lintels, beams and joists.
    - Lightweight masonry vaults, or a traditional covering made out of a reed and plaster deck, or brick deck under ceramic curved tiles (for the case of roofs).
    - RC beams and joists with ceramic vaults.
- The following elements can be found to be used for adding strength to the buildings:
    - Quoins (solid corner masonry/stone blocks).
    - Plinths (square slabs at base of columns).
    - Floor and wall timber ties or timber ring beams.
    - Timber lintels.
    - Stone frames around openings.
    - Iron ties.
- A large percentage of the façades have balconies with a usual depth of 0.4 m.

Basset-Salom & Guardiola-Víllora (2014) highlight that uniformly squared stone blocks can be found almost exclusively in monumental buildings and mansions.

Regarding the churches that could be found in Lorca at the time of the earthquake, most of which were built between the 15th and 18th centuries, Romão *et al.* (2013) bring attention to the complexity of their structural configuration and geometry, as well as to the heterogeneity of their materials. Further, they emphasize that their degree of maintenance is variable, but often poor. Finally, they describe the use of five types of masonry:

- Small and medium size irregular stones with mortar.

- Two-leaf (*i.e.*, two-layered) wall with an outer leaf made of regular cut stone and an internal one made of small and medium size irregular stones with mortar.
- Brickwork.
- Regular cut stone.
- Three-leaf wall with regular cut stone leaves of similar thickness.

According to Romão *et al.* (2013), the reinforced concrete (RC) buildings in Lorca are mostly residential, but commercial spaces located at street level are frequently observed. Further, basements (often partially-underground) used for parking purposes are common as well. The number of storeys is usually between three and six, and only very few buildings are taller than ten storeys. From the structural point of view, Romão *et al.* (2013) describe two cases: RC columns and beams with floors made by one-way precast concrete joists with RC topping, on one hand, and RC columns, no beams, and floors consisting in flat or waffle slabs, on the other. Benavent-Climent *et al.* (2014) mention the use of wide (flat) beams as being common practice too. External walls, parapets and interior partition walls are usually made of masonry.

In spite of the very detailed descriptions of the building typologies that could be found in Lorca at the time of the earthquake, information regarding the relative quantities of each typology is scarce in publications directly related to the earthquake. It is possible, however, to combine the information contained in the RISMUR ("Seismic Risk of the Autonomous Community of the Murcia Region) and SISMIMUR ("Civil Protection Special Plan in view of the Seismic Risk in the Murcia Region") projects together with data from the 2011 census to get an idea of the overall level of vulnerability of the building stock in Lorca. The resulting distribution of buildings by year of construction and EMS-98 vulnerability class are shown in Figure A2.3.31 and 32. As can be observed, it is estimated that slightly more than 50% of the residential buildings in Lorca belonged to the two most vulnerable classes (A and B).
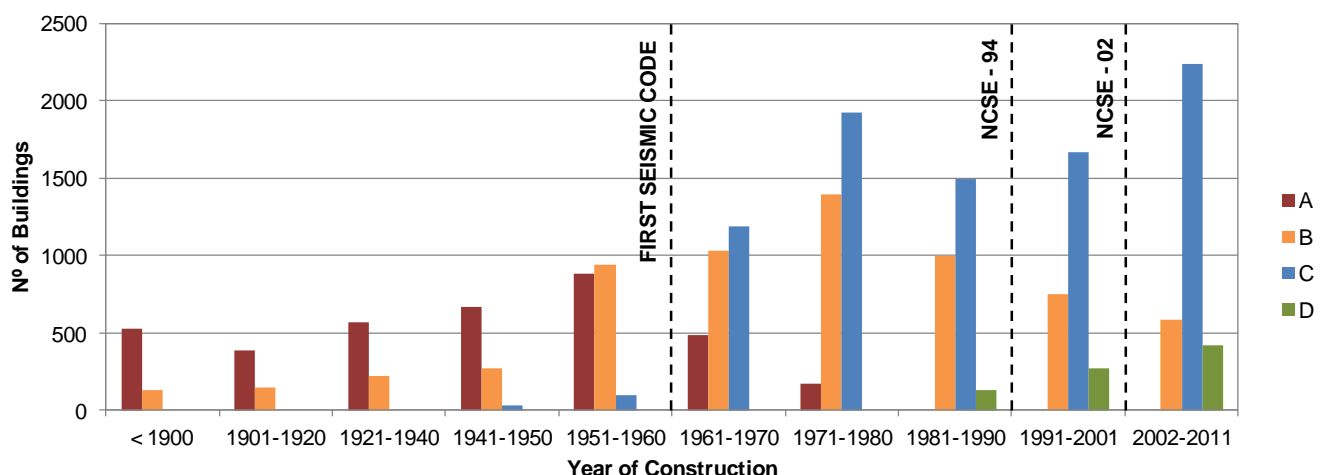
Figure A2.3.31. Number of residential buildings in the municipality of Lorca per year of construction and EMS-98 vulnerability class, estimated from the available data. Vertical dashed lines indicate the introduction of the first Spanish seismic code (1962) and the codes of 1994 and 2002.
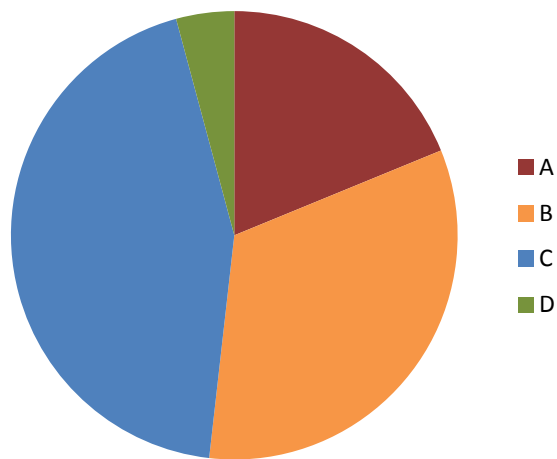
Figure A2.3.32. Estimated percentage of residential buildings belonging to each EMS-98 vulnerability class at the moment of the 2011 Lorca earthquake.

It should be noted that the quantities shown in Figure A2.3.31 correspond to the whole municipality of Lorca, and not just to the city of Lorca itself, and therefore their significance lies in the overall distribution among different categories and not in the absolute values themselves. While the whole municipality of Lorca comprised over 19,000 buildings, the city of Lorca itself and, in particular, the area in which the damage of the earthquake was more severe, comprises only around 8,000 buildings.

Regarding their representativeness, it should be noted that the 2011 census took place after the earthquake, in November 2011. Nevertheless, this information is used because it is probably closer to the situation in May 2011 than the equivalent information from the 2001 census. Further, the information corresponds only to residential buildings. Murphy Corella (2005) reports that these make up 95.64% of the total building stock of the Murcia region. Finally, work carried out by Murphy Corella (2005) was based on the whole of the Murcia region, and it is being assumed herein that this applies directly to the municipality of Lorca, and that all of Lorca's building stock corresponds to an urban environment.

In order to assign overall vulnerability levels within smaller districts in the Murcia region, the SISMIMUR project establishes the following criteria:

- High vulnerability: more than 45% of the building stock corresponds to class A.
- Medium vulnerability: more than 50% of the building stock corresponds to classes A or B combined.
- Low vulnerability: more than 40% of the building stock corresponds to class C.

According to these criteria, the SISMIMUR project assigns a medium vulnerability level to the area in which Lorca is located.

A2.3.7.3 Prior damage and retrofit

Feriche *et al.* (2012) mention that some heritage buildings, particularly churches, have undergone restoration interventions during the last century with some detrimental

consequences. For example, the addition of a compression layer of reinforced concrete in the roofs of heritage buildings has probably increased the stresses over the masonry and, at the same time, increased the mass of the building. Further, the incorporation of metallic braces that have afterwards become rusty has caused the rocks in which they are embedded to break.

Romão *et al*. (2013) make similar observations regarding the church of Santiago, whose dome and transept area were strengthened in the 1960s using reinforced concrete with the aim of providing some kind of diaphragm action. This church suffered quite significant damage.

In contrast, Basset-Salom & Guardiola-Víllora (2014) mention that the residential and commercial unreinforced stone or brick masonry of Lorca's city centre have seldom had any intervention to improve their seismic vulnerability. Exceptions to these observations include the use of ring beams, quoins and iron ties in a reduced number of buildings.

As an interesting detail of a damaging intervention, the Master Plan for the Recovery of Lorca's Cultural Patrimony (In "Plan Director para la Recuperación del Patrimonio Cultural de Lorca (Murcia)", http://www.lorca.es/) makes reference to the merlons of the battlements of the tower of Lorca's castle, which were only added in 1972 and were the first elements to fail, even during the foreshock (Jurado Jiménez, 2012).

A2.3.8 Damage observations

A2.3.8.1 Damage states

Most information regarding damage caused to buildings by the 2011 Lorca earthquake makes use of the European Macroseismic Scale (EMS-98; Grünthal, 1998), which classifies damage into five grades. Further, numerous statistics regarding the post-earthquake tagging are available as well. For details regarding the European Macroseismic Scale and the tagging codes, please refer to Section 2.

A2.3.8.2 Damage statistics

It is relevant to point out the existing level of discrepancy amongst the different statistics that can be found in the literature. In some cases, this is clearly due to the different dates in time in which these were developed (especially those referring to the aftermath soon after the main shock), but in others the cause of differences is unknown.

According to Goula *et al*. (2011), 7,839 buildings had been assessed by 21st May 2011 for fast tagging (assignment of green, yellow and red tags, for damage ranging from null or negligible to serious and extensive). As can be observed in Table A20.2.8, around 10% of the assessed buildings were classified as having moderate to heavy damage. It should be noted that a green tag does not imply absence of damage, and green tagged buildings can present cracks and several other minor problems.

Table A2.3.8. Post-earthquake tagging by 21st May 2011, according to Goula *et al.* (2011). Gray tagging corresponds to buildings which were in ruins before the earthquake.

Tag	N° Buildings	% Buildings
Green	6998	89.3%
Yellow	465	5.9%
Red	309	3.9%
Gray	67	0.9%

Numbers are slightly different within the report prepared by Cabañas Rodríguez *et al.* (2011), who also report the tagging corresponding to 7,839 buildings, but for whom buildings with yellow and red tags represent 8.1% and 4.8% of the total, respectively. They present the information disaggregated by districts. Four districts out of a total of thirty-five suffered damages in over 40% of their building stock, and around 45% of the districts had more than 20% of their building stock tagged as yellow or red. Even though the number of "traditional" and "technological" buildings is provided, tagging information is not separated according to this classification.

The most encompassing statistics can be found in Feriche *et al.* (2012), Benavent-Climent *et al.* (2014) and Donaire Ávila *et al.* (2012), who express that at least 80% of the building stock of the city of Lorca was affected by the earthquake to some extent. All authors coincide in the fact that these statistics correspond to 6,416 inspected buildings out of the 7,852 to 7,890 existing buildings in the area. According to Feriche *et al.* (2012), the damage to the building stock in terms of the European Macroseismic Scale (EMS-98) was as summarized in Table A2.3.9 (left), while according to Benavent-Climent et al. (2014) and Donaire Ávila et al. (2012), the damage observed for the same set of buildings was as summarized in Table A20.2.9 (right).

Table a2.1.9. Damage grades of 6,416 inspected buildings, according to Feriche *et al.* (2012), left, and Benavent-Climent et al. (2014) and Donaire Ávila et al. (2012), right.

N° Buildings	Damage Grade	Authors' Description
4035	1 - 2	Minor damage.
1328	2 - 3	Moderate damage.
689	3 - 4	Moderate to serious damage.
329	4 - 5	Had to be demolished.

N° Buildings	Damage Grade	Authors' Description
4035	2	-
1328	3	-
689	4	Mostly the case of four-storey buildings.
329	5	

The information contained in the tables above is briefly summarized by Rodríguez-Escudero *et al.* (2014) and Martínez-Díaz *et al.* (2012), who report serious damage observed in 1,164 buildings (slightly above the sum of 689 and 329 in the tables), according to data from the Municipality of Lorca by November 2011. Regarding the over 300 buildings that needed to be demolished, Alfaro *et al.* (2012) report that demolition work "was still in progress several months after the main event".

Donaire Ávila *et al.* (2012) provide some insight with respect to the damage suffered by RC buildings built from 1994 to 2002, *i.e.*, according to the NCSE-94 code, and from 2003 to 2008, *i.e.*, built according to the NCSE-02 code. They report 755 and 373 damaged buildings for each group. Figure A2.3.33 shows the number of damaged buildings with EMS-98 damage grade equal to or larger than 3. The authors highlight that the number of buildings designed to code which suffered substantial to very heavy damage is clearly not negligible.
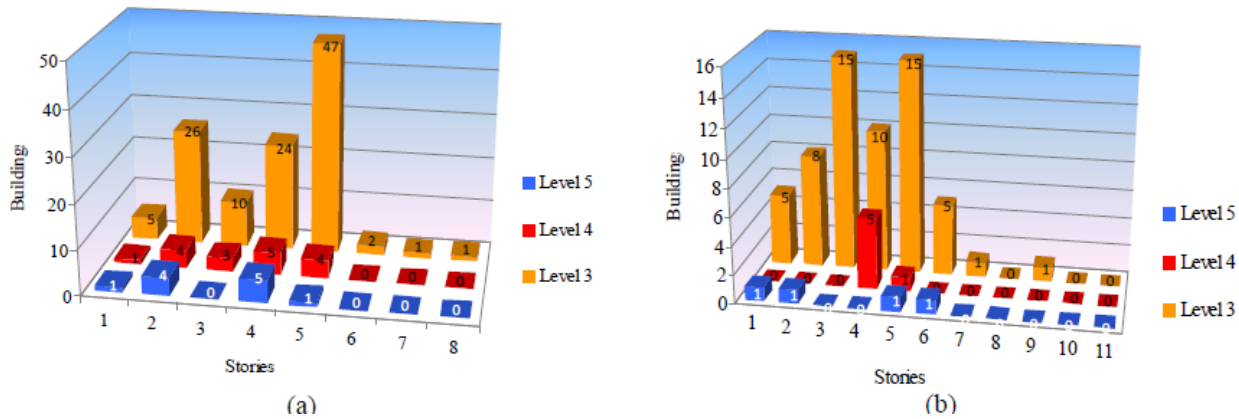
Figure A2.3.33. Number of damaged buildings with EMS-98 damage grade equal to or larger than 3: (a) built between 1994 and 2002; (b) built between 2003 and 2008. (Donaire Ávila *et al.*, 2012).

The vulnerability of RC buildings was clearly demonstrated by the two complete collapses observed, as described by Romão *et al.* (2013). Only one of these occurred during the main shock, while the other took place almost a week after the earthquake when it was about to be demolished. This latter structure, called the "Grial" building, suffered from excessive residual deformations, and from inadequate confinement at the top extreme of the ground storey columns.

The RC building that collapsed during the main shock was located in La Viña neighbourhood, an area that was particularly damaged, as reported in the Damage Distribution section. This building was a 10-year old, 3-storey residential structure, with a partially subterranean parking lot constructed on a slope. The collapse was due to the short column effect of the parking level columns, as it became clear from a neighbouring building with similar characteristics whose columns exhibited damage associated to this phenomenon (Cabañas Rodríguez *et al.*, 2011). While collapsing, the building across the street was hit and damaged. The figure below shows the collapsed building.

Figure A2.3.34. Building located in La Viña neighbourhood which collapsed during the main shock (Meteoweb, 2016). A street runs in between the two buildings shown.

Basset-Salom & Guardiola-Víllora (2014) studied in some detail 65 façades from 50 unreinforced masonry residential buildings located within the historic city centre, 93% of which had timber floors while only 7% had RC floors (RC beams and joists with ceramic vaults) instead. Of these buildings, 46% suffered negligible or slight damage (EMS-98 grade 1), 36% suffered moderate damage (EMS-98 grade 2), 18% suffered substantial to heavy damage (EMS-98 grade 3); worse levels of damage, corresponding to EMS-98 grades 4 and 5, were not observed. The authors report as well the types of failure mechanism that prevailed in each case, based on the classification catalogue developed by D'Ayala & Speranza (2003). As can be observed in the figures that follow, most of the assessed buildings suffered from in-plane mechanisms H or H2.

Figure A2.3.35. Classification of failure mechanisms in masonry according to D'Ayala & Speranza (2003), from Basset-Salom and Guardiola-Víllora (2014).

159
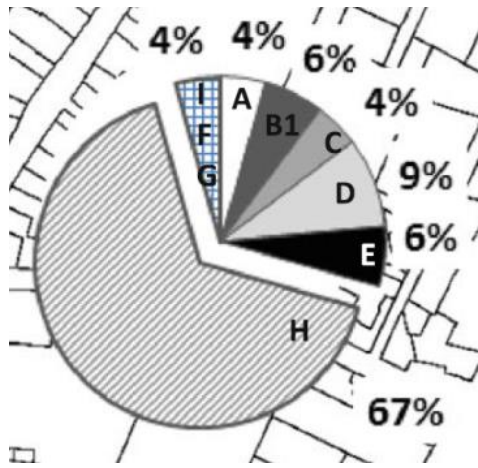
Figure A2.3.36. Failure mechanisms observed in the 50 buildings studied by Basset-Salom & Guardiola-Víllora (2014).

Heritage buildings suffered significant damage during the earthquake. Feriche *et al.* (2012) and Romão *et al.* (2013) describe in detail the most common types of damage observed in churches and other types of historical buildings, which are:

- Partial or total collapse of roofs, towers and walls.
- Significant damage or collapse of belfries.
- Cracking within a wall and in between perpendicular walls.
- Partial or total collapse of arches, vaults and walls.
- Detachment of façades and ornaments.
- Cracking of buttresses and arches.
- Vertical displacement of the keystones in arches.

Basset-Salom & Guardiola-Víllora (2014) highlight that some of the heritage buildings that had to be demolished were listed in the Catalogue of Protected Buildings of 1994.

The possible examples of damages in churches are several, but that of the Church of Santiago is of particular interest not only due to its severity but also to the fact that said building had been retrofitted in the 1960s. At that time, the dome and transept area were strengthened using reinforced concrete with the aim of providing some kind of diaphragm action (Romão *et al.*, 2013; Feriche *et al.*, 2012). During the main shock, the dome, roof and vaults collapsed, as shown in Figure A2.3.37.

As mentioned in the Damage States section, non-structural elements such as masonry infills, parapets and ledges, were particularly vulnerable during the earthquake and their failure was responsible for deaths and severe damage. Collapses of non-structural walls surrounding elevator shafts were reported, as well as severe deformation of elevator door frames (Goula *et al.*, 2011). Detachment of air conditioning units due to failure of the façades that were holding them was observed.

Figure A2.3.37. Collapse of the transept area of the Church of Santiago (Wikipedia).

Goula *et al.* (2011) report that seven out of seventeen (41%) pre-school and primary school buildings and three out of eight (38%) secondary school buildings suffered from damage that limited their re-occupation after the earthquake. Three out of four health centers suffered from significant non-structural damage, while the fourth one presented severe structural problems. In view of this, Goula *et al.* (2011) highlight the need for decreasing the vulnerability of primary importance constructions in the area.

Finally, and as reported earlier in the Landslides section, some of the damage observed can be attributed to soil and rocks instability, though not on a significant scale.

A2.3.8.3 Observed weaknesses

Numerous publications make reference to systematic weaknesses observed in the different kinds of constructions. According to Feriche *et al.* (2012), the following weaknesses were systematically observed in heritage buildings (mostly churches): excessive stiffness, low ductility and lack of connection between vertical and horizontal elements.

With regards to unreinforced masonry residential buildings, Romão *et al.* (2013) put emphasis on their geometrical irregularities, heterogeneity of their materials and their frequent lack of conservation, while Basset-Salom & Guardiola-Víllora (2014) report observation of poor quality rubble stones, inadequate bond between stones and mortar, and weak connections between the different leafs of the same wall. Cabañas Rodríguez *et al.* (2011) highlight the poor connection between perpendicular walls.

Romão *et al.* (2013), Cabañas Rodríguez *et al.* (2011) and Goula *et al.* (2011) extensively describe the weaknesses found in RC buildings, which can be summarized as follows:

- Soft storeys at ground level, mainly due to the architectural regulations of the city, which impose that commercial spaces have greater interstorey heights than residential ones, and to the use of masonry exterior walls in all floors except the ground level.
- Short column effects due both to partially underground basements and interaction with masonry infills.
- Inadequate shear reinforcement in columns: a typical spacing of the transverse reinforcement of around 20 to 30 cm and no densification in plastic hinge regions was observed.
- Non-structural masonry infills interacting with structural ones and attracting seismic forces due to their stiffness and lack of separation from the latter, while not being designed for it.
- Insufficient building separation leading to pounding between adjacent buildings.

Regarding non-structural elements such as exterior masonry walls and parapets, Romão *et al.* (2013) report an inadequate seismic performance related to inadequate connection of these elements to the structures, and the interaction between structural and non-structural elements clearly not having been accounted for during the design stage, as mentioned above. Cabañas Rodríguez *et al.* (2011) explain that the NCSE-94 building code, which was in force between 1996 and 2004, only required parapets and ledges to be confined with concrete in areas where the design PGA (in rock) was above 0.16 g, which was higher than that corresponding to Lorca in the same code. This threshold was reduced to 0.12 g in the NCSE-02 code and, therefore, buildings designed after 2004 should have complied with this requirement.

A2.3.8.4 Damage distribution

Several authors highlight the uneven distribution of damage within the city of Lorca (*e.g.*, Alguacil *et al.*, 2014). Cabañas Rodríguez *et al.* (2011) and Benito Oterino *et al.* (2012) report a concentration of damage in some districts of La Viña neighbourhood (southwestern zone of the city, districts 1013 and 1024 of Figure A2.3.38), and district 1027 of the neighbourhood of the Fuerzas Armadas avenue. These authors find a significant correlation between the number of damaged buildings and the soil type, and they observe an increase of damage for buildings located on soft sedimentary soils of the Guadalentín valley. Around 20% of the buildings located on this type of soil were damaged, as shown in Table A2.3.10, in which soils are classified into four categories, IA, IB, II and III, ranging from hard to soft. Figure A2.3.38 superimposes the yellow and red tagged buildings with this soil classification and the administrative districts of the city. Note that this soil classification is slightly different from that shown previously in Figure A2.3.10 (Navarro *et al.*, 2014), but there exists overall consistency between the two. Further, Navarro *et al.* (2014) coincide as well on the influence of unconsolidated Quaternary formations on the level of damage observed, and highlight the case of the neighbourhoods of La Viña (to the south) and La Alberca and La Alameda (close to the Guadalentín river), also shown in the figure below.

Table A2.3.10. Number of damaged buildings per soil type, from Cabañas Rodríguez *et al.* (2011).

Soil Type	N° Buildings	Damaged Buildings	% of Buildings Damaged
IA (hard)	369	24	6.50%
IB	1006	74	7.36%
II	2013	127	6.31%
III (soft)	3374	664	19.68%
All	6762	889	13.15%
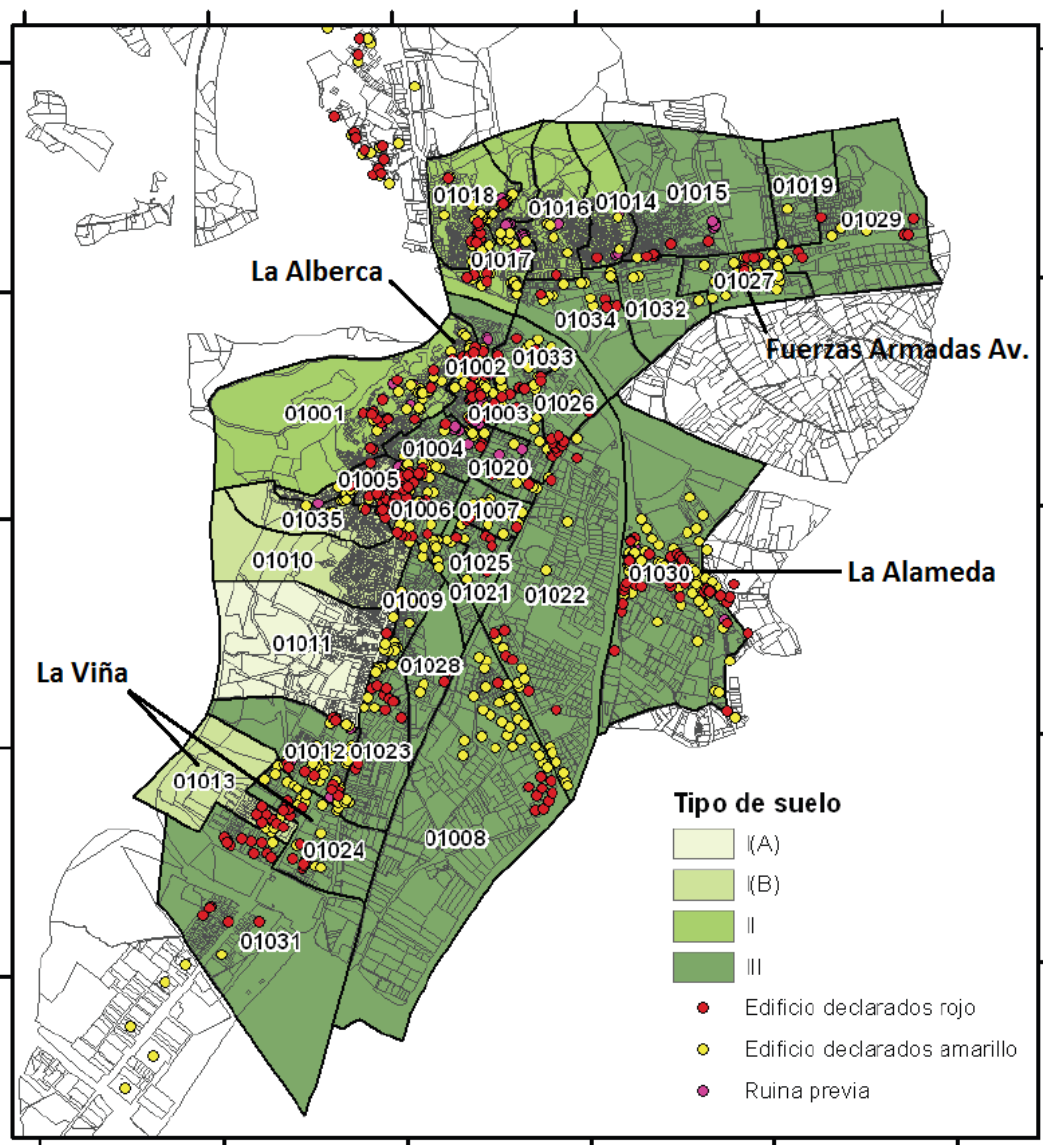
Figure A2.3.38. Yellow and red tagged buildings superimposed to the basic soil types in the city (darker shades of green correspond to softer soils) and its administrative districts, from Benito Oterino *et al.* (2012).

Several authors coincide as well in believing that directivity effects contributed to the significant level of damage that occurred within the city of Lorca, despite the small magnitude of the main shock (López-Comino *et al.*, 2012; Pro *et al.*, 2014; Rueda *et al.*, 2011).

A2.3.9 Casualties and losses

A2.3.9.1 Numbers of dead and injured

Most sources, including the website of the National Geographic Institute (Instituto Geográfico Nacional, IGN) of Spain, indicate that 9 people died due to the 2011 Lorca earthquake (Cabañas Rodríguez *et al.*, 2011; Cabañas *et al.*, 2014; López-Comino *et al.*, 2012; Rodríguez-Escudero *et al.*, 2014), though reference to 10 casualties can be found as well (*e.g.*, EM-DAT International Disaster Database).

Discrepancy can also be observed in what regards the number of injuries, though most sources coincide in citing a number around 300 and 400 people (Cabañas Rodríguez *et al.*, 2011; Cabañas *et al.*, 2014; López-Comino *et al.*, 2012; Rodríguez-Escudero *et al.*, 2014; EM-DAT International Disaster Database).

Regarding those left homeless, the number raises to 15,000, according to the EM-DAT International Disaster Database.

A2.3.9.2 Causes of casualties

Most of the deaths and injuries observed were due to falling objects and non-structural elements such as parapets, external masonry walls and cornices (Pro *et al.*, 2014; Romão *et al.*, 2013), whose failure was systematically observed during this event. In particular, Regalado & Lloret (2011) report that seven out of the nine fatalities can be attributed to this cause.

Several authors (*e.g.*, Alfaro *et al.*, 2012) suggest that the death toll would have been a lot higher had the foreshock that alarmed the population not occurred.

Information regarding the number of casualties associated to the RC building which collapsed during the main shock have not been found. Nevertheless, a local newspaper makes reference to one woman having died due to this collapse, and her son having been found still alive under the debris (Laverdad, 2011).

A2.3.9.3 Estimates of economic losses

Figures for economic losses are quite varied and, in many cases, it is not clear exactly which kind of losses are being considered.

Martínez-Díaz *et al.* (2012) and Rodríguez-Escudero *et al.* (2014) make reference to an estimation of economic losses from the Municipality of Lorca by November 2011 of more than 1,200 million Euros. No details are given of whether these losses are direct or integral.

In an online publication from December 2011, the European Parliament says that a request from Spain for 21.1 million Euros from the European Union Solidarity Fund was approved, and that the total direct cost of the damage caused by the earthquake was estimated in 842.8 million Euros.

This value is similar to the 700 million Euros reported by Olcina Cantos (2011), who specifies that 50 million of which correspond to losses in the historic or artistic patrimony of the city.

A more recent document (2014) from the Spanish Insurance Compensation Consortium (Consorcio de Compensación de Seguros), a public corporate entity attached to the Ministry of Economy and Competitiveness, reports a total value of insurance claims for damage due to the earthquake of around 498 million Euros. Table A2.3.11 shows the disaggregation of the insured losses.

Table A2.3.11. Disaggregation of insured losses by type of damage, from Consorcio de Compensación de Seguros (2014). Values are given in Euros updated to December 2013.

Type of Damage / Risk Class	N° Files	Claims	
		Euros	%
Death	4	136,322	0.0%
Permanent Disability	5	75,854	0.0%
Dwellings and Dwelling Communities	24,996	415,172,739	83.4%
Offices	365	7,362,734	1.5%
Commerces	2,096	67,573,680	13.6%
Industries	202	6,911,276	1.4%
Cars	375	704,168	0.1%
Civil Engineering Works	1	25,241	0.0%
TOTAL	28,044	497,962,014	

It should be noted that a newspaper from the region of Murcia highlights that a big percentage of the properties were not insured, and that this additional demolition and reconstruction costs are falling on the government (Murcia Today, 2011).

All the figures provided above are well above the 200 million US dollars losses reported by the International Disaster Database (EM-DAT).

A2.3.10 Discussion and conclusions

This earthquake occurred on 11th May 2011, at 16.47 UTC (18.47 local time), very close to the city of Lorca, south-eastern Spain, preceded by a **M**4.5 foreshock at 15.05 UTC (17.05 local time), which caused only minor damage. The main shock, on the other hand, reached a maximum EMS-98 intensity of VII and caused losses of around one thousand million Euros to the city of Lorca, nine deaths, and injuries to hundreds of people. The main reasons for the high losses were:

- the proximity of the epicentre to the town (1.8 to 6.0 kilometres, depending on the estimation of the epicentral coordinates),
- the shallowness of the hypocentre (less than 6 km deep),
- directivity effects,
- site amplification effects, and
- vulnerability of the building stock.

Regarding the latter, it is relevant to highlight that, in spite of there being a history of evolution of the Spanish seismic design building codes since the 1960s, a series of weaknesses were systematically observed in the building stock. In particular, reinforced concrete buildings suffered from short column effects and soft storeys, as well as from a lack of adequate seismic gaps in between adjacent structures. Of particular relevance was that their masonry infills and parapets proved to be poorly linked to the structure, either in default or in excess, for failure of these elements was the cause of most casualties. Similarly, structural masonry structures presented problems related to the inadequate bond between stones and mortar, weak connections between the different leafs of the same wall and between vertical and horizontal elements, as well as a combination of excessive stiffness and low ductility. Furthermore, it should also be noted that around 25% of the building stock existing in the municipality of Lorca at the time of the earthquake had been built before the publication of the first code.

Neither surface ruptures nor liquefaction were observed, as expected from its low hazard around the epicentral area. Hundreds of slope instabilities were identified. These were responsible for some very localized damage to buildings, but were not the cause of the widespread losses that took place.

This earthquake was triggered by the effects of groundwater extraction, though the characteristics of the event are consistent with the natural seismicity of the area. This means that human activity may have had an influence on the time and way in which accumulated tectonic stresses were released, but these had nevertheless most likely been building up naturally over several centuries.

A2.3.11 References

A2.3.11.1 Bibliography

Abrahamson, N. & W. Silva (2008). Summary of the Abrahamson & Silva NGA ground-motion relations. *Earthquake Spectra* **24**(1), 67-97.

Akkar, S. & J.J. Bommer (2010). Empirical Equations for the prediction of PGA, PGV, and spectral accelerations in Europe, the Mediterranean region, and the Middle East. *Seismological Research Letters* **81**, 195-206.

Alfaro, P., J. Delgado, F.J. García-Tortosa, L. Lenti, J.A. López, C. López-Casado & S. Martino (2012). Widespread landslides induced by the Mw 5.1 earthquake of 11 May 2011 in Lorca, SE Spain. *Engineering Geology* **137-138**, 40–52.

Alguacil, G., F. Vidal, M. Navarro, A. García-Jerez & J. Pérez-Muelas (2014). Characterization of earthquake shaking severity in the town of Lorca during the May 11, 2011 event. *Bulletin of Earthquake Engineering* **12**(5), 1889–1908.

Armijo, R. (1977). La zona des failles Lorca-Totana (Cordillères Bétiques, Espagne). Étude tectonique et neotectonique. Thèse IIIème cycle, Univ. Paris VII: 229 p.

Arnedo Pena, A. (2010). *How does the system of implementation of European standards works in Spain.* Polish Road Congress Conference, Warsaw, Poland, June 2010. http://www.pkd.org.pl/pliki/eurokody_Arnedo.pdf

Avouac, J.P. (2012). Earthquakes: Human-induced shaking. *Nature Geoscience* **5**(11), 763–64.

Baker, J.W. (2007). Quantitative classification of near-fault ground motions using wavelet analysis. *Bulletin of the Seismological Society of America* **97**, 1486-1501.

Basset-Salom, L. & A. Guardiola-Víllora (2014). Seismic performance of masonry residential buildings in Lorca's city centre, after the 11th May 2011 earthquake. *Bulletin of Earthquake Engineering* **12**(5), 2027–48.

Belvaux, M., A. Macau, S. Figueras, X. Goula & T. Susagna (2014). Recorded ground motion and estimated soil amplification for the May 11, 2011 Lorca earthquake. *Earthquake Spectra* IN PRESS. DOI 10.1193/122212EQS354M

Benavent-Climent, A., A. Escobedo, J. Donaire-Avila, E. Oliver-Saiz & A.L. Ramírez-Márquez (2014). Assessment of expected damage on buildings subjected to Lorca earthquake through an energy-based seismic index method and nonlinear dynamic response analyses. *Bulletin of Earthquake Engineering* **12**(5), 2049–73.

Benito Oterino, M.B., M.E. Jiménez Peña, M.J. García Rodríguez, J.M Gaspar Escribano & J. García Mayordomo (2005). *Riesgo sísmico en la región de Murcia RISMUR - Volumen 5: Evaluación del riesgo sísmico.* RISMUR Report, 103 pp.

Benito Oterino, B., A. Rivas Medina, J.M. Gaspar Escribano & P. Murphy (2012). El terremoto de Lorca (2011) en el contexto de la peligrosidad y el riesgo sísmico en Murcia. *Física de La Tierra* **24**, 255-287.

Bommer, J.J., G. Georgallides & I.J. Tromans (2001). Is there a near-feld for small-to-moderate magnitude earthquakes? *Journal of Earthquake Engineering* **5**(3), 395-423.

Bommer, J.J., P.J. Stafford & J.E. Alarcón (2009). Empirical equations for the prediction of the significant, bracketed, and uniform duration of earthquake ground motion. *Bulletin of the Seismological Society of America* **99**(6), 3217-3233.

Bouchon, M. & J. Baker (1996). Seismic response of a hill; the example of Tarzana, California. *Bulletin of the Seismological Society of America* **86**(1, A), 66-72.

Bousquet, J.C. & H. Phillip (1976). Observations micro-tectoniques sur la compresion nord-sud quaternaire des Cordillères Betiques Orientales (Espagne Méridional - Arc de Gibraltar). *Bull. Soc. Géol. France* **18**, 711-724.

Cabañas, C., B. Benito, M. López, M.E. Jiménez, P. Gómez González, S. Alvarez & L. Cabañas Rodríguez (1999). Banco de datos de movimiento fuerte del suelo: aplicaciones. *Física de la Tierra* **11**, 113-139.

Cabañas, L., J.M. Alcalde, E. Carreño & J.B. Bravo (2014). Characteristics of observed strong motion accelerograms from the 2011 Lorca (Spain) earthquake. *Bulletin of Earthquake Engineering* **12**(5), 1909–32.

Cabañas Rodríguez, L., E. Carreño Herrero, A. Izquierdo Álvarez, J.M. Martínez Solares, R. Capote del Villar, J.J. Martínez-Díaz, B. Benito Oterino, J. Gaspar Escribano, A. Rivas Medina, J. García Mayordomo, R. Pérez López, M.A. Rodríguez Pascua & P. Murphy Corella (2011). *Informe del sismo de Lorca del 11 de Mayo de 2011*. Report of the Instituto Geográfico Nacional, Madrid, Spain. http://digital.csic.es/handle/10261/62381.

Calais, E., C. DeMets, J-M. Nocquet (2003). Evidence for a post-3.16-Ma change in Nubia-Eurasia-North America plate motions? *Earth and Planetary Science Letters* **216**, 81-92.

Campbell K.W. & Y. Bozorgnia (2008). NGA ground motion model for the geometric mean horizontal component of PGA, PGV, PGD and 5% damped linear elastic response spectra for periods ranging from 0.01 to 10 s. *Earthquake Spectra* **24**(1), 139-171.

CEN (2004). *Eurocode 8: Design of structures for earthquake resistance - Part 1: General rules, seismic actions and rules for buildings*. European Committee for Standardization, Brussels, Belgium.

Chiou B.S.-J. & R.R. Youngs (2008). An NGA Model for the average horizontal component of peak ground motion and response spectra. *Earthquake Spectra* **24**(1), 173-215.

Consorcio de Compensación de Seguros (2014). *Estadística riesgos extraordinarios. Serie 1971-2013*. Available online at: http://www.consorseguros.es/web/c/ document_library/get_file?uuid=548d4f59-b6c5-40dd-b06b-98dbcefd790f&groupId=10124

D'Ayala, D. & E. Speranza (2003). Definition of collapse mechanisms and seismic vulnerability of historic masonry buildings. *Earthquake Spectra* **19**(3), 479–509.

DeMets, C., R.G. Gordon, D.F. Argus & S. Stein (1994). Effect of recent revisions to the geomagnetic reversal time scale on estimates of current plate motions, *Geophys. Res. Lett.* **21**, 2191–2194.

Dengler, L. A., & J. W. Dewey (1998). An intensity survey of households affected by the Northridge, California, earthquake of 17 January, 1994, *Bulletin of the Seismological Society of America* **88**, 441-462.

d'Estevou, P. & C. Montenat (1985). Evolution structurale de la zone Betique orientale (Espagne) du Tortonian à l' Holocène. *Comptes-rendus des séances de l'Académie des sciences. Série 2, Mécanique-physique, chimie, sciences de l'univers, sciences de la terre* **300**(8), 363-368.

Donaire Ávila, J., A. Benavent Climent, A. Escobedo Ruiz, E. Oliver Saiz, A.L. Ramírez Márquez & M. Feriche Fernández-Castanys (2012). Damage assessment on building structures subjected to the recent near-fault earthquake in Lorca (Spain). In *Proceedings of the 15th World Conference on Earthquake Engineering*, Lisbon, Portugal, September 24-28.

Feriche, M., F. Vidal, G. Alguacil, C. Aranda, J. Pérez-Muelas, M. Navarro & A. Lemme (2012). Performance of cultural heritage of Lorca (Spain) during the two small earthquakes of May 11th, 2011. In *Proceedings of the 15th World Conference on Earthquake Engineering,* Lisbon, Portugal, September 24-28.

García-Mayordomo, J., J.M. Insua-Arévalo, J.J. Martínez-Díaz, A. Jiménez-Díaz, R. Martín-Banda, S. Martín-Alfageme, J.A. Álvarez-Gómez, M. Rodríguez-Peces, R. Pérez-López, M.A. Rodríguez-Pascua, E. Masana, H. Perea, F. Martín-González, J. Giner-Robles, E.S. Nemser, J. Cabral, QAFI compilers (2012). The quaternary active faults database of Iberia (QAFI v.2.0). *Journal of Iberian Geology* **38**(1), 285-302.

Gaspar-Escribano, J. M. & B. Benito (2007). Ground-motion characterization of low-to-moderate seismicity zones and implications for seismic design: Lessons from recent Mw 4.8 damaging earthquakes in southeast Spain. *Bulletin of the Seismological Society of America* **97**(2), 531–44.

Giardini, D., G. Grünthal, K.M. Shedlock & P. Zhang (1999). The GSHAP global seismic hazard map. *Annali di Geofisica* **42**(6), 1225-1228.

Giardini, D., G. Grünthal, K.M. Shedlock & P. Zhang (2003). The GSHAP global seismic hazard map. In: Lee, W., H. Kanamori, P. Jennings & C. Kisslinger (eds.): International handbook of earthquake & engineering seismology, International Geophysics Series **81**B, Academic Press, Amsterdam, 1233-1239.

Giardini, D., J. Woessner, L. Danciu, H. Crowley, F. Cotton, G. Gruenthal, R. Pinho, G. Valensise, S. Akkar, R. Arvidsson, R. Basili, T. Cameelbeck, A. Campos-Costa, J. Douglas, M. B. Demircioglu, M. Erdik, J. Fonseca, B. Glavatovic, C. Lindholm, K. Makropoulos, F. Meletti, R. Musson, K. Pitilakis, K. Sesetyan, D. Stromeyer, M. Stucchi & A. Rovida (2013). *Seismic Hazard Harmonization in Europe (SHARE): Online data resource*, doi:10.12686/SED-00000001-SHARE.

González, P.J. & J. Fernández (2011). Drought-driven transient aquifer compaction imaged using multitemporal satellite radar interferometry. *Geology* **39**(6), 551–54.

González, P.J., K.F. Tiampo, M. Palano, F. Cannavó & J. Fernández (2012). The 2011 Lorca earthquake slip distribution controlled by groundwater crustal unloading. *Nature Geoscience* **5**(11), 821–25.

Goula, X., J. Irizarry, S. Figueras, A. Macau, A.H. Barbat, L.M. Carreño, N. Lantada, J. Valcarcel (2011). *El terremoto de Lorca del 11 de Mayo de 2011. Informe de la inspección y de los trabajos de campo realizados.* Monografies tècniques, Barcelona, IGC.

Grünthal, G. (ed.) (1998). *European Macroseismic Scale 1998 (EMS-98).* Cahiers du Centre Europeen de Geodynamique et de Seismologie 15, Centre Europeen de Geodynamique et de Seismologie, Luxembourg.

Jiménez-Munt, I., R. Sabadini, A. Gardi (2003). Active deformation in the Mediterranean from Gibraltar to Anatolia inferred from numerical modeling and geodetic and seismological data. *Journal of Geophysical Research* **108**.

Jurado Jiménez, F. (2012). Torre del Espolón: de ruina a primer monumento recuperado en Lorca (Murcia). *Alberca: Revista de La Asociación de Amigos Del Museo Arqueológico de Lorca* **10**, 39–52.

Keefer, D.K. (1984). Landslides caused by earthquakes. *Geological Society of America Bulletin* **95**(4), 406–421.

Kempton, J.J. & J.P. Stewart (2006). Prediction equations for significant duration of erthquake ground motions considering site and near-source effects. Earthquake Spectra **22**(4), 985-1013.

Khazaradze, G., J. Gárate, E. Suriñach, J.M. Davila, E. Asensio (2008). Crustal deformation in south-eastern Betics from CuaTe-Neo GPS network. *Geo-Temas* **10**, 1023-1026.

Koulali, A., D. Ouazar, A. Tahayt, R.W. King, P. Vernant, R.E. Reilinger, S. McClusky, T. Mourabit, J.M. Davila & N. Amraoui (2011). New GPS constraints on active deformation along the Africa–Iberia plate boundary. *Earth and Planetary Science Letters* **308**, 211–217.

López-Comino, J.A., F.L. Mancilla, J. Morales & D. Stich (2012). Rupture directivity of the 2011, Mw 5.2 Lorca earthquake (Spain). *Geophysical Research Letters* **39**(3): n/a–n/a.

Martínez-Díaz, J.J. (2002). Stress field variety related to fault interaction in a reverse oblique-slip fault: the Alhama de Murcia fault, Betic cordillera, Spain. *Tectonophysics* **356**, 291-305.

Martínez-Díaz, J.J., E. Masana & M. Ortuño (2012). Active tectonics of the Alhama de Murcia fault, Betic Cordillera, Spain. *Journal of Iberian Geology* **38**(1), 253-270.

Martínez Díaz, J.J., C. Canora Catalán & J.A. Álvarez Gómez (2005). *Riesgo sísmico en la región de Murcia RISMUR - Volumen 4: Mapa de representación de máxima acumulación de esfuerzos en las fallas activas de la comunidad autónoma de la región de Murcia*. RISMUR Report, 50 pp.

Martínez-Díaz, J.J., M. Bejar-Pizarro, J.A. Álvarez-Gómez, F.L. Mancilla, D. Stich, G. Herrera & J. Morales (2012). Tectonic and seismic implications of an intersegment rupture. *Tectonophysics* **546-547**, 28–37.

Martínez-Díaz, J.J., M.A. Rodríguez-Pascua, R. Pérez López, J. García Mayordomo, J.L. Giner Robles, F. Martín-González, M. Rodríguez Peces, J.A. Álvarez Gómez & J.M. Insua Arévalo (2011). *Geological preliminary field report of the Lorca earthquake (5.1 Mw, 11th May 2011)*. Report of the Instituto Geológico y Minero de España (IGME), Spanish Group of Tectónica Activa, Paleosismicidad y Riesgos Asociados de la Universidad Complutense de Madrid (UCM), Universidad Autónoma de Madrid (UAM) and Universidad Rey Juan Carlos de Madrid (URJC).

Martinez Guevara, J.B. & S. Fernandez Navarro-Soto (1986). *Catálogo sísmico de la región de Murcia (Sismicidad histórica hasta el siglo XVIII)*. Report of the Instituto Geografico Nacional, Spain.

Martinez Solares, J.M. & J. Mezcua (2002). *Catálogo sísmico de la Península Ibérica (880 a.C. - 1900)*. Monography of the Instituto Geográfico Nacional, Spain.

Masana, E., J.J. Martínez-Díaz, J.L. Hernández-Enrile & P. Santanach (2004). The Alhama de Murcia fault (SE Spain), a seismogenic fault in a diffuse plate bundary: Seismotectonic implications for the Ibero-Magrebian region. *Journal of Geophysical* Research 109(B1), n/a-n/a.

Mezcua, J., R.M. Garcia Blanco, & J. Rueda (2008). On the strong ground motion attenuation in Spain. *Bulletin of the Seismological Society of America* **98**(3), 1343-1353.

Milutinovic, Z.V. & G.S. Trendafiloski (2003). *RISK-UE - An advanced approach to earthquake risk scenarios with applications to different European towns - WP4: Vulnerability of current buildings*. RISK-UE Report, 110 pp.

Montenat, C., P.O. D'Estevou & P. Masse (1987). Tectonic-sedimentary characters of the Betic Neogene Bassins evolving in a crustal transcurrent shear zone (SE Spain). *Bull. Centres Rech. Explo. Prod. Elf Aquitaine.* **11**, 1-22.

Morales, J., J.V. Cantavella, F.L. Mancilla, L. Lozano, D. Stich, E. Herraiz, J.B. Martín, J.A. Lopez-Comino & J.M. Martínez-Solares (2014). The 2011 Lorca seismic series: Temporal evolution, faulting parameters and hypocentral relocation. *Bulletin of Earthquake Engineering* **12**(5), 1871–1888.

Morel, J.L. & M. Meghraoui (1996). Gorringe-Alboran-Tell tectonic zone: a transpression system along the Africa-Eurasia plate boundary. *Geology* **24**, 755-758.

Murphy Corella, P. (2005). *Riesgo sísmico en la región de Murcia RISMUR - Volumen 3: La vulnerabilidad de la edificación de la región de Murcia.* RISMUR Report, 60 pp.

Navarro, M., A. García-Jerez, F.J. Alcalá, F. Vidal & T. Enomoto (2014). Local site effect microzonation of Lorca town (SE Spain). *Bulletin of Earthquake Engineering* **12**(5), 1933–1959.

NCSE-02 (2002). *Norma de Construcción Sismorresistente: Parte general y edificación - Real decreto 997/2002, de 27 de Septiembre.* Published in BOE **244**, 35898-35967.

Olcina Cantos, Jorge (2011). Lecciones tras el desastre de Lorca (terremotos del 11 de Mayo de 2011). *Estudios Geográficos* **72**(271), 717–724.

Pro, C., E. Buforn, S. Cesca, C. Sanz de Galdeano & A. Udías (2014). Rupture process of the Lorca (southeast Spain) 11 May 2011 (M W = 5.1) earthquake. *Journal of Seismology* **18**, 481–95.

Regalado, F. & V. Lloret (2011). *Análisis y reflexiones sobre los terremotos del 11 de mayo del 2011 acontecidos en Lorca (sugerencias para el futuro).* Report of the Equipo Técnico de Florentino Regalado y Asociados y Regalado Arquitectos.

Rodríguez-Escudero, E., J.J. Martínez-Díaz, J.A. Álvarez-Gómez, J.M. Insua-Arévalo & R. Capote del Villar (2014). Tectonic setting of the recent damaging seismic series in the southeastern Betic Cordillera, Spain. *Bulletin of Earthquake Engineering* **12**(5), 1831–1854.

Rodríguez-Peces, M.J., J. García-Mayordomo & J.J. Martínez-Díaz (2014). Slope instabilities triggered by the 11th May 2011 Lorca earthquake (Murcia, Spain): Comparison to previous hazard assessments and proposition of a new hazard map and probability of failure equation. *Bulletin of Earthquake Engineering* **12**(5), 1961–1976.

Romão, X., A.A. Costa, E. Paupério, H. Rodrigues, R. Vicente, H. Varum & A. Costa (2013). Field observations and interpretation of the structural performance of constructions after the 11 May 2011 Lorca earthquake. *Engineering Failure Analysis* **34**, 670–692.

Rueda, J., J. Mezcua, R.M. García-Blanco (2011). Directivity effects of the May 11, 2011 Lorca (Spain) Mw=5.1 earthquake. InAGU Fall Meeting Abstracts **1**, p. 2277.

Serpelloni, E., G. Vannucci, S. Pondrelli, A. Argnani, A. Casula, M. Anzidei, P. Balde & P. Gasperini (2007). Kinematics of the Western Africa-Eurasia plate boundary from focal mechanisms and GPS data. *Geophysical Journal International* **169**, 1180-1200.

Tapia, M., T. Susagna & X. Goula (2007). Curvas predictivas del movimiento del suelo en el oeste del Mediterráneo. 3er Congreso Nacional de Ingeniería Sísmica, Girona, Spain, May 2007.

Tsige Aga, M. & I. García Flores (2005). *Riesgo sísmico en la región de Murcia RISMUR - Volumen 2: Caracterización geotécnica y análisis de efecto local.* RISMUR Report, 39 pp.

United Nations, ed. (2011). *Human Development Report 2011 - Sustainability and equity: A better future for all*. Report of the United Nations Development Programme (UNDP). Palgrave Macmillan, New York, United States.

United Nations, ed. (2013). *Human Development Report 2013 - The rise of the South: Human progress in a diverse world*. Report of the United Nations Development Programme (UNDP). Palgrave Macmillan, New York, United States.

United Nations, ed. (2014). *Human Development Report 2014 - Sustaining human progress: Reducing vulnerabilities and building resilience*. Report of the United Nations Development Programme (UNDP). Palgrave Macmillan, New York, United States.

A2.3.11.2 Web references

Accessed on 27 January 2016:

Actualidad Volcánica: http://www.avcan.org/

European Parliament: http://www.europarl.europa.eu/

GeoAzur: https://geoazur.oca.eu

GeoForschungsZentrum: http://geofon.gfz-potsdam.de/

Global Centroid-Moment -Tensor (CMT) Project: http://www.globalcmt.org/

Instituto Geográfico Nacional: http://www.ign.es/

Instituto Nacional de Estadística: http://www.ine.es/

International Seismological Centre: http://www.isc.ac.uk/

Laverdad (2011): http://www.laverdad.es/murcia/20110511/local/ lorca/terremoto-lorca-201105111711.html

Ministerio de Fomento: http://www.fomento.gob.es/

Murcia Today (2011): http://murciatoday.com/ reconstruction-work-still-in-progress-4-years-after-lorca-earthquake_25885-a.html#.VXw_ TTGUeOc

Quaternary Active Faults Database of Iberia (QAFI) v.2: http://info.igme.es/qafi/

RISMUR Project: http://www.112rm.com/dgsce/planes/rismur.php

SISMIMUR Project: http://www.112rm.com/dgsce/planes/sismimur/sismimur.php

United States Geological Service: http://earthquake.usgs.gov/earthquakes/

A2.4 August 2011 M5.3 Trinidad (Colorado) Earthquake, USA

This earthquake occurred on 23rd August 2011, at 05.46 UTC (22nd August 2011, 23.46 local time), and was the largest to take place in Colorado in around half a century (Matthews, 2011; Morgan & Morgan, 2011). It was part of a sequence that started with a series of small foreshocks the day before, was followed by over 500 events in the following four months, and is believed to have been induced by deep injection of wastewater in the Raton Basin (Rubinstein *et al.*, 2014). The main shock was widely felt and caused significant damage to masonry buildings in the scarcely populated towns of Segundo, Valdez, Cokedale and Trinidad, all located within 20 km of the epicentre.

A2.4.1 Tectonic and seismic setting

A2.4.1.1 Tectonic setting

The epicentre of this earthquake was located within the Raton sedimentary Basin, at the base of the Sangre de Cristo Mountains, the southernmost sub-range of the Rocky Mountains, along the border of the states of Colorado and New Mexico. The Rocky Mountains make up an effective boundary between the active shallow regions of the United States, to the West, and the stable continental regions, to the East. Overall, the state of Colorado is subject to a regional tectonic setting of east–west extension (Rubinstein *et al.*, 2014).

The most relevant fault in the area is the extensional Sangre de Cristo fault, over the Rockies (Figure A2.4.1), which is part of the Rio Grande Rift system and is the closest known to be active during the Quaternary Period (Rubinstein *et al.*, 2014). Quaternary deposits around the area of this fault and to its West show the occurrence of multiple paleoseismic events with individual displacements of 1.7 to 2.9 metres, and fourteen faults around the state of Colorado are believed to be capable of generating maximum credible earthquakes with magnitudes ranging from **M**6.25 to 7.5 (Sheehan *et al.*, 2003).

In spite of this significant tectonic activity across the western side of the state of Colorado, there is little evidence for faulting within the low-lying Raton Basin, except for some isolated buried faults reported by Rubinstein *et al.* (2014), making reference to Johnson (1969), Robson & Banta (1987), and Scott & Pillmore (1993), which are not part of the U.S. Geological Survey (USGS) Quaternary Fault and Fold Database (see Web references), and are believed by the authors to be inactive. As shown in Figure A2.4.2, the lineation of the foreshocks, main shock and aftershocks is consistent with the strike of one of these faults. Nevertheless, Rubinstein *et al.* (2014) believe that the 2011 earthquake swarm had its origin along the planes of unknown faults, not expected to be directly related to these previously mapped ones, though both structures are consistent with the regional tectonic stresses.
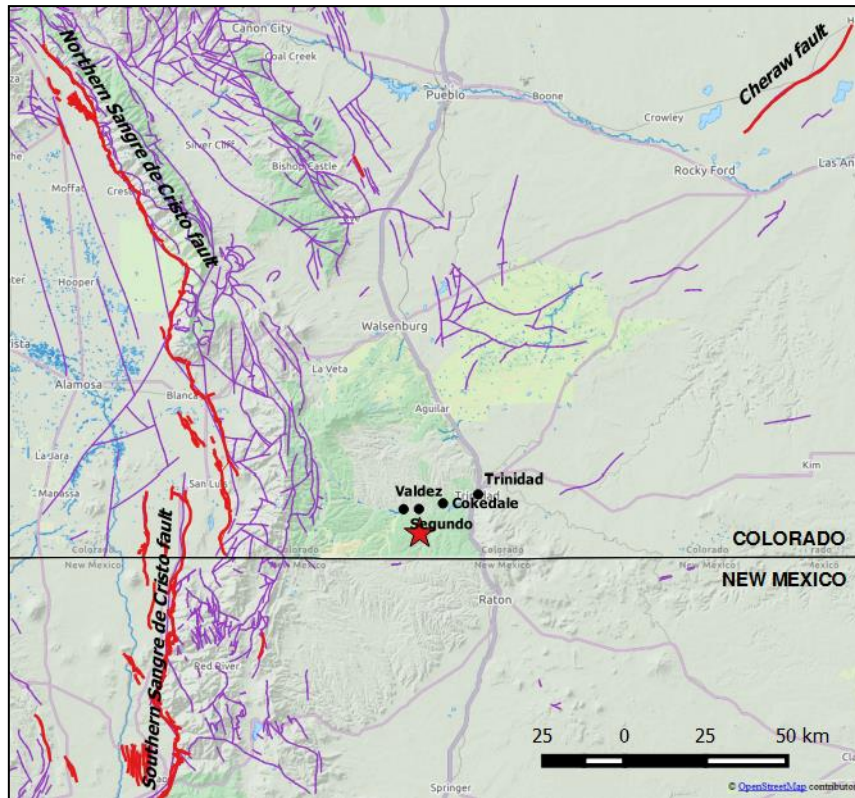
Figure A2.4.1. Quaternary faults (red) and fault traces (violet) close to the Raton Basin. The four locations marked are those at which damage was observed during the 2011 Trinidad earthquake. Faults locations from the Quaternary Fault and Fold Database of the United States (USGS) and the Mineral Resources Online Spatial Data (USGS).
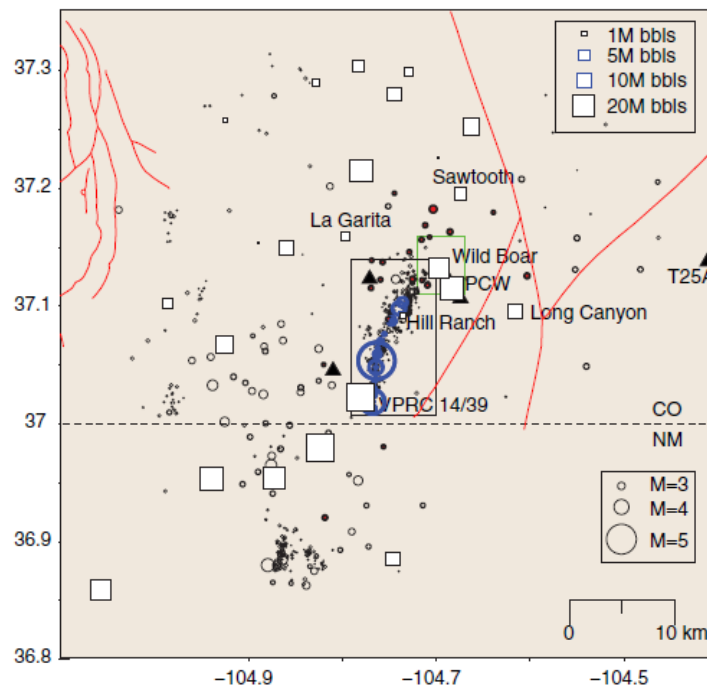
Figure A2.4.2. Seismicity from August 2011 to 15th December 2011 (blue circles), and location of injection wells (white squares). Faults (red lines) to the East of the epicentres shown are those believed to be buried and inactive. From Rubinstein *et al.* (2014).

A2.4.1.2 Regional and local seismicity

In spite of having faults believed to be capable of generating earthquakes of magnitudes up to 7.5 (Sheehan *et al.*, 2003), Colorado is usually considered a region of minor seismic activity. In particular, the Raton Basin is, or was before the turn of the century, one of the most aseismic areas of the state.

According to the United States Geological Service (USGS), the first known reference to an earthquake in Colorado dates from 7th December 1870. During this event, an observer in Fort Reynolds, 30 km to the east of Pueblo, noticed that bottles which were originally separated by over 2 cm, were suddenly pulled together. The largest known historical earthquake to have taken place in Colorado occurred on 7th November 1882, had an estimated moment magnitude of 6.6 ± 0.6, and was the first ever to cause damage at Denver, where walls cracked and plaster fell from walls (USGS; Sheehan *et al.*, 2003). A large increase in the seismic activity within the state of Colorado was observed during the 1960s, after a well was drilled for the disposal of waste fluids at the Rocky Mountain Arsenal, northeast of Denver (USGS). These and most of the significant earthquakes in the state had their epicentres around the north-central or western areas.

Within the Raton Basin, the most relevant earthquakes observed before 2011 were the August-September 2001 and August-September 2005 sequences, whose epicentres were located on the Colorado side and on the New Mexico side of the central region of the basin, respectively. The 2001 swarm included eight shocks with magnitudes larger than or equal to 4.0, with the two largest being M_{bLg} 4.0 and 4.5. The largest earthquake ever recorded in the basin before the **M**5.3 2011 event was a **M**5.0 which occurred as part of the 2005 sequence, in August that year (USGS; Rubinstein *et al.*, 2014). These sequences represented a significant change in the seismic behaviour of the Raton Basin, whose activity before August 2001 was widely distributed and infrequent, and observed mostly around its north-eastern margin (Rubinstein *et al.*, 2014). Sixteen earthquakes with magnitudes equal to or larger than 3.8 occurred within the basin between August 2001 and 2013, while only one had taken place in the preceding three decades. Rubinstein *et al.* (2014) believe that this increase in the seismic activity in the area can be linked to wastewater injection, but Matthews (2011) highlights that analysis carried out by the USGS and the Colorado Geological Service were not conclusive.

Before 2001, relevant earthquakes in the area include a **M**4.6 event on 2nd October 1966 northeast of Trinidad, the 1973 swarm, whose two largest events were a **M**3.1 and a **M**4.2, west or northwest of Trinidad, a **M**3.2 in 1983, northeast of Trinidad, and three events with magnitudes equal to or larger than 3.2 in 1996, also to the northeast of Trinidad (USGS; Matthews, 2011).

Figure A2.4.3 shows the seismicity in Colorado between 1870 and 1992, as reported by Sheehan *et al.* (2003).
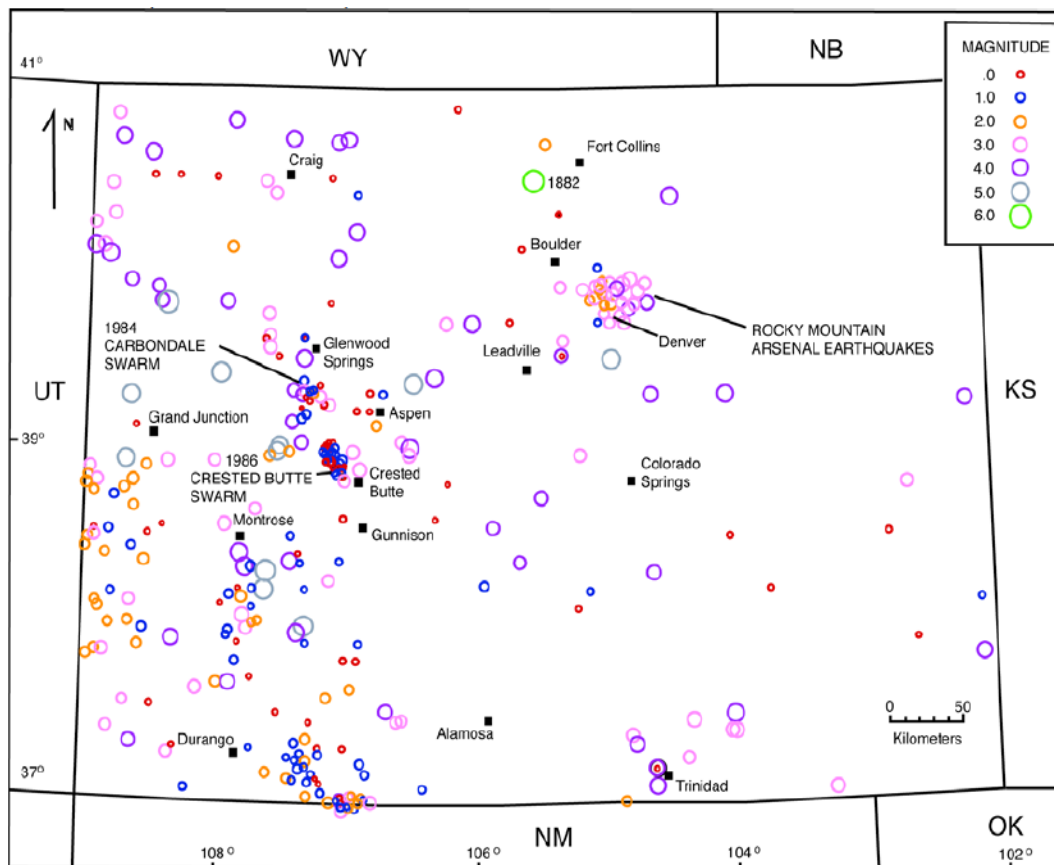
Figure A2.4.3. Seismicity of the state of Colorado between 1870 and 1992. From Sheehan *et al.* (2003), after Bott & Wong (1995).

A2.4.1.3 Seismic hazard

Figure A2.4.4 shows extracts of the probabilistic seismic hazard maps for the United States of 2008 and 2014, elaborated by the USGS. Values shown correspond to peak ground acceleration (PGA) on rock with a 10% probability of exceedance in 50 years. The Raton Basin area is marked in red. Table A2.4.1 presents a summary of the PGA values expected at Segundo, Valdez, Cokedale and Trinidad, which are the locations that experienced damage during the 2011 Trinidad earthquake. The table also reports the corresponding values obtained from the Global Seismic Hazard Assessment Program (GSHAP; Giardini *et al.*, 1999; Giardini *et al.*, 2003), which are closer to those of the 2014 USGS hazard map than to those of the 2008 one. In any case, all values support the idea that seismic hazard is moderate to low in the area of the Raton Basin. It should be noted that the USGS national seismic hazard maps do not take into consideration non-tectonic seismic activities and, therefore, the 2011 Trinidad sequence had no effect over the change from the 2008 map to the 2014 one.
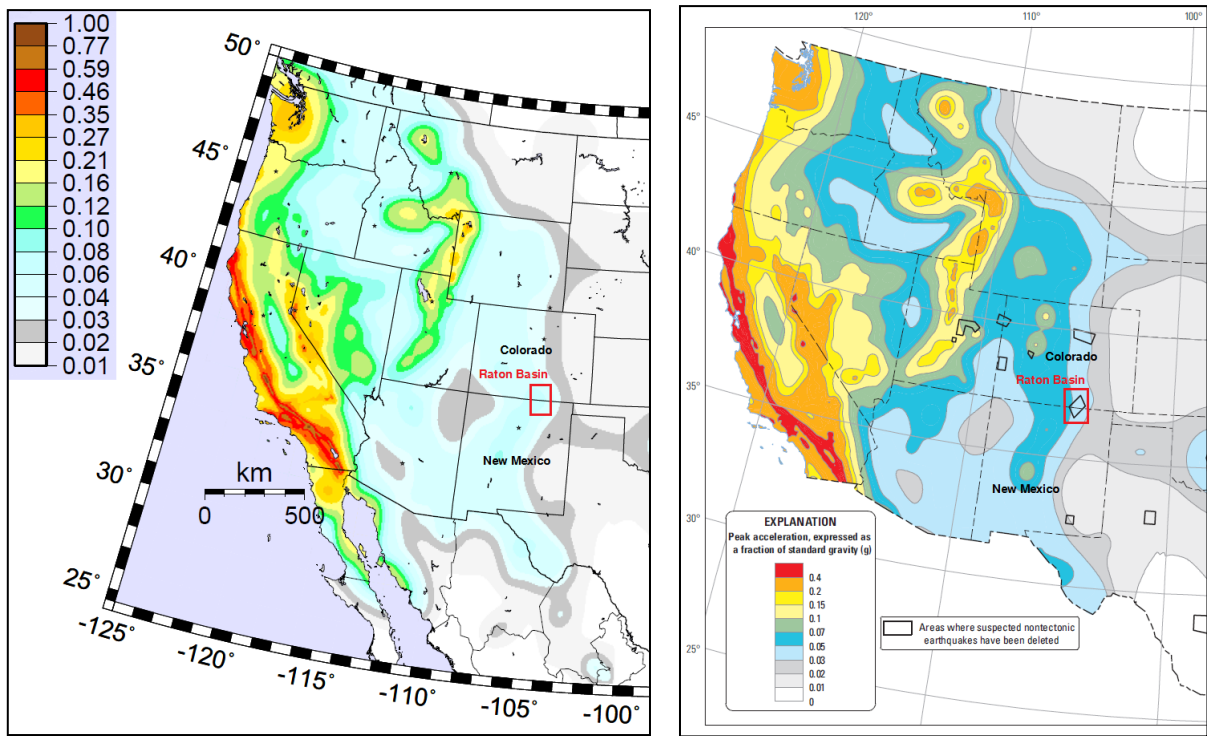
Figure A2.4.4. Extract of the 2008 (left) and 2014 (right) hazard maps for the United States, elaborated by the USGS (2015). Values correspond to peak ground acceleration (g) on rock with a 10% probability of exceedance in 50 years.

Table A2.4.1. Peak ground acceleration (PGA, g) values on rock with a 10% probability of exceedance in 50 years according to the 2008 and 2014 USGS hazard maps, and results from the Global Seismic Hazard Assessment Program (GSHAP), at locations in which damage was observed after the 2011 Trinidad earthquake.

PLACE	USA 2008	USA 2014	GSHAP
Segundo	0.0648	0.0417	0.0466
Valdez	0.0629	0.0405	0.0431
Cokedale	0.0590	0.0383	0.0395
Trinidad	0.0551	0.0365	0.0367

A2.4.2 Earthquake source characteristics

A2.4.2.1 Location, depth and time

The main shock occurred on 23rd August 2011, at 05.46 UTC (22nd August 2011, 23.46 local time).

Several organizations and agencies report their own estimations of the epicentral coordinates and hypocentral depth. The information reported in the websites of the National Earthquake Information Center (NEIC) of the United States Geological Service (USGS), the Global Centroid Moment Tensor Project (GCMT) and the International Seismological Centre (ISC) is summarized in Table A2.4.2. Cells marked as (*f) correspond to parameters that were held fixed while inversion was carried out to retrieve those that

177

remain. Table A2.4.2 also includes the epicentral coordinates and hypocentral depths calculated by Barnhart *et al.* (2014) and Rubinstein *et al.* (2014).

Table A2.4.2. Epicentral coordinates and hypocentral depths from different sources.

	Agency / Publication	Latitude	Longitude	Depth (km)
NEIC	National Earthquake Information Center, USGS	37.0630 ° N	104.7010 °W	4.00
GCMT	Centroid Global Centroid Moment Tensor Project (**)	37.1200 ° N	104.5900 °W	12.00
ISC	International Seismological Service (inversion)	37.0680 ° N	104.6482 °W	10 (*f)
	Barnhart *et al*. (2014)	37.0381 ° N	104.7530 °W	5.10 (*f)
	Rubinstein *et al*. (2014)	37.0540 ° N	104.7600 °W	3.50

(*f) fixed parameter used for inversion

(**) centroid (not-hypocentral) location

Rubinstein *et al.* (2014) shed some light over the variability observed in the estimations of the hypocentral depths. According to the authors, standard arrival-time location techniques place the main shock hypocenter at 4.3 km depth, though with a two standard deviation uncertainty of ± 15.0 km. Analyses of In-SAR images support this small value, indicating that slip was concentrated within a zone of approximately 2.5 to 6.0 km in depth. Finally, computed synthetic seismograms for two well-recorded smaller earthquakes that were close to the main shock match best the recorded surface waves when hypocentral depths of 3.0 and 4.0 km are used for their generation. Based on all these observations and on the fact that most aftershocks have hypocentral depths between 4.0 and 8.0 km, and these are better constrained than for the main shock due to the availability of more stations, Rubinstein *et al.* (2014) conclude that a hypocentral depth of the main shock between 3.0 and 4.0 km is most likely.

The map in Figure A2.4.5 shows the different estimations of the epicentral coordinates enumerated above. Note that coordinates reported by the GCMT correspond to the location of the centroid, and not the hypocentre.

A2.4.2.2 Magnitude

Estimations of magnitude made by the same agencies are reported in Table A2.4.3.

Table A2.4.3. Estimations of moment magnitude (**M**), body-wave magnitude (mb) and surface-wave magnitude (Ms).

	Agency	M	mb	Ms
NEIC	National Earthquake Information Center, USGS	5.3	5.0	-
GCMT	Global Centroid Moment Tensor Project (1)	5.4	5.0	5.4
ISC	International Seismological Service (inversion)	-	5.1	5.0
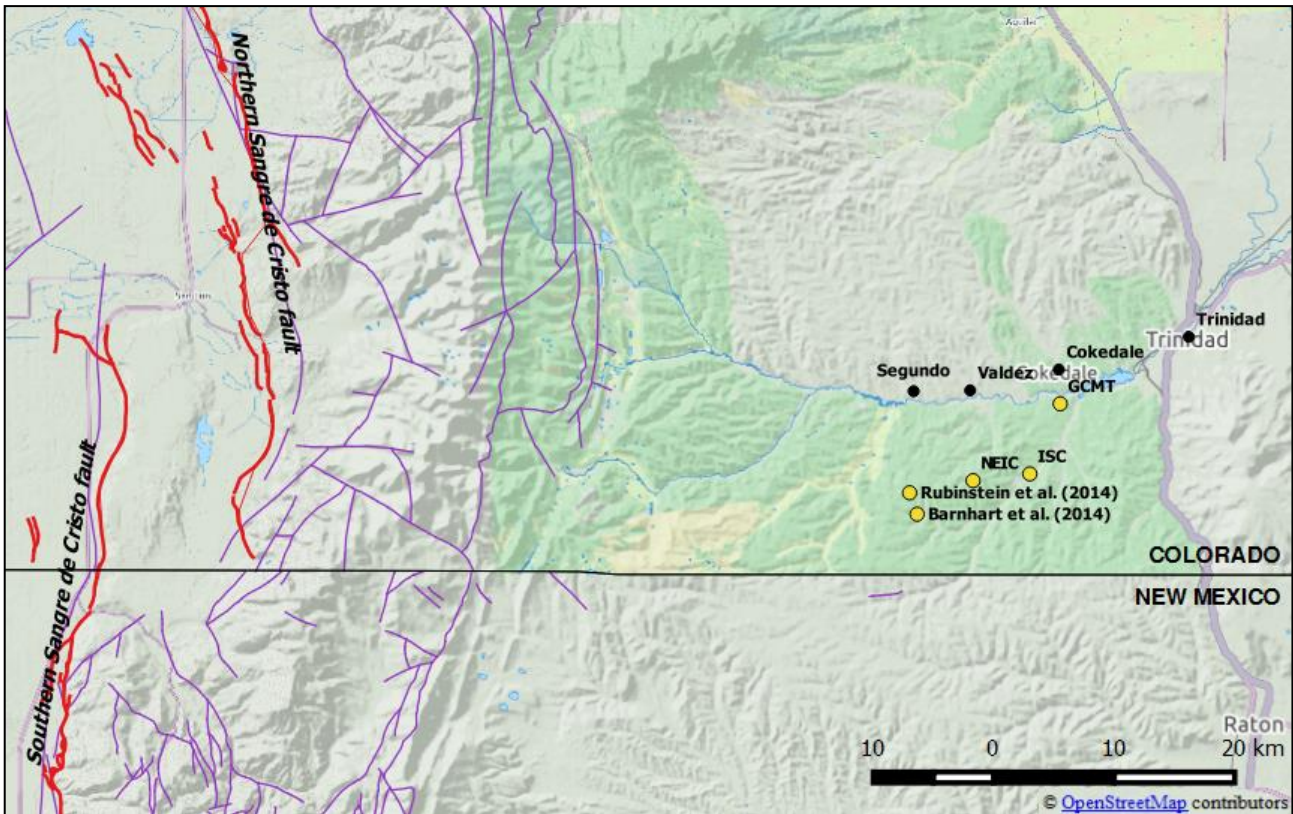
Figure A2.4.5. Estimation of epicentral coordinates (yellow circles). Faults in the area marked in red and violet, as described earlier.

A2.4.2.3 Style-of-faulting

All sources indicate a normal mechanism on a fault striking to the north-northeast (USGS; Barnhart *et al.*, 2014; Rubinstein *et al.*, 2014). According to Rubinstein *et al.* (2014), the main shocks of the swarms that took place in 2001 and 2005 in the Raton Basin also presented the same mechanism at a similar strike, which is consistent with the ambient stress. Said authors also note that the whole 2011 sequence had epicentres along two intersecting lineations. While the southern lineation strikes nearly north-south, the northern one strikes closer to northeast-southwest. The authors believe that these planes are faults different from the ones with similar strikes lying to the East of the basin (Figure A2.4.2). Further, they suggest that it is possible that the different lineations be a consequence of lack of precision in the localization of the events. Table A2.4.4 summarizes the fault plane solutions calculated by the USGS and the GCMT, while Figure A2.4.6 shows the corresponding plot for the centroid moment tensor (GCMT).

Table A2.4.4. Fault plane solutions and fault planes from different sources. Fault planes marked in gray are the preferred solution in each case.

Fault Plane 1			Fault Plane 2			Source
Strike	Dip	Rake	Strike	Dip	Rake	
185	38	-103	21	53	-80	Regional Moment Tensor NEIC (USGS)
203	38	-75	4	53	-101	GCMT
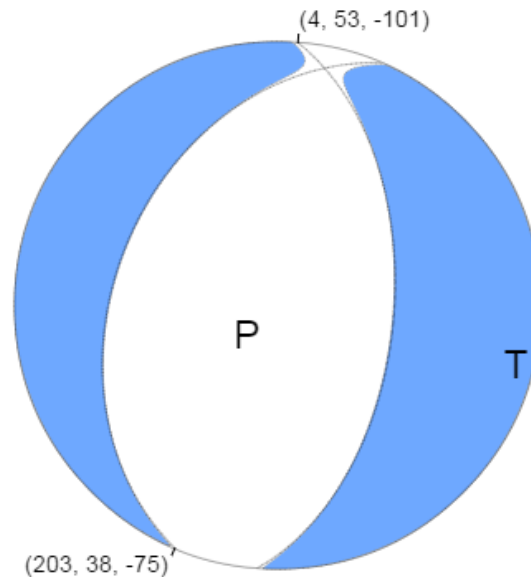
Figure A2.4.4. GCMT centroid moment tensor for the main shock. From the USGS website.

A2.4.2.4 Stress drop

Barnhart *et al.* (2014) report a stress drop of 0.07 MPa, which they say is much lower than expected for intraplate normal faulting events.

A2.4.2.5 Foreshocks and aftershocks

The **M**5.3 main shock was preceded by a foreshock sequence which started on 21st August 2011. By means of a manual scanning of the seismic records at a station to the southeast of Trinidad, Rubinstein *et al.* (2014) identified 36 foreshock events, the first of which was a **M**~1.1, which was the smallest detected. The three strongest foreshocks (Figure A2.4.7) were a **M**4.7 and two events of ML 2.9 and 3.0, all of which occurred within the 24 hours before the main shock (Barnhart *et al.*, 2014; Morgan & Morgan, 2011; Rubinstein *et al.*, 2014). According to the USGS, the **M**4.7 event reached a MMI of IV at La Junta, Manzanola, Trinidad and Weston. According to Rubinstein *et al.* (2014), the earliest foreshocks had epicentres towards the north, while foreshocks following the **M**4.7 event were mostly concentrated to the south.

After the **M**5.3 main shock, the USGS located 584 aftershocks that took place within the Raton Basin between 23rd August and 15th December 2011. Rubinstein *et al.* (2014) point out that the sequence decayed quickly, and most aftershocks occurred within approximately one month of the main shock. According to Barnhart *et al.* (2014), the aftershock sequence exhibits statistical properties (such as the b-value of the Gutemberg-Richter relation and the Omori-Utsu decay constant) expected for intraplate earthquakes. Most of the aftershocks occurred at very shallow depths (Rubinstein *et al.*, 2014). The location of some of the most significant ones, according to the USGS, is shown in Figure

A2.4.7. The largest reported macroseismic intensity for these events was MMI V, which corresponds to moderate shaking and very light damage (Did You Feel It?, USGS).
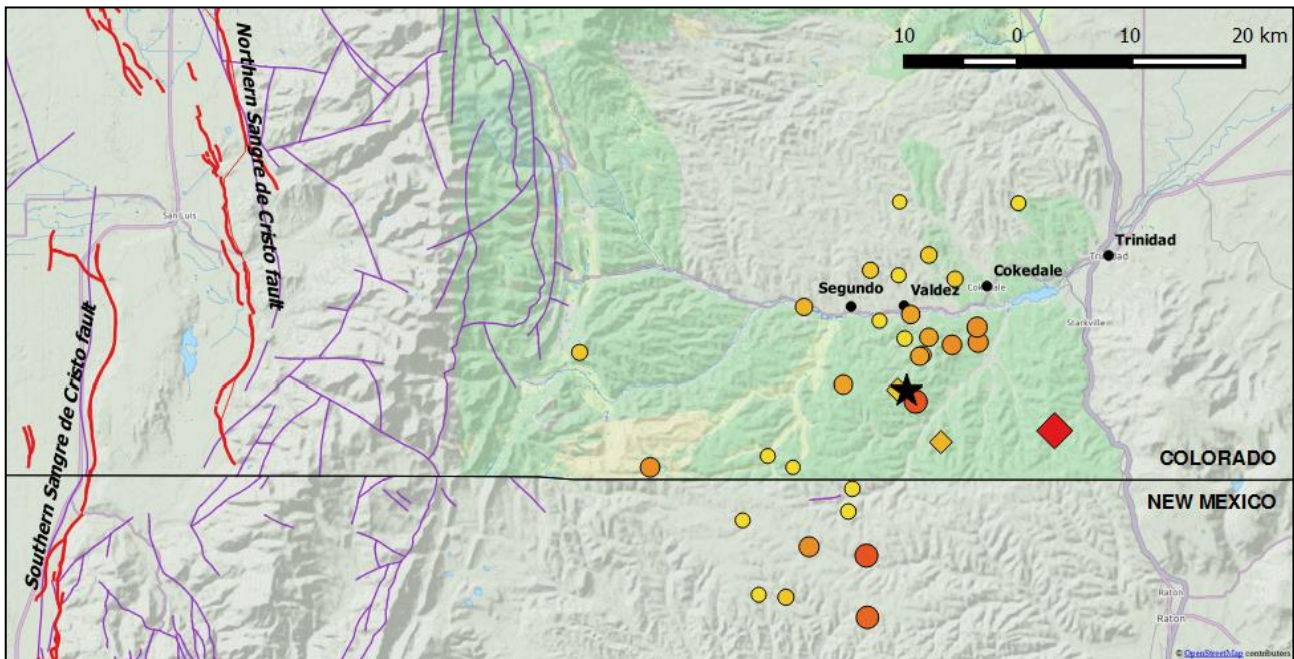
Figure A2.4.7. Most significant foreshocks (rhombuses) and aftershocks (circles), with colour scale representing magnitude (2.5: yellow, 4.7: red). The black star is the epicentre of the main shock, according to the USGS. Epicentral coordinates of all events according to the USGS. Faults in the area marked in red and violet, as described earlier.

A2.4.2.6 Nature of earthquake

While some authors are cautious in labelling the 2011 Trinidad earthquake sequence as induced (*e.g.*, Matthews, 2011) others present significant arguments supporting this hypothesis (Barnhart *et al.*, 2014; Rubinstein *et al.*, 2014). In any case, it is well known that the Raton Basin is a coal-bearing sedimentary basin which is being actively exploited for the production of gas and the disposal via injection of wastewater (Matthews, 2011). However, according to Rubinstein *et al.* (2014), increased seismic activity in the basin since 2001 is directly related only to deep injection of wastewater and not to gas production. They get to this conclusion by means of three separate analyses. Firstly, a statistical analysis of the change in the earthquake rate that occurred in the area in 2001 suggests that it is highly unlikely that such a change be due to random fluctuations of the ambient seismicity. Secondly, they observed a significant spatial correlation between the location of the injection wells and the epicentres of the seismic events taking place since 2001, an observation which matches that of Barnhart *et al.* (2014), who found a strong correlation between the seismicity in the Raton Basin and regions of subsidence observed in InSAR time series analysis. Finally, Rubinstein *et al.* (2014) note that total injection volumes and the number of earthquakes taking place present similar trends.

A2.4.3 Geology and ground conditions in the affected area

A2.4.3.1 Regional geology and topography

This earthquake occurred within the Raton Basin, a coal-bearing sedimentary basin in which 2.0-2.5 km of Cretaceous and Tertiary sedimentary rocks overlie a Precambrian crystalline basement (Barnhart *et al.*, 2014). The basin itself presents a flat topography, but lies at the base of the Sangre de Cristo Mountains, the southernmost subrange of the Rocky Mountains. It is approximately 150 km long in the north–south direction, and 75 km wide at its maximum (Rubinstein *et al.*, 2014).

A2.4.3.2 Site conditions in the affected area

Figure A2.4.8 presents an east-west stratigraphic cross section across the southern part of the Raton Basin, while Figure A2.4.9 describes the corresponding formations and soil types. As can be observed, sandstone and shale, two types of clastic sedimentary rock, are predominant in all formations.
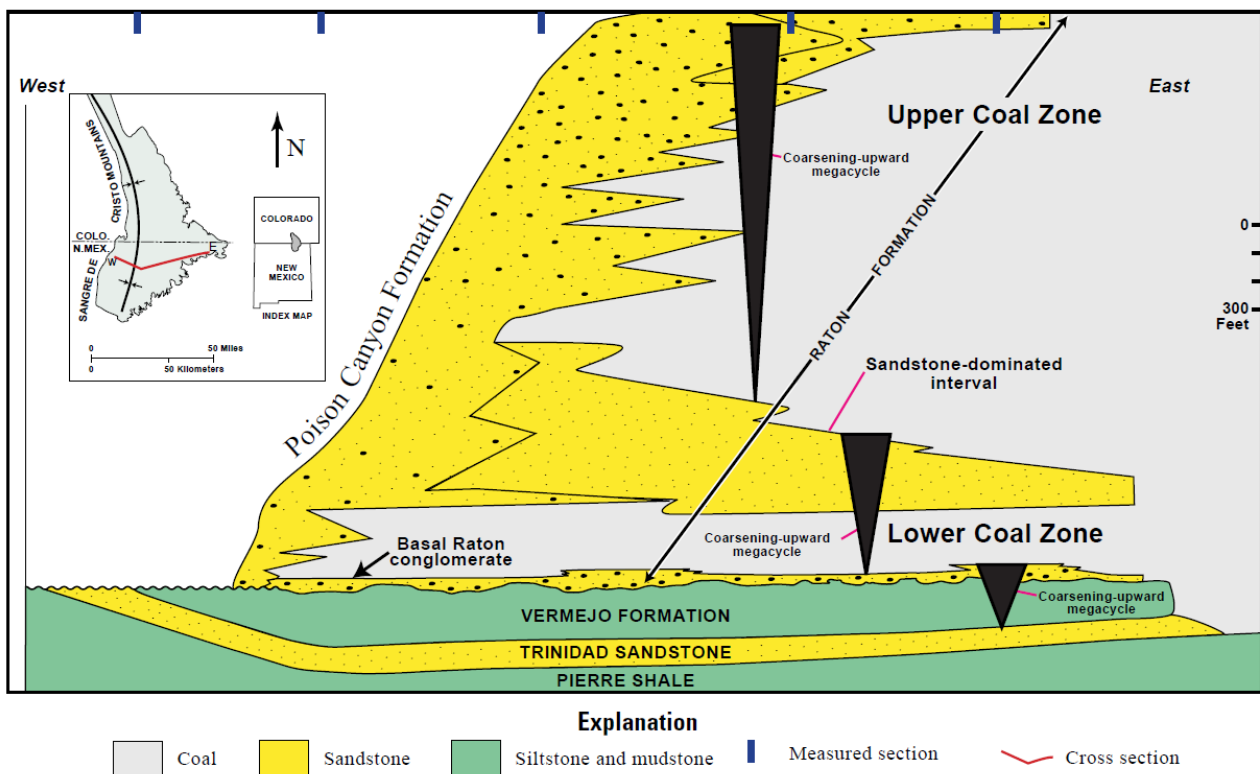
Figure A2.4.8. East-west stratigraphic cross section across the southern part of the Raton Basin. From Flores (1987) and Flores & Bader (1999), in Johnson & Finn (2001).

AGE		FORMATION NAME	GENERAL DESCRIPTION	LITH-OLOGY	APPROX. THICKNESS IN FEET
TERTIARY	PALEOCENE	POISON CANYON FORMATION	SANDSTONE–Coarse to conglomeratic beds 13–50 feet thick. Interbeds of soft, yellow-weathering clayey sandstone. Thickens to the west at expense of underlying Raton Formation		500+
		RATON FORMATION	Formation intertongues with Poison Canyon Formation to the west UPPER COAL ZONE–Very fine grained sandstone, siltstone, and mudstone with carbonaceous shale and thick coal beds BARREN SERIES–Mostly very fine to fine-grained sandstone with minor mudstone, siltstone, with carbonaceous shale and thin coal beds LOWER COAL ZONE–Same as upper coal zone; coal beds mostly thin and discontinuous. Conglomeratic sandstone at base; locally absent		0(?)–2,100 ← K/T boundary
MESOZOIC	UPPER CRETACEOUS	VERMEJO FORMATION	SANDSTONE–Fine to medium grained with mudstone, carbonaceous shale, and extensive, thick coal beds. Local sills		0–380
		TRINIDAD SANDSTONE	SANDSTONE--Fine to medium grained; contains casts of *Ophiomorpha*		0–300
		PIERRE SHALE	SHALE--Silty in upper 300 ft. Grades upward to fine-grained sandstone. Contains limestone concretions		1800-1900

Figure A2.4.9. Generalised stratigraphic column for Cretaceous and Tertiary rocks in the Raton Basin. From Flores & Bader (1999), modified from Pillmore (1969), Pillmore & Flores (1987), and Flores (1987), in Johnson & Finn (2001).

To our knowledge, measured V_{s30} values for the Raton Basin area are not readily available in the literature. However, based on the work by Wills & Silva (1998), Wills & Clahan (2006) report a series of relationships between Californian geologic units and their corresponding V_{s30} values, which can be used as a reference herein. Table A2.4.5 summarizes those corresponding to geologic units which can be comparable to those of the Raton Basin. As can be observed, V_{s30} values can be expected to range approximately between 300 and 600 m/s. These values are in agreement with those estimated by the United States Geological Survey (USGS) V_{s30} Map Server (Figure A2.4.10) using topographic slope as a proxy. The map in Figure A2.4.10 was generated using the correlations derived by Wald & Allen (2007) for active tectonic regions. These were preferred here over those for stable shield regions given the proximity to the Rocky Mountains which suggests conditions might be closer to those of western and not eastern USA.

Table A2.4.5. Relationship between geologic units comparable to those of the Raton Basin and their shear-wave velocities (Wills & Clahan, 2006).

Geologic description	Mean V_{s30}
Tertiary (mostly Miocene and Pliocene) shale and siltstone units such as the Repetto, Fernando, Puente, and Modelo Formations of the Los Angeles area	390
Tertiary (mostly Miocene, Oligocene, and Eocene) sandstone units such as the Topanga Formation in the Los Angeles area and the Butano sandstone in the San Francisco Bay area	515
Cretaceous sandstone of the Great Valley Sequence in the central Coast Ranges	566

Figure A2.4.10. Estimation of V_{s30} in the Raton Basin using topographic slope as a proxy. From the USGS V_{s30} Map Server (USGS, 2015).

According to Rubinstein *et al.* (2014), the hydraulic head within the Cretaceous layers lies, on average, approximately 500 m below the surface, and is approximately 4.9 MPa naturally underpressured. Due to this, wastewater injection throughout much of the Colorado portion of the Raton Basin can be done via gravity feed.

A2.4.4 Ground motions

A2.4.4.1 Intensity observations

Four locations were reported to have suffered structural damage in their building stocks. From most severe to least, these are: Segundo, Valdez, Cokedale and Trinidad (Morgan & Morgan, 2011). According to the written report at the USGS website, the Modified Mercalli Intensities (MMI) at these sites were VII (very strong shaking, moderate damage) at Segundo, VI (strong shaking, minor damage) at Cokedale and Valdez, and V (moderate shaking, minor damage) at Trinidad. The main shock was felt in most of eastern and central Colorado and in parts of south-western Colorado. It was also felt widely in south-western Nebraska, western Kansas and north-eastern New Mexico, and felt in a few places in Texas, at Cheyenne, Wyoming and at Omaha, Nebraska.

In spite of the intensity at Segundo being reported as VII, the two MMI ShakeMaps produced by the USGS do not reach this intensity level. Figure A2.4.11 (top) shows the

automatically calculated ShakeMap, while Figure A2.4.11 (bottom) presents the revised version. As can be observed, the automatically calculated version reaches values closer to VII, while the revised one only gets to IV-V. This difference is most likely due to aggregation of Did You Feel It? reports by zip codes and the incorporation of instrumental intensities derived from recorded peak ground acceleration values. In any case, and as it will become clear in the section regarding damage observations, the MMI VII value assigned to Segundo probably has its origin in the damage assessment carried out by the Colorado Geological Survey, and reported in Morgan & Morgan (2011).
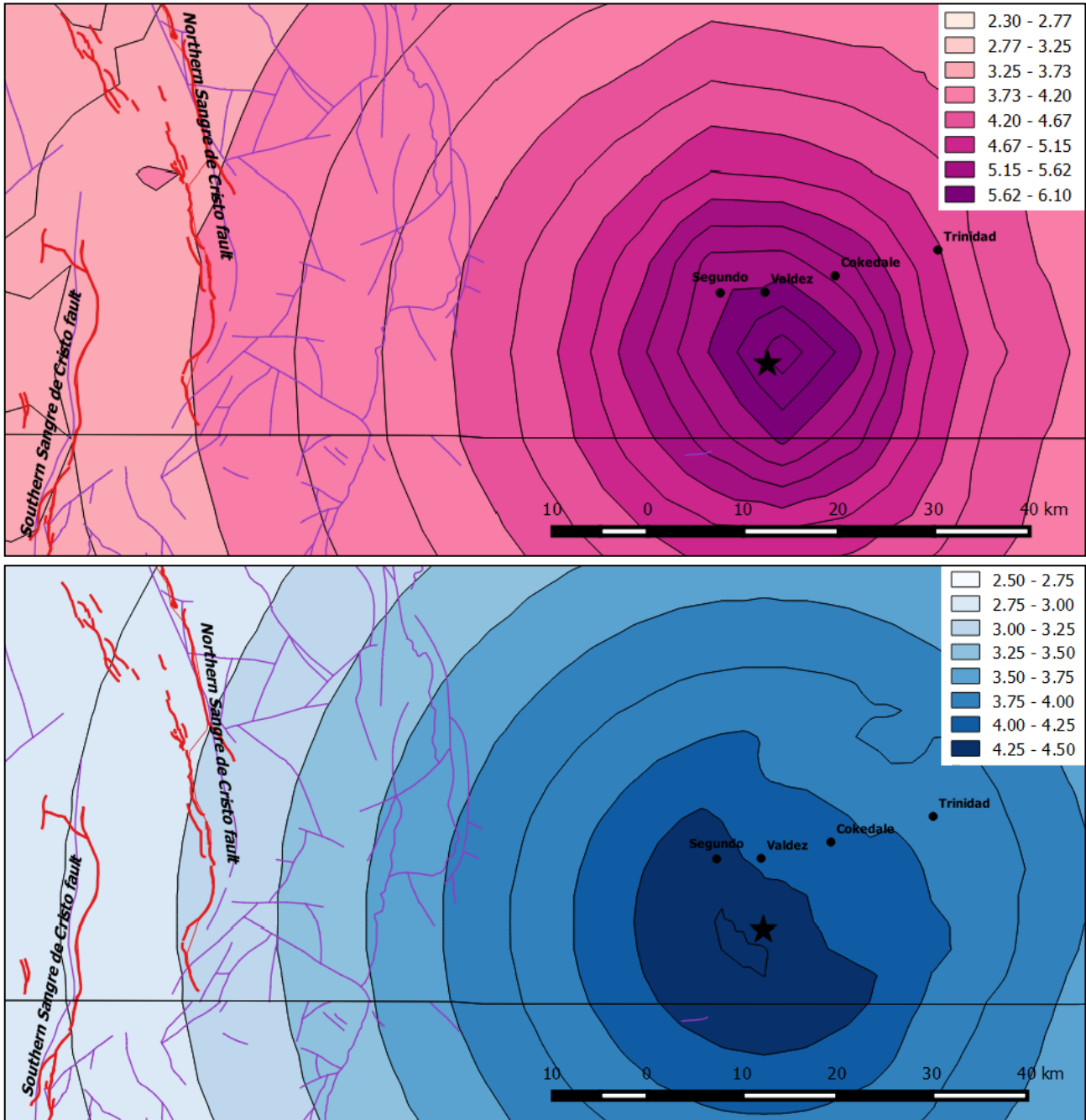
Figure A2.4.11. USGS ShakeMaps in terms of Modified Mercalli Intensities (MMI): initial automatic calculation (top), and revised calculation (bottom). The black star is the epicentre of the main shock, according to the USGS.

A2.4.4.2 Ground motion recordings

Information on ground motion recordings for this earthquake is scarce. The website of the USGS provides information on peak ground acceleration (PGA), peak ground velocity (PGV) and pseudo-spectral acceleration at 0.3, 1.0 and 3.0 seconds at some locations. The maximum recorded PGA was 2.26% g, and was observed at station T25A, around 26 km away from their estimated epicentral coordinates, close to the city of Trinidad. The list of highest recorded PGA values continues with 1.50% g registered 280 km away (station KSCO). All remaining recorded values are smaller than 0.27% g (station Q24A, 213 km). The two largest values of PGV were 1.43 and 1.23 cm/s, registered at KSCO and T25A stations, respectively. The maximum observed pseudo-spectral acceleration values were 4.26% g, 2.14% g and 0.53% g, at 0.3, 1.0 and 3.0 seconds, respectively.

Figure A2.4.12 shows the recorded peak ground acceleration values (maximum of the two as-recorded components), according to the USGS.
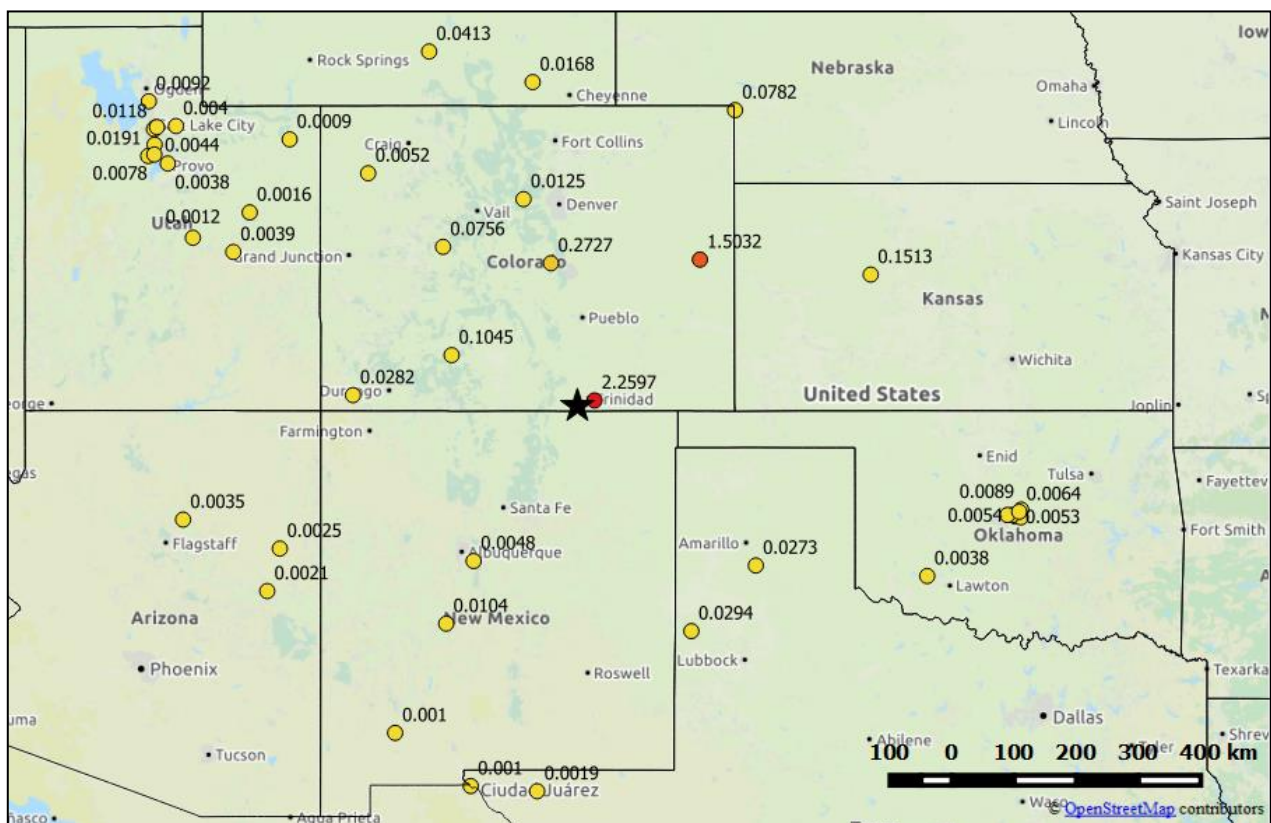
Figure A2.4.12. Recorded peak ground accelerations (% g) according to the USGS. The black star is the epicentre of the main shock.

A2.4.4.3 Inferred shaking levels

The website of the United States Geological Service (USGS) provides two different ShakeMaps for the 2011 Trinidad earthquake. ShakeMaps present estimations of the ground shaking based on the magnitude, location, fault dimensions, style of faulting, site conditions and, where available, observations from recording stations and/or macroseismic intensity observations.

The initial automatically calculated ShakeMap (Figure A2.4.13, left) suggests a maximum 10% g PGA within a 15 km diameter circle around the epicentre, slightly shifted to the East. Values provided in the revised map (Figure A2.4.13, right) are significantly higher. Values within the same 15 km diameter circle around the epicentre are larger than 36% g. Station T25A, with its 2.26% g, lies within an area of this map in which a value of 6% g is estimated.
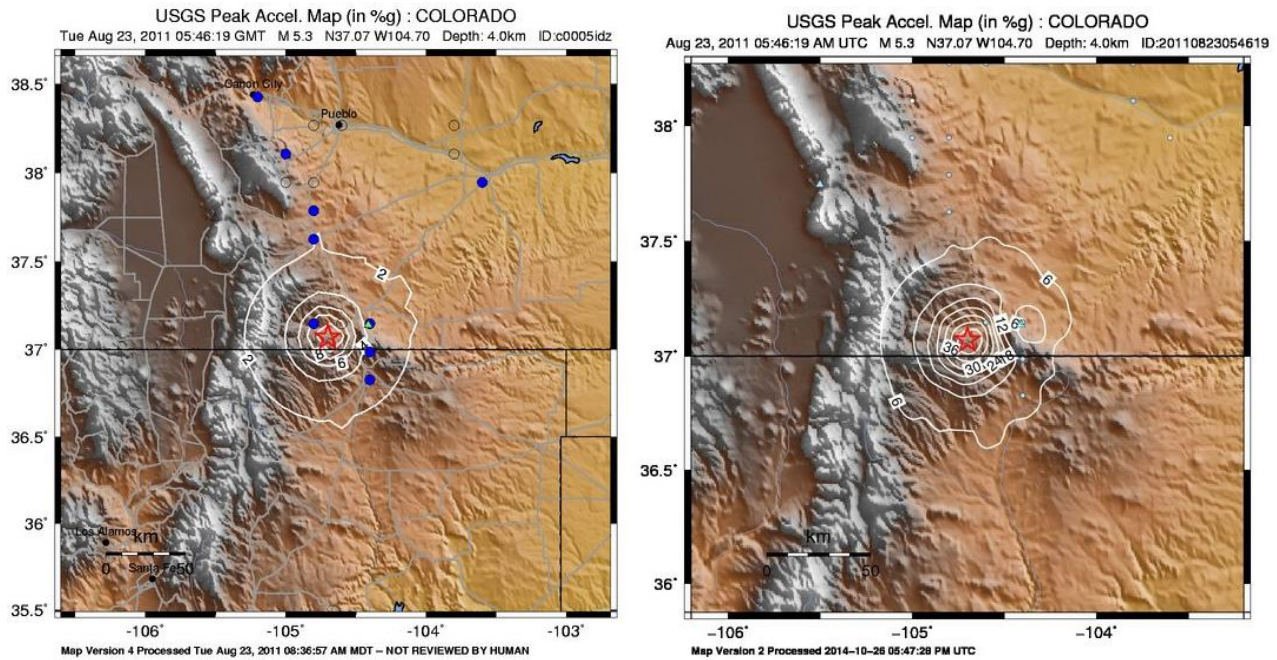
Figure A2.4.13. USGS ShakeMaps in terms of peak ground acceleration: initial automatic calculation (left), and revised calculation (right). Note the difference in scale between the two figures (USGS, 2015).

Comments regarding these discrepancies have not been found in the literature. A possible explanation may lie in the extremely reduced exposure of building stock and population in the area: 98, 47, 129 and 9,096 inhabitants by 1st April 2010 in Segundo, Valdez, Cokedale and Trinidad, respectively. This reduced exposure makes each building reported to have suffered damage a very large proportion of the total, perhaps leading to the assignation of slightly biased macroseismic intensity values, then used to derive the ShakeMaps. It is then possible that the difference between the two ShakeMaps be due to the influence of the incorporation of potentially biased information from damage assessments in the revised version.

A2.4.4.4 Duration of ground shaking

According to Morgan & Morgan (2011), in Segundo, the most severely-hit town, the resident whose house experienced the most severe damage said the earthquake lasted for "about a minute".

Estimations of earthquake significant durations can be obtained by means of prediction equations such as those of Bommer *et al.* (2009) and Kempton & Stewart (2006). V_{s30} values reported by Wills & Clahan (2006) for Californian geologic units comparable to those of the Raton Basin are used (Figure A2.4.5), though a larger range from 180 to 800 m/s is included in Figure A2.4.14 for completeness. Closest distances from the fault rupture are not known with precision, so epicentral distances to Segundo (6.80 km) and station T25A (26.35 km), as well as an arbitrary 50.00 km case are used to estimate the significant duration of this earthquake. A 1.50 km depth to the top of rupture is used, based on the work by Barnhart *et al.* (2014). Results shown in Figure A2.4.14 are well below the duration reported by Morgan & Morgan (2011). This agrees with the observations of Barnhart *et al.* (2014), who noted that the main shock was "unexpectedly long for a **M**5.3 event".
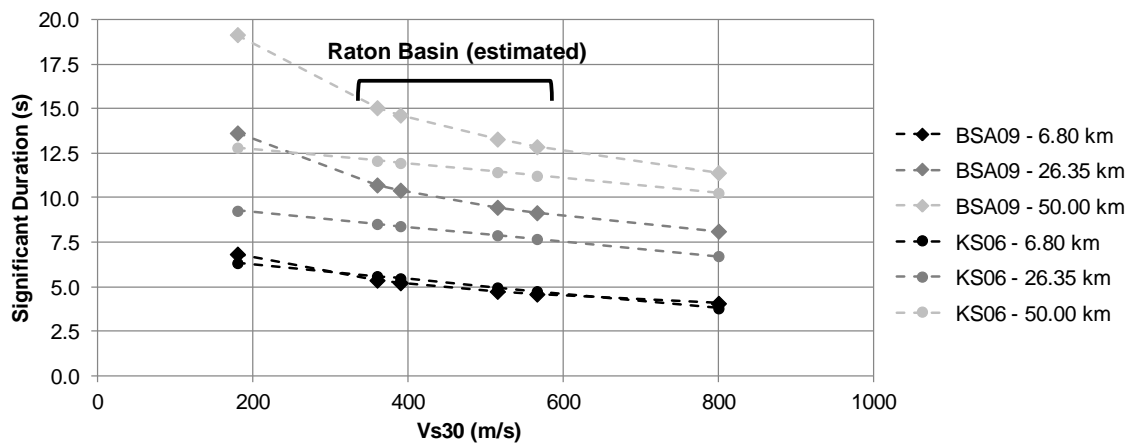
Figure A2.4.14. Estimation of the significant duration of the main shock, using prediction equations by Bommer *et al.* (2009, BSA) and Kempton & Stewart (2006, KS).

A2.4.5 Collateral earthquake hazards

A2.4.5.1 Surface rupture

Surface rupture not reported for this earthquake.

A2.4.5.2 Landslides

Morgan & Morgan (2011) report rockfalls covering the State Highway 12, a road approximately 1.5 km east of Segundo. Some of the rock fragments were larger than 1.8 m, but damage to the pavement seems to have been null or minimum. The rocks were quickly removed.

A2.4.5.3 Liquefaction

In their report on the damage assessment carried out by the Colorado Geological Survey, Morgan & Morgan (2011) raise the question of whether the house that suffered the most severe damage had experienced issues associated to liquefaction. The authors report that the residents said the ground "seemed to rotate", and interpret this as a possible

consequence of liquefaction. However, given the extremely low phreatic level (500 m, according to Rubinstein *et al.*, 2014), liquefaction seems unlikely, and the residents' description most likely refers to the motion of the ground due to Rayleigh waves.

A2.4.6 Exposed population

A2.4.6.1 Socio-economic setting

According to the 2014 Human Development Report (United Nations, 2014), the Human Development Index (HDI) for the United States in 2013 was 0.914, while its Inequality-adjusted HDI (IHDI) was 0.755. This located the USA in the 5th place in the world's ranking, while the Netherlands ranks 4th. Table A2.4.6 compares the HDI and IHDI for both countries from the last three Human Development Reports (United Nations, 2011; United Nations, 2013; United Nations, 2014). The column "Adj. HDI" provides the HDI values given in the 2014 report for previous years, adjusted for data consistency in time.

Table A2.4.6. Human Development Index and Inequality-adjusted Human Development Index for the United States and the Netherlands.

Report	Data	Unites States of America				Netherlands			
		HDI	IHDI	Rank	Adj. HDI	HDI	IHDI	Rank	Adj. HDI
2011	May 2011	0.910	0.771	4	0.911	0.910	0.846	3	0.914
2013	October 2012	0.937	0.821	3	0.914	0.921	0.857	4	0.915
2014	November 2013	0.914	0.755	5	-	0.915	0.854	4	-

Table A2.4.7 presents a comparison between the United States and the Netherlands in terms of GDP, GDP per capita and unemployment rate.

Table A2.4.7. Gross domestic product (GDP), GDP per capita and unemployment rate for the United States and the Netherlands, according to the World Economic Outlook Database 2015.

Indicator	Units	Unites States		Netherlands	
		2011	2014	2011	2014
Gross domestic product, current prices	Billions of US dollars	15,517.925	17,418.925	894.576	866.354
Gross domestic product per capita, current prices	US dollars	49,724.999	54,596.653	53,589.909	51,372.963
Unemployment rate	% of total labor force	8.942	6.150	4.980	7.395

During the mid-19th century, mining was the most significant economic activity in the state of Colorado, but it was slightly overshadowed when irrigated agriculture developed and raising livestock acquired importance by the late 19th century. Early industries grew around these activities. Nowadays, agricultural products produced in Colorado include cattle, wheat, dairy products, corn, and hay. Industrial and service sectors, as well as scientific research, expanded significantly during the second half of the 20th century. Modern industries in the state include food processing, transportation equipment, machinery, and chemical products.

The large economic crisis that began in 2008 had a significant impact on the United States, causing high unemployment, an increasing federal debt, and inflation. In 2011, the Gross Domestic Product (GDP) increased in 43 of the 50 states of the USA. The state of Colorado presented a 1.9% increase in its GDP, a value that positioned it within the second to highest quintile (Bureau of Economic Analysis, U.S. Department of Commerce). During the year 2012, the state of Colorado ranked 15th with respect to GDP per capita, whose value was an 8% higher than that of the USA as a whole.

A2.4.6.2 Population density and distribution

The Raton Basin is sparsely populated (Matthews, 2011). Table A2.4.8 shows the population by 1st April 2010 of the four most affected towns. According to Gridded Population of the World v.3.0, population density in the year 2010 around Segundo and Valdez and the Raton Basin in general was estimated to be less than 10 people per square kilometre. Around Cokedale, values are closer to 20 people/km^2. Trinidad is more populated, and reaches a density of around 100 people/km^2 in some areas.

Table A2.4.8. Population of the four towns which were most affected by this earthquake.

City	Population 1st April 2010
Segundo	98
Valdez	47
Cokedale	129
Trinidad	9,096

In the same way there is disagreement between the initial automatically calculated ShakeMaps and intensity estimations, the USGS PAGER exposure report generated within the first hour of the earthquake differs slightly from its revised version, generated after nine hours of the event. As shown in Figure A2.4.15 (left), initial estimations included an exposure of 23 people to MMI VII, while adjusted estimations eliminate this exposure level altogether (Figure A2.4.15, right).
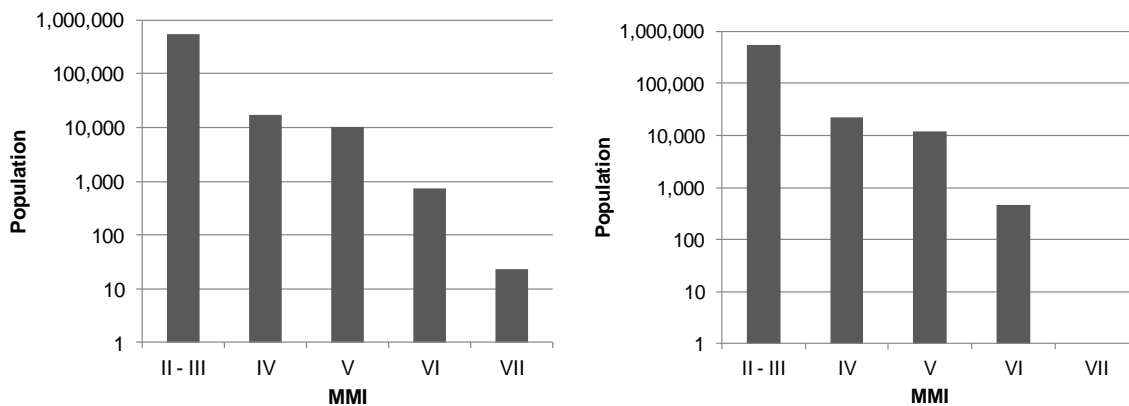
Figure A2.4.15. Estimation of total population exposed to different Modified Mercalli Intensities (MMI) one hour after the main shock (left) and nine hours after the main shock (right) (USGS, 2015.

A2.4.6.3 Time of day of earthquake

The main shock occurred on 22nd August 2011, 23.46 local time. Given the type of damage and the absence of casualties, the time of occurrence of the event did not have a significant impact over its consequences.

A2.4.7 Characteristics of exposed building stock

A2.4.7.1 Seismic design codes

While Cutcliffe (2000) believes that it was the 1906 San Francisco earthquake which marked the start of a real interest in earthquake engineering and seismic design in the United States, Freeman (1932) stated a quarter of a century later that "the art of constructing earthquake-resisting buildings is still in the formative stage, that there are differences of opinions among experts and that there is much deficiency in important data". Further, he points at the 1925 Santa Barbara earthquake to have been more significant in raising awareness on the subject. It was this devastating event that prompted the first edition of the Uniform Building Code (UBC) in 1927, which contained the first written seismic design provisions for a regional level, but which did not become mandatory until 1961 (Beavers, 2002).

As recapitulated by Beavers (2002), the origin of seismic design codes and building codes in general in the USA started in a fragmented fashion, by regions or states. For example, the Uniform Building Code (UBC) just mentioned above was typically used west of the Mississippi river. The National Building Code of the Building Officials and Code Administrators (BOCA) (known as the BOCA Code) was, instead, used in the upper midwest and northeast. It was first published in 1950, including seismic design provisions. In the south, the Standard Building Code (SBC) of the Southern Building Code Congress International (SBCCI) was used. Seismic design provisions were included in the SBC in 1976, by referencing ANSI A58.1, but "were not mandatory unless local authorities required seismic design, which was rarely the case", until 1988. The 1987 edition of the BOCA Code also incorporated the provisions of ANSI A58.1, and made them mandatory.

The ANSI A58.1 standard of the American National Standards Institute (ANSI) was first published in 1945, and was the first standard to consider earthquake loads (Beavers, 2002). However, seismic hazard did not have a role in ANSI A58.1, which only had a map showing the locations of destructive earthquakes of the past until its 1972 edition, in which a seismic hazard description similar to the 1949 USCGS (United States Coast and Geodetic Survey) map was incorporated. The 1972 edition of ANSI A58.1 was also the first one to outline modern wind design provisions (Fratinardo & Schroeder, 2015; Ghosh, 2008), evolving from more basic guidelines developed in the 1950s (Huston, 2007).

The 1949 hazard map was the first one to encompass the whole of the contiguous USA, and it was based on "the premise that similar earthquakes will occur in the future where

they have occurred in the past" (Beavers, 2002). For reasons that are not fully clear, this map was withdrawn in 1952, and replaced with a map that only showed the location of known past significant earthquakes. In the 1970s, the responsibility of producing hazard maps passed on to the USGS (United States Geological Survey), who published the first map developed in the form of probabilistic estimates of maximum acceleration contours on rock in 1976, and which, as highlighted by Beavers (2002), represented a significant paradigm shift. It should be noted, however, that the first edition of the ATC3-06, which in 1985 evolved into the National Earthquake Hazards Reduction Program (NEHRP) Recommended Provisions for Seismic Regulations for New Buildings and Other Structures, used a truncated version of this map in 1978, not allowing for values above 0.4g to be considered. This map was used for almost 20 years, given the inability to reach consensus on a different map that took place in between 1988 and 1994. It was finally updated by the USGS in 1997, after a four-year project called Project 97, during which large efforts were invested in giving a voice to all the professionals and sectors involved. Since then, the USGS hazard map has been updated in 2002, 2008 and 2014.

The way in which seismic loads were considered evolved significantly from the simple use of a 7.5%-10.0% of the building's weight as a lateral load (1927 edition of the UBC), with the progressive incorporation of significant factors such as soil type and capacity, seismic zonation, natural period of vibration of the structure, and importance of the building.

In 1988, ANSI combined with ASCE to update and re-designate ANSI A58.1-1982 to ASCE 7, which is now the most significantly recognised standard by all earthquake regulations, codes, standards, procedures and guidelines for basic seismic design in the USA (Beavers, 2002). Furthermore, ASCE 7 is also the "de facto" national wind design standard (Fratinardo & Schroeder, 2015). The International Building Code (IBC), whose first edition in 2000 was based in the NEHRP Provisions, makes reference to ASCE 7 for the definition of seismic and wind loads. Regarding the latter, it should be noted that, according to ASCE 7-05 (ASCE, 2005), the area affected by the 2011 Trinidad earthquake corresponds to a so-called "special wind region", prone to tornado-like wind speeds.

The IBC 2012 is currently in force in the state of Colorado and is "to be applied to all state-owned buildings and physical facilities including capital construction and controlled maintenance construction projects" (State of Colorado, 2014). No regulation referring to privately-owned buildings has been found.

The Building Code Effectiveness Grading Schedule (BCEGS), developed by the Insurance Services Office (SO), indicates that the overall level of code enforcement across the state of Colorado is relatively low when compared to the country as a whole and to states like California, in which awareness with respect to seismic risk is much greater. Figure A2.4.16 shows the distribution of communities by BCEGS class number for the United States as a whole and for the state of Colorado. Within this classification schedule, classes 1-3 correspond to the maximum enforcement levels, while class 10 indicates no enforcement at all. These figures agree with statements of Beavers (2002) and Cutcliffe (2000), who highlight that, due to their relative lack of seismic activity, the effort to incorporate good

seismic design practises in building codes has been more challenging in the central and eastern USA, when compared to other areas of the country.
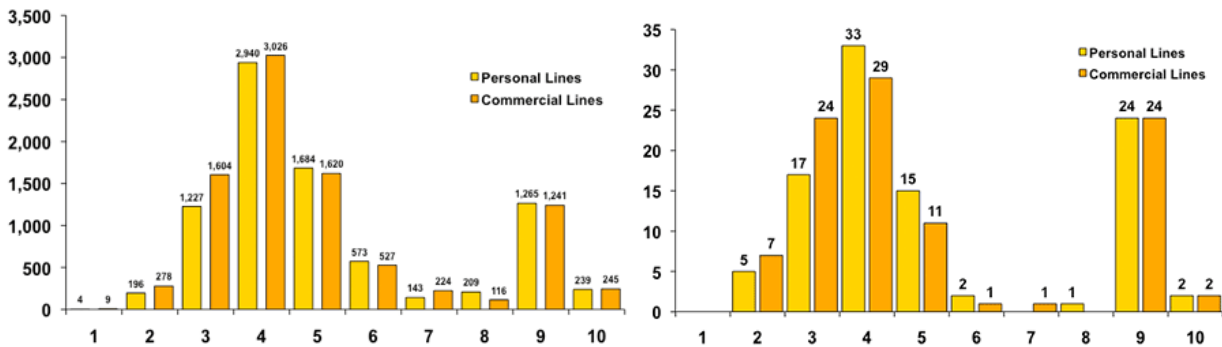
Figure A2.4.16. Distribution of communities by BCEGS class number for the whole of the United States (left) and the state of Colorado (right). Personal lines include 1- and 2-family dwellings. Commercial lines include all other buildings. Classes 1-3: maximum enforcement. Class 10: no enforcement ISO Mitigation (2015)

A2.4.7.2 Building typologies

Information regarding building typologies in the state of Colorado is scarce to null. For this reason, data regarding typologies at the country level were collected from the PAGER Inventory Database v2.0 (Jaiswal & Wald, 2008). Figure A2.4.17 shows that the structure of most of the buildings in the USA consists of light wood frames (61.2%), and unreinforced brick masonry (19.3%) in a smaller proportion. The remaining 19.4% is mostly made up of heavy wood frames and mobile homes (Figure A2.4.18). From available pictures of damage caused by the 2011 Trinidad earthquake it seems possible to infer that light wood frames and unreinforced brick masonry are probably the most likely building typologies in the affected area.

W1: Wood stud-wall frame with plywood/gypsum board sheathing.
UFB3: Unreinforced brick masonry in lime mortar
Other
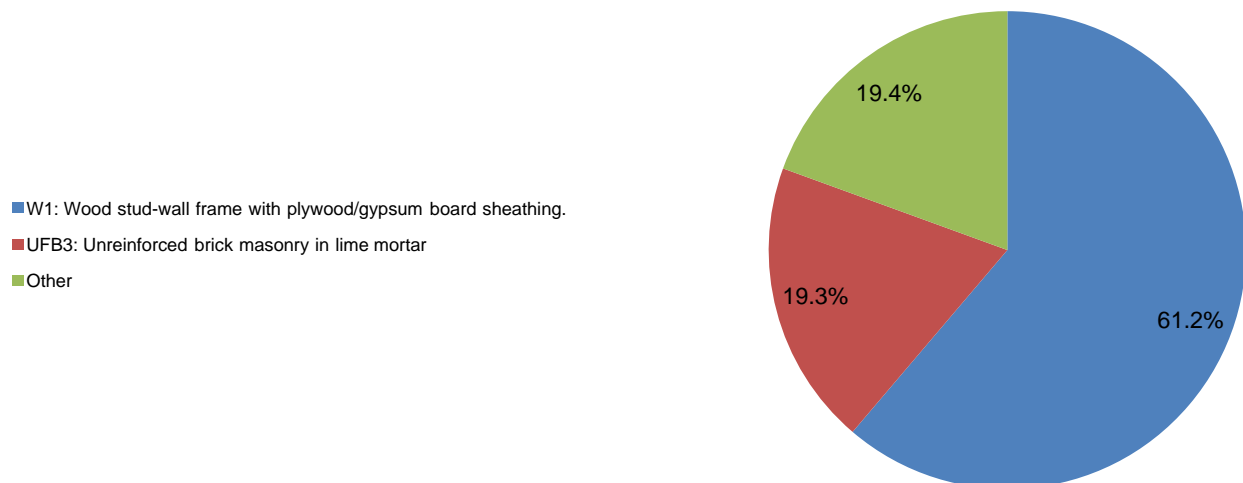
Figure A2.4.17. Proportion of buildings in the United States belonging to each typology. The subcategories within class "Other" are expanded upon in the figure below (Jaiswal & Wald, 2008).

- ■ W2: Wood frame, heavy members (with area > 5000 sq. ft.)
- ■ S1L: Steel moment frame low-rise
- ■ S2L: Steel braced frame low-rise
- ■ S3: Steel light frame
- ■ S4L: Steel frame with cast-in-place concrete shear walls low-rise
- ■ S5L: Steel frame with unreinforced masonry infill walls low-rise
- ■ C1L: Ductile reinforced concrete moment frame with or without infill low-rise
- ■ C2L: Reinforced concrete shear walls low-rise
- ■ C3L: Nonductile reinforced concrete frame with masonry infill walls low-rise
- ■ PC1: Precast concrete tilt-up walls
- ■ PC2L: Precast concrete frames with concrete shear walls low-rise
- ■ RM1L: Reinforced masonry bearing walls with wood or metal deck diaphragms low-rise
- ■ RM2L: Reinforced masonry bearing walls with concrete diaphragms low-rise
- ■ MH: Mobile homes

Figure A2.4.18. Breakdown of the "Other" class in the figure above. To determine the percentage that each of these sub-categories represents of the total in the USA, multiply the value in this figure by 0.194 (Jaiswal & Wald, 2008).

A2.4.7.3 Prior damage and retrofit

No details on prior damage or retrofit available.

A2.4.8 Damage observations

A2.4.8.1 Damage states

Given the relatively low level of damage observed, there are no reports making use of standardised damage scales for this earthquake. However, from the qualitative descriptions, it is possible to believe that most damage observed corresponded to Grade 2 in the European Macroseismic Scale (EMS-98; Grünthal, 1998). For details regarding the latter, please refer to Chapter 2.

A2.4.8.2 Damage statistics

As mentioned earlier, the four locations in which structural damage was observed were, from most severe to least, Segundo, Valdez, Cokedale, and Trinidad (Morgan & Morgan, 2011, see locations in Figure A2.4.11). According to Matthews (2011), forty-six structures were damaged, beyond repair in only two cases. It seems that one of this cases was reported in Segundo, but Morgan & Morgan (2011) state that this could not be verified, due to the will of the owners of the property to remain anonymous.

Located at approximately 6.8 km from the epicentre, both Segundo and Valdez saw several displaced/pulled-away façades and chimneys, significant cracks in masonry walls, and masonry blocks and bricks collapsing and causing additional damage due to their fall. Offsets of façades and walls reported by Morgan & Morgan (2011) range from 1 cm to 5 cm. Figs. II.4.19 and 20 show some examples of this kind of damage.

Figure A2.4.19. Damage observed at Segundo: on the left, the exterior wall pulled away approximately 2.5 cm from the interior wall; on the right, the front of this brick building collapsed (Morgan & Morgan, 2011).

Figure A2.4.20. Major brick damage to a home in Segundo (left) and to a garage in Valdez (right) (Morgan & Morgan, 2011).

Figure A2.4.21. A 3 metres long vertical crack in the building of the Cokedale post office/city hall (left); cracked plaster on a façade in Segundo (Morgan & Morgan, 2011).

Cracked plaster was observed in all four towns mentioned, being the case of the 3 metres vertical crack at the Cokedale post office/city hall building the worst (Figure A2.4.21).

Nevertheless, the town mayor of Cokedale (located at approximately 11.5 km from the epicentre) reported "no significant damage" to the residences in the area (Morgan & Morgan, 2011).

Regarding Trinidad, located at approximately 21 km from the epicentre, Morgan & Morgan (2011) only report a plaster and metal siding fall from the front of a coffee shop.

A2.4.8.3 Observed weaknesses

No reports of systematic weaknesses were found in the literature. However, the kind of damage observed and the statements by Beavers (2002) and Cutcliffe (2000) regarding the challenges faced by the efforts to incorporate good seismic design practises in the central and eastern USA suggest that the lack of seismic design of masonry structures was the main cause of the damage observed.

A2.4.8.4 Damage distribution

There are no details available with respect to the distribution of damage within the towns. Nevertheless, it should be noted that the towns which suffered the most damage are significantly small (less than 100 people in Segundo, and less than 50 people in Valdez).

A2.4.9 Casualties and losses

A2.4.9.1 Numbers of dead and injured

No casualties reported.

A2.4.9.2 Causes of casualties

No casualties reported.

A2.4.9.3 Estimates of economic losses

According to Morgan & Morgan (2011), none of the damaged structures were covered by earthquake insurance, and the economic loss was expected to exceed 100,000 US dollars. This figure is in agreement with the estimation from USGS PAGER (2015) according to which the economic loss was not expected to exceed one million US dollars.

A2.4.10 Discussion and conclusions

This earthquake occurred on 23rd August 2011, at 05.46 UTC (22nd August 2011, 23.46 local time), and was the largest to take place in Colorado in around half a century. It was part of a sequence that started with a series of small foreshocks the day before, was

followed by over 500 events in the following four months. Whilst tectonic earthquakes have been known to occur in the Raton Basin area, this event is believed to have been induced by deep injection of wastewater in the Raton Basin.

The main shock was widely felt and caused significant damage to masonry buildings in the scarcely populated towns of Segundo, Valdez, Cokedale and Trinidad, all located within 20 km of the epicentre. Rockfalls occurred at the State Highway 12, a road approximately 1.5 km east of Segundo, causing minimum disruption and no damage to buildings. No casualties were reported.

In spite of there being some disagreement amongst different estimations of the ground motion level to which the damaged structures were subject, an accelerograph recorded near the town of Trinidad suggests that it was not particularly high. It is thus likely that the significant damage observed be due to the lack of seismic design of masonry structures in the area, in spite of their (possible) wind design.

A2.4.11 References

A2.4.11.1 Bibliography

American Society of Civil Engineers, Structural Engineering Institute (2005). *Minimum Design Loads for Buildings and Other Structures, ASCE/SEI 7-05*. Reston, VA, United States.

Barnhart, W.D., H.M. Benz, G.P. Hayes, J.L. Rubinstein & E. Bergman (2014). Seismological and geodetic constraints on the 2011 M_w5.3 Trinidad, Colorado earthquake and induced deformation in the Raton Basin. *J. Geophys. Res. Solid Earth* **119**, 7923–7933.

Beavers, J.E. (2002). A review of seismic hazard description in US design codes and procedures. *Prog. Struct. Eng. Mater.* **4**, 46–63.

Bommer, J.J., P.J. Stafford & J.E. Alarcón (2009). Empirical equations for the prediction of the significant, bracketed, and uniform duration of earthquake ground motion. *Bulletin of the Seismological Society of America* **99**(6), 3217-3233.

Bott, J.D.J. & I.G. Wong (1995). The 1986 Crested Butte earthquake swarm and its implications for seismogenesis in Colorado. *Bull. Seismol. Soc. Am.* **85**, 1495-1500.

Cutcliffe, S.H. (2000). Earthquake resistant building design codes and safety standards: The California experience. *GeoJournal* **51**, 259–262.

Flores, R.M. (1987). Sedimentology of Upper Cretaceous and Tertiary siliciclastics and coals in the Raton Basin, New Mexico and Colorado, in Lucas, S.G. & Hunt, A.P., eds., Northeastern New Mexico. New Mexico Geological Society 38th Annual Field Conference, 255–264.

Flores, R.M. & Bader, L.R. (1999). A summary of Tertiary coal resources of the Raton Basin, Colorado and New Mexico, chap. SR of Fort Union Coal Assessment Team, 1999 Resource Assessment of Selected Tertiary Coal Beds and Zones in the Northern Rocky Mountains and Great Plains Region. U.S. Geological Survey Professional Paper 1625-A [available only on CD-ROM].

Fratinardo, V.F. & S.A. Schroeder (2015). Historical study of the wind design provisions of ASCE 7. *Structures Congress 2015*, 829–839.

Freeman J.R. (1932). *Earthquake Damage and Earthquake Insurance*. 1st edition. New York: McGraw-Hill.

Ghosh, S.K. (2008). Searching for simplicity: The evolution of wind provisions in standards and codes in the United States. *RCI Interface*, 13–21.

Giardini, D., G. Grünthal, K.M. Shedlock & P. Zhang (1999). The GSHAP global seismic hazard map. *Annali di Geofisica* **42**(6), 1225-1228.

Giardini, D., G. Grünthal, K.M. Shedlock & P. Zhang (2003). The GSHAP global seismic hazard map. In: Lee, W., H. Kanamori, P. Jennings & C. Kisslinger (eds.): International handbook of earthquake & engineering seismology, International Geophysics Series 81 B, Academic Press, Amsterdam, 1233-1239.

Grünthal, G. (ed.) (1998). *European Macroseismic Scale 1998 (EMS-98)*. Cahiers du Centre Europeen de Geodynamique et de Seismologie 15, Centre Europeen de Geodynamique et de Seismologie, Luxembourg.

Huston, E. (2007). SEAW's handbook of a rapid-solutions methodology for wind design. *Struct. Mag.*, 61–64.

Jaiswal, K. & D.J. Wald (2008). Creating a Global Building Inventory for Earthquake Loss Assessment and Risk Management. USGS Open File Report 2008-1160. Available electronically at http://pubs.usgs.gov/of/2008/1160/.

Johnson, R. (1969). *Geologic map of the Trinidad quadrangle, south-central Colorado*. U.S. Geol. Surv. Misc. Geol. Investig. Map I-558.

Johnson, R.C. & T.M. Finn (2001). *Potential for a basin-centered gas accumulation in the Raton Basin, Colorado and New Mexico - Geologic studies of basin-centered gas systems*. U.S. Geological Survey Bulletin 2184-B, US Department of the Interior, US Geological Survey. Available only online: http://geology.cr.usgs.gov/pub/bulletins/b2184-b/ .

Kempton, J.J. & J.P. Stewart (2006). Prediction equations for significant duration of erthquake ground motions considering site and near-source effects. Earthquake Spectra **22**(4), 985-1013.

Matthews, V. (2011). The Trinidad, Colorado earthquakes. *Colorado Geological Survey*.

Morgan, M.L. & K.S. Morgan (2011). Preliminary damage report of the August 22, 2011 Mw 5.3 earthquake near Trinidad, Colorado. *Colorado Geological Survey*.

Pillmore, C.L. (1969). Geology and coal deposits of the Raton coal field, Colfax County, New Mexico. *The Mountain Geologist* **6**, 125–142.

Pillmore, C.E. & R.M. Flores (1987). Stratigraphy and depositional environments of the Cretaceous-Tertiary boundary clay and associated rocks, Raton Basin, New Mexico and Colorado, in Fassett, J.E. & Rigby, J.K., Jr., eds., The Cretaceous-Tertiary Boundary in the San Juan and Raton Basins, New Mexico and Colorado. *Geological Society of America* **209**, 111–130.

Robson, S. & E. Banta (1987). *Geology and hydrology of deep bedrock aquifers in eastern Colorado*. USGS Water-Resources Investig. Rept. 85-4240, 22 pp.

Rubinstein, J.L., W.L. Ellsworth, A. McGarr & H.M. Benz (2014). The 2001-present induced earthquake sequence in the Raton Basin of northern New Mexico and southern Colorado. *Bull. Seismol. Soc. Am.* **104**, 2162–2181.

Sheehan, A.F., J.D. Godchaux & N. Hughes (2003). Colorado Front Range seismicity and seismic hazard. *Engineering Geology in Colorado: Contributions, Trends and Case Histories*.

Scott, G. R. & C. L. Pillmore (1993). *Geologic and structure-contour map of the Raton 30′× 60′ quadrangle, Colfax and Union Counties, New Mexico, and Las Animas County, Colorado*. U.S. Geol. Surv. Misc. Geol. Investig. Map I-2266.

State of Colorado (2014). *Building code compliance policy: Coordination of approved building codes, plan reviews and building inspections*. Office of the State Architect, State Buildings Programs, Policies and Procedures, Colorado, United States.

United Nations, ed. (2011). *Human Development Report 2011 - Sustainability and equity: A better future for all*. Report of the United Nations Development Programme (UNDP). Palgrave Macmillan, New York, United States.

United Nations, ed. (2013). *Human Development Report 2013 - The rise of the South: Human progress in a diverse world*. Report of the United Nations Development Programme (UNDP). Palgrave Macmillan, New York, United States.

United Nations, ed. (2014). *Human Development Report 2014 - Sustaining human progress: Reducing vulnerabilities and building resilience*. Report of the United Nations Development Programme (UNDP). Palgrave Macmillan, New York, United States.

Wald, D.J. & T.I. Allen (2007). Topographic slope as a proxy for seismic site conditions and amplification. *Bull. Seismol. Soc. Am*. **97**, 1379–1395.

Wills, C.J. & K.B. Clahan (2006). Developing a map of geologically defined site-condition categories for California. *Bull. Seismol. Soc. Am*. **96**, 1483–1501.

Wills, C.J. & W. Silva (1998). Shear wave velocity characteristics of geologic units in California. *Earthquake Spectra* **14**, 533–556.

A2.4.11.2 Web references

Gridded Population of the World (GPW): http://sedac.ciesin.columbia.edu/data/collection/ gpw-v3

ISO Mitigation: http://www.isomitigation.com/index.php/bcegs/facts-and-figures-about-bcegs-grades-around-the-country.

United States Bureau of Economic Analysis: http://www.bea.gov/

United States Geological Survey (USGS): http://earthquake.usgs.gov/

United States Geological Survey (USGS) Mineral Resources Online Spatial Data: http://mrdata.usgs.gov/geology/state/

United States Geological Survey (USGS) Quaternary Fault and Fold Database: http://earthquake.usgs.gov/hazards/qfaults/

United States Geological Survey (USGS) V_{s30} Map Server: http://earthquake.usgs.gov/hazards/apps/vs30/

World Economic Outlook Database 2015: http://www.imf.org/external/pubs/ft/weo/2015/01/ weodata/index.aspx

A2.5 November 2011 M5.6 Prague (Oklahoma) Earthquake, USA

This earthquake occurred on 6th November 2011, at 03.53.10 UTC (5th November 2011, 22.53.10 local time), and is the largest to have ever occurred in the history of Oklahoma. It was part of a sequence that includes a **M**4.8 foreshock around 21 hours earlier, a **M**4.0 that occurred only 10 minutes after the main shock and a **M**4.8 on 8th November 2011, which was the biggest of its more than one thousand aftershocks. The whole sequence is widely believed to have been induced by the activities of deep injection of wastewater that have been going on in the area for decades. The main shock and other strong events were extensively felt and caused significant fear in the population, as well as different levels of damage, particularly in the area enclosed by the cities/towns of Prague, Sparks, Meeker and Shawnee.

A2.5.1 Tectonic and seismic setting

A2.5.1.1 Tectonic setting

This earthquake occurred within the Cherokee Platform, in the centre of the state of Oklahoma, 60 km to the east of Oklahoma City. The whole area belongs to the large stable continental region of the central and eastern United States. In contrast with active continental regions, stable continental areas are characterised by a relatively lower seismic activity and low strain rates (Klose & Seeber, 2007), and by the fact that earthquakes tend to be felt over much larger areas (USGS).

The state of Oklahoma is subject to a horizontal compressive stress oriented from east to west (Darold & Holland, 2015; Witze, 2015). Witze (2015) determined a mean and a median orientation of the maximum horizontal stress of N83.2°E and N84.8°E, respectively, with a standard deviation of 21.3°. This direction of horizontal stresses causes faults oriented northwest to southeast or northeast to southwest to be more likely to rupture than faults with orientations significantly different from these.

The slow rates of deformation and limited knowledge of the fault geometry that characterise stable continental regions often prevent unambiguous attribution of an earthquake to a given fault structure. Nevertheless, in view of the location of all the events in the sequence and the suspicion of their connection with the extraction and injection activities carried out in the surrounding oil field, it is believed that the 2011 Prague earthquake occurred on the Wilzetta fault (Figure A2.5.1), an 200-km long strike-slip subsurface fault running in the NNE-SSW direction, an orientation which favours the occurrence of earthquakes within the present stress regime, as described above (Keranen *et al.*, 2013; Northcutt & Campbell, 1995; USGS; OGS).
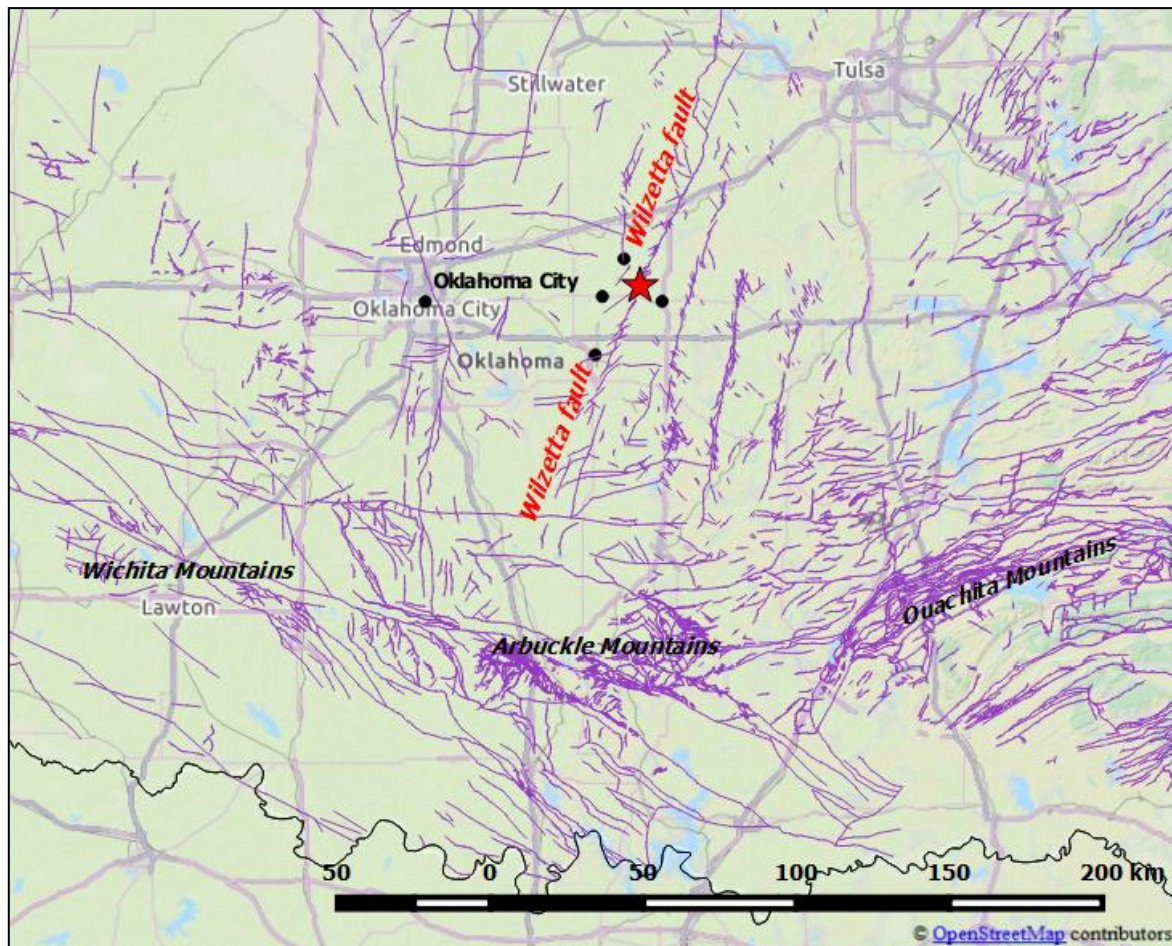
Figure A2.5.1. Faults in the area around the epicentre (red star, according to the USGS) of the 2011 Prague earthquake, according to the Oklahoma fault database. From the Oklahoma Geological Survey (Darold & Holland, 2015; Northcutt & Campbell, 1995).

A2.5.1.2 Regional and local seismicity

Seismicity rates in the area known as the central and eastern United States (CEUS), to which Oklahoma belongs, are generally low, as should be expected for such low intraplate strain rates (Hough & Page, 2015). The Meers fault, located along the Whichita mountains (Figure A2.5.1), is the only fault within the state of Oklahoma with documented Quaternary surface rupture. According to Hough & Page (2015), there is evidence of two earthquakes of **M**6.5-7 having occurred along this fault within the past 3,400 years, though modern seismicity rates associated with it have been extremely low.

A recent study by Hough & Page (2015) indicates that the earliest earthquake known to have occurred within Oklahoma according to the recently compiled Central and Eastern United States Seismic Source Characterization for Nuclear Facilities (CEUS-SSC) catalogue occurred on 22nd October 1882, and had its epicentre in eastern Oklahoma. Hough & Page (2015) believe that this event was associated with the Ouachita structural belt (Figure A2.5.1). The CEUS-SSC catalogue estimates a moment magnitude of **M**5.6 for this event, while Hough & Page (2015) estimate a significantly lower **M**4.8 instead.

Only six events larger than **M**3.5 occurred in Oklahoma between 1900 and 1940, and no events larger than **M**3.5 occurred between 1940 and 1950 (Hough & Page, 2015). A relevant **M**5.5 event took place on 9th April 1952, with epicentre to the west of Oklahoma City. Although damage was not extensive, people located close to the epicentral area were noticeably alarmed (USGS).

The relatively low seismicity rates inferred from the information above has seen a significant increase in recent years. Keranen *et al.* (2013) report an increase by a factor of 40 in the number of earthquakes per year recorded within Oklahoma between 2008 and 2013, compared to 1976-2007. Hough & Page (2015) report an increase factor of 100 when the compared periods are 2010-early 2015 and 1900-2009, considering events with magnitude equal to or larger to **M**3.5. This drastic change in the observed seismicity becomes evident in Figure A2.5.2, which shows the epicentres of events registered since 1970 grouped by colours according to their time of occurrence.
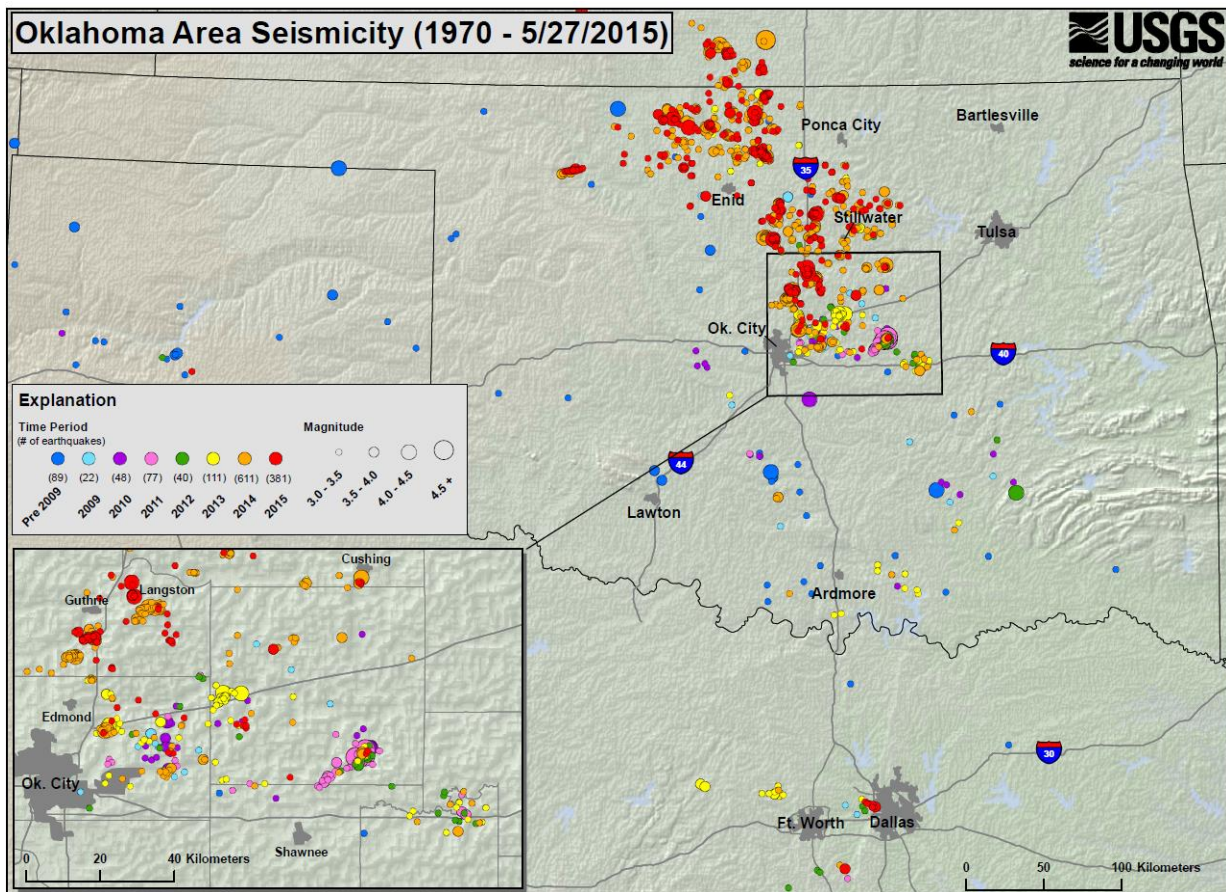
Figure A2.5.2. Seismicity map of Oklahoma according to the United States Geological Survey. Events between 1970 and 27th May 2015 are grouped by colours (USGS, 2015)

A2.5.1.3 Seismic hazard

Figure A2.5.3 shows extracts of the probabilistic seismic hazard maps for the United States of 2008 and 2014, elaborated by the United States Geological Survey (USGS). Values

shown correspond to peak ground acceleration (PGA) on rock with a 10% probability of exceedance in 50 years. The area affected by the 2011 Prague earthquake and the state of Oklahoma are marked in red. Table A2.5.1 presents a summary of the PGA values expected at Meeker, Prague, Shawnee and Sparks, which are the most relevant locations to describe the damage experienced as a consequence of the 2011 Trinidad earthquake. The table also reports the corresponding values obtained from the Global Seismic Hazard Assessment Program (GSHAP; Giardini *et al.*, 1999; Giardini *et al.*, 2003), which are very close to the average between those of the 2014 USGS hazard map than to those of the 2008 one. In spite of the discrepancies, all values support the idea that seismic hazard is moderate to low in the affected area. It should be noted that the USGS national seismic hazard maps do not take into consideration non-tectonic seismic activities and, therefore, the 2011 events around the area of Prague had no effect over the change from the 2008 map to the 2014 one.
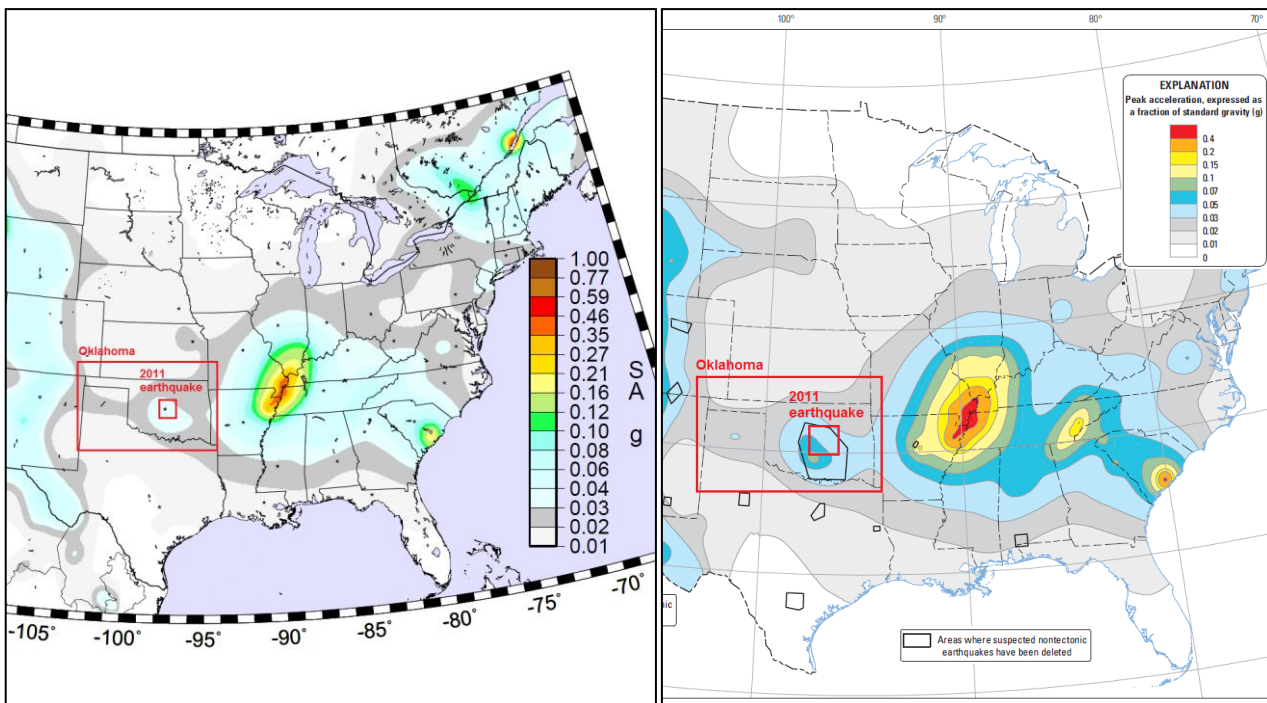
Figure A2.5.3. Extract of the 2008 (left) and 2014 (right) hazard maps for the United States, elaborated by the USGS (2015). Values correspond to peak ground acceleration (g) on rock with a 10% probability of exceedance in 50 years.

Table A2.5.1. Peak ground acceleration (PGA, g) values on rock with a 10% probability of exceedance in 50 years according to the 2008 and 2014 USGS hazard maps, and results from the Global Seismic Hazard Assessment Program (GSHAP), at locations in which damage was observed after the 2011 Trinidad earthquake.

PLACE	USA 2008	USA 2014	GSHAP
Meeker	0.0328	0.0412	0.0371
Prague	0.0312	0.0390	0.0349
Shawnee	0.0342	0.0444	0.0394
Sparks	0.0310	0.0382	0.0350

A2.5.2 Earthquake source characteristics

A2.5.2.1 Location, depth and time

The main shock occurred on 6th November 2011, at 03.53 UTC (5th November 2011, 22.53 local time).

Several organizations and agencies report their own estimations of the epicentral coordinates and hypocentral depth. The information reported in the websites of the National Earthquake Information Center (NEIC) of the United States Geological Service (USGS), the Global Centroid Moment Tensor Project (GCMT) and the International Seismological Centre (ISC) is summarized in Table A2.5.2. Cells marked as (*f) correspond to parameters that were held fixed while inversion was carried out to retrieve those that remain. Table A2.5.2 also includes the epicentral coordinates and hypocentral depth calculated by Holland (2013) and Sun & Hartzell (2014).

Table A2.5.2. Epicentral coordinates and hypocentral depths from different sources.

	Agency / Publication	Latitude	Longitude	Depth (km)
NEIC	National Earthquake Information Center, USGS	35.5320 °N	96.7650 °W	5.20
GCMT	Centroid Global Centroid Moment Tensor Project (**)	35.6100 °N	96.7200 °W	12.00 (*f)
ISC	International Seismological Centre - GEM catalogue	35.5330 °N	96.7050 °W	10.00
OGS	Oklahoma Geological Service	35.5316 °N	96.7714 °W	3.1 - 5.2
Holland (2013)		35.5220 °N	96.7800 °W	3.10
Sun & Hartzell (2014)		35.5301 °N	96.7773 °W	5.00

(*f) fixed parameter used for inversion

(**) centroid (not-hypocentral) location

Regarding the variability in the estimated depths, a shallow hypocentre seems more likely given that Keranen *et al.* (2013) report the depths of 83% of the aftershocks of this event being less than 5 km, and highlight that 30% of the early aftershocks (which represent 20% of the total) were located within the sedimentary units into which fluids are injected. Furthermore, Sun & Hartzell (2014) infer a slip model for the main shock in which a first patch of highly-concentrated slip is located at a depth range between 3.0 and 5.5 km, and a second deeper one can be observed between 7.5 and 9.5 km.

The map in Figure A2.5.4 shows the different estimations of the epicentral coordinates enumerated above. Note that coordinates reported by the GCMT correspond to the location of the centroid, and not the hypocentre.

A2.5.2.2 Magnitude

Estimations of magnitude made by the same agencies are reported in Table A2.5.3.
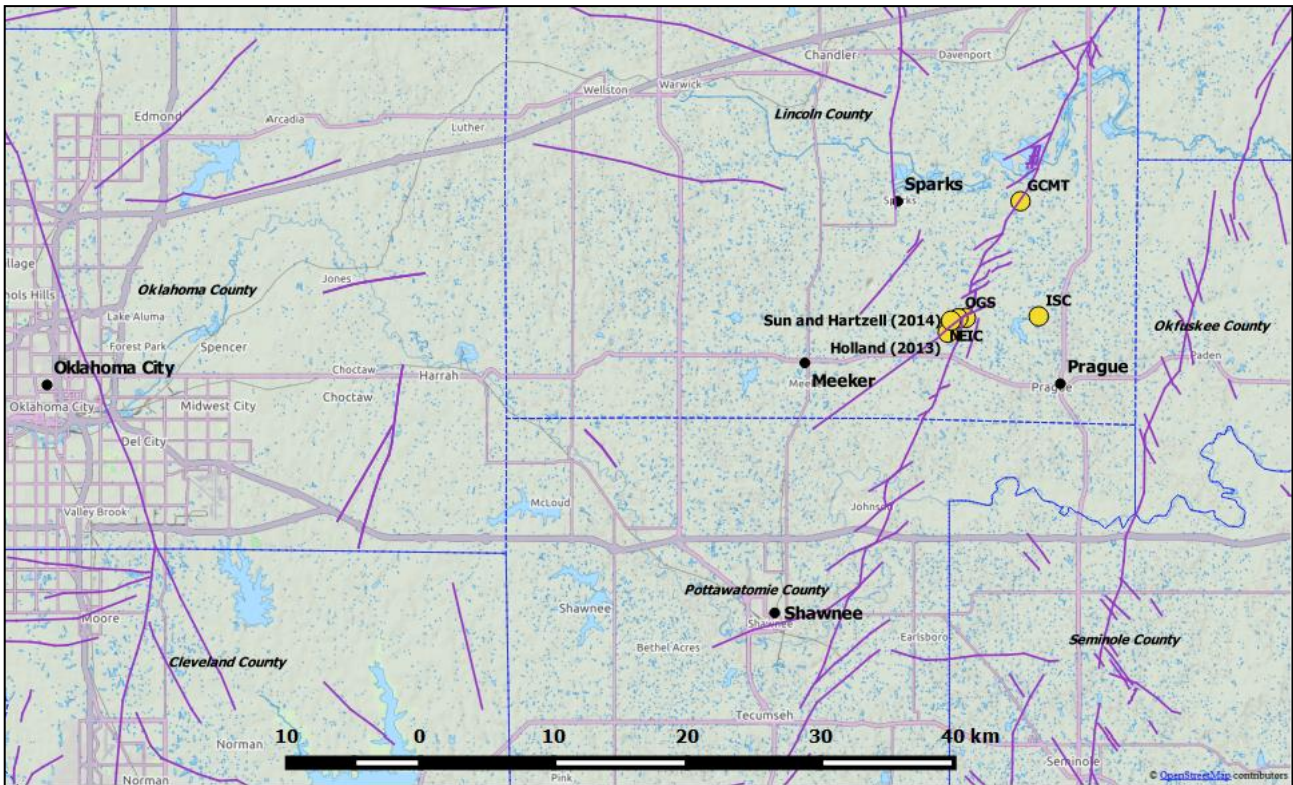
Figure A2.5.4. Estimation of epicentral coordinates (yellow circles). Faults in the area marked in violet, according to the Oklahoma fault database.

Table A2.5.3. Estimations of moment magnitude (**M**), body-wave magnitude (mb) and surface-wave magnitude (Ms).

	Agency	M	mb	Ms
NEIC	National Earthquake Information Center, USGS	5.6	5.2	5.6
GCMT	Global Centroid Moment Tensor Project (1)	5.7	5.2	5.7
ISC	International Seismological Service (inversion)	5.7	-	-
OGS	Oklahoma Geological Service	5.6	5.2	5.6
Holland (2013) and Sun & Hartzell (2014)		5.6	-	-

A2.5.2.3 Style-of-faulting

All sources indicate a strike-slip mechanism on a fault striking to the northeast. Furthermore, Holland (2013) demonstrates that the vast majority of the events that made up the 2011 Prague sequence, as well as the vast majority of the events occurring in the area in general, are the result of strike-slip motion on steeply dipping faults, as shown in Figure A2.5.5.

Table A2.5.4 summarizes the fault plane solutions calculated by the USGS, the GCMT, Holland (2013) and Sun & Hartzell (2014). Note that, being the dip very close to 90° in all cases, a 55° strike and a 235° strike are practically equivalent.
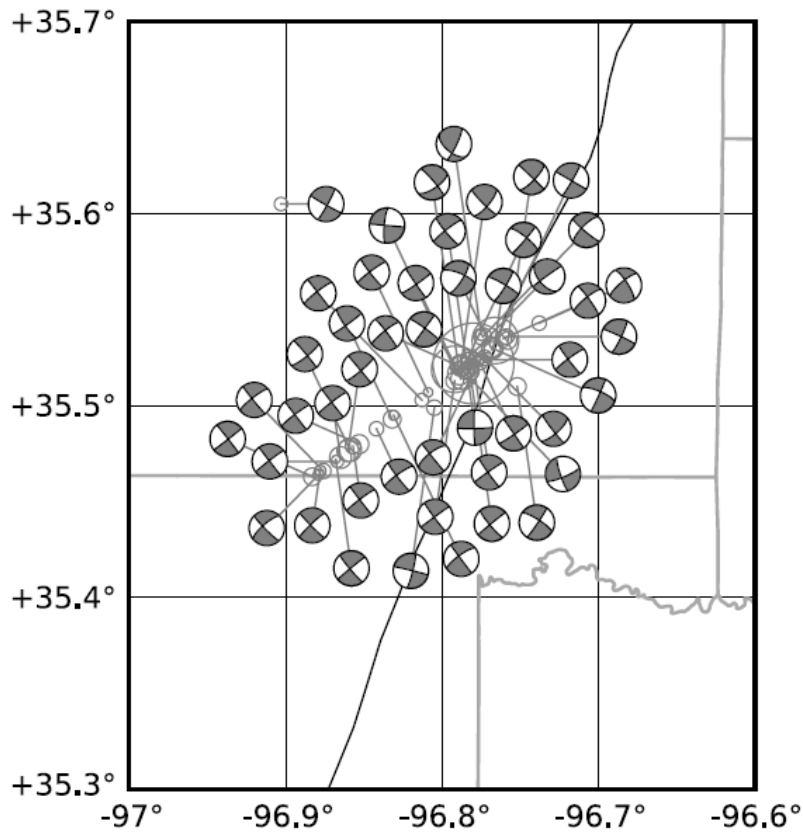
Figure A2.5.5. Focal mechanisms of 47 events of the 2011 Prague earthquake sequence following the **M**4.8 foreshock of 5th November 2011. From(Holland (2013).

Table A2.5.4. Fault plane solutions and fault planes from different sources. Fault planes marked in gray are the preferred solution in each case.

Fault Plane 1			Fault Plane 2			Source
Strike	Dip	Rake	Strike	Dip	Rake	
324	86	-4	55	86	-176	Regional Moment Tensor NEIC (USGS)
324	88	-2	54	88	-178	GCMT
235	85	-175	-	-	-	Holland (2013) and Sun & Hartzell (2014)

A2.5.2.4 Stress drop

According to the slip model inferred by Sun & Hartzell (2014), two large slip patches could be identified for the main shock: one located around the hypocentre, at a depth range between 3.0 and 5.5 km, and a second one between 7.5 and 9.5 km (Figure A2.5.6). The average stress drops were 9 MPa (90 bars) for the shallower patch and 1.6 MPa (16 bars) over all areas of slip.
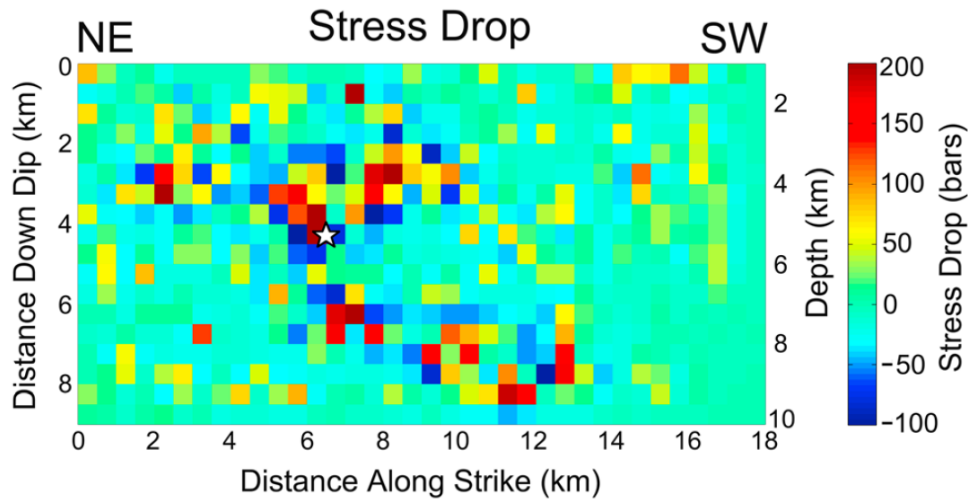
Figure A2.5.6. Static stress drop (1 bar = 0.1 MPa) on the fault due to the main shock. From Sun & Hartzell (2014).

A2.5.2.5 Foreshocks and aftershocks

According to the Oklahoma Geological Survey (OGS), the main shock of 6th November 2011 was preceded by multiple foreshock events, the largest of which was a **M**4.8 which occurred around 21 hours earlier. It was then followed by thousands of aftershocks, including a **M**4.0 that occurred only 10 minutes after the main shock and a **M**4.8 on 8th November 2011, which was the biggest. The OGS reports that the aftershocks in the Prague area followed the normal Omori Law time--decay that is typical of natural seismicity.

Keranen *et al.* (2013) report the occurrence of 1183 aftershocks. During the whole sequence, they observe the progressive rupture of three fault planes, and believe that the **M**4.8 foreshock of 5th November 2011 triggered the rest of the sequence, including the main shock. Figure A2.5.7 shows their reported locations for several of the events in the sequence.

A2.5.2.6 Nature of earthquake

A significant number of studies link the 2011 Prague earthquake sequence to deep fluid injection of waste water (Hough & Page, 2015; Keranen *et al.*, 2013; Llenos & Michael, 2013; Sumy *et al.*, 2014; Sun & Hartzell, 2014; Witze, 2015). In particular, Sun & Hartzell (2014) point out that the relatively low peak slip and stress drop support this assertion. A statement by the Oklahoma Geological Survey from March 2013 exposes the lack of agreement on the issue, for it concludes that "the interpretation that best fits current data is that the Prague earthquake sequence was the result of natural causes", based mainly on the fact that tectonic earthquakes have been known to occur in the area and that measurements carried out by the Oklahoma Corporation Commission (OCC) indicate that the geological formations in the area are under-pressured. However, a joint statement of the Oklahoma Geological Survey and the United States Geological Survey from May 2014 states their conviction that the recent changes in earthquake rates in Oklahoma do not

seem to be due to typical natural fluctuations, and that they are likely linked to waste water injection. Regarding the reference to previous seismicity observed in the area, Hough & Page (2015) acknowledge the evidence that natural intraplate earthquakes tend to be temporally clustered, but also believe that the apparent cluster of activity in Oklahoma since 2009 is not consistent with the level of natural rate fluctuations seen in the past.
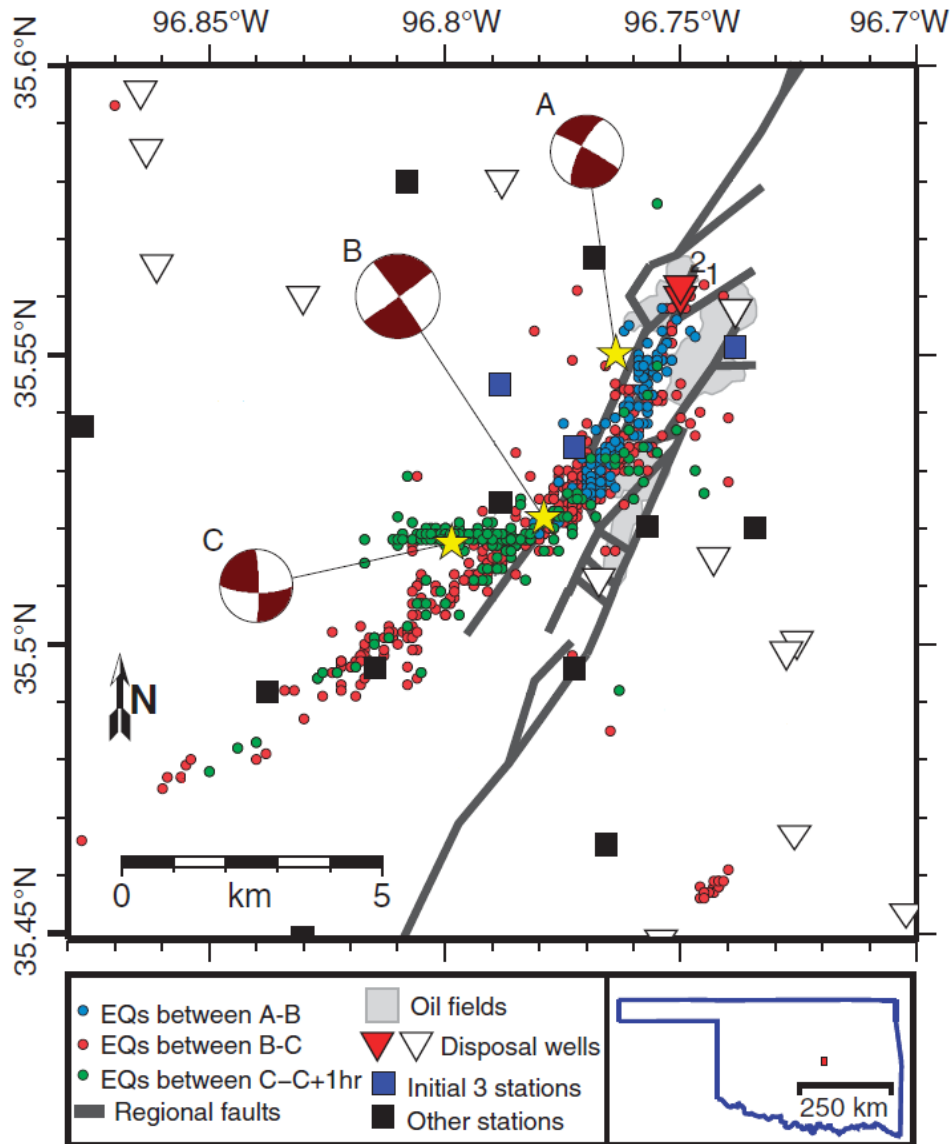
Figure A2.5.7. Location of the main **M**4.8 foreshock (marked as A), the **M**5.6 main shock (marked as B), the **M**4.8 aftershock (marked as C), and several other foreshocks (blue dots) and aftershocks (red and green dots). From Keranen *et al.* (2013).

Though claiming that the 2011 Prague sequence was induced, Keranen *et al.* (2013) believe that the faults were heavily loaded with tectonic stress and that fluid injection acted as a trigger, for the scalar moment released exceeds the value expected as a function of the volume of injected fluid by several orders of magnitude. Sumy *et al.* (2014) support this view and suggest that it was the **M**4.8 foreshock that was directly induced by fluid injection and then triggered the main shock and its aftershocks.

A2.5.3 Geology and ground conditions in the affected area

A2.5.3.1 Regional geology and topography

The most affected region, a triangle enclosed by the towns of Prague, Shawnee and Sparks as vertices, is located in a low-lying area in the middle of the state of Oklahoma, within the geologic province known as the Cherokee Platform (Northcutt & Campbell, 1995). The whole state slopes gradually downwards from west to east, and its main topographic features are the Wichita mountains, the Arbuckle mountains, the Ouachita mountains and the Ozark mountains, marked in the map of Figure A2.5.8 as the Wichita, Arbuckle, Ouachita and Ozark uplifts, respectively. The western part of the state is part of the United States' High Plains, a large relatively flat region lying at a significantly high altitude.

As shown in the map in Figure A2.5.9, different affected cities lie over different kinds of geologic units (Johnson, 2008). The city of Prague lies over Pennsylvanian sediments, which consist mostly of marine shale, with interbedded sandstone, limestone, and coal, and whose thickness can vary between 0.6 and 1.5 km. The city of Meeker is located in an area where Permian sediments consisting of shallow-marine, deltaic and alluvial deposits of red sandstone and shale, instead. Their thickness can vary between 0.3 and 2.0 km. Due to their proximity to two rivers, the cities of Sparks and Shawnee lie over quaternary deposits of sand, silt, clay and gravel, whose thickness varies between 8.0 and 30.0 metres.
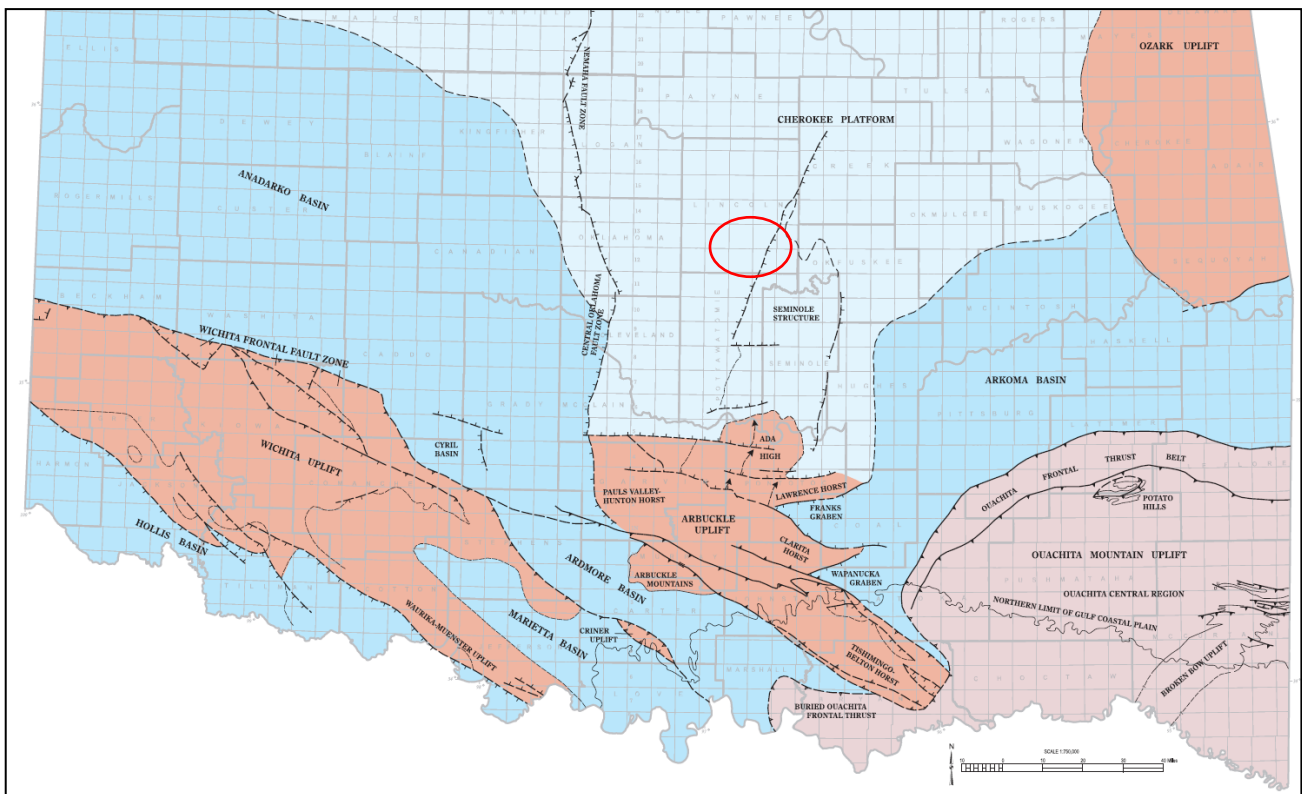
Figure A2.5.8. Geologic provinces of Oklahoma. The red circle marks the area affected by the 2011 Prague earthquake. From Northcutt & Campbell (1995).

Figure A2.5.9. Geologic map of sediments and sedimentary rocks of the area affected by the 2011 Prague earthquake. Permian (P): shallow-marine, deltaic and alluvial deposits of red sandstone and shale predominate, generally between 0.3 and 2.0 km thick; subdivided into lower (P1) and upper (P2, P3 and P4) units. Penssylvanian (|P): mostly marine shale, with interbedded sandstone, limestone, and coal, generally between 0.6 and 1.5 km thick; subdivided into lower (|P1), middle (|P2) and upper (|P3) units. Quaternary (Q): sand, silt, clay and gravel in flood plain and terrace deposits of major rivers, generally 8.0 to 30.0 m thick. Black dots indicate the locations of cities affected by the 2011 Prague earthquake, and the red star indicates the epicentre, as determined by the United States Geological Survey. From Johnson (2008).

A2.5.3.2 Site conditions in the affected area

Figure A2.5.10 presents a schematic cross section across the Wilzetta fault system, which is believed to be where the 2011 Prague event was originated. According to the figure, a top layer of interbedded sandstone and shale overlays an alternation of clay, clay shale and limestone (Keranen *et al.*, 2013). This cross section is consisted with the geologic units described above.

To our knowledge, measured V_{s30} values are not available in the literature for central Oklahoma. For this reason, three different sources that can help form a picture of the site conditions around the affected area are herein reported. In their probabilistic seismic hazard assessment of the Arcadia Dam, located to the northeast of Oklahoma city, Holland *et al.* (2013) present shear wave velocity models to a depth of 30 metres for two specific sites, which were determined by means of active-source multichannel analysis of surface wave (MASW) studies. The location of these sites is shown in Figure A2.5.11. Shear wave velocities at the ADOK station vary increasingly from 300 m/s at the top to 800 m/s at a depth of 30 metres, and yield a V_{s30} value of 621 m/s. Shear wave velocities measured to the east of the Arcadia Dam are much lower: they vary between 180 m/s at the surface and 400 m/s at a depth of 30 metres, and yield a much lower V_{s30} value of 281 m/s. This level of variability is somehow in agreement with the map generated by the United States Geological Survey (USGS) V_{s30} Map Server (Figure A2.5.11) using topographic slope as a proxy, by means of the correlations derived by Wald & Allen (2007) for stable shield

regions. According to this map, Prague and Shawnee would be characterised by V_{s30} values of around 350 to 400 m/s, while the area round Sparks seems to vary along a larger range between 450 and 700 m/s. Finally, the relationships between Californian geologic units and their corresponding V_{s30} values reported by Wills & Clahan (2006) can be used as a reference. Not all the geologic formations reported by Keranen *et al.* (2013) can be represented by the aforementioned study, but those of relevance are summarized in Table A2.5.5. As can be observed, V_{s30} values can be expected to range approximately between 300 and 600 m/s, a range that is in agreement with the two previous sources.
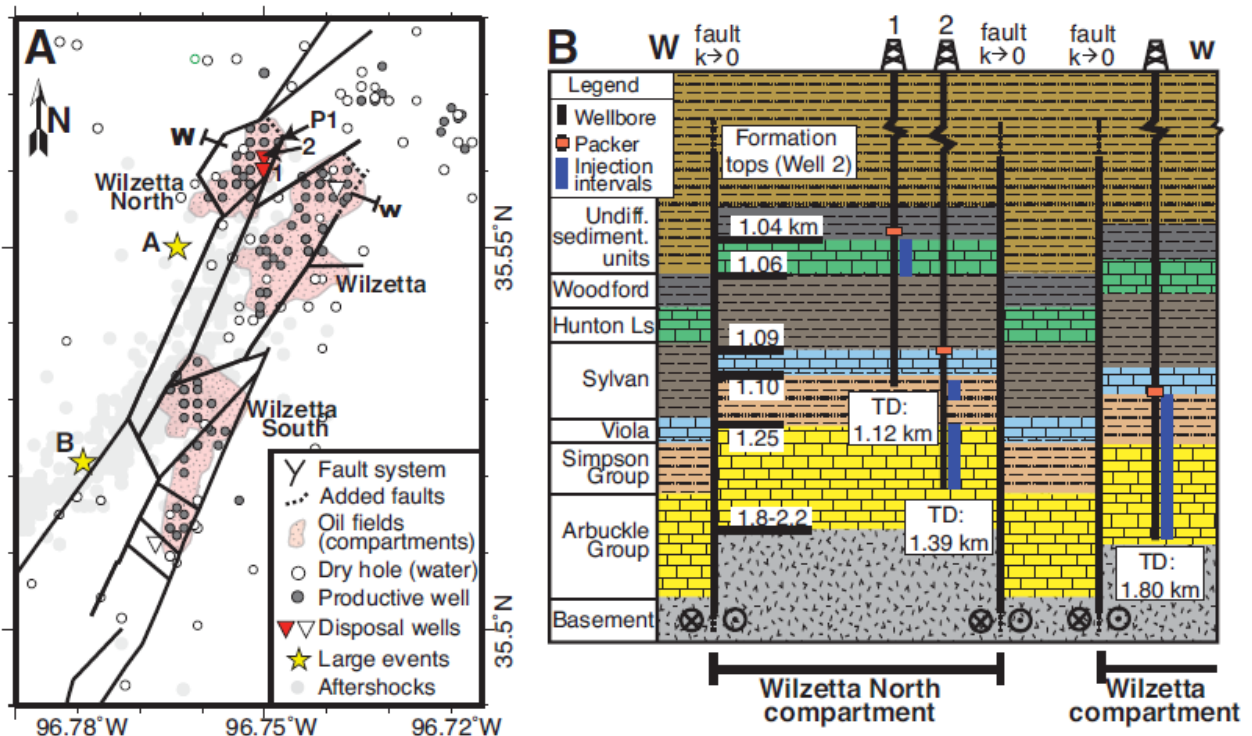
Figure A2.5.10. Schematic cross section across the Wilzetta fault system. Location of crossed section is marked over the map on the left. Starts marked as A and B are the epicentres of the **M**4.8 foreshock and the main event, respectively. The city of Prague lies to the southeast of this structure, while the city of Sparks lies to its northwest. Oil fields and wells are indicated as well. From Keranen *et al.* (2013).

Table A2.5.5. Relationship between geologic units comparable to those of the area affected by the 2011 Prague earthquake and their shear-wave velocities. From Wills & Clahan (2006).

Geologic description	Mean V_{s30}
Tertiary (mostly Miocene and Pliocene) shale and siltstone units such as the Repetto, Fernando, Puente, and Modelo Formations of the Los Angeles area	390
Tertiary (mostly Miocene, Oligocene, and Eocene) sandstone units such as the Topanga Formation in the Los Angeles area and the Butano sandstone in the San Francisco Bay area	515
Cretaceous sandstone of the Great Valley Sequence in the central Coast Ranges	566

Figure A2.5.11. Estimation of V_{s30} in the area using topographic slope as a proxy. From the USGS V_{s30} Map Server (USGS, 2015). Location of the two available site-specific studies are marked in blue.

A2.5.4 Ground motions

A2.5.4.1 Intensity observations

According to Keranen *et al*. (2013) and the USGS, an area of approximately 65 km^2 in the immediate vicinity of the epicentre experienced shaking of intensity VIII (severe shaking, extensive damage in poorly built constructions) in the Modified Mercalli scale. The USGS reports the largest damage to have occurred in the area between the cities of Shawnee and Sparks. The Modified Mercalli Intensity (MMI) at these sites and at Castle, Indianola, McLoud, Sentinel and Tupelo was VI (strong shaking, minor damage), while intensity VII (very strong shaking, moderate damage) is reported for Meeker and Prague. It was felt in at least seventeen states of the central United States, from southern Wisconsin to southern Texas, and from eastern Colorado to the Memphis, Tennessee area. A resident of Shawnee told Fox News that him and his family felt it strongly, and that it was hard to keep their balance and walk (Fox News).

The automatically calculated USGS ShakeMap (Figure A2.5.12, top) reaches the value of VIII in the MMI scale reported for the epicentral area, but its revised version (Figure A2.5.12, bottom) does not and only shows a maximum of VI-VII. It is possible that these initially higher values be due to the influence of Did You Feel It? reports of significant shaking at places like Shawnee, Prague, Meeker and Sparks, which might have led to an overestimation of the damage in the significantly under-populated epicentral area. This explanation is consistent with the peak ground acceleration ShakeMaps corresponding to each of the intensity ShakeMaps: the initial estimations for PGA reach levels of up to more

212

than 1 g, while the final estimations only get to 0.34 g instead. Though no accelerograms seem to be available for areas so close to the epicentre, values larger than 0.34 g seem unlikely for this kind of event, given the relatively limited extend of the damage in the surrounding towns.
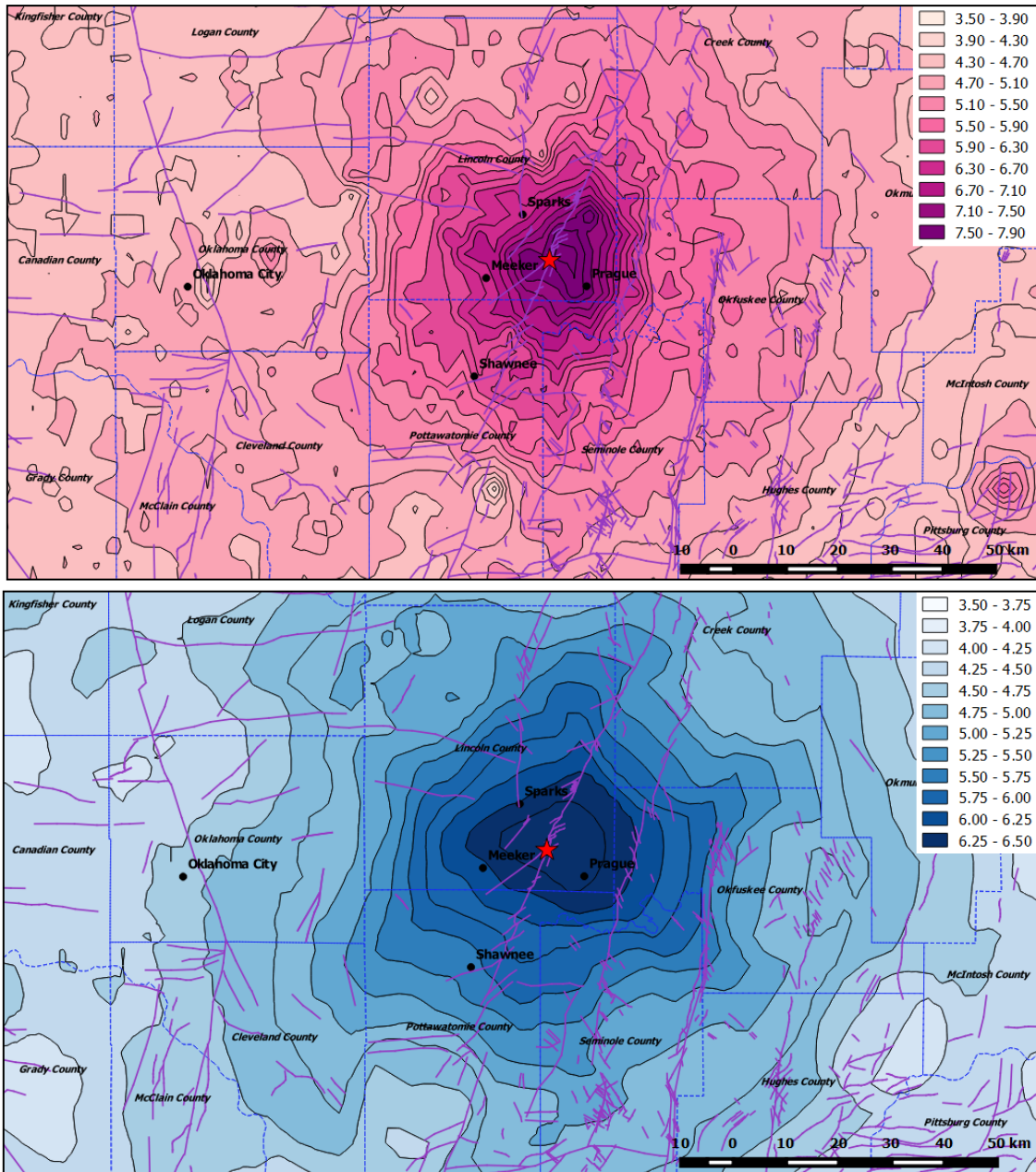
Figure A2.5.12. USGS ShakeMaps (2015) in terms of Modified Mercalli Intensities (MMI): initial automatic calculation (top), and revised calculation (bottom). The red star is the epicentre of the main shock.

A2.5.4.2 Ground motion recordings

Six three-component accelerograms are available for this event from the Center for Engineering Strong Motion Data (CESMD), one of which was recorded 68 km away from the epicentre, while the rest correspond to a range of epicentral distances between 580

and 680 km. Further, information regarding maximum horizontal peak ground accelerations is available for 37 stations from the USGS website. Table A2.5.6 summarizes the location, epicentral distance and recorded peak ground accelerations (PGA). For the case of the six accelerograms obtained from the CESMD, PGA is reported for the three components, while only the value provided by the USGS website can be reported in the remaining cases. Figure A2.5.13 shows the plots for the acceleration time-histories recorded at station 2406, located in Oklahoma City, 68 km away from the epicentre.
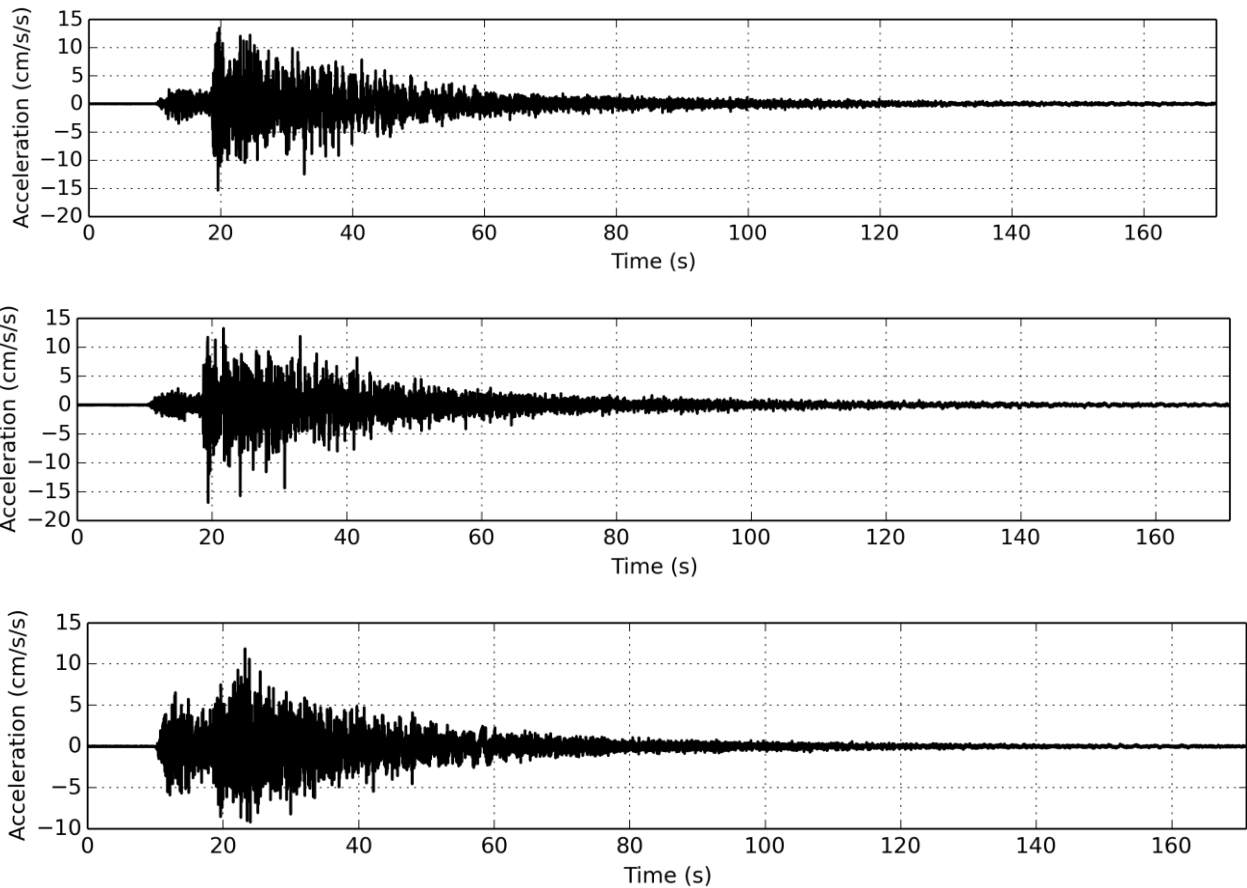
Figure A2.5.13. Horizontal (top and centre) and vertical (bottom) acceleration time-histories recorded for the main shock at station 2406, in Oklahoma City, 68 km away from the epicentre. Waveform data from the Center for Engineering Strong Motion Data (CESMD, 2015).

Table A2.5.6. Main characteristics of waveforms and recording stations for 43 records of the main shock. Epicentral distances as reported by the sources.

Station	Station Name	Latitude	Longitude	Epi. Dist. (km)	PGA (cm/s²)			Source
					Horiz. 1	Horiz. 2	Vertical	
2406	OK Oklahoma City - VAMC, Bldg 3	35.4840 ° N	97.4950 °W	68.1	15.346	16.900	11.857	(A)
2458	AR Lepanto - FS	35.6130 ° N	90.3300 °W	581.8	1.020	1.167	0.512	(A)
2495	MO Poplar Bluff - FS	36.7370 ° N	90.3980 °W	586.8	2.054	1.312	0.482	(A)
2457	Dexter- Fire Station 2	36.7960 ° N	89.9660 °W	625.9	0.954	1.638	0.683	(A)
7403	MO St. Louis - Cochran VAMC, Bldg 6	38.6430 ° N	90.2320 °W	674.1	1.222	1.447	0.468	(A)
2491	St. Louis - Visitors Ctr	38.6260 ° N	90.1910 °W	676.3	3.162	3.272	0.827	(A)

(A) Processed records downloaded from the CESMD Strong Motion Center (http://www.strongmotioncenter.org).

Table A2.5.6. Main characteristics of waveforms and recording stations for 43 records of the main shock. Epicentral distances as reported by the sources (*continued*).

Station	Station Name	Latitude	Longitude	Epi. Dist. (km)	PGA (cm/s²)			Source
					Horiz. 1	Horiz. 2	Vertical	
V35A	Meyer Ranch, Chandler, OK	35.7630 ° N	95.8380 °W	25.6	54.048	-	-	(B)
OK002	Wilshire Boulevard, Harrah, OK	35.5490 ° N	96.1970 °W	39.6	30.699	-	-	(B)
OK005	Luther Middle School, Luther, OK	35.6550 ° N	96.1910 °W	41.0	21.315	-	-	(B)
OK001	Jones High School, Jones, OK	35.5610 ° N	96.2890 °W	47.8	23.876	-	-	(B)
OK009	Oakdale Elementary School, Edmond, OK	35.5810 ° N	96.4230 °W	60.0	26.722	-	-	(B)
2406	OK:Oklahoma City;VA Medical Ctr.	35.4840 ° N	96.4950 °W	66.6	11.872	-	-	(B)
V36A	Jenks, OK	35.7860 ° N	94.9420 °W	76.3	12.961	-	-	(B)
U35A	Pawnee, OK	36.3710 ° N	95.7320 °W	91.2	11.296	-	-	(B)
TUL1	Leonard, OK	35.9100 ° N	94.7920 °W	94.1	8.972	-	-	(B)
W37B	Quinton, OK	35.1390 ° N	94.4320 °W	125.7	19.958	-	-	(B)
V37A	Hulbert, OK	35.8830 ° N	94.1410 °W	148.4	9.304	-	-	(B)
X37A	Clayton, OK	34.5890 ° N	94.3710 °W	162.1	3.345	-	-	(B)
WMOK	Wichita Mountains, Oklahoma	34.7380 ° N	97.7810 °W	203.7	4.818	-	-	(B)
HHAR	Hobbs, AR	36.2820 ° N	92.9400 °W	264.4	9.445	-	-	(B)
MIAR	Mount Ida, Arkansas	34.5450 ° N	92.5760 °W	307.4	1.418	-	-	(B)
W40A	Ferguson Farm, Pottsville, AR	35.1920 ° N	92.0690 °W	334.1	1.076	-	-	(B)
WLAR	White Oak Lake, AR	33.6880 ° N	92.1120 °W	389.4	1.120	-	-	(B)
KSU1	Kansas State University-Konza Prairie	39.1010 ° N	95.6090 °W	394.9	0.484	-	-	(B)
WHTX	Lake Whitney, Meridian, TX	31.9910 ° N	96.4560 °W	398.2	0.733	-	-	(B)
WHAR	Wooly Hollow, AR	35.2900 ° N	91.2880 °W	403.4	0.707	-	-	(B)
UALR	University of Arkansas, Little Rock	34.7750 ° N	91.3430 °W	407.6	0.512	-	-	(B)
FCAR	Ozark Folk Center, AR	35.8900 ° N	91.1240 °W	417.6	4.170	-	-	(B)
ABTX	Abilene, Hawley, TX	32.6240 ° N	98.6430 °W	418.0	2.717	-	-	(B)
MGMO	Mountain Grove, MO	37.1540 ° N	91.2690 °W	437.8	1.904	-	-	(B)
CBKS	Cedar Bluff, Kansas	38.8140 ° N	98.7370 °W	448.9	0.797	-	-	(B)
NATX	Nacogdoches, Texas	31.7600 ° N	93.6610 °W	460.7	0.814	-	-	(B)
CCAR	Cane Creek, AR	33.9170 ° N	90.7720 °W	487.4	0.621	-	-	(B)
LCAR	Lake Charles, AR	36.0690 ° N	90.1540 °W	506.2	0.746	-	-	(B)
CCM	Cathedral Cave, Missouri	38.0560 ° N	90.2450 °W	562.6	0.944	-	-	(B)
MSTX	Muleshoe, TX	33.9700 ° N	101.7720 °W	575.7	1.259	-	-	(B)
PBMO	Stasrv: unknown station	36.7790 ° N	89.4300 °W	582.0	1.432	-	-	(B)
536A	Bastrop TX	30.0760 ° N	96.0650 °W	606.4	0.433	-	-	(B)
MPH	Memphis-Engineering Bdg, Tennessee	35.1230 ° N	88.9320 °W	618.2	0.362	-	-	(B)
FVM	French Village, Missouri	37.9810 ° N	89.4270 °W	623.4	0.348	-	-	(B)
HKT	Hockley, Texas	29.9620 ° N	94.8380 °W	624.2	0.045	-	-	(B)
PVMO	Portageville, Missouri	36.4140 ° N	88.7000 °W	639.9	1.117	-	-	(B)
KSCO	Kaye Shedlock's, Cheyenne Wells, CO	39.0110 ° N	101.6270 °W	646.2	0.592	-	-	(B)

(B) Data from the USGS (http://earthquake.usgs.gov/earthquakes/eventpage/usp000jadn#impact_shakemap). Waveforms not directly available.

Figure A2.5.14 and Figure A2.5.15 show the pseudo-acceleration and displacement response spectra for the six records whose waveforms are available, separated according

to epicentral distance for clarity. All the spectra were obtained using the OpenQuake ground motion toolkit (Weatherill, 2014).
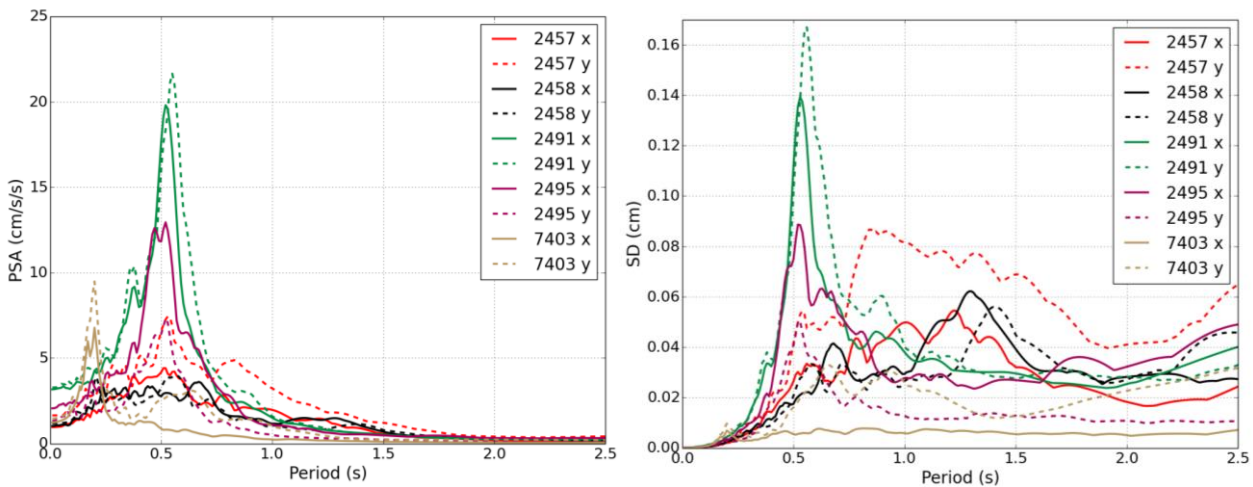
Figure A2.5.14. Pseudo-acceleration (left) and displacement (right) response spectra for each of the two horizontal components (x, y) of the five accelerograms recorded between 580 and 680 km. Waveform data from the CESMD.
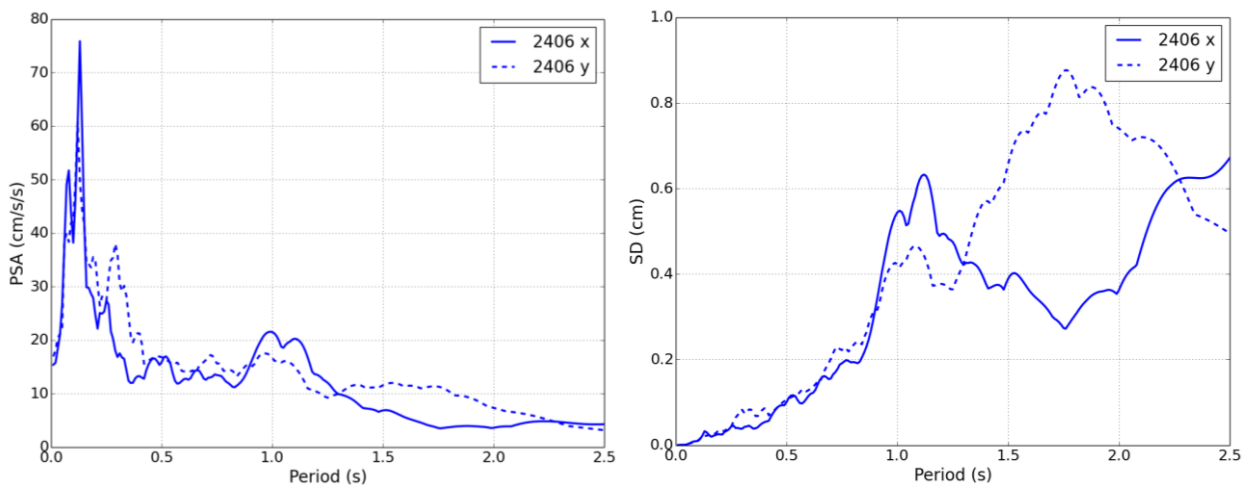
Figure A2.5.15. Pseudo-acceleration (left) and displacement (right) response spectra for each of the two horizontal components (x, y) of the accelerogram recorded at 68 km (station 2406). Waveform data from the CESMD.

A2.5.4.3 Inferred shaking levels

In order to generate a more complete characterisation of the earthquake, the USGS combines information from recording stations and reports of felt intensity. Given that the closest available peak ground acceleration information was recorded 25 km away from the epicentre, it is relevant to observe the PGA values estimated by the USGS from felt intensity. The map in Figure A2.5.16 shows the acceleration ShakeMap generated by the USGS, together with recorded PGA values (squares) and inferred values for specific locations (circles). According to theses estimations, Prague probably experienced around 26-30% g, Sparks 22% g, Meeker, 20-22% g, and Shawnee 8% g.
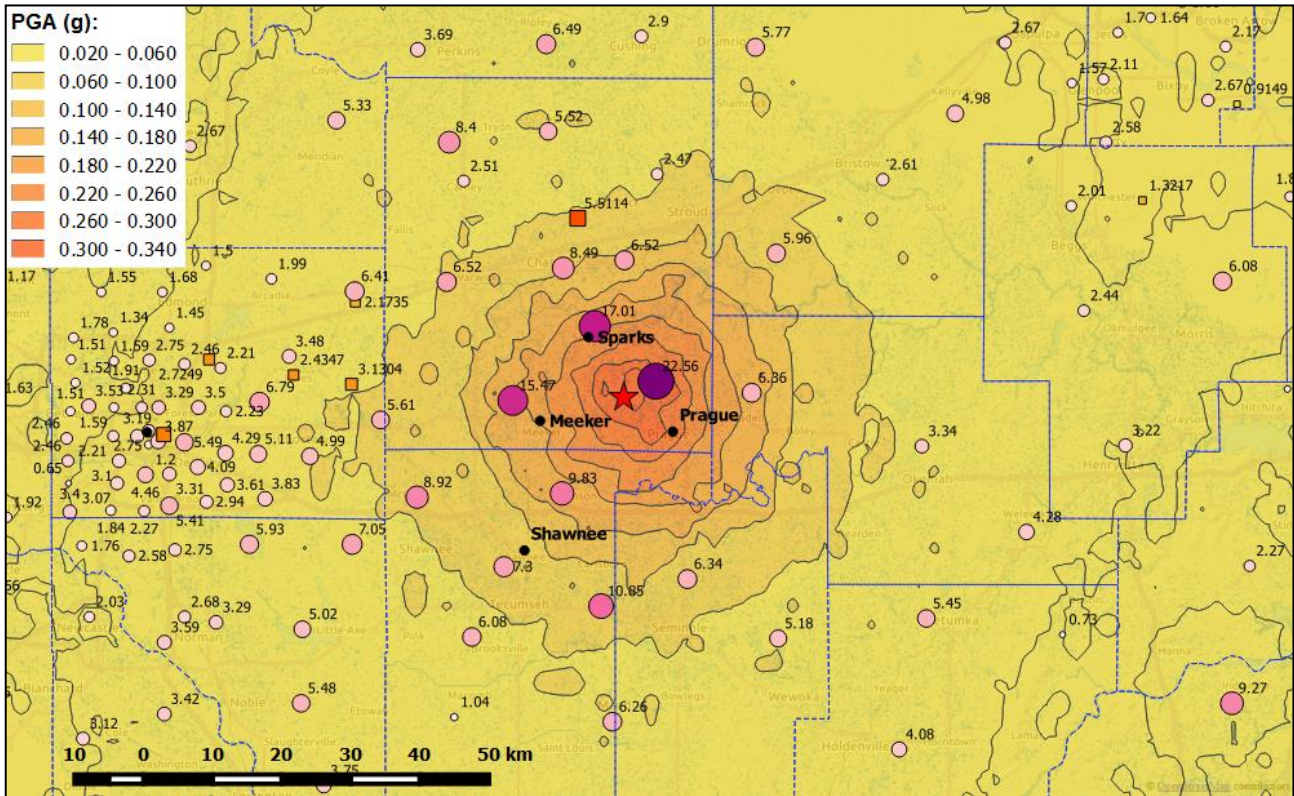
Figure A2.5.16. Maximum PGA values (% g): recorded (squares) and inferred from intensity (circles, USGS). The contour lines (g) correspond to the revised version of the PGA ShakeMap developed by the USGS.

A2.5.4.4 Duration of ground shaking

The significant duration of a waveform is defined as the time lapse between the release of the 5% and 95% of the Arias Intensity. The significant duration of the six records from the CESMD database was calculated for each horizontal component using the OpenQuake ground motion toolkit (Weatherill, 2014). Results are shown in Table A2.5.7.

Table A2.5.7. Significant duration (in seconds) of the ground motions available from the RESORCE database (Akkar *et al*., 2014).

Station	Station Name	Latitude	Longitude	Repi (km)	X component	Y component
2406	OK Oklahoma City - VAMC, Bldg 3	35.4840 ° N	97.4950 °W	68.1	39.1	41.3
2458	AR Lepanto - FS	35.6130 ° N	90.3300 °W	581.8	31.3	33.4
2495	MO Poplar Bluff - FS	36.7370 ° N	90.3980 °W	586.8	35.9	48.7
2457	Dexter- Fire Station 2	36.7960 ° N	89.9660 °W	625.9	38.1	33.5
7403	MO St. Louis - Cochran VAMC, Bldg 6	38.6430 ° N	90.2320 °W	674.1	57.0	56.8
2491	St. Louis - Visitors Ctr	38.6260 ° N	90.1910 °W	676.3	68.3	55.9

Estimations of earthquake significant durations can be obtained by means of prediction equations such as those of Bommer *et al*. (2009) and Kempton & Stewart (2006). For the former, a 1.5 km depth to the top of the rupture was used, based on the slip model of Sun & Hartzell (2014) and the fact that Keranen *et al*. (2013) reports that there was no surface

rupture for this event. A series of distances were considered, including an approximation to the distances to the cities of Sparks, Prague and Meeker, as well as the distance to recording station 2406, located in Oklahoma City, and an average 600 km distance to represent the remaining five stations for which the significant duration could be calculated. In view of the lack of information regarding the site conditions at the recording stations, a range of values of V_{s30} was also considered, including the known values for ADOK station (620 m/s) and Arcadia dam (280 m/s), and values that would approximately correspond to the cities of Prague and Shawnee (375 m/s) and some locations in Sparks (700 m/s), according to the V_{s30} map generated by the United States Geological Survey (Figure A2.5.11). Results obtained are plotted in Figure A2.5.17.

As can be observed, the significant duration calculated for Station 2406 (around 40 seconds) is double than estimated for a distance of 68 km in all soil conditions considered. It is interesting to note that the Earth Institute at Columbia University reports a statement by seismologist Katie Keranen, who said the shaking lasted "for about 20 seconds", a number much closer to the predictions than to that calculated for Station 2406 (The Earth Institute, Columbia University). A resident of the town of Broken Arrow, located approximately 100 km away from the epicentre, told the CNN that the ground shaking lasted "for a full minute". This duration is significantly larger than that predicted by the Bommer *et al.* (2009) and Kempton & Stewart (2006) equations, though not necessarily inaccurate, in view of the observations just made for Station 2406. Regarding the remaining five stations, calculated values are significantly closer to the predictions of the Bommer *et al.* (2009) equation than to those of the Kempton & Stewart (2006) equation.
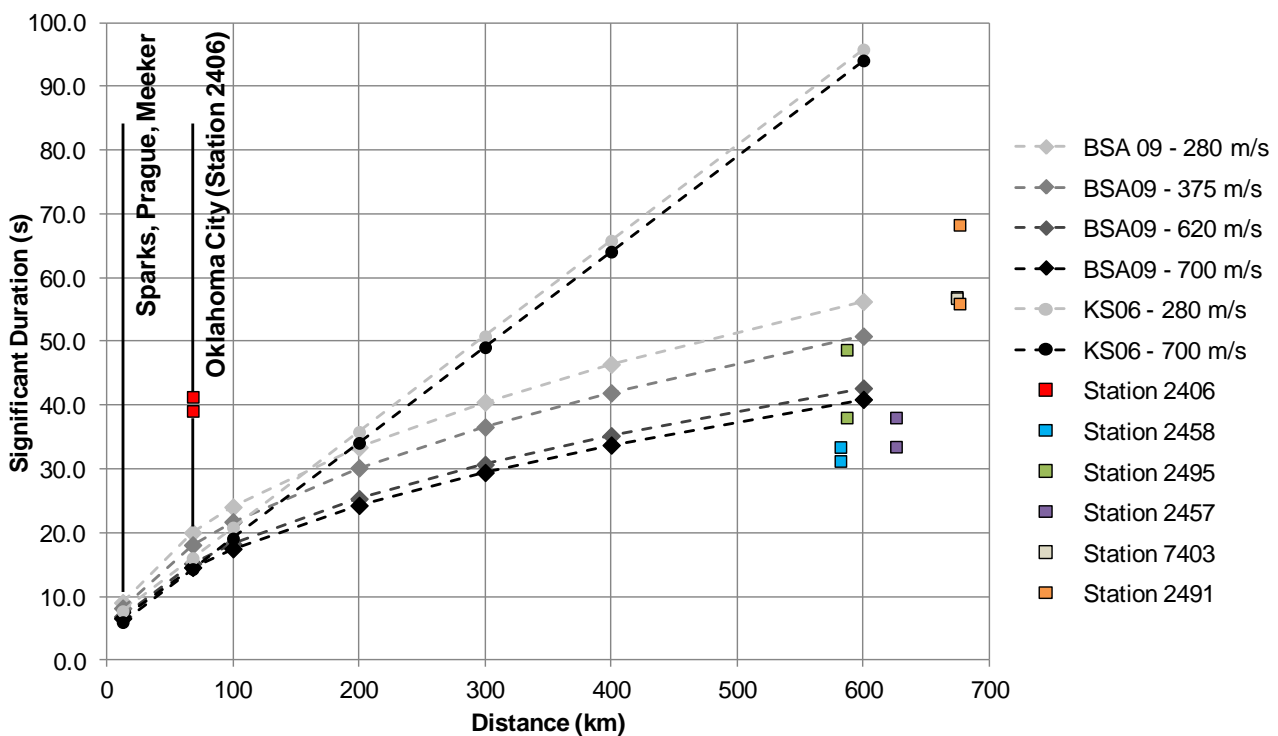
Figure A2.5.17. Estimation of the significant duration of the main shock, using prediction equations by Bommer *et al.* (2009, BSA) and Kempton & Stewart (2006, KS), and significant duration calculated for the two horizontal components of the six available accelerograms.

A2.5.5 Collateral earthquake hazards

A2.5.5.1 Surface rupture

According to Keranen *et al.* (2013), there was no surface rupture for this event. Sun & Hartzell (2014) report a peak slip at the hypocentre of 70 cm, though the slip distribution is quite heterogeneous.

A2.5.5.2 Landslides

The Christian Science Monitor (see Web references) reports a rock fall of the size of a sport-utility vehicle along a rural county road.

A2.5.5.3 Liquefaction

No liquefaction reported for this event.

A2.5.6 Exposed population

A2.5.6.1 Socio-economic setting

According to the 2014 Human Development Report (United Nations, 2014), the Human Development Index (HDI) for the United States in 2013 was 0.914, while its Inequality-adjusted HDI (IHDI) was 0.755. This located the USA in the 5th place in the world's ranking, while the Netherlands ranks 4th. The following table compares the HDI and IHDI for both countries from the last three Human Development Reports (United Nations, 2011; United Nations, 2013; United Nations, 2014). The column "Adj. HDI" provides the HDI values given in the 2014 report for previous years, adjusted for data consistency in time.

Table A2.5.8. Human Development Index and Inequality-adjusted Human Development Index for the United States and the Netherlands.

Report	Data	Unites States of America				Netherlands			
		HDI	IHDI	Rank	Adj. HDI	HDI	IHDI	Rank	Adj. HDI
2011	May 2011	0.910	0.771	4	0.911	0.910	0.846	3	0.914
2013	October 2012	0.937	0.821	3	0.914	0.921	0.857	4	0.915
2014	November 2013	0.914	0.755	5	-	0.915	0.854	4	-

Table A2.5.9 presents a comparison between the United States and the Netherlands in terms of GDP, GDP per capita and unemployment rate. Some of the man economic sectors of Oklahoma include energy production, aviation, transportation equipment, food processing, electronic and telecommunications. In 2014, the state of Oklahoma ranked third in the national natural gas marketed production and fourth in the national production of dry natural gas (dry natural gas production equals the marketed production minus the extraction loss), according to the United States Energy Information Administration (EIA).

Furthermore, it ranked fifth in the total national energy production in 2013. Overall, the trade, transportation and utilities sector accounts for 19.1% of Oklahoma's GDP, followed by the government sector and financial activities, which represent 15.5% and 14.2% of the GDP, respectively (Evans, 2015). Though agriculture, forestry, fishing and hunting represent only 1.1% of the GDP, Oklahoma ranks fifth in cattle production and fifth as well in production of wheat in the whole of the United States.

Table A2.5.9. Gross domestic product (GDP), GDP per capita and unemployment rate for the United States and the Netherlands, according to the World Economic Outlook Database 2015.

Indicator	Units	Unites States		Netherlands	
		2011	2014	2011	2014
Gross domestic product, current prices	Billions of US dollars	15,517.925	17,418.925	894.576	866.354
Gross domestic product per capita, current prices	US dollars	49,724.999	54,596.653	53,589.909	51,372.963
Unemployment rate	% of total labor force	8.942	6.150	4.980	7.395

The large economic crisis that began in 2008 had a significant impact on the United States, causing high unemployment, an increasing federal debt, and inflation. In 2011, the Gross Domestic Product (GDP) increased in 43 of the 50 states of the USA. The state of Oklahoma presented a 1.0% increase in its GDP, a value that positioned it within the third to highest quintile (Bureau of Economic Analysis, U.S. Department of Commerce). During the year 2012, the state of Oklahoma ranked 37th with respect to GDP per capita, whose value was a 15% lower than that of the USA as a whole.

A2.5.6.2 Population density and distribution

The area around the epicentre of this event is sparsely populated. Table A2.5.10 shows the population by 1st April 2010 of some of the most affected towns. According to the United States Census 2010 (U.S. Census Bureau, 2012), population density in the year 2010 around the areas of Prague, Sparks and Meeker was between 37 and 53 people/km^2, taking into consideration the area and population of the census county divisions, instead of just the urban areas. The area around the town of Shawnee is more densely populated, with an average of around 131 people/km^2. The density of housing units per area is around 16.9 to 22.5 housing units /km^2 and 54.5 housing units /km^2, in each case.

Table A2.5.10. Population of some relevant towns in the epicentral area (only urban population considered) (Quickfacts,2015).

City	Population 1st April 2010
Oklahoma	580,008
Shawnee	29,857
Sparks	169
Meeker	1,145
Prague	2,386

The USGS PAGER exposure report generated 35 hours after the earthquake estimates that approximately eight thousand people were exposed to shaking of intensity between VII and VIII in the Modified Mercalli Intensity (MMI) scale, while seventy-nine thousand and around 2.6 million were exposed to MMI VI and V, respectively (Figure A2.5.18). Note that these numbers are much larger than those of Table A2.5.10 because Table A2.5.10 reports strictly on the urban population of the enumerated towns, while the USGS PAGER exposure report considers all of the exposed population.
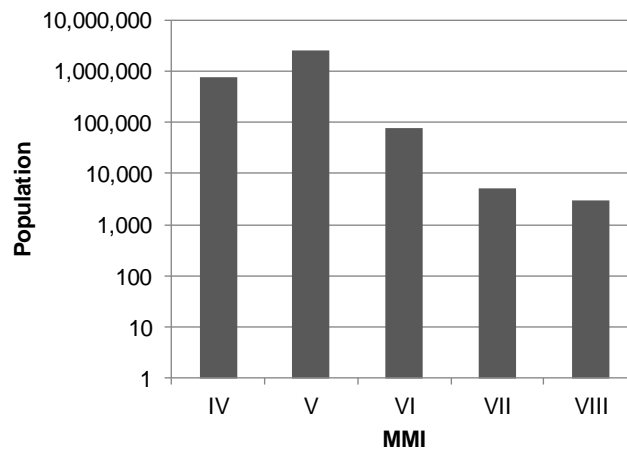
Figure A2.5.18. Estimation of total population exposed to different Modified Mercalli Intensities (MMI) 35 hours after the main shock. Data from PAGER (USGS, 2015)

A2.5.6.3 Time of day of earthquake

The main shock occurred on 5th November 2011, 22.53 local time. In general, the time of occurrence of the event did not have a significant impact over its consequences. Nevertheless, it should be noted that the occupants of a house in Sparks whose chimney collapsed and caused severe damage to the roof (Figure A2.5.23) did not suffer any injuries because they were sleeping in their bedroom and the chimney caused damage to the living room.

The time of occurrence of the **M**4.8 aftershock of 8th November 2011 02.46 UTC was slightly more relevant, for it having taken place at night prevented the occurrence of multiple injuries as a consequence of ceiling tiles falling inside classrooms at Meeker High School.

A2.5.7 Characteristics of exposed building stock

A2.5.7.1 Seismic design codes

While Cutcliffe (2000) believes that it was the 1906 San Francisco earthquake which marked the start of a real interest in earthquake engineering and seismic design in the United States, Freeman (1932) stated a quarter of a century later that "the art of

constructing earthquake-resisting buildings is still in the formative stage, that there are differences of opinions among experts and that there is much deficiency in important data". Further, he points at the 1925 Santa Barbara earthquake to have been more significant in raising awareness on the subject. It was this devastating event that prompted the first edition of the Uniform Building Code (UBC) in 1927, which contained the first written seismic design provisions for a regional level, but which did not become mandatory until 1961 (Beavers, 2002).

As recapitulated by Beavers (2002), the origin of seismic design codes and building codes in general in the USA started in a fragmented fashion, by regions or states. For example, the Uniform Building Code (UBC) just mentioned above was typically used west of the Mississippi river. The National Building Code of the Building Officials and Code Administrators (BOCA) (known as the BOCA Code) was, instead, used in the upper midwest and northeast. It was first published in 1950, including seismic design provisions. In the south, the Standard Building Code (SBC) of the Southern Building Code Congress International (SBCCI) was used. Seismic design provisions were included in the SBC in 1976, by referencing ANSI A58.1, but "were not mandatory unless local authorities required seismic design, which was rarely the case", until 1988. The 1987 edition of the BOCA Code also incorporated the provisions of ANSI A58.1, and made them mandatory.

The ANSI A58.1 standard of the American National Standards Institute (ANSI) was first published in 1945, and was the first standard to consider earthquake loads (Beavers, 2002). However, seismic hazard did not have a role in ANSI A58.1, which only had a map showing the locations of destructive earthquakes of the past until its 1972 edition, in which a seismic hazard description similar to the 1949 USCGS (United States Coast and Geodetic Survey) map was incorporated. The 1972 edition of ANSI A58.1 was also the first one to outline modern wind design provisions (Fratinardo & Schroeder, 2015; Ghosh, 2008), evolving from more basic guidelines developed in the 1950s (Huston, 2007).

The 1949 hazard map was the first one to encompass the whole of the contiguous USA, and it was based on "the premise that similar earthquakes will occur in the future where they have occurred in the past" (Beavers, 2002). For reasons that are not fully clear, this map was withdrawn in 1952, and replaced with a map that only showed the location of known past significant earthquakes. In the 1970s, the responsibility of producing hazard maps passed on to the USGS (United States Geological Survey), who published the first map developed in the form of probabilistic estimates of maximum acceleration contours on rock in 1976, and which, as highlighted by Beavers (2002), represented a significant paradigm shift. It should be noted, however, that the first edition of the ATC3-06, which in 1985 evolved into the National Earthquake Hazards Reduction Program (NEHRP) Recommended Provisions for Seismic Regulations for New Buildings and Other Structures, used a truncated version of this map in 1978, not allowing for values above 0.4g to be considered. This map was used for almost 20 years, given the inability to reach consensus on a different map that took place in between 1988 and 1994. It was finally updated by the USGS in 1997, after a four-year project called Project 97, during which large efforts were

invested in giving a voice to all the professionals and sectors involved. Since then, the USGS hazard map has been updated in 2002, 2008 and 2014.

The way in which seismic loads were considered evolved significantly from the simple use of a 7.5%-10.0% of the building's weight as a lateral load (1927 edition of the UBC), with the progressive incorporation of significant factors such as soil type and capacity, seismic zonation, natural period of vibration of the structure, and importance of the building.

In 1988, ANSI combined with ASCE to update and re-designate ANSI A58.1-1982 to ASCE 7, which is now the most significantly recognised standard by all earthquake regulations, codes, standards, procedures and guidelines for basic seismic design in the USA (Beavers, 2002). Furthermore, ASCE 7 is also the "de facto" national wind design standard (Fratinardo & Schroeder, 2015). The International Building Code (IBC), whose first edition in 2000 was based in the NEHRP Provisions, makes reference to ASCE 7 for the definition of seismic and wind loads. Regarding the latter, it should be noted that most of the state of Oklahoma is located within an area of the United States known as "tornado alley", characterised by the frequent occurrence of tornadoes due to the interaction between big masses of air with significantly different humidity contents and temperature. According to FEMA-543 (FEMA, 2007), the area around Oklahoma City has seen over 26 tornadoes of categories F3 to F5 ("severe" to "incredible") per 10,000 km2 between 1950 and 1998, one of the highest rates across all of the USA.

In 2009, the state of Oklahoma created the Oklahoma Uniform Building Code Commission (OUBCC), whose purpose was and continues to be to develop state minimum-requirement building codes. All jurisdictions in the state of Oklahoma can either adopt these minimum requirements or more restrictive ones. The OUBCC has adopted (with some modifications) the International Building Code (now in its 2015 version) and the 2009 edition of the International Residential Code (IRC), a stand-alone code addressing the requirements for residential one- and two-family homes and town houses.

The Building Code Effectiveness Grading Schedule (BCEGS), developed by the Insurance Services Office (SO), indicates that the overall level of code enforcement across the state of Colorado is relatively low when compared to the country as a whole and to states like California, in which awareness with respect to seismic risk is much greater. Figure A2.5.19 shows the distribution of communities by BCEGS class number for the United States as a whole and for the state of Oklahoma. Within this classification schedule, classes 1-3 correspond to the maximum enforcement levels, while class 10 indicates no enforcement at all. These figures agree with statements of Beavers (2002) and Cutcliffe (2000), who highlight that, due to their relative lack of seismic activity, the effort to incorporate good seismic design practises in building codes has been more challenging in the central and eastern USA, when compared to other areas of the country. Furthermore, this is also consistent with the statement by Witze (2015), who points out that the buildings in Oklahoma in particular might not be constructed to standards that consider seismic risk.
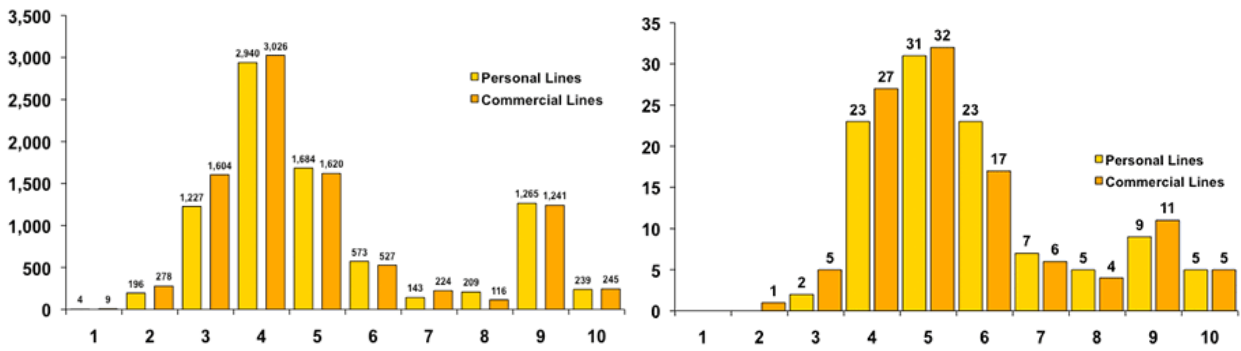
Figure A2.5.19. Distribution of communities by BCEGS class number for the whole of the United States (left) and the state of Oklahoma (right). Personal lines include 1- and 2-family dwellings. Commercial lines include all other buildings. Classes 1-3: maximum enforcement. Class 10: no enforcement (ISO Mitigation, 2015)

A2.5.7.2 Building typologies

Information regarding building typologies in the state of Oklahoma is scarce to null. For this reason, data regarding typologies at the country level were collected from the PAGER Inventory Database v2.0 (Jaiswal & Wald, 2008). Figure A2.5.20 shows that the structure of most of the buildings in the USA consists of light wood frames (61.2%), and unreinforced brick masonry (19.3%) in a smaller proportion. The remaining 19.4% is mostly made up of heavy wood frames and mobile homes (Figure A2.5.21). From available pictures of damage caused by the 2011 Prague earthquake it seems possible to infer that light wood frames and unreinforced brick masonry are probably the most likely building typologies in the affected area. Furthermore, Witze (2015) makes direct reference to the latter, when she states that "*many scientists [...] are concerned about how old brick-and-mortar structures would hold up in a large earthquake*" in Oklahoma.

W1: Wood stud-wall frame with plywood/gypsum board sheathing.
UFB3: Unreinforced brick masonry in lime mortar
Other
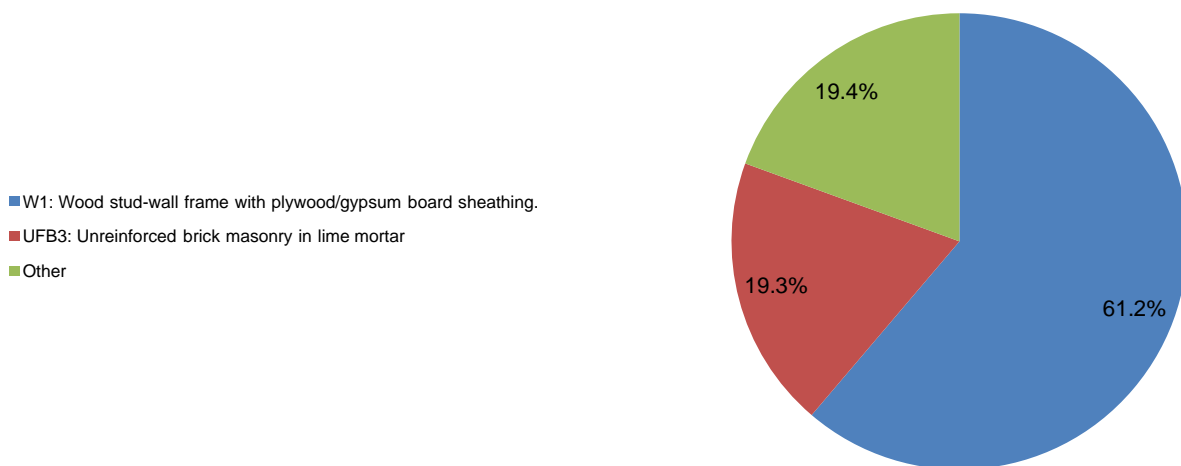
Figure A2.5.20. Proportion of buildings in the United States belonging to each typology. The subcategories within class "Other" are expanded upon in the figure below. Data from Jaiswal & Wald (2008).

- ■ W2: Wood frame, heavy members (with area > 5000 sq. ft.)
- ■ S1L: Steel moment frame low-rise
- ■ S2L: Steel braced frame low-rise
- ■ S3: Steel light frame
- ■ S4L: Steel frame with cast-in-place concrete shear walls low-rise
- ■ S5L: Steel frame with unreinforced masonry infill walls low-rise
- ■ C1L: Ductile reinforced concrete moment frame with or without infill low-rise
- ■ C2L: Reinforced concrete shear walls low-rise
- ■ C3L: Nonductile reinforced concrete frame with masonry infill walls low-rise
- ■ PC1: Precast concrete tilt-up walls
- ■ PC2L: Precast concrete frames with concrete shear walls low-rise
- ■ RM1L: Reinforced masonry bearing walls with wood or metal deck diaphragms low-rise
- ■ RM2L: Reinforced masonry bearing walls with concrete diaphragms low-rise
- ■ MH: Mobile homes

Figure A2.5.21. Breakdown of the "Other" class in the figure above. To determine the percentage that each of these sub-categories represents of the total in the USA, multiply the value in this figure by 0.194 (Jaiswal & Wald, 2008).

A2.5.7.3 Prior damage and retrofit

No details on prior damage or retrofit available.

A2.5.8 Damage observations

A2.5.8.1 Damage states

The Oklahoma Geological Survey does not know of any publicly available report on damage caused by this event that makes use of standardised damage scales (OGS, 2015, personal communication). However, from the qualitative descriptions found in online media it is possible to believe that most damage observed would correspond to Grades 2 and 3 in European Macroseismic Scale (EMS-98; Grünthal, 1998). For details regarding the latter, please refer to Chapter 2.

A2.5.8.2 Damage statistics

Information regarding damage caused by the 2011 Prague earthquake is scarce and contradictory at some points. According to the USGS, fourteen houses were "destroyed" in the Shawnee-Sparks area (Figure A2.5.12), but other reports and the images available from online media suggest damage was significantly less significant than implied by the description of the USGS. According to a situation update by the Oklahoma Department of Emergency Management with date 6th November 2011 04.30 pm local time (*i.e.* 17-18 hours after the main shock), twelve houses in the Lincoln County "sustained minor damage", most of which involved cracks in plasterboards, damage to brick façades, and toppling of chimneys. This statement is in agreement with that of Joey Wakefield, from the Lincoln County Emergency Management team, who told News 9 that most of the damage

observed was superficial, and specified "we are seeing a lot of fireplaces falling over, bricks falling, sheet rock cracked" (News 9).

Some of the instances of damage most encountered in the media are the collapse of one of the towers of Benedictine Hall at St. Gregory's University in Shawnee, a chimney which toppled and damaged the roof of a house in Sparks, a house whose façade bricks almost completely detached from the wood-frame structure, and the buckling of US Highway 62 between Meeker and Prague.

Figure A2.5.22 shows the damage to Benedictine Hall, a five-storey administrative building at St. Gregory's University, in Shawnee, built in 1915, one of whose 7-8 metre four towers collapsed (Reuters). According to Brad Collins, spokesman for the University, and as can be observed in Figure A2.5.22, the other three towers also sustained damage (Fox News).

Figure A2.5.22. Damage to one of the towers of Benedictine Hall at St. Gregory's University in Shawnee. Photos by Jim Beckel, from http://newsok.com/gallery/articleid/3621379/pictures/1555036.

The roof of a house in Sparks was damaged due to the chimney toppling over it during the main shock (Figure A2.5.23). According to News OK (see Web references), the occupants of the house were not in the room at that moment and were not injured. Numerous cracks can be observed on the walls as well.

As shown in Figure A2.5.24, the façade bricks of a house in Sparks almost completely detached from its wood-frame structure. News 9 (see Web references) reports quite extensively on this case, but does not mention any structural damage to the house.

The main shock also caused US Highway 62 to buckle in three locations between Meeker and Prague (USGS, CNN, The Earth Institute, Columbia University). According to The Christian Science Monitor (see Web references), the road was rapidly patched and reopened to traffic some hours after the earthquake.

According to the Oklahoma Department of Emergency Management, by 6th November 2011 04.30 pm local time the Oklahoma Department of Transportation had found no

damage to bridges within a 80-km radius of the epicentre, and the U.S. Army Corps of Engineers had reported no problems at dam sites within an approximate 120-km radius of the epicentre.

Figure A2.5.23. Damage to a house in Sparks. The chimney toppled over the roof. Photos by Sue Ogrocki(2015)

Figure A2.5.24. Façade bricks detached from the wood-frame structure of a house in Sparks

The total number of houses damaged due to the main shock is not clear, for the only numerical reference is the 12-14 homes mentioned earlier. Besides the cases described above, online media report numerous broken windows and mirrors, cracks to masonry and plasterboards, and collapsed chimneys. However, Joey Wakefield, from the Lincoln County Emergency Management team, reported a much larger number of homes affected with earthquake-related damage following the strongest **M**4.8 aftershock of 8th November 2011 02.46 UTC. According to Mr. Wakefield, his office had received reports of 94 homes damaged due to the "recent earthquakes". Gibson & Medley (2011) highlight the possible influence of cumulative damage on these numbers.

The **M**4.8 aftershock caused damage to ceiling tiles and metal framework in five classrooms, the library, the auditorium and the cafeteria at Meeker High School. The Meeker City Hall and two other structures were reported to have experienced some kind of damage as a consequence of this aftershock as well.

A2.5.8.3 Observed weaknesses

No reports of systematic weaknesses were found in the literature. However, the kind of damage observed and the statements by Beavers (2002) and Cutcliffe (2000) regarding the challenges faced by the efforts to incorporate good seismic design practises in the central and eastern USA suggest that the lack of seismic design of masonry structures and, perhaps, non-structural components, was the main cause of the damage observed.

It should be noted that a commonly observed failure was the toppling or complete collapse of masonry chimneys/fireplaces. Apart from the case reported above (Figure A2.5.23), other chimneys were also severely damaged, as shown in Figure A2.5.25.

Figure A2.5.25. Complete collapse of a fireplace in the interior of a house in Sparks (left, News 9), and collapse of the top of a chimney of a house.

A2.5.8.4 Damage distribution

There are no details available with respect to the distribution of damage within the towns. Joey Wakefield, from the Lincoln County Emergency Management team, highlighted that

though damage reports were being received from all over Lincoln County, the area with a higher concentration was around the epicentre, as expected (Gibson & Medley, 2011).

A2.5.9 Casualties and losses

A2.5.9.1 Numbers of dead and injured

The USGS and the Oklahoma State Department of Health report at least two injured in the Shawnee-Sparks area: one in Lincoln County (where the epicentre was located), and the other one in Pottawatomie County, to the south of the above (Figure A2.5.12). Reuters highlights that the Oklahoma Health Department reported that there were no serious injuries, that the two injuries that occurred were minor, and that neither of them required hospitalization. However, CNN reports at least one person having been taken to a hospital in Prague with minor injuries.

A2.5.9.2 Causes of casualties

According to a situation update by the Oklahoma Department of Emergency Management with date 6th November 2011 04.30 pm local time, the cause of the injury at Lincoln County was that the person involved hit his head when trying to run out of his home during the main shock, while the victim of the injury at Pottawatomie County cut her foot on broken glass after the earthquake.

A2.5.9.3 Estimates of economic losses

According to the International Business Times (see Web references), the 2011 Prague earthquake caused losses of around one million U.S. dollars. This figure is significantly smaller than the estimation from USGS PAGER (see Web references), according to which losses were expected to range between ten and one-hundred million U.S. dollars instead. This range of losses had a 33% probability, while losses smaller than one million and between one and 10 million had a 4% and a 17% probability.

The estimation from USGS PAGER is somehow in agreement with the twelve million insured losses reported by Daniell & Vervaeck (2012), which contrasts quite significantly with the statement by Bankrate.com (see Web references), according to which less than 1% of Oklahomans had proper earthquake insurance.

A2.5.10 Discussion and conclusions

This earthquake occurred on 6th November 2011, at 03.53.10 UTC (5th November 2011, 22.53.10 local time), and is the largest to have ever occurred in the history of Oklahoma. It was part of a sequence that includes a **M**4.8 foreshock around 21 hours earlier, a **M**4.0 that occurred only 10 minutes after the main shock and a **M**4.8 on 8th November 2011, which was the biggest of its more than one thousand aftershocks. Whilst tectonic earthquakes

have been known to occur in Oklahoma, including a **M**5.5 in 1952, the whole sequence is widely believed to have been induced by the activities of deep injection of wastewater that have been going on in the area for decades.

The main shock and other strong events were extensively felt and caused significant fear in the population, who were not used to ground shaking. The most affected area is that enclosed by the cities/towns of Prague, Sparks, Meeker and Shawnee, very close to the epicentre. The overall extent of the damage is somehow unclear, for some sources describe around fourteen houses being "destroyed", while some others only talk about "minor damage". Given the lack of official systematic damage and economic losses reports it is difficult to reach to a conclusion on the matter. However, descriptions and images available through online media suggest that most damage was related to the toppling and collapse of masonry chimneys, and cracks in masonry and plasterboard. It should also be noted that figures of damage seem to go significantly larger when consequences of the strongest aftershock are taken into consideration as well.

A2.5.11 References

A2.5.11.1 Bibliography

Bommer, J.J., P.J. Stafford & J.E. Alarcón (2009). Empirical equations for the prediction of the significant, bracketed, and uniform duration of earthquake ground motion. *Bulletin of the Seismological Society of America* **99**(6), 3217-3233.

Daniell, J. & A. Vervaeck (2012). *CATDAT Integrated Historical Global Catastrophe Database - Damaging Earthquakes Database 2011- The Year in Review*. Available online at http://earthquake-report.com/2012/01/09/catdat-damaging-earthquakes-database-2011-annual-review/

Darold, A.P. & A.A. Holland (2015). *Preliminary Oklahoma optimal fault orientations*. Open File Report OF4-2015, Oklahoma Geological Survey. 1 pp.

Evans, M. (2015). *Oklahoma economic indicators*. Oklahoma Employment Security Commission - Economic Research and Analysis Division. 26 pp.

FEMA (2007). *FEMA 543, Design Guide for Improving Critical Facility Safety from Flooding and High Winds: Providing Protection to People and Buildings*.

Giardini, D., G. Grünthal, K.M. Shedlock & P. Zhang (1999). The GSHAP global seismic hazard map. *Annali di Geofisica* **42**(6), 1225-1228.

Giardini, D., G. Grünthal, K.M. Shedlock & P. Zhang (2003). The GSHAP global seismic hazard map. In: Lee, W., H. Kanamori, P. Jennings & C. Kisslinger (eds.): International handbook of earthquake & engineering seismology, International Geophysics Series 81 B, Academic Press, Amsterdam, 1233-1239.

Gibson, T. & R. Medley (2011). Monday earthquake rocks Lincoln County, damages high school. News OK. Available online at http://newsok.com/article/3621379.

Grünthal, G. (ed.) (1998). *European Macroseismic Scale 1998 (EMS-98)*. Cahiers du Centre Europeen de Geodynamique et de Seismologie 15, Centre Europeen de Geodynamique et de Seismologie, Luxembourg.

Holland, A.A. (2013). Optimal Fault Orientations within Oklahoma. *Seismol. Res. Lett.* **84**, 876–890.

Holland, A.A., C.R. Toth & E.M. Baker (2013). *Probabilistic seismic hazard assessment and observed ground motions for the Arcadia, Oklahoma, Dam site*. Oklahoma Geological Survey, The University of Oklahoma, Special Publication 2013-01. Available online at http://wichita.ogs.ou.edu/documents/SP2013-01/SP2013-01_PSHA-Arcadia.pdf

Hough, S.E. & M. Page (2015). A Century of Induced Earthquakes in Oklahoma? *Bull. Seismol. Soc. Am.* **105**(6), -.

Jaiswal, K. & D.J. Wald (2008). Creating a Global Building Inventory for Earthquake Loss Assessment and Risk Management. USGS Open File Report 2008-1160. Available electronically at http://pubs.usgs.gov/of/2008/1160/.

Johnson, K.S. (2008). *Geologic history of Oklahoma*. Educational Publication 9: 2008, Oklahoma Geological Survey.

Kempton, J.J. & J.P. Stewart (2006). Prediction equations for significant duration of erthquake ground motions considering site and near-source effects. Earthquake Spectra **22**(4), 985-1013.

Keranen, K.M., H.M. Savage, G.A. Abers & E.S. Cochran (2013). Potentially induced earthquakes in Oklahoma, USA: Links between wastewater injection and the 2011 Mw 5.7 earthquake sequence. *Geology* **41**, 699–702.

Klose, C.D. & L. Seeber (2007). Shallow seismicity in stable continental regions. *Seismol. Res. Lett.* **78**, 554–562.

Llenos, A.L. & A.J. Michael (2013). Modeling Earthquake Rate Changes in Oklahoma and Arkansas: Possible Signatures of Induced Seismicity. *Bull. Seismol. Soc. Am.* **103**, 2850–2861.

Northcutt, R.A. & J.A. Campbell (1995). *Geological provinces of Oklahoma*. Open-File Report OF5-95, Oklahoma Geological Survey.

Sumy, D.F., E.S. Cochran, K.M. Keranen, M. Wei & G.A. Abers (2014). Observations of static Coulomb stress triggering of the November 2011 M 5.7 Oklahoma earthquake sequence. *J. Geophys. Res. Solid Earth* **119**, 1904–1923.

Sun, X. & S. Hartzell (2014). Finite-fault slip model of the 2011 M $_w$ 5.6 Prague, Oklahoma earthquake from regional waveforms. *Geophys. Res. Lett.* **41**, 4207–4213.

United Nations, ed. (2011). *Human Development Report 2011 - Sustainability and equity: A better future for all*. Report of the United Nations Development Programme (UNDP). Palgrave Macmillan, New York, United States.

United Nations, ed. (2013). *Human Development Report 2013 - The rise of the South: Human progress in a diverse world*. Report of the United Nations Development Programme (UNDP). Palgrave Macmillan, New York, United States.

United Nations, ed. (2014). *Human Development Report 2014 - Sustaining human progress: Reducing vulnerabilities and building resilience*. Report of the United Nations Development Programme (UNDP). Palgrave Macmillan, New York, United States.

U.S. Census Bureau (2012). *United States 2010 Census of Population and Housing - Population and Housing Unit Counts - Oklahoma*. U.S. Department of Commerce - Economics and Statistics Administration - U.S. Census Bureau, Washington D.C.

Wald, D.J. & T.I. Allen (2007). Topographic slope as a proxy for seismic site conditions and amplification. *Bull. Seismol. Soc. Am.* **97**, 1379–1395.

Weatherill, G. A. (2014). *OpenQuake ground motion toolkit - User guide.* Global Earthquake Model (GEM). Technical Report.

Wills, C.J. & K.B. Clahan (2006). Developing a map of geologically defined site-condition categories for California. *Bull. Seismol. Soc. Am.* **96**, 1483–1501.

Witze, A. (2015). Artificial quakes shake Oklahoma. *Nature* **520**, 418–419.

A2.5.11.2 Web references

Accessed on 21 December 2015:

Bankrate: http://www.bankrate.com/finance/insurance/earthquake-insurance-sturdier-home-coverage-1.aspx

Center for Engineering Strong Motion Data (CESMD): http://www.strongmotioncenter.org/

Central and Eastern United States Seismic Source Characterization for Nuclear Facilities (CEUS-SSC) Project: http://www.ceus-ssc.com/

CNN: http://edition.cnn.com/2011/11/06/us/oklahoma-earthquake

Fox News: http://www.foxnews.com/us/2011/11/06/52-magnitude-earthquake-strikes-oklahoma/

Gridded Population of the World (GPW): http://sedac.ciesin.columbia.edu/data/collection/ gpw-v3

International Business Times: http://www.ibtimes.com/oklahoma-earthquake-swarm-2015-sharp-turnaround-oklahoma-officials-confirm-link-1892086

ISO Mitigation: http://www.isomitigation.com/index.php/bcegs/facts-and-figures-about-bcegs-grades-around-the-country.

News 9: http://www.news9.com/story/15972293/earthquake-rattles-communities-in-lincoln-county

News OK: http://newsok.com/gallery/articleid/3621379/pictures/1555036

Oklahoma Department of Emergency Management, Situation Update: https://www.ok.gov/ OEM/Emergencies_&_Disasters/2011/Earthquake_Event_-_November_6,_2011/ 20111106_Earthquake_Situation_Update_.html

Oklahoma Geological Survey: http://www.ou.edu/ogs/

Oklahoma Geological Survey, Statement of March 2013: http://www.ogs.ou.edu/earthquakes/OGS_PragueStatement201303.pdf

Oklahoma Geological Survey and United States Geological Service, Joint Statement of May 2014: http://earthquake.usgs.gov/contactus/golden/newsrelease_05022014.php

Oklahoma Uniform Building Code Commission (OUBCC): https://www.ok.gov/oubcc/

Quickfacts: http://quickfacts.census.gov/.

Reuters: http://www.reuters.com/article/2011/11/07/us-quake-usa-oklahoma-idUSTRE7A50A020111107 #wfgJM5G1CcKDqvtL.97

The Christian Science Monitor: http://www.csmonitor.com/USA/Latest-News-Wires/2011/1106/Rare-Oklahoma-earthquake-damages-14-buildings

The Earth Institute, Columbia University: http://www.earth.columbia.edu/articles/view/3072

United States Bureau of Economic Analysis: http://www.bea.gov/

United States Energy Information Administration (EIA): http://www.eia.gov/state/rankings/

United States Geological Survey (USGS): http://earthquake.usgs.gov/

United States Geological Survey (USGS) Mineral Resources Online Spatial Data: http://mrdata.usgs.gov/geology/state/

United States Geological Survey (USGS) PAGER: http://earthquake.usgs.gov/earthquakes/pager/events/us/b0006klz/index.html

United States Geological Survey (USGS) Quaternary Fault and Fold Database: http://earthquake.usgs.gov/hazards/qfaults/

United States Geological Survey (USGS) V_{s30} Map Server: http://earthquake.usgs.gov/hazards/apps/vs30/

World Economic Outlook Database 2015: http://www.imf.org/external/pubs/ft/weo/2015/01/weodata/index.aspx

APPENDIX III:

Detailed information on the selected case histories can be found herein.

A3.1 April 1992 M5.4 Roermond Earthquake, The Netherlands

This earthquake occurred on 13th April 1992, at 01.20 UTC (03.20 local time), very close to the city of Roermond, in the south of the Netherlands. Apart from a smaller event that occurred 0.2 seconds earlier, no other foreshock activity had been observed. It is the strongest earthquake to have been recorded in the Netherlands and north-western Europe to date, though its size and statistical probability of occurrence are in clear agreement with the tectonics of the region. It was felt over a large area extending to places located over 500 km away from the epicentre. Significant losses were registered in the Netherlands and Germany, mainly in masonry buildings. Landslides and liquefaction phenomena were observed, though they did not contribute to the damage to the building stock. One death and 45 injured people were reported.

A3.1.1 Tectonic and seismic setting

A3.1.1.1 Tectonic setting

The 1992 Roermond earthquake originated from the rupture at the depth continuation of the Peel Boundary (or Peelrand) fault, which defines the northeast border of the Roer Valley Graben, and whose southwest limit is the Feldbiss Fault Zone (Ahorner, 1994; Camelbeeck & Meghraoui, 1996; Vanneste *et al.*, 2013). To the northwest, the Roer Valley Graben widens into the West Netherlands Basin, while to the southeast it narrows and finally disappears, extending for around 145 km overall. The Roer Valley Graben is the central graben of the Lower Rhine Graben (or Lower Rhine Embayment), a system of grabens and horsts separated by NW-SE trending normal faults (Figure A3.1.1) located in the triple frontier comprising the Netherlands, Germany, and Belgium (Vanneste *et al.*, 2013). The direction of the regional maximum compressive stress is parallel to these faults, causing the Roer Valley Graben to be subject to extensional tension forces perpendicular to its axis and to give place to thick sedimentary basins (Braunmiller *et al.*, 1994; Camelbeeck & van Eck, 1994; Ewald *et al.*, 2006). It is believed that this intraplate stress field is a consequence of the interaction between the Eurasian and the African tectonic plates (Ahorner, 1994).

Figure A3.1.2 presents a simplified cross-section through the Roer Valley Graben near the area of Roermond. During the 1992 earthquake, the western block moved down with respect to the eastern one (Ahorner, 1994).
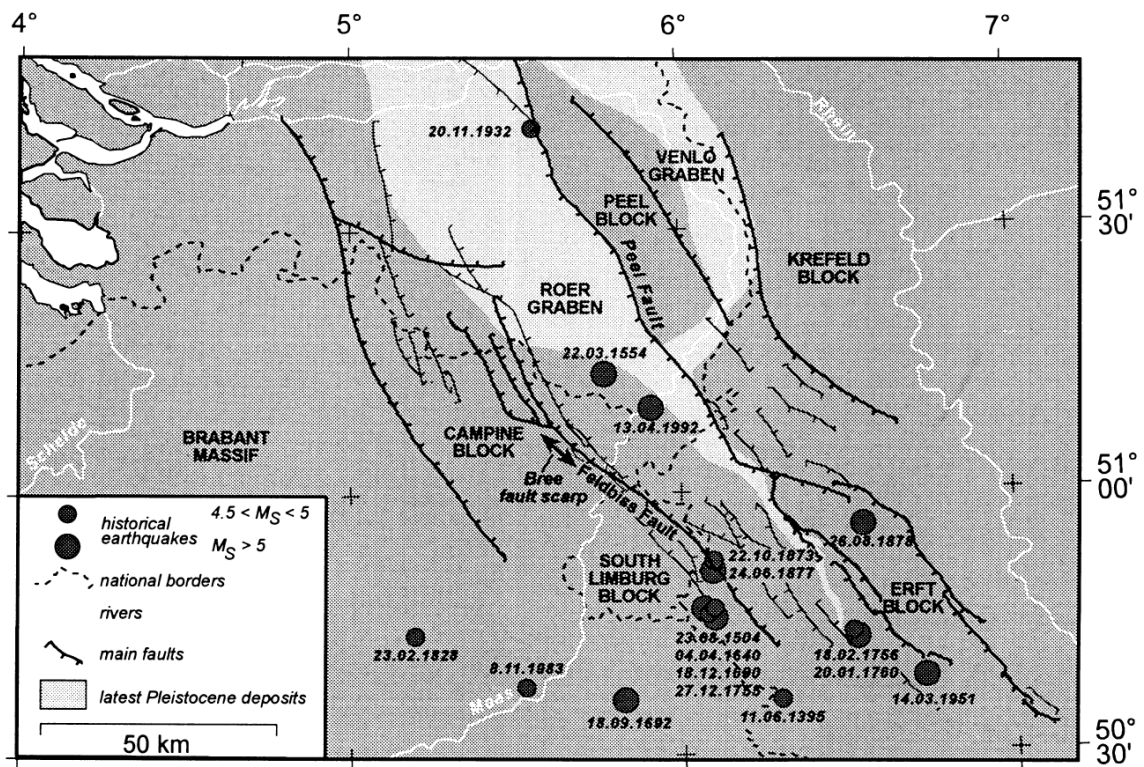
Figure A3.1.1. Quaternary faults along the Roer Valley. Main historical earthquakes with magnitude **M** larger than 4.5 shown. From Camelbeeck & Meghraoui (1998).
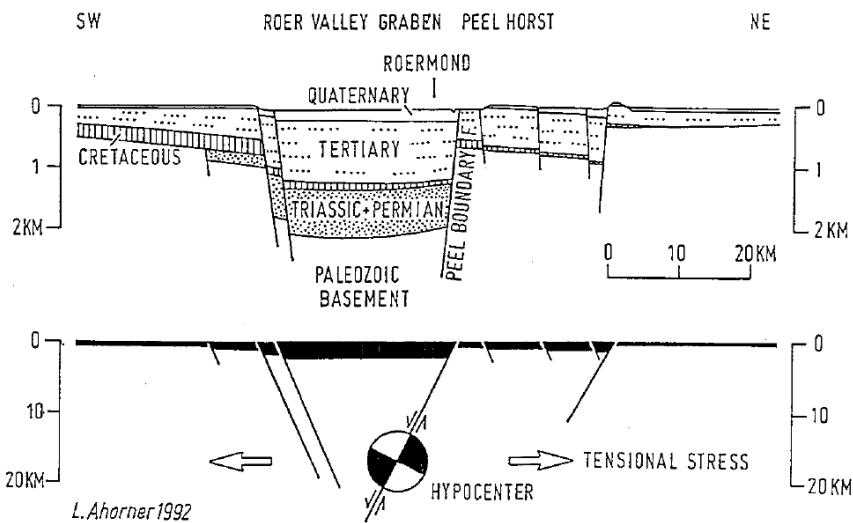
Figure A3.1.2. Simplified cross-section through the Roer Valley Graben near Roermond. From Ahorner (1994).

A3.1.1.2 Regional and local seismicity

Though being the most active tectonic region in north-western Europe and presenting a rather continuous seismic activity, the Roer Valley Graben is characterized by low deformation rates and long recurrence times for large seismic events (Camelbeeck *et al.*, 1994; Ewald *et al.*, 2006; Vanneste *et al.*, 2013).

235

According to Vanneste *et al.* (2013), and as shown in Figure A3.1.3, seven earthquakes with surface-wave magnitude Ms larger than or equal to 5.0 and epicentres within the Roer Valley Graben have been recorded since 1350, including the 1992 Roermond one. Before the latter, the last equally damaging earthquake was that of 18th February 1756 near Düren (Germany) which, with an estimated magnitude of Ms 5.7 and a maximum epicentral intensity of VIII MSK, was the most important event of a seismic series that lasted almost four years (Braunmiller *et al.*, 1994; Vanneste *et al.*, 2013). Most of the observed events are concentrated around certain areas, especially to the south, and very few events have been recorded in the northern Roer Valley Graben.
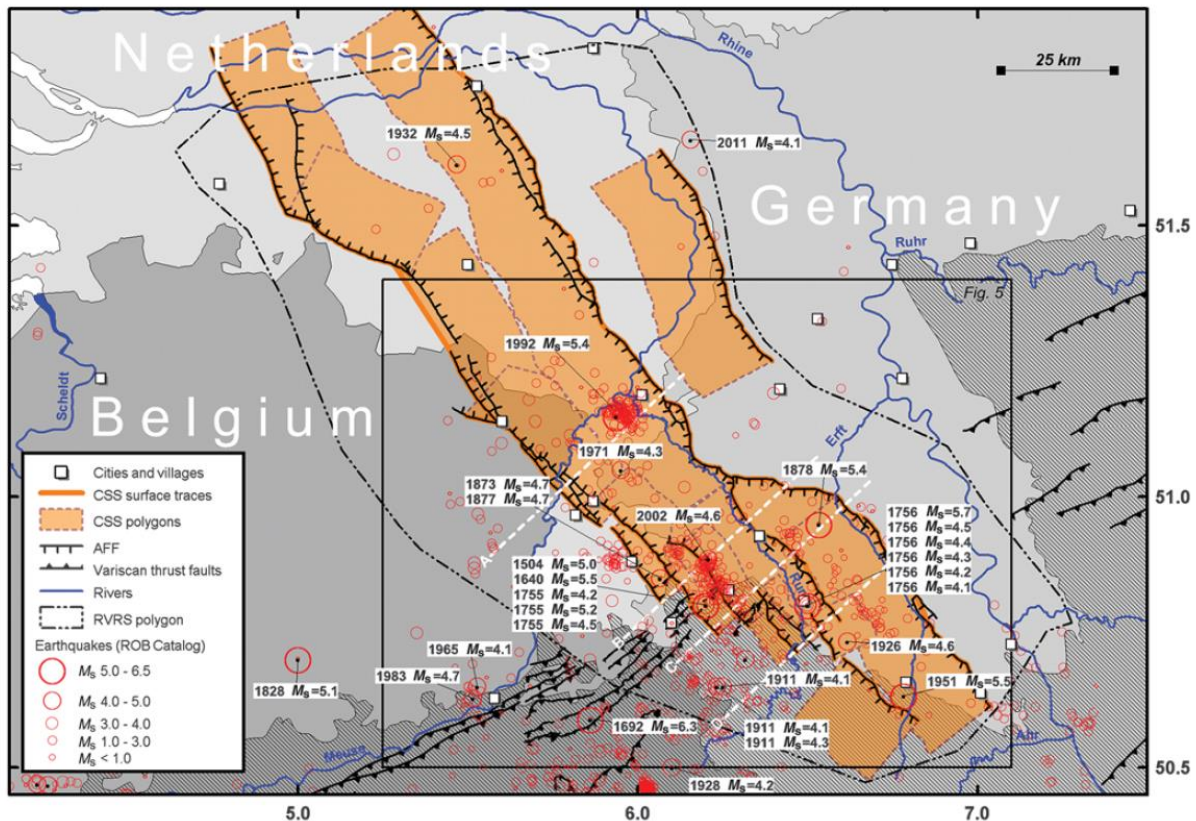
Figure A3.1.3. Historical and instrumental seismicity (1350-2011) in the Lower Rhine Graben according to the catalog of the Royal Observatory of Belgium, overlying the seismogenic sources defined by Vanneste *et al.*, (2013). From Vanneste *et al.*, (2013).

Atakan *et al.* (2000) draw attention to the importance of taking into consideration paleoseismic studies when defining recurrence periods of seismic events. While addressing the question of whether the faults along the Roer Valley Graben are capable of producing an earthquake larger than the 1992 Roermond one, Camelbeeck & Meghraoui (1996) concluded that the return period of a **M**6.5 event estimated only from historical and instrumental seismicity data (40,000 years) is significantly longer than if determined taking into consideration palaeoseismic data (two or three possible occurrences during the last 12,000 years).

A3.1.1.3 Seismic hazard

Information regarding the seismic hazard in the Roer Valley Graben can be found spread amongst national hazard maps of each of the countries involved and regional studies.

In 1984, Ahorner & Rosenhauer (1986) generated a seismic hazard map for Germany and adjacent regions in which it can be seen that the macroseismic intensity expected for Roermond and a series of cities in between the latter and Koblenz is around 7.25-7.50 in the MSK scale (MSK-81; Medvedev *et al.*, 1981) for a return period of 10,000 years (FigureA3.1.4). According to Rosenhauer & Ahorner (1994), it became clear at that time that the Lower Rhine Embayment belonged to the most active seismic zone in western and central Europe. When incorporating the 1992 Roermond earthquake to the seismic catalogue, Rosenhauer & Ahorner (1994) observed an increase in the annual probability of experiencing a VII MSK intensity at Roermond from 0.00049 to 0.00024, and concluded that the inclusion of the 1992 earthquake had moderate effects on the overall seismic hazard. At the same time, de Crook (1994) stated that the influence is, actually, negligible. However, the current seismic hazard map for Germany (Grünthal *et al.*, 1998, Figure A3.1.5) presents similar values of EMS-98 intensity expected in a much shorter return period of 475 years (10% probability of exceedance in 50 years).
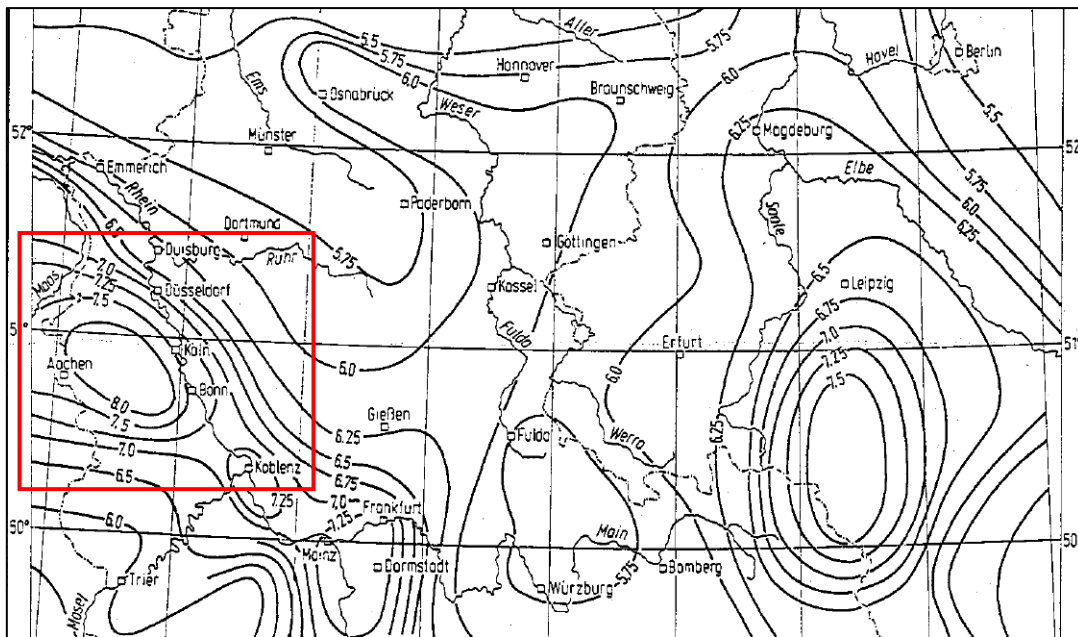
Figure A3.1.4. Extract of the hazard map of Ahorner & Rosenhauer (1986), from Rosenhauer & Ahorner (1994). Isolines correspond to MSK intensity values with a 10,000 years return period. The red rectangle frames the area most affected by the 1992 earthquake.

Figure A3.1.6 shows the outcome of a probabilistic seismic hazard analysis carried out by de Vos (2010) for the southern Netherlands. The expected PGA on rock with a 10% probability of exceedance in 50 years according to this study is around 100 cm/s^2 (0.102 g) for Roermond and most of the area affected by the 1992 earthquake. This value is in relatively good agreement with those of the official seismic hazard map for Belgium, on

which the microzonation for Eurocode 8 for this country is based (Figure A3.1.7, Leynaud *et al.*, 2000).
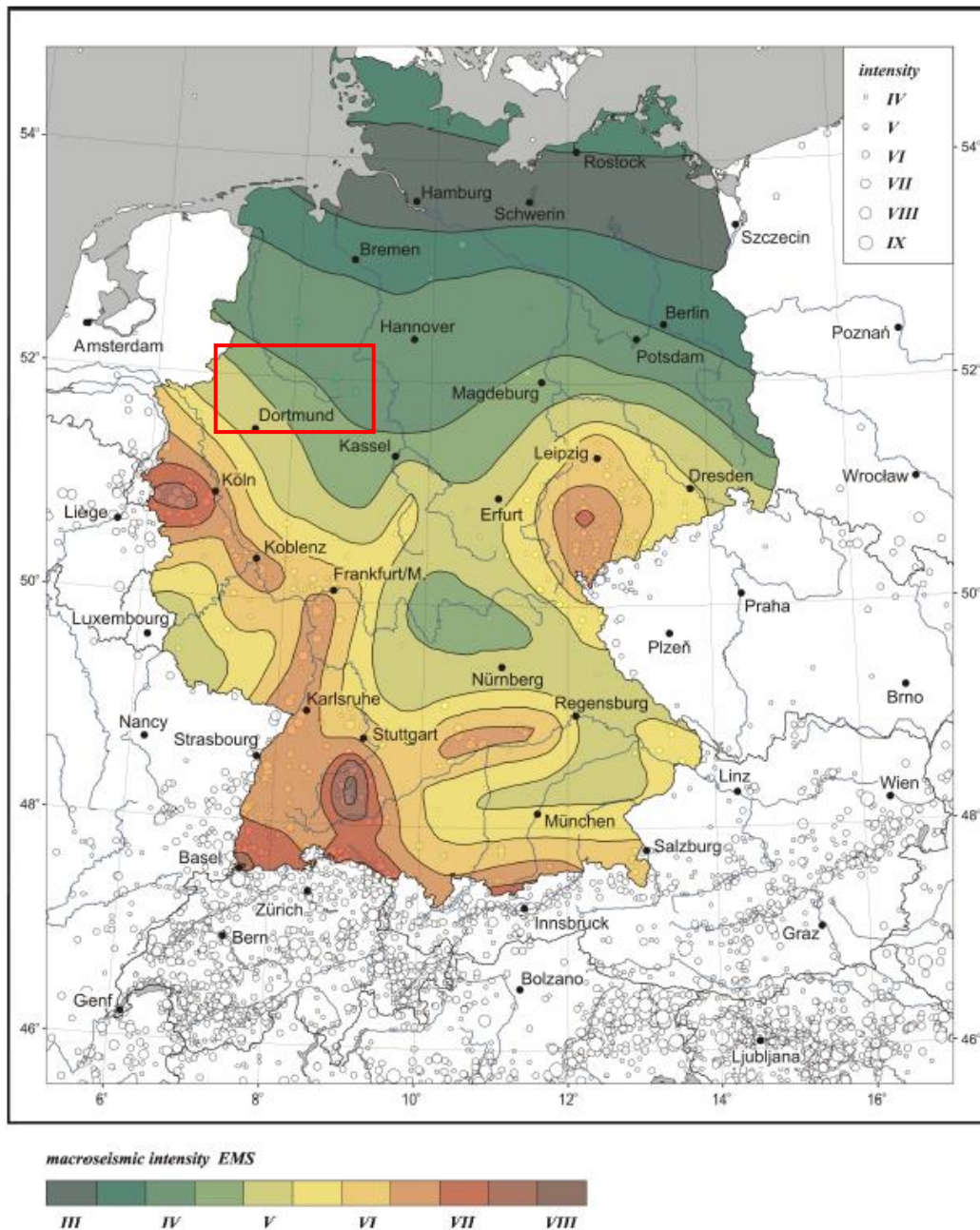
Figure A3.1.5. Seismic hazard in Germany in terms of European Macroseismic Scale (EMS-98) intensities for a 10% probability of exceedance in 50 years. From Grünthal *et al.* (1998). The red rectangle frames the area most affected by the 1992 earthquake.

Within the seismic hazard zonation map of the Netherlands (de Crook, 1996, Figure A3.1.8), it is not clear whether Roermond falls in zone C or D, being the corresponding design PGA in rock (10% probability of exceedance in 50 years) 0.05 g and 0.10 g, respectively. The Royal Netherlands Meteorological Institute (KNMI) is preparing an update of this map (Brouwer *et al.*, 2010).
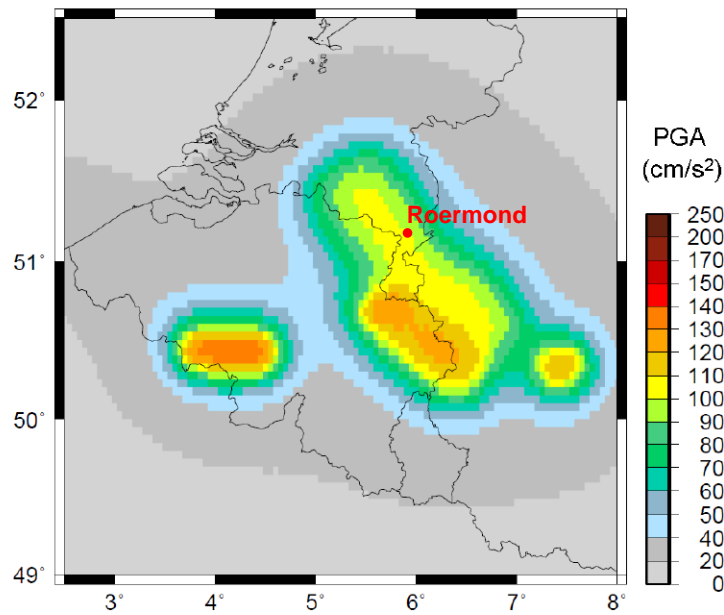
Figure A3.1.6. PGA on rock with 10% probability of exceedance in 50 years (475 years return period) for the southern Netherlands. From de Vos (2010).
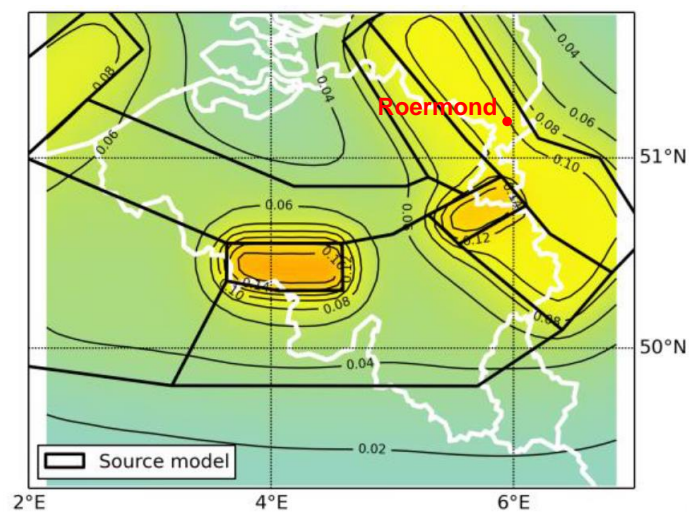
Figure A3.1.7. Official hazard map for Belgium (Leynaud *et al.*, 2000): PGA on rock with 10% probability of exceedance in 50 years (475 years return period) for Belgium. Image from Vanneste *et al.* (2014).

Figure A3.1.9 shows the 5% damped uniform hazard spectra on rock from the SHARE (Seismic Hazard Harmonization in Europe) project (Giardini *et al.*, 2013) for the closest available coordinates to some of the cities which suffered relevant damage: Roermond and Herkenbosch, in the Netherlands, and Heinsberg and Cologne, in Germany. The corresponding PGA values on rock with a 10% probability of exceedance in 50 years are, in order, 0.113 g, 0.105 g, 0.121 g, and 0.089 g. The Global Seismic Hazard Assessment Program (GSHAP) yields significantly lower values of 0.070 g, 0.071 g, 0,084 g and 0,085 g, respectively (Giardini *et al.*, 1999; Giardini *et al.*, 2003).
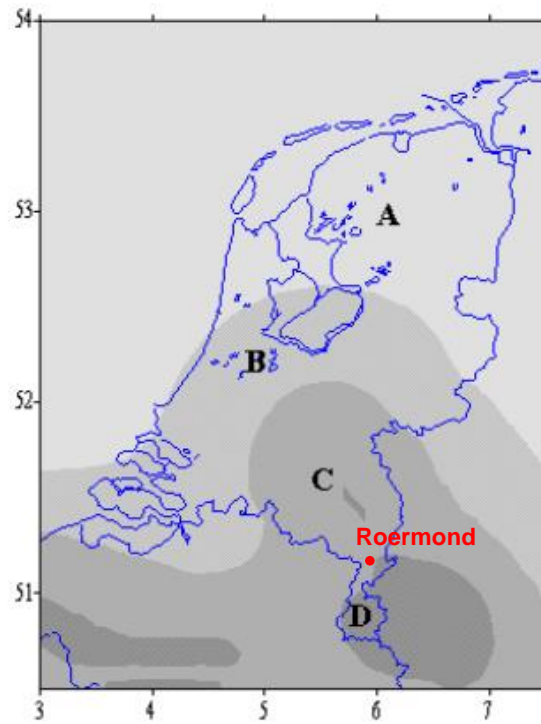
Figure A3.1.8. Hazard zonation in the Netherlands, from the work of de Crook (1996). For a 10% probability of exceedance in 50 years, the design PGA values on rock are 0.010 g (zone A), 0.022 g (zone B), 0.050 g (zone C) and 0.100 g (zone D). Image from Brouwer *et al.* (2010).
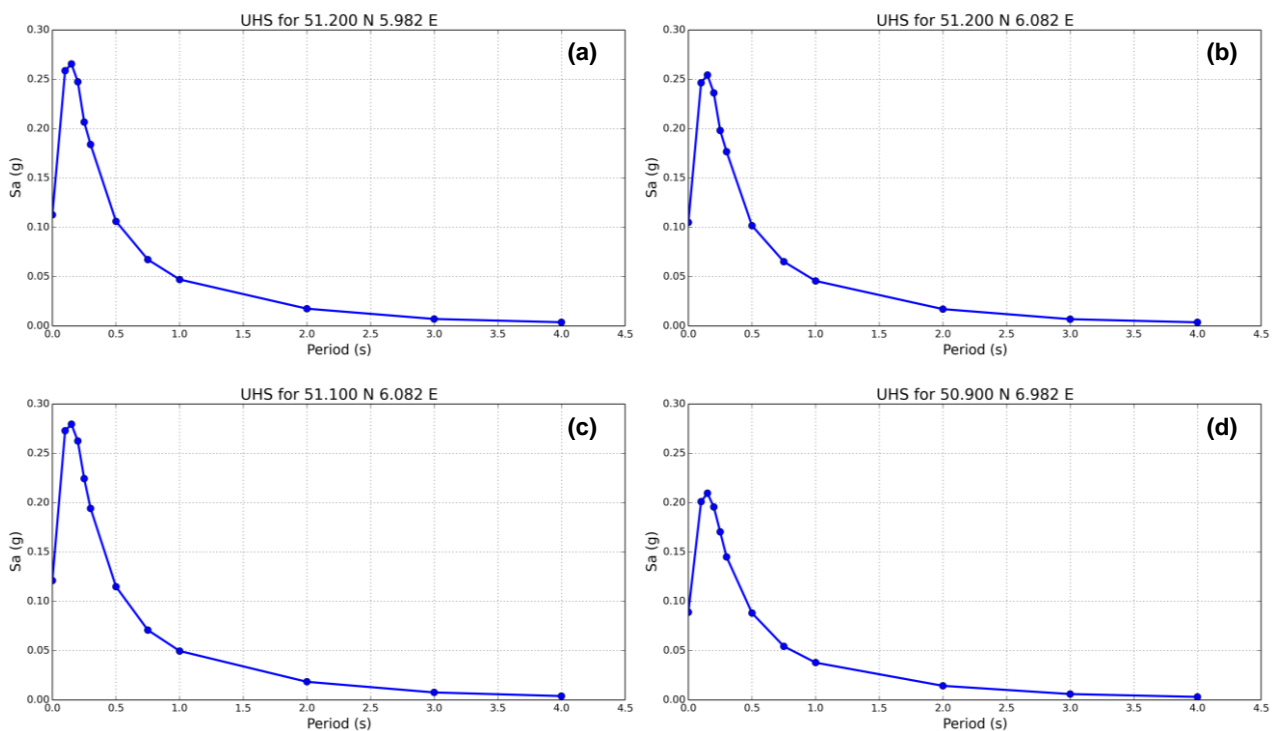
Figure A3.1.9. Uniform Hazard Spectra for the closest available coordinates to the cities of (a) Roermond (Netherlands), (b) Herkenbosch (Netherlands), (c) Heinsberg (Germany) and (d) Cologne (Germany), according to SHARE. Values correspond to PGA and spectral acceleration in rock with a 10% probability of exceedance in 50 years (mean).

The Worldwide Seismic Design Tool of the United States Geological Survey (USGS) make use of the results from GSHAP to estimate the spectral accelerations at 0.2 and 1.0 seconds with a 2% probability of exceedance in 50 years shown in Table A3.1.1. It should be noted that these values result from significant approximations and are therefore classified within the lowest reliability category of the USGS database.

Table A3.1.1. Spectral accelerations at 0.2 and 1.0 seconds with a 2% probability of exceedance in 50 years, according to GSHAP. "UFC+GSHAP" and "EUCode+GSHAP" make reference to different estimation methods

Location	Latitude	Longitude	Case	Sa(0.2) (g)	Sa(1.0) (g)
Roermond	51.200	5.982	UFC+GSHAP	0.350	0.140
			EUCode+GSHAP	0.370	0.150
Herkenbosch	51.200	6.082	UFC+GSHAP	0.360	0.140
			EUCode+GSHAP	0.370	0.150
Heinsberg	51.100	6.082	UFC+GSHAP	0.420	0.17
			EUCode+GSHAP	0.430	0.170
Cologne	50.900	6.982	UFC+GSHAP	0.430	0.170
			EUCode+GSHAP	0.450	0.180

A3.1.2. Earthquake source characteristics

A3.1.2.1 Location, depth and time

The main shock occurred on 13th April 1992, at 01.20 UTC (03.20 local time).

Several organizations and agencies report their own estimations of the epicentral coordinates and hypocentral depth. The information reported in the websites of the Royal Netherlands Meteorological Institute (KNMI), the Royal Observatory of Belgium (ROB), the National Earthquake Information Center (NEIC) of the United States Geological Service (USGS), the Global Centroid Moment Tensor Project (GCMT), the International Seismological Centre (ISC) and the GEM Earthquake Consequences Catalogue is summarized in Table A3.1.2. Cells marked as (*f) correspond to parameters that were held fixed while inversion was carried out to retrieve those that remain. Table A3.1.2 also includes the epicentral coordinates and hypocentral depths calculated by Ahorner (1994) and Camelbeeck *et al.* (1994). Note that in some cases it is not clear whether the reported coordinates correspond to the epicentre or to the centroid of the moment tensor solution.

There appears to be no agreement with respect to the hypocentral depth. Scherbaum (1994) carried out a series of stochastic simulations of the strong ground motion of this earthquake considering three different hypocentral depths (13, 21 and 25 km) and concluded that the shallow source is the most inconsistent with the observations. Meidow & Ahorner (1994) recognize the difficulties of justifying a maximum observed epicentral intensity of VII with a shallow hypocentre, but believe the reduced intensity levels are due to the influence of the sedimentary graben fill on the attenuation of the seismic waves. By adjusting the epicentral intensity to account for this influence, Meidow & Ahorner (1994)

calculate a depth of 17 km, which they find more accurate than the 26 km they would obtain without said adjustment. Braunmiller *et al.* (1994) estimated the source mechanism of the earthquake considering a hypocentral depth of 18 km and 13 km and observed an slightly better fit with the former than with the latter. It should be noted that Ahorner (1994) and Camelbeeck *et al.* (1994) provide their estimations with a variability of ± 3 km and ± 1 km, respectively, therefore overlapping in the range 16.4-17.6 km.

Table A3.1.2. Epicentral coordinates and hypocentral depths from different sources

Agency / Publication		Latitude	Longitude	Depth (km)
KNMI	Royal Netherlands Meteorological Institute	51.1620 ° N	5.9330 ° E	15.40
ROB	Royal Observatory of Belgium	51.1480 ° N	5.9370 ° E	19.00
NEIC	National Earthquake Information Center, USGS	51.1530 ° N	5.7980 ° E	21.20
GCMT	Global Centroid Moment Tensor Project	51.5600 ° N	5.6300 ° E	15.00
ISC	International Seismological Centre (inversion)	51.1391 ° N	5.7587 ° E	21.20 (*f)
GEM	GEM Earthquake Consequences Database	51.1500 ° N	5.9300 ° E	15.00
Ahorner (1994)		51.1700 ° N	5.9250 ° E	14.60
Camelbeeck *et al*. (1994)		51.1633 ° N	5.9533 ° E	17.40

(*f) fixed parameter used for inversion

The map in Figure A3.1.10 shows the different estimations of the epicentral coordinates enumerated above. Note the good agreement amongst the positions reported by KNMI, ROB, GEM, Ahorner (1994) and Camelbeeck *et al.* (1994), in contraposition with those of GCMT, ISC and NEIC.
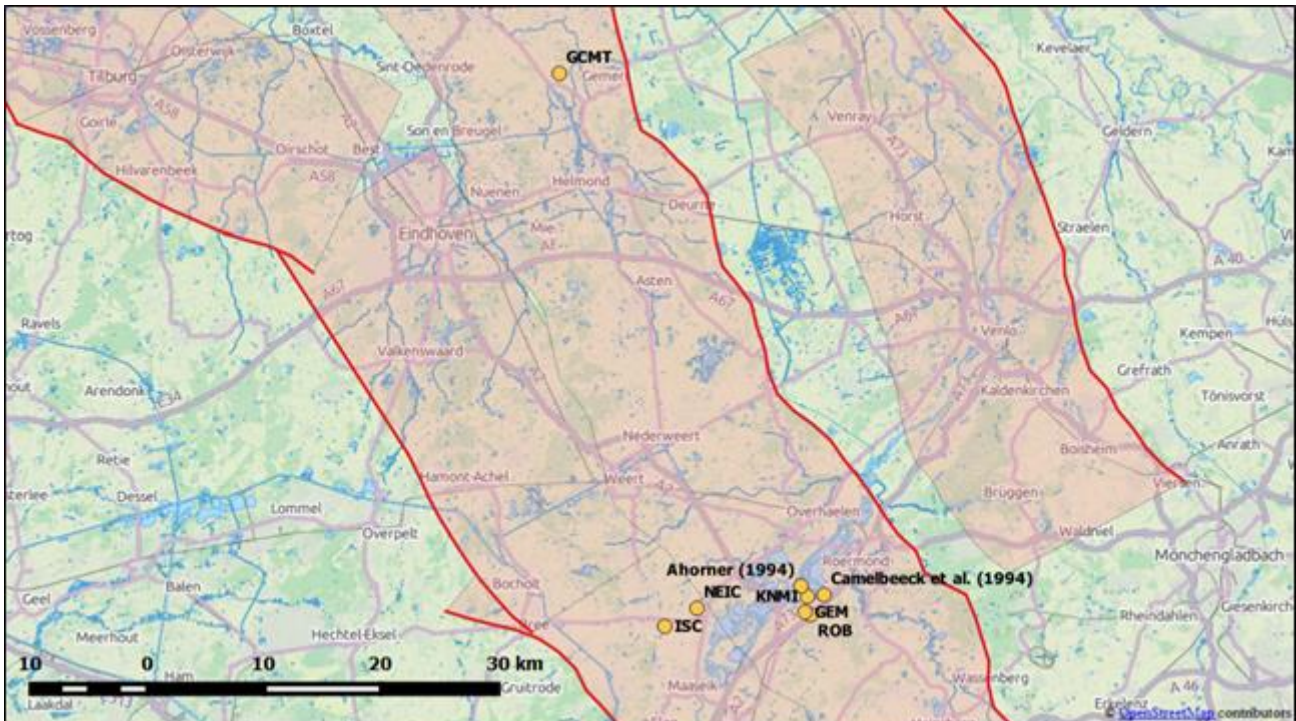
Figure A3.1.10. Estimation of epicentral coordinates (yellow circles). Red lines represent the surface traces of the main faults in the area. Red areas represent the projection of the faults planes. Faults position from SHARE (Giardini *et al.*, 2013).

A3.1.2.2 Magnitude

Estimations of magnitude made by the same agencies and studies are reported in Table A3.1.3.

Table A3.1.3. Estimations of moment magnitude (**M**), body-wave magnitude (mb), local magnitude (M_L) and surface-wave magnitude (Ms)

Agency		M	mb	ML	Ms
KNMI	Royal Netherlands Meteorological Institute	-	-	5.8	-
ROB	Royal Observatory of Belgium	5.3	-	5.8	5.4
NEIC	National Earthquake Information Center, USGS	5.4	5.5	5.9	5.2
GCMT	Global Centroid Moment Tensor Project	5.3	5.4	-	5.0
ISC	International Seismological Centre (inversion)	-	5.3	-	5.6
GEM	GEM Earthquake Consequences Database	5.4	-	-	-
Ahorner (1994)		5.3	-	5.9	-
Camelbeeck *et al.* (1994)		5.4	-	5.8	-

A3.1.2.3 Style-of-faulting

All sources agree in the focal mechanism being almost purely normal, and identify the Peel Boundary Fault as the responsible for this earthquake. However, the strike of the preferred nodal plane varies between 124° and 143° for different authors. Camelbeeck & van Eck (1994) believe this variation is due to different local velocity models being used and different focal depths being assumed. The estimation of the strike by Ahorner (1994) is 124° (Figure A3.1.11). The author recognizes that there is a slight misalignment between this value and the 145° of the near-surface trace of the Peel Boundary fault, but believes that a change of orientation is taking place at depth.
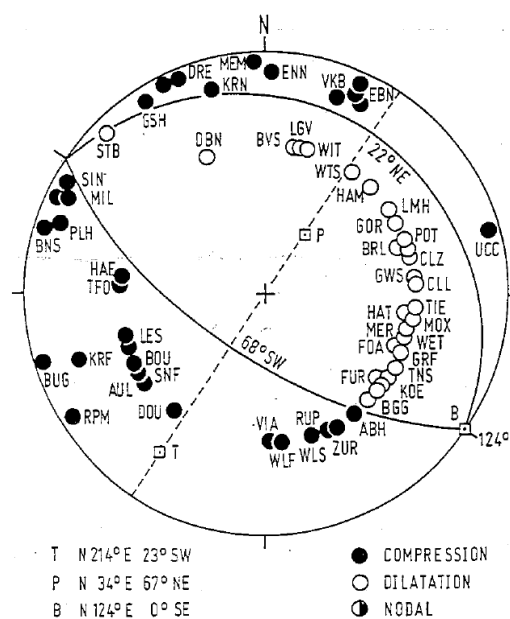
Figure A3.1.11. Fault plane solution for the main shock, from Ahorner (1994)

Table A3.1.4 summarizes the fault plane solutions calculated by different authors. In many cases, only the fault plane is reported.

Table A3.1.4. Fault plane solutions and fault planes from different sources. Fault planes marked in gray are the preferred solution in each case.

Fault Plane 1			Fault Plane 2			Source
Strike	Dip	Rake	Strike	Dip	Rake	
143	68	-87	314	22	-98	NEIC (USGS)
143	68	-87	314	22	-98	GCMT
124	68	-90	124	22	-90	Ahorner (1994)
127	70	-92	n/a	n/a	n/a	Camelbeeck et al. (1994)
139	58	263	n/a	n/a	n/a	Braunmiller et al. (1994) - 13 km depth assumed
138	58	262	n/a	n/a	n/a	Braunmiller et al. (1994) - 18 km depth assumed

A3.1.2.4 Stress drop

Ahorner (1994) reports a stress drop of 4.4 MPa. Camelbeeck et al. (1994) estimate a significantly larger value of 9.7 MPa, with a variation of ± 6.4 MPa. The 4.4 MPa of Ahorner (1994) fall within the lower bound of the latter, while the 12 MPa resported by Pelzing (1994) fall within the upper bound. Grünthal & Grosser (1992) estimate it to be between 1 and 7 MPa.

A3.1.2.5 Foreshocks and aftershocks

The main shock was preceded by a smaller event that occurred 0.2 seconds earlier. According to Ahorner (1994), its magnitude was M_L 4.8, while for Oncescu et al. (1994) it was closer to M_L 4.0, "approximately two units smaller than the main shock". Ahorner (1994) estimated their hypocentral locations being 51.168°N 5.927ºE 14.0 km deep and 51.170ºN 5.925ºE 14.6 km deep for the foreshock and main shock, respectively, and concluded that they were significantly close to each other. Apart from this one previous event, no other foreshock activity had been observed (Camelbeeck et al., 1994).

Over 200 aftershocks were detected (Oncescu et al., 1994b), but the seismic activity decreased rapidly, with 50 events being detected during the first four hours and another 50 events during the next twenty (Camelbeeck & van Eck, 1994). Twenty-nine aftershocks with M_L equal to or larger than 2.0 were detected until 17th May 1992, with four of them being larger than 3.0 (Ahorner, 1994). The plot in Figure A3.1.12 shows the number of events observed per day during the first month after the main shock. As shown in the map of Figure A3.1.13, this activity was observed both in the direct vicinity of the epicentre and within a localized area 40 km south-east of the main shock, along the axis of the Roer Valley Graben (Camelbeeck & van Eck, 1994).
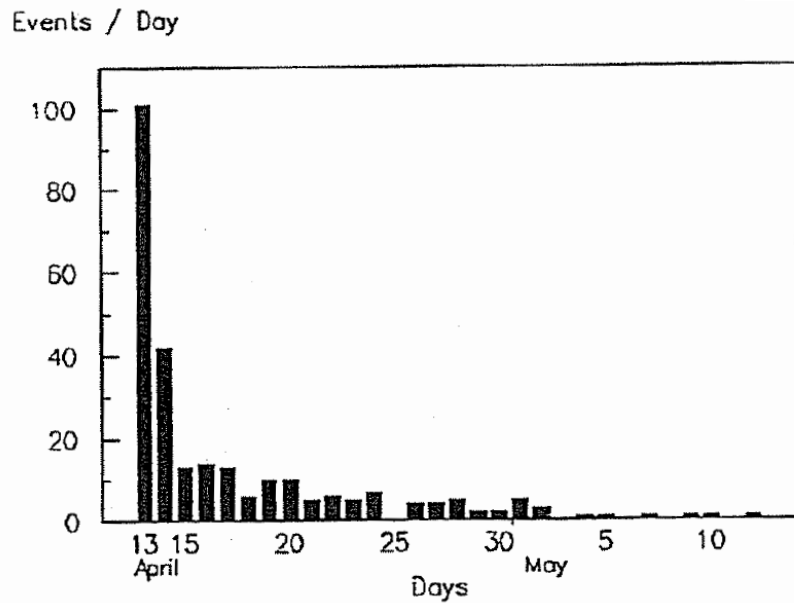
Figure A3.1.12. Number of events observed per day during the first month after the main shock. From Camelbeeck *et al*. (1994).
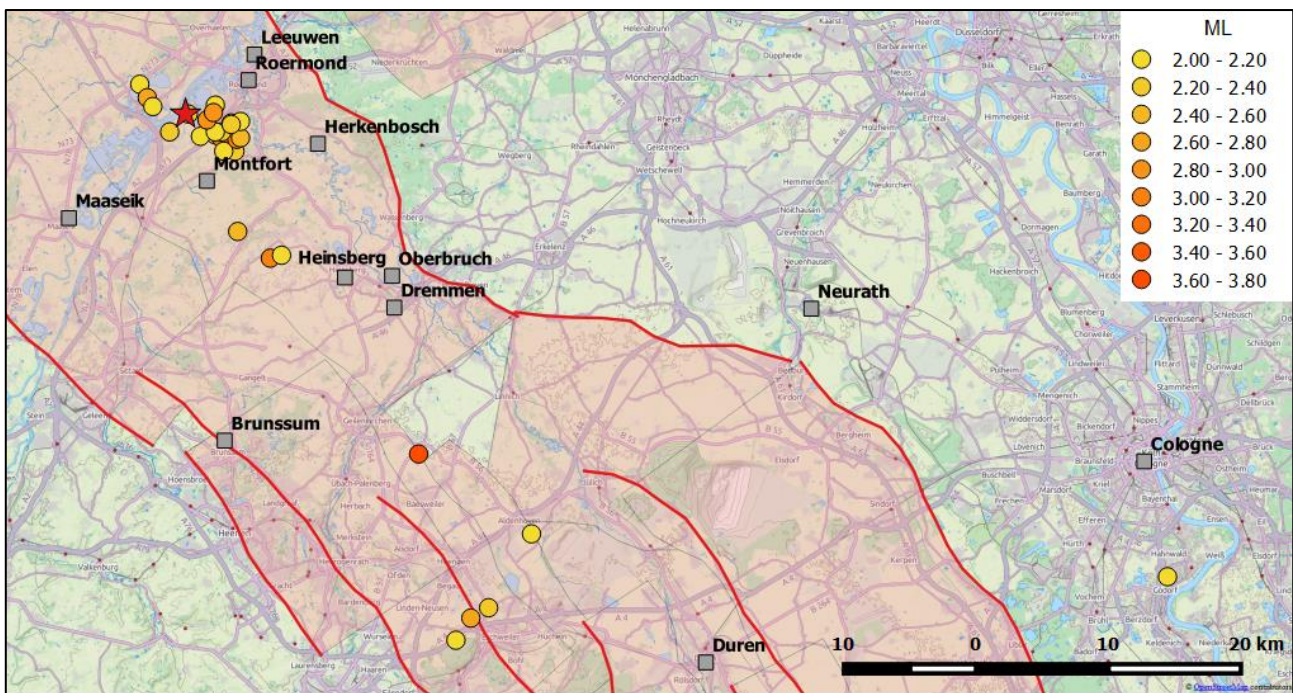
Figure A3.1.13. Location of aftershocks with ML equal to or larger than 2.0, according to Ahorner (1994). The red star marks the epicentre of the main shock, according to the same author.

A3.1.2.6 Nature of earthquake

This is a tectonic earthquake. According to Camelbeeck & van Eck (1994), although this event is one of the largest observed in western Europe in the 20th century, its size and location are in fully agreement with state-of-the-art knowledge of seismic hazard in the region.

A3.1.3 Geology and ground conditions in the affected area

A3.1.3.1 Regional geology and topography

The city of Roermond and most of the cities who suffered significant damage during the 1992 Roermond earthquake are located within the Roer Valley Graben, the central graben of the Lower Rhine Graben, located in the triple frontier comprising the Netherlands, Germany, and Belgium. The area lacks relevant topographic features, with the exception of a few isolated fault scarps (Evers, 2000).

The Lower Rhine Graben forms part of the European Cenozoic Rift System. It originated in the Early Tertiary (Oligocene) and was later filled with different layers of sediments of variable depth (Vanneste *et al.*, 2013). In the central Roer Valley Graben, the thickness of Neogene deposits can vary between 500 m and 900 m from west to east, while outside of the central area the depth of the deposits is generally less than 200 m. The largest thickness of Neogene sediments is located in the northwest sector, where they can reach to up to 1200 m. In the southeast, thicknesses progressively decrease. Younger Quaternary deposits are generally more than 100 m thick in all the graben, with the largest thickness being over 200 m in the northern areas. According to Ewald *et al.* (2006), the basin reaches a maximum overall depth of 1900 m. Figure A3.1.14 shows the general topography of the area and the depth of the sedimentary basin of the Roer Valley Graben, to the south of Roermond.
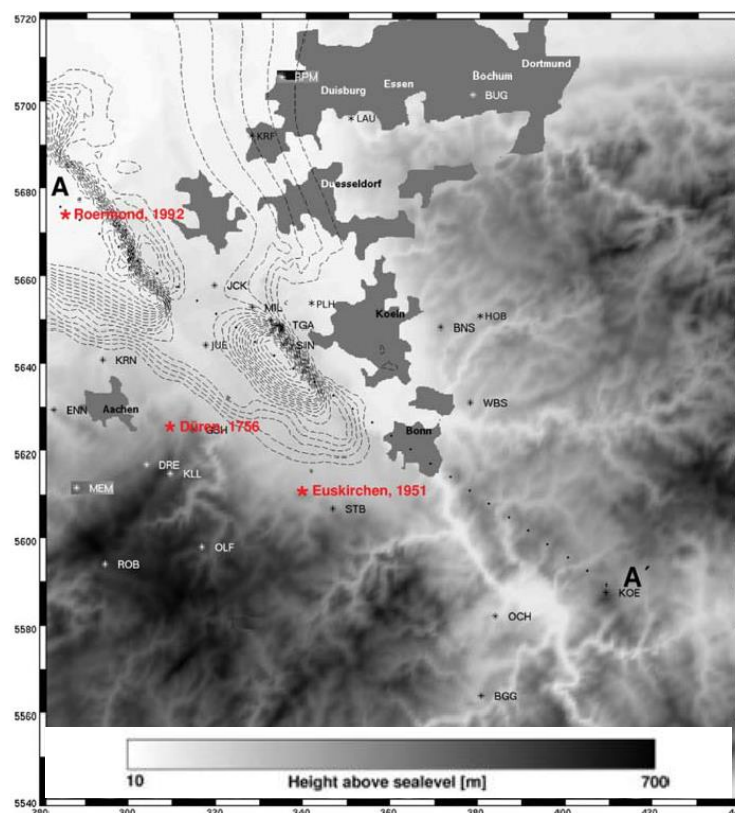
Figure A3.1.14. Topography (grey scale) and sedimentary basin depths of the Roer Valley Graben, to the south of Roermond. The sedimentary basin depth is indicated by dashed isolines in 100 m intervals. Epicentres of the 1992 Roermond earthquake and other two relevant events marked with red stars. Relevant urban settlements marked in gray (Ewald *et al.*, 2006).

A3.1.3.2 Site conditions in the affected area

As mentioned above, the Roer Valley Graben is filled with different layers of sediment. According to Schokker & Koster (2004), the oldest are an alternation of marine, coastal and fluvial materials deposited during the Tertiary and Early Quaternary. The withdrawal of the sea from the area left medium- to coarse-grained sediments from the Rhine-Meuse river depositional system. After this system disappeared in the second half of the Middle Pleistocene, the graben has been filled with local fine-grained sand, silt and peat. Figure A3.1.15 shows simplified geological cross sections of the Roer Valley Graben. Site effects are likely to be observed in this kind of geological structure (Ewald *et al.*, 2006; Horrent *et al.*, 1994).
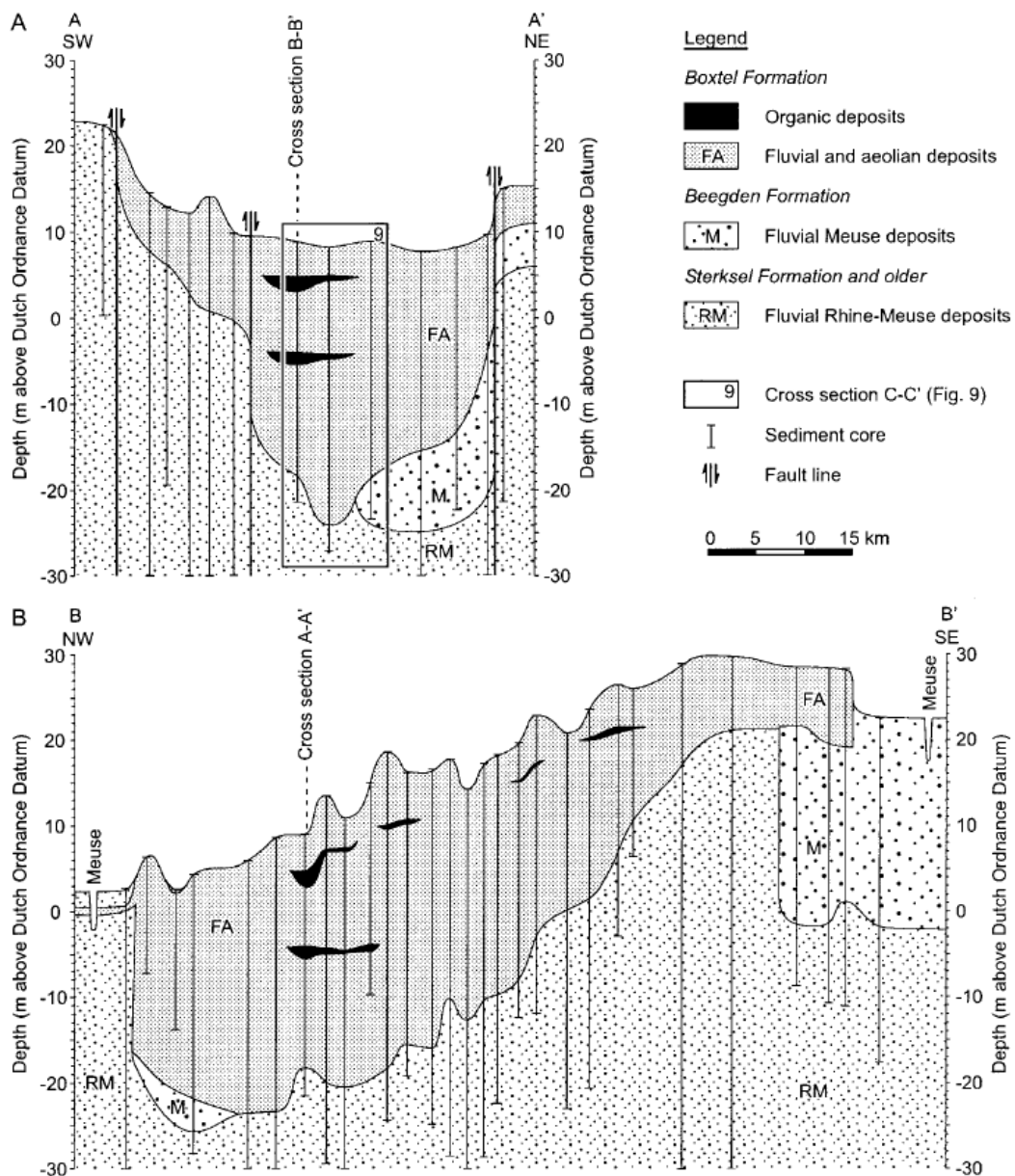
Figure A3.1.15. Simplified SW-NE (top) and NW-SE (bottom) geological cross sections showing the Middle and Upper-Pleistocene deposits in the Roer Valley Graben. FA: fluvial and aeolian fine-grained deposits. M: coarse-grained fluvial Meuse deposits. RM: medium- to coarse-grained fluvial Rhine-Meuse deposits (Schokker & Koster, 2004).

Davenport *et al.* (1994) and Nieuwenhuis (1994) report very shallow groundwater table levels in some areas of the Roer Valley Graben, of around 2.0 m and 3.5 m, respectively. The combination of loose sands and a water table at shallow depth suggests a significant likelihood of susceptibility to the occurrence of liquefaction. A study carried out by Lap (1987) concluded that the area around and to the south of Roermond presents a significant liquefaction potential, as shown in the map of Figure A3.1.16. This study also concluded that no liquefaction was to be expected in the area of Brunssum (25 km south of the epicentre) but, according to Maurenbrecher *et al.* (1994), the fact that the soil in the area has been reworked should suggest otherwise.
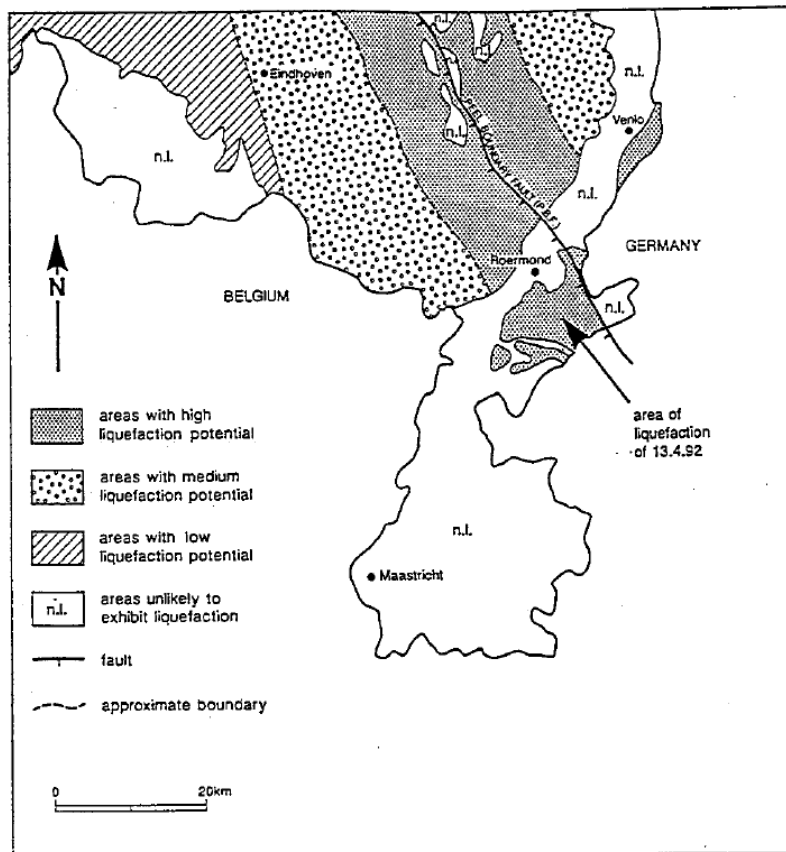
Figure A3.1.16. Susceptibility to liquefaction under a **M**6 earthquake along the Peel Boundary Fault. From Davenport *et al.* (1994), after Lap (1987).

A3.1.4 Ground motions

A3.1.4.1 Intensity observations

Haak *et al.* (1994) carried out a significant effort to gather personal and community reports of macroseismic intensity from Belgium, Czech Republic, France, Germany, the Netherlands and the United Kingdom and homogenise them with the aim of elaborating the macroseismic intensity map of the 1992 Roermond earthquake. Different countries had used different intensity scales (MSK-64; Medvedev *et al.*, 1965; EMS-92, Grünthal, 1993; MSK-81, Medvedev *et al.*, 1981), and the final map was produced in terms of MSK-81 (Medvedev *et al.*, 1981), whose equivalence with the European Macroseismic Scale EMS-

98 is, roughly, one to one (Musson *et al.*, 2010). Low intensity areas were difficult to delimitate as a consequence of most people being asleep and not woken up by the shaking. Interpolation was needed for the intensity III isoline for areas such as the North Sea and the English Channel. The maximum observed intensity was VII ("damaging"), but the authors estimated a theoretical epicentral intensity of 7.4 (between "damaging" and "heavily damaging"), based on the average isoseismal radii. According to Meidow & Ahorner (1994), this were 6 km for intensity VII ("damaging"), 42 km for VI ("slightly damaging"), 102 km for V ("strong"), 179 km for IV ("largely observed"), 322 km for III ("weak") and 440 km for II ("scarcely felt"). Figure A3.1.17 shows the resulting map, which was adopted as well by the Royal Netherlands Meteorological Institute (KNMI). The inner isoseismals show an elongation in the southeast direction.
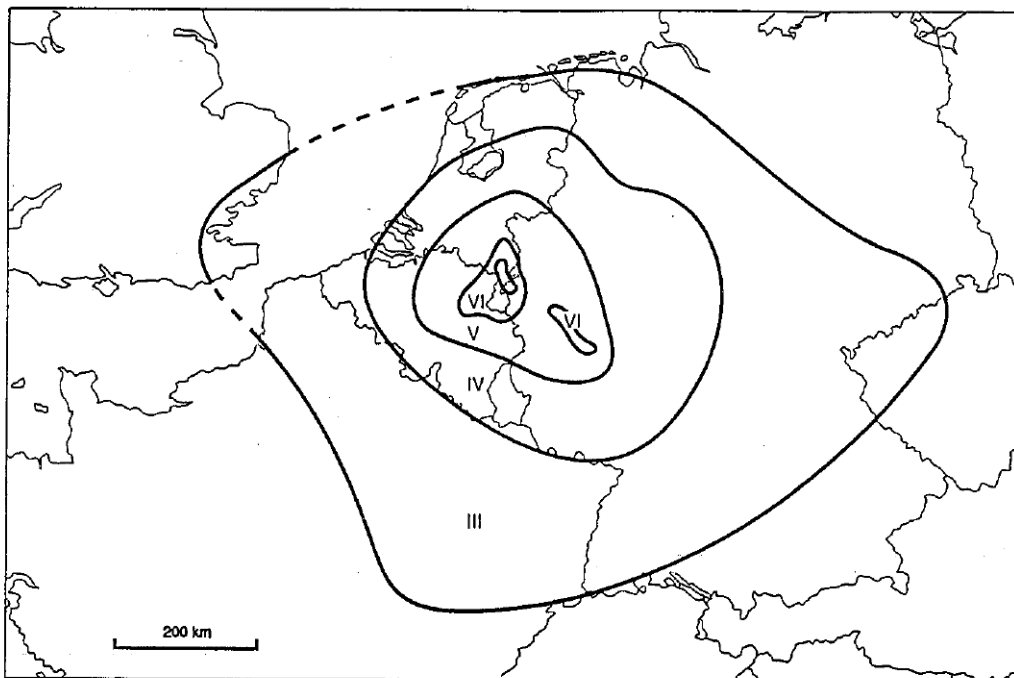
Figure A3.1.17. Isoseismal map of the 1992 Roermond earthquake. Intensities expressed in the MSK-81 scale. From Haak *et al.* (1994).

According to Meidow & Ahorner (1994), a maximum observed magnitude of VII MSK is "unusually low" when compared to other large seismic events in the Lower Rhine Embayment, and believe this is due to the absorption effect of the very thick sedimentary layers in the area, which reach a 1.5 km thickness near the epicentre.

Macroseismic reports were received from places located more than 500 km away from the epicentre, such as Berlin, Munich, Zürich and south-east England (Ahorner, 1994; Meidow & Ahorner, 1994). The event was felt over an area of approximately 600,000 km^2 (Ahorner, 1994). Islands of intensity V that can be explained by local site conditions were observed.

A3.1.4.2 Ground motion recordings

Due to the limited range of the instruments at the permanent stations around the Roermond area, most of them saturated and, consequently, there are no near-field records available for the 1992 Roermond main shock. The exact limit epicentral distance from which records are available is somewhere between 50 and 100 km, depending on the source (Camelbeeck *et al.*, 1994; Gariel *et al.*, 1994; Scherbaum, 1994). For this report, it was possible to have access to three records from the German network by means of the RESORCE European ground motion database (Akkar *et al.*, 2014). Figures A3.1.18 to 20 show plots of their corresponding acceleration time-histories.
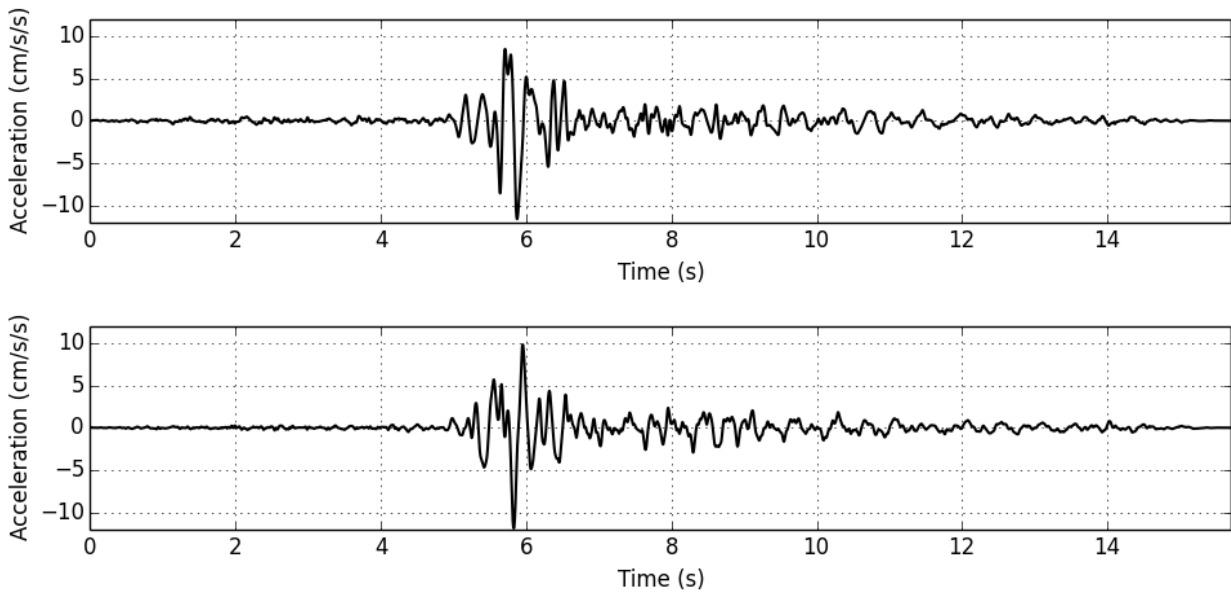
Figure A3.1.18. Horizontal acceleration time-histories recorded for the main shock at station GSH, in Germany. Waveform data from RESORCE database (Akkar *et al.*, 2014).
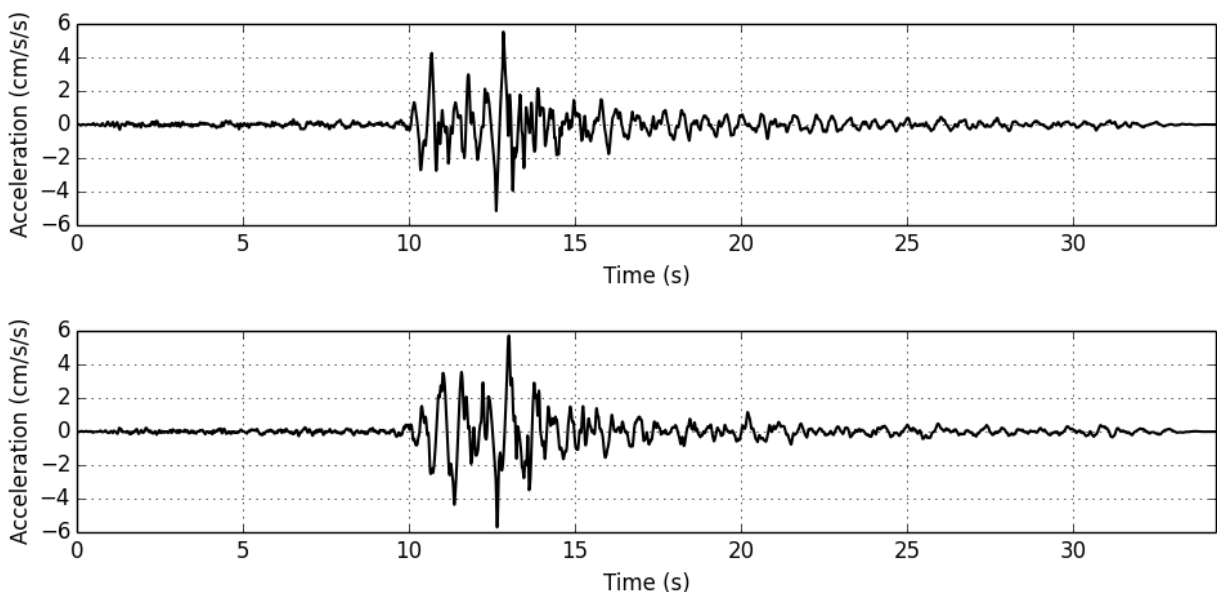
Figure A3.1.19. Horizontal acceleration time-histories recorded for the main shock at station OLF, in Germany. Waveform data from RESORCE database (Akkar *et al.*, 2014).
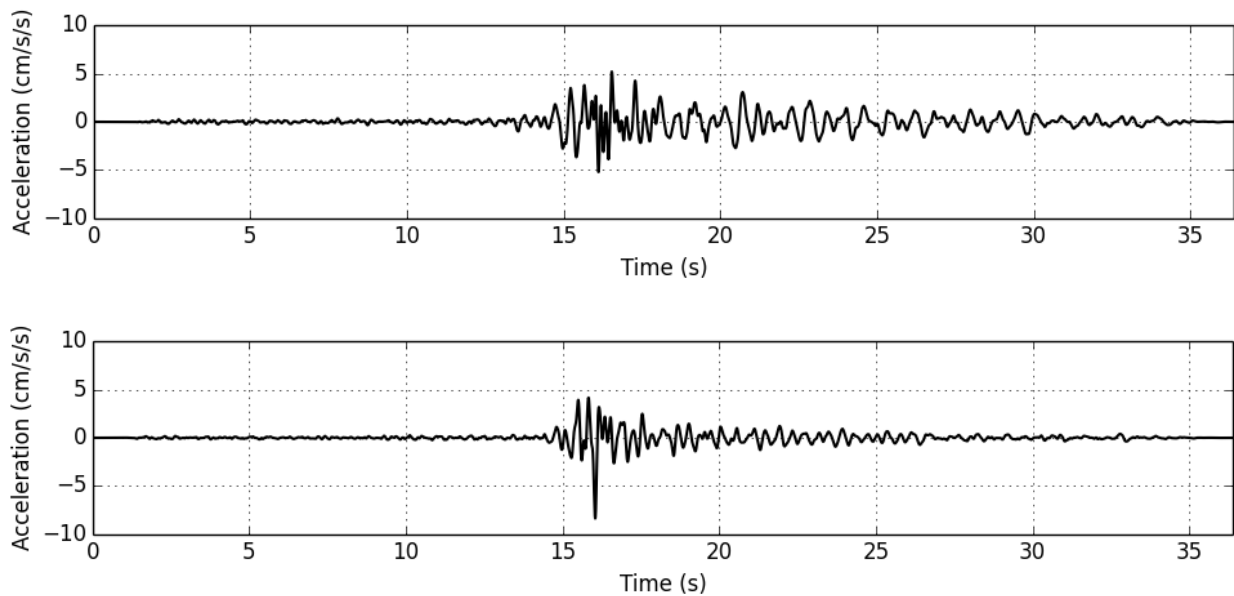
Figure A3.1.20. Horizontal acceleration time-histories recorded for the main shock at station WBS, in Germany. Waveform data from RESORCE database (Akkar *et al.*, 2014).

The pseudo-acceleration and displacement response spectra shown in Figure A3.1.21 were obtained using the OpenQuake ground motion toolkit (Weatherill, 2014). Table A3.1.5 summarizes some of the main characteristics of the waveforms and the recording stations of these 3 records and other 5 that could be collected from the literature (Helm *et al.*, 1994; Meidow & Ahorner, 1994). Indicated epicentral distances are calculated with respect to the epicentral coordinates of Ahorner (1994).
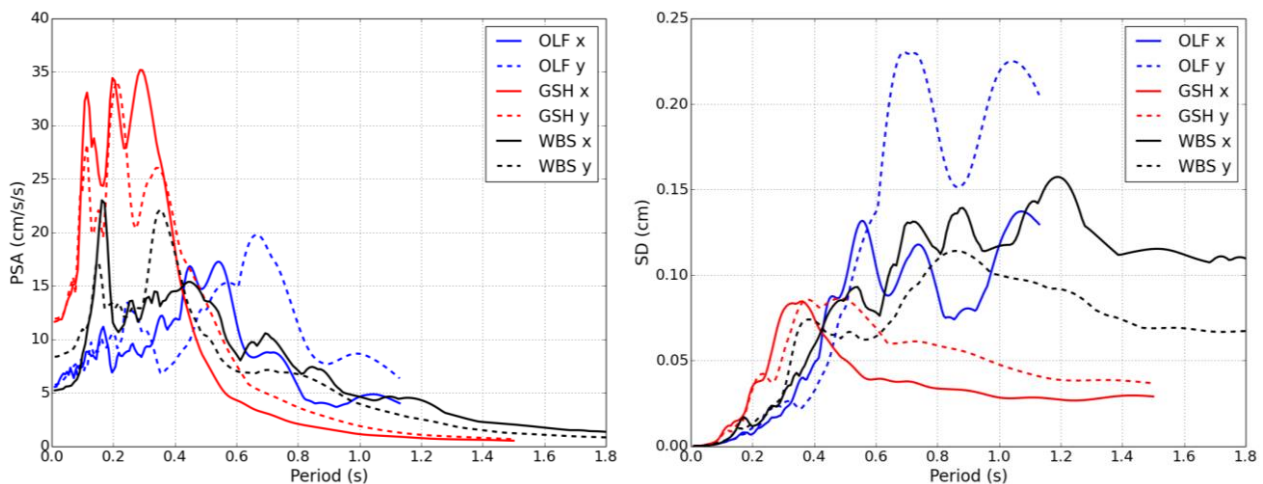
Figure A3.1.21. Pseudo-acceleration (left) and displacement (right) response spectra for each of the two horizontal components (x, y) of the three records available from the RESORCE database (Akkar *et al.*, 2014).

By comparing records from stations KKW, BGG and KOE shown in the table above, all of which correspond to, approximately, the same epicentral distance, Meidow & Ahorner (1994) highlight the influence of site amplification. Stations BGG and KOE are located on

firm rock outside the Middle Rhine Valley, while station KKW is located on soft soil within the basin. The maximum recorded peak ground acceleration is clearly larger on the latter.

Table A3.1.5. Main characteristics of waveforms and recording stations for 8 records of the main shock. Sources: RESORCE database (R, Akkar *et al.*, 2014), Meidow & Ahorner (MA, 1994), and Helm *et al.* (Hea, 1994). Note: the exact location of station KKW (Mülhem-Kärlich) is not available, and the coordinates corresponding to the Mülhem-Kärlich power station are reported.

Station	Country	Latitude	Longitude	Repi (km)	Soil	PGA X (cm/s²)	PGA Y (cm/s²)	Source
GSH	Germany	50.737	6.377	58.0	B, V_{s30}= 660 m/s	11.603	11.874	R
OLF	Germany	50.496	6.421	83.0	B, V_{s30}= 660 m/s	5.524	5.715	R
WBS	Germany	50.808	7.286	103.0	B, V_{s30}= 660 m/s	5.202	8.348	R
KKW	Germany	50.408	7.490	138.9	soft	44.000	-	MA
BGG	Germany	50.206	7.337	146.2	rock	22.000	-	MA
KOE	Germany	50.425	7.732	151.6	rock	8.000	-	MA
Surbourg	France	48.915	7.852	286.0	loess, quaternary	9.100	10.000	Hea
Hoffen	France	48.942	7.964	287.3	loess, quaternary	3.400	3.800	Hea

On a similar line, Braunmiller *et al.* (1994) comment that stations located within the sedimentary basin of northern Germany show large low-frequency oscillating signals, and, in a more general observation, that attenuation of high frequency signals differs significantly for different source-receiver paths. Furthermore, they observe a relatively high complexity in the body-wave part of the seismograms at distances between 100 and 1,500 km, which they claim is due to the different heterogeneous crustal structures along the travel paths.

A3.1.4.3 Inferred shaking levels

In view of the lack of records in the epicentral area for the main shock, Gariel *et al.* (1994) used the accelerograms of the aftershocks recorded by the temporary stations deployed after the main event to generate synthetic horizontal accelerograms of the former by means of the empirical Green's function method. Table A3.1.6 presents the peak ground acceleration values calculated by the authors for each of the six stations they studied. A particularly high value of 0.35 g for station HLN strikes the eye as surprising. The authors say that, while it is possible that the assumption of linearity adopted when using the empirical Green's function method may be responsible for an unrealistically high result, this value is somehow supported by the fact that the town of Haelen, where the station is located, suffered from significant damage. Furthermore, one of the turbines of the local power plant moved during the main shock. Nevertheless, it is possible that the actual acceleration values may have been slightly smaller, especially because of possible non-linear effects caused by the alluvial soils in the area. Peak ground accelerations calculated for the other stations range from 0.06 to 0.18 g, which the authors claim is in agreement with what could be expected for this event. Figure A3.1.22, in which observed and

computed acceleration values are compared with those predicted by the Boore & Joyner (1982) attenuation model, supports this statement.

Table A3.1.6. Peak ground acceleration values calculated by Gariel *et al.* (1994) using the empirical Green's function method. $Repi_1$ is the epicentral distance calculated with respect to the epicentral coordinates defined by Ahorner (1994), while $Repi_2$ is the value provided by Gariel *et al.* (1994).

Station	Country	Latitude	Longitude	$Repi_1$ (km)	$Repi_2$ (km)	PGA X (cm/s²)	PGA Y (cm/s²)
ODL	Netherlands	51.146	6.000	5.9	5.0	150.0	175.0
HLN	Netherlands	51.236	5.957	7.7	6.2	174.0	350.0
THN	Netherlands	51.160	5.845	5.7	8.6	60.0	72.0
KIN	Belgium	51.146	5.776	10.7	13.4	110.0	130.0
STP	Netherlands	51.194	5.728	14.0	14.8	-	120.0
MAS	Belgium	51.097	5.712	16.9	15.1	80.0	57.0
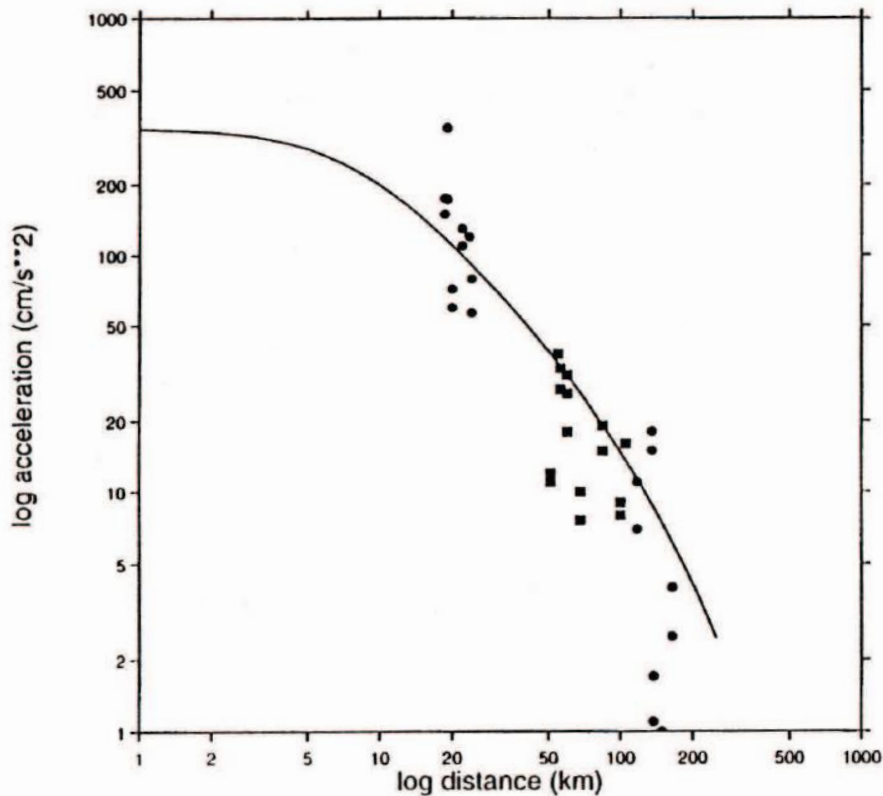
Figure A3.1.22. Comparison between observed and computed peak ground acceleration values in Belgium (dots) and Germany (squares) and values predicted by the Boore & Joyner (1982) attenuation model. From Gariel *et al.* (1994).

Given that no records are available for the area around Brunssum, where significant earthquake-triggered landslides were observed, Alkema *et al.* (1994) carried out estimates of the peak ground acceleration based on different ground motion prediction equations, as shown in Table A3.1.7.

Table A3.1.7. Peak horizontal accelerations at the location of the landslides in Brunssum, 25 km away from the epicentre, estimated from different ground motion prediction equations (GMPEs). From Alkema *et al.* (1994).

GMPE	PGA (g)
Ambraseys (1990)	0.07
Chiaruttini & Siro (1981)	0.14
Campbell (1981)	0.05
Campbell (1985)	0.05
Joyner & Boore (1981)	0.07
Joyner & Boore (1988)	0.07

The website of the United States Geological Service (USGS) provides two different ShakeMaps for the 1992 Roermond earthquake. ShakeMaps present estimations of the ground shaking based on the magnitude, location, fault dimensions, style of faulting, site conditions and, where available, observations from recording stations and/or macroseismic intensity observations. Due to the lack of availability of these data, the map shown in Figure A3.1.23 was generated using the Californian ground-motion prediction equation of Boore *et al.* (1997), which is based on as-recorded horizontal components. As can be observed, the maximum PGA predicted is 0.22 g, which is significantly below the 0.35 g calculated by Gariel *et al.* (1994) for station HLN. Estimations for stations KIN, ODL, STP match relatively well the contour lines, while values calculated by Gariel *et al.* (1994) for THN and MAS are significantly lower than those of the ShakeMap.
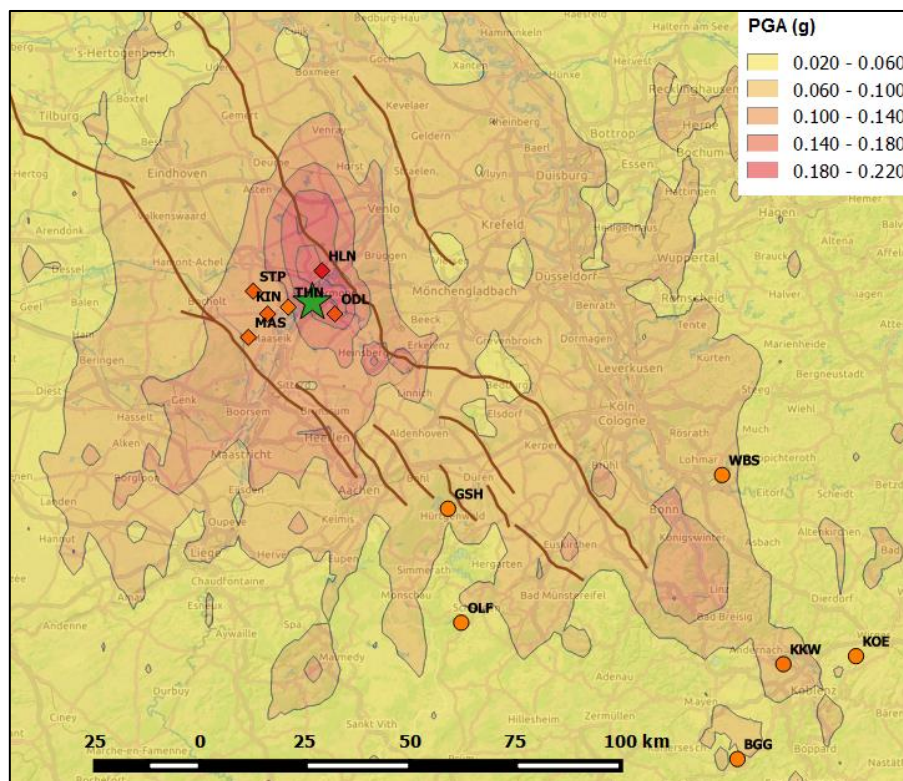
Figure A3.1.23. USGS ShakeMap (option 1) in terms of peak ground acceleration. The green star marks the epicentre of the main shock, according to Ahorner (1994). Circles indicate stations for which records are available (see Table A3.1.5). Rhombuses correspond to stations for which estimations are available (see Table A3.1.6 (USGS, 2015).

The map shown in Figure A3.1.24 is an alternative to the previous one, and it constitutes an estimation generated based on the macroseismic intensity map of Haak *et al.* (1994). This ShakeMap presents higher peak ground acceleration values around the epicentral area, which support the 0.35 g calculated by Gariel *et al.* (1994). Estimations from these authors for stations KIN and STP match relatively well the contour lines, while those for stations ODL, THN and MAS are significantly lower than those of the ShakeMap.
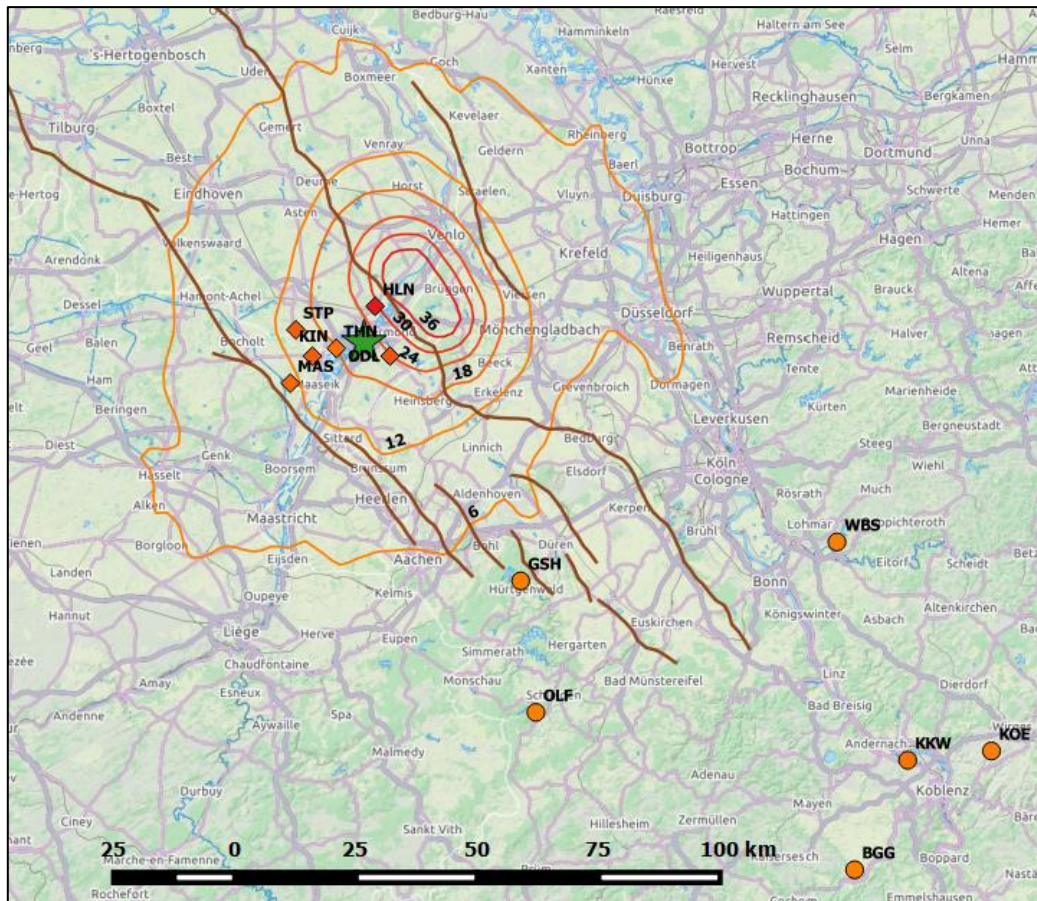
Figure A3.1.24. USGS ShakeMap (option 2) in terms of peak ground acceleration. Values of the contour lines correspond to percentages of g. The green star marks the epicentre of the main shock, according to Ahorner (1994). Circles indicate stations for which records are available (see Table A3.1.5). Rhombuses correspond to stations for which estimations are available (see Table A3.1.6). USGS ShakeMap available from http://earthquake.usgs.gov/earthquakes/eventpage/ usp00055q3#impact_shakemap:atlas_atlas19920413012000.

A3.1.4.5 Duration of ground shaking

The significant duration of a waveform is defined as the time lapse between the release of the 5% and 95% of the Arias Intensity. The significant duration of the three records from the RESORCE database (Akkar *et al.*, 2014) was calculated for each component using the OpenQuake ground motion toolkit (Weatherill, 2014). Results are shown in Table A3.1.8.

Table A3.1.8. Significant duration (in seconds) of the ground motions available from the RESORCE database (Akkar *et al.*, 2014).

Station	Repi (km)	X component	Y component
OLF	83.0	8.6	6.4
GSH	58.0	4.1	3.8
WBS	103.0	13.5	8.2

Gariel *et al.* (1994) highlight that the duration of strong accelerations observed in their synthetic records is "only a few seconds", but do not provide values.

Ewald *et al.* (2006) carried out 3D modelling simulations of wave propagation during the 1992 Roermond earthquake in the Lower Rhine Embayment, and concluded that there is a strong correlation between the duration of shaking and the depth of the basin. Figure A3.1.25 shows the shaking durations they calculated. No details with respect to the definition of duration being used are provided.
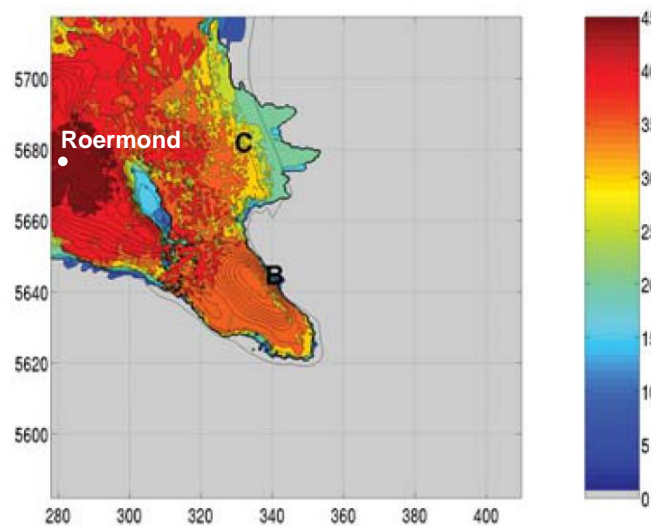
Figure A3.1.25. Shaking duration for the 3D simulation of the 1992 Roermond earthquake by Ewald *et al.* (2006).

According to The New York Times (1992), the earthquake lasted for more than 20 seconds, though no specification with respect to the location they are referring to is given.

Estimations of earthquake significant durations can be obtained by means of prediction equations such as those of Bommer *et al.* (2009) and Kempton & Stewart (2006). For the former, two alternative depths to the top of the rupture were used, based on estimations of fault rupture parameters by Ahorner (1994) and Camelbeeck *et al.* (1994). Table A3.1.9 shows the results obtained for the three records from the RESORCE database (Akkar *et al.*, 2014). In all cases, the epicentral distance was considered instead of the closest distance from the fault rupture, due to lack of information and the fact that the rupture size is small compared to the distance to the stations considered. In general, significant

durations calculated from the waveforms seem to be systematically smaller than the estimations of Kempton & Stewart (2006). Estimations obtained using the equation of Bommer *et al.* (2009) are closest to the real values, being more accurate at larger distances.

Table A3.1.9. Estimation of significant duration (in seconds) of the ground motions available from the RESORCE database (Akkar *et al.*, 2014) using prediction equations by Bommer *et al.* (2009, BSA09) and Kempton & Stewart (2006, KS06). For BSA09, estimations of fault rupture parameters by Ahorner (1994, A94) and Camelbeeck *et al.* (1994, C94) were used.

Station	Repi (km)	FROM WAVEFORMS		FROM PREDICTION EQUATIONS		
		X component	Y component	BSA09-A94	BSA09-C94	KS06
OLF	83.0	8.6	6.4	10.8	9.6	16.1
GSH	58.0	4.1	3.8	9.0	8.0	12.3
WBS	103.0	13.5	8.2	12.1	10.8	19.1

Values of Vs_{30}, which are needed for both prediction equations used here, are not known for the area around the epicentre. A range between 180 m/s and 659.6 m/s (the value corresponding to stations OLF, GSH, and WBS) was considered, and the resulting values for a null distance to the fault rupture lie between 1.8 and 5.6 seconds. These are significantly smaller than those shown in Figure A3.1.25, supporting the observation of Ewald *et al.* (2006) regarding the relevance of the influence of the basin geometry on the duration of the shaking.

A3.1.5 Collateral earthquake hazards

A3.1.5.1 Surface rupture

No surface rupture observed (Vanneste *et al.*, 1999).

A3.1.5.2 Landslides

While Davenport *et al.* (1994) state that the only reported landslides induced by the 1992 Roermond earthquake in the Netherlands occurred at Brunssum, Meidow & Ahorner (1994) report the occurrence of landslides in Leeuwen as well (Figure A3.1.26). According to the latter study, those that occurred in Germany were only small, mostly from shore lines of artificial lakes. No damage to buildings or infrastructure due to landslides was reported.

The most significant landslides observed were those of Brunssum, 25 km to the south of the epicentre. The largest of those was 200 m wide and 25 m long, and occurred 300 m away from the smaller one (Alkema *et al.*, 1994). The area had suffered from a previous slide in 1955, which occurred without any seismic trigger (Maurenbrecher *et al.*, 1994). The overall slope in the area is gentle, of around 1 in 5, but locally stepped, and it consists of loose, reworked, uniformly graded, fine quartz sands. No ground-motion records are available for this area, but Alkema *et al.* (1994) estimate it to have been between 0.05 g

and 0.14 g, from empirical attenuation relationships. According to the authors, these values are significantly smaller than those that would be necessary to destabilize these slopes. This, in combination with the groundwater table being almost at the surface at the foot of the slope, and taking into consideration the locally reworked nature of the ground, leads Alkema *et al*. (1994) and Maurenbrecher *et al*. (1994) to believe that liquefaction at the foot of the slope may have been the cause of the landslides in Brunssum. Hack *et al*. (2007) point out that no clear indications of liquefaction were observed in their vicinity, though remains of sand volcanoes were found several kilometres away, possibly indicating that liquefaction phenomena may have occurred, at least in some points. The liquefaction study of Lap (1987) had concluded years earlier that no liquefaction was to be expected in the area of Brunssum.
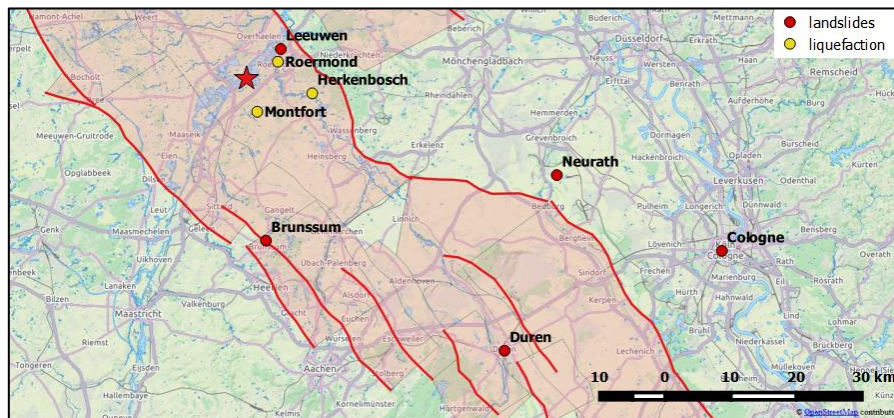
Figure A3.1.26. Map of geotechnical effects triggered by the 1992 Roermond earthquake. Data from Meidow & Ahorner (1994) and Nieuwenhuis (1994). The red star marks the epicentre of the main shock, according to Ahorner (1994).
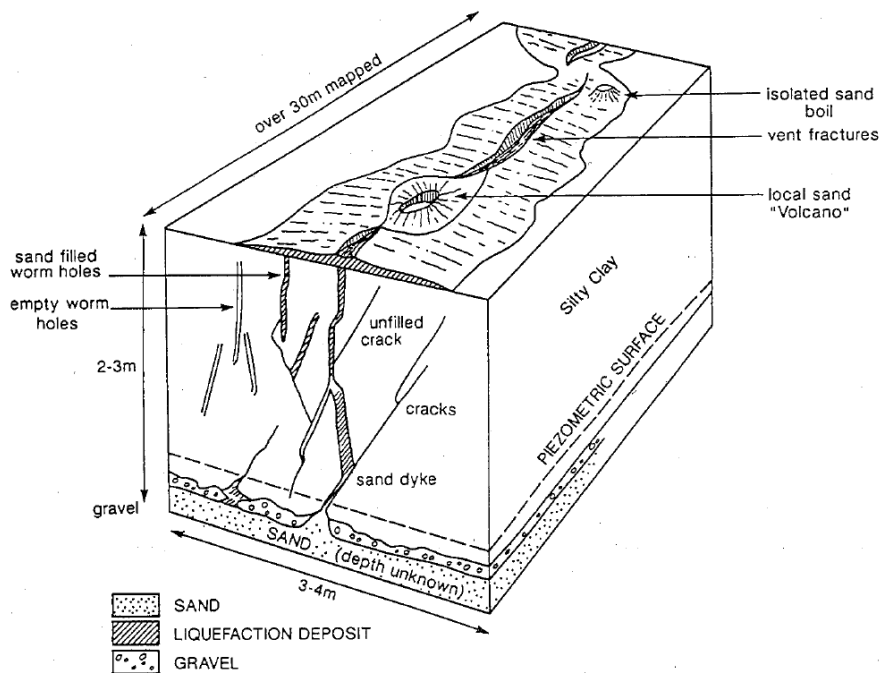
Figure A3.1.27. Liquefaction structures observed at Herkenbosch. From Davenport *et al*. (1994).

A3.1.5.3 Liquefaction

According to Nieuwenhuis (1994), evidence of liquefaction in the form of fracture vents and sand boils was observed at three places within a 10 km radius from the epicentre: near Herkenbosch, near Montfort, and to the north of Roermond (Figure A3.1.26). As can be observed in Figure A3.1.16, all these areas had been identified as being susceptible to liquefaction. However, no liquefaction was observed in areas further north also marked as highly or moderately susceptible. Hack *et al.* (2007) mention that remains of sand volcanoes were found "several kilometres" away from the landslides in Brunssum.

None of the farms located around Herkenbosch suffered from damage due to liquefaction, but Nieuwenhuis (1994) believes that significant damage would have occurred, had the liquefied area exceeded 1% of the total area. No comments regarding damage to buildings due to liquefaction in other areas have been found.

Figure A3.1.27 shows a diagram of the kind of effects observed at Herkenbosch. Groundwater levels at the time of the earthquake were close to the surface (Davenport *et al.*, 1994).

A3.1.6 Exposed population

A3.1.6.1 Socio-economic setting

According to the 2014 Human Development Report (United Nations, 2014), the Human Development Index (HDI) for the Netherlands, Germany and Belgium was 0.915, 0.911 and 0.881, respectively, placing these countries 4th, 6th and 21st in the world's ranking. Their Inequality-adjusted HDIs (IHDI) were 0.854, 0.846 and 0.806, respectively as well. Tables A3.1.10-11 compare the HDI and IHDI for the three countries for the years 1993 (around the time of the earthquake) and 2013. IHDI values are not available for reports generated before 2010. The column "Adj. HDI" provides the HDI values given in the 2014 report for 1993, adjusted for data consistency in time. As can be observed, the Netherlands and Germany present a relatively similar level of human development, while that of Belgium seems to be smaller (Tables A3.1.10-11).

Table A3.1.10. Human Development Index and Inequality-adjusted Human Development Index for Germany and the Netherlands.

Report	Germany				Netherlands			
	HDI	IHDI	Rank	Adj. HDI	HDI	IHDI	Rank	Adj. HDI
1993	0.957	-	12	0.782	0.970	-	9	0.826
2014	0.911	0.846	6	-	0.915	0.854	4	-

Table A3.1.11. Human Development Index and Inequality-adjusted Human Development Index for Belgium and the Netherlands.

Report	Belgium				Netherlands			
	HDI	IHDI	Rank	Adj. HDI	HDI	IHDI	Rank	Adj. HDI
1993	0.952	-	16	0.805	0.970	-	9	0.826
2014	0.881	0.806	21	-	0.915	0.854	4	-

In 1992, the European Monetary System suffered a significant crisis. The effects of this crisis over the gross domestic product (GDP) of the Netherlands, Germany and Belgium becomes apparent in Table A3.1.12, which shows the GDP annual percent change before and after 1992. In the case of Germany and Belgium, this percentage became negative, while for the Netherlands it decreased significantly, though staying positive. The GDP per capita, estimated from the combination of the total GDP (data from the World Economic Outlook Database 2015) and the 1990 population (United Nations data, as reported in Gridded Population of the World v.3.0), is very similar for the three countries in 1992.

In spite of the financial crisis, Gariel *et al.* (1994) describe the area affected by the 1992 Roermond earthquake as highly urbanized and industrialized. Twelve years later, Ewald *et al.* (2006) describe the whole Lower Rhine Embayment as being "densely populated and highly industrialized with large petrochemical and chemical plants".

Table A3.1.12. Gross domestic product (GDP), GDP per capita, annual percent change and population of Germany, Belgium and the Netherlands.

Indicator	Units	Germany		Netherlands		Belgium	
		1992	2014	1992	2014	1992	2014
GDP, current prices	Billions of US dollars	1,971.377	3,859.547	321.928	866.354	224.842	534.672
GDP, annual percent change	%, before year	2.200	1.607	2.030	0.875	1.490	1.043
	%, after year	-1.180	1.620	0.760	1.559	-1.460	1.341
GDP, current prices	US dollars	24,818.115	47,589.972	21,530.785	51,372.963	22,558.664	47,721.586
Population (*)	1000 People	79,433	81,100	14,952	16,864	9,967	11,204

(*) Population data:

For 1992: 1990 UN data, as reported in the Gridded Population of the World (GPW v.3.0) website.

For 2014: 2014 data, from the World Economic Outlook Database 2015.

A3.1.6.2 Population density and distribution

Given the proximity of the epicentre to several urban agglomerations and the extent to which the earthquake was felt, defining the exact number of people exposed to significant shaking during the 1992 Roermond seismic event is not simple. Nevertheless, it is clear that the area is (and was) densely populated (Ewald *et al.*, 2006), as can be observed in Figure A3.1.28, which shows the population density in 1990 according to data from Gridded Population of the World v.3.0.

Figure A3.1.28 also shows the cities and districts that observed either the largest damage or some kind of geotechnical issue. The most damaged locations were Roermond (57,000 people, 2015), Herkenbosch (4,000 people in 2015, a district within Roerdalen, with 20,000 people), Heinsberg (41,000 people in 2015), whose most affected districts were Oberbruch and Dremmen, and Bonn (311,000 people in 2015). Damage was also reported in Cologne (1 million people in 2015) and Maaseik (25,000 people in 2015). It should be noted that Cologne and Bonn are part of a large metropolitan area with a population of around 10 million people.

The USGS EXPO-CAT database (Allen *et al.*, 2009) estimates that around 91,000 people were exposed to a MMI intensity of VII, of which around 65% (59,000) was urban population. The plot on the left of Figure A3.1.29 shows the total (urban plus rural) estimations for different intensity levels while the plot on the right shows in detail the exposure to MMI VI and larger.
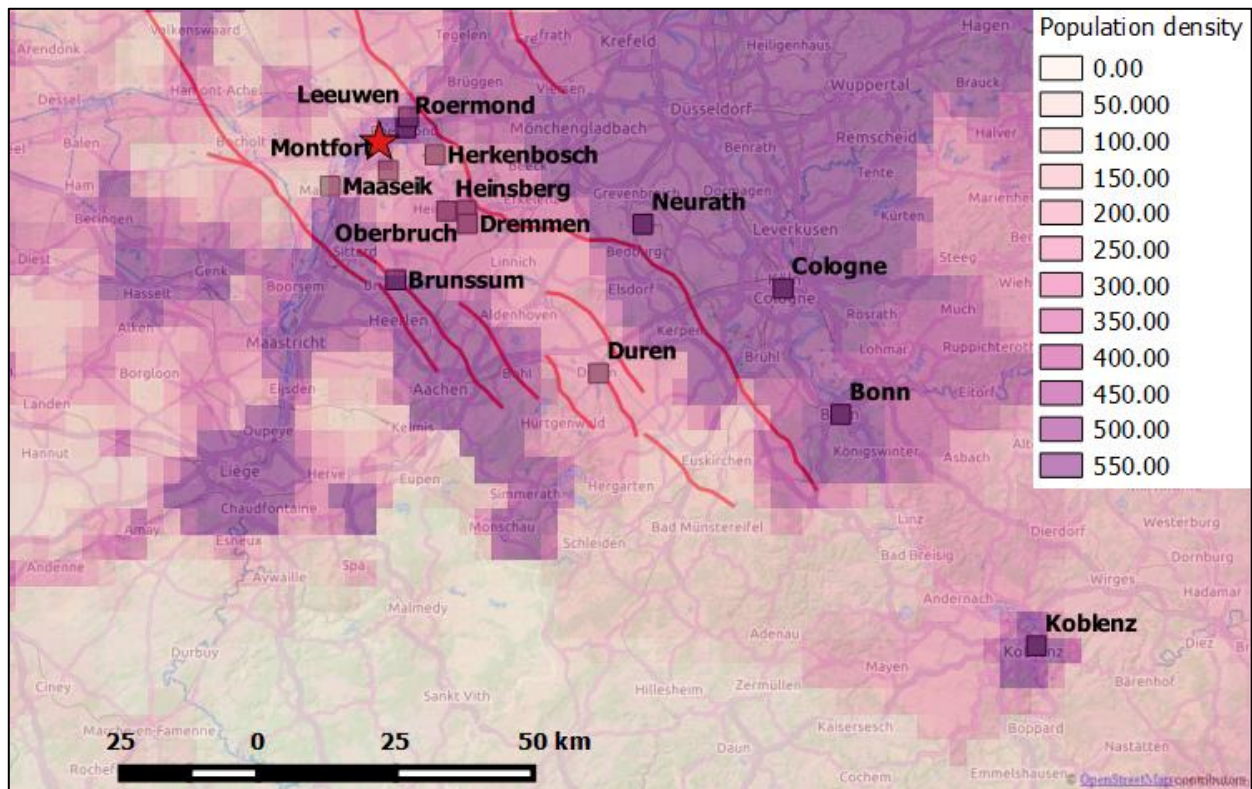
Figure A3.1.28. Population density (persons/km^2) around the Roermond area in 1990. Data from Gridded Population of the World (GPW v.3.0). The red star marks the epicentre of the main shock, according to Ahorner (1994).
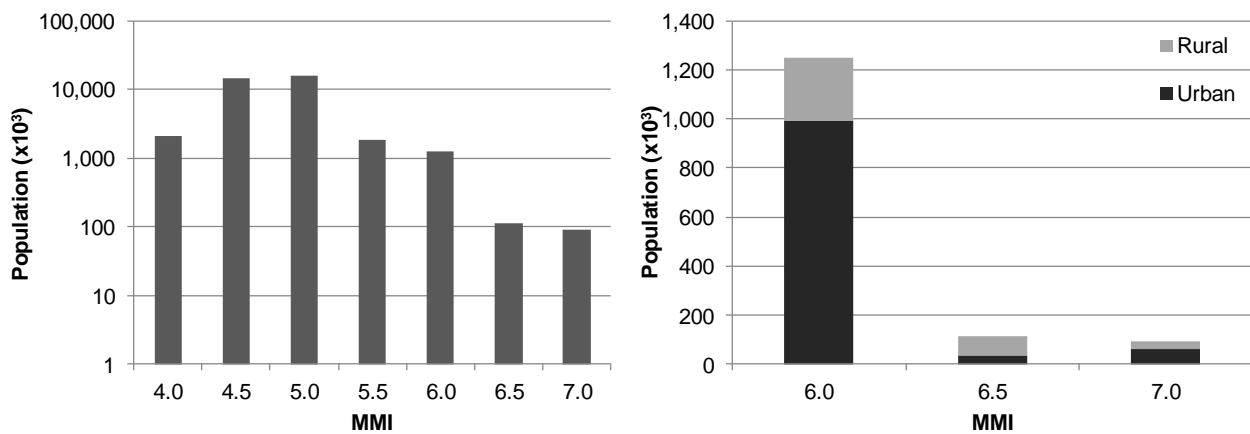
Figure A3.1.29. Left: estimation of total (urban plus rural) population exposed to different Modified Mercalli Intensities (MMI). Right: disaggregation of rural and urban population exposed to MMI VI and larger. Data from the USGS EXPO-CAT database (Allen *et al.*, 2009).

A3.1.6.3 Time of day of earthquake

According to the website of the Royal Netherlands Meteorological Institute and the GEM Earthquake Consequences Database, the number of casualties would have been significantly larger had the earthquake taken place during the day-time and not in the middle of the night, as it did. This is due to the fact that very few people were on the streets, and most injuries were caused by debris falling over those who were evacuating buildings.

A3.1.7 Characteristics of exposed building stock

A3.1.7.1 Seismic design codes

In the Netherlands, the first Building Act or Decree ("Bouwbesluit") came into force in 1992, and contained all the technical requirements applicable for the whole country. It was updated in 2003 and in 2012, when it stopped making reference to the old Dutch TGB NEN 6700 series of building regulations and adopted the Eurocodes instead. The TGB series of standards first appeared in 1972 and were updated in 1990, changing their previous deterministic perspective into a probabilistic one. In particular, the 6700 series specified the requirements to ensure the safety and serviceability of structures, both during their construction and in their subsequent use. However, the NEN 6702 code, which refers to loadings and deformations, did not specify seismic load values in the text itself, and only contained a reference to a zonation map elaborated in terms of modified Mercalli intensities and Eurocode 8 (in its latest version) in its comments regarding special projects (Brouwer *et al.*, 2010).

The current hazard zonation map for the Netherlands was elaborated by de Crook (1996), is based on an earthquake catalogue compiled up to 1993. The study was carried out in terms of macroseismic intensities, which were then translated into design peak ground

accelerations. The Royal Netherlands Meteorological Institute (KNMI) is preparing an update of this map (Brouwer *et al.*, 2010).

According to Brouwer *et al.* (2010), in the Netherlands there is no legal obligation to take into consideration seismic actions in the design of buildings and, in general, Dutch engineers believe that wind loading is always governing the design of standard structures, over earthquake loading.

The first seismic code of the Federal Republic of Germany was the DIN 4149, introduced in 1981, and then revised in 1992 to be applied to the reunified country. Its latest version dates from 2005 (DIN, 2005), and follows the Eurocode 8 (CEN, 2004) text (Brouwer *et al.*, 2010), though it does not pretend to be its implementation, which is DIN EN 1998 (DIN, 2010) instead. In spite of having been withdrawn, DIN 4149:2005-04 is still being applied, since DIN EN 1998 is not in the lists of the Technical Building Regulations of the country. Brouwer *et al.* (2010) highlight that, as opposed to the case of the Netherlands, taking into account seismic loads is mandatory in Germany, especially in the area around the Lower Rhine Embayment, which is one of the most seismically active areas of the country.

In Belgium, the first investigations aimed at estimating ground motion levels for the safety of new buildings date from the 1970s and were motivated by the construction of the first nuclear reactors in the country (Vanneste *et al.*, 2014). The first study encompassing the country as a whole was that of van Gils & Zaczek (1978). Investment in seismic hazard assessments and the development of a seismic network in Belgium increased after the 1983 Liège earthquake, which caused two deaths, several injuries and considerable damage. In the 1990s, the GSHAP project (Giardini *et al.*, 1999; Giardini *et al.*, 2003) allowed for an actualization, but it was not until the year 2000 that a new seismic hazard map (Leynaud *et al.*, 2000) was elaborated thanks to a cooperation between the Liège University and the Royal Observatory of Belgium (ROB). This map has served as the basis for the seismic zonation map included in the Belgian national annex (BIN, 2002) to Eurocode 8 (CEN, 2004), which became in force in 2012 as the NBN-ENV 1998 standard, which replaced the previous NBN ISO 3010:1993. The latter was a Belgian application of the ISO 3010 norm from the International Organization for Standardization, which contains guidelines for the design of structures taking into consideration seismic loads.

A3.1.7.2 Building typologies

Information regarding building typologies in the Roer Valley Graben is scarce to null. For this reason, data regarding typologies at the country level were collected from the PAGER Inventory Database v2.0 (Jaiswal & Wald, 2008) for the Netherlands, Belgium and Germany, and summarized in Figures A3.1.30-32. As can be observed, unreinforced masonry is the most common typology in the Netherlands and Belgium for urban, rural, residential and non-residential buildings. Reinforced concrete frames with low ductility capacities represent only a small percentage of the urban residential buildings, but are more frequent for non-residential buildings, for which steel is also an alternative. Unreinforced masonry is very common in Germany, but a larger proportion of ductile

reinforced concrete frames and reinforced masonry walls with concrete diaphragms can be observed. Unfortunately, the typology of around 50% of the building stock has not been identified, and is marked as "unknown" in Figure A3.1.32.
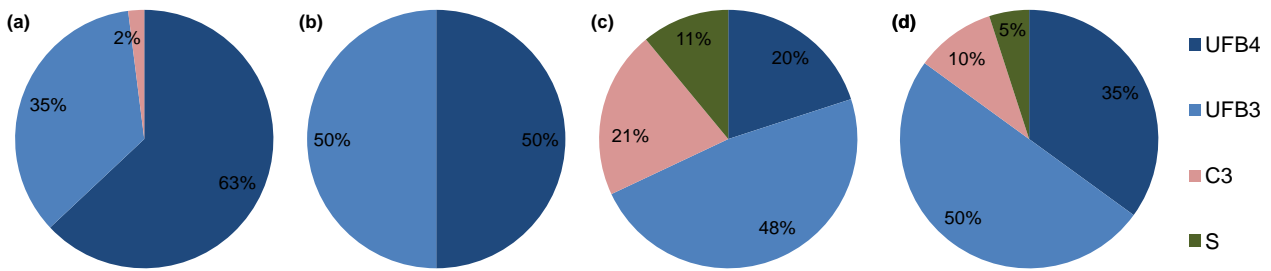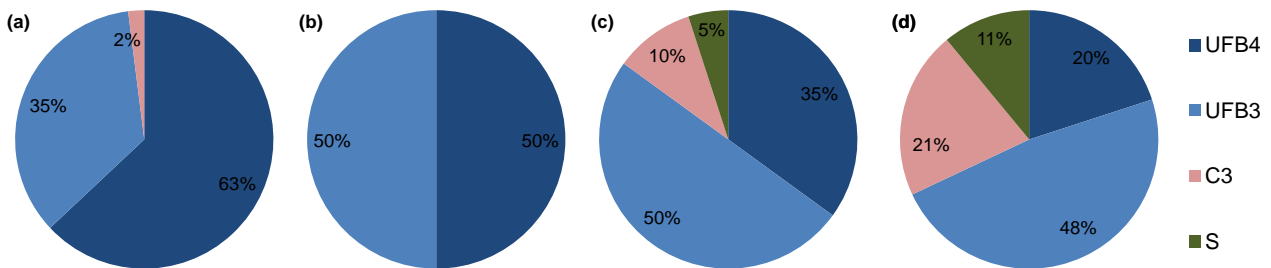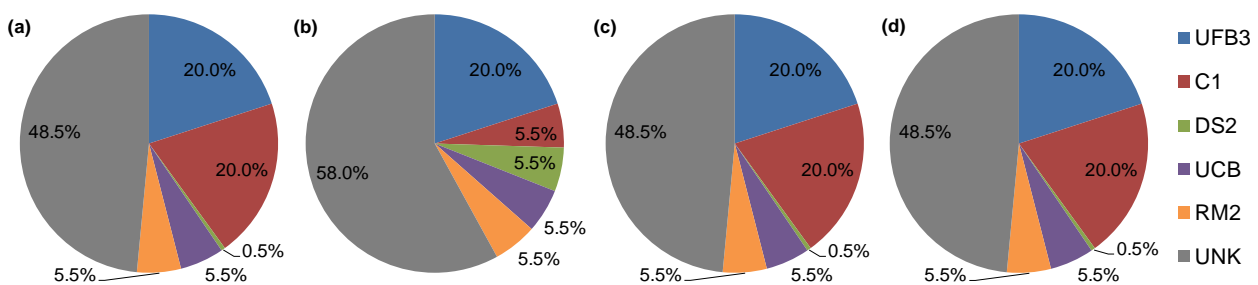

Figure A3.1.30. Proportion of buildings in the Netherlands belonging to each typology: (a) urban and residential, (b) rural and residential, (c) urban and non-residential, and (d) rural and non-residential. UFB4: unreinforced fired brick masonry, cement mortar. UFB3: unreinforced brick masonry in lime mortar. C3: non-ductile reinforced concrete frame with masonry infill walls. S: steel. Data from Jaiswal & Wald (2008).

Figure A3.1.31. Proportion of buildings in Belgium belonging to each typology: (a) urban and residential, (b) rural and residential, (c) urban and non-residential, and (d) rural and non-residential. UFB4: unreinforced fired brick masonry, cement mortar. UFB3: unreinforced brick masonry in lime mortar. C3: non-ductile reinforced concrete frame with masonry infill walls. S: steel. Data from Jaiswal & Wald (2008).

Figure A3.1.32. Proportion of buildings in Germany belonging to each typology: (a) urban and residential, (b) rural and residential, (c) urban and non-residential, and (d) rural and non-residential. UFB3: unreinforced brick masonry in lime mortar. C1: ductile reinforced concrete moment frame with or without infill. DS2: rectangular cut stone masonry block with lime mortar. UCB: concrete block unreinforced masonry with lime or cement mortar. RM2: reinforced masonry bearing walls with concrete diaphragms. UNK: not specified (unknown). Data from Jaiswal & Wald (2008).

According to the Dutch Census 2011 (Schulte Nordholt *et al.*, 2014), by 1990 approximately 9.7%, 30.6% and 59.7% of the dwellings had been constructed before 1920,

between 1920 and 1960, and after 1960, respectively (Figure A3.1.33). This distinction is relevant for future reference to damage statistics reported in Pappin *et al.* (1994).
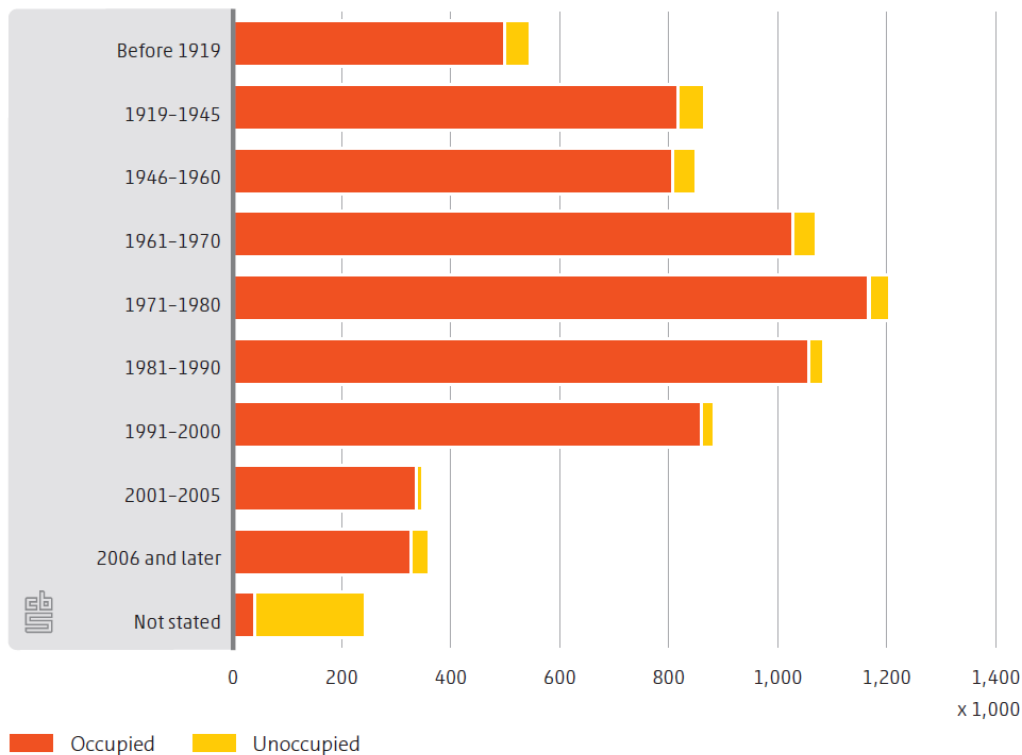

Figure A3.1.33. Dwellings in the Netherlands by period of construction and occupancy status. From the Dutch Census 2011 (Schulte Nordholt *et al.*, 2014).

Residential single- and multi- family houses built in the Netherlands between the beginning of the 18th century and the mid-20th century usually consist of timber diaphragms and solid or cavity walls. RC diaphragms with cavity walls became more common only after the end of the Second World War. Mixed floor systems consisting on timber ground floor and attic and concrete first floor can also be found in residential terraced houses. From the 1960s onwards, the use of timber or steel frames with timber shear panels for single-family houses spread, though this typology always represented a very small percentage of the buildings built each year.

According to Koopman (2007), houses dating to the first two decades after the Second World War were usually 3 to 4 storey multi-family buildings, 70% of which were built with brick masonry load bearing walls, and 30% of which were built with large concrete blocks, or panel building systems, or using in-situ concrete. Floors and horizontal roofs were usually made of a combination of prefabricated non-reinforced concrete elements and in-situ concrete, with the reinforcement placed in the latter. Sloped roofs were constructed in timber and covered in tiles. Façades were usually made of brickwork.

Since the mid-1960s, higher-rise buildings up to 10-storeys high became more common (Koopman, 2007). Most structures built in the late 1960s and 1970s were carried out with in-situ concrete. Light blocks were used for non-bearing partition walls. Floors were either casted in-situ using steel tunnel moulds as well, or were made of a combination of 50 mm

265

thick prefabricated concrete slab flooring elements over which in-situ concrete was placed. Most façades were prefabricated, either in timber or in masonry, the latter usually consisting of an inner layer of gas concrete blocks and an outer layer of brick. The use of precast structural reinforced concrete walls gained more popularity in the 1980s.

Mixed residential-commercial buildings in the Netherlands usually consist of solid walls or calcium silicate unreinforced masonry walls in the upper floors, with many of the walls replaced at ground floor with steel frames or precast reinforced concrete columns. Hollow block slabs, with cast-in-place structural walls, replaced with reinforced concrete frames at the ground floor became more common after the Second World War, while their precast walls and columns alternative spread from the 1970s onwards.

Regarding the situation of Germany, Tyagunov *et al.* (2006) say that, though pre-code buildings are dominant in quantity, the generally good workmanship with which they were built prevents them from being as vulnerable as could be expected. In their multi-risk assessment of the city of Cologne, Germany, Grünthal *et al.* (2006) highlight that the largest part of its building stock is not more than 50 years old, as the city was severely damaged during the Second World War. As a consequence, around 80% of the structures can be assigned to a C vulnerability class within the EMS-98 scale, in which A and F correspond to the most and least vulnerable classes, respectively. Figure A3.1.34 shows the proportions of the total building stock that can be assigned to each typology (on the left) and each EMS-98 vulnerability class (on the right). As can be observed, masonry is the most common structural type in Cologne, an observation which matches the information of Jaiswal & Wald (2008, Figure A3.1.32).

A3.1.7.3 Prior damage and retrofit

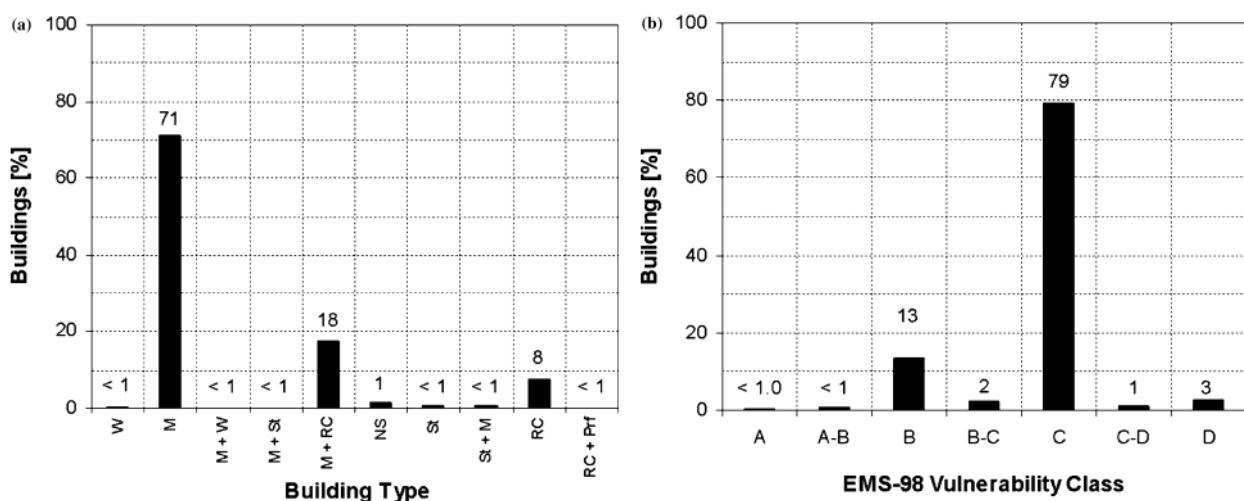No details on prior damage or retrofit available.

Figure A3.1.34. Proportion of buildings in Cologne, Germany, belonging to each typology (a) and to each EMS-98 vulnerability class (b). W: wooden. M: masonry. St: steel. RC: reinforced concrete. NS: natural stone. Prf: Prefabricated (Grünthal *et al.*, 2006).

A3.1.8 Damage observations

A3.1.8.1 Damage states

The most comprehensive statistics regarding the damage caused by the 1992 Roermond earthquake can be found in the work by Pappin *et al.* (1994), who used a damage scale very similar to that of the MSK intensity scale (MSK-64, Medvedev *et al.*, 1965). This damage scale is described in Table A3.1.13.

Table A3.1.13. Definition of damage levels used in the study of Pappin *et al.* (1994).

Damage Level		Definition for load-bearing masonry
D0	Undamaged	No visible damage
D1	Slight damage	Hairline cracks
D2	Moderate damage	Cracks 5-20 mm
D3	Heavy damage	Cracks 20 mm or wall material dislodged
D4	Partial destruction	Complete collapse of individual wall or individual roof support
D5	Collapse	More than one wall collapsed or more than half of roof

A3.1.8.2 Damage statistics

According to Camelbeeck & van Eck (1994), the level of damage caused by the main shock was relatively low if compared to that observed due to other seismic events in the region. Braunmiller *et al.* (1994) state that no fatal building collapses occurred. In the epicentral area, numerous walls and roofs collapsed, and chimneys and Church towers cracked (Davenport *et al.*, 1994). Small cracks formed in walls and plaster, and pieces of plaster fell down (Meidow & Ahorner, 1994). According to The New York Times (1992), telephone lines were cut, electricity supplies were interrupted and water mains were damaged in some areas. The GEM Earthquake Consequences Database reports 1400 buildings damaged by shaking, out of which 100 were believed to have been damaged beyond repair. Several vehicles were damaged due to falling objects.

Meidow & Ahorner (1994) mention Roermond (Netherlands), Herkenbosch (Netherlands) and Heinsberg (Germany) as the most affected places. In the latter, Oberbruch and Dremmen saw more than 100 and about 30 significantly damaged buildings, respectively, making them the most affected districts. Furthermore, about 50 buildings in the surrounding villages suffered extensive damage as well. Around this area, many uppermost part of gables fell down and large cracks opened in walls. Three houses had to be torn down due to the large likelihood of an imminent collapse, while other eight buildings had to be temporarily evacuated. Many other walls and chimneys were in risk of imminent collapse as well. Meidow & Ahorner (1994) point out that the most vulnerable buildings suffered the most significant damage. In Dremmen, the roof of the Marienkloster chapel partially collapsed.

Around 500 buildings were damaged in Herkenbosch. As can be observed in Figure A3.1.35, a large proportion of buildings suffered from a combination of types of damage (Maurenbrecher & de Vries, 1995).
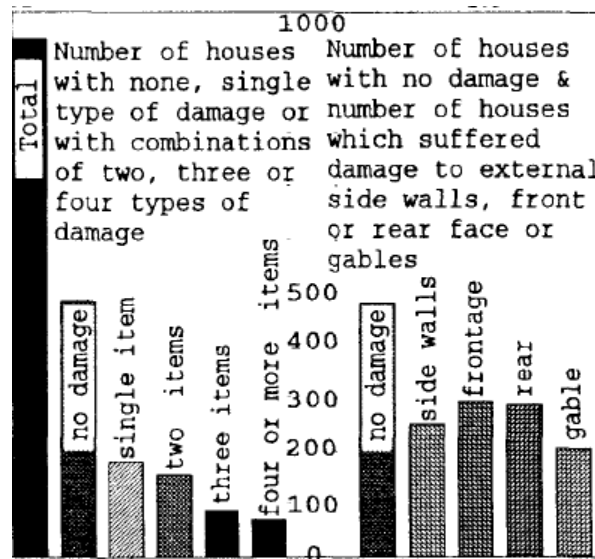

Figure A3.1.35. Damage observed in Herkenbosch, the Netherlands, according to questionnaires filled out by the population. From Maurenbrecher & de Vries (1995).

According to Davenport *et al.* (1994), many historic buildings in the city of Roermond were seriously damaged. These include the Munsterkerk and Minderbroederskerk churches, some ornate roofs near the railway station, and brickwork of the Vroom & Dreesmann department store. Damage to building foundations was also documented.

More than 150 churches were damaged in Germany, many of them around Heinsberg, but also in regions as distant as Cologne, Bonn and Koblenz, located at approximately 75 km, 95 km and 150 km away from the epicentre, respectively (Meidow & Ahorner, 1994). Six finials broke out off their embeddings in the 13th century cathedral in Cologne, and one stone weighting around 500 kg fell from the top of a 60 m tower, striking a whole in the roof of the transept. In Bonn, more than 60 private and public buildings suffered from damages including the collapse of chimneys and cracking of walls. Damage to plaster was widespread all over the town. Figure A3.1.36 shows examples of damage observed in Bonn.

Meidow & Ahorner (1994) point out that most of the damage observed at distances larger than 20 km consisted on small cracks in chimneys and walls, as well as plaster falling off walls and ceilings, though islands of higher damage like those mentioned above occurred at more distant locations.

The most systematised statistics regarding damage caused by this earthquake have been gathered by Pappin *et al.* (1994), who report on the damage ratios observed during a three-day visit to the affected area by the UK-based Earthquake Engineering Field Investigation

Team (EEFIT). This group of experts rapidly found that the only building typology to regularly occur in sufficient numbers for statistics to be relevant was residential masonry, and, therefore, decided to focus on it. They subdivided the full typology into those built before 1920, those built between 1920 and 1960, and those built after 1960, and observed that the first were the only ones who had systematically experienced high levels of damage. For this reason, information regarding the three groups was collected during the initial stages of the survey, while later stages only focused on buildings built before 1920.

Figure A3.1.36. Damage to a residential house (left) and a car (right) in the city of Bonn (Germany). Photos copyright of Seismic Workgroup, St.-Michael-Gymnasium Monschau (2005)

Figures A3.1.37-38 show the damage ratios obtained for this category, using the damage scale defined in Table A3.1.13, in the first case, and simply grouping results into "no damage" and "some level of damage" categories, in the second. As can be observed, the largest proportion of damaged buildings was observed in Oberbruch, Germany. It should be noted that Herkenbosch, a town which clearly experienced severe damage, was not part of the survey. From the plots in Figure A3.1.39, which present the corresponding results for residential masonry buildings built after 1920, it becomes apparent that, in general, these buildings suffered far less damage than those built before 1920.
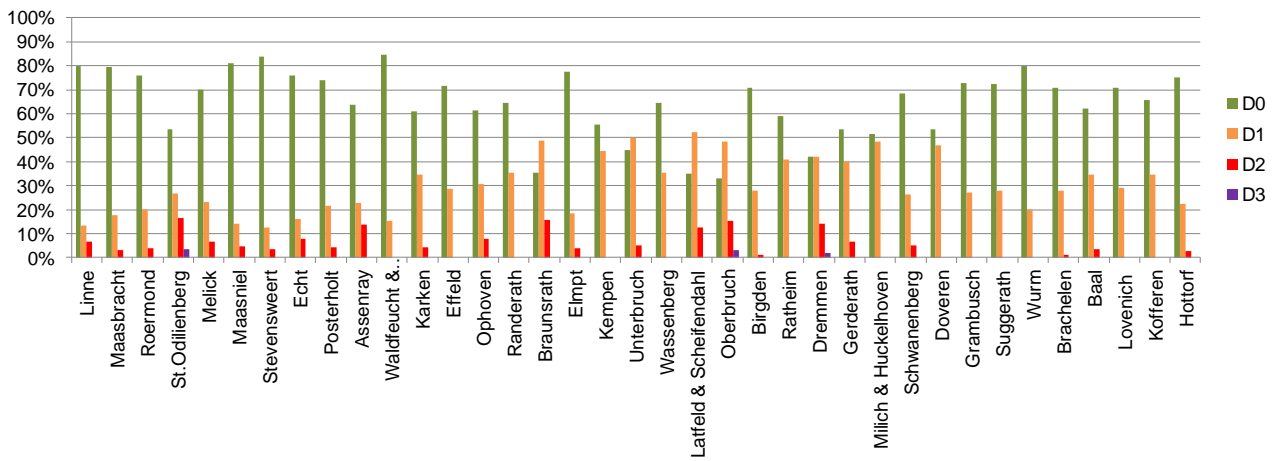
Figure A3.1.37. Damage ratios observed by the Earthquake Engineering Field Investigation Team (EEFIT, Pappin *et al.*, 1994) for residential masonry buildings built before 1920. Locations ordered from closest to most distant from the epicentre, as defined by Ahorner (1994).
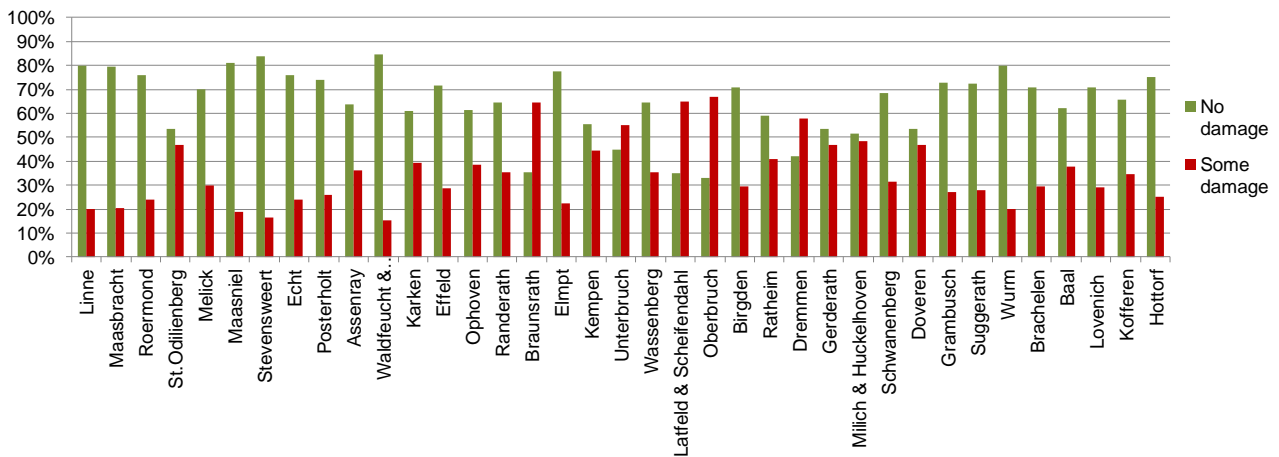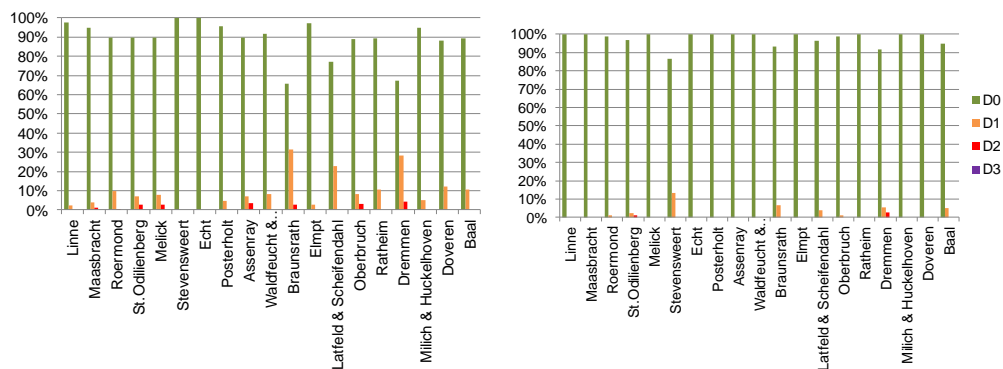

Figure A3.1.38. Damage ratios observed by the Earthquake Engineering Field Investigation Team (EEFIT, Pappin *et al.*, 1994) for residential masonry buildings built before 1920. Locations ordered from closest to most distant from the epicentre, as defined by Ahorner (1994).

Figure A3.1.39. Damage ratios observed by the Earthquake Engineering Field Investigation Team (EEFIT, Pappin *et al.*, 1994) for residential masonry buildings built between 1920 and 1960 (left), and after 1960 (right). Locations ordered from closest to most distant from the epicentre, as defined by Ahorner (1994).

270

A3.1.8.3 Observed weaknesses

No details regarding systematic causes of failure and damage were found in the literature. However, from the results of Pappin *et al.* (1994) it becomes clear that older masonry buildings were significantly more vulnerable than more modern ones. Furthermore, and as observed during other small-to-moderate magnitude earthquakes (*e.g.*, Sargeant *et al.*, 2008), the frequency with which damage to chimneys was observed is also a sign of an increased vulnerability of these structures (Figure A3.1.40).

Figure A3.1.40. D2 (left) and D3 (right) damage to chimneys (Schwarz *et al.*, 2010).

A3.1.8.4 Damage distribution

The 1992 Roermond earthquake was felt in places located over 500 km away from the epicentre, such as Berlin, Munich, Zürich and southeast England (Ahorner, 1994). Intensity V effects (*e.g.*, people waking up, some frightened people, hanging objects swinging considerably, china and glasses clattering, etc.) were observed in locations as far as Luxemburg, Frankfurt, Siegen and Kassel, at 174 km, 227 km, 150 km and 248 km from the epicentre, respectively. According to Meidow & Ahorner (1994), these islands of intensity V are due to local site conditions.

Significant damage was observed in the Netherlands and Germany, but not so much in Belgium (Horrent *et al.*, 1994). Figure A3.1.41 shows the location of the cities and towns which suffered significant damage, as described above. The location of the cities studied by the Earthquake Engineering Field Investigation Team (EEFIT; Pappin *et al.*, 1994) are also included, though a detail of the area is presented in Figure A3.1.42. Some degree of correlation can be observed between the results of Pappin *et al.* (1994) and the estimated PGA values from the USGS ShakeMap. Meidow & Ahorner (1994) report local observations of MSK intensities VI to VII from Bonn to Koblenz. As can be observed, the trend of damage seems to be elongated to the south-east and shifted eastwards with

respect to the instrumental epicentre. According to Meidow & Ahorner (1994), this can be explained both through soil amplification and the specific geometry and dynamics of the earthquake source.
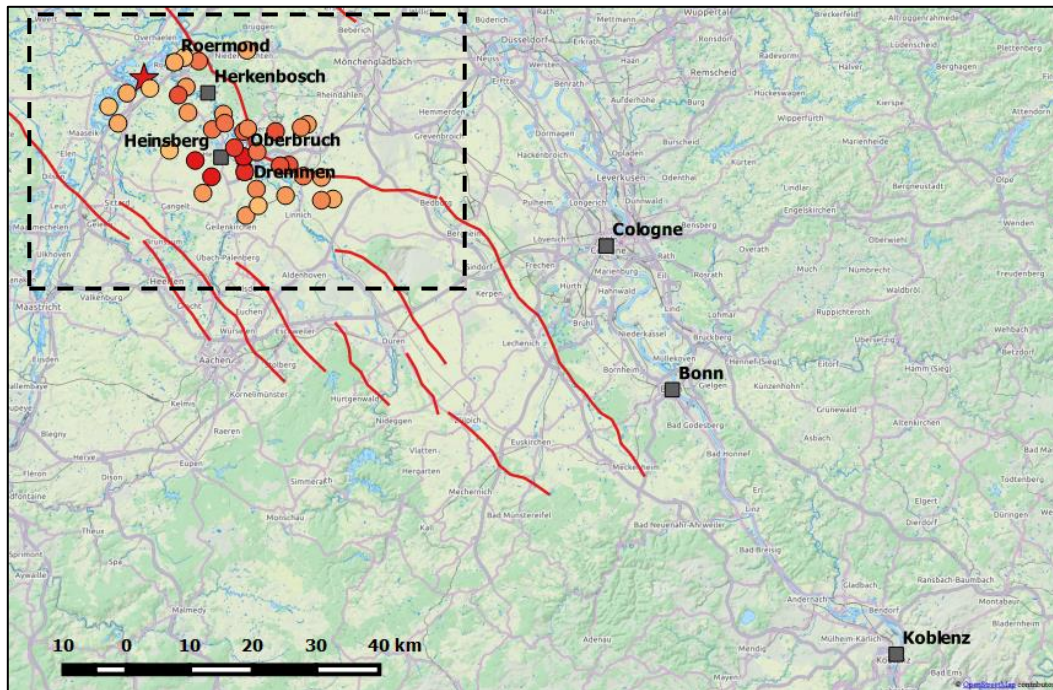

Figure A3.1.41. Location of cities and towns which suffered significant damage. Orange-to-red dots corresponds to the cities studied by the EEFIT (Pappin *et al.*, 1994).
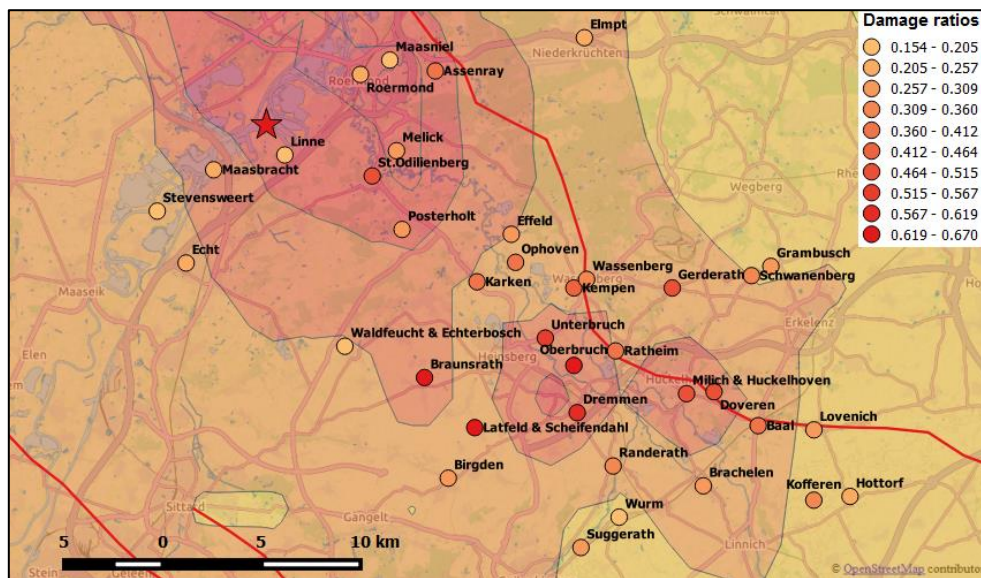

Figure A3.1.42. Location of cities studied by the EEFIT (Pappin *et al.*, 1994) over PGA ShakeMap from the USGS (see Inferred shaking levels section). Colour of dots represents the extent of damage to residential masonry buildings built before 1920 according to the specified scale (ratio makes reference to any kind of damage, *i.e.*, the summation of D1, D2 and D3 damage ratios).

Figure A3.1.43 shows the locations of damaged churches, as reported by Meidow & Ahorner (1994). Slight and moderate damage occurred in regions with MSK macroseismic intensities of V-VI and VI, respectively, while heavy damage took place in regions with intensity larger than VI.
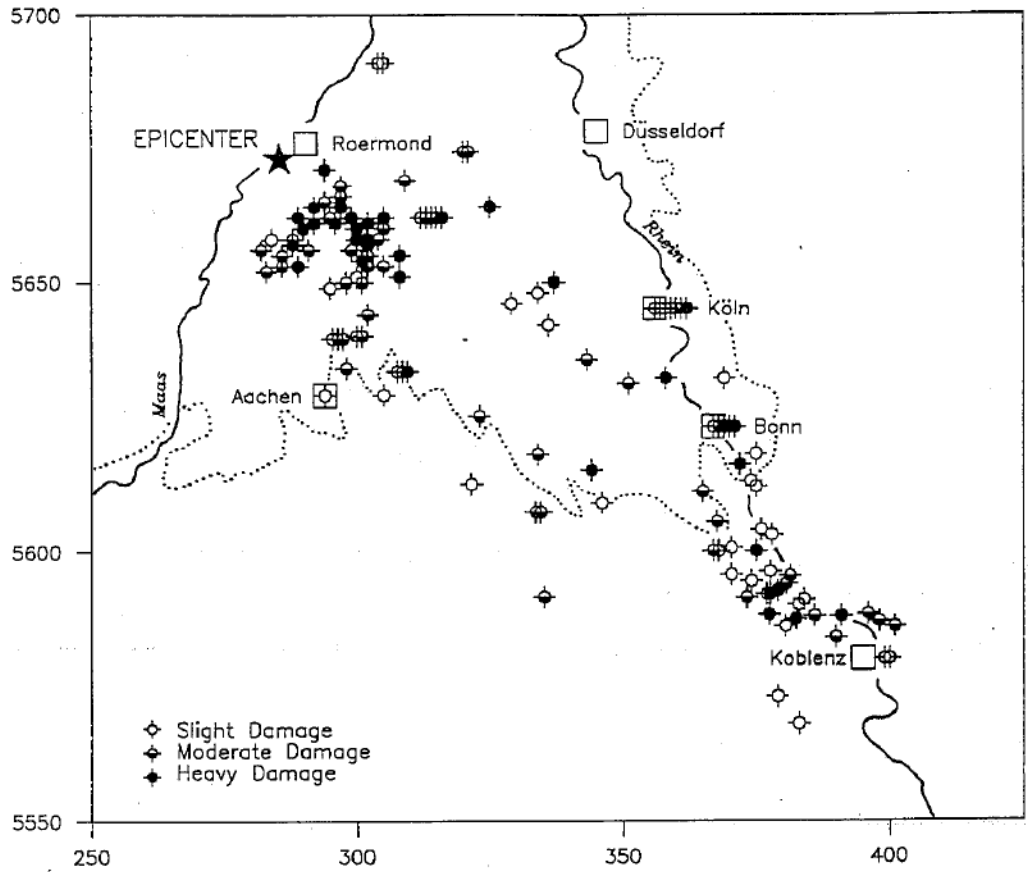

Figure A3.1.43. Location of churches damaged by the earthquake. Slight damage: fine cracks in plaster, fall of small pieces of plaster, and loosening of pinnacles or similar construction parts. Moderate damage: small cracks in walls and vaults, cracks between church tower and nave, and falling of pinnacles. Heavy damage: large and deep cracks in walls and vaults, and damage to load-bearing parts. From Meidow & Ahorner (1994).

Ewald *et al.* (2006) carried out 3D modelling simulations of wave propagation during the 1992 Roermond earthquake in the Lower Rhine Embayment, and concluded that there is a strong correlation between the high observed macroseismic intensities and the contours of the sedimentary basin. Meidow & Ahorner (1994) point out that the thick sediments (over 500 m) in the area close to the epicentre acted decreasing the ground motions in the epicentral area, while relatively larger macroseismic intensities can be observed where sedimentary layers have thicknesses of up to 100 m. They also conclude that the shape of the isoseismals is strongly influenced by local site conditions. Ahorner (1994) also observed that stations located on layers of unconsolidated sediments suffered from amplification effects, but give no indication with respect to the location of these stations. Through the analysis of a series of aftershocks, Horrent *et al.* (1994) concluded that site effects were significant because systematic amplifications were observed at the same

stations for events varying in location and source mechanism. They observed particularly high amplifications at station HLN, which is located north of Roermond, quite close to the Peel Boundary Fault trace, the same station for which (Gariel *et al.*, 1994) computed large accelerations (0.35 g).

A3.1.9 Casualties and losses

A3.1.9.1 Numbers of dead and injured

Only one death was reported for this earthquake, and it corresponds to a 79-year-old woman in Bonn who died of a heart attack apparently triggered by the tremor (USGS, GEM Earthquake Consequences Database).

Twenty and twenty-five people were reported injured in Roermond and Heinsberg, respectively. Of the latter, four were in serious condition (USGS, GEM Earthquake Consequences Database). Meidow & Ahorner (1994) also mention some minor injuries being reported at distant towns such as Euskirchen (82 km) and Langenfeld (71 km), but provide no further details.

According to the GEM Earthquake Consequences Database, 200 people were left homeless. This number was estimated based on damage statistics of the building stock.

A3.1.9.2 Causes of casualties

As mentioned earlier, the registered death was due to a medical condition triggered by fear resulting from the ground shaking.

Several sources (*e.g.*, Meidow & Ahorner, 1994; GEM Earthquake Consequences Database; The New York Times, 1992) point out that the registered injuries were caused by falling parts of chimneys, masonry and roofing tiles. Meidow & Ahorner (1994) also mention that some people were slightly injured due to shattering of window glasses.

A3.1.9.3 Estimates of economic losses

According to the GEM Earthquake Consequences Database, Munich Re estimated the total direct losses to be 206 million US$, of which 120 million correspond to Germany, 50 million correspond to the Netherlands, and 6 million correspond to Belgium. The remaining 30 million correspond to insured losses in Germany. Insured losses in the Netherlands and Belgium are not known.

The Royal Netherlands Meteorological Institute (KNMI) reports a total loss of 275 million guilders, of which 170 million correspond to damage in the Netherlands. With the official conversion rate of 1999, these values are approximately 125 and 77 million Euros, respectively.

Braunmiller *et al.* (1994) report an estimated damage in the epicentral region (Roermond, Herkenbosch and Heinsberg) of around 130 to 200 million US$. Hinzen & Oemisch (2001) report an overall value of 125 US$, which is on the lower bound of the estimation by Braunmiller *et al.* (1994) for the epicentral area alone.

Meidow & Ahorner (1994) report that first estimates of damage to public buildings in the district of Heinsberg reached approximately 500,000 DM (around 256 thousand Euros, with the official conversion rate of 1999). Further, they report the repair costs for the cathedral in Cologne to be around 50,000 DM (around 25.6 thousand Euros)

A3.1.10 Discussion and conclusions

This earthquake occurred on 13th April 1992, at 01.20 UTC (03.20 local time), very close to the city of Roermond, in the south of the Netherlands. Apart from a smaller event that occurred 0.2 seconds earlier, no other foreshock activity had been observed. It is the strongest earthquake to have been recorded in the Netherlands and north-western Europe to date, though its size and statistical probability of occurrence are in clear agreement with the tectonics of the region.

It was felt over a large area extending to places located over 500 km away from the epicentre, and reached a maximum MSK-81 (very similar to EMS-98) intensity of VII. Significant losses were registered in the Netherlands and Germany, and in a much lesser extent in Belgium. Residential masonry buildings built before 1920 and churches were the most affected constructions. No damage reports were found for buildings designed to modern codes.

Landslides and liquefaction phenomena were observed, though they did not contribute to the damage to the building stock.

The characteristics of the basin of the Roer Valley seem to have played a significant role in the ground motion levels, as well as in the duration of the shaking.

One death was reported, albeit this being attributed to a medical condition triggered by fear resulting from the ground shaking. An additional 45 injuries were also reported, which were caused by falling parts of chimneys, masonry and roofing tiles.

A3.1.11 References

A3.1.11.1 Bibliography

Ahorner, L. (1994). Fault-plane solutions and source parameters of the 1992 Roermond, the Netherlands, mainshock and its stronger aftershocks from regional seismic data. *Geol. En Mijnb.* **73**, 199–214.

Ahorner, L. & W. Rosenhauer (1986). Regionale erdbebengefährdung. In: Realistische seismische lastannahmen für bauwerke. Abschluβbericht an das Institut für Bautechnik Berlin - König und Heunisch, Bratende Ingenieure, Frankfurt/Erdbebenstation Bensberg der Universität Köln / Institut für Geophysik der Universität Stuttgart. 334 pp.

Akkar, S., M.A. Sandıkkaya, M. Senyurt, A. Azari Sisi, B.Ö. Ay, P. Traversa, J. Douglas, F. Cotton, L. Luzi, B. Hernandez & S. Godey (2014). Reference database for seismic ground-motion in Europe (RESORCE). *Bulletin of Earthquake Engineering* **12**(1), 311-339.

Alkema, D., M. Mosselman & I. Paulussen (1994). Earthquake-triggered landslides at the Brunssummerheide, Limburg, the Netherlands: preliminary studies following the 1992 Roermond earthquake. *Geol. En Mijnb.* **73**, 387–391.

Allen, T.I., D.J. Wald, P.S. Earle, K.D. Marano, A.J. Hotovec, K. Lin & M.G. Hearne (2009). An Atlas of ShakeMaps and population exposure catalog for earthquake loss modeling. *Bull. Earthq. Eng.* **7**, 701–718.

Atakan, K., V. Midzi, B.M. Toiran, K. Vanneste, T. Camelbeeck & M. Meghraoui (2000). Seismic hazard in regions of present day low seismic activity: uncertainties in the paleoseismic investigations along the Bree Fault Scarp (Roer Graben, Belgium). *Soil Dyn. Earthq. Eng.* **20**, 415–427.

BIN (2002). NBN-ENV 1998-1-1: 2002 NAD-E/N/F, Belgische toepassingsrichtlijn Eurocode 8: Ontwerp en dimensionering van aardschokbestendige structuren – Deel 1-1: Algemene regels – Aardschokken en algemene richtlijnen voor structuren.

Bommer, J.J., P.J. Stafford & J.E. Alarcón (2009). Empirical equations for the prediction of the significant, bracketed, and uniform duration of earthquake ground motion. *Bulletin of the Seismological Society of America* **99**(6), 3217-3233.

Boore, D.M. & W.B. Joyner (1982). The empirical prediction of ground motion. *Bulletin of the Seismological Society of America* **72**, S43-S60.

Boore, D.M., W.B. Joyner & T.E. Fumal (1997). Equations for estimating horizontal response spectra and peak acceleration from western North American earthquakes: a summary of recent work. Seismological Research Letters **68**(1), 128-153.

Braunmiller, J., T. Dahm & K.-P. Bonjer (1994). Source mechanism of the 1992 Roermond earthquake from surface-wave inversion of regional data. *Geophys. J. Int.* **116**, 663–672.

Brouwer, J.W.R., T. Van Eck, F.H. Goutbeek & A.C.W.M. Vrouwenvelder (2010). The meaning of Eurocode 8 and induced seismicity for earthquake engineering in the Netherlands. Fifth International Conference on Recent Advances in Geotechnical Earthquake Engineering and Soil Dynamics and Symposium in Honor of Professor I. M. Idriss, San Diego, California, May 24-29.

Camelbeeck, T. & T. van Eck (1994). The Roer Valley Graben earthquake of 13 April 1992 and its seismotectonic setting. *Terra Nova* **6**, 291–300.

Camelbeeck, T. & M. Meghraoui (1996). Large earthquakes in Northern Europe more likely than once thought. *EOS* **77**, 405–409.

Camelbeeck, T. & M. Meghraoui (1998). Geological and geophysical evidence for large palaeo-earthquakes with surface faulting in the Roer Graben (northwest Europe). *Geophys. J. Int.* **132**, 347–362.

Camelbeeck, T., T. van Eck, R. Pelzing, L. Ahorner, J. Loohuis & H.W. Haak (1994). The 1992 Roermond earthquake, the Netherlands, and its aftershocks. *Geol. En Mijnb.* **73**, 181–197.

CEN (2004). Eurocode 8: Design of Structures for Earthquake Resistance - Part 1: General rules, seismic actions and rules for buildings.

Davenport, C.A., J.M.J. Lap, P.M. Maurenbrecher & D.G. Price (1994). Liquefaction potential and dewatering injection structures at Herkenbosch: field investigations of the effect of the 1992 Roermond earthquake, the Netherlands. *Geol. En Mijnb.* **73,** 365–374.

De Crook, T. (1994). Earthquake hazard for Roermond, the Netherlands. *Geol. En Mijnb.* **73**, 425–429.

De Crook, T. (1996). A seismic zoning map conforming to Eurocode 8, and practical earthquake parameter relations for the Netherlands. *Geol. En Mijnb.* **75**, 11–18.

De Vos, D. (2010). *Probabilisitic Seismic Hazard Assessment for the Southern part of the Netherlands*. MSc. thesis. Utrecht University.

DIN (2005). DIN 4149:2005-04: Bauten in deutschen Erdbebengebieten - Lastannahmen, Bemessung und Ausführung üblicher Hochbauten.

DIN (2010). DIN EN 1998-1:2010-12: Eurocode 8: Auslegung von Bauwerken gegen Erdbeben - Teil 1: Grundlagen, Erdbebeneinwirkungen und Regeln für Hochbauten.

Evers, L. (2000). An extended abstract on geophysical investigations for fault identification in paleoseismology. Royal Netherlands Meteorological Institute. Available online at http://www.knmi.nl/~evers/paleoseismology/paleoseis.html.

Ewald, M., H. Igel, K.-G. Hinzen & F. Scherbaum (2006). Basin-related effects on ground motion for earthquake scenarios in the Lower Rhine Embayment. *Geophys. J. Int.* **166**, 197–212.

Gariel, J.C., C. Horrent, D. Jongmans & T. Camelbeeck (1994). Strong ground motion computation of the 1992 Roermond earthquake, the Netherlands, from linear methods using locally recorded aftershocks. *Geol. En Mijnb.* **73**, 315–321.

Giardini, D., G. Grünthal, K.M. Shedlock & P. Zhang (1999). The GSHAP global seismic hazard map. *Annali di Geofisica* **42**(6), 1225-1228.

Giardini, D., G. Grünthal, K.M. Shedlock & P. Zhang (2003). The GSHAP global seismic hazard map. In: Lee, W., H. Kanamori, P. Jennings & C. Kisslinger (eds.): International handbook of earthquake & engineering seismology, International Geophysics Series **81**B, Academic Press, Amsterdam, 1233-1239.

Giardini, D., J. Woessner, L. Danciu, H. Crowley, F. Cotton, G. Gruenthal, R. Pinho, G. Valensise, S. Akkar, R. Arvidsson, R. Basili, T. Cameelbeck, A. Campos-Costa, J. Douglas, M. B. Demircioglu, M. Erdik, J. Fonseca, B. Glavatovic, C. Lindholm, K. Makropoulos, F. Meletti, R. Musson, K. Pitilakis, K. Sesetyan, D. Stromeyer, M. Stucchi & A. Rovida (2013). *Seismic Hazard Harmonization in Europe (SHARE): Online data resource*, doi:10.12686/SED-00000001-SHARE.

Grünthal, G. (ed.) (1993). *European Macroseismic Scale 1992 (updated MSK scale)*. European Seismological Commission, Subcommission on Engineering Seismology, Working Group Macroseismic scale.

Grünthal, G. & H. Grosser (1992). Roermond erdbeben vom 13 April 1992: Zu physikalischen herdparametern und zur makroseismischen herdtiefenschätzung. In: Report by the Arbeitsgruppe Wisstechn. Task force und Erdebebenkatastrophenforschung. Hannover: 2/1-2/4.

Grünthal, G., D. Mayer-Rosa & W.A. Lenhardt (1998). Abschätzung der Erdbebengefährdung für die D-A-CH-Staaten-Deutschland, Österreich, Schweiz. *Bautechnik* **75**, 753–767.

Grünthal, G., A.H. Thieken, J. Schwarz, K.S. Radtke, A. Smolka & B. Merz (2006). Comparative Risk Assessments for the City of Cologne – Storms, Floods, Earthquakes. *Nat. Hazards* **38**, 21–44.

Haak, H.W., J.A. van Bodegraven, R. Sleeman, R. Verbeiren, L. Ahorner, H. Meidow, G. Grünthal, P. Hoang-Trong, R.M.W. Musson, P. Henni, Z. Schenková & R. Zimová (1994). The macroseismic map of the 1992 Roermond earthquake, the Netherlands. *Geol. En Mijnb.* **73**, 265–270.

Hack, R., D. Alkema, G.A.M. Kruse, N. Leenders & L. Luzi (2007). Influence of earthquakes on the stability of slopes. *Eng. Geol.* **91**, 4–15.

Helm, J.A., M. Bour & P. Hoang-Trong (1994). Accelerometer recordings of the 1992 Roermond earthquake, the Netherlands, and ground motion simulations using the empirical Green's function method. *Geol. En Mijnb.* **73**, 331–337.

Hinzen, K.-G. & M. Oemisch (2001). Location and magnitude from seismic intensity data of recent and historic earthquakes in the northern Rhine area, Central Europe. *Bull. Seismol. Soc. Am.* **91**, 40–56.

Horrent, C., D. Jongmans & T. Camelbeeck (1994). Local ground motion variations observed in the region of Roermond, the Netherlands, from aftershocks of the April 1992 earthquake. *Geol. En Mijnb.* **73**, 323–330.

Jaiswal, K. & D.J. Wald (2008). Creating a Global Building Inventory for Earthquake Loss Assessment and Risk Management. USGS Open File Report 2008-1160. Available electronically at http://pubs.usgs.gov/of/2008/1160/.

Kempton, J.J. & J.P. Stewart (2006). Prediction equations for significant duration of erthquake ground motions considering site and near-source effects. Earthquake Spectra **22**(4), 985-1013.

Koopman, F.W.A. (2007). General Overview of the Problems, Needs and Solutions in the Dutch Urban Building Envelopes. *In:* COST C16 Improving the Quality of Existing Urban Building Envelopes, E. Melgaard, G. Hadjimichael, M. Almeida, and L.G.W. Verhoef, eds. (IOS Press).

Lap, J.M.J. (1987). Earthquake-induced liquefaction potential in the area south of Eindhoven, the Netherlands. *Mem. Centre Eng. Geol. Netherlands* **47**, 40 pp.

Leynaud, D., D. Jongmans, H. Teerlynck & T. Cambelbeeck (2000). Seismic hazard assessment in Belgium. *Geol. Belg.* **3**, 67–86.

Maurenbrecher, P.M. & G. de Vries (1995). Assessing damage for Herkenbosch, The Netherlands, due to the Roermond earthquake of April 13, 1992. Trans. *Built Environ.* **14**, 397–404.

Maurenbrecher, P.M., D.G. Price & W. Verwaal (1994). Technical note on the 1992 Brunssummerheide landslide in Limburg, the Netherlands. *Geol. En Mijnb.* **73**, 393–398.

Medvedev, S., W. Sponheuer & V. Karnik (1965). *Seismic intensity scale, MSK 1964.* Acad. Sci. USSR, Sov. Geophys. Comm., 13 pp.

Medvedev, S., W. Sponheuer & V. Karnik (1981). Report of the ad-hoc panel meeting of experts on the updating of the MSK-64 seismic intensity scale. *Gerlands Beitr. Geophys* **90**, 261-268.

Meidow, H. & L. Ahorner (1994). Macroseismic effects in Germany of the 1992 Roermond earthquake and their interpretation. *Geol. En Mijnb.* **73**, 271–279.

Musson, R.M., G. Grünthal & M. Stucchi (2010). The comparison of macroseismic intensity scales. *J. Seismol.* **14**, 413–428.

Nieuwenhuis, J.D. (1994). Liquefaction and the 1992 Roermond earthquake, the Netherlands. *Geol. En Mijnb.* **73**, 357–364.

Oncescu, M.-C., T. Cambelbeeck & H. Martin (1994a). A note on the foreshock of the 1992 Roermond earthquake, the Netherlands. *Geol. En Mijnb.* **73**, 229–233.

Oncescu, M.-C., T. Camelbeeck & H. Martin (1994b). Source parameters for the Roermond aftershocks of 1992 April 13–May 2 and site spectra for P and S waves at the Belgian seismic network. *Geophys. J. Int.* **116**, 673–682.

Pappin, J.W., A.R. Coburn & C.R. Pratt (1994). Observations of damage ratios to buildings in the epicentral region of the 1992 Roermond earthquake, the Netherlands (extended abstract). *Geol. En Mijnb.* **73**, 299–302.

Pelzing, R. (1994). Source parameters of the 1992 Roermond earthquake, the Netherlands, and some of its aftershocks recorded at the stations of the Geological Survey of NorthRhine-Westphalia. *Geologie en mijnbouw* **73**, 215-223.

Rosenhauer, W. & L. Ahorner (1994). Seismic hazard assessment for the Lower Rhine Embayment before and after the 1992 Roermond earthquake. *Geol. En Mijnb.* **73**, 415–424.

Sargeant, S.L., P.J. Stafford, R. Lawley, G. Weatherill, A.-J.S. Weston, J.J. Bommer, P.W. Burton, M. Free, R.M.W. Musson, T. Kuuyuor & T. Rossetto (2008). Observations from the Folkestone, U.K., Earthquake of 28 April 2007. *Seismol. Res. Lett.* **79**, 672–687.

Scherbaum, F. (1994). Modelling the Roermond earthquake of 1992 April 13 by stochastic simulation of its high-frequency strong ground motion. *Geophys. J. Int.* **119**, 31–43.

Schokker, J. & E.A. Koster (2004). Sedimentology and facies distribution of Pleistocene cold-climate aeolian and fluvial deposits in the Roer Valley Graben(southeastern Netherlands). *Permafr. Periglac. Process.* **15**, 1–20.

Schulte Nordholt, E., J. van Zeijl, L. Hoeksma & Centraal Bureau voor de Statistiek (2014). *Dutch census 2011: analysis and methodology*. Statistics Netherlands, The Hague.

Schwarz, J., S. Beinersdorf, H. Meidow & L. Ahorner (2010). *Magnitudenorientierter Erdbebenkatalog für deutsche und angrenzende Gebiete - EKDAG - erweiterter Ahorner-Katalog - Version 1.0*. SeismoGeologisches Büro Dr. Meidow & Earthquake Damage Analysis Center (Bauhaus-Universiät, Weimar).

Tyagunov, S., G. Grünthal, R. Wahlström, L. Stempniewski & J. Zschau (2006). Seismic risk mapping for Germany. *Nat. Hazards Earth Syst. Sci.* **6**, 573–586.

Van Gils J.M. & Zaczek, Y. (1978). La séismicité de la Belgique et son application en génia parasismique. *Annales des Travaux Publics de Belgique* **6**, 1-38.

Vanneste, K., M. Meghraoui & T. Camelbeeck (1999). Late Quaternary earthquake-related soft-sediment deformation along the Belgian portion of the Feldbiss Fault, Lower Rhine Graben system. *Tectonophysics* **309**, 57–79.

Vanneste, K., T. Camelbeeck & K. Verbeeck (2013). A Model of Composite Seismic Sources for the Lower Rhine Graben, Northwest Europe. *Bull. Seismol. Soc. Am.* **103**, 984–1007.

Vanneste, K., B. Vleminckx, K. Verbeeck & T. Camelbeeck (2014). Development of seismic hazard maps for Belgium. Workshop: Results of the European Project SHARE: Seismic Hazard Harmonization in Europe.

Weatherill, G. A. (2014). *OpenQuake ground motion toolkit - User guide*. Global Earthquake Model (GEM). Technical Report.

A3.1.11.2 Web references

Accessed on 9 June 2015:

GEM Earthquake Consequences Database: http://gemecd.org/

Global Centroid-Moment -Tensor (CMT) Project: http://www.globalcmt.org/

Gridded Population of the World (GPW): http://sedac.ciesin.columbia.edu/data/collection/ gpw-v3

International Seismological Centre: http://www.isc.ac.uk/

Royal Netherlands Meteorological Institute: http://www.knmi.nl/index_en.html

Royal Observatory of Belgium: http://seismologie.oma.be/

Seismic Workgroup, St.-Michael-Gymnasium Monschau, (2005): http://seismic.mgm-monschau.de/english/artikel/artikel_1_3.php).

Statistics Netherlands: http://statline.cbs.nl/

The New York Times (1992): http://www.nytimes.com/1992/04/14/news/14iht-quak.html).

United States Geological Service (USGS): http://earthquake.usgs.gov/earthquakes/

USGS EXPO-CAT database: http://earthquake.usgs.gov/research/pager/data/expocat.php

World Economic Outlook Database 2015: http://www.imf.org/external/pubs/ft/weo/2015/01/ weodata/index.aspx